Architecture and processes of deep-marine sandbodies, Ainsa basin, Spanish Pyrenees

Nicole Joanna Bayliss

2010

University College London

Thesis submitted for examination for the award of Doctor of Philosophy (Ph.D.)

DECLARATION

I, Nicole Joanna Bayliss, confirm that the work presented in this thesis is my own. Where information has been derived from other sources, I confirm that this has been indicated in the thesis.

Signed: ___________________________________

ABSTRACT

The integration of sedimentology, architectural element analysis and stratigraphy has been applied to characterise the complex depositional history of the Ainsa basin fill, and document the evolution of the proximal parts of eight, channelised deep-marine systems of the Hecho Group. The Eocene Ainsa basin provides an opportunity to research three-dimensional organisation through an entire deep-marine slope to proximal basin-floor fill, and records a range of depositional processes and sedimentary environments in a spatio-temporal framework.

The Hecho Group can be divided into two tectono-sequences, TS-I and TS-II. TS-I accumulated during a period of strong flexural subsidence ahead of the main thrust front during a foredeep setting, whereas TS-II represents a more mature stage of basin development, characterised by anticlinal uplift as the basin became detached and evolved into a complex thrust-top basin. Four discrete systems and their constituent sandy sequences compose each tectono-sequence. The sequences comprising TS-I show very little lateral migration due to high basin-scale accommodation; however, westward lateral offset stacking is observed in the sandy sequences of TS-II due to the development of intrabasinal growth anticlines. These structurally controlled trends demonstrate that the timing of tectonic processes operated at frequencies consistent with the accumulation of the depositional systems.

Depositional systems range between ~60–700 m thick, and were deposited in a number of deep-marine settings that include mid-slope canyons, lower-slope erosional channels and proximal basin-floor channel systems. Temporal variation in depositional style and architecture between systems reflects the tectonic regimes operating during the accumulation of the tectono-sequences. Alternatively, the 22 sandy sequences were controlled by the ~400 kyr Milankovitch frequency with higher-frequency orbital bands influencing the accumulation of channel complexes and channel fill elements.

An important outcome of this study is the recognition of a complex hierarchical interaction between global climatic and tectonic drivers, operating at a variety of time scales to control the timing of coarse clastic sediment supply and the architectural styles of depositional systems.

TABLE OF CONTENTS

LIST OF FIGURES

LIST OF TABLES

ACKNOWLEDGEMENTS

I would like to thank my supervisor, Professor Kevin T. Pickering (UCL), for the opportunity to pursue research in the Ainsa basin, and for supporting my ideas and research directions. I enjoyed the numerous reconnaissance field trips we conducted, and assisting you in field-based courses.

I am very grateful for the help and guidance I received from Dr John J. Millington, former second supervisor (Shell UK), particularly in understanding the stratigraphy of the study area and the valuable suggestions on various topics.

Thank you to various industry professionals for your guidance on selected areas of research and encouragement.

I appreciate all the fun times and interesting discussions with my friends, Tom, Clare and Kanchan.

Thank you to my family for their patience and moral support throughout my studies. A special thank you to Mum and Nan who have understood the obstacles I have encountered and provided unconditional love and support. Thanks Dad, for the ultimate field tool (my beloved Rocky), which allowed me to cover terrain I never thought possible.

I am very grateful to my Minnie-rat for the great company she provided during the long nights of constructing geological maps and sedimentary logs.

Thank you to my husband for his valuable assistance and exceptional understanding in my pursuit of this degree.

CHAPTER 1

INTRODUCTION

1.1. BACKGROUND

The primary focus of this Ph.D. thesis is the sedimentary and stratigraphic evolution of the Eocene deep-marine siliciclastic fill of the Ainsa basin, Spanish Pyrenees. The deep-marine systems of the Ainsa basin have played an important role in understanding deep-marine processes and products, and the development of stratigraphic concepts and generic models (e.g., Mutti, 1977, 1983, 1985; Mutti & Normark, 1987, 1991; Remacha *et al*., 1991, 1995, 1998, 2003, 2005, 2008; Schuppers, 1993; Clark, 1995; Millington & Clark, 1995a,b; Clark & Pickering, 1996; Dreyer *et al*., 1999; Pickering & Corregidor, 2000, 2005; Remacha & Fernandez, 2003, 2005; Fernandez *et al*., 2004; Melick *et al*., 2004; Falivene *et al*., 2006a,b, 2010; Bakke *et al*., 2008; Das Gupta & Pickering, 2008; Heard & Pickering, 2008; Heard *et al*., 2008; Labourdette *et al*., 2008; Sutcliffe & Pickering, 2009). This can be attributed to the increasing interest and activity of the oil and gas industry in deep water environments, and a more recent demand to interpret smaller-scale depositional bodies and stacking patterns due to the advancements in three-dimensional seismic data. Although this project does not attempt to directly apply to the industry, there is a requirement for more detailed outcrop studies to improve interpretations and predictions in reservoir architecture, heterogeneity and connectivity. The Ainsa basin provides an opportunity to research three-dimensional organisation through an entire deep-marine slope and proximal basin-floor fill, recording a range of depositional processes and sedimentary environments in an evolutionary framework.

Many publications on deep-marine systems have addressed lithofacies distributions, stratal geometries, characterisation of architectural elements, sequence stratigraphic patterns and depositional models of composite sequences, often third- or fourth-order stratigraphic cycles (*sensu* Haq *et al*., 1987) and higher (e.g., Ricci Lucchi, 1985; Sinclair, 2000; Johnson *et al*., 2001; Hickson & Lowe, 2002; McCaffrey *et al*., 2002; Eschard *et al*., 2003; Gardner *et al*., 2003; Anderson *et al*., 2006; Hodgson *et al*., 2006; Hubbard *et al*., 2008). Despite placing such observations into a simplified spatial and temporal context, similar investigations on the evolution of entire basin fills or second order stratigraphic cycles are infrequent, if not absent from such research. Additionally, the processes controlling sedimentation in foreland basins, such as regional/local tectonics, eustasy and climate, and the variety of frequencies at which they operate, are rarely integrated into these sedimentary and stratigraphic studies to constrain the timing and cause of sediment supply (Willis, 2000; Mutti *et al.*, 2003; Payros *et al.*, 2007; Maestro, 2008). The interaction between tectonic processes and climate change is more commonly treated as separate areas of interest (Blair & Bilodeau, 1988; Heller *et al.*, 1988; Flemings & Jordan, 1990; Zoetemeijer *et al.*, 1992, 1993; Butler & Grasso; 1993; Posamentier & Allen, 1993; Houston, 2000; Marzo & Steel, 2000; Clevis *et al.*, 2004a,b; Simpson, 2006; Naylor & Sinclair, 2007). The assessment of how deep-marine systems and sequences evolve through time is paramount to interpreting the depositional history of a complex basin fill and the mechanics responsible for the configuration. Thus, the stratigraphic evolution of the Ainsa turbidite system (a second order stratigraphic sequence comprising eight deep-marine systems), can lend insight into the complexity of factors that influence the hierarchical organisation of stacking patterns in a complete deep-marine succession.

1.2. RESEARCH AIMS AND OBJECTIVES

The principal aim of this study is to integrate sedimentological descriptions and interpretations of deep-marine sandy systems into a temporal and spatial framework to provide a better understanding of the stratigraphic evolution of the Ainsa basin and a synthesis of architectural styles for the history of the basin fill. The hierarchy of depositional elements will be investigated in the context of tectono-climatic signals and the different frequencies at which those processes operate; however, radiometric and geochemical studies is beyond the scope of this study and relevant information will be sourced from various publications. Despite the considerable amount of research on the deep-marine clastic systems in the Ainsa basin, this project intends to bridge the gap between previous research and to present a unique data set that investigates the complex depositional history of the Ainsa basin. Several objectives have been assigned to the project to attain the goals outlined:

(1) Study the stratigraphy of the Ainsa basin defining deep-marine sandy systems and sequences, documenting environments of deposition, and compiling palaeocurrent measurements
(2) Create geological maps of the deep-marine sandy systems in the Ainsa basin, which have previously received little attention in publications, with particular focus on the Banastón and Morillo systems.
(3) Describe the range of deposits and depositional processes in the Ainsa basin through detailed sedimentary logging and quantitative analyses of lithofacies.
(4) Document lateral and vertical lithofacies distributions, and geometrical relationships by constructing correlation panels and interpreting photomosaics.
(5) Delineate architectural elements and classify the hierarchical stacking patterns of depositional bodies to develop a deep-marine channelised hierarchy that can be quantitatively characterised.
(6) Identify the three-dimensional depositional characteristics in deep-marine slope to proximal basin-floor systems and create depositional models of the Banastón and Morillo systems that integrate structural and stratigraphic elements.
(7) Develop generic models of channel fills and stacking patterns at various scales to produce a synthesis of architectural styles and depositional trends in the Ainsa basin.
    - Assess the influence of thrust-related topography on basin fill architecture.
    - Consider the factors controlling the timing of sediment supply and the hierarchical organisation of depositional bodies in the Ainsa basin, and evaluate the significance of each parameter in the stratigraphic evolution of the basin.
(8) Describe the depositional history and tectono-stratigraphic evolution of the Ainsa basin using results from the above objectives.
    - Integrate the regional stratigraphic and structural evolution of the South Pyrenean foreland basin by reviewing previous work and constructing palaeogeographic reconstructions to determine how the basin fill evolved with time.

1.3. THESIS OUTLINE

This thesis consists of seven chapters sequentially organised to present results and interpretations that address the aims and objectives. Chapter 1 provides a general background to the nature of the study. The geological setting of the study area and an introduction to previous stratigraphic nomenclature and concepts are included. This information is designed to form a foundation to expand upon and is integrated into successive chapters to support the interpretations outlined in the thesis. Chapter 2 presents the field-based techniques carried out to acquire the data set and a summary of geographical locations visited. Chapter 3 describes the lithofacies classification scheme that was used to analyse the range of deposits and depositional processes in the Ainsa basin, followed by a description of facies associations and types of mass transport deposits (MTDs) observed in the study area. A review of deep-marine architectural elements and hierarchical stacking patterns forms the second part of this chapter. Chapters 4–6 systematically document sedimentary and stratigraphic observations of deep-marine systems in the Ainsa basin. They are assembled chronologically to build a temporal framework for the later part of the thesis. Chapter 4 details the results and interpretation of the four sandy systems that comprise the Lower Hecho Group (which includes the Fosado, Los Molinos, Arro and Gerbe systems). An overview of the structural framework during deposition of the Lower Hecho Group is provided in this chapter to assess the early morphological configuration of the basin and contribute to the tectono-stratigraphic evolution of the Ainsa basin (final chapter). Chapter 5 is concerned with the lower division of the Upper Hecho Group and predominantly investigates the erosional slope to proximal basin-floor sequences in the Banastón system, and the influence of intrabasinal structural highs on depositional architectures. A sedimentological synopsis of the Ainsa system is discussed at the end of the chapter. Chapter 6 considers the way in which deep-marine systems change their architectural style as the basin infills, documenting observations from the youngest systems in the Ainsa basin, the Morillo and Guaso systems (upper division of the Upper Hecho Group). An emphasis is placed on the Morillo system, where a geological map, correlation panels and depositional models are presented with the interpretations. Furthermore, the interaction between sedimentation patterns and seafloor topography is discussed in detail. Chapter 7 forms the discussion to the study. It is designed to interpret the observations made in Chapters 4–6 and outline conclusions reached from this study in order to construct the depositional history of the Ainsa basin. The interplay between tectonic processes and global climate change at a variety of temporal and spatial scales is also addressed. The final chapter (Chapter 8) concludes with future research and an overview of results obtained from the study.

1.4. GEOGRAPHICAL SETTING

The Pyrenees are an east–west trending linear mountain chain of Alpine age, forming the northeast edge of the Iberian Peninsula. They extend from Provence in Southern France, westwards to the Cantabrian ranges of Northern Spain, and are ~1500 km long with an average width of ~200 km (Schellart, 2002). The central part of the range lies between the Mediterranean Sea and the Bay of Biscay, separating France and Spain (Fig. 1.1).

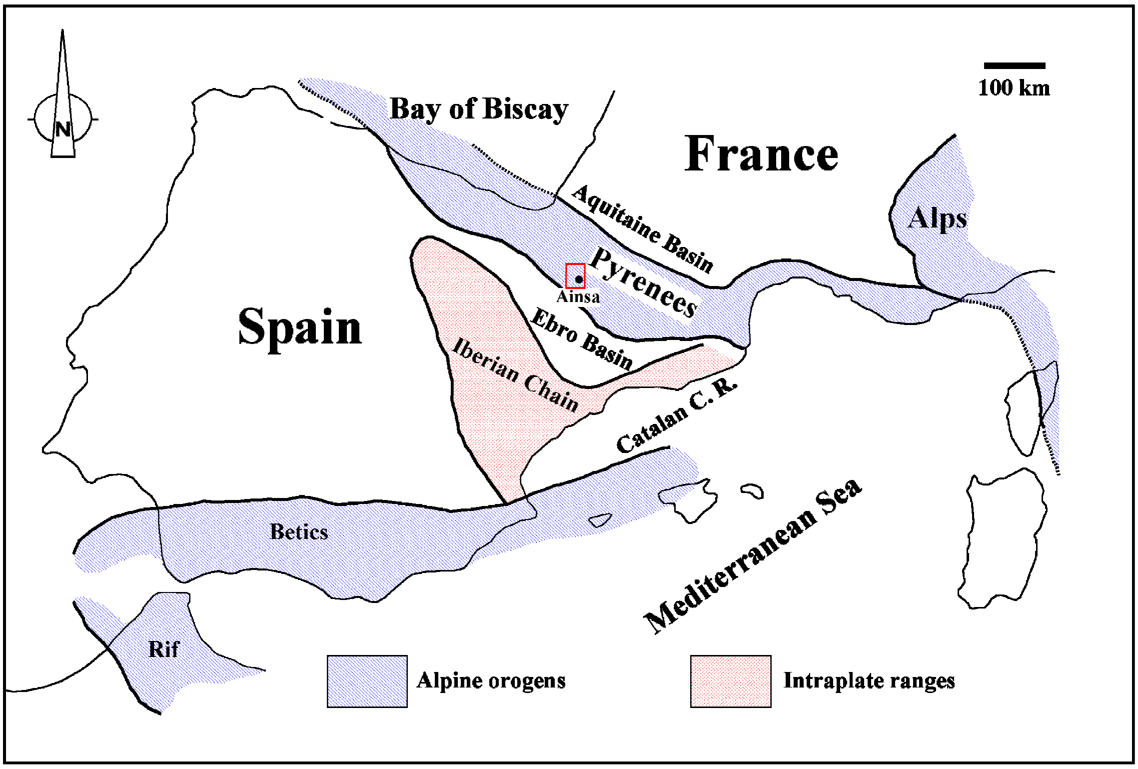

Fig. 1.1. Geographical location of the Pyrenees and the study area (redrawn and modified after Santanach, 1997).

The study area is located in the south-central Pyrenees, situated in the province of Huesca, within the Sobrarbe region of Northeastern Spain. The outcrops are positioned around the towns of Ainsa and Boltaña, in a mountainous region with elevation ranges between 500 m and 1,300 m above sea level. The vegetation is characterised by low-lying shrubbery, which become denser at higher altitudes. The area is typical of a Mediterranean climate, with temperatures ranging from -5 degrees Celsius to 30 degrees Celsius. Rainfall is moderate from autumn to spring.

1.5. GEOLOGICAL SETTING

1.5.1. INTRODUCTION TO THE PYRENEES

The Pyrenees formed as a fold and thrust belt orogen as a result of the north–south continental collision between the Iberian and Eurasian plates in the Santonian (Late Cretaceous) to Early Miocene time (Muñoz *et al.*, 1986; Muñoz, 1992; Puigdefàbregas *et al.*, 1992). Compressional movements were in response to the closure of the Tethys Sea, and the opening of the Central Atlantic Ocean and Bay of Biscay (Dercourt *et al.*, 1986), resulting in a ~35° anticlockwise rotation of Iberia (Vergés *et al.*, 2002). The partial subduction of the Iberian plate underneath the European plate (Fig. 1.2; Séguret & Daigneres, 1986; Choukroune & ECORS Team, 1989) has been well documented by different geophysical techniques, including deep seismic reflection data (ECORS Pyrenees Team, 1988), seismic tomography (Souriau & Granet, 1995) and magnetotellurics (Ledo *et al.*, 2000). The most intense period of shortening and deformation occurred during the Early/Middle Eocene to Oligocene time (Puigdefàbregas *et al.*, 1992; Vergés *et al.*, 1998, 2002). The cessation of tectonic activity along the Iberian-European plate boundary occurred in the Miocene (Huyghe *et al.*, 2009).

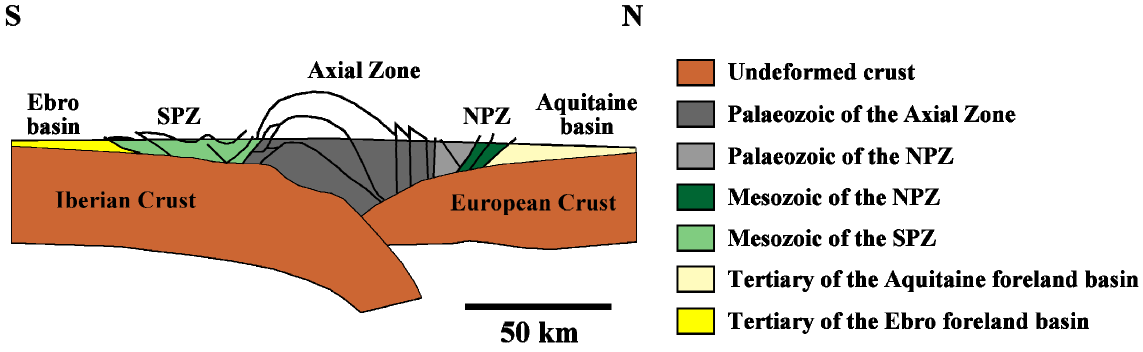

Fig. 1.2. Crustal scale cross-section based on the ECORS-Pyrenees seismic profile (redrawn and modified after Muñoz, 1992). See Figure 1.3 for location of section.

The Pyrenees mountain range began an area of inversion that was superimposed on east–west trending, Triassic–Cretaceous, extensional to transtensional rift systems (Coney *et al.*, 1996). Prior to the Alpine compression, Early Cretaceous rift basins had developed, which contained thick sequences of marls and limestones. These basins were shortened and strained during the Late Cretaceous to Early Miocene time, and were subsequently incorporated into the Pyrenean thrust system (Puigdefàbregas *et al.*, 1992). Deformation was characterised by partly inverted extensional faults, footwall short-cut faults and hangingwall fault-propagation folds. Syn-inversion, strongly subsiding basins developed in front of the inverted extensional faults and were infilled with Late Cretaceous turbidites (Garcia-Senz *et al.*, 2000).

The Pyrenees orogen is an asymmetric, bivergent mountain belt, primarily consisting of a series of east–west trending fold and thrust systems (Vergés *et al.*, 2002), with major northeast–southwest fault lines superimposed on the main structural trend (Payros *et al.*, 1999). The southern, and most significant system developed on top of the subducted Iberian plate, and is characterised by south-vergent thrusts. The northern system developed on top of the Eurasian plate (Vergés *et al.*, 2002), and is represented by north-vergent thrusts. The tectonic deformation was diachronous due to an oblique plate convergence, initiating in the east and propagating westwards. Thus, significant structural variations are observed laterally through the mountain range (Teixell, 1998), but five major structural zones can be identified after Vergés *et al.* (1995). These zones are, from north to south, the Aquitaine Foreland Basin, the North Pyrenean Zone, the Axial Zone, the South Pyrenean Zone and the Ebro Foreland Basin (Fig. 1.3; *sensu* Schellart, 2002).

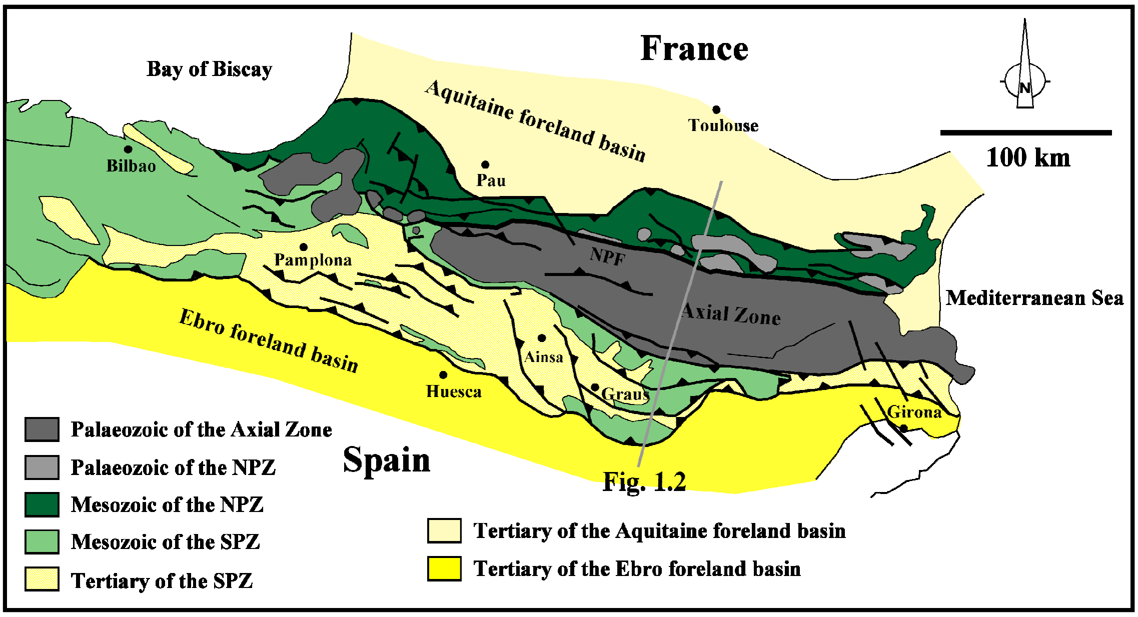

Fig. 1.3. Five structural zones of the Pyrenees (redrawn and modified after Schellart, 2002). NPF, North Pyrenean Fault; NPZ, North Pyrenean Zone; SPZ, South Pyrenean Zone. The location of the section in Figure 1.2 is shown.

The *Aquitaine Foreland Basin* is situated on the Eurasian plate and was formed by flexural subsidence from the weight of the thrusting in the North Pyrenean zone. The basin is filled with tectonically undisturbed synorogenic sediments, with the oldest sediment dating from the Late Cretaceous (Schellart, 2002). The *North Pyrenean Zone* consists of north-verging thrusts deforming Hercynian basement and Mesozoic to Late Eocene cover sediments. The zone is bounded to the south by the North Pyrenean Fault; a major strike-slip fault which developed during the sinistral displacement of Iberia during the Middle Cretaceous (Santanach, 1997). The North Pyrenean Fault is considered to be the axis of the collisional belt and present boundary between the Iberian and European plates, although the fault does die out to the west and no longer represents the plate boundary (Muñoz, 1992; Teixell, 1998). The *Axial Zone* consists of Palaeozoic rocks that were deformed from the Hercynian orogenic episodes in the Late Carboniferous (Williams, 1985;Vissers, 1992). The zone forms a south-vergent antiformal stack of basement thrust sheets, which typically show characteristics of thick-skinned tectonics (Schellart, 2002). The *South Pyrenean Zone* is a zone of south-vergent thrusts, which deformed by thin-skinned tectonics with a décollement level in the Triassic evaporites (Muñoz *et al.,* 1986). The décollement zone emerges at the South Pyrenean Frontal Thrust, the Sierras Marginales (Exteriores), north of the Ebro foreland basin (Schellart, 2002). Deformation of the South Pyrenean Zone involved thrusting over the foreland of autochthonous rocks in a piggyback sequence (Santanach, 1997), which commenced in the Early Eocene and continued until the Early Miocene (Labaume *et al.*, 1985; Vergés *et al.*, 1995). The study area is located in the South Pyrenean Zone. The *Ebro foreland basin* is the youngest southern foreland basin of the Pyrenees, and contains an asymmetrical sedimentary fill, which thickens northwards (Riba *et al*., 1983). The basin formed under the weight of South Pyrenean thrust system, and consists of tectonically undisturbed sediments of Tertiary age that directly overlie Hercynian basement (Schellart, 2002).

ECORS Pyrenees Team (1988) documented the initial results from the first deep seismic reflection profile across an entire orogenic belt. The ECORS-Pyrenees profile is a nearly continuous, ~225 km long reflection seismic survey across the central Pyrenees, extending from the Ebro basin in Spain to the Aquitaine basin in France. The primary objective of the survey was to understand geometrical relationships between structures in order to constrain possible tectonic models for the formation of the Pyrenean chain. The profile illustrates the subduction of the Iberian plate beneath the

European plate, and has been the basis for the construction of crustal-scale balanced cross-sections. However, the key observation made by ECORS Pyrenees Team (1988) in relation to this study was the thin-skinned tectonic style in the southern Pyrenees, showing that the basement rocks underlying the South Pyrenean Frontal Thrust were not involved in Eocene (Pyrenean) deformation. They also interpreted major northward-dipping reflectors within the Axial Zone that are connected to the décollement of the Tremp basin (part of the South Pyrenean foreland basin) and emerge in the frontal thrust zone of the Montsec and Sierras Marginales (Exteriores) thrusts. This work has formed the foundation to understanding the evolution of the South Pyrenean Zone and the sedimentation patterns in the South Pyrenean foreland basin (discussed below).

1.5.2. RATES OF SHORTENING

Total shortening of the Pyrenees, calculated from balanced and restored cross-sections, is estimated between 120 km (Roure *et al.*, 1989), 147 km (Muñoz, 1992) and 165 km (Fitzgerald *et al.*, 1999) for the eastern and central Pyrenees. These estimates are mainly based on the restoration of the ECORS-Pyrenees deep reflection seismic survey (ECORS Pyrenees team, 1988); other areas of the Pyrenees may yield different total shortening estimates due to the variation in convergence between Iberia and Europe (Schellart, 2002). The estimated total shortening for the western part of the Central Pyrenees is on the order of 75–80 km (Teixell, 1998).

Vergés *et al.* (1995) calculated shortening rates for the South Pyrenean Zone based on balanced cross-sections and palinspastic maps from eastern Pyrenean sections. Three different periods were revealed and have subsequently been attributed to the emplacement of various thrust sheets by Vergés *et al.* (2002). The first period (Late Cretaceous to Palaeocene time) shows a very slow rate of shortening, less than 0.5 mm yr^{-1}, and has been related to the development of the uppermost thrust sheets during tectonic inversion of pre-existing rifted Mesozoic basins, involving the upper Pedraforca, Bóixols and Turbón thrust sheets. This period was followed by a relatively fast rate of shortening, up to 4.5 mm yr^{-1}, during the second period (Early to Middle Eocene time), which was correlated to the emplacement of the lower Pedraforca thrust sheet and the South-Central Pyrenean Unit. From the Middle Eocene to Middle Oligocene, rates of shortening varied from 1.5 to 2.6 mm yr^{-1}. This third period was associated with deformation in the transition zone between thinned and undeformed crusts (Vergés *et al.*, 2002). The North Pyrenean Zone is characterised by an average shortening rate of ~1 mm yr^{-1} throughout deformation, although the Early to Middle Eocene time represented intensified deformation. These combined rates of shortening support an average convergence rate between the northeastern part of the Iberian plate and the European plate of ~6 mm yr^{-1} during the most rapid period of plate collision in the Early to Middle Eocene (Burbank, *et al.*, 1992a; Vergés *et al.*, 1995). This time period is significant because it represents the age of the sediments investigated in this thesis.

1.5.3. EVOLUTION OF THE PYRENEES

The evolution of the Iberian and Eurasian plate boundary began in the Early Mesozoic and developed as: (a) a rifted margin during the extensional and transtensional Mesozoic times; (b) a collisional margin during the Tertiary, and (c) a large passive margin during the Late Miocene and Quaternary (Ziegler, 1988; Srivastava *et al.*, 1990; Vergés *et al.*, 2002). The Pyrenean orogenic episode can be divided into two separate phases, an earlier Cretaceous phase of sinistral strike-slip movements as the Iberia plate was rotated in an anticlockwise direction (Fischer, 1984), and a Palaeocene to Oligocene compressional phase, dominated by north–south shortening (Williams & Fischer, 1984; Farrell *et al.*, 1987).

1.5.3.i. Pre-collisional history

The oldest rocks exposed in the Pyrenees form the Hercynian basement and are exposed in the Axial Zone and in the North Pyrenean Zone. The rocks are Cambrian to Carboniferous in age and have been affected by metamorphism during the Hercynian orogeny (Williams, 1985;Vissers, 1992).

During early Permian times, volcanism and intrusions of granitic bodies into the Hercynian basement was in response to an extensional phase (Zwart, 1979). Deposition of Permian redbeds occurred in small fault-bound basins as the erosional product of the newly exposed mountains. In Triassic time, clastics, carbonates and evaporites were deposited and an intracontinental rift environment existed due to an overall extensional regime (Puigdefàbregas & Souquet, 1986; Vergés *et al.*, 2002). During Jurassic times, a widespread carbonate platform had extended over most of the Pyrenees (Peybernes & Souquet, 1984). Opening of the Central Atlantic Ocean in the Early Cretaceous caused a left-lateral, transtensional movement of the Iberian plate, with respect to the Eurasian plate, resulting in the opening of the Bay of Biscay (Puigdefàbregas & Souquet, 1986).

The Pyrenean rift connected the Bay of Biscay with the Tethys Ocean in the east (Vergés *et al.,* 2002). The formation of pull-apart basins linked to transtensional motion of the Iberian plate boundary during this time led to the renewed production of carbonate platforms and the first deposition of true Pyrenean clastics. The tectonic regime changed to transpressional during the Late Cretaceous, and resulted in down-faulting tectonics that created a regional unconformity with retreating, erosional basin margins (Schellart, 2002). The end of this regime is marked by a shallowing-upward sequence consisting of turbidites, marls and marine redbeds.

1.5.3.ii. Tertiary collisional history: evolution of the South Pyrenean foreland basin

The continental collisions of the Iberian and European plates produced the formation of the Pyrenean orogen (Muñoz *et al*., 1986; Puigdefàbregas *et al*., 1992; Vergés *et al.,* 2002). During the Tertiary times, rearrangement of the Iberian and Eurasian plates led to the replacement of the Mesozoic basins with northern and southern Tertiary foreland basins, with the axial zone between (Schellart, 2002). In the southern Pyrenees, tectonic loading and lithospheric flexure gave rise to an extensive South Pyrenean foreland basin (Poblet *et al*., 1998), which developed in front of the southward-advancing thrust front (Farrell *et al*., 1987). A pattern of outward depocentre migration is observed from the Late Cretaceous onwards, as a consequence of thrust propagation towards the foreland. The focus of this study is concerned with part of the South Pyrenean foreland basin; therefore, only the evolution of the south-central Pyrenees and the associated foreland basin is discussed herein.

During the Palaeocene, the emergence of the mountain chain led to erosion and subsequent deposition of non-marine redbeds. This was followed with the development of a shallow carbonate shelf extending from the east, which was rapidly replaced with more deep-marine deposits including hemipelagics and carbonate turbidites in the west (Léon-Gonzalez, 1972). During this period, the first foreland basin geometry was established in the east, while Mesozoic basins still prevailed in the west (Schellart, 2002). From the Eocene times, the Pyrenees developed into a true fold and thrust belt orogen, and a complete South Pyrenean foreland basin developed (Seguret, 1972). The basin was flanked in the north by active thrust sheets and in the south by carbonates (Barnolas *et al.,* 1991). The sediment was supplied from the rising mountain range in the north and was axially fed into the basin. Deltaic deposition prevailed in the centre of the basin (Tremp–Ager basin), while the deposition of siliciclastics turbidites were in the east (Vic basin) and west (Ainsa–Jaca basin). As the southern Pyrenees thrust sheets propagated southwards, the South Pyrenean foreland basin synchronously shifted towards the foreland (Labaume *et al.*, 1985). Contemporaneously, the basin also shifted westwards, due to progressive infilling of the basin from east to west. The basin developed as an underfilled, marine basin until the late Lutetian to Bartonian times. The uplift of the western Pyrenees marked the transition of the basin into an overfilled stage, when a deltaic system prograded westwards over much of the area**.** The extensive carbonate system in the south was no longer present during this time (Schellart, 2002) and an intermontane foreland basin existed (Vergés and Burbank, 1996). During the Oligocene, sedimentation was predominantly fluvial in the South Pyrenean foreland basin. The southward advancement of active thrust sheets in the southern Pyrenees deformed and incorporated the northern basin margin into the deformation front. Early Miocene molasses were deposited unconformably above the thrusts and folds of the deformation front, and were subsequently deformed (Labaume *et al.*, 1985). From the Oligocene to early Miocene times, sedimentation shifted to the Ebro foreland basin, characterised by a large central lake (Anadón *et al.*, 1979; Luzón, 2005).

1.6. THE SOUTH-CENTRAL PYRENEES

1.6.1. INTRODUCTION

The study area is situated within the South Pyrenean foreland basin in the south-central Pyrenees (Fig. 1.4), which is part of the South Pyrenean thrust system. The south-central Pyrenees extends from the Segre fault system in the east to the Pamplona fault in the west (Payros *et al*., 1999; Remacha *et al*., 2003; Ruiz *et al*., 2006), and consists of: (1) Palaeozoic (Hercynian) basement rocks of the Axial Zone in the north, comprising a south-verging antiformal stack; (2) a Mesozoic pre-orogenic succession; (3) a syn-orogenic succession comprising Late Cretaceous–Tertiary sedimentary rocks deposited during basin inversion and thrust advancement (Remacha *et al*., 2003). Two main south-verging thrust units that are part of the South Pyrenean Zone are recognised in the south-central Pyrenees: (1) the Lakora-Eaux Chaudes / South-Central Pyrenean Unit (SCPU; *sensu lato* Séguret, 1972; Muñoz *et al.*, 1994, 1998); (2) the Larra-Boltaña / Gavarnie-Sierras Exteriores unit (Farrell *et al*., 1987; Verges & Muñoz, 1990; Muñoz, 1992; Muñoz *et al.,* 1994, 1998; Nijman, 1998; Maestro, 2008). These thrust units are related to specific tectonic stages in the evolution of the south-central Pyrenees, discussed in Section 1.6.4.

1.6.1.i. The South-Central Pyrenean Unit (SCPU)

The development of the SCPU is related to the evolution of the South Pyrenean foreland basin, and involves the emplacement of thrust sheets during various tectonic stages in the evolution of the south-central Pyrenees. The SCPU was responsible for controlling the geometry and configuration of the basin, and facies distributions during filling. The unit is located in the eastern part of the south-central Pyrenees, bounded by the Segre fault system in the east, and the imbricate thrust system defining the boundary with the Gavarnie thrust sheet in the west (see Fig. 1.4; Farrell *et al.*, 1987; Verges & Muñoz, 1990; Burbank *et al.*, 1992b; Muñoz, 1992; Muñoz *et al.,* 1994, 1998; Nijman, 1998; Dreyer *et al.*, 1999; Fernández *et al.*, 2004; Falivene *et al.*, 2006b). The Ebro foreland basin forms the southern–southeastern margin and the Nogueres zone defines the northern extent. The Nogueras zone consists of a duplex of basement-involved lower thrust sheets comprising cover and basement rocks of the Axial Zone (Burbank *et al.*, 1992a,b), which developed into a pronounced antiformal stack at the rear of the cover thrust sheets (Nijman, 1998). The SCPU is formed by the southward emplacement of three major structural units, which consist of the Bóixols, Montsec and Sierras Marginales thrust sheets, from north to south, respectively. These are equivalent to the lower and upper Pedraforca thrust sheets in the eastern Pyrenees (Vergés *et al.*, 1992; Vergés & Burbank, 1996). Thrusts were generated by tectonic inversion of pre-existing Cretaceous normal faults (Roure *et al.*, 1989). Development of the Bóixols thrust sheet initiated in the Late Cretaceous time (Simó & Puigdefàbregas 1985; Simó, 1986), whereas the Montsec and Sierras Marginales thrust sheets were emplaced during the Eocene, representing a phase of major shortening (Mutti *et al.*, 1985; Burbank *et al.*, 1992a). Balanced cross-sections indicate a minimum of 7.5 km of shortening occurred along the Sierras Marginales and Montsec thrust sheets (Burbank *et al.*, 1992b).

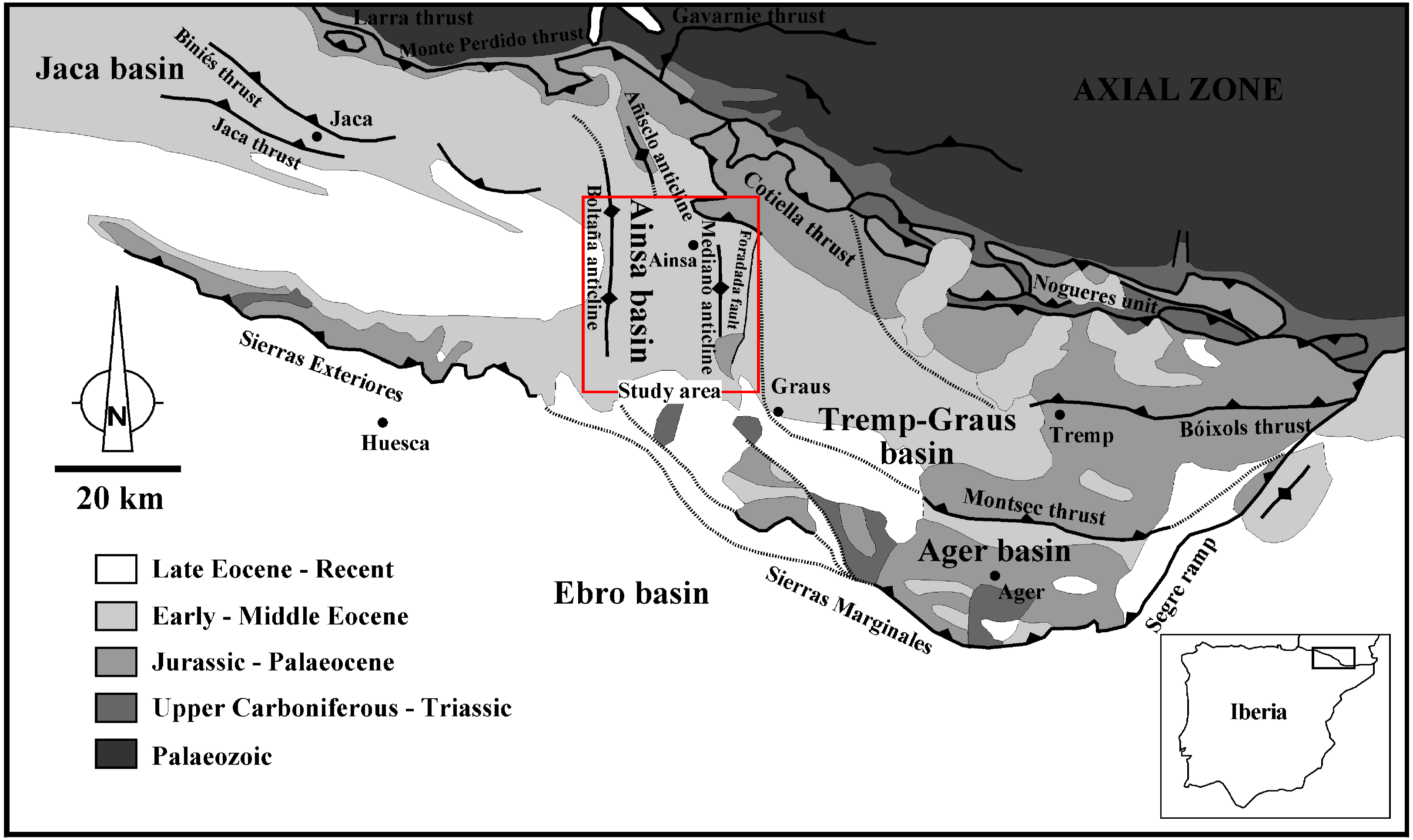

Fig. 1.4. Simplified geological map of the south-central Pyrenees showing major geological units and location of the study area (redrawn and modified after Choukroune & Seguret, 1973; Remacha & Fernández, 2003).

1.6.1.ii. Structural trends

Tectonic deformation developed diachronously along the strike of the Pyrenees due to an oblique plate convergence, initiating in the east and propagating westwards (Payros *et al.*, 1999). This tectonic trend is reflected in the pattern of structural deformation, subsidence trends and the palaeogeographic evolution of the foreland basin (Mutti *et al.*, 1985; Puigdefàbregas & Souquet, 1986; Puigdefàbregas *et al.*, 1992).

The main structural trend of the south-central Pyrenees is west-northwest–east-southeast, whereas traverse structures generally trend north–south to northeast–southwest. To the north of the South Pyrenean Zone, Hercynian basement rocks of the Axial Zone, together with Triassic rocks, comprise the duplex system (Cámara & Klimowith, 1985; Farrell *et al.*, 1987; Remacha *et al.*, 2003). Triassic (Keuper) evaporites provide a detachment level through which a series of splays form a foreland-verging cover thrust system (Remacha *et al.*, 2003). Mesozoic and Tertiary sediments were thrusted and folded in the South Pyrenean Zone and South Pyrenean foreland basin (Choukroune & Seguret, 1973; Farrell *et al.*, 1987). East–west trending thrusts constitute the frontal ramps and define the southward propagation of the thrust front, whereas north–south trending structures (thrusts and folds) represent extensions of lateral and oblique ramps, and reflect the lateral propagation of deformation. The frontal ramps are connected to the orogenic wedge through a shallow hinterland-dipping detachment thrust. The ECORS profile documented the thin-skinned style of tectonics operating in the South Pyrenean thrust system during the Eocene and depicted thrust splays that branch from a common décollement plane (ECORS Pyrenees team, 1988). Cover thrusts developed as a forward-breaking sequence (in which younger, deeper faults deformed overlying thrust sheets), where older (upper) thrusts formed in the east and north of the western part of the south-central Pyrenees, propagating to the south and west as progressively younger (lower) thrusts (Fig. 1.5; Farrell *et al.*, 1987; Remacha *et al.*, 2003).

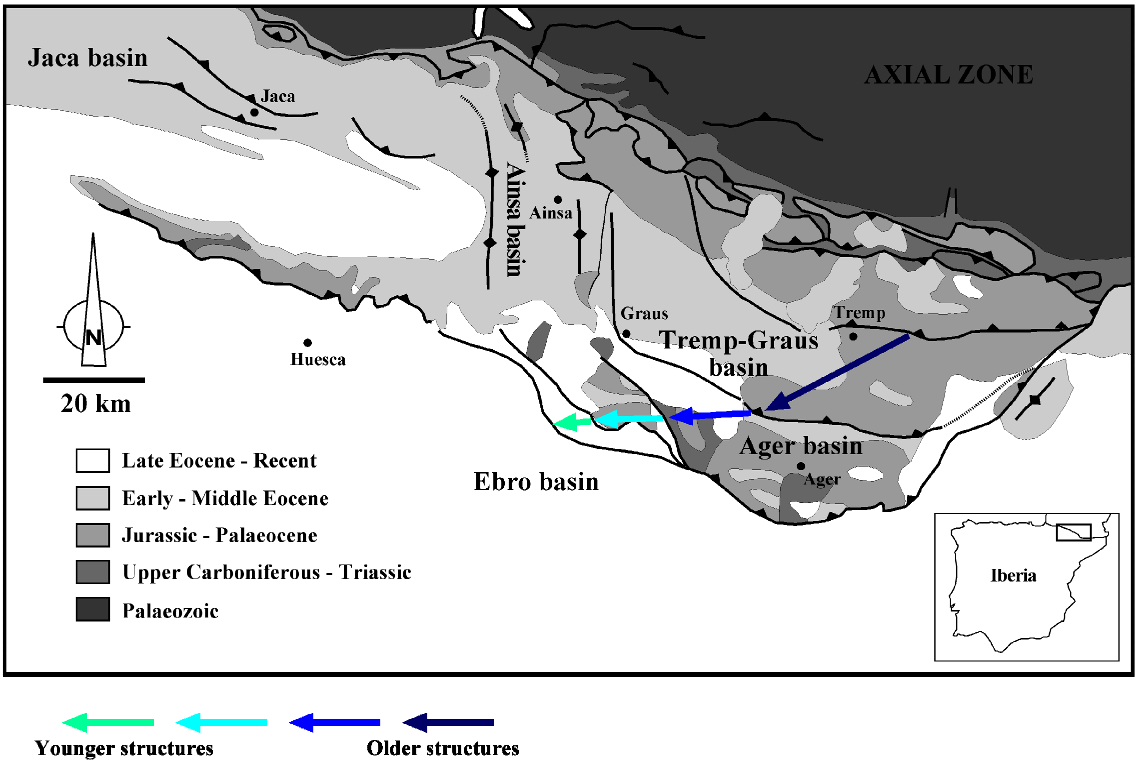

Fig. 1.5. Sequence of thrusting in the south-central Pyrenees (redrawn and modified after Choukroune & Seguret, 1973; Remacha & Fernández, 2003). Arrows point from older (right) to younger (left) thrust sheets. The pattern of thrusting influences stratigraphic trends in the South Pyrenean foreland basin.

1.6.2. Palaeogeographic sectors of the South Pyrenean foreland basin

The study area is situated in the east-southeast–west-northwest trending South Pyrenean foreland basin, collectively named the Tremp–Pamplona basin (Mutti *et al.*, 1988). This Tertiary foreland basin trended parallel to the Pyrenean Axial Zone, and opened towards the Atlantic Ocean. The Ebro Massif formed the southern margin. The Segre oblique ramp confined the basin in the east (Farrell *et al.*, 1987), and the Roncesvalles fault defined the basin in the west (Remacha *et al.*, 2003). A complex system of frontal and lateral ramps defining the Southern Pyrenees was responsible for the structural segmentation of the foreland basin into subsequent piggyback sub-basins, each characterised by a different depositional environment (Puigdefàbregas *et al.*, 1992). Consequently, three main palaeographical sectors can be identified from facies associations within the basin fill (Fig. 1.6; Mutti *et al.*, 1972, 1985, 1988). For the clarity of this study, the sub-basins are referred to basins themselves. The *eastern sector* or *Tremp–Ager basin* extends from the Tremp–Ager region in the east, westwards to the general area of Tierrantona. The sector is characterised by an east–west succession of alluvial, deltaic, nearshore and shelfal deposits of the Montañana Group (Nijman & Nio, 1975; Friend *et al.,* 1981; Mutti *et al.,* 1985). The east–west trending, south-verging Montsec thrust partly divides this sector into two further sub-basins, named the Ager basin and the Tremp–Graus basin (Payros *et al*., 1999). The *central sector* or *Ainsa–Jaca basin* lies between the area of Tierrantona in the east, and Jaca in the west. The eastern and central sectors are bounded by a complex system of lateral ramps and detachments accommodating differential movements within the SCPU. This boundary is marked a palaeogeographic shelf break, and the subsequent change in facies associations due to the structural oversteepening of the delta front. Major submarine erosional surfaces and shelf edge failures characterise this eastern boundary, which correlate westwards to a thick deep-water clastic succession, collectively named the Hecho Group (Mutti *et al.,* 1972). Although the Ainsa–Jaca basin represented a contiguous basin during deep-marine sedimentation, the present day Boltaña anticline roughly divides the Ainsa–Jaca basin into two parts. The structure broadly coincides with the change from more channelised deposits in the east (Ainsa basin) to less-confined, more sheet-like, lobe and related deposits in the west (Jaca basin). The Boltaña anticline formed as a syn-sedimentary structural high, but did not represent a significant sea floor high physically compartmentalizing the Ainsa and Jaca basins; therefore, the naming of the two sub-basins is adopted mainly for convenience. The *western sector* or *Pamplona Basin* extends from Jaca to Pamplona, and consists of a thick succession of basin plain deposits, sporadically interbedded with re-sedimented carbonate units/megaturbidites (Soler & Puigdefabregas 1970; Mutti *et al*., 1972; Labaume *et al.,* 1987; Payros *et al.,* 1999; Puigdefabregas 2003). The northern border was formed by the active Lakora-Eaux Chaudes thrust sheet (Labaume *et al*., 1985; Teixell, 1992; Remacha *et al.,* 2003), and the south was flanked by an extensive carbonate platform (Puigdefàbregas & Souquet, 1986; Barnolas *et al*., 1991). In the Early to Middle Eocene, the South Pyrenean foreland basin evolved with mainly non-marine and marginal marine environments in the eastern sector (Tremp–Ager basin), whilst farther west there was an overall transition to deep-marine environments in the Ainsa–Jaca basin and distal basin-floor environments in the Pamplona basin (Mutti *et al*., 1988).

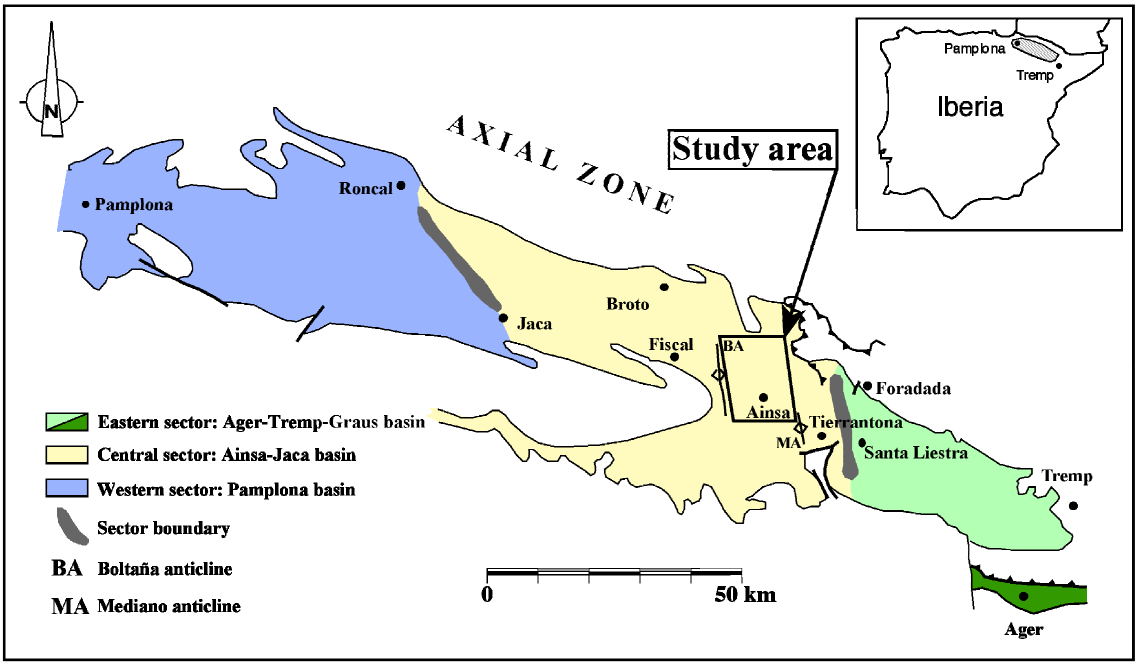

Fig. 1.6. Map of the main palaeogeographic sectors of the Tremp–Pamplona basin, south-central Pyrenees (redrawn and modified after Mutti *et al.*, 1985). The Montsec thrust further divides the Tremp–Ager basin (eastern sector) into 2 sub-basins, named the Ager basin and the Tremp–Graus basin. The study area is located in the central sector, named the Ainsa–Jaca basin. Note the Tremp–Pamplona basin trends parallel to the axial zone of the Pyrenean mountain belt.

1.6.3. STRATIGRAPHY OF THE SOUTH PYRENEAN FORELAND BASIN

The eastern sector of the South Pyrenean foreland basin predominantly consists of Eocene fluvio-deltaic deposits of the Montañana Group (*sensu* Nijman & Nio, 1975). These deposits grade westward into the contemporaneous deep-marine Hecho Group (*sensu* Mutti *et al.*, 1972) in the central sector of the basin (study area), which are also referred to as the San Vicente Formation (*sensu* Van Lunsen, 1970; Nijman &Nio, 1975). Throughout the three main palaeogeographic sectors of the South Pyrenean foreland basin, unconformity bound units have been defined (e.g., Mutti *et al.*, 1972, 1984, 1985, 1988; Nijman & Nio, 1975; Nijman, 1998; Remacha *et al.*, 1998, 2003; Pickering & Bayliss, 2009). The correlation of sequence boundaries within and between the sub-basins is controversial. The subdivision of the stratigraphy in this study attempts to retain the original group names where possible, but is modified to represent a more detailed stratigraphic framework of the Ainsa basin fill (Fig. 1.7).

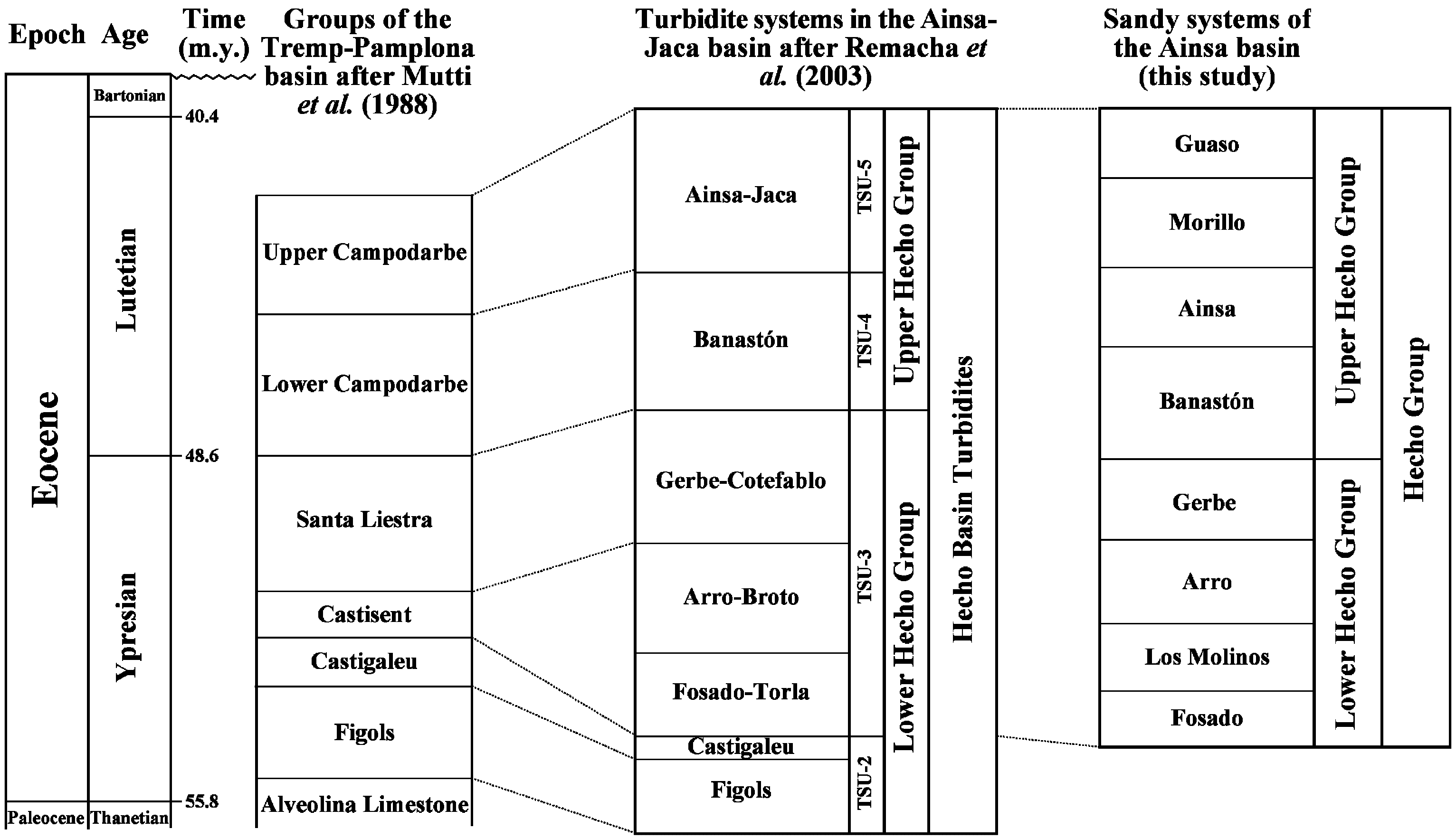

Fig. 1.7. Stratigraphic divisions in the Tremp-Pamplona basin and component sub-basins, as defined by various authors. The focus of this study is concerned with the deep-marine sandy systems of the Hecho Group in the Ainsa basin. Ages taken from Abrués *et al*. (1998), and have been updated using the timescale of Gradstein *et al*. (2004). TSU, tectono-sedimentary unit.

Mutti *et al*. (1985) recognised three stages of evolution within the Tremp–Pamplona basin. The first stage is represented by the fluvio-deltaic deposits of the Figols and Montañana sequences, situated in the eastern sector of the basin. These deposits barely reach the central sector, which provides some indication that the axis of the Tremp–Graus sub-basin was lying farther to the north during the early stages of evolution. The intermediate stage, consisting of the Castisent, Santa Liestra and Banastón sequences, are recorded in both the eastern sector (shallow-water deposits) and the central sector (deep-water deposits) of the basin. This period is marked by the rapid south-directed shift in the Tremp–Graus basin axis. The third stage, expressed by the Ainsa, Morillo and Guaso sequences, is not very well developed in the Tremp–Graus basin and is focused to the central sector of the basin. This stage of evolution is marked by strong synsedimentary tectonic deformation that controlled the architecture and spatial distribution of each coarse-clastic system in the Ainsa–Jaca sub-basin (see below for more detail). Figure 1.8 summarises the stratigraphic transitions within the eastern and central sectors of the South Pyrenean foreland basin.

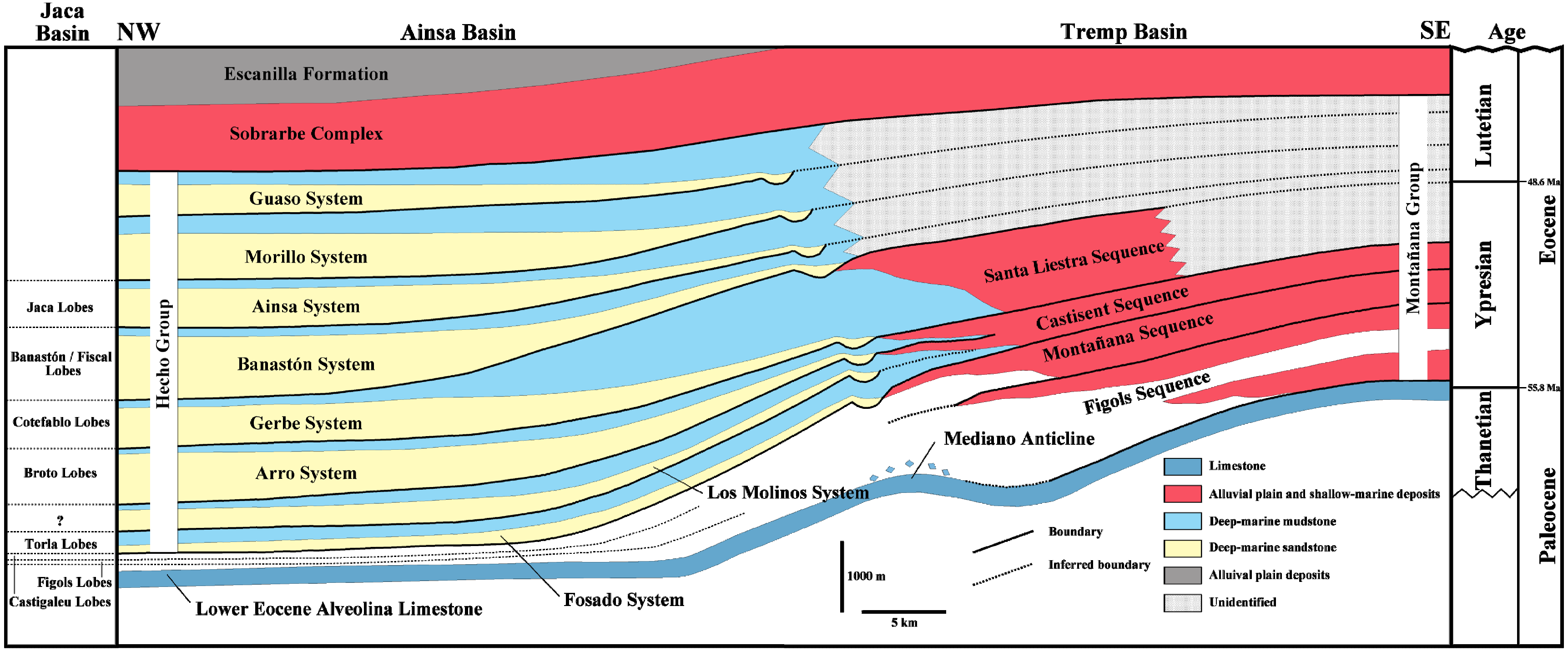

Fig. 1.8. Stratigraphic transitions between the eastern and central sectors of the Eocene Tremp-Pamplona Basin (redrawn and modified after Mutti *et al*., 1985). Ages taken from Abrués *et al*. (1998) and updated using the timescale of Gradstein *et al*. (2004). The nomenclature of stratigraphic divisions is used in this study.

1.6.4. EVOLUTION OF THE SOUTH-CENTRAL PYRENEES

Three major evolutionary tectonic stages can be identified in the south-central Pyrenees (Table. 1.1; Remacha *et al*., 2003), which form part of the South Pyrenean thrust system and are related to the syntectonic sedimentary evolution of the South Pyrenean foreland basin (Mutti *et al*., 1985; Puigdefàbregas & Souquet, 1986; Remacha *et al*., 2003). The tectonic regime during the deposition of the deep-marine systems in the Ainsa basin was characterised by a strong compressive deformation related to these stages, which exerted a primary control on the deposition of the coarse clastics.

Tectonic Stage	Thrusting Units
Stage I Upper Tectonic Complex: Ancestral orogen	Inversion of earlier structures / Lakora-Eaux Chaudes / South-Central Pyrenean Unit
Stage II Lower Tectonic Complex: Development of new cover thrusts	Larra-Boltaña / Gavarnie / enlargement of the lateral ramp zone of the South-Central Pyrenean Unit
Stage III Pyrenean molasse stage: Continued compression	Gavarnie – Biniés / Oroz-Betelu

Table 1.1. Tectonic stages in the south-central Pyrenees with related thrusting units. Data compiled from Remacha *et al*. (2003).

Stage I spans from the Middle Santonian to Thanetian and generally involves the inversion of pre-existing extensional faults and basins. The initiation of detachment and thrust propagation in the South-Central Pyrenean Unit (SCPU) and the Lakora (Eaux-Chaudes) thrusts (Seguret, 1972; Teixell, 1992) are also recorded in this stage. All these structures are considered to be the ancestral Pyrenees orogen and are collectively named the upper (older) tectonic complex (Fig. 1.9). This complex remained active during stage II with the generation of new cover thrusts. Towards the end of stage I, shallow-marine limestones developed across most of the basin west of the SCPU, deepening to the west towards the Bay of Biscay.

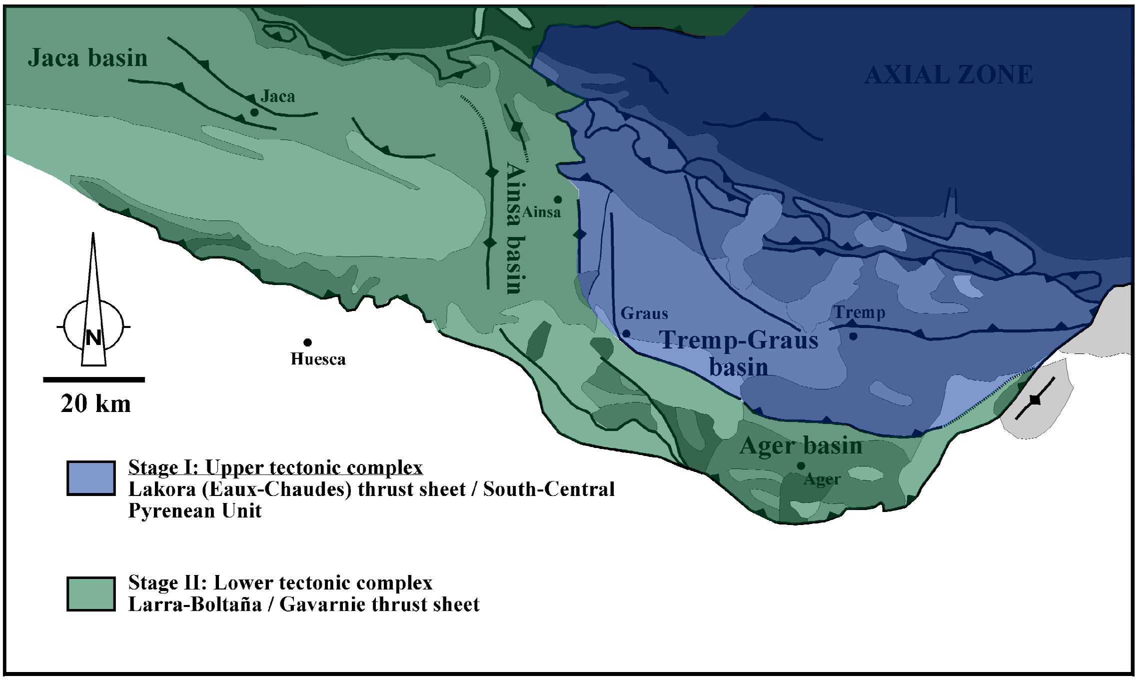

Fig. 1.9. Two main evolutionary stages in the south-central Pyrenees (redrawn and modified after Choukroune & Seguret, 1973; Remacha & Fernández, 2003). Note the upper tectonic complex was still active in stage II with the enlargement of the lateral zone of SCPU.

Stage II marks a major basin reorganisation and occurred during the Early Eocene, from the Ypresian to Late Lutetian. This period is characterised by very strong subsidence and basin axis shift, controlled by loading during the progressive detachment and thrust propagation in stage I, involving the Nogueres unit and Lakora-Eaux Chaudes thrust sheet (Remacha *et al.,* 2003). Shallow-marine limestones and marls belonging to the Ager Group mark the onset of this stage, which are soon followed by the delta complex of the Montañana Group and the time-equivalent Hecho Group siliciclastics: a stage when the basin was underfilled. This stage involves two phases of structural evolution, which directly relate to the evolution of the Hecho Group in the Ainsa basin—the focus of this study.

Phase I developed from the Ypresian to Bartonian and involved the generation of new cover thrusts within the upper tectonic complex, enlarging the lateral ramp zone of the SCPU. The sequence of thrusting consist of, from east to west, the Foradada, Atiart and Los Molinos thrusts, and the Mediano detachment fold (Mutti *et al*., 1988; Remacha *et al*., 2003). Figure 1.10 details the sequence of thrusts associated with the lateral ramp zone of the SCPU.

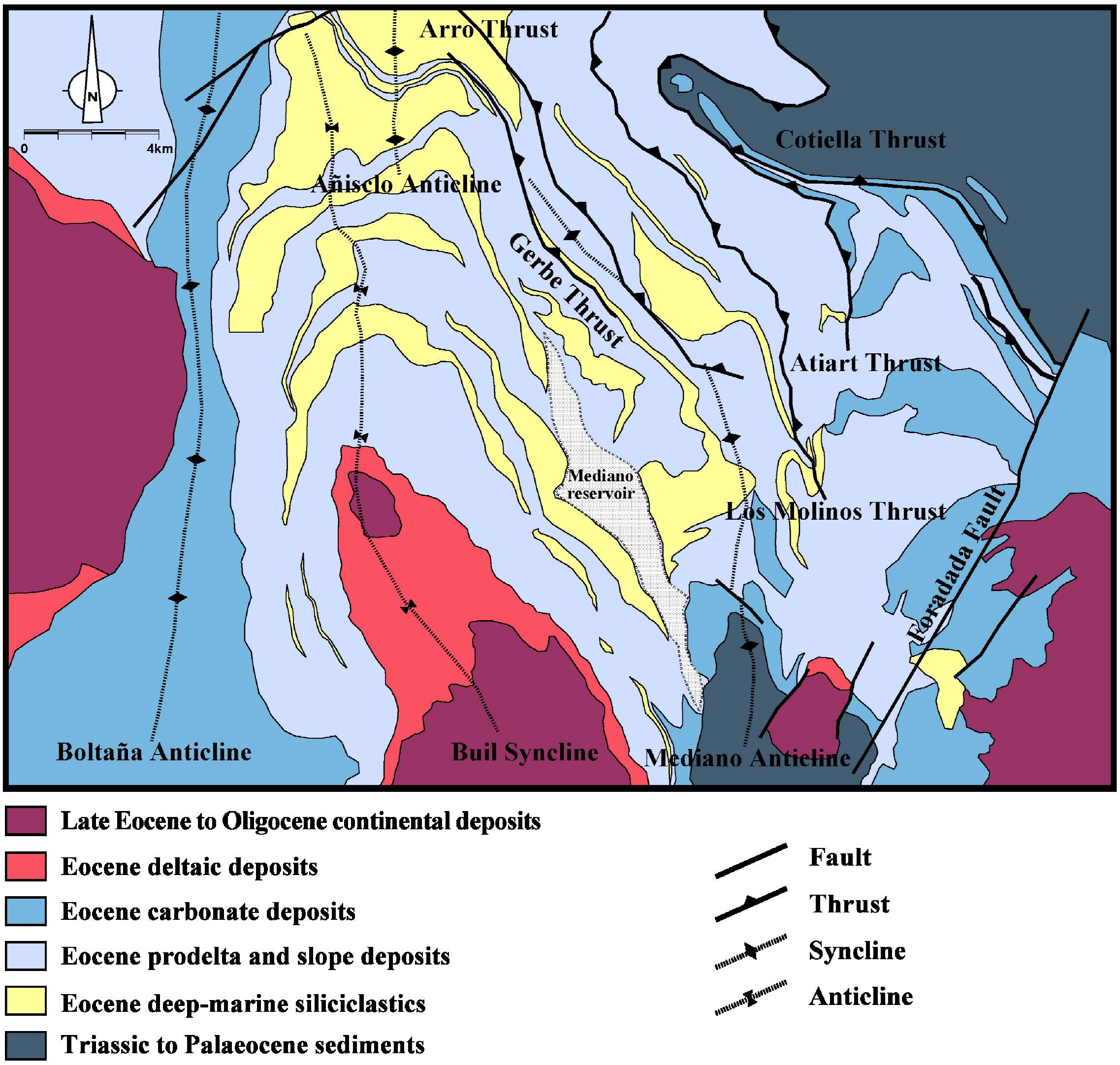

Fig. 1.10. Simplified geological map of the Ainsa basin, showing the lateral ramp zone of the SCPU (modified and redrawn after Poblet *et al*., 1998).

Phase II occurred from the Lutetian to Priabonian and is characterised by the development of the lower (younger) tectonic complex (Fig. 1.9). The initiation of phase II is marked by the onset of the Larra-Boltaña cover thrust and associated folds (Teixell, 1990, 1992, 1996), followed by the development of the Gavarnie-Sierras Exteriores thrust sheet (Labaume, 1983), which included the Biniés cover thrust and associated thrust-ramp anticline (Remacha *et al*., 2005). These structures were accompanied by the reactivation of structures of the upper tectonic complex; such structures were mainly out-of-sequence thrusts related to the lateral ramp zone of the SCPU, including the Arro and Gerbe thrusts sheets (Fig. 1.10; Remacha *et al*., 2003).

Within the SCPU, the end of stage II marks the transition of a simple foredeep into segmented thrust-top basins, including the Tremp–Graus, Ainsa and Jaca basins.

Stage III developed from the Late Lutetian to the Miocene time when the basin became overfilled and a progradational facies trend from shallow- to marginal-marine deposits to alluvial deposits is observed (Dreyer *et al.,* 1999). Widespread continental conditions existed throughout the basin towards the end of this stage, marking the end of marine sedimentation. The Gavarnie and the Oroz-Betelu basement-involved thrusts were responsible for this change, leading to the western closure of the basin and emersion of the inner Pyrenean orogenic wedge. This resulted in the reduction of accommodation and a closure of connections between the foreland basin and the Atlantic Ocean (Remacha *et al*., 2003). This phase is commonly referred to as the molasse stage (Payros *et al.,* 1999; Schellart, 2002; Vergés *et al.,*1998). Inversion and uplift of the Iberian and Catalan Coastal ranges closed the Ebro basin to the southwest and southeast, transforming it into a tectonically-silled basin (Gasper-Escribano *et al.,* 2001).

1.7. TREMP–AGER BASIN

The Tremp–Graus and Ager basins form the eastern (proximal) sector of the South Pyrenean foreland basin, and developed as thrust-top basins on top of the allochthonous SCPU (Payros *et al*., 1999). The sedimentary fills are characterised by an east–west succession of alluvial, deltaic, nearshore and shelfal deposits of the Eocene fluvio-deltaic Montañana Group (Nijman & Nio, 1975; Friend *et al.,* 1981; Mutti *et al.,* 1985; Marzo *et al*., 1988), derived from the rising orogen. The Montañana Group grades westward into the adjacent deep-marine Ainsa Basin (the study area). The east–west trending, south-verging Montsec thrust partly divides the proximal foreland basin into two sub-basins, named the Ager basin and the Tremp–Graus basin (Payros *et al*., 1999). Although the Tremp–Ager basin can be referred to as one sedimentary basin, the Montsec thrust sheet represented a synsedimentary feature during sedimentation, progressively separating the two sub-basins by the Montsec Range (Nijman, 1998). It is, therefore, convenient to refer to the Tremp–Graus as the proximal foreland basin from herein. The Tremp–Graus basin is bounded to the south by the Montsec Range and to the north by the southern termination of the Nogueres Zone (Nijman, 1998). The basin is defined in the east by the Segre fault system (Farrell *et al*., 1987; Nijman, 1998) and deepens to the northwest-west into the Ainsa basin, which is situated in the footwall of the Montsec thrust sheet.

Eocene sediments of the Tremp–Graus basin overlie a thick Mesozoic succession of syn-compressional deep-marine sediment of the Vallcarga basin, deposited during an earlier Late Cretaceous phase of subsidence driven by the creation of the South Pyrenean foreland basin and the emplacement of the Bóixols thrust sheet. This syn-inversion basin preserves the first record of longitudinal (northwestward) clastic sediment transport, parallel to the orogenic axis (Simó, 1986; Nijman, 1989). The succession is characterised by an overall regressive megasequence from the Santonian and Campanian turbidites (Mascarell Member) via slope sediments (Pumanyons Member) of the Vallcarga sequence, shallow-marine sediments of the Maastrichtian Arén sequence overlain by nearshore shelf sandstones, and non-marine, red-bed, fluviatile sediments of the Tremp Formation (Simó & Puigdefàbregas, 1985; Nijman, 1998). Basin inversion lasted ~10 Myr, from ~75–65 Ma (Simo & Puigdefàbregas, 1985). As the tectonic style changed to thrust tectonics in the Early Eocene, a pattern of outward (southward) depocentre shift from the Cretaceous to Eocene is observed. This was a result of thrust migration from the Bóixols to the Montsec thrust sheet, with increasing crustal shortening and upper crustal detachment (Puigdefàbregas & Souquet, 1986). The process of depocentre migration and basin detachment was accompanied by an increase in clastic supply and coarsening-upward grain size trends during deposition in the Eocene–Oligocene (Nijman, 1998, fig. 6), and resulted in the southward migration of the depocentre to the Ebro basin during the Oligocene–Miocene (Friend *et al*., 1979, 1981; Santanach, 1997; Nijman, 1998).

The Tremp–Graus basin developed into a piggy-back basin on top of the Montsec thrust sheet in the Early to Middle Eocene. Southward translation of the Montsec thrust sheet formed an emergent frontal ramp, forming the intermediate part of the SCPU (ECORS, Pyrenees team, 1988; Mutti *et al*., 1988). It was represented by a number of folds that produced topographic highs during sedimentation (Farrell *et al*., 1987). As the thrust front propagated from east to west, growth of the Mediano anticline initiated during the Ypresian (Puigdefàbregas *et al*., 1975; Farrell *et al*., 1987; Remacha *et al*., 2003), and represented a shelf break between the deep-marine Ainsa basin in the west. The Mediano anticline continued to grow as an anticlinal feature in the Lutetian, controlling the spatial distribution of sediment in the Ainsa basin and restricted connectivity with the Tremp–Graus basin. The progressive detachment of the Montsec thrust sheet and the resultant tectonic uplift segmented the Tremp–Graus basin into a piggyback setting, diminishing relative subsidence and accelerating filling (Bentham &

Burbank, 1996). Prominent surface expressions of this thrust-top phase are represented by growth anticlines developed in the Middle to Late Eocene, as documented by de Boer *et al*. (1991). However, total movement on the Montsec thrust sheet was limited and can be estimated at ~8 km (Williams & Fischer, 1984; Williams, 1985).

Deposition in the Tremp–Graus basin occurred in a variety of terrestrial and shallow-marine settings during the Eocene with the deposition of the upper Ypresian to upper Lutetian Montañana Group (Nijman & Nio, 1975; Nijman, 1981, 1998; de Boer *et al*., 1991). Figure 1.11 illustrates the palaeodrainage pattern in the Eocene, showing traverse (southwestward) prograding alluvial fans merging with an axial fluvial system flowing parallel to the orogenic axis (Friend *et al*., 1981; Simó, 1986; Marzo *et al*., 1988; Nijman, 1989, 1998; Clevis *et al*., 2004a). The alluvial fans and fan deltas in the northeastern flanks of the basin delivered mud- to boulder-grade sediment from the rear of the SCPU, whereas the fluvial systems supplied sand and mud from the southwest. Source areas were situated in the rising Axial Zone of the Pyrenees in the north and northeast, and sediment transport routes were controlled by synsedimentary structures related to forward propagation of the thrust front (Nijman, 1998). Thus, the Montañana Group is partitioned into several tectonically-controlled megasequences, characterised by unconformities flanking the basin margins (Nijman, 1998; Clevis *et al*., 2004b). Njman (1998) recognised eight megasequences of the Montañana Group, ~150–400 m thick (see Nijman, 1998, fig. 13 &16). The megasequences are interpreted as being aperiodic, spanning time intervals between 400 and 1,400 Kyr (Nijman, 1998), and although they can be related to third-order sea-level fluctuations, predominant structural control is indicated by sharp basin axis shifts and prominent unconformities (Nijman, 1998; Clevis *et al*., 2004a). Due to the northwestward change in water depth in the Tremp–Graus basin, each megasequence grades basinwards into slope and basin-floor siliciclastic systems of the Hecho Group (*sensu* Mutti *et al*., 1972) in the Ainsa–Jaca basin (Fig. 1.12). The sedimentary motif observed in the Montañana Group can, therefore, be reflected in the character of the deep-marine sediments in the Ainsa basin. The sedimentary trends across the two basins will be fully investigated in this study.

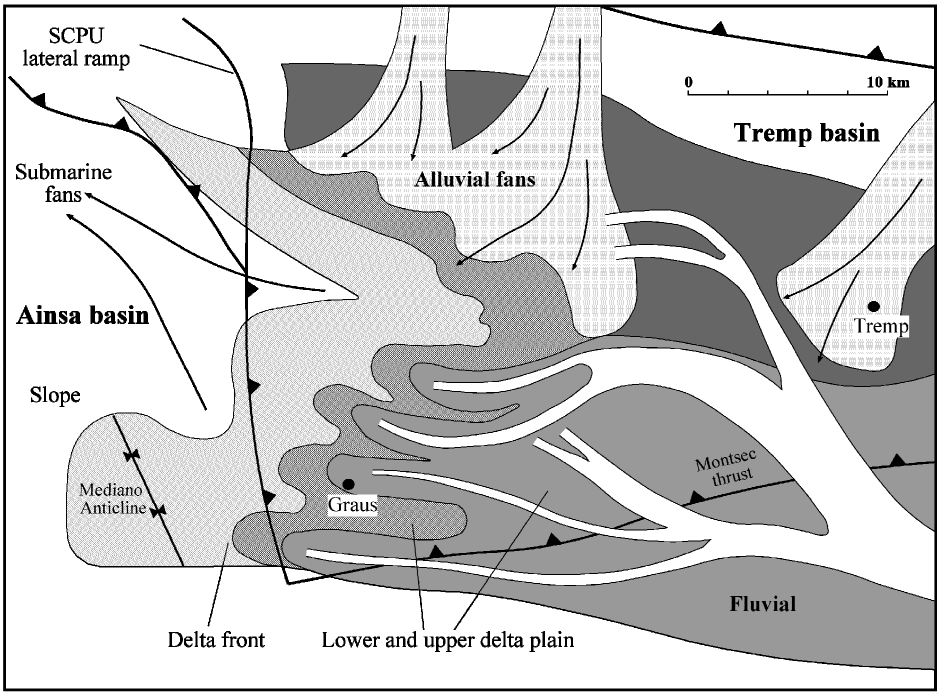

Fig. 1.11. Palaeodrainage organisation in the Eocene Tremp basin during deposition of the Montañana Group. The basin consisted of two depositional systems; transverse alluvial fans and an axial fluvio-delta system, which collectively supplied sediment to the deep-marine Hecho Group in the Ainsa basin via the lateral ramp zone of the SCPU. Redrawn and modified after Nijman (1998) and Clevis *et al.* (2004b).

Megasequences of the Tremp-Ager basin (Nijman, 1998)				**Sandy systems of the Ainsa basin (this study)**		
UM-E	**Upper Montañana Group**	**Montañana Group**		**Guaso**	**Upper Hecho Group**	**Hecho Group**
UM-D				**Morillo**		
UM-C				**Ainsa**		
UM-B				**Banastón**		
UM-A				**Gerbe**	**Lower Hecho Group**	
MM	**Middle Montañana Group**			**Arro**		
MLM?	**Lower Montañana Group**			**Los Molinos**		
LLM?				**Fosado**		

Fig. 1.12. Correlation between stratigraphic divisions in the Tremp–Ager basin and the Ainsa basin interpreted in this study.

1.8. THE AINSA BASIN: STUDY AREA

1.8.1. GEOLOGICAL SETTING

The syn-tectonic Ainsa basin is located within a zone of deformation defined by an oblique thrust and fold system that separates two of the major thrust units in the south-central Pyrenees: the Montsec thrust sheet (which forms the intermediate part of the SCPU and accommodates a portion of the overall shortening) and the Gavarnie-Sierras Exteriores thrust sheet (Farrell *et al*., 1987; Verges & Muñoz, 1990; Muñoz, 1992; Muñoz *et al.*, 1994, 1998; Nijman, 1998; Dreyer *et al*., 1999; Fernández *et al*., 2004; Falivene *et al*., 2006b). The Ainsa basin is situated to the west of the Montsec thrust sheet on top and in the eastern part of the Gavarnie thrust sheet (Verges & Muñoz, 1990; Muñoz, 1992; Dreyer *et al*., 1999). An east–west trending hanging-wall anticline associated with the Sierras Marginales (Exteriores) thrust defines the southern boundary. The north and eastern margins are deformed by a west to southwest-vergent imbricate thrust system and related folds accommodating differential movement on the SCPU (refer to Fig. 1.10; Nijman & Nio, 1975; Muñoz *et al*., 1994, 1998: Dreyer *et al*., 1999). These structures are genetically related to the growth of the Montsec thrust sheet, and, therefore, the tectonic evolution of the Tremp–Graus basin (Séguret, 1972; Nijman & Nio, 1975), located to the east of the Ainsa basin. The boundary between the Tremp–Graus and Ainsa basin is structurally complex and defined by a change in the direction of movement along the detachment fault during the piggyback phase of each sub-basin. In the east (Tremp–Graus basin), displacement of the SCPU is directed southwards, whereas to the west (Ainsa basin), deformation consists of the southwest-vergent imbricate thrust system (Nijman & Nio, 1975; Muñoz *et al*., 1994; Teixell, 1996). The western margin is defined by the Boltaña anticline, a synsedimentary fold that was connected to the development of the basement-involved Gavarnie thrust sheet (Holl & Anastasio, 1995; Huyghe *et al*., 2009). All these structures define a small basin, ~25 km wide and ~40 km long, with a north to northwest structural and depositional trend (Dreyer *et al.*, 1999). Figure 1.13 illustrates the timing of deformation during deposition of the Ainsa basin fill.

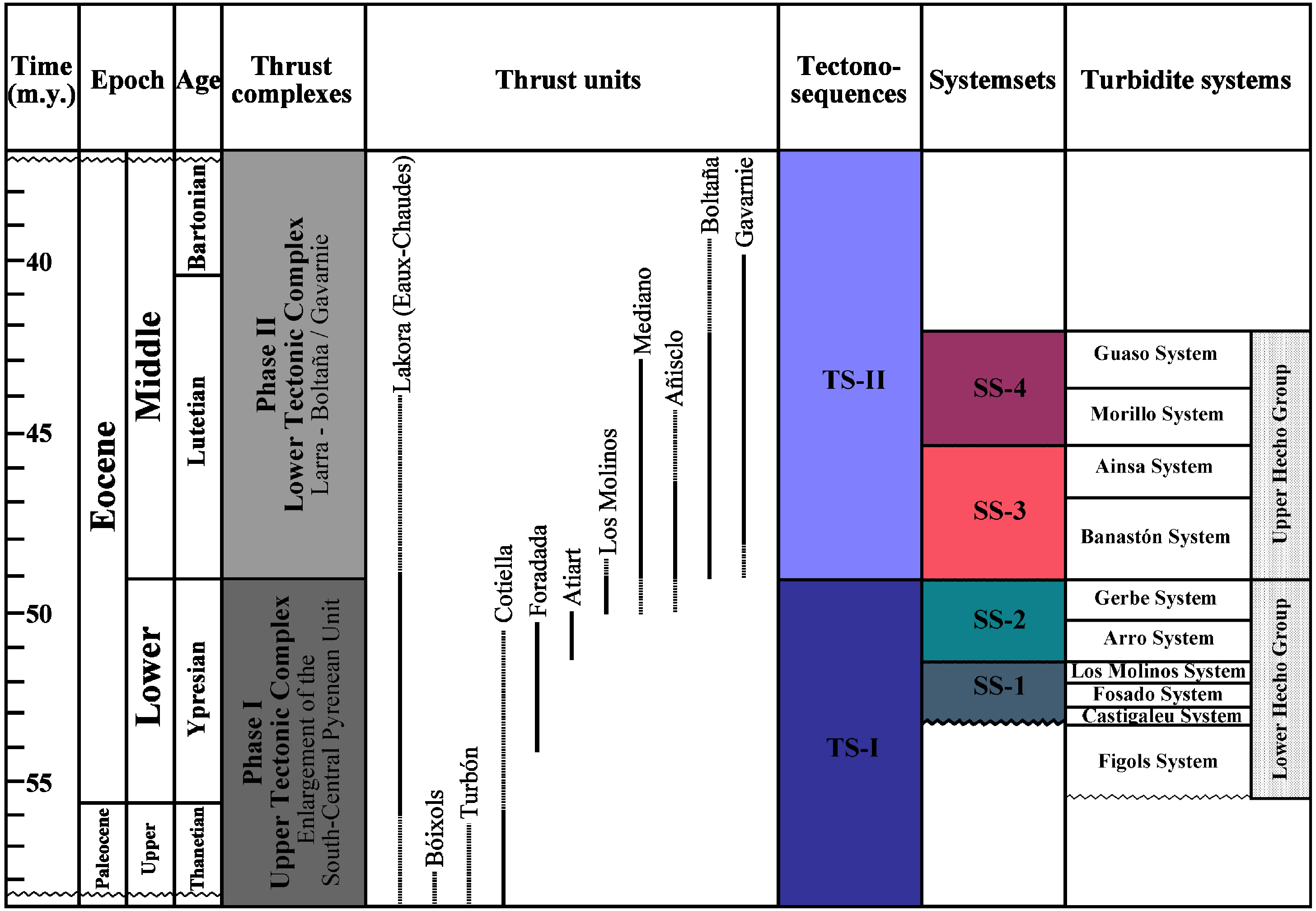

Fig. 1.13. Timing of deformation and classification of tectonic phases during the deposition of tectonosequences, system sets and systems in the Ainsa basin (timing of thrust complexes and units complied from Remacha *et al*., 1998; Verges *et al*., 2002. Timescale after Gradstein *et al*., 2004).

1.8.1.i. Depositional overview

The pre-thrusting sequence in the Ainsa basin comprises ~1.5 km of Mesozoic–Palaeocene (Tethyan) shallow-marine carbonates and siliciclastics (Garrido-Megías, 1973), which overlie Triassic evaporates and shales that provide a detachment level for folds and thrusts (Muñoz *et al.*, 1986; Remacha *et al*., 2003; Fernández *et al*., 2004). The Mesozoic and Palaeocene sediment are overlain by the Ypresian Alveolina Limestone, which represents a widespread transgressive event over the South Pyrenean foreland basin (Fernández *et al*., 2004). As the Pyrenees developed into a true fold and thrust belt orogen and thrusting propagated towards the foreland, ~4 km of syn-tectonic fill accumulated in the Ainsa basin during the late Ypresian to Lutetain stages (Seguret, 1972; Labaume *et al*., 1985; Payros *et al*., 1999; Pickering & Corregidor, 2000, 2005; Remacha & Fernandez, 2003; Fernandez *et al*., 2004; Remacha *et al*., 2005). The succession primarily consists of lower-slope marly and deep-marine turbidite sandstone of the Hecho Group. These are overlain by <1 km of shallow- to marginal-marine sediment belonging to the Sobrarbe deltaic complex (*sensu stricto* Dreyer *et al*., 1999), which accumulated from the middle part of Lutetian to the lower Bartonian (Muñoz *et al*., 1998). This complex represents structural uplift and overall shallowing in the area as the Ainsa basin became part of the deformation front. The final part of the Eocene basin fill consists of an alluvial redbed succession of the Escanilla Formation (Bentham *et al*., 1992; Bentham & Burbank, 1996). Oligocene alluvial fan conglomerates of the Collegats Formation overlie a major unconformity in the basin (Dreyer *et al*., 1999) and represent the youngest synorogenic depositional record of the South Pyrenean thrust and fold belt evolution (Nijman, 1998). Overall, the Ainsa basin deposits comprise a broadly transgressive–regressive sequence.

1.8.1.ii. Tectonic phases

The depositional history of the Ainsa basin is inherently linked to the synsedimentary tectonic evolution of the south-central Pyrenees and can be related to the two tectonic phases discussed above. The Early Eocene, from the Ypresian to middle Lutetian, is characterised by very strong flexural subsidence of the area laterally adjacent to the active SCPU and the subsequent formation of the Ainsa basin (Dreyer *et al*., 1999; Fernández *et al*., 2004). Consequently, the basin originated as a foredeep to the south and west of the Montsec thrust sheet (Fernández *et al*., 2004), being controlled by the emplacement of the Lakora (Eaux-Chaudes)-SCPU tectonic complex. Dreyer *et* *al*. (1999) interpreted the study area (Ainsa basin) as a transitional foredeep setting in this early stage (Ypresian–early Lutetian), primarily responding to synclinal flexing of an underlying sole thrust during a 'subsidence-dominated' phase (phase I), involving lithospheric loading ahead of the main thrust front. By contrast, phase II of structural growth is characterised by anticlinal uplift (Muñoz *et al*., 1994) and a shift towards an 'uplift-dominated' phase in response to detachment and accelerated movement on the underlying sole thrust (Remacha *et al*., 1998; Dreyer *et al*., 1999).

The Ainsa basin evolved into a piggyback setting as the southern Pyrenean front propagated towards the foreland (Farrell, 1984; Williams & Fischer 1984; Puigdefàbregas & Souquet, 1986; Muñoz, 1992; Vergés *et al*., 1995; Meigs *et al*., 1996; Teixell, 1996; Meigs & Burbank, 1997; Vergés *et al*., 2002 Remacha *et al*., 2003; Fernández *et al*., 2004) and incorporated the basin into the deformation front (Muñoz *et al*., 1994, 1998) during tectonic phase II. The thin-skinned evolution of the fold and thrust belt involved the southwards movement of thrust sheets in response to the expansion of the southern Pyrenean front (ECORS Pyrenees team, 1988), reflecting the growth of the Pyrenean orogenic wedge. In summary, the emplacement of the lower tectonic complex (Larra-Boltaña / Gavarnie thrust sheets; refer to Fig.1.9) in the south-central Pyrenees, and coeval deposition of the Upper Hecho Group in the Ainsa–Jaca basin, signifies the transition between a simple foredeep setting into a complex thrust-top (piggyback) basin developed above a basal detachment within Middle Triassic evaporites (DeCelles & Giles, 1996). This records the initiation of an 'uplift-dominated' phase (tectonic phase II) in the study area, where southwards propagation of basement-involved thrusting in the Middle Eocene (Remacha *et al*., 2003; Fernández *et al*., 2004; Huyghe *et al*., 2009; see Chapter 1 for more detail) incorporated the basin into the hanging wall of the Gavarnie-Sierras Exteriores thrust sheet (Verges & Muñoz, 1990; Muñoz, 1992; Dreyer *et al*., 1999; Remacha *et al*., 2003; Fernández *et al*., 2004). The southward advancement of the thrust front was contemporaneous with kinematically-linked lateral (westward) movement of deformation, expressed as a series of oblique folds and thrust ramps (Muñoz *et al*., 1994, 1998; Huyghe *et al*., 2009), which indicated the delineation of the basin (Dreyer *et al*., 1999). The surface expression of this phase is represented by the development of the generally north–south-orientated Mediano, Añisclo and Boltaña anticlines in the study area that detached over the same Triassic evaporites as the Gavarnie-Sierras Exteriores thrust sheet (Puigdefàbregas *et al*., 1992; Barnolas & Teixell, 1994; Muñoz *et al*., 1998; Fernández *et al*., 2004; Falivene *et al*., 2006b).

1.8.1.iii. Synsedimentary tectonics and intrabasinal structural highs

The sediments in the Ainsa basin are deformed by syn-sedimentary and post-depositional tectonics. The depositional history of the Ainsa basin is inherently linked to the evolution of the South Pyrenean thrust system and thrust sheet advancement (Williams & Fischer, 1984; Williams, 1985). Intra-basinal deformation associated with the southward propagation of the thrust front (Farrell, 1984; Williams & Fischer 1984; Puigdefàbregas & Souquet, 1986; Muñoz, 1992; Muñoz *et al.*, 1994, 1998) controlled the spatial distribution and temporal evolution of sediment in the basin, and can be directly related to the regional style of deformation in the southern Pyrenees. Discriminating the timing and sequence of deformational structures in the Ainsa basin is, therefore, essential to understanding the stratigraphic trends in the deep-marine siliciclastic fill. However, the present tectonic structures are late-stage features, representing considerable tightening and amplification of earlier seafloor highs. Assessing the magnitude of thrust-related topography during deep-marine sedimentation in the Eocene forms a key area of research in this study. Muñoz *et al*. (2003) studied the palaeomagnetic history of the Gavarnie thrust sheet in the Ainsa basin and determined a regional clockwise rotation up to 80º in Lower Eocene sediments to accommodate for southward thrusting. The study postulated that rotation was coeval with the development of the major thrust ramp anticlines, the Mediano, Añisclo and Boltaña anticlines, and the growth of extensional faults westwards in the Montsec thrust sheet. Thus, the present orientation of these tectonic features probably developed obliquely to the orientation of the early-stage, synsedimentary structures. A brief description of the main structures in the Ainsa basin is outlined below; smaller scale structural features have also been investigated and are defined in geological maps presented in this thesis.

The *Mediano anticline* is an approximately north–south trending, east-verging, asymmetric detachment fold (Holl & Anastasio, 1993; Poblet *et al*., 1998), ~20 km long, ~9 km wide, and plunges ~10° towards its northern termination (Poblet *et al*., 1998; Fernández *et al*., 2004). The structure is located within the western lateral ramp zone of the SCPU, forming the western part of the Montsec thrust sheet (Muñoz *et al.*, 1994, 1998) and defining the eastern margin of the Ainsa basin. A detailed palaeomagnetic study of the Mediano anticline, combined with the identification of significant unconformities, suggests fold initiation at ~52 Ma, with significant development by ~42 Ma (Holl & Anastasio, 1993). The structure developed into a detachment fold in the late Ypresian (during tectonic phase I), but developed into a fault-propagating fold with renewed deformation during tectonic phase II in the Lutetian (Bentham & Burbank, 1996; Vergés & Burbank, 1996; Remacha *et al*., 2003). This tectonic period was characterised by continued movement on the Montsec thrust sheet, propagating to the south and west (Farrell *et al*., 1987, their fig. 6) and resulted in the segmentation of the Tremp–Graus basin into a piggyback setting (Bentham & Burbank, 1996). Thus, the Mediano anticline represents a thrust ramp anticline and defines the boundary between the Tremp–Graus basin and the Ainsa basin. It can be interpreted as a synsedimentary feature that was active as a seafloor topographic high during the deposition of the deep-marine sediments in the Ainsa basin (Holl & Anastasio, 1993; Poblet *et al*., 1998). Poblet *et al*. (1998) suggested that the Mediano anticline was still active during the deposition of the Escanilla Formation in the Late Eocene.

The *Boltaña anticline* is a north–south trending, west verging fault-propagating fold developed above a blind thrust (Muñoz *et al*., 1998). The anticline formed as a syn-sedimentary feature within the Ainsa basin during the early/middle Lutetian (during tectonic phase II) until the early Priabonian (~50–36 Ma) (Mutti, 1985; Mutti *et al*., 1985; Puigdefàbregas & Souquet, 1986; Holl & Anastasio, 1993; Anastasio & Holl, 2001; Fernández *et al*., 2004; Bentham & Burbank, 1996). This anticline is a regional scale asymmetric anticline located above the western oblique ramp of the Gavarine thrust sheet (Holl & Anastasio, 1995), defining the present western margin of the Ainsa basin and exposing mainly Eocene and older carbonate sequences. The area occupied by the present Boltaña anticline was likely a depocentre during Cretaceous sedimentation, controlled by extensional faulting in a half-graben (Farrell, 1984). This suggests tectonic inversion during thrusting in the southern Pyrenees in the Late Cretaceous to Palaeocene (Farrell *et al*., 1987; Remacha *et al*., 2003). The Boltaña anticline forms part of the Larra-Boltaña thrust system, and is connected to the Larra thrust through the Monte Perdido thrust (Remacha *et al*., 2003). The emplacement of the Larra-Boltaña system was coupled with the early stages of the emplacement of the Gavarnie (Labaume, 1983) and the Oroz-Betelu basement-involved thrusts (Remacha & Fernández, 2003), and contributed to the segmentation of the basin into the Ainsa and Jaca basins during phase II of structural evolution of the Ainsa basin. Although the Boltaña anticline was a growing seafloor high during accumulation of the deep-marine basin fill, there was uninterrupted connectivity between the Ainsa and Jaca basin throughout most of the depositional history of the South Pyrenean foreland basin (Mutti, 1985; Mutti *et al*., 1985; Dreyer *et al*., 1999; Pickering & Corregidor, 2005, Pickering & Bayliss, 2009). However, a quantitative study of bioturbation intensity in fine-grained sediment in the Ainsa basin suggests the existence of a subtle submarine sill or ridge between the two sub-basins during deposition in the Eocene (Heard *et al*., 2008). This is also supported by palaeocurrent data in this study. Late stage uplift and tightening of the Boltaña anticline resulted in the erosion of any physically continuity of deep-marine deposits of the Hecho Group.

The onset of the *Añisclo anticline* is coeval with the development of the Boltaña anticline in the Lutetian; it formed to the east of the Boltaña anticline where the hanging-wall of the lateral ramp is deformed giving rise to the fault-propagating fold (Remacha *et al*., 2003). The Añisclo anticline is a north–south trending, west verging fold, plunging ~25° towards its southern termination (Fernández *et al*., 2004).

The *Buil syncline* is a north–south trending open syncline, ~10 km wide, and plunges ~7° to the south (Fernández *et al*., 2004). The large-scale folding of the deep-marine sediments in the Ainsa basin into the Buil syncline represent a post-fill tectonic feature, although initial folding developed during the Lutetian (Poblet *et al*., 1998), and created a topographic low between seafloor highs (the surrounding anticlines). The structure is bounded to the east by the Mediano anticline, to the north by the Añisclo anticline and to the west by the Boltaña anticline. The Buil syncline opens to the north around the Añisclo anticline to form two synclines, the San Vicente syncline (to the east) and the Boltaña anticline (to the west).

1.8.2. AGE DATING

Age dating of the Ainsa basin based on micropalaeontological data suggest that the entire deep-marine stratigraphy accumulated during the late Ypresian to middle Lutetian (Puigdefàbregas *et al*., 1975; Labaume *et al*., 1987; Payros *et al*., 1999; Remacha & Fernández, 2003; Pickering & Corregidor, 2005; Remacha *et al*., 2005; Das Gupta & Pickering, 2008), with the overlying deltaic sediments having been ascribed to the middle Lutetian to early Bartonian stages (Muñoz *et al*., 1998; Dreyer *et al*., 1999). The deep-marine deposits span ~8–10 Myr (using the timescale of Gradstein *et al*., 2004). This age dating is consistent with palaeomagnetic data derived from the Montañana Group in the Tremp–Graus basin (broadly contemporaneous with the Hecho Group in the Ainsa–Jaca basin), which determined a mid/late Ypresian–middle Lutetian age for the fluvio-deltaic sediments. Additionally, the analysis of planktonic foraminifera in the more distal deep-marine sediments in the Pamplona basins yielded a similar age range of late Ypresian to middle Lutetian (Payro *et al.*, 1999, their Fig. 6).

1.8.3. SEDIMENT ACCUMULATION RATES

Heard *et al*. (2008) conducted spectral analysis on bioturbation intensity data in fine-grained sediment in the Ainsa basin, which yielded a prominent power peak that was compared to the obliquity (41 kyr) Milankovitch frequency. A ~30 cm ky^{-1} sediment accumulation rate for the sedimentary section analyzed was then calculated using this cyclity. This is consistent with ~40 cm ky^{-1} (not corrected for compaction; Sadler, 1981) obtained from an independent age model for the deep-marine sediments in the Ainsa basin, which suggests that ~4 km of sediment accumulated in ~10 Myr (Pickering & Corregidor, 2005; Pickering & Bayliss, 2009). A higher sedimentation rate is expected for the entire basinal stratigraphy because of the addition of mass transport deposits and thick sandy packages that would have been deposited at much greater rates than the finer-grained sediment (Heard *et al.*, 2008). Bentham and Burbank (1996) used magnetostratigraphy to estimate an average sediment accumulation rate of ~40 cm ky^{-1} for the Ainsa basin during the Lutetian. They postulated that despite rapid subsidence in the basin (~40 cm ky^{-1}), the sediment supply was sufficient to fill the subsiding basin.

1.8.4. STRATIGRAPHY OF THE AINSA BASIN

1.8.4.i. The Hecho Group

The infill of the Ainsa basin comprises ~4 km of deep-marine deposits of the Hecho Group, which accumulated in the Ainsa–Jaca basin in the Early to Middle Eocene (Labaume *et al.*, 1985; Pickering & Corregidor, 2005; Remacha & Fernández, 2003). The Hecho Group unconformably overlies the Castigaleu Group (predominantly comprising shelf carbonates and marls), and records a major tectonic phase and deepening of the Ainsa–Jaca basin (Mutti *et al.*, 1988). The group represents a foreland-propagating turbidite wedge, showing progressive onlap to the south as the thrust front propagated towards the foreland. This indicates a strong tectonic control on basin geometry, accommodation and sediment supply during the Eocene. The turbidite wedge is defined in the east by the western lateral ramp zone of the SCPU and in the west by the western boundary of the South Pyrenean foreland basin. The foredeep infill extends downdip for ~190 km (Remacha *et al*., 2003), and is 10–70 km wide (Teixell, 1992).

1.8.4.ii. Tectono-sequences

The tectono-sequences in the Ainsa basin comprise part of the four major depositional units identified in the basin fill (Fig. 1.14; Arbués *et al*., 1998, 2007; Muñoz *et al*., 1998), which are at the same temporal scale as the contemporaneous non-marine and marginal marine sediments in the Tremp–Graus basin (Burbank *et al*., 1992). An angular unconformity defines the base of each unit, which can be traced towards the hinterland forming a subaerial unconformity (Arbués *et al*., 2007). It is postulated that each unit represents a 2–5 Myr cycle, comparable to the lowstand systems tract of a 3rd-order composite sequence of 2–4 Myr duration (Mitchum, 1985; Mitchum & Van Wagoner, 1991; Van Wagoner, 1996; Vail, 1987). However, due to the strong tectonic control on sedimentation (Mutti *et al*., 1988, 1994) in the Eocene and the ambiguity associated with precisely timing the duration of each cycle, it is likely that a compressional tectonic driver was responsible for the depositional cycles. As the thrust front propagated towards the foreland, the Ainsa basin was segmented into the four major depositional cycles, developed during periods of uplift and oversteepening, causing suberial erosion and basin depocentre shift towards the foreland. Arbués *et al*. (2007) estimated a 10 km displacement of the basin depocentre during thrust activity. The major phases of thrust activity are, therefore, reflected in the internal organisation and character of the depositional units and the bounding unconformities.

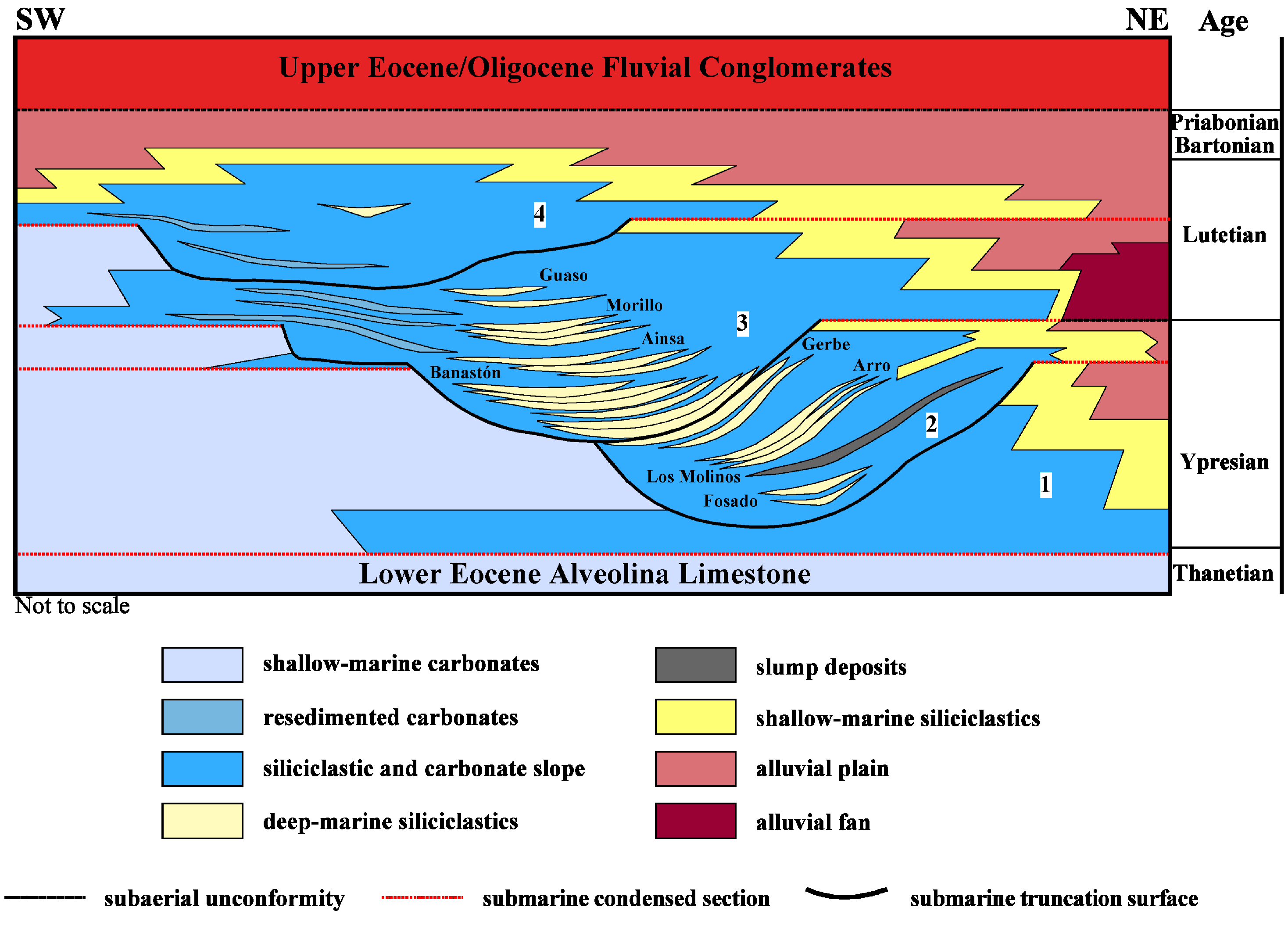

Fig. 1.14. Stratigraphy of the Ainsa basin (redrawn after Abrues *et al.*, 1998), showing unconformities and the stacking of sandy systems. The basin fill is divided into depositional cycles, numbered 1–4.

The Hecho Group can be subdivided into two tectono-sequences, which represent the middle two cycles of the four unconformity-bound depositional units identified in the Ainsa basin (depositional cycles 2 and 3 in Fig. 1.14). Other researchers have also identified two distinct successions that divide the Ainsa basin deep-marine deposits (Muñoz *et al*., 1994, 1998; Fernández *et al*., 2004; Pickering & Corregidor, 2005). The tectono-sequences are related to the two discrete tectonic phases (involving part of the upper tectonic complex and the lower tectonic complex, as mentioned above) operating in the south-central Pyrenees, and divide the Hecho Group into the Lower Hecho Group and the Upper Hecho Group, respectively (refer to Fig. 1.3; *sensu* Remacha *et al*., 2003). The boundary between the Lower and Upper Hecho Groups indicates the transition between a simple foredeep basin into a complex thrust-top (piggyback) basin, containing the Ainsa and the Jaca sub-basins (Remacha *et al*., 2003). The tectono-sequences developed during a major phase of thrust propagation and subsequent basin reorganisation, involving basin depocentre shift towards the foreland and an increase in slope gradient. The base of each tectono-sequence is defined by an angular unconformity, which is a submarine depression, or canyon, excavated by mass wasting during the thrust activity, uplift and slope oversteepening. They form regional unconformities extending from the delta to the basin floor (Remacha *et al*., 2003; Arbués *et al*., 2007). The sedimentological trends and characteristics observed in the two successions, and how they directly relate to the tectonic complexes is documented in this study.

1.8.4.iii. Deep-marine systems

The Hecho Group can be further subdivided into eight siliciclastic depositional systems ('sandy systems'), equally partitioned into the Lower and Upper Hecho Group (see Fig. 1.13 & Fig. 1.14). The sandy systems are separated vertically by up to several tens-of-metres of mainly fine-grained sediment, predominantly consisting of marlstones with subordinate, thin-bedded sandstones, herein termed 'inter-system sediment'. These sandy systems are considered as higher frequency cycles comparable to 4th-order sequence stratigraphic cycles. The sandy systems comprising tectono-sequence I show an aggradational stacking pattern, whereas the younger systems of tectono-sequence II are both structurally less deformed and show a southwestward shift in depositional axis towards the foreland due to thrust advancement and development of syn-depositional structural highs. This suggests a first-order tectonic control on accommodation and deposition in the Ainsa basin.

Each sandy system typically contains 2–6 sandy sequences (a total of 22 sequences throughout the basin), from ~30–160 m thick and characterised by a lower sandy division followed by an upper muddy division. The sandy systems record various stages in the evolution of the foreland basin and were deposited and preserved in various deep-marine settings, which from the oldest to youngest are: (1) Fosado (two sequences, FI–II) — mid-slope channels; (2) Los Molinos (one sequence: LMI) — slope apron with mid-slope channels; (3) Arro (three sequences: ArI–III) — upper/mid-slope canyon to lower-slope channels; (4) Gerbe (two sequences: GbI–II) — upper/mid-slope canyon to lower-slope erosional channels; (5) Banastón (six sequences: BI–VI) — lower-slope canyon–channel transition to proximal basin-floor channels; (6) Ainsa (three sequence: AI–III) — lower-slope erosional channels to proximal basin-floor channels; (7) Morillo (three sequences: MI–III) — mid-slope canyon to lower-slope, structurally-confined channels; (8) Guaso (two sequences: GI–II) — low-gradient, structurally-confined channels. The naming of the sandy systems refers to the type locality where representative sections can be found. A revised stratigraphic framework of the Ainsa basin is presented in this study, including the grouping of systems into system sets.

1.8.5. CONTROLS ON SEDIMENTATION

The accumulation of the Early/Middle Eocene deep-marine sediments in the Ainsa basin were coincident with maximum rates of shortening and thrust front advancement (Verges *et al.*, 1998), and broadly contemporaneous with maximum rates of tectonic subsidence in the Ainsa basin (Bentham & Burbank, 1996). The first-order control on basin accommodation was created by tectonic-induced subsidence of the Ainsa–Jaca basin during the Early/Middle Eocene in response to lithospheric loading by thrust sheets associated with the South Pyrenean Zone (Labaume *et al.*, 1985; Vergés *et al.*, 1995; Santanach, 1997). This resulted in uplift of source areas in the north/northeast (Nogueres zone; Burbank *et al.*, 1992a,b) and rapid deepening of the Ainsa–Jaca basin from a shallow-marine mixed carbonate and clastic shelf to water depths in the range ~400–800 m, as suggested by micropaleontological data (Pickering & Corregidor, 2000, 2005; Pickering & Fadell, 2004). Climate could have played an important role in sediment supply; palynofloral and microfaunal data obtained within the Ainsa basin suggests a very warm perennially humid climate with significant precipitation during the Middle Eocene (Pickering & Fadell, 2004; Pickering & Corregidor, 2005). Such favourable climatic conditions would have enhanced weathering and released large volumes of siliciclastic sediment into the foreland.

Discrete tectonic regimes are reflected in the stratigraphy of the Ainsa basin (with the formation of tectono-sequences), and are expressed as abrupt changes in sedimentation styles and depositional trends. The evolution of sedimentary environments, spatial distribution of facies and hierarchical organisation of stacking patterns were strongly controlled by the compressional tectonic activity and the evolution of the South Pyrenean foreland basin. The sandy systems of the Ainsa basin occur stratigraphically at the base of each sequence of the Montañana Group in the Tremp–Graus basin; they are correlative with unconformities that separate the fluvio-deltaic deposits, and are associated with tectonically-induced periods of relative sea-level fall (Mutti *et al*., 1985, 2003). However, a global climatic driver (eustatic sea-level change) can be interpreted as the fundamental cause of higher-frequency depositional cycles (e.g., sandy sequences) observed in the Ainsa basin (Pickering & Bayliss, 2009). The interaction between global climate change and tectonic processes operating at a variety of temporal and spatial scales is investigated in this study to elucidate the control on sedimentation.

1.8.6. PALAEOFLOW

Sediment dispersal patterns in the South Pyrenean foreland basin followed the structural directions of the south-central Pyrenees. The deep-marine sediments in the Ainsa basin were fed throughout most of the basin history from a structural confined eastern/southeastern point source, controlled by the development of the western lateral ramp zone of the SCPU (flowing ~270–300^{o}). However, due to the progressive development of the Mediano anticline, the Guaso and Morillo systems were fed from a more southern sediment source within a structurally lower frontal ramp area (Dreyer *et al*., 1999), being diverted around the prominent seafloor high. As the sediment gravity flows entered the basin, flows were deviated to the north (~320^{o}), flowing axially through the basin depocentre. The growth of the Boltaña anticline during deposition of the Upper Hecho Group deflected palaeoflow more westerly across the seafloor high into the Jaca basin (~270^{o}). Figure 1.15 illustrates the mean palaeoflow in each of the eight sandy systems (see following chapters for more complex dispersal patterns).

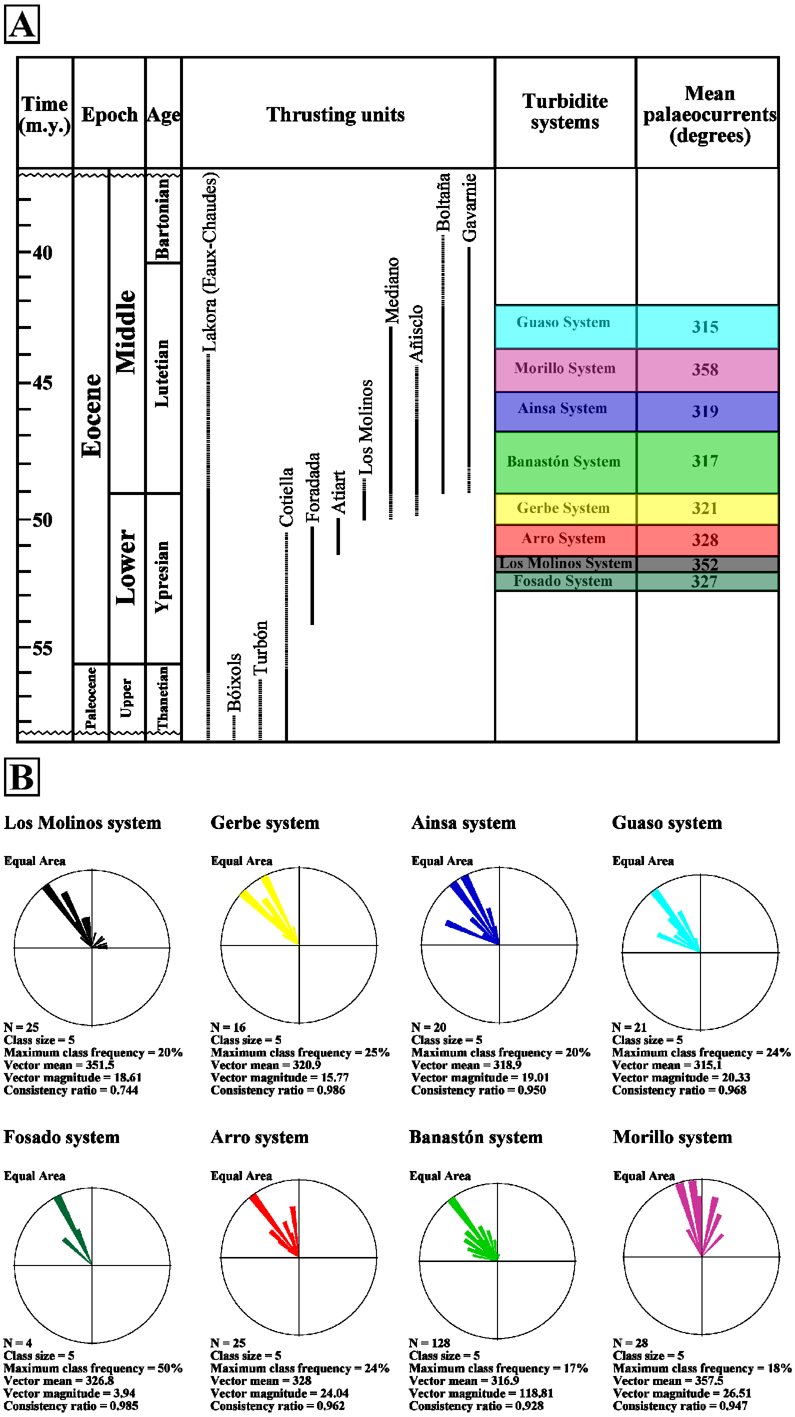

Fig. 1.15. (A) Timing of deformation during deposition of the turbidite systems in the Ainsa basin (data compiled from Remacha et al., 1998; Verges et al. 2002), showing mean palaeocurrent directions obtained from sole structures. Timescale after Gradstein et al. (2004). (B) Rose diagrams depicting mean palaeoflow for each turbidite system in the Ainsa basin.

1.9. JACA BASIN

The Jaca basin is a Tertiary deep-marine basin that forms part of the central sector of the South Pyrenean foreland basin. It is the down-dip (distal) counterpart of the Ainsa basin (Ypresian–Lutetian in age), consisting of less-confined, more sheet-like sandy deposits within outer-fan lobe, lobe-fringe, fan-fringe and distal basin floor environments. The basin floor complex was predominantly fed from a single entry point located to the east/southeast, except for the latest stages of turbidite sedimentation (see below). Fluvio-deltaic sediment originating from the Montañana Group located in the Tremp–Graus basin was transferred eastwards via the deep-marine Ainsa basin. Sedimentation patterns and confinement were partly controlled by the western lateral ramp zone of the SCPU and the Boltaña anticline (Remacha & Fernández, 2005), with sediment dispersals following the main structural trends.

The Jaca depocentre was bordered by the active Lakora (Eaux-Chaudes) thrust on the hinterland (northern) side (Labaume *et al.*, 1985; Teixell, 1992) and carbonate platforms on the southern cratonic margin (Puigdefàbregas & Souquet, 1986; Barnolas *et al.*, 1991). The syn-tectonic sedimentary fill shows a south-directed onlap pattern (Mutti *et al.*, 1984; Labaume *et al.*, 1985), which is consistent with the southward advancement of thrust sheets (Schellart, 2002). The present geographic separation of the Ainsa–Jaca basin by the Boltaña anticline prevents any physical correlation between these two areas. Additionally, the Boltaña anticline broadly coincides with the change from more channelised deposits in the east (Ainsa basin) to the less confined, more sheet-like deposits in the west (Jaca basin). It is, therefore, convenient to separate the Ainsa–Jaca basin into the constituent sub-basins. The western part of the Jaca basin grades into distal basin plain deposits of the Pamplona basin (Mutti *et al.*, 1988; Payros *et al.*, 1999, 2006, 2007). The Sierras Exteriores thrust sheet presently defines the southern margin of the basin (Labaume, 1983), whereas the northern margin is bounded by the Larra-Boltaña cover thrust system and the Oroz-Betelu basement thrust (Teixell, 1990, 1992, 1996; Remacha & Fernández, 2005).

The older turbidite systems of the Hecho Group in the Ainsa basin, have been correlated with five principal systems in the Jaca basin (refer to Fig. 1.8). In each system, the first name denotes the type locality of the channelised deposits in the Ainsa basin, and the second name refers to the type locality of the depositional lobes in the Jaca basin (Mutti *et al.*, 1985). A distinctive feature of the Hecho Group in the Jaca basin is the occurrence of a number of very thick megaturbidites (<250 m thick), interbedded with the siliciclastic turbidites (nine recognised by Labaume, 1983; Labaume *et al*., 1985, 1987; 13 recognised by Payros *et al.* 1999). These megaturbidites extend for considerable distances along the Jaca basin, and provide useful marker beds throughout the basin (e.g., Payros *et al*., 1999; Remacha *et al*., 2005). They are thicker in the basin plain area and dramatically thin updip to more proximal lobe environments (Remacha *et al*., 2003). The megaturbidites are derived from the southern carbonate margin and occur as time-stratigraphic clusters, which can be correlated with relative sea-level lowstands and phases of tectonic activity (*sensu* Payros *et al*., 1999). It can be interpreted that they were emplaced by cohesive debris flows, which evolved into high-density turbidite currents (Payros *et al*., 1999). In the younger, upper Lutetian part of the Hecho Group, an additional northerly-derived, confined sediment system is recognised (the Rapitán turbidite channel after Remacha *et al*., 1991; 1995), west of the Boltaña anticline in the Jaca basin. The deep-marine clastic system was sourced from internal highs constructed by the Gavarnie thrust sheet, and exclusively entered the Jaca basin due to tectonic separation of the sub-basins during the growth of the Boltaña anticline (Remacha *et al*., 2003) during tectonic phase II (see Section 1.8.1.ii). The sedimentary fill of the Jaca basin is outside the scope of this study.

CHAPTER 2

METHODOLOGY

2.1. INTRODUCTION

The Ainsa basin provides an opportunity to research three-dimensional organisation through an entire deep-marine slope and proximal basin-floor fill, and records a range of depositional processes and sedimentary environments. The focus of this Ph.D. study was to exploit the diversity of outcrops in the Ainsa basin and analyze the entire siliciclastic fill in order to understand the depositional evolution of the basin. A number of field-based techniques were employed during this investigation that involved numerous excursions to the study area resulting in ~10 months of cumulative fieldwork (including a short reconnaissance study).

2.2. GEOLOGICAL MAPPING

2.2.1. MAPPING OVERVIEW

The study area encompasses ~20 km^2 surrounding the tourist town of Ainsa in the south-central Pyrenees, Spain, extending from Laspuña town in the north to Formigales village in the south. The elevation of this region varies between 500 m to 1,300 m above sea level. The areas chosen for mapping were not based on accessibility or outcrop availability, but on the premise that the six deep-marine sandy systems in question had previously received little/no attention in publications. However, emphasis was placed on mapping the Banastón and Morillo systems because detailed geological maps of the stratigraphically adjacent sandy systems (the Ainsa and Guaso systems) had previously been undertaken as part of other research projects conducted at University College London, and the integration of these maps yielded a complete facies map for the Upper Hecho Group. The composite map offered valuable information on the depositional history of the Ainsa basin during the upper part of the deep-marine siliciclastic fill. In order to elucidate the stratigraphic evolution of the Ainsa basin in a temporal and spatial framework, less detailed mapping of the Lower Hecho Group, comprising Fosado, Los Molinos, Arro and Gerbe systems, permitted the construction of a simplified geological map of the entire deep-marine sediments of the Ainsa basin (by merging all available maps).

2.2.2. MAPPING THE BANASTÓN AND MORILLO SYSTEMS

A total of four months of fieldwork was spent to collectively map the Banastón and Morillo systems (see Appendix A). The primary focus of the mapping project was to determine the stratigraphic organisation in the Ainsa basin and to evaluate the range of deep-marine environments by investigating facies distributions. Geological attributes such as sequence boundaries, palaeocurrents and prominent structural features assisted in this process. Mapping significant folds and thrusts in the Ainsa basin was required to assess the influence of intrabasinal tectonics on facies distributions and depositional architectures. Defining structures also facilitated the construction of accurate correlation panels through structurally complex sections. Figure 2.1 shows the colour coding and symbols used in the geological maps.

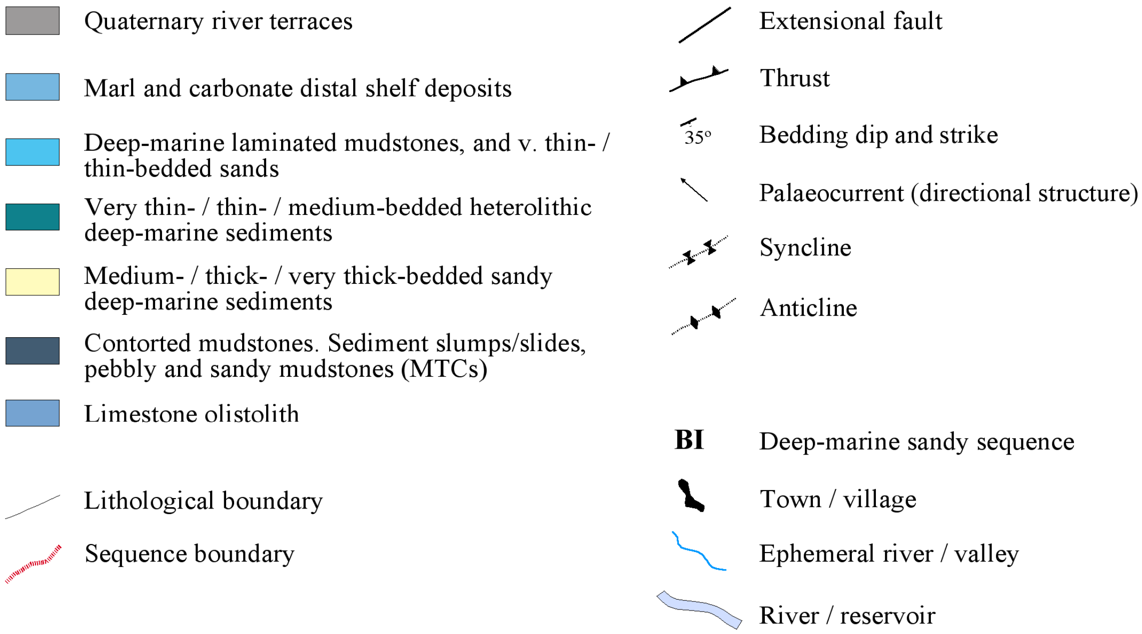

Fig. 2.1. Key for colour coding and symbols used in the geological maps of the Banastón and Morillo systems.

A simplified facies scheme was employed for the purpose of mapping, and was later used with a detailed classification scheme for mass transport deposits (the constituents of mass transport complexes) in correlation panels and photo interpretations. Reconnaissance fieldwork was required to classify the mappable lithological units into facies classes. These facies classes were mainly distinguished by sediment textures and bed thicknesses: (1) Marl and carbonate distal shelf deposits comprise fine-grained, thin- to medium-bedded, nodular limestone interbedded with *Nummulites*-rich marls (verified by thin-section analysis). This facies class is located on the flanks of major anticlines; (2) Deep-marine laminated mudstones and very thin- / thin-bedded sandstones are primarily represented as siltstone-mudstone couplets interbedded with subordinate sandstones, >80% mud grade and <20% sand grade. These deposits are commonly found between depositional sequences (forming inter-sequence sediment) and lateral to sandy depocentres representing overbank environments; (3) Very thin- / thin- / medium-bedded, heterolithic, deep-marine sediments comprise disorganised and organised sandstone-mudstone couplets, 30–50% sand grade and <70% mud grade (mostly silt). This group predominantly defines marginal and/or off-axis environments lateral to sandy depocentres, and also forms the upper division of channelised sandy successions; (4) Medium- / thick- / very thick-bedded sandy, deep-marine sediments include disorganised and organised gravels, pebbly sands, and sandstone-mudstone couplets, consisting of >50% sand grade and <25% pebble grade. This facies class constitutes channel-axis and/or channel thalweg deposits of channelised sandy depocentres; (5) Mass transport complexes (MTCs) include disorganised muddy gravels (10–50% mud grade and >25% pebble grade) and gravelly, contorted muds (50–90% mud grade and <25% pebble grade), typically with visco-plastically deformed rafts of disrupted bedding. MTCs typically range from metres to tens-of-metres thick, and are composite units consisting of a number of beds/events. They are mainly found stratigraphically below the main channelised sandy succession of depositional sequences and define sequence boundaries; (6) Limestone olistolith blocks are identified as exotic, angular to subangular blocks of pure carbonate (marl). They are usually located within MTCs and have dimensions measuring up to tens-of-metres. See Chapter 3 for a detailed description of facies, facies associations, transport and depositional processes within the Ainsa basin.

Geological mapping of the Banastón and Morillo systems at a scale of 1:20,000 consisted of detailed field-based outcrop and aerial photograph interpretation. Reconnaissance fieldwork involved traversing large stream sections, valleys, ridges and road cuttings to assess the size of the mapping area and gain preliminary information, such as facies types and distributions, structural deformation and sequence stratigraphic patterns, in order to subdivide the area into workable units. Initial positioning in the field at any given locality was determined by referencing a 1:40,000 topographic map of the region (prior to familiarisation of the area). Aerial photographs were subsequently employed to examine the mapping area and assist with the interpretation of geological features (See Figs. A1, A3, A4, A6, A7 and A9). The aerial photographs were obtained from a cartographic company (Azimut, S.A.) in Madrid. They are black and white orthophotographs, 1:20,000 in scale, with each photograph covering an area of ~4.5 km^2. Stereopairs were used as a visualisation tool to examine the general topology and major landmarks by creating stereographic projections to yield a three-dimensional image through a stereoscope. Due to vertical exaggeration of the three-dimensional images, minor features are accentuated; therefore, the orthophotographs were particularly effective in tracing faults, key boundaries and other structures that are difficult to visualise from ground level. Although geological features and landmarks were located on the aerial photographs, fieldwork was essential to "ground truth" these observations so that the image data was related to real features on the ground. Despite the fact that more detailed observations could be made in the field, including the analysis of facies, architectural elements and depositional environments, frequent calibration of photographic images with ground interpretation was required to fixate locations and increase the accuracy of the maps. Furthermore, the aerial photographs were used as base maps because of the lack of fine topographic map detail for the area.

Various techniques were employed during the course of field mapping, mainly consisting of traversing well-exposed sections through predetermined routes (e.g., through a stream, valley or road cutting) and tracing large-scale lithological units and sequence boundaries. The mapping area was partitioned into discrete geographic sectors to organise and regulate data acquisition. These sectors often represented deep-marine environments within specific sandy sequences in which to document detailed facies distributions. Angular unconformities were identified as significant erosional surfaces representing cut-downs up to several tens-of-metres, and were typically overlain by thick MTCs. These erosional events are interpreted as sandy sequence boundaries. The overlying MTCs formed key stratigraphic horizons that determined first-order (sequence-scale) correlative surfaces. Second-order correlation between lithological units was achieved by tracing markers beds throughout the available outcrops (see Section 2.5 for more detail). Prominent structural features were also mapped, including basin-bounding anticlines and thrusts. All observations were traced onto the relevant orthophotographs using triacetate overlays. Symbols were used to delineate facies classes, and dashed lines were drawn to infer contacts and structures until further mapping had conclusively determined the geological features. Due to distortions between orthophotos residing after orthorectification (developed from scale variations as the focal point of each photo differs), aerial photographs were chosen where the mappable area was as close to the centre of the photograph (the principal point) as possible, and the least amount of orthophotos required to map key features were used. This was to maintain consistency in the dimensions of features and their representation when mapped. At each locality visited, often defined as a continuous sedimentary succession (and used for sedimentary logging), brief descriptions, bedding measurements (dip and strike) and palaeocurrents were recorded in field notebooks. A handheld GPS unit was used in the field to mark waypoints at each locality and follow tracks during correlation in order to precisely locate geographic positions and prominent geological features. Roads and dirt tracks in the study area were exploited to maintain time efficient access to the outcrops.

A number of problems were encountered during field mapping, namely terrain inaccessibility and the frequency of poorly exposed regions. These issues were partly overcome by constructing sedimentary logs to correlate geological attributes between geographically separated sections. This was required to support facies distributions and the identification of key boundaries. Figure 2.2A illustrates a densely vegetated region in the mapping area where hiking trails and river sections exposed continuous sedimentary sections that were used to create sedimentary logs for correlation purposes. Where complete inaccessibility prevailed, photogeology and remote mapping on prominent topographic ridges offering panoramic views were carried out. The majority of the ridges investigated in this thesis represented mappable sandy units due to their resistance to erosion, and often delineated sequence boundaries (Fig. 2.2B). This facilitated remote mapping and the identification of predominant structural trends (the trend of the ridgelines are topographic expressions of tectonic fabrics). Areas of no exposure were usually caused by high mud content in the eroded rock. In which case, inferences on facies classes and boundaries were made from the identification of floats or boulders, vegetation changes and topographic breaks. In most circumstances, the stratigraphic significance of the locality implied a facies class, e.g., the base of sandy sequences were usually defined by MTCs.

Once field mapping and aerial photograph interpretation had been completed, fair copy maps were produced on triacetate (see Figs. A2, A5, A8 and A10). These maps were digitised using Macromedia Freehand (a drawing software). Electronic copies of the four maps, comprising the Banastón, Ainsa, Morillo and Guaso systems, were subsequently integrated to form a complete facies map of the Upper Hecho Group. The same key for colour coding and symbols presented in Figure 2.1 was used.

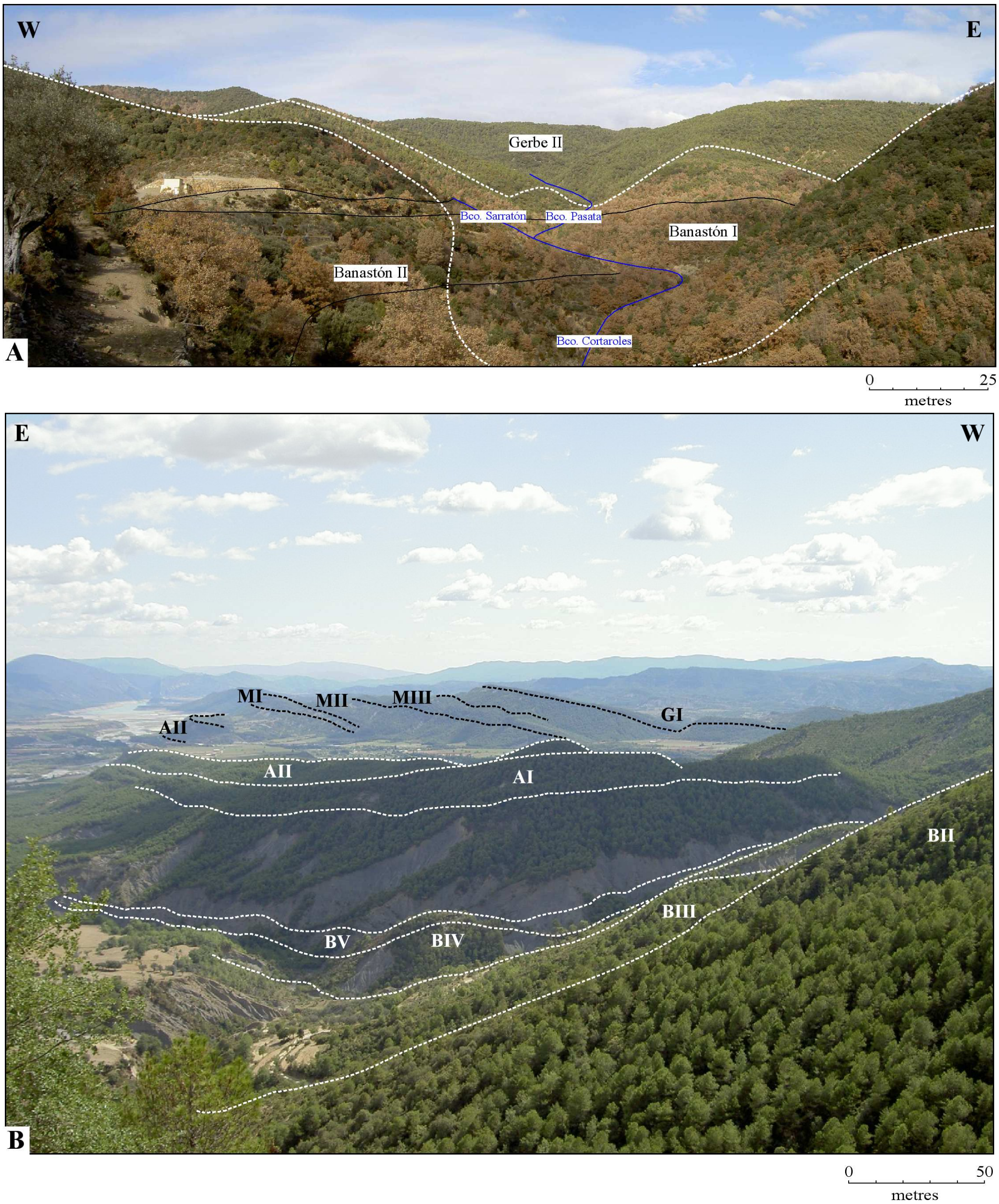

Fig. 2.2. Mapping topographic ridges. (A) View east of San Vicente village illustrating the complexity of mapping sandy sequence boundaries due to the lack of outcrop. Sedimentary logging was completed through river and hiking trail traverses. Dashed white lines represent sequence boundaries; blue lines are river sections; black lines define hiking trails. (B) View north of San Vicente village showing sandy ridges delineating sequence boundaries. Dashed lines define sequence boundaries; abbreviations denote depositional sequences.

2.2.3. CONSTRUCTING A SIMPLIFIED GEOLIGLCAL MAP OF THE AINSA BASIN

A total of three weeks of fieldwork was spent mapping the four oldest deep-marine siliciclastic systems (the Fosado, Los Molinos, Arro and Gerbe systems) belonging to the Lower Hecho Group. The purpose of this project was to complete mapping in the Ainsa basin so that a simplified geological map of the entire deep-marine siliciclastic fill could be constructed. The same mapping techniques undertaken in the detailed mapping of the Banastón and Morillo systems were employed in order to record similar geological attributes in the Lower Hecho Group. Base maps comprised 1:40,000 topographic maps with triacetate overlays, and aerial photographs were used to assist with interpretation. The outline of each siliciclastic system and main structural elements were documented; however, the detailed outcrop pattern or MTCs and minor (heterolithic) sandbodies were not recorded. The observations were then digitised (using Macromedia Freehand) and compiled with the facies map of the Upper Hecho Group to produce a ~15 km^2 composite map of the deep-marine sediments in the study area (see Fig. 2.3 for the colour coding and symbols used in the composite map).

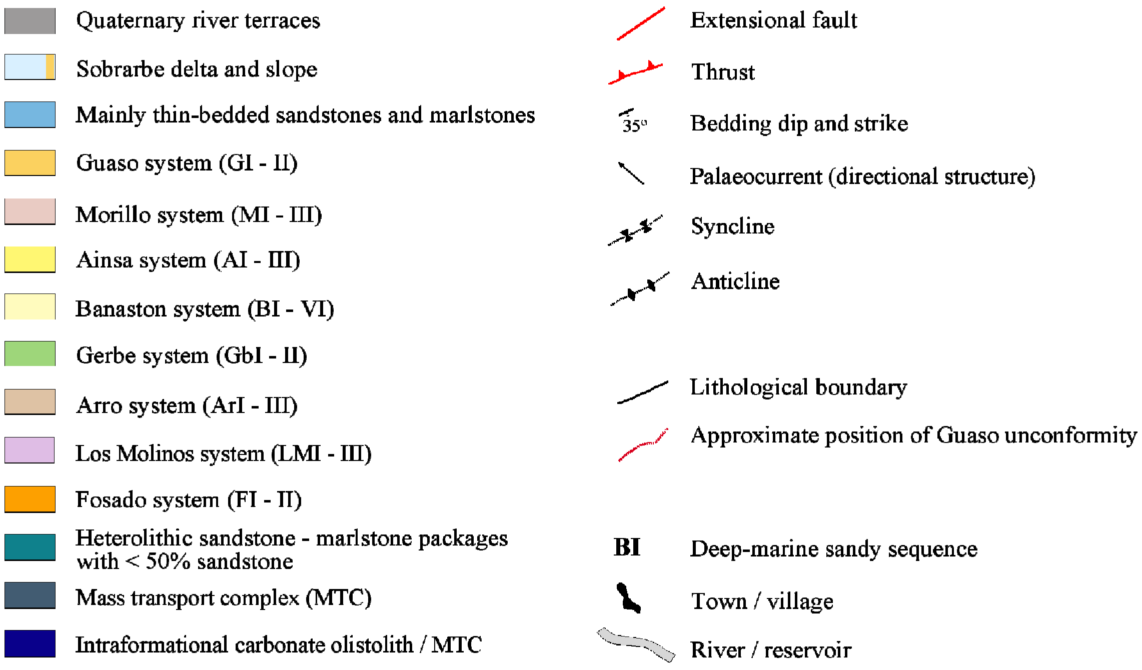

Fig. 2.3. Key for colour coding and symbols used in the simplified map of the Ainsa basin.

2.2.4. PALAEOFLOW ANALYSIS

Numerous palaeoflow measurements were recorded at localities visited whilst field mapping and sedimentary logging. Compiling a large data set of palaeoflow measurements was used to identify the spatial distribution and stratigraphic correlation of depositional bodies, define basin margins and understand the influence of basin-floor topography on facies distributions. Sole marks, mainly flutes and grooves, and ripple azimuths were dominantly used to obtain the measurements. The data were rotated to account for bedding dip so that the pre-tectonic orientation of the palaeoflow indicators could be determined. Equal area rose diagrams were then constructed to illustrate the results. Furthermore, using the geological maps as overlays and referencing the calculated mean palaeoflow from various depositional environments, outlines of sandy depocentres (of sandy systems and sequences) were conveyed. These depositional models lent insight into basin geometry, the position of basin-floor obstacles and the spatial arrangement of depositional sequences within siliciclastic systems.

2.3. SEDIMENTARY LOGGING

2.3.1. INTRODUCTION

Sedimentary logging is the most widely applied technique to display the character of sedimentary successions, define type sections and determine stratigraphic thicknesses. An extensive sedimentary logging project was undertaken in the Ainsa basin to predominantly characterise lithology in deep-marine siliciclastic systems, sequences and depositional environments, in order to produce a synthesis of facies associations, depositional processes, and palaeoenvironmental interpretations. This technique was also used for correlating between geographically separated regions through the analysis of key sedimentary attributes in detailed facies descriptions. Each recorded sedimentary succession generally denoted a particular deep-marine environment; however, in some geographically areas, several sedimentary sections were measured for the construction of correlations panels. This facilitated the recognition of geometrical relationships at a number of scales, and the analysis of architectural elements.

Detailed (bed-by-bed) sedimentary logs were compiled from ~4,000 m of measured section from 46 locations, which includes all eight sandy systems in the Ainsa basin (Fig. 2.4 & Table 2.1). The ~70,000 beds that were recorded were classified into 30 facies divisions for description and analysis. The main lithologies observed in the investigation are shale (mudstone), siltstone and sandstone comprising ~51%, ~28% and ~21% of the measured sections, respectively.

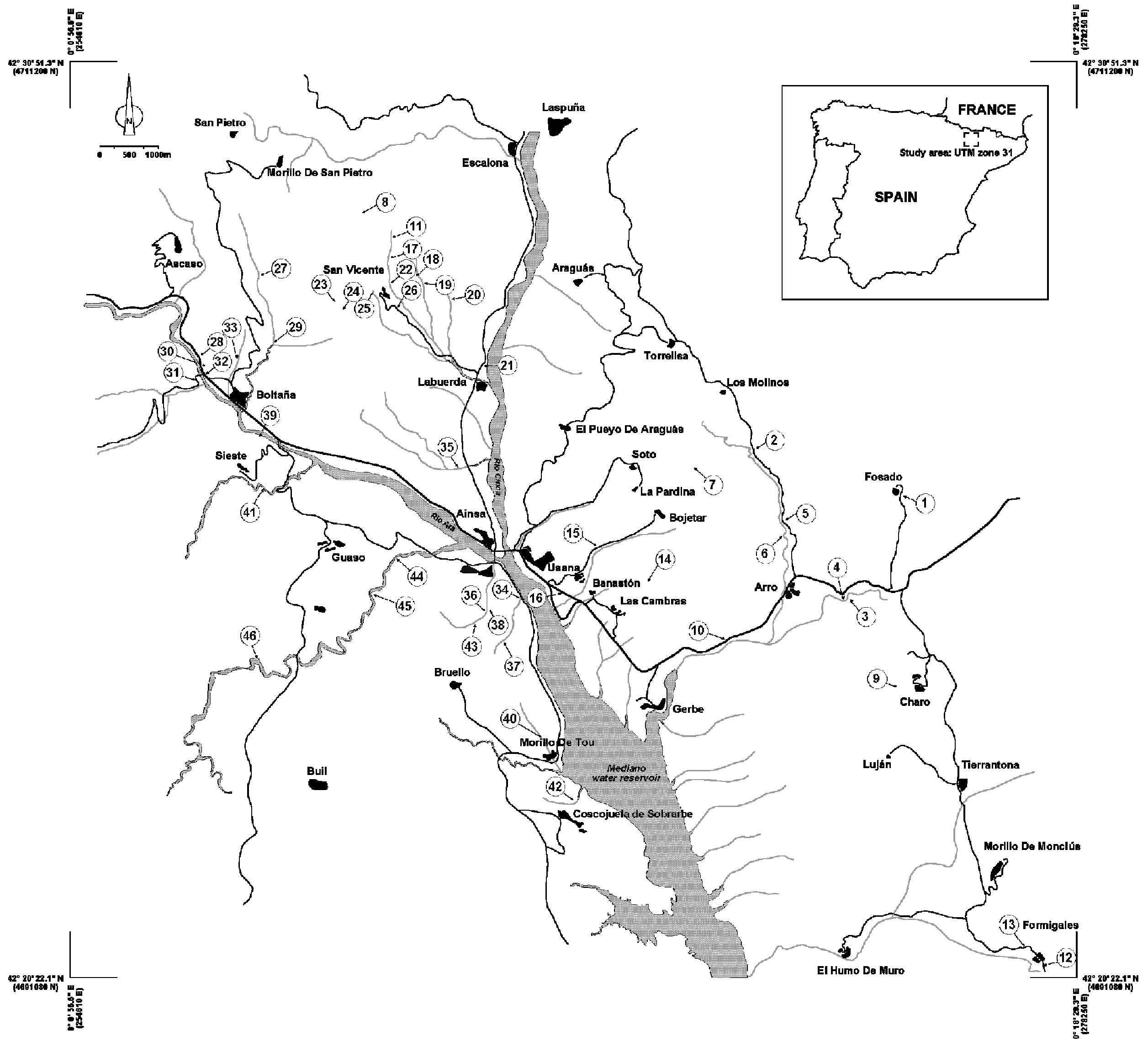

Fig. 2.4. Geographical map of the study area, showing the localities of measured sections. For a summary of the main characteristics of each section see Table 2.1.

Locality No.	Latitude (N)	Longitude (E)	Location Description	Depositional Element	Total Measured (m)
1	42° 25'	0° 15' 17.650"	Southeast of Fosado	Fosado channel complex axis	50
2	42° 26'	0° 12' 50.623"	Southeast of Los Molinos	Los Molinos slope apron sequence	100.37
3	42° 24'	0° 14' 22.762"	Rio Nata	Arro sequence axis	212.53
4	42° 24'	0° 14' 22.676"	Old road section adjacent to Rio	Arro sequence axis	101.33
5	41° 31'	0° 15' 44.147"	Road section adjacent to Bco. Sierre	Arro sequence axis	137.33
6	41° 31'	0° 15' 40.003"	Bco. Sierre	Arro sequence axis	160.89
7	42° 25'	0° 11' 49.870"	Santa Catalina, east of La Pardina	Arro channel complex margin	59.18
8	42° 29'	0° 6' 44.399"	As Faixas ridge, north of San	Arro sequence axis	239.17
9	42° 23'	0° 15' 8.906"	Tozal de Charo, west of Charo	Gerbe canyon sequence	116.51
10	42° 23'	0° 12' 11.261"	N-260 road section, near Gerbe	Gerbe I channel complex axis	35.35
11	42° 28'	0° 6' 36.950"	Bco. Pasata, San Vicente	Gerbe II sequence axis	149.6
12	42° 20'	0° 17' 56.220"	Formigales	Banastón canyon sequence	10
13	42° 20'	0° 17' 47.285"	Northwest of Formigales	Banastón gully complex	20
14	42° 24'	0° 11' 0.013"	San Martin ridge, east of Banastón	Banastón III mass transport	19.7
15	42° 24'	0° 10' 3.449"	Bco. d’Usana	Banastón V channel axis	13.4
16	42° 24'	0° 9' 36.053"	N-260 road section, near Usana	Banastón VI mass transport	30.35
17	42° 28'	0° 6' 36.796"	Bco. a Pasata, San Vicente	Banastón I sequence axis	98.44
18	42° 28'	0° 7' 7.234"	Path adjacent to Bco. Pantiellos	Banastón I channel complex margin	42
19	42° 28'	0° 7' 9.858"	Bco. Pantiellos	Banastón II sequence margin	99.4
20	42° 28' 6.470"	0° 7' 38.985"	Bco. Biñés	Banastón I & II sequence	110
21	42° 27'	0° 8' 5.650"	Labuerda road section	Banastón I & II sequence	87.4
22	42° 28'	0° 6' 38.635"	Bco. Cortaroles, San Vicente	Banastón II sequence axis	160.11

Table 2.1. List of measured sections, GPS readings, locality description, representative depositional elements and the thickness of each measured section (categorised in stratigraphic order, starting with the oldest sedimentary successions visited).

Locality No.	Latitude (N)	Longitude (E)	Location Description	Depositional Element	Total Measured (m)
23	42° 28'	0° 6' 12.528"	San Miguel, San Vicente	Banastón II sequence axis	72.31
24	42° 28' 5.250"	0° 6' 11.905"	San Miguel, San Vicente	Banastón III sequence axis	77.32
25	42° 28'	0° 6' 21.229"	Bco. Pinar, San Vicente	Banastón III complex off-axis	46.16
26	42° 28'	0° 6' 26.618"	San Vicente road section	Banastón III sequence	29.29
27	42° 27'	0° 4' 42.416"	Bco. San Martin, Boltaña	Banastón IV sequence axis	124.59
28	42° 27'	0° 3' 22.907"	N-260 road section, Boltaña	Banastón IV sequence off-axis	62.37
29	42° 27'	0° 4' 43.216"	Bco. San Martin, Boltaña	Banastón V sequence off-axis	97.01
31	42° 27'	0° 3' 25.351"	N-260 road section, Boltaña	Banastón V sequence axis	97.66
32	42° 26'	0° 3' 24.332"	A1604 road section/Bco. Ferrera,	Banastón VI sequence off-axis	97.71
33	42° 27'	0° 3' 26.017"	N-260 road section, Boltaña	Banastón VI sequence axis	160.89
34	42° 27'	0° 4' 4.461"	Bco. Xabierre, Boltaña	Banastón VI sequence	98.57
35	42° 24'	0° 8' 54.837"	Bco. Buchosa, Ainsa	Ainsa I sequence axis	31.5
36	42° 26'	0° 7' 48.545"	Bco. Forcaz, north of Ainsa	Ainsa II sequence margin	99
37	42° 24'	0° 8' 17.164"	Bco. Ranito, Ainsa	Morillo I channel margin	23.15
38	42° 23'	0° 8' 37.388"	Bco. Buchosa, Ainsa	Morillo I channel complex margin	32.01
39	42° 24' 3.794"	0° 8' 10.190"	Path parallel to Bco. Ranito, Ainsa	Morillo I sequence margin	200
40	42° 26'	0° 4' 18.084"	Path parallel to Rio Ara, Sieste	Morillo I sequence off-axis	87.41
41	42° 22'	0° 9' 4.913"	Bco. Cotón, Morillo de Tou	Morillo I & II sequence margins	148.07
42	42° 25'	0° 4' 7.579"	Rio Sieste, Sieste	Morillo I, II & III sequence axes	258.56
43	42° 22' 5.660"	0° 9' 36.004"	Bco. Fuen Mazana, Coscojuela de	Morillo II & III sequence axes	199.35
42	42° 24' 3.607"	0° 8' 2.764"	Path parallel to Bco. Ranito, Ainsa	Morillo II sequence margin	102.57
43	42° 25'	0° 6' 46.955"	Rio Ena, El Grado	Morillo II complex margin	59.08
44	42° 24'	0° 6' 39.758"	Rio Ena, El Grado	Guaso I sequence axis	77.2
45	42° 23'	0° 4' 56.182"	Rio Ena, southwest of Latorrecilla	Gully complex	6.2

Table 2.1. (Continued)

2.3.2. METHODOLOGY FOR SEDIMENTARY LOGGING

The localities chosen for measurement were relatively continuous, well-exposed, representative sections, showing very little structural deformation and limited vegetation (see Table 2.1 for the main characteristics of each location studied). Discontinuous and short sedimentary successions were excluded from the study. The majority of sections were traverses through valleys, rivers or matured road cuttings, which offered excellent exposures and good accessibility. Sedimentary logging was completed by recording bed thicknesses with a metric measuring tape at a scale of 5 mm, i.e., every bed/structure with a thickness ≥5 mm was documented. The true stratigraphic thickness for each section was ascertained incrementally by measuring bed thicknesses normal to bedding; the average sedimentary log completed was ~100 m thick. At each locality, the lithology, bed thickness, grain size, sandstone to mudstone ratio and sedimentary attributes, including fossils and sedimentary structures, were recorded in a fieldwork book. Grain sizes were estimated using the Udden-Wentworth classification scheme (Wentworth, 1922) and bed thicknesses were defined according to Ingram (1954). In structurally deformed locations, beds or distinctive lithological packages were traced across the structures so that sedimentary sections were not repeated. Highly deformed outcrops were not used in the study.

The geological characteristics acquired from the sedimentary successions were graphically represented using Macromedia Freehand. Figure 2.5 illustrates the symbols used in the sedimentary logs. Statistical analysis was preformed on the bed thickness and lithology data.

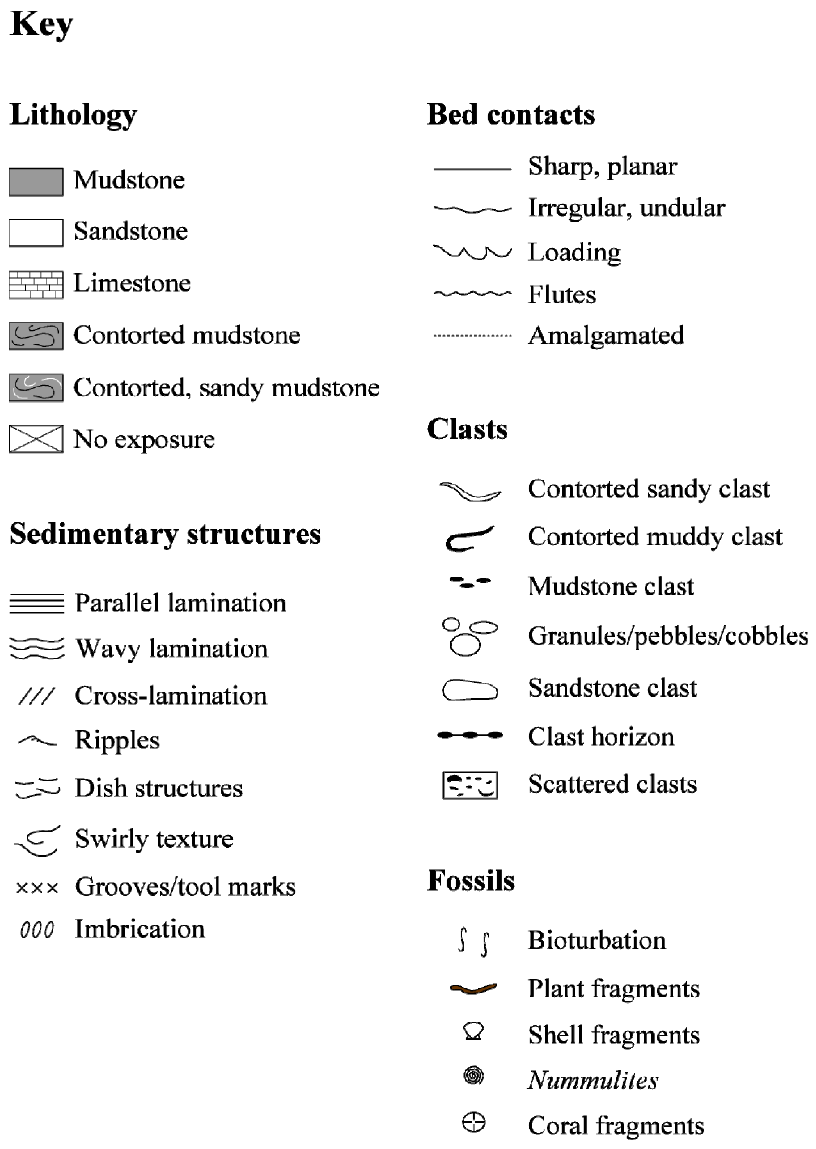

Fig. 2.5. Key for symbols used in sedimentary logs.

2.4. TRACE FOSSIL ANALYSIS

For each deep-marine environment within the six depositional sequences of the Banastón system, trace fossils were analyzed on well-exposed bedding planes of sandstone beds at varying intervals during sedimentary logging of representative sections. The trace fossils were identified at an ichnogenus or ichnospecies level depending on the preservation of the structures and degree of weathering of the outcrop. The qualitative abundance of bioturbation was also observed. The identified trace fossils were arranged into morphological groups according to Książkiewicz (1977), with further modifications by Uchman (1995), and then assigned to ethological groups (*sensu* Seilacher, 1964). The trace fossils were then classified into pre- and post-depositional structures, and the number of graphoglyptid ichnotaxa was determined. The aim of this study was to characterise sedimentary environments in the deep-marine Banastón system by trace-fossil assemblages, and determine possible ecological and taphonomical controls on trace-fossil distributions and behaviours. Ichnological analysis was also undertaken in the underlying and overlying deep-marine systems in the Ainsa basin, but at a depositional system level and non-specific to deep-marine environments.

2.5. CONSTRUCTION OF CORRELATION PANELS

Sedimentary logging permitted the correlation and interpretation between geographically partitioned localities so that correlations panels of various depositional environments in the Banastón and Morillo systems could be constructed. Detailed correlation panels are essential to understanding lateral and vertical facies distributions, lateral thickness variations and sequence stratigraphic patterns. They can lend insight into stratal geometries, the characterisation of architectural elements and the identification of basin depocentres. The integration of detailed sedimentological descriptions (documented in sedimentary logs) and interpretations (illustrated in correlation panels) of deep-marine sandy systems provides a better understanding of architectural styles and hierarchical stacking of depositional elements in the history of a basin fill. Furthermore, two-dimensional representation of depositional characteristics in structurally complex regions, such as at the flanks of intrabasinal highs, can elucidate the influence of seafloor structures on sedimentation.

High-resolution correlation panels were constructed from direct physical tracing of key correlative surfaces and stratigraphic packages using a hierarchical approach. Three orders of correlation were used to subdivide sedimentary successions into discrete, contemporaneous units, similar to the method described by Remacha and Fernández (2003). MTCs defining the base of depositional sequences formed key stratigraphic horizons that determined first-order (sequence-scale) surfaces in which to constrain second- and third-order correlations. Second-order partitioning within lithological units was achieved by tracing markers beds throughout the available outcrops, which facilitated the subdivision of sandy successions into smaller-scale units (~5–20 m thick). Marker beds varied between siliciclastic systems and depositional environments. For example, thin-bedded siltstones that weathered to an orange appearance (possibly rich in iron) were used as precise timelines to correlate within homogenous overbank deposits in the Banastón system (Fig. 2.6). Other marker beds consisted of very thick-bedded sandstone, often amalgamated to form large units, and heavily bioturbated surfaces that could be traced laterally over long distances. Characteristic geological attributes, including lithology, texture, bed-thickness trends, sedimentary structures and geometrical relationships, documented in chronological arrangements within second-order packages defined third-order correlation. Albeit, high-resolution (metre-scale) correlation was achieved, pervasive bed-by-bed scale tracing was rarely attained due to limited outcrop availability and structural deformation. Additionally, the tracing of time-equivalent packages was carried out in a conservative manner to account for the across flow (and in some panels, downflow) variations in stratigraphic thicknesses and key attributes.

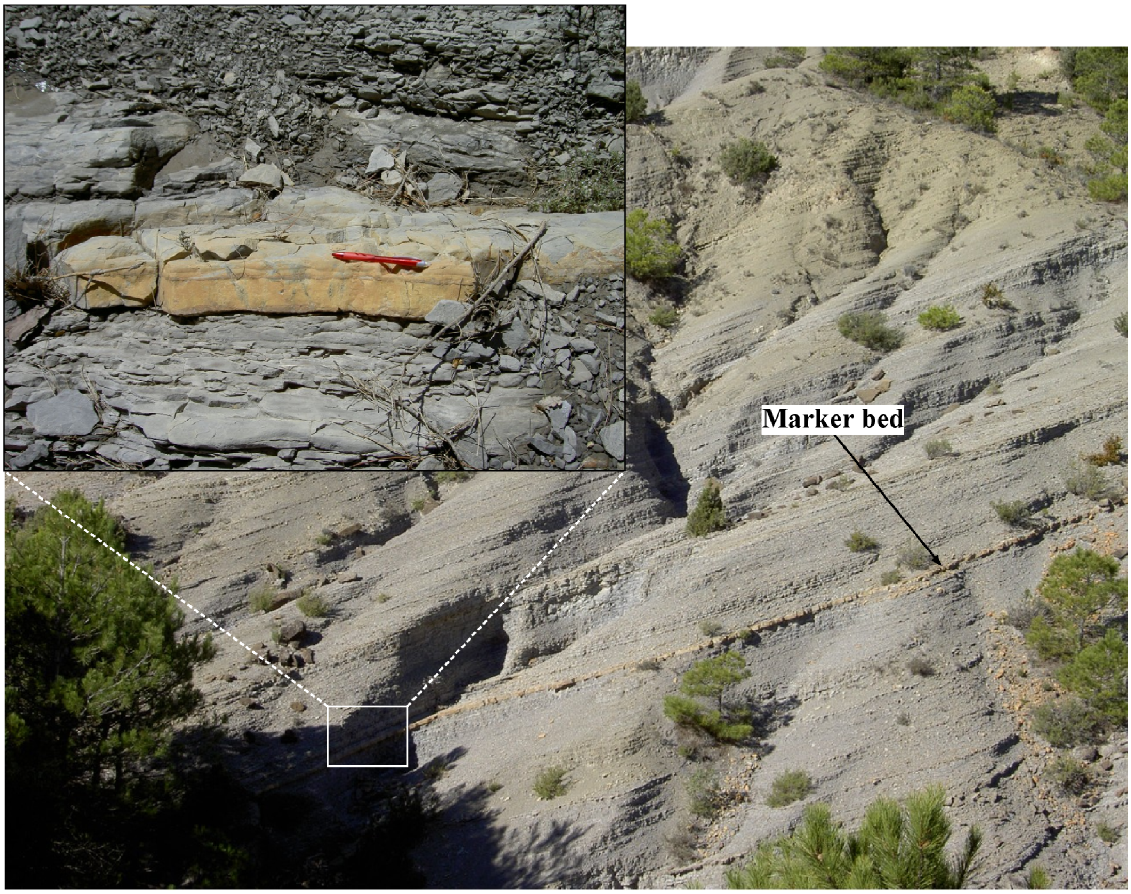

Fig. 2.6. Marker bed used for correlating between outcrops in overbank deposits in the Banastón III sequence, Barranco Biñés area. Similar marker beds were also employed to correlate in the Banastón II sequence. These beds are exclusive to overbank environments in the Banastón system and do not continue laterally into sandy channel-axis environments. Pencil for scale is ~15 cm long.

2.6. STRUCTURAL TECHNIQUES

The timing and kinematics of intrabasinal compressional structures is crucial in understanding the tectono-stratigraphic evolution of thrust-top basins. Mapping and interpreting prominent structural features in the Ainsa basin and assessing the influence of intrabasinal tectonics on the stratigraphy was used to evaluate the contribution of tectonic processes in controlling sedimentation.

The measurement of crystal fiber slickenside lineations preserved on thrust planes provided inferences on the direction of thrusting. Thrust lines were mainly identified in the field by the presence of overturned bedding in deformed strata, with older sediment overlying younger sediment. Mapping the thrusts in the study area and characterizing the timing of deformation allowed kinematic regimes and the pattern of structural movement to be determined. An extensive database of bedding measurements recorded during field mapping was used to interpret the location of large-scale folding in the study area; the orientation of the fold axes and associated plunges were measured. In order to examine the spatial and temporal control of intrabasinal tectonics on the stratigraphic evolution of the Ainsa basin fill, geological maps and correlation panels were used to document and interpret facies patterns, geometries and stratigraphic thickness variations across structural highs. The timing of structural growth with respect to the development of sandy depocentres (siliciclastic systems and sequences) was based on stratal arrangements. Periods of structural growth and non-growth were recognised through onlap patterns and thickness changes over the structures.

CHAPTER 3

FACIES DESCRIPTIONS, INTERPRETATIONS AND STRATIGRAPHIC HIERARCHY

3.1. INTRODUCTION

3.1.1. CONTROLS ON DEEP-MARINE SILICICLASTIC SYSTEMS

Sequence-stratigraphic concepts and their related predictive models have highlighted the variability in turbidite systems and the controls militating their development. Deep-marine systems reflect the complex interplay between a wide variety of allocyclic and autocyclic controls (Fig. 3.1). Posamentier and Kolla (2003) stated that controls on deep-marine systems can be grouped into two categories: those which control the occurrence of sediment into deep-water systems, and those which control the style of sedimentation. Although it seems viable to separate each variable, controls are rarely mutually exclusive and are more commonly interdependent (Reading & Richards, 1994; Emery & Myers, 1996). As a result, a wide spectrum of system types can exist, such that no single model can be applied to describe the variability in facies distribution, stratigraphic architecture, stratal geometry, depositional style and environment. Richards and Bowman (1998) attempted to categorise the variability of deep-marine systems based on the following key parameters:

(a) the method of sediment supply to the system;
(b) the number of entry points to the basin;
(c) the dominant grain size of the system.

These three factors, when considered in combination, provide inferences on the controls influencing all characteristics of the system. This classification framework was used to determine end-members within a hybrid association of system types. The scheme distinguishes between different types of single point-source submarine 'fans', multiple point-source ramps, and line-sourced, slope-apron systems (Richards *et al.*, 1996). This method facilitates the comparison between systems, and the analysis of controls operating within. The aim of this study is not to produce similar generic models, but to highlight the controls influencing the spatial and temporal distribution of depositional elements at a variety of scales within a mixed sand–mud, channel–levee system (representing one apex on one ternary diagram of the classification scheme of Richards & Bowman, 1998) and attempt to deconvolve the controls driving system development. In understanding these controls and evaluating them in a scalar hierarchy, the application of sequence stratigraphy in the characterisation of deep-marine systems becomes a useful tool.

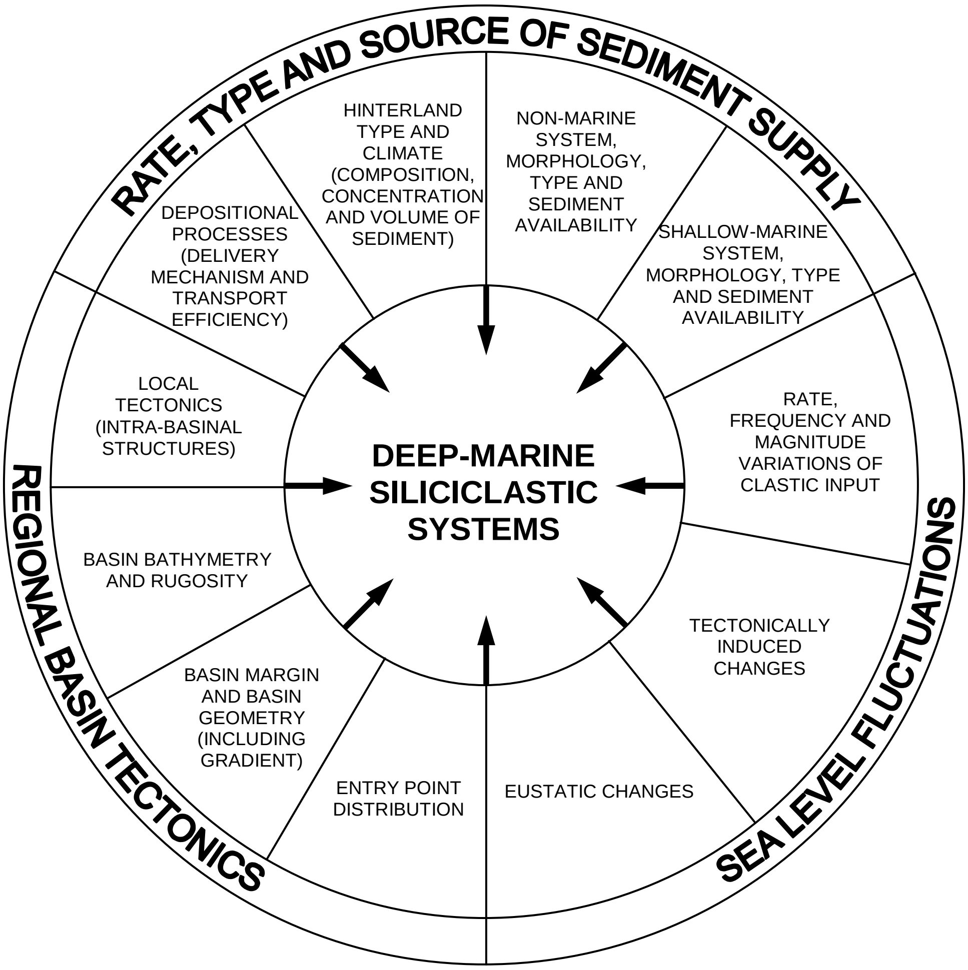

Fig. 3.1. Controls on the development of deep-marine systems. The complex interplay between a number of autocyclic and allocyclic controls determines the characteristics of a system and allows a wide spectrum of system types to operate. (Redrawn and modified after Richards & Bowman, 1998; Richards *et al.,* 1998).

3.1.2. INTRODUCTION TO ARCHITECTURAL ELEMENTS

The organisation of architetural elements into hierarchical classification schemes were originally employed in non-marine environments to characterise various scales of sedimentological observations (Brookfield, 1977; Miall, 1985). This method has proven to be valuable in the description and interpretation of deep-marine sediments (Gosh &

Lowe, 1993; Pickering *et al*., 1995; Clark & Pickering, 1996; Hickson & Lowe, 2002; Anderson *et al*., 2006; Hubbard *et al*., 2008). A hierarchical approach to sequence stratigraphy is adopted in this study to determine the depositional history of the Ainsa basin. The analysis of architectural elements in the Ainsa basin modifies the methods of Gosh and Lowe (1993) and Pickering *et al*. (1995) to organise complex stratigraphic and sedimentological observations in order to interpret architectural styles of depositional bodies at a range of scales, and to make inferences on the complexity of factors influencing the nature of slope and basin-floor systems. The approach to depositional characterisation follows a bounding surface hierarchy scheme (*sensu* Miall, 1985; Pickering *et al*., 1995), which allows the sedimentary fill in the Ainsa basin to be delineated at various scales. The architectural elements are classified using facies, facies associations and architectural geometry. The scalar hierarchy of channelised elements (the stacking of channelforms), and the stratigraphy of the Ainsa basin, can then be defined. This scheme forms the structural basis of this chapter.

3.1.3. CLASSIFICATION OF THE AINSA BASIN

The concept of architectural elements in turbidite systems was initially introduced by Mutti and Normark (1987); they defined large-scale features, such as channels, overbank deposits and lobes, by facies associations and a classification of the hierarchy of events. The classification scheme categorised the Ainsa basin into a foreland-propagating, structurally-controlled Type C basin, which formed as a succession of turbidite systems (comprising the Hecho Group; this study). Tectonic processes were the primary control on basin configuration and duration.

The Hecho Group may be considered a turbidite complex *sensu* Mutti and Normark (1987), where it is defined as a basin-fill succession composed of several stacked turbidite systems (termed sandy/depositional systems in this study). The Hecho Group is a foreland-propagating turbidite wedge; it shows a south-directed onlap, which is consistent with the direction of thrust sheet advancement (Labaume *et al.*, 1985), indicating a strong tectonic control on basin geometry, accommodation and sediment supply. Each system contains Type I deposits *sensu* Mutti and Normark (1987) that represent deposition within a highly efficient sediment dispersal pattern, and the formation of erosional canyons and channels. Type I deposits are characteristic of tectonically-controlled narrow basins, which enhance the transport of siliciclastic sediments. The channel fill elements composing each turbidite system can be referred to as mixed erosional-depositional channel fills (*sensu* Mutti and Normark, 1991). These elements are discussed in more detail later.

The first depositional environment to form in the majority of sandy systems is defined by an upper/mid-slope canyon, comprising coarse-grained channel fill elements dominated by mass transport deposits situated above a pre-developed erosional surface. Downflow, these elements pass into lower-slope, erosional channels and proximal basin-floor channel systems. These major elements form the main depositional settings in the Ainsa basin in a continuous depositional profile (Fig. 3.2). The lower stage of growth of each system is represented by a sandy phase, which transitionally passes upward into an upper muddy stage of growth (*sensu* Mutti, 1985).

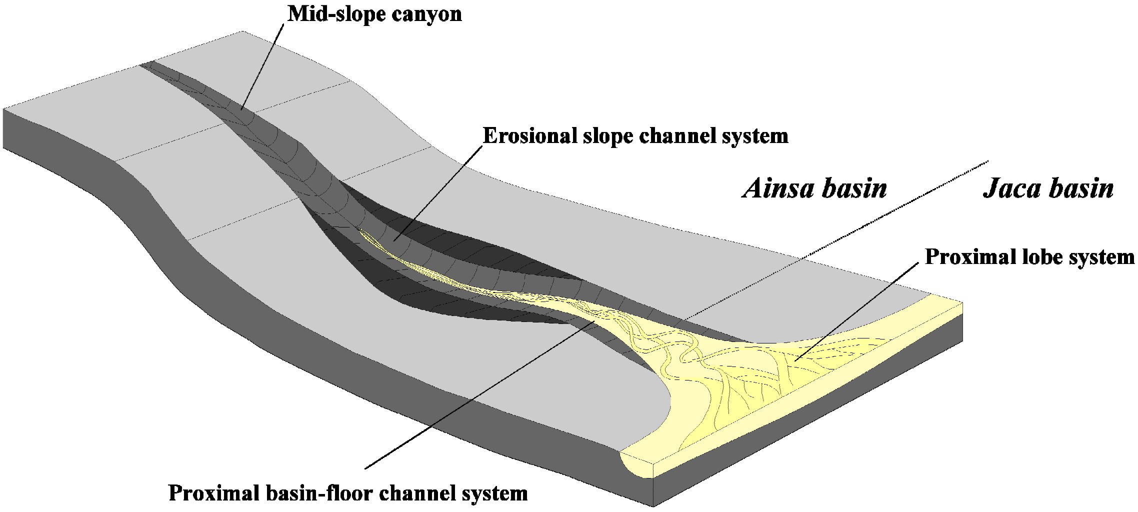

Fig. 3.2. Schematic representation of the deep-marine settings in the Ainsa basin.

3.2. FACIES CLASSIFICATIONS

The facies scheme used in this study is a modification of Pickering *et al.* (1986, 1989) as it can be adapted to multiple sediment grades and is hierarchical in its assignments. As noted by Pickering *et al.* (1986, 1989), ‘facies’ refers to various types of sediment or bodies of sedimentary rock with specific characteristics that are physical, biological and chemical in nature. For sediment gravity flow deposits, individual facies are scaled directly to the scale of single flow deposits (beds). Common facies definitions in this study included textural trends, relative thicknesses and internal organisation. Several *facies classes* (A–H) were defined, which contain subsequent *facies groups* in a hierarchical organisation — 30 facies groups for this study. Facies class A–E are divided into organised and disorganised facies, where clear indications of stratification, grading and sedimentary structures are representative of organised facies. Facies class F comprises exotic clasts and contorted strata; facies class G is biogenic muds (Pickering *et al.*, 1986, 1989). Throughout this study, facies groups were mainly distinguished in the field by grain size, using the Udden-Wentworth classification scheme (Wentworth, 1922), and bed thicknesses from Ingram (1954):

Laminae, <1cm;
Very thin beds, 1–3 cm;
Thin beds, 3–10 cm;
Medium beds, 10–30 cm;
Thick beds, 30–100 cm;
Very thick beds, >100 cm.

In an effort to maintain simplicity, the terminology for modern unconsolidated sediments is used where the terms gravel, sand, mud, silt and clay are representative of the ancient lithified rock types conglomerate, sandstone, mudstone, siltstone and claystone, respectively (Pickering *et al.*, 1986, 1989). Pictorial representations of type facies are found in the following chapters related to the sandy systems in the Ainsa basin.

The data acquired while measuring sections is summarised on Table 3.1 according to facies. In total, 70,194 beds were measured constituting 4,118 m of thickness. Beds averaged 6.3 cm in thickness with minimum and maximum thicknesses of 1 and 3,460 cm, respectively. Only 1.8% of the beds measured were amalgamated. Subsequent plots assist in analysing the measured data. Figure 3.3 indicates that the majority of facies measured by bed belong to facies class C, D and E; however, thickness of measured facies varies across all facies. If the average thickness of beds is considered (total thickness divided by the number of beds, Fig. 3.3), there is a general decrease from facies class A to H as would be expected for this type of basin. A large number of thin beds were measured in the basin, which is evident in Figure 3.4. A well behaved trend indicates that the number of beds measured according to bed thicknesses decreases to very thick beds. Analysing this trend with the previous, the general association of very thick beds with facies class A is apparent; similarly, very thin beds with facies class D and E. Beds were also identified as being amalgamated with the majority of amalgamation occurring in facies class A, B and C (Fig. 3.5).

Facies	Bed Thickness (cm)			Number of Beds				Thickness		
	Average	S.D.	Min/max	Total	% of class	% of all classes	% amalgamated	Total (m)	% of class	% of all classes
Class A	209.2	388.0	12/3460	466	100	0.70	47.0	974.81	100	23.67
A1.1	126.8	15.6	55/240	16	3.4	0.02	100	20.29	2.08	0.49
A1.2	111.5	47.3	35/310	10	2.1	0.01	30.0	11.15	1.14	0.27
A1.3	381.3	441.9	12/3460	207	44.4	0.29	1.4	789.36	80.98	19.17
A1.4	50.9	24.2	15/120	43	9.2	0.06	81.4	21.87	2.24	0.53
A2.1	158.3	384.9	20/1290	20	4.3	0.03	90.0	31.65	3.25	0.77
A2.2	64.8	15.3	55/95	6	1.3	0.01	100	3.89	0.40	0.09
A2.3	80.3	38.2	35/220	31	6.7	0.04	87.1	24.89	2.55	0.60
A2.4	49.2	25.2	12/145	75	16.1	0.11	82.7	36.93	3.79	0.90
A2.5	60.0	25.3	15/155	58	12.4	0.08	84.5	34.78	3.57	0.84
Class B	31.8	26.9	2/160	802	100	1.10	39.7	254.80	100	6.19
B1.1	40.1	23.9	8/160	422	52.6	0.60	58.1	169.21	66.41	4.11
B1.2	6.1	1.7	2/9	260	32.4	0.37	0.8	15.96	6.26	0.39
B2.1	59.2	23.0	14/145	101	12.6	0.14	67.3	59.82	23.48	1.45
B2.2	51.6	9.8	38/70	19	2.4	0.03	15.8	9.81	3.85	0.24
Class C	7.4	15.7	1/295	18706	100	26.60	3.8	1340.82	100	32.56
C1	31.1	16.1	12/125	84	0.4	0.12	26.2	26.14	1.95	0.63
C2.1	147.1	47.6	15/295	73	0.4	0.10	72.6	107.36	8.01	2.61
C2.2	48.1	15.5	20/98	1069	5.7	1.52	35.7	513.81	38.32	12.48
C2.3	17.7	6.1	10/38	1951	10.4	2.78	12.6	344.67	25.71	8.37
C2.4	5.5	1.7	2/12	3115	16.7	4.44	0.1	175.44	13.08	4.26
C2.5	2.0	0.2	2/5	4798	25.6	6.84	0	97.24	7.25	2.36
C2.6	1.0	0.0	1/1	7616	40.7	10.85	0	76.16	5.68	1.85

Table 3.1. Summarised statistics of measured section data organised by facies class.

Facies	**Bed Thickness (cm)**			**Number of Beds**				**Thickness**		
	Average	**S.D.**	**Min/max**	**Total**	**% of class**	**% of all classes**	**% amalgamated**	**Total (m)**	**% of class**	**% of all classes**
Class D	1.6	1.1	1/18	19680	100	28.00	0	313.49	100	7.61
D1	4.0	1.5	2/8	1504	7.6	2.14	0	57.73	18.42	1.40
D2.1	2.4	1.1	1/18	5390	27.4	7.68	0	127.90	40.80	3.11
D2.2	1.0	0.0	1/1	12786	65.0	18.22	0	127.86	40.79	3.10
Class E	2.4	1.8	1/21	29110	100	41.50	0	713.84	100	17.33
E1.1	7.4	3.7	2/20	905	3.1	1.29	0	57.44	8.05	1.39
E1.2	3.2	1.8	1/13	3517	12.1	5.01	0	115.24	16.14	2.80
E2	2.1	1.4	1/21	24688	84.8	35.17	0	541.16	75.81	13.14
Class F	216.6	276.2	10/1700	290	100	0.40	3.8	481.59	100	11.69
F1	298.9	265.3	10/1060	96	33.1	0.14	0	84.37	17.52	2.05
F2	204.8	276.4	12/1700	194	66.9	0.28	5.7	397.22	82.48	9.64
Class G*	2.6	0.7	2/4	1101	100	1.60	0	33.17	100	0.81
Class H*	15.1	9.8	3/45	39	100	0.10	38.5	5.90	100	0.14
All Facies	6.3	44.4	1/3460	70194	n/a	n/a	1.8	4118.42	n/a	n/a

* One facies in class G and H

Table 3.1. Continued from previous page.

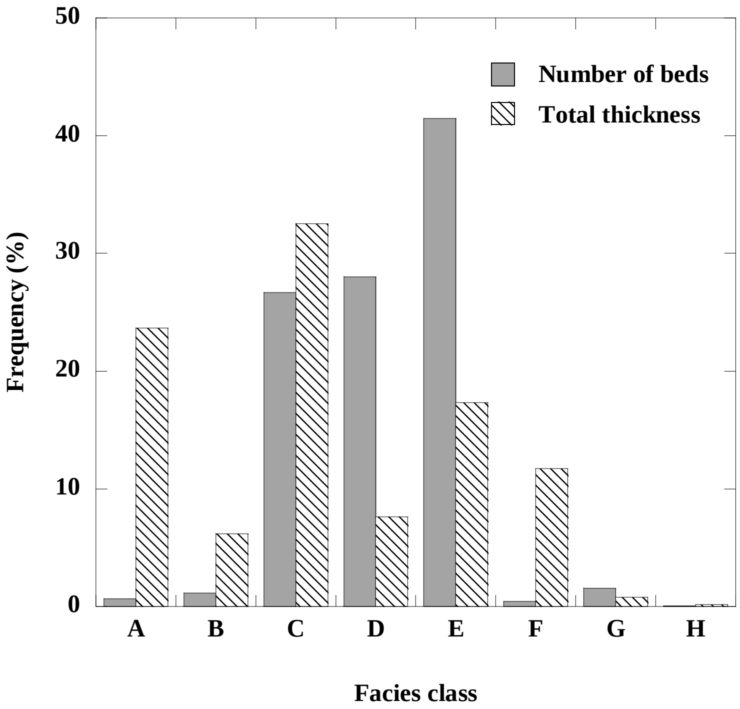

Fig. 3.3. Abundances of facies classes, reported by number of beds and total thickness, for all facies measured. Relative relationships between facies classes for average bed thicknesses can be concluded. Here, facies class A shows much larger beds than facies class E.

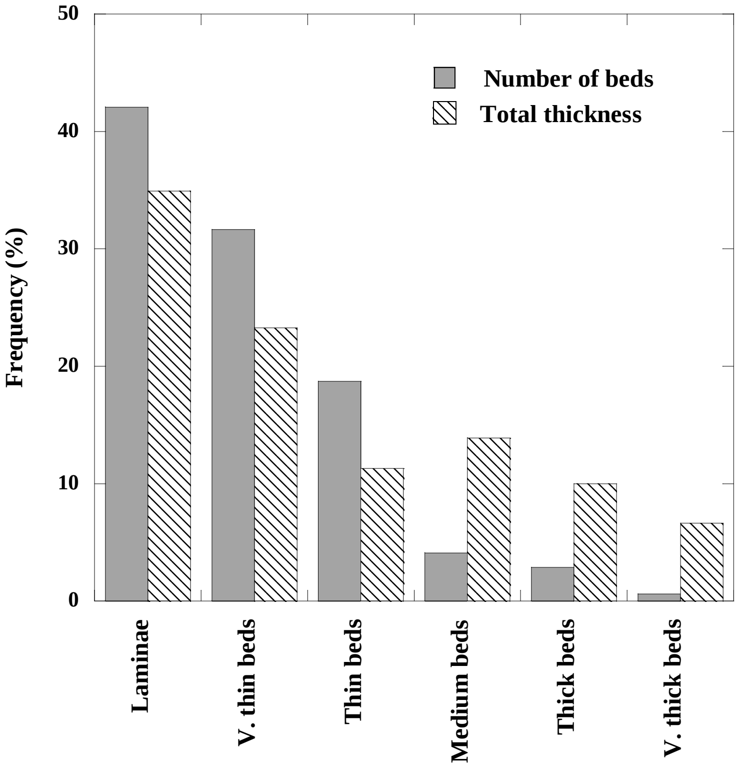

Fig. 3.4. Relative proportions of beds and total bed thicknesses for thickness categories from all facies classes. Medium to very thick beds show a noticeable increase in the thickness to number of beds ratio compared to laminae to thin bed thicknesses, indicating the abundance of thin beds in the basin.

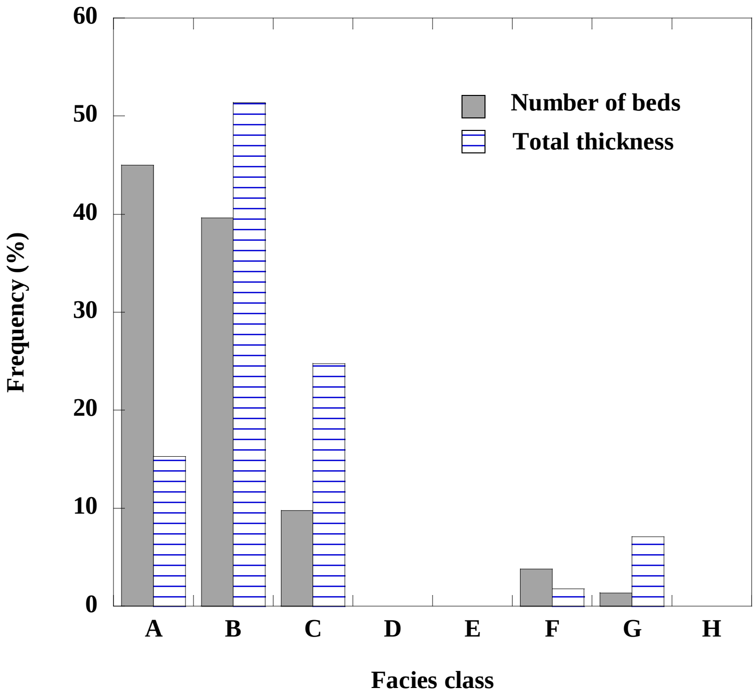

Fig. 3.5. Bed amalgamation according to facies class reported by the number of beds and total thickness. The majority of amalgamation between beds occurs in facies class A–C.

3.2.1. Facies Class A: gravels, muddy gravels, gravelly muds, pebbly sands, 25% gravel-grade

Facies class A is the coarsest facies class in the Ainsa basin. There is a notable amount of Facies A1.3, which is a facies with a muddy matrix (Fig. 3.6). This is attributed to an abundance of muddy beds measured throughout the basin. Matrixes of this facies class may be of sand or mud, or facies may be supported by clasts (Pickering *et al.*, 1989). Figure 3.7 shows that the majority of beds measured of this facies class are thick to very thick.

3.2.1.i. Facies Group A1 – Disorganised gravels, muddy gravels, gravelly muds and pebbly sands

3.2.1.i.a. Facies A1.1 – Disorganised gravel

Description: Clast supported, massive, thick bedded sandy gravel (Pickering *et al.*, 1989). Disorganised gravels account for 0.49% of the total thickness of the beds measured in the Ainsa basin. The matrix of this facies type is one of sand or mud, but more commonly sand. Sediments composing this facies contain clasts ranging from fine pebble- to boulder-grade, where the angularity of the clasts is angular to well-rounded and sorting is poor. There is no well defined fabric to disorganised gravels.

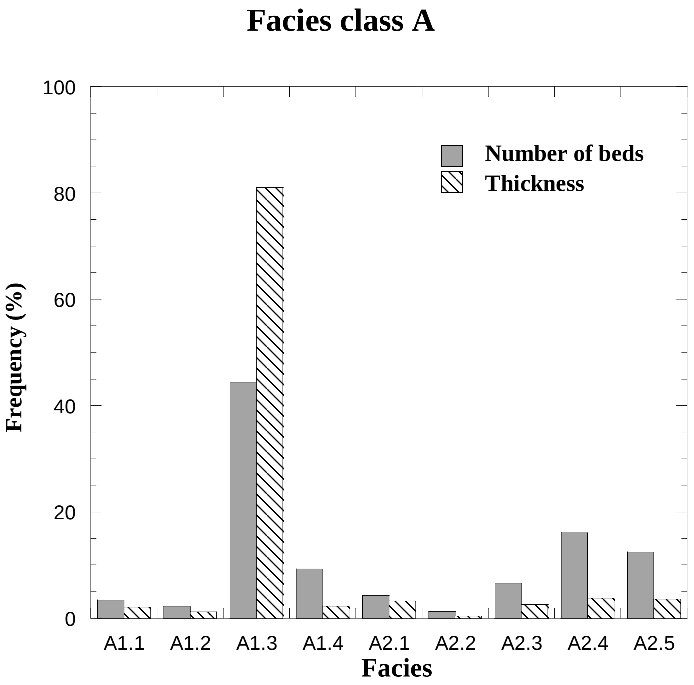

Fig. 3.6. Facies of class A by number of beds and thickness, presented as proportions of all measured sections.

A) Number of beds

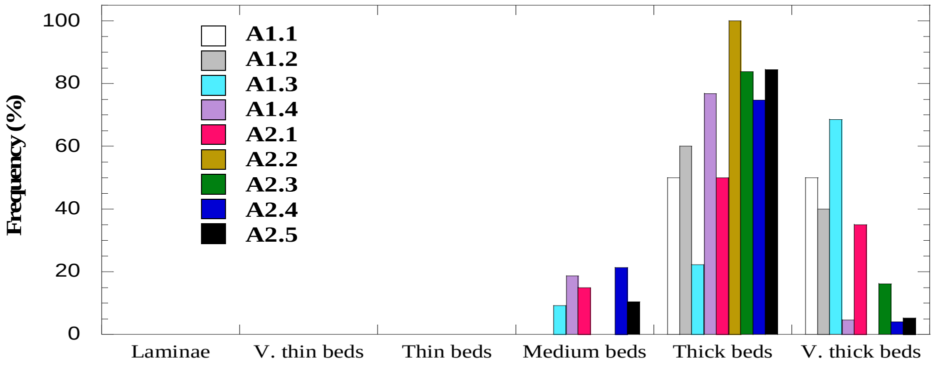

B) Thickness

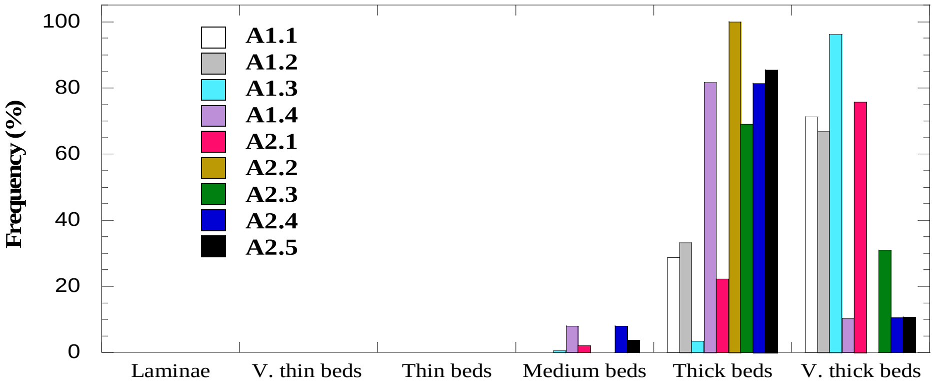

Fig. 3.7. Relative proportions of the number of beds (A) and thickness (B) for each facies according to bed thickness.

Bedding takes on multiple geometries where basal geometries can be flat-based or deeply scoured and bedding tops are irregular to wavy, resulting in depositional bodies that laterally degrade and thin in a lenticular fashion, which can be gradual or abrupt. These beds commonly have bedding thicknesses in the order of 0.5 to 5 m with random beds attaining thickness of tens-of-metres. These beds are found associated with other facies of Group A1.

Interpretation: These facies are emplaced by concentrated density flows, inflated sand/gravel flows and debris flows coming to rest where slopes are decreasing due to intergranular friction and cohesion (Hiscott & James, 1985; Stanley *et al.*, 1978, Winn & Dott, 1979).

3.2.1.i.b. Facies A1.2 – Disorganised muddy gravel

Description: Structureless, matrix supported muddy gravel, typically referred to as a debris flow, with bed thickness up to very thick and a mud-grade content of 10–50% (Pickering *et al.*, 1989). This facies amounts to 0.27% of the total thickness of the beds measured in the Ainsa basin. Clasts vary in size, composition, and angularity. Polymodal distributions of clast size are common with compositions from igneous, sedimentary, metamorphic, lithified biogenic material or unlithified sediment sources. Throughout bedding, large cobbles and boulders may appear as evenly distributed, grading, or extruding from within the bed into the overlying sediments. Fabrics are rare in existence and take on parallel to sub-parallel lamination form.

The bedding of disorganised muddy gravels ranges from medium bedded to very thick bedded. Beds show low-relief planar tops and bases in outcrop, with little evidence for erosive bases; however, many beds are inferred to have abrupt/blunt terminations at their downdip extents.

Interpretation: Disorganised muddy gravels can originate from local or distant source areas, and occur as the result of mass failures where in-place sediments collapse (multiple clast compositions) and flow until coming to rest due to frictional forces and cohesion. These sediments are found on degrading slopes near slope to basin floor transitions (Stanley *et al.*, 1978; Mutti & Ricci Lucchi, 1972; Winn & Dott, 1979; Labaume *et al.*, 1983; Hiscott & James, 1985).

3.2.1.i.c. Facies A1.3 – Disorganised gravelly mud

Description: This facies is distinguished by having a 50–95% mud-grade content that is matrix supported and structureless with highly irregular bedding (Pickering *et al.,* 1989). It totals 19.17% of the total thickness of the beds measured in the Ainsa basin. It carries many similar attributes of Facies A1.2 and can also have beds in the tens-of-metres. Clasts exhibit a range in size and follow a polymodal distribution. An abundance of silt-mud chips and slabs are present in this facies along with clast compositions as described in Facies A1.2.

Thicknesses of beds range from decimetres to metres for this facies. Beds are typically laterally discontinuous and show high levels of irregularity in bedding shape. Punctual changes in the level of internal organisation are readily apparent along with variations of matrix content and bed shape.

Interpretation: This facies is emplaced on lower slopes by cohesive mud flows coming to rest when frictional and cohesive forces overtake the kinetic forces of the flow (Stanley *et al.,* 1978; Mutti & Ricci Lucchi, 1972; Winn & Dott, 1979; Labaume *et al.,* 1983; Hiscott & James, 1985).

3.2.1.i.d. Facies A1.4 – Disorganised pebbly sand

Description: This facies is dominated by a sand matrix, but includes large clasts dispersed randomly in beds that can be tens-of-metres thick (Pickering *et al.,* 1989). In this study, 0.53% of measured thickness in the Ainsa basin is assigned to this facies type. Clasts are found to randomly concentrate into ribbons and irregular patches within the sandy matrix. Concentrations can be on the order of one pebble in thickness. Clasts vary in size from fine to coarse with a regularity of mudstone clasts and occasional cobbles and boulders. Larger clasts show no indication of grading, stratification or preferred orientation.

Bedding commonly ranges from 0.5 to 5 m in thickness and is lenticular and laterally continuous in nature. Bedding surfaces are poorly defined when clasts are weakly present and readily identified with increasing clast concentration. Scouring along bed bases is common, as is loading and large sole marks. Bed top surfaces tend to be more continuous and flat. Beds with high concentrations of mudstone clasts are best identified as mud-flake breccia.

Interpretation: High concentration turbidity currents are the transport mechanisms for disorganised pebbly sand. As flow decelerates, intergranular friction of the flow increases causing the pebble-sand mixture to deposit as grain deposition (Winn & Dott, 1979; Walker, 1978).

3.2.1.ii. Facies Group A2 – Organised gravels and pebbly sands

3.2.1.ii.a. Facies A2.1 – Stratified gravel

Description: Stratified gravels are well stratified, clast-supported, imbricated, lenticular in shape and up to several metres in thickness (Pickering *et al.,* 1989). This facies constitutes 0.77% of the total thickness of measured section in the study area. Clasts can be coarse pebble-grade to large sand clast over one metre in diameter. Commonly, clasts are well rounded to angular about the size classification of coarse pebbles.

Bed thickness averages 1.6 m for this facies type. Erosive bed bases occur with this facies; tops of beds tend to be continuous, but will show irregularity in geometry. Internal erosive surfaces with poor lateral extent are common.

Interpretation: These deposits are formed from concentrated density flows. Grain-by-grain deposition occurs first, followed by traction transport processes (Winn & Dott, 1979).

3.2.1.ii.b. Facies A2.2 – Inversely graded gravel

Description: These deposits are primarily identified by the apparent inverse grading in bedding with well developed clast imbrication and poor sorting (Pickering *et al.*, 1989). Beds reach maximum thicknesses of several metres. In the studied area, this facies accounts for 0.09% of the total thickness of all measured sections. Clast size varies from fine- to coarse-pebble, with large clast sizes as the most common.

Thickness of bedding averages between 0.5–4 m. Beds show erosion on the base surfaces and are lenticular. They thin laterally and can develop complexity in bed shape due to variable clast concentrations. Where beds are towards the upper threshold of thickness, the lower 5–20% of the bed typically contains smaller clasts than that part of the bed immediately overlying, creating a noted change in grain size within a bed.

Interpretation: Inversely graded gravels are transported by concentrated density flows that undergo late-stage flow transformations. Increased intergranular friction causes rapid deposition where grain interaction leads to imbrication and inverse grading (Winn & Dott, 1979).

3.2.1.ii.c. Facies A2.3 – Normally graded gravel

Description: These deposits are clast-supported and normally graded with bed thicknesses up to several metres (Pickering *et al.*, 1989). They comprise 0.60% of the total measured thickness of measured outcrop in the study area. Erosion is commonly associated to this facies. Clast can vary in size from fine- to coarse-pebbles and may contain cobbles. As they are normally graded, larger clasts are located at the base of beds and transition to smaller clasts at bed tops. This may be seen as transitions from coarse pebbles to fine pebbles or sand, and less commonly from cobbles to granule sand in very thick beds. Imbrication does occur in this facies; however, it is less common than in Facies A2.2.

Bed thickness ranges from 0.5 to several metres on average. Erosion is prominent on bed base surfaces and causes variations in thickness of the bed where local, deep-scour events take place. Upper bed surfaces are characterised as irregular in geometry. In general, beds are lenticular in shape and laterally discontinuous.

Interpretation: These deposits are formed from concentrated density flows where deposition occurs from grain-by-grain emplacement from suspension (Winn & Dott, 1979; Mutti & Ricci Lucchi, 1972). Unlike Facies A2.2, traction transport of clasts does not occur during deposition.

3.2.1.ii.d. Facies A2.4 – Normally graded pebbly sand

Description: This facies is identified by having normal grading with pebble or smaller clasts at bed base locations (Pickering *et al.*, 1989). In the Ainsa basin, this facies type constitutes 0.90% of the total thickness of measured outcrop. Common bed thicknesses range from decimetres to several metres with scour structures that produce irregular appearances. If clasts are present, they tend to be on the order of granules to medium-sized pebbles.

These facies are typically found in amalgamated sandy units. Bed contacts can be difficult to distinguish when clast concentrations are minimal or non-existent and beds are amalgamating together. Overall, these deposits tend to be lenticular in shape, show erosion in basal surfaces and have irregular tops.

Interpretation: This facies is formed from concentrated density flows where rapid burial occurs during grain-by-grain deposition from suspension (Winn & Dott, 1979).

3.2.1.ii.e. Facies A2.5 – Graded stratified pebbly sand

Description: These deposits are much like Facies A2.4 with the exception that stratification occurs in the beds (Pickering *et al.,* 1989; Winn & Dott, 1979). This study shows that 0.84% of the total measured thickness of the Ainsa basin constitutes this facies type. Beds are commonly lens-like in shape with repetitive patterns of fining upward grain sizes. Overall, the entirety of a bed shows a fining upwards pattern. Stratification in these deposits can be parallel, oblique or repetitive. Incorporated clasts range in size from granules to pebbles and are rounded to angular. The coarser of the clasts (greater than very-fine pebbles) are restricted to the lower parts of beds.

Beds are usually located in amalgamated sandy units where bed contacts can be difficult to distinguish when pebbly strands occur high in beds. Amalgamated packages are on the order of tens-of-metres.

Interpretation: These pebbly sands are formed from concentrated density flows that become dilute with time for a respective location. Initial deposition occurs rapidly by grain-by-grain deposition from suspension. As sediment is accumulated, stratification appears when grains are transported via bedload prior to burial (Winn & Dott, 1979).

3.2.2. Facies Class B: sands, >80% sand grade, <5% pebble grade

This facies class is divided into two groups, organised and unorganised, based on sedimentary structures present (Pickering *et al.,* 1989). The majority of the thickness measured in the basin attributed to this facies belongs to Facies B1.1 where thick beds prevail (Fig. 3.8). However, on multiple occasions this facies was measured in thinner beds, as noted in the spike in thin beds for Facies B1.2 in figure 3.9.

3.2.2.i. Facies Group B1 – Disorganised sands

3.2.2.i.a. Facies B1.1 – Thick to medium-bedded, disorganised sands

Description: This facies is identified as laterally continuous, medium to thick beds that are vacant of grading and commonly have fluid-escape structures. These beds compose 4.11% of the total measured thickness in the Ainsa basin for this study. Composition consists of >80% sand-grade and <5% pebble-grade (Pickering *et al.,* 1989). Dish structures are the common fluid-escape features in this facies for well sorted sands and tend to occur in the upper half of the beds. Poorly sorted sands show fluid escape along pillars and sheets.

Uniform to highly irregular medium to thick beds are typical where pinch and swell geometries can form from intrastratal flow or collapse of overlying units creating pseudo-clasts. Bases of beds usually show coarse-tail grading with small pebbles and granules in thin layers.

Interpretation: Two theories are given for the deposition of these deposits: concentrated density flows (Pickering *et al.,* 1989; Mutti, 1992; Lowe, 1997; Hiscott *et al.,* 1997) or inflated sand flows (Shanmugam, 2000; Shanmugam *et al.,* 1997). In the first case, sediments are transported down slope and rapidly decelerate, eliminating the possibility of tractional structure development. For inflated sand flows, intergranular friction in concentrated dispersion causes mass deposition. Either theory allows the possibility for open grain collapse and the formation of fluid-escape features.

3.2.2.i.b. Facies B1.2 – Thin-bedded, coarse-grained sands

Description: This facies is recognised as thin beds composed of very coarse-grained sands with no internal structure or grading. In the study area, 0.39% of the total thickness of outcrop measured is of this facies type. Pebbles are rare in this facies, but can occur in strings within beds. Angular silt and mud clasts may be found in this facies as well.

Beds show wedge-shaped or pinch-and-swell geometries with distinct tops, and are irregular in nature. If pebble clasts are present, they may extrude into overlying sediments.

Interpretation: These facies are transported beneath turbidity currents or strong bottom currents as bed-load and come to rest from grain-by-grain deposition (Mutti, 1977).

Facies class B

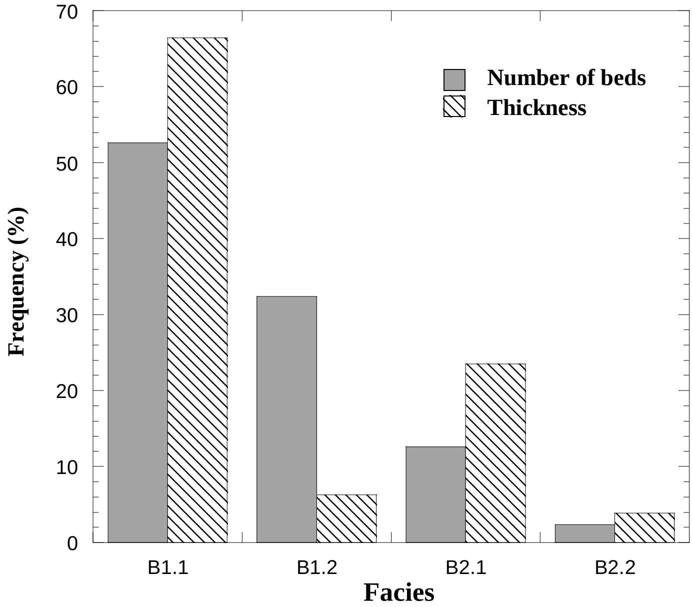

Fig. 3.8. Facies of class B by number of beds and thickness, presented as proportions of all measured sections.

A) Number of beds

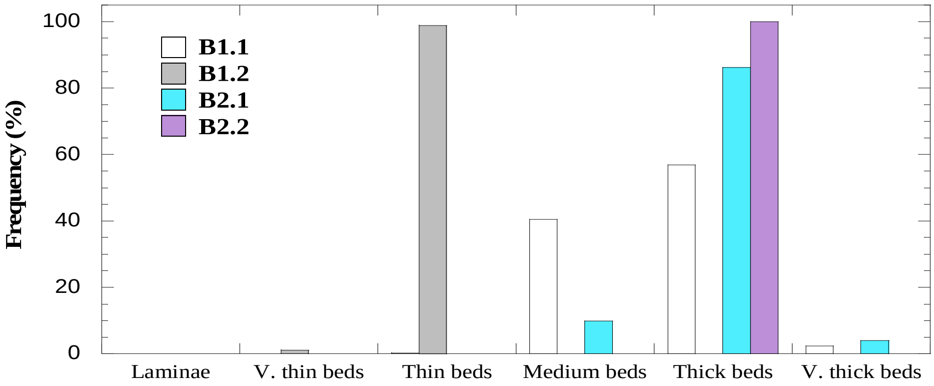

B) Thickness

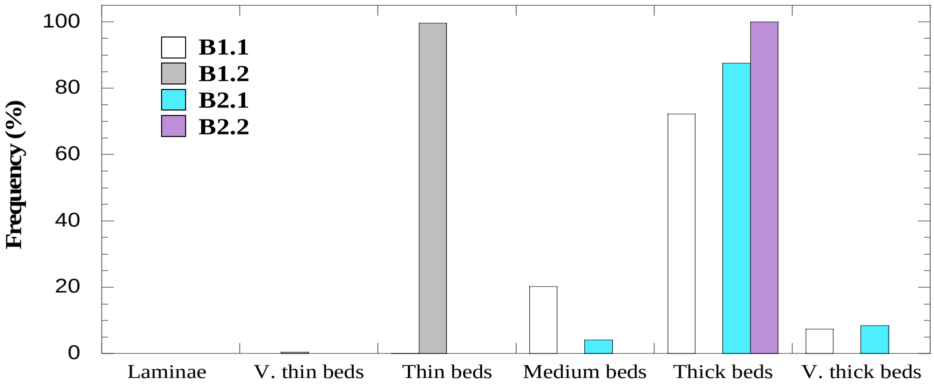

Fig. 3.9. Relative proportions of the number of beds (A) and thickness (B) for each facies according to bed thickness.

3.2.2.ii. Facies Group B2 – Organised sands

3.2.2.ii.a. Facies B2.1 – Parallel stratified sands

Description: This facies is commonly recognised by its thick to very thick, normally graded beds that contain inversely stratified layers on the order of tens of centimetres (Pickering *et al.,* 1989). In the study area, these deposits comprise 1.45% of the total measured thickness. The internal, stratified sand bands show inverse grading and are interlaced by structureless sands of medium to very-coarse grains.

Bedding in this facies type can range from medium to very thick with parallel-sided to highly irregular nature. Bed bases are typically near-horizontal erosional surfaces; bed tops grade into silts with ripple laminations. Alternatively, and more commonly, these beds are amalgamated.

Interpretation: Parallel stratified sands are deposited by concentrated density flows where the bands of inverse grading are due to downward sweeps of large turbulent eddys (Hiscott & Middleton, 1979, 1980; Hiscott, 1994) and structureless sands are attributed to rapid grain-by-grain deposition (Lowe, 1982).

3.2.2.ii.b. Facies B2.2 – Cross stratified sands

Description: This facies is best identified by the presence of cross stratification sets in beds ranging in dimension from 10 to 25 cm thick. This facies accounts for 0.24% of the total thickness of measured outcrop. Cross stratified sets may occur as solitary sets or cosets with internal lamination angles similar to the angle of repose. Grain size is on the order of granule-grade to coarse-grained sands. Sands in this facies are very well sorted.

Beds show a lens shape, but are irregular and amalgamated. Bed bases are erosive and bed tops are distinctively defined. Beds are typically thick to very thick.

Interpretation: This facies are deposited by bed-load transport or via strong basal currents in confined channels (Pickering *et al.,* 1989; Mutti, 1977; Hubert, 1966; Lowe, 1982). Grains are deposited through intermittent suspension transport over crests of bedforms. Alternatively, the grains can follow the same depositional process into scours rather than over crests.

3.2.3. FACIES CLASS C: SANDSTONE-MUDSTONE COUPLETS AND MUDDY SANDS, 20–80% SAND GRADE, <80% MUD-GRADE

This facies class is best compared to the scheme of Bouma (1962), where beds generally trend from sandier bases to muddy tops. This class is also divided into organised and unorganised groups with the basis for discrimination being bed thickness and textural homogeneity, respectively (Pickering *et al.*, 1989). Figure 3.10 shows a well correlated trend of increasing number of beds measured to lessening thickness. This is attributed to an increase in overall measurements of thin, muddier beds that resided between sandier units. Figure 3.11 depicts a clear trend of facies moving towards thinner beds for muddier contents.

3.2.3.i. Facies Group C1 – Disorganised muddy sands

3.2.3.i.a. Facies C1 – Mottled muddy sands

Description: This facies is commonly identified by having irregular concentrations of coarse material layered within fine grained sands of very thin- to medium-bed thickness (Pickering *et al.,* 1989). In this study, 0.63% of the total measured thickness is associated to this facies type. In rare occasions, normal or inverse grading is apparent. Bioturbation is regularly associated with this facies and hinders the presence of physical structures.

Bedding is characterised by either sharp or gradational tops and bases, and show poor to moderate sorting. Typical bed thicknesses range from <1 cm to ~20 cm.

Interpretation: Mottled muddy sands are transported by strong bottom currents that cause repetitive, short-lived bedload transport. Coarse grained material is emplaced by grain-by-grain deposition; finer grained material through depositional mixing by burrowers (Stow, 1984; Stow & Piper, 1984).

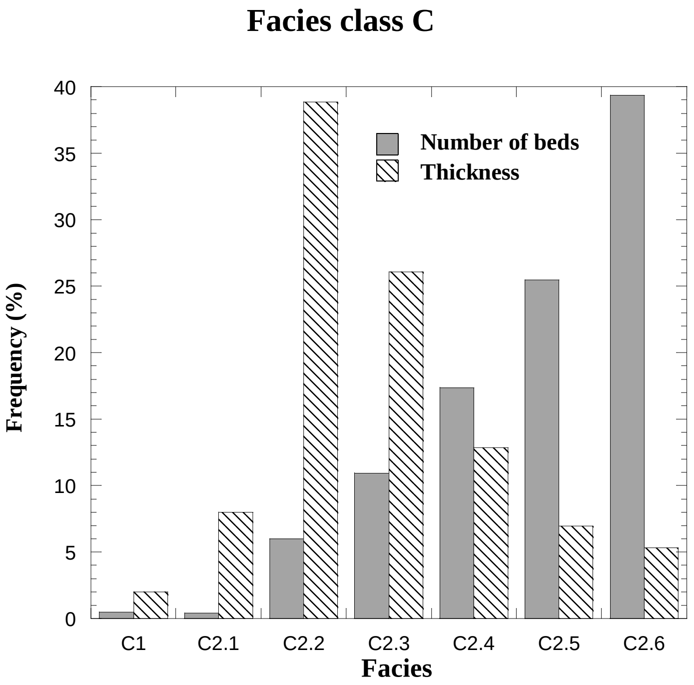

Fig. 3.10. Facies of class C by number of beds and thickness, presented as proportions of all measured sections.

A) Number of beds

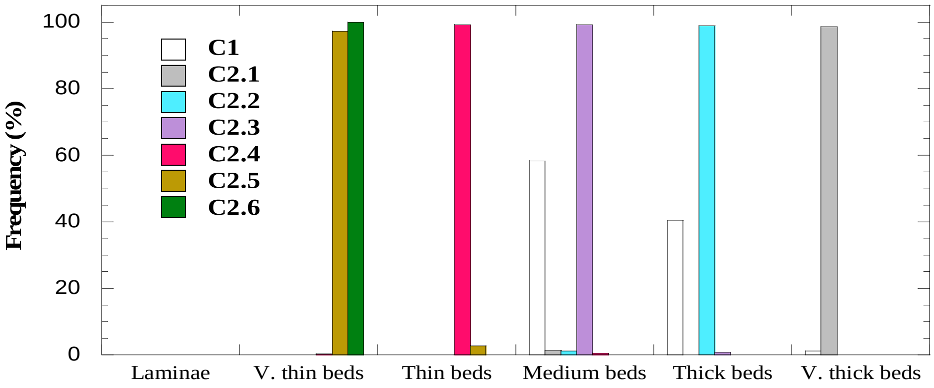

B) Thickness

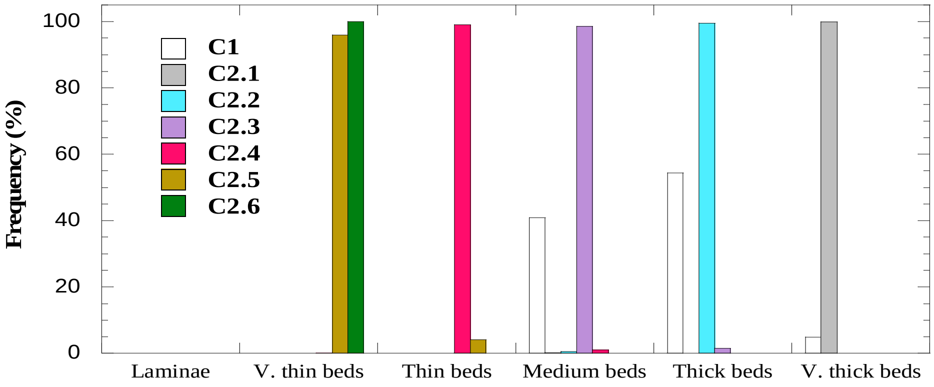

Fig. 3.11. Relative proportions of the number of beds (A) and thickness (B) for each facies according to bed thickness.

3.2.3.ii. Facies Group C2 – Organised sandstone-mudstone couplets

3.2.3.ii.a. Facies C2.1 – Very-thick to thick bedded sandstone-mudstone couplets

Description: This facies is classified by having very-thick to thick bedding (>100 cm) with Bouma (1962) division Ta commonly appearing at the base with occasional gravel. Erosion is associated with this facies type, which constitutes 2.69% of the total thickness of measured outcrop in the study area.

Interpretation: This facies is deposited from flows migrating between concentrated density flows and turbidity currents (Pickering *et al.,* 1989; Lowe, 1982, 1997; Bouma *et al.,* 1997; Hiscott *et al.,* 1997; Shanmugam, 1997, 2000).

3.2.3.ii.b. Facies C2.2 – Thick bedded sandstone-mudstone couplets

Description: This facies is best noted by bed thicknesses of 30 to 100 cm of Bouma (1962) division Ta. This facies amounts to 12.48% of the total thickness of the outcrop measured in this study. Erosion and scour on bedding bases is common.

Interpretation: Deposition of this facies occurs from turbidity currents (Pickering *et al.,* 1989; Lowe, 1982, 1997; Bouma *et al.,* 1997; Hiscott *et al.,* 1997).

3.2.3.ii.c. Facies C2.3 – Medium bedded sandstone-mudstone couplets

Description: Medium bedded sandstone-mudstone couplets are indicative of Bouma (1962) division Tb, and have bed thicknesses in the range of 10 to 30 cm. This facies represents 8.37% of total thickness measured in this study.

Interpretation: Turbidity currents similar in concentration and velocity of those which deposit Facies C2.2 are accountable for this facies deposition (Pickering *et al.,* 1989; Lowe, 1982, 1997; Bouma *et al.,* 1997; Hiscott *et al.,* 1997).

3.2.3.ii.d. Facies C2.4 – Thin bedded sandstone-mudstone couplets

Description: These deposits are noted by Bouma (1962) division Tc and have bed thicknesses of 3 to 10 cm. Bed bases are absent of erosion or scour. In this study, 4.26% of total measured thickness is of this facies type.

Interpretation: These facies are deposited from low-concentration, low-velocity turbidity currents (Hiscott & Pickering, 1984; Pickering & Hiscott, 1985, Pickering *et al.,* 1989; Lowe, 1982, 1997; Bouma *et al.,* 1997; Hiscott *et al.,* 1997).

3.2.3.ii.e. Facies C2.5 – Very-thin bedded sandstone-mudstone couplets

Description: These very-thin bedded sands commonly have 1 to 3 cm thick beds, which are sheet like. Ripples with low amplitudes (<2 cm) and long wavelengths (<10 cm) can occur in this facies. This facies represents 2.36% of total measured outcrop thickness for the study area.

Interpretation: These facies are deposited from low-concentration, low-velocity turbidity currents (Pickering *et al.,* 1989; Lowe, 1982, 1997; Bouma *et al.,* 1997; Hiscott *et al.,* 1997).

3.2.3.ii.f. Facies C2.6 – Laminae sandstone-mudstone couplets

Description: These sands are characterised by bed thicknesses of <1 cm and are generally referred to as laminae. Bedding is sheet-like with planar bases. In the study area, 1.85% of total measured section thickness forms this facies type.

Interpretation: This facies is deposited from very dilute turbidity currents (Pickering *et al.,* 1989).

3.2.4. FACIES CLASS D: SILTS, SILTY MUDS, AND SILT-MUD COUPLETS, >80% MUD, >40% SILT, 0–20% SAND

Sediments of this facies are predominately that of silt- and clay-grade (Pickering *et al.,* 1989). The number of beds to thickness ratio seems to remain constant for the first two facies in this class with a noticeable decrease in thickness of beds for Facies D2.2 (Fig. 3.12). Sediment grade is reflected in bed thickness of very thin to thin beds (Fig. 3.13).

3.2.4.i. Facies Group D1 – Disorganised silts and silty muds

3.2.4.i.a. Facies D1 – Mottled silt and mud

Description: This facies is distinguished as thin beds, laminae, lenses and mottles of silt in mud that rarely shows organisation and is commonly bioturbated. In this study, 1.40% of the total measured thickness is of this facies type. Normal or inverse grading can occur in this facies on scales from laminae to tens of centimetres where sorting is poor to moderate (Pickering *et al.,* 1989). Bed tops and bases can be sharp or gradational with bed shape primarily irregular.

Interpretation: This facies is transported by long-lived bottom currents and deposited through grain-by-grain deposition. Post-depositional bioturbation has removed most original sedimentary structures (Piper & Brisco, 1975; Stow, 1984; Stow & Piper, 1984).

3.2.4.ii. Facies Group D2 – Organised silts and muddy silts

3.2.4.ii.a. Facies D2.1 – Graded stratified silt

Description: Graded stratified silt consists of thin- to medium-bedded silts and silty muds which occur as discrete beds of interlaminated units of mud and silt that can be described by the Bouma (1962) scheme. This facies shows normal grading from silt- to clay-grade (Pickering *et al.*, 1989). Bed soles are scoured and sharp; bed tops are gradational. In this study, 3.11% of the total measured thickness is comprised of this facies.

Interpretation: This facies is transported via turbidity currents and emplaced through grain-by-grain deposition. Lamination is achieved by traction transport after initial deposition (Piper, 1973, 1978; Stow & Piper, 1984; Pickering, 1982, 1984).

3.2.4.ii.b. Facies D2.2 – Thin regular silt and mud laminae

Description: Facies D2.2 occurs as thin to medium beds of mud with horizontal silt laminae. Silt to mud ratios are on the order of 2:1 to 1:2. Laminae are typically grouped where silt becomes finer grained upwards through intervals. Sharp to gradational tops and bases of silt laminae are common. Grain size is on the order of medium to fine silt and clay. This facies amounts to 3.10% of the total measured thickness of outcrop measured in this study.

Interpretation: Transportation of this facies is through turbidity currents or rarely through weak bottom currents. Deposition occurs as slow uniform fallout from suspension (Stow & Bowen, 1980, Piper, 1973, 1978; Pickering, 1982; Stow & Sshanmugam, 1980).

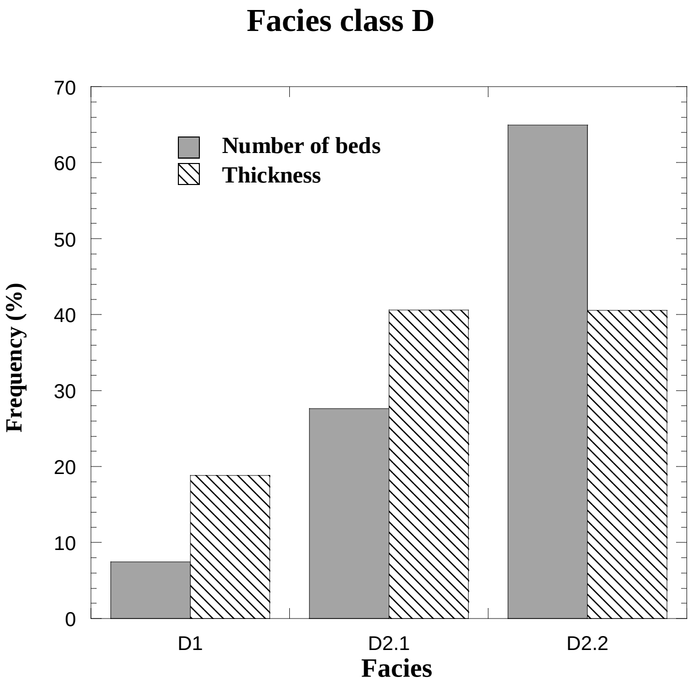

Fig. 3.12. Facies of class D by number of beds and thickness, presented as proportions of all measured sections.

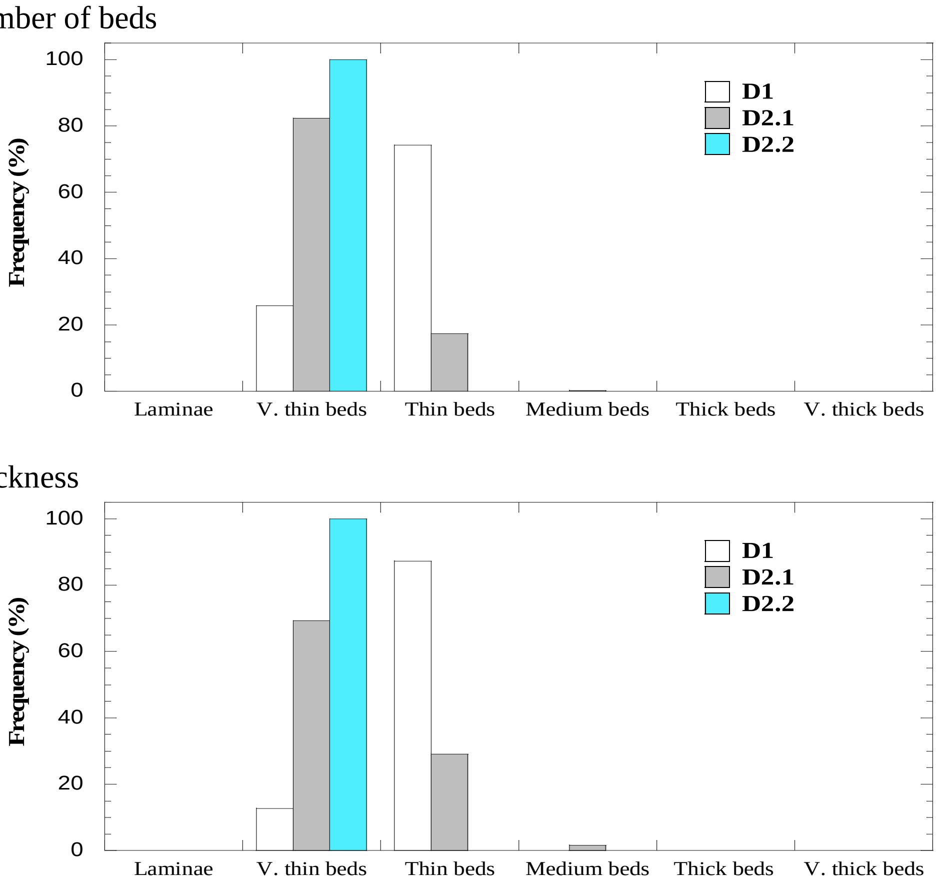

Fig. 3.13. Relative proportions of the number of beds (A) and thickness (B) for each facies according to bed thickness.

3.2.5. FACIES CLASS E: >95% MUD-GRADE, <40% SILT-GRADE, <5% SAND AND COARSER-GRADE, <25% BIOGENICS

This facies class is comprised mainly of silty clays and clays, which can be up to metres thick containing beds of laminae- to very thick-scale (Pickering *et al.*, 1989). Scours on bases do occur in this facies class, although more commonly, layers are parallel. Figure 3.14 shows that the majority of beds measured are classified under Facies E2 where organisation of silty clays and clays prevails. Figure 3.15 goes on to show that although beds can be upwards of tens-of-metres, the majority are of smaller beds thickness.

3.2.5.i. Facies Group E1 – Disorganised muds and clays

3.2.5.i.a. Facies E1.1 – Structureless muds

Description: Facies E1.1 is composed of structureless muds on the order of one to tens-of-metres thick with weakly defined to absent bedding (Pickering *et al.*, 1989). Occasionally, colour banding may locally develop. Muds are clay, or mixed silt- and clay-grade with uniform composition. This facies comprises 1.39% of the total measured thickness in the study area.

Interpretation: A likely transport method is a thick, muddy turbidity current with rapid deposition occurring (Piper, 1978; Stow, 1984; Pickering & Hiscott, 1985).

3.2.5.i.b. Facies E1.2 – Mottled muds

Description: This facies is recognised as thin to thick intervals of uniform mud that show poor bedding (Pickering *et al.*, 1989). Intermittent primary structures of wavy, indistinct or fine parallel layering may exist. Silty intervals can occur in this facies; however, the dominant material is clay-grade. The amount of total measured thickness in this study attributed to this facies is 2.80%.

Interpretation: This facies is transported as suspended load in bottom currents and deposited through particle settling. Post-depositional activity includes extensive bioturbation (Stow, 1984; Gonthier *et al.*, 1984).

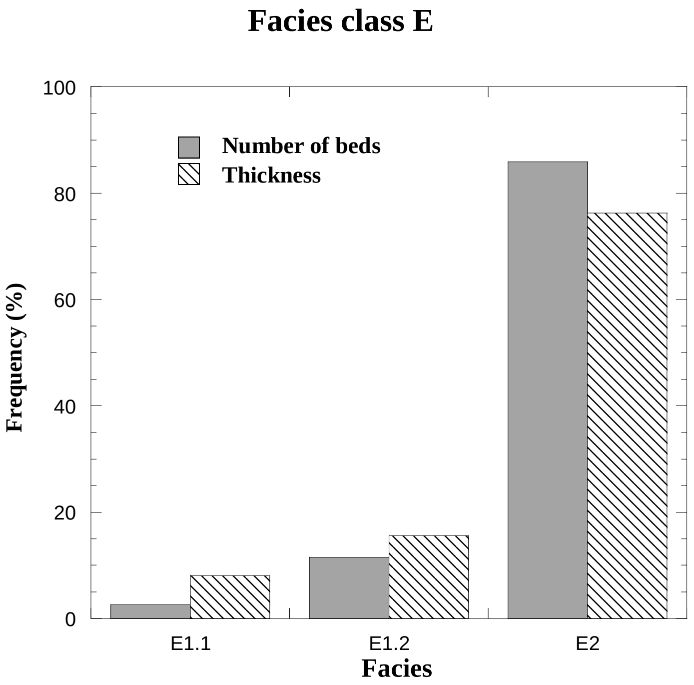

Fig. 3.14. Facies of class E by number of beds and thickness, presented as proportions of all measured sections.

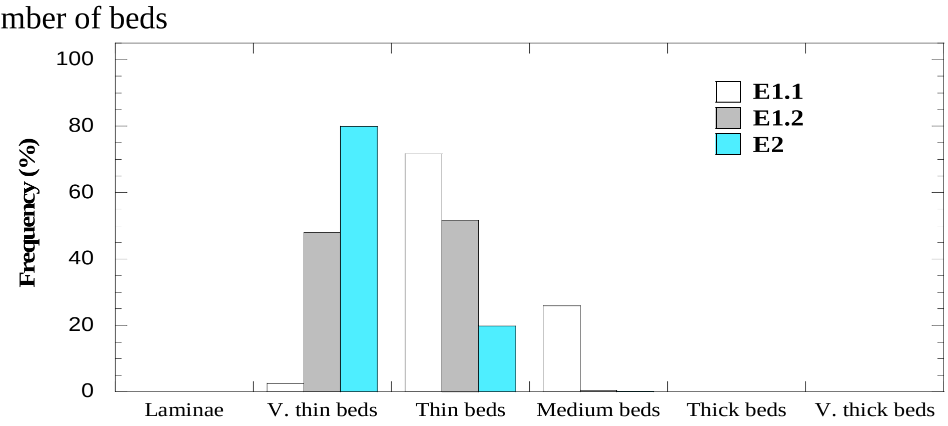

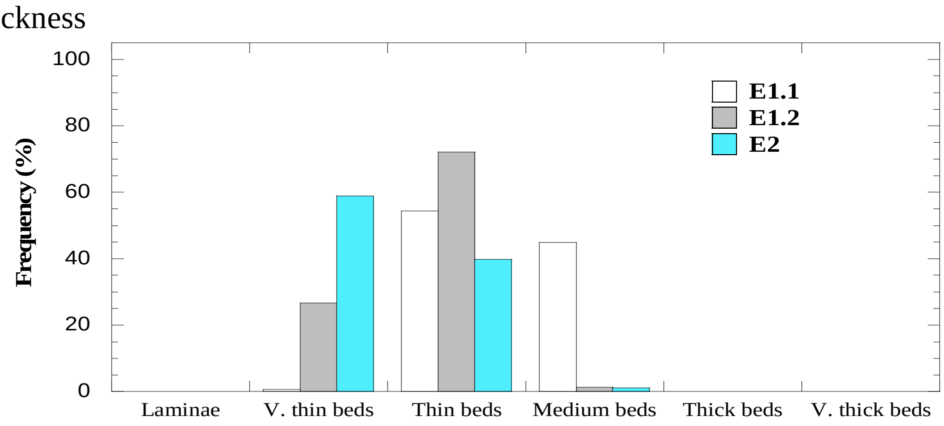

Fig. 3.15. Relative proportions of the number of beds (A) and thickness (B) for each facies according to bed thickness.

3.2.5.ii. Facies Group E2 – Organised muds

3.2.5.ii.a. Facies E2 – Laminated muds and clays

Description: Facies E2 shows some internal organisation (parallel lamination) of mud and clays (Pickering *et al.,* 1989). Clay-grade and fine silt-grade sediments constitute the majority of this facies. Bed thicknesses range between 1 to 10 cm, but total sections can be tens-of-metres thick. Bioturbation is generally absent. This facies accounts for 13.14% of the total measured thickness of the outcrop measured in this study.
Interpretation: This facies arises from production of organic material in the water column or via transport of hemipelagic material through oceanic currents. The mechanism for deposition is grain-by-grain settling (Piper, 1978; Stow, 1984).

3.2.6. Facies Class F: chaotic deposits

Chaotic deposits constitute a mixture of sediments with no apparent order commonly sourced from large-scale downslope mass movements (Pickering *et al.,* 1989). A variety of clasts are found within this facies class from single isolated clasts to olistoliths. The majority of facies measured in facies class F belong to the sandier slumps and slides of Facies F2 (Fig. 3.16). The thickness of these facies tends to be very thick, as noted by figure 3.17, and no beds exist for medium bed thickness.

3.2.6.i. Facies Group F1 – Contorted mudstones

3.2.6.i.a. Facies F1 – Muddy slumps and slides

Description: This facies includes folded and contorted layers of irregular shape with thicknesses of centimetres to tens-of-metres (Pickering *et al.*, 1989). In this study, 2.05% of the total measured thickness of outcrop is of this facies type. Variation is high for internal structure and grain size, with dominant grain size waning towards mud-grade. Commonly, lateral continuity is preserved in coarser-grained beds. Tops and bases of beds range from smooth-planar to highly irregular. Internal surfaces may be visibly present, which are representative of glide or shear surfaces.
Interpretation: Slide and slumps transport these sediments which come to rest as frictional forces overtake gravitational forces (Ricci Lucchi, 1975; Pickering, 1982, 1984).

3.2.6.ii. Facies Group F2 – Contorted sandstones

3.2.6.ii.a. Facies F2 – Sandy slumps and slides

Description: Facies F2 is similar to Facies F1 with the distinction that grain size is increased. Internal structure varies widely in this facies that is composed of intraformational marly and heterolithic sediments. Layers are irregular in shape and can be up to tens-of-metres in thickness. Bed tops and bases vary from planar to irregular. This facies amounts to 9.64% of the total measured thickness of the outcrop measured in this study.

Interpretation: Slide and slumps transport these sediments, which come to rest as frictional forces overtake gravitational forces (Ricci Lucchi, 1975; Pickering, 1982, 1984).

3.2.7. FACIES CLASS G: BIOGENIC MUDS (25–50% BIOGENICS)

Biogenic input (calcareous and siliceous) and terrigenous sources form the key components to this facies class (Pickering *et al.*, 1989). They typically form thin to very-thin beds as indicated in Figure 3.18, as they are deposited slowly over a period of time and undergo moderate bioturbation. They are often homogeneous, but can show grading to lamination. They have a turbiditic origins (hemiturbidites) and form by tractional and fallout processes (mud and lime-mud fallout of hydraulically sorted carbonate particles) of low concentration turbidity currents (Pickering *et al.*, 1989).

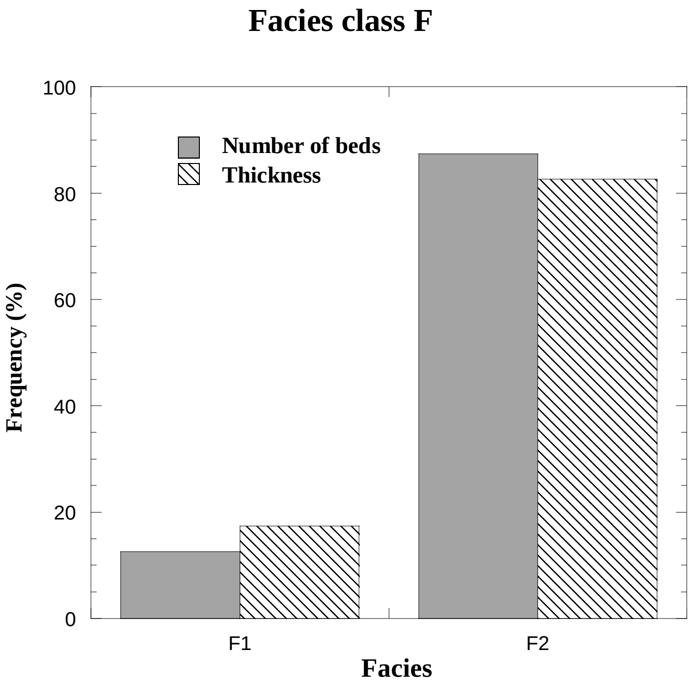

Fig. 3.16. Facies of class F by number of beds and thickness, presented as proportions of all measured sections.

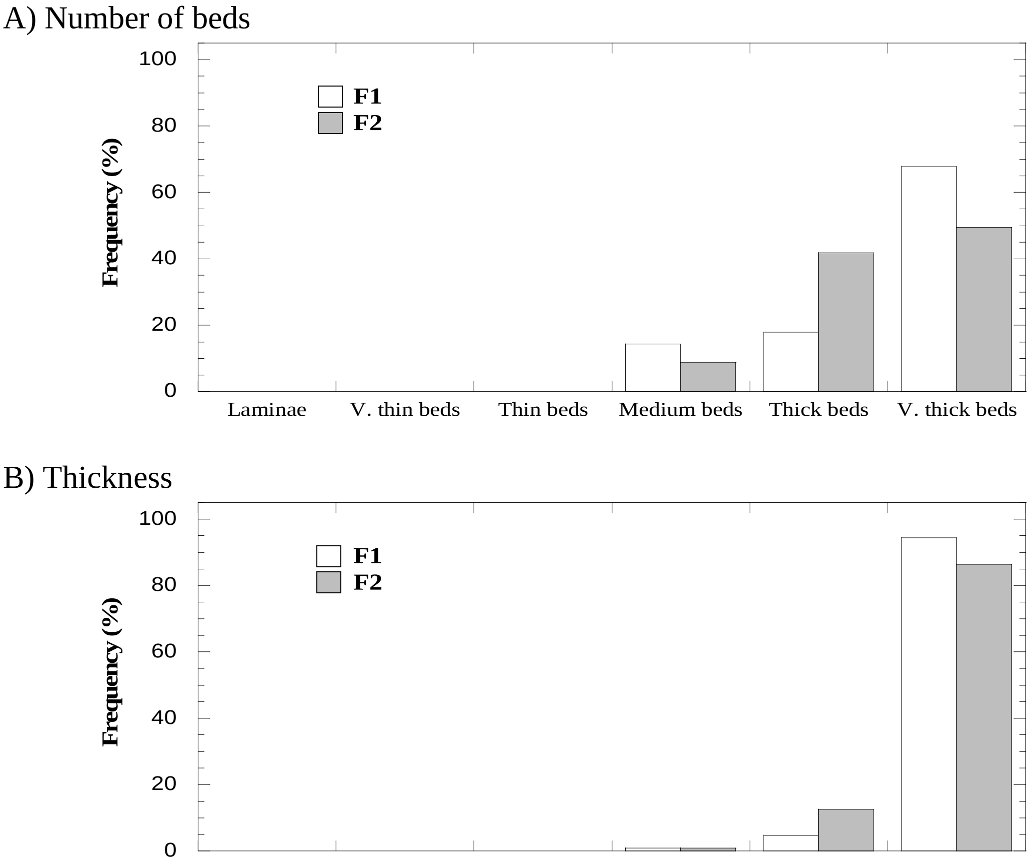

Fig. 3.17. Relative proportions of the number of beds (A) and thickness (B) for each facies according to bed thickness.

A) Number of Beds

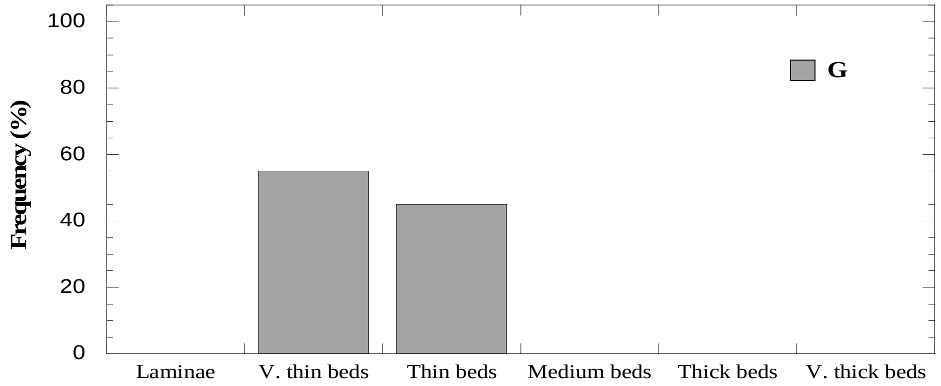

B) Thickness

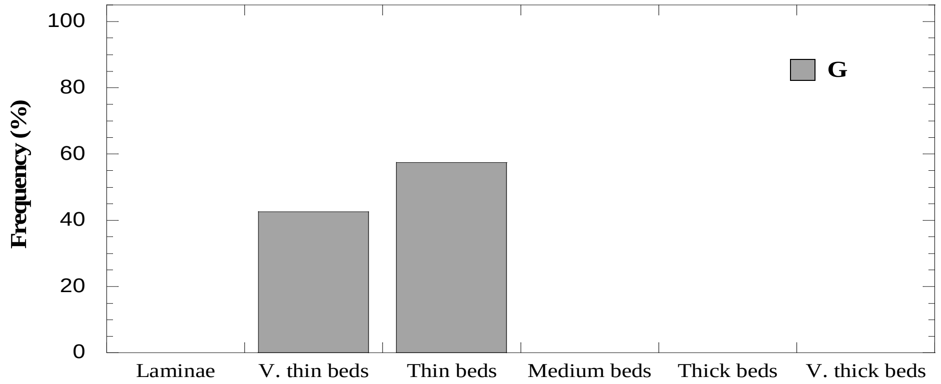

Fig. 3.18. Relative proportions of the number of beds (A) and thickness (B) for each facies according to bed thickness.

3.2.7.i. Facies Group G1 – Biogenic mud

3.2.7.i.a. Facies G1 – Biogenic mud

Description: This facies is noted as 25 to 50% biogenic content mixed with silt, clay and sand (Pickering *et al.*, 1989). Typically, there is no evidence of grading and sediments are poorly sorted. Bedding, if present, is poorly defined and not easily identifiable. Structures are absent. In the study area, 0.81% of total measured section thickness is of this facies type.

Interpretation: Mode of transport is through very low concentrated turbidity currents and bottom water currents. Deposition is on a grain-by-grain basis or through aggregate settling in the water column (Pickering, 1982; Stanley & Maldonado, 1981; Wang & Hesse, 1996).

3.2.8. FACIES CLASS H

This facies class is located in upper-slope environments and represents distal delta facies (Fig. 3.19).

A) Number of beds

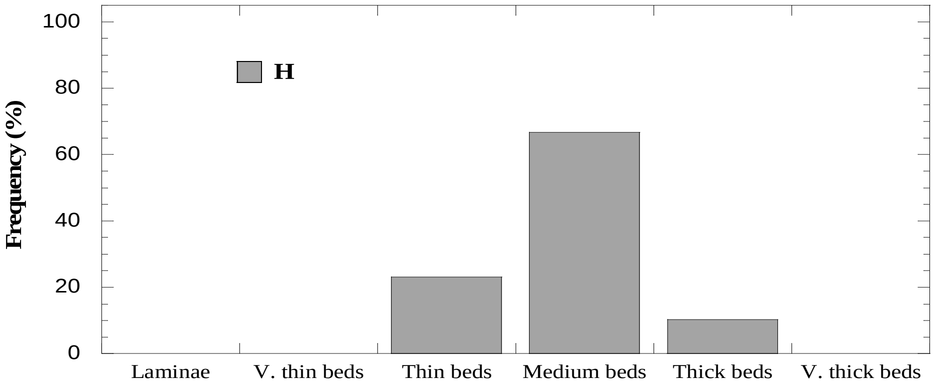

B) Thickness

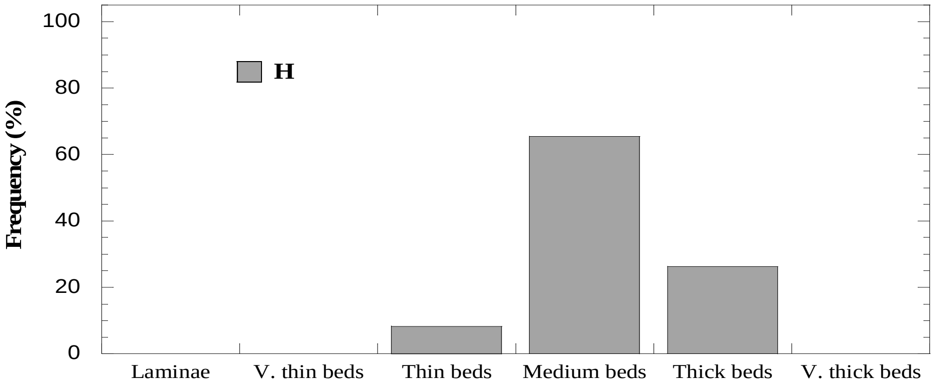

Fig. 3.19. Relative proportions of the number of beds (A) and thickness (B) for each facies according to bed thickness.

3.2.8.i. Facies Group H1 – Nummulitic sand

3.2.8.i.a. Facies H1 – Gully/slope nummulitic sand

Description: Facies H1 is identified as having abundant, well developed nummulities nested in sandstones. Grain size of the sandstone ranges from very-fine to fine grained. Silt content is high and sorting is poor in this facies. Beds may achieve 2 m in thickness with sharp to gradational bases and more gradational tops. A small amount, 0.14%, of the total measured thickness of outcrop in this study is of this facies type.

Interpretation: This facies is deposited as suspension fallout from low concentration turbidity currents.

3.3. MASS TRANSPORT COMPLEX CLASSIFICATIONS

The Ainsa basin contains an abundance of chaotic deposits, referred to by Pickering and Corregidor (2005) as mass transport complexes (MTCs). Commonly, they contain deformed rafts of disrupted bedding, cobble-pebble conglomerates, pebbly mudstones, mud-flake breccias, and pebbly sandstones. These deposits represent a range of flow processes, including sediment slides, slumps, turbidity currents, concentrated density flows and debris flows (Pickering and Corregidor, 2005). Furthermore, the Ainsa basin contains a number of deposits with attributes that are ambiguous, and can be interpreted as representing various flow properties. Such deposits can be considered hybrids of sediment gravity flows, showing properties of both turbidity currents and debris flows. (e.g., slurry flows of Lowe *et al*., 2003). They can also be derived from flow transformations and multiphase flows (e.g., Sohn *et al.,* 2002).

An adaptation to the classification of Pickering and Corregidor (2005) is made for this study where the term mass transport deposit (MTD) is used rather than mass transport complex (MTC). This substitution is made as “complex” implies that multiple depositional events have occurred; “deposit” refers to only a single process/failure event. It therefore follows that MTC will be used, in a hierarchical manner, such that two or more MTDs comprise a MTC (see section 3.5), whereas a MTD consists of a single facies type.

In the study area, MTCs are commonly identified at the base of sequences (Fig. 3.20), marking the earliest events of depositional cycles, which may have influenced subsequent deposition (Pickering and Corregidor, 2005). Three possibilities associated with the creation of topography from MTDs can be described: (1) upper- and mid-slope failure that occurs to initiate a MTD creates large excavations that act as conduits for channels or channel complexes to flow within the confines of the eroded space (e.g., Hackbarth & Shew 1994); (2) in previously created conduits on slope or base-of-slope settings, MTDs may create localised ridges or obstacles of various shapes that act to confine/deflect turbidites in a ponded setting; (3) in deposition, the upper part of MTDs may form an irregular top surface creating localised depressions that subsequent turbidity currents can deposit sediments into. These three examples for the generation of topography suggest MTDs have a significant impact on the geometry and distribution of sandbodies at various scales in slope and base-of-slope environments.

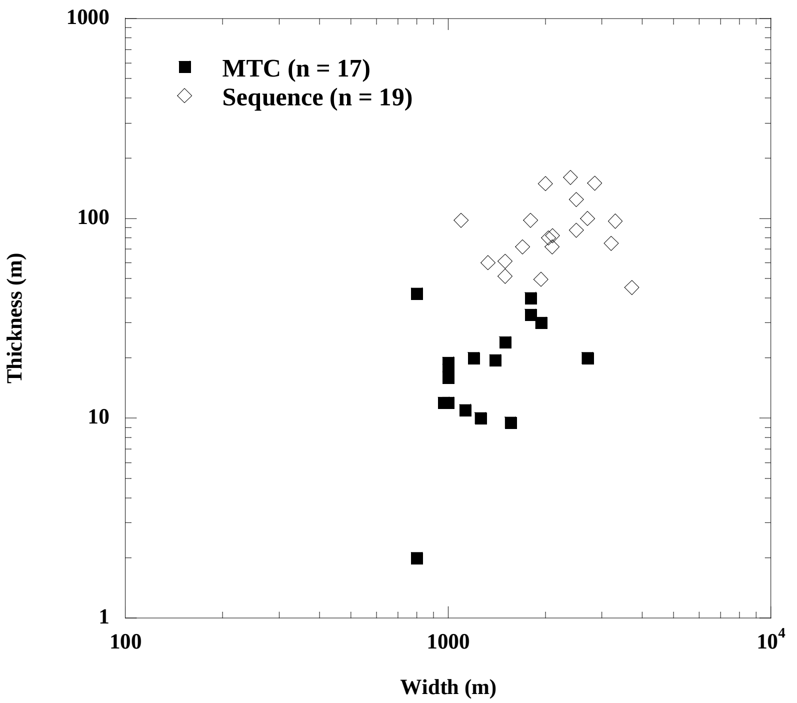

Fig. 3.20. Comparison of dimensions: MTCs versus sequences. MTC mainly define the base of sequences and generally occupy the entire width of each sequence, as identified in the graph.

Mass transport deposits may be sourced intra-basinally or from extra-basinal locations (Fig. 3.21). The composition of the mass failure and other environmental parameters (i.e. slope gradients) combine to develop the flow competency of MTDs. It may be possible to determine the source distance of various MTDs based on flow processes; however, a simplified technique is examined herein where the composition of a MTD is compared to possible source areas to suggest an origin. Refer to type Ic below (Section 3.3.1.iii) for an example of an easily identified relationship between composition and source area.

Three types of MTDs are defined in this study (types I–III), with further categorisation of type I into muddy slides/slumps (type Ia)**Error! Bookmark not defined.**, sandy slides/slumps (type Ib), and carbonate mass flows (type Ic); type II into pebbly mudstones (muddy debrites; type IIb), pebbly and sandy mudstones (sandy debrites; type IIa) and clast-supported mudstones (pebble-rich debrites; type IIc); and type III as pebbly sandstones. These designations cover a broad range of categories and include various facies described above.

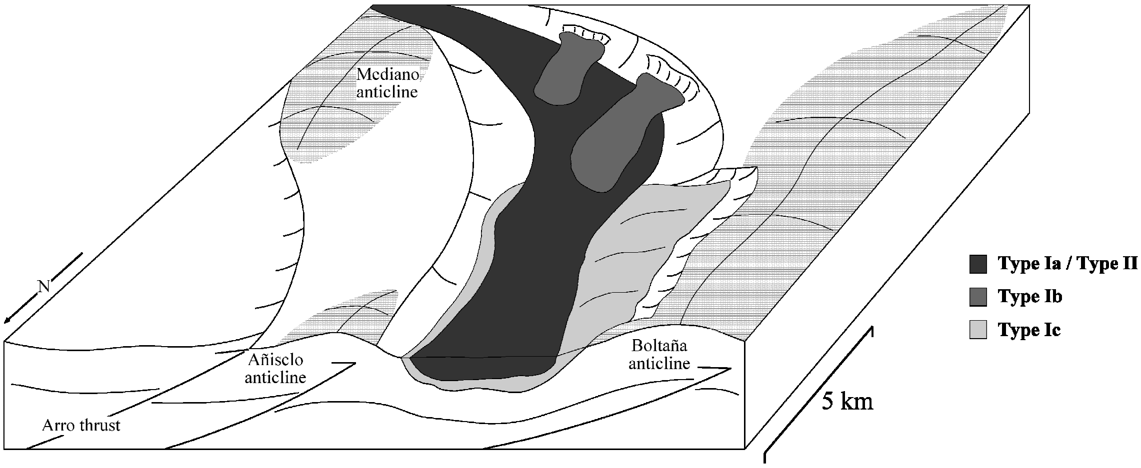

Fig. 3.21. Type classifications for MTDs. Type Ia are sourced from up-dip locations of the mid- and upper-slope; type Ib are caused by localised slope instability; type Ic consist entirely of carbonates, originating in elevated areas; and type II are extra-basinally sourced.

3.3.1. Type I MTDs

3.3.1.i. Type Ia

Muddy slides and slumps mainly consist of folded and contorted layers of irregular shape, with thicknesses of centimetres to metres in the study area (facies F1). Top and base surfaces vary from smooth-planar to highly irregular, and internal surfaces may be visibly present that are representative of glide or shear surfaces. These deposits are typically found in mid- to upper-basin slope environments and have a high composition of muds/marls (see figures 3.22 and 3.23).

It is interpreted that these MTDs are very cohesive and formed irregular sea floor topography that created accommodation for subsequent turbidites to infill.

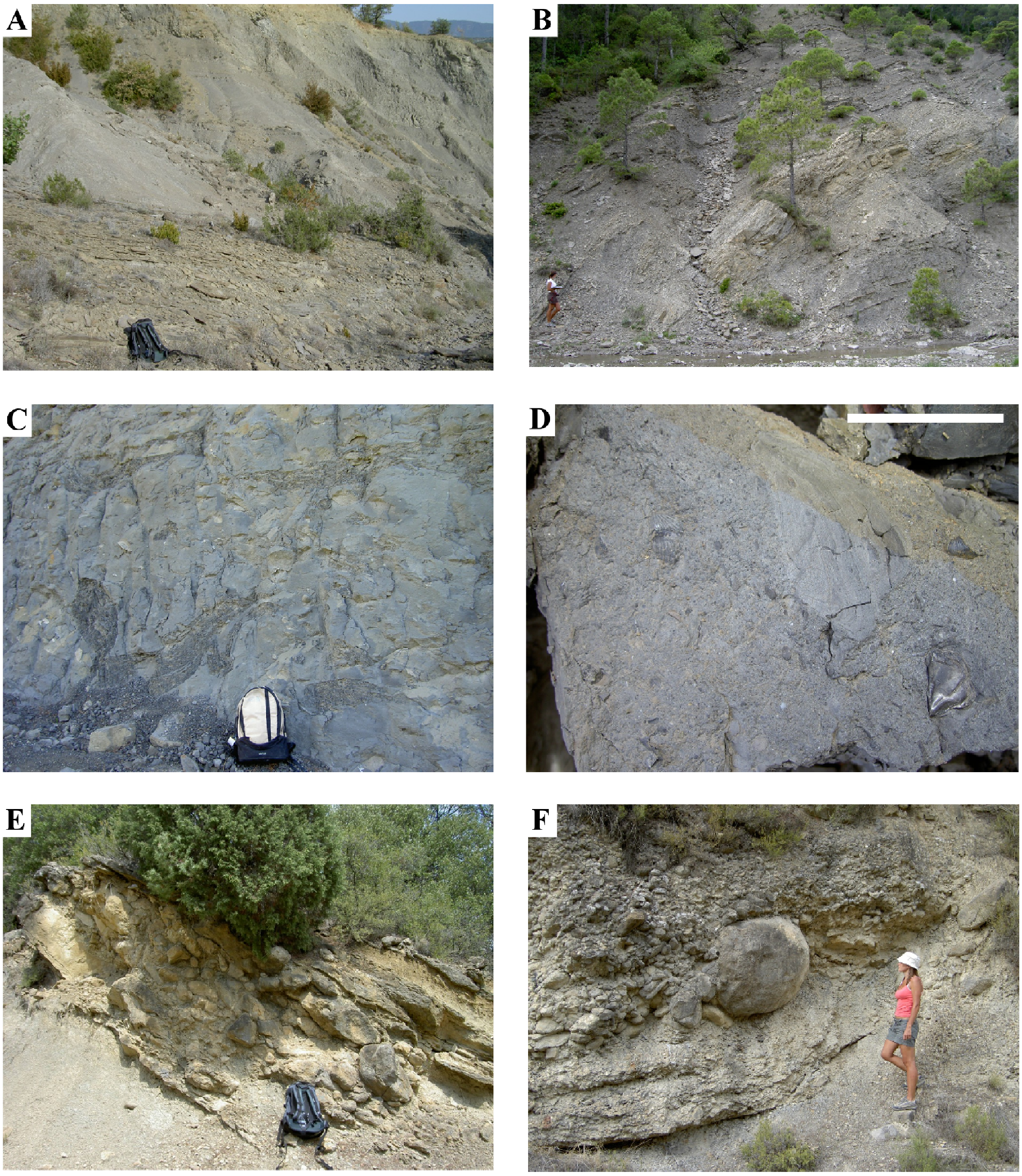

Fig. 3.22. Representative MTDs from each depositional system comprising tectono-sequence I. (A) Muddy slump deposit (facies F1; type Ia MTD) located stratigraphically above the Fosado channel complex, locality 1. (B) Muddy slump deposit (facies F1; type Ia MTD), Los Molinos system, locality 2. (C) Muddy slump deposit (facies F1; type Ia MTD) containing deformed mud rafts, Arro system, locality 5. (D) Mollusc fragments incorporated into the muddy, nummulitic matrix of a slump, Arro system, locality 5. Scale bar is 10 cm long. (E) Scour infilled by sand clasts and boulders (facies A1.1; type II MTD), Charo canyon (Gerbe system), locality 9. (F) Gravel barform (facies A1.1; type II MTD), Gerbe system, locality 10.

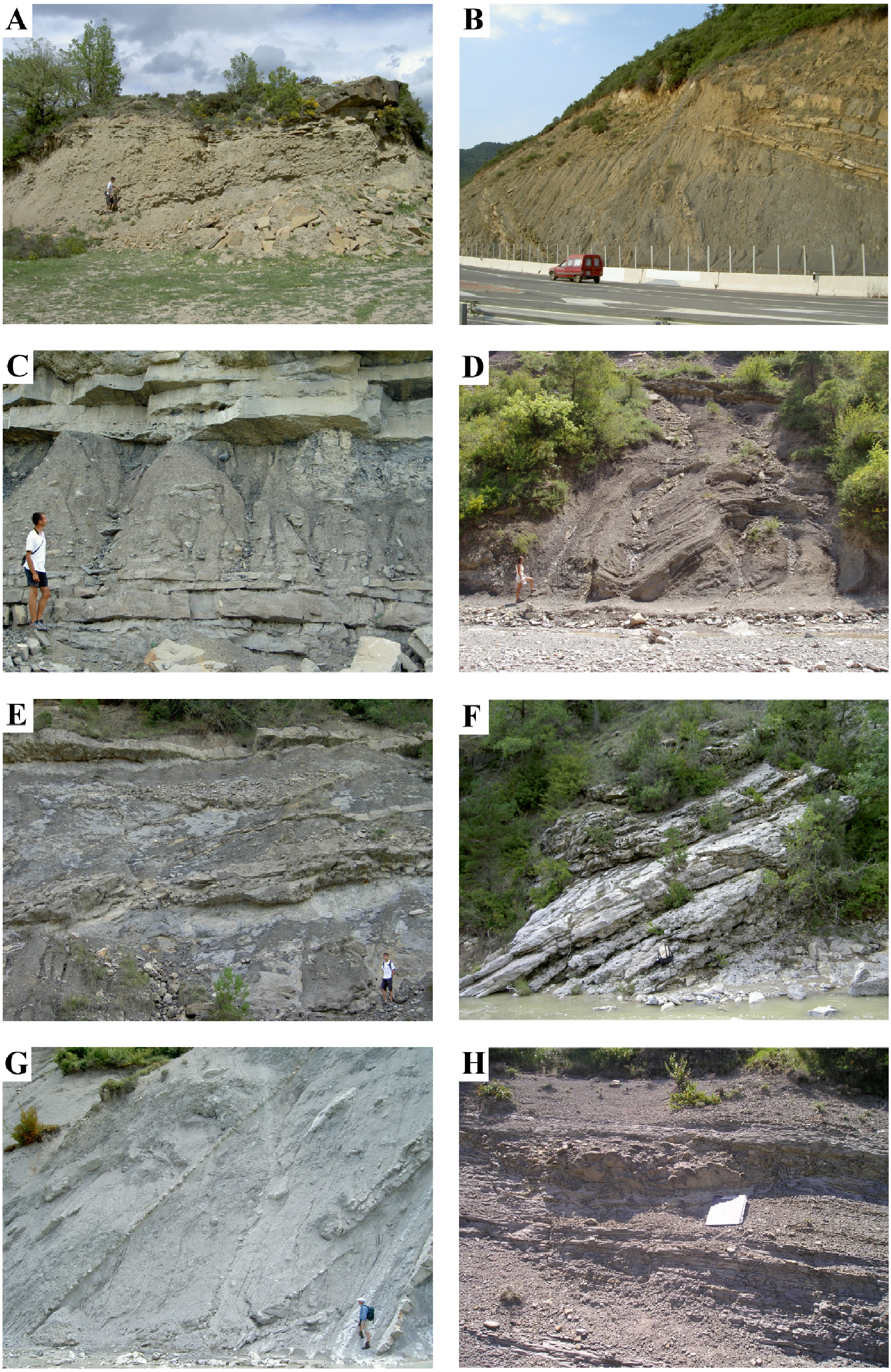
A
B
C
D
E
F
G
H

Fig. 3.23. Representative MTDs from each depositional system comprising tectono-sequence II. (A) Stratified gravelly mudstone (facies A2.1; type II MTD), Banastón V, locality 15. (B) Pebbly, sandy mudstone (facies A1.2; type II MTD), Banastón V, locality 31. (C) Pebbly mudstone (facies A1.3; type II MTD), Ainsa I, Quarry section. (D) Muddy slump deposit (facies F1; type Ia MTD), Ainsa II, locality 36. (E) Amalgamated type II MTDs, forming a MTC, base of Morillo I, locality 42. (F) Carbonate mass flow deposit (type Ic MTC), Morillo II, locality 42. (G) Sandy slump deposit (facies F2, type Ia MTD), base of Guaso I, Rio Ena. (H) Pebbly mudstone (facies A1.2; type II MTD), base of Guaso I, Sarreta Brello ridge.

3.3.1.ii. Type Ib

Sandy slides and slumps occur between thick sandbodies and generate irregular surfaces upon which successive sandy units accumulate. They are commonly found in mid-to upper-basin slope environments, range in thickness from metres to tens-of-metres and comprise intraformational fine-grained marls and heterolithic sediments or extrabasinal collapsed carbonate platform deposits (see facies F2). Specific to the study area, sandy slides and slumps created significant topography on the seafloor through vertical to semi-vertical stacking, causing turbidity currents to deviate around the seafloor highs, which resulted in onlap of turbidites against the depositional highs (see figures 3.22 and 3.23).

These MTDs are interpreted as sediment slides or slumps sourced from intra-channel mass wasting processes in mid- and upper-slope settings situated above the active lateral ramp zone of the SCPU. The source for these types of MTDs is within the depositional environments of the Ainsa basin and can be attributed to localised slope instability, which preferentially deposits these sandy slides and slumps in channel off-axis and margin environments.

3.3.1.iii. Type Ic

Carbonate mass flow events are relatively infrequent within the basin, but the deposits represent a considerable proportion of the total thickness of the basin stratigraphy. These MTDs are predominantly composed of carbonate sediments and clasts interpreted to have derived from carbonate platforms. An example of this type of MTD in the study area is found in the Morillo system in Rio Sieste (Fig. 3.23) that has many petrographic and textural similarities with the Roncal megabed documented in the Jaca basin (Labaume *et al.*, 1983, 1985, 1987). The Roncal megabed contains a lower carbonate megabreccia, an intermediate mud-dominated chaotic interval, and an upper carbonate megaturbidite comprising 200 m of thickness (Labaume *et al.*, 1987).

Type Ic MTDs are derived from the collapse of carbonate mounds or platforms located within the basin. For the example given above, the MTD can be interpreted as being sourced from the mass failure of the Boltaña anticline area during a period of tectonic activity and slope instability (see Chapter 6).

3.3.2. TYPE II MTDS

3.3.2.i. Type IIa

Pebbly and sandy mudstones (sandy debrites, facies A1.2) are matrix supported muddy gravels with bed thicknesses of a few metres to tens-of-metres. They have mud-grade contents of 10–50%, and often show cumulative basal erosion of up to tens-of-metres. The gravels incorporated into this type of MTD originate from igneous, sedimentary, metamorphic, lithified biogenic material, or unlithified sediment sources. Many of the well-rounded pebbles are covered in *Gastrochaenolites* borings produced by molluscs (such as *Lithophaga*) showing that they resided for at least some time in the littoral zone. Irregular tops are common to these deposits, which create topography for thin heterolithic sediments to infill (Fig. 3.22 and 3.23). This type of MTD typically forms the upper division of a bipartite deposit with a type IIc MTD forming the lower division (Fig. 3.24). The base of the lower division is characterised by flutes and grooves followed by a clast-supported mudstone layer showing rare pebble imbrication (type IIc MTD). The upper division is characterised by a matrix-supported pebbly mudstones, often comprising intraformational thin-bedded rafts of heterolithic sediment (a type IIa or type IIb MTD).

These deposits result from mass failure of upper-slope and outer shelf to littoral zone sediments, which get redeposited in deeper water. Multi-granular flow, as described by Parsons et al. (2001) and Sohn et al. (2002), is suggested as a transport mechanism for most of type II MTDs due to their composite nature, where sediments may have undergone a transitional state of flow between debris flow, concentrated density flow and turbidity currents. In this model, debris flows are interpreted to have travelled on and behind a water-rich, gravelly sand bed prior to deposition, forming a multiphase flow (Fig. 3.24).

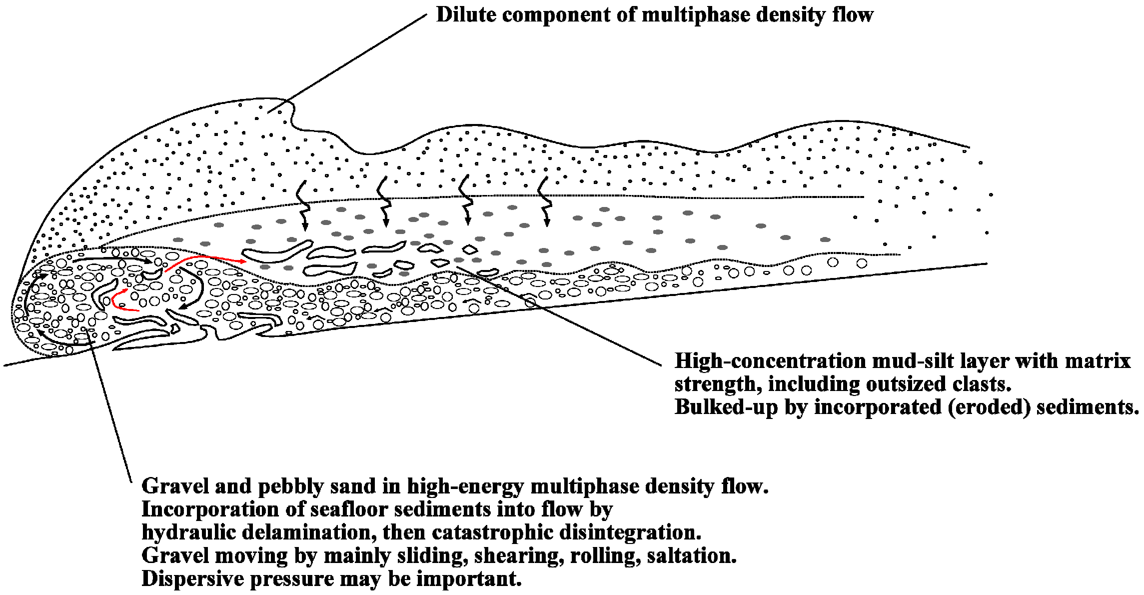

Dilute component of multiphase density flow

High-concentration mud-silt layer with matrix strength, including outsized clasts.
Bulked-up by incorporated (eroded) sediments.

Gravel and pebbly sand in high-energy multiphase density flow.
Incorporation of seafloor sediments into flow by
hydraulic delamination, then catastrophic disintegration.
Gravel moving by mainly sliding, shearing, rolling, saltation.
Dispersive pressure may be important.

Fig. 3.24. Depositional flow processes for multiphase flows..

3.3.2.ii. Type IIb

Pebbly mudstones (muddy debrites) are matrix supported, structureless deposits consisting of 50–95% mud-grade content (facies A1.3). Thicknesses of these deposits range from decimetres to tens-of-metres with distinct changes of internal organisation (Fig. 3.22 and 3.23). The processes associated with this type are similar to that of type IIa indicating that the only noticeable difference is the mud content and the lack of intraformational heterolithic sediment.

3.3.2.iii. Type IIc

Clast-supported mudstones (pebble-rich debrites) are typically decimetres to a few metres thick, and form the lower division of a bipartite deposit (facies A1.1). These MTDs are composed of extra-formational material such as well-rounded pebbles, shallow-marine shells and reworked *Nummulites* (Fig. 3.22 and 3.23). Pebbles may consist of limestone, chert, sandstone or igneous rock. There is a range of internal complexity to this type of MTD where the lower part may have erosional bases overlain by clast-supported pebble-grade conglomerates showing inverse grading, whereas the upper parts are more chaotic and poorly developed, often showing no grading.

Type IIc MTDs are interpreted as the likely products of flow transformations or the lower divisions of mutiphase density flows created by abrupt momentum changes, from strongly erosive, high-energy turbidity currents carrying well-rounded pebbles as a basal concentrated layer or traction carpet.

3.3.3. TYPE III MTDS

Pebbly sandstone MTDs (Facies A1.4, A2.1, A2.2, A2.3, A2.4 and A2.5) are the thinnest type of MTDs defined, having thicknesses from decimetres to metres. This type generally comprises the highest proportion of sand-grade sediments of all types defined, and contains well-rounded pebbles from extra-formational locations with angular to rounded, intra-formational silt-mud clasts (Pickering and Corregidor, 2005). The bases of these types typically define the erosive bases of channels and other erosional architectural elements.

These deposits are thought to be the products from concentrated density flows that underwent late-stage flow transformations. During high-energetic times, these flows were strongly erosive, carrying pebbles and entraining intra-formational, fine-grained silty and muddy sands. As this process continued, the MTD became over-laden with respect to gravelly sediments and rapidly deposited the load over a relatively short distance.

3.4. FACIES ASSOCIATIONS

Sediment gravity flow deposits define the second order hierarchical division in the Ainsa basin (see section 3.5) and facies types define the fundamental units of a depositional body in architectural element analysis. Facies associations for the Ainsa basin, and therefore, deep-marine sandy systems, are representative of the temporal and spatial arrangement of facies (see above section 3.2) in the sedimentary record. Several facies associations are defined, which encompass the variety of deposits found in the basin due to the range of depositional processes through time. The associations presented below integrate the modified facies scheme of Pickering *et al.* (1989) and the mass transport complex classification of Pickering and Corregidor (2005).

3.4.1. FACIES ASSOCIATION 1 (FA1)

FA1 is characterised by discontinuous, lens-shaped gravels, pebbly sandstones and MTDs (facies A1.1, A1.2, A1.3, A2.1, A2.2, A2.3, F1 and F2). These deposits can be stacked together to form thick MTCs, which typically reside at the base of sequences and form topography upon which sandbodies accumulate. Alternatively, they may represent periods of bypass during channel development where erosive flows leave lag deposits. In either case, these deposits have irregular tops and are commonly erosive, with cumulative erosion of tens-of-metres. Internally, thin-bedded sandstones and mudstones are folded, attenuated and partially disaggregated with an abundance of incorporated *Nummulites*. Thin- to thick-bedded, laterally discontinuous sandstone packages are commonly dispersed between the gravelly sediment.

FA1 occurs in a variety of deep-marine environments; however, they are most commonly associated with canyon-fills and the base of channelised slope sequences. They originate from the collapse of upper- to lower-slope settings during the excavation of slope sediments and mark the onset of significant sediment supply to the basin. Transport mechanisms include concentrated density flows, hyper-concentrated density flows, MTD processes (slides, slumps, debris flow processes) and multiphase flows. The base of these deposits commonly represents sequence boundaries in the stratigraphic record (see section 3.5 below). At outcrop, these deposits often form prominent, mappable ridges, and in plan view they could extend for kilometres.

3.4.2. FACIES ASSOCIATION 2 (FA2)

FA2 comprises thick-bedded, very coarse-grained, amalgamated sandstones (facies A1.1, A1.4, A2.1, A2.2, A2.4 and A2.5). These deposits are typically lens-shaped and laterally discontinuous. They are frequently erosive, creating irregular bases and convex-upward geometry. Groove casts and load structures are common. These deposits may contain conglomerates, which are typically well-stratified or graded, and rarely ungraded and disorganised. Internally, erosional surfaces commonly form inclined imbricated clast horizons. Downslope, this facies association becomes more laterally extensive and forms channel-mouth and/or proximal lobe deposits that comprise relatively unconfined, thick- to thin-bedded sandstones.

This facies association is interpreted to represent the filling phase of channel fill elements, with the deposition turbidity currents and concentrated density flows. This association of facies is typically found stratigraphically above and temporally adjacent to FA1. Basal contacts could represent sequence boundaries were FA1 is absent. At outcrop, these deposits are laterally more extensive in both cross-section and dip-section when compared to FA1. When mapped in plan view, the outer boundary of these deposits should encompass FA1.

3.4.3. FACIES ASSOCIATION 3 (FA3)

FA3 is characterised by medium-bedded, fine- to medium-grained, cross or planar laminated sandstones that are laterally discontinuous (Facies B1.2, C1, C2.2, C2.3 and C2.4). Individual beds have well developed sharp tops and bases, and are typically associated with small amounts of erosion on the order of tens of centimetres. Sandstone-mudstone couplets showing partial to full Bouma sequences are typical of these deposits commonly occur in rippled sands within marginal environments. Internally, stratification is well developed and planar to cross stratification common. Planar laminated intervals may contain laminae with high carbonaceous content.

FA3 is transported by turbidity currents and represents the back-filling phase of channel formation. During this time, flows commonly splay from primary conduits into marginal areas as the channels become overfilled. FA3 is located stratigraphically above both FA1 and FA2, but may be temporally adjacent to either. Unit thicknesses of FA3 are less than those of FA1 and FA2; however the areal extent of FA3 is much larger. Surfaces bounding this facies association can represent bed- to sequence-scale surfaces.

3.4.4. FACIES ASSOCIATION 4 (FA4)

FA4 comprises thin-bedded, ripple-laminated sandstones, with laminated siltstones and mudstones (Facies B1.2, C1, C2.4, C2.5, C2.6, D1, D2.1, D2.2, E1.1, E1.2, G). Deposits typically have sharp bases and gradational tops, and show normal grading with little to no associated erosion. Commonly, they are bipartite or tripartite with basal cross-laminated sandstone that grade into parallel laminated siltstones and structureless or parallel laminated mudstones. For bipartite beds, the basal sandstone is not present.

These deposits represent channel abandonment facies and overbank sediment deposited during the waning flow stages, or after avulsion has occurred. They are transported by low-concentration, low-velocity turbidity currents, and are located stratigraphically above all previously discussed facies associations (ideally). This facies association marks the tops of classically defined channel fills as the tail end of Bouma sequences (1962). These deposits may amalgamate to show large unit thicknesses in outcrop when compared to other associations.

3.4.5. FACIES ASSOCIATION 5 (FA5)

FA5 is characterised by bioturbated muds and laminated siltstones with subordinate thin-bedded, fine-grained sandstone lenses (Facies C1, C2.5, C2.6, D1, D2.1, D2.2, E1.2, E2, F2 and G). These deposits represent the intersystem or intersequence deposits and are volumetrically significant within the Ainsa basin. The ratio of siltstone to mudstone is such that most mudstone intervals are thicker than the underlying siltstones. Typically, these deposits comprise laminated siltstones overlain by graded mudstones, and occasionally, a very thin hemipelagic cap. Bioturbation is intense in these deposits, which may form fully homogenised units. Where original fabric persists, common deposits are composed of graded-stratified siltstones, graded mudstones, and biogenic mudstones (hemipelagites / hemiturbidites). Pervasive microfaulting also occurs in this facies association.

FA5 deposits can accumulate packages up to several tens-of-metres thick between sandy units. At outcrop these deposits are readily identified, as they are comprised of mainly mud/marls that form large valleys between sandy ridges. These units are deposited from low concentration turbidity currents through grain-by-grain deposition from suspension, followed by traction transport to produce lamination. The mud caps are deposited from suspension as flocs, with no subsequent traction transport.

3.4.6. FACIES ASSOCIATION 6 (FA6)

FA6 is dominated by marlstone, bedded sandy marlstone (including nummulitic packstones of centimetre-scale), and sediment slides/slumps (Facies C2.6, D2.1, D2.2, E2 and F1) representative of slope and base-of-slope facies that thin basinward in a wedge-like manner from the prodelta front.

These units are thick in the proximal parts of the foredeep in the Ainsa basin and thin downcurrent towards the Jaca basin forming a slope wedge, which is commonly characterised by sediment creep and slump features. This facies association can be considered as the terminal zone of deltaic deposition, recording background hemipelagic sedimentation (Mutti *et al*., 2003), deposition from low concentration turbidity currents and sediment creep or sliding.

3.4. ARCHITECTURAL ELEMENTS

3.4.1. INTRODUCTION

Applying architectural elements (previously introduced) to deep-marine systems can greatly assist in stratigraphic interpretation and deciphering depositional histories. An architectural element is, as defined by Miall (1985), a body of rock characterised by geometry, facies composition and scale that illustrates a single or group of processes existing within a depositional system. Within this study, the facies composition associated to an architectural element is comprised of a facies association (see section 3.4). In addition to the composition of an element, defining the bounding surfaces is important in distinguishing the scale of each element because the surfaces can be defined in a hierarchical manner (see section 2.6).

3.4.2. ARCHITECTURAL GEOMETRY

The architectural geometries of depositional elements are designed to be scale-invariant and therefore apply to various deep-marine basins. The definition of these geometries in two-dimensions, typically cross-section, is easily identifiable; likewise, plan view patterns are also readily established. Describing a three-dimensional pattern is difficult, but does assist in absolute geometrical definition. In this study, the combination of using both cross-section and plan view patterns to create pseudo three-dimensional elements is preferred (Fig. 3.25 and 3.26).

The geometries of channelforms show a concave-upward, erosional base and a mounded (convex-upward) top. Channelforms are thickest in the axis (after deposition, in cross-sectional view) and thin laterally, which can occur abruptly or gradually over several kilometres. In plan form, channelforms follow ribbon-like patterns that may be linear or wavy over a few kilometres, and may increase or decrease in width at any point along their length. Channelforms are most commonly linked to FA2. Alternatively, lobeforms are lens-shaped elements that are more laterally extensive (in cross-section) than channelforms. In plan form, they are narrowest at their origin point and resemble a tear drop shape where they become wide and rounded with distance down flow. They are thickest in their centre (in cross-section) and gradually thin laterally. In plan form, they follow a similar pattern. FA3 is the predominant facies association to these elements. Levee elements are commonly associated with channelform elements. Classically, they have a gull-wing morphology in cross-section (see Fig. 3.25). In plan form, they may extend for kilometres in length (following a channelform), and are linear or wavy. These elements are commonly associated with FA4. Barforms are found within channelforms and lobeforms. They tend to occur in the centre of erosive channelforms (as mid-channel bar elements) or on the edges of depositional channelforms (as lateral accretion elements). Mid-channel bar elements may form extensive depositional bodies, tens-of-metres in length and width, and are typically amalgamated. Lateral accretion elements are commonly stacked laterally against one another (in cross-section) to form a package of sediment (Fig. 3.25), deposited within the interior bends of meandering channels. Barforms are not extensive in dip or strike dimension and form on a scale of tens-of-metres. They are thickest in their centre and may have variations of coarsening or fining upwards trends. FA1, FA2 and FA3 can be associated to barform elements. Scour and fill elements are identified by an erosional base that has been filled with a fining upwards sequence of deposits. These elements are on the order of decimetres to tens-of-metres in length. In plan form, they commonly take on a similar shape to lobeforms, but show both up-flow and down-flow depositional wedging. They can also form localised crescent shaped scours on the seafloor (Fig. 3.26). FA1 and FA2 are related to these elements. Mounds are fairly large elements most commonly comprised of MTDs. The base of mounds can be erosional or wavy due to loading; tops are mounded. In plan form, they are greater in length than width, and have a somewhat oval shape that varies with each deposit. These elements can be tens-of-metres thick and extend in plan form for several kilometres. They are commonly comprised of FA1. Sheets and drapes are depositional elements and have the greatest lateral extent of all architectural elements. They can be tens-of-metres thick and extend in plan form for hundreds of metres or more. Sheet elements tend to be more planar in their stacking pattern, where drape elements follow the underlying topography. These elements are related to FA4 and FA5.

3.4.3. BOUNDING SURFACES

The surfaces that bound architectural elements are typically interpreted in both plan and cross-sectional views. Combining these interpretation results in a three dimensional surficial representation of an element. As previously discussed, these surfaces can be classified by type (conformable, erosional, depositional, etc.) and by order, where a surface of one order naturally embodies all surfaces of subsequent orders. The idea of naturally ordering surfaces according to these properties defines the traditional aspect of hierarchy, which will be discussed in the next section.

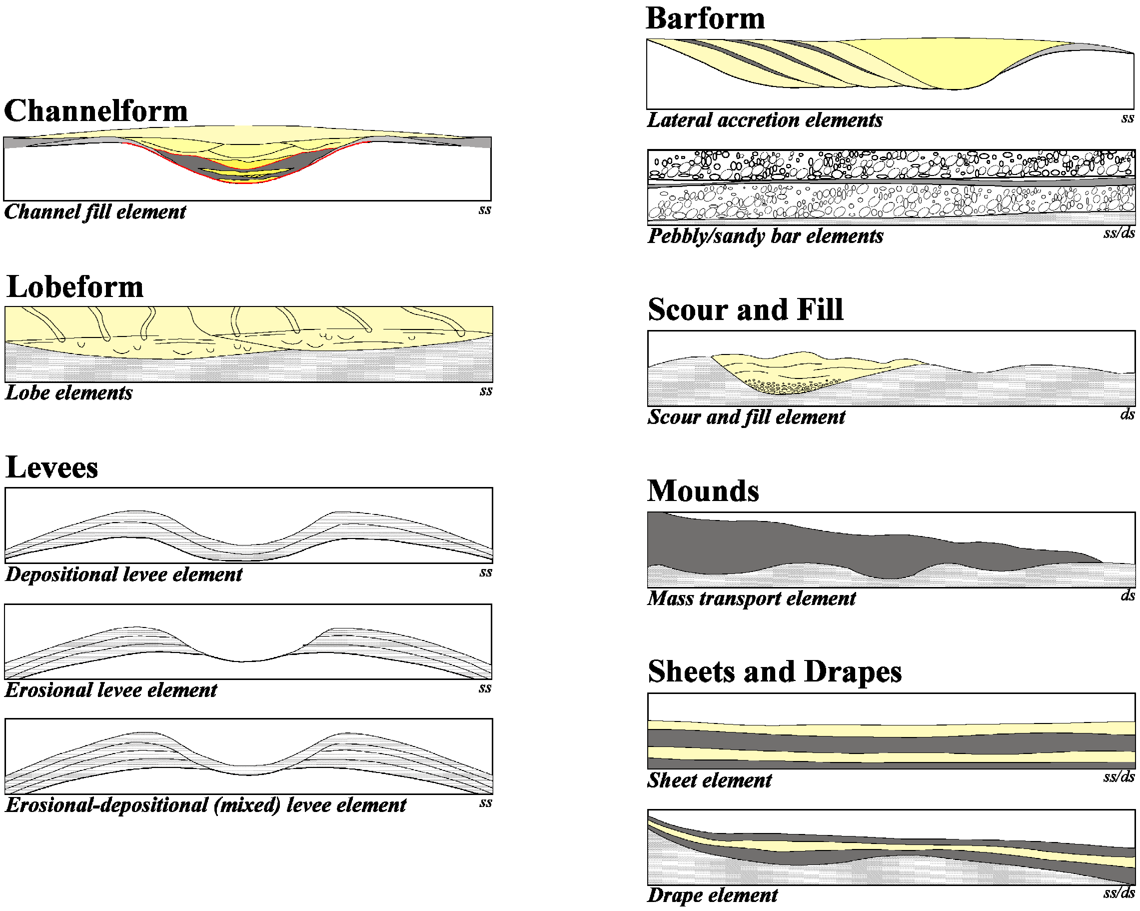

Fig. 3.25. Sectional classification of deep-marine architectural elements (architectural elements terminology adapted from Stow & Mayall, 2000). Note that some architectural elements form the building blocks for composite depositional bodies, e.g., channelforms form the fundamental unit for the deep-marine hierarchy in the Ainsa basin. ss, strike section; ds, dip section.

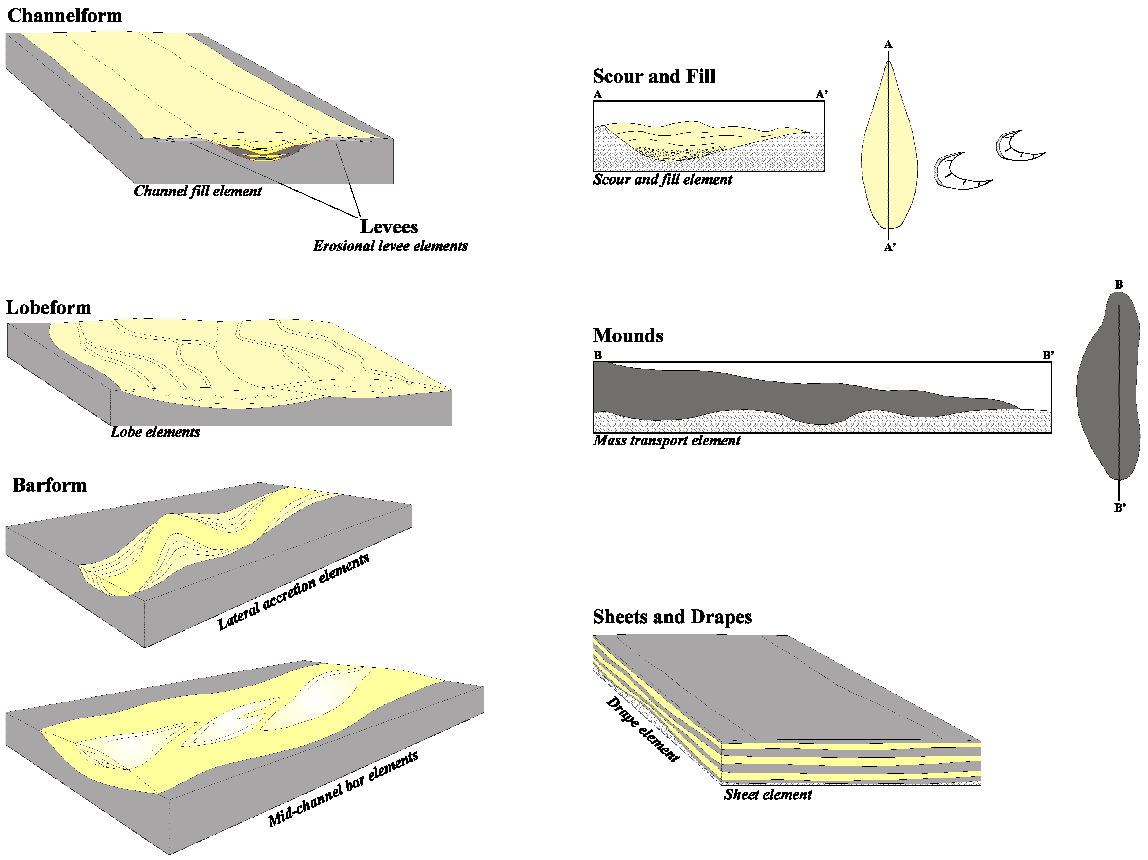

Fig. 3.26. Plan form classification of deep-marine architectural elements (terminology modified after Pickering *et al.*, 1995; Clark & Pickering, 1996). Note that some architectural elements form the building blocks for composite depositional bodies, e.g., channelforms form the fundamental unit for the deep-marine hierarchy in the Ainsa basin. ss, strike section; ds, dip section.

3.5. HIERARCHY

3.5.1 INTRODUCTION

Hierarchy is a tool used to differentiate and correlate key surfaces throughout the stratigraphy in a graduated manner, such that each surface can be genetically related to other interpreted surfaces. These surfaces were previously noted in section 3.4 as a way to establish bounding surfaces for architectural elements. In deep-marine environments, the channel is the largest autocyclic element that can be indentified, and as it occurs at a number of levels, the bounding surfaces must be introduced to delineate scaling (Miall, 1985).

For the purpose of this study, the applied hierarchy scheme (Fig. 3.27) is basin specific and describes a physical hierarchy, with some inferences on depositional processes in the Ainsa basin. Due to the confinement in the basin, depositional bodies tend to stack vertically in a channelised environment so that the determination of hierarchical levels is particularly difficult to determine. Effectively, the hierarchy proposed by Van Wagoner *et al.* (1990) is modified to apply to the Ainsa basin. Other versions of hierarchy rely on basic dimensions in unconfined settings to establish assignments to surfaces; erosion and other processes associated with vertical stacking do not allow this simplistic approach.

In the study area, outcrops are well exposed in very localised, mainly axially-dominated environments, and non-exposed or poorly exposed for other environments. Therefore, hierarchy, established from field observations and measured section logs, was catered to axial environments. Full dimensional analysis was not tangible due to limited outcrop widths, thus only approximated widths are provided. Additionally, vertical successions do not attain the upper hierarchical orders due to lack of exposure; only channel-level and lower thicknesses are fully captured for measured outcrops. A unique factor challenging hierarchy classification was the incorporation of abundant MTCs, which are not normally present in other basins.

3.5.2. LAMINA/LAMINASETS

Lamina and laminasets are 1st order hierarchical divisions representing the smallest identifiable packages of sediment (Campbell, 1967). They are commonly uniform in composition and lack internal layering (Van Wagoner *et al.,* 1990).

3.5.3. BEDS

Beds are a 2nd order division and are the fundamental building block for sedimentary bodies and are bounded by two surfaces, on the top and base, called bedding surfaces (Campbell, 1967). Beds typically develop over short time durations, therefore, they can be considered a time stratigraphic unit, which allows for interbasinal correlation (Van Wagoner *et al.,* 1990). Beds are representative deposits of MTDs, multiphase density flows, hyperconcentrated density flows, concentrated density flows and turbidites. Beds are comprised of one or more laminae sets.

3.5.4. BEDSETS

Bedsets (Fig. 3.28) are a 3rd order division comprised of one or more genetically related beds. Bedsets are distinguished as the beds over and underlying them are different in composition, texture or sedimentary structure (Van Wagoner *et al.,* 1990).

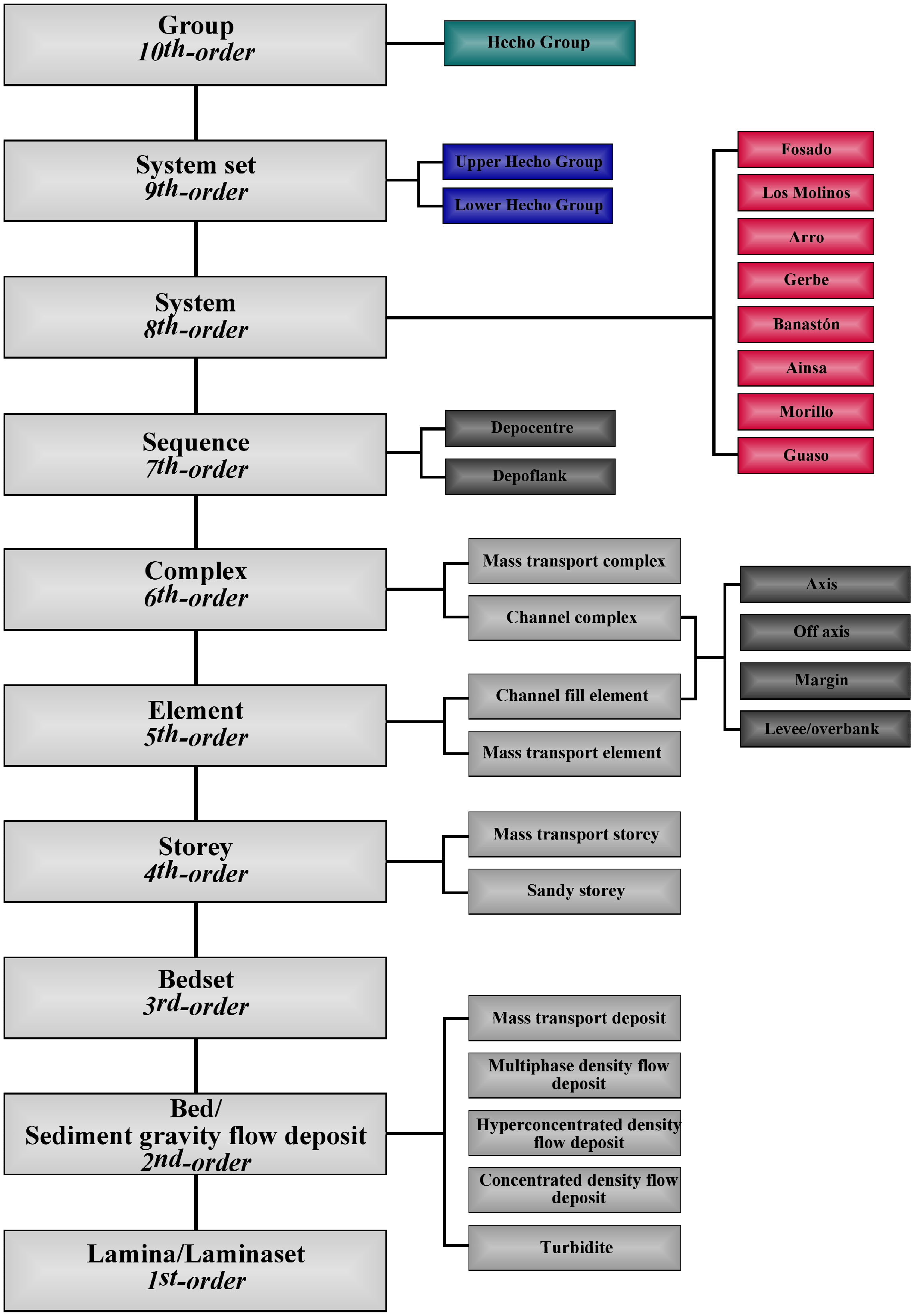

Fig. 3.27. Hierarchy of the Ainsa basin. This ordering system forms the hierarchical framework of the physical stratigraphy of the basin. Coloured backgrounds indicate the

base of each hierarchical element and not the erosional cutdown. CDD, concentrated density-flow deposit; MTD, mass transport deposit.

3.5.5. STOREY

Storeys (Fig. 3.28 and 3.29) are 4th order and were originally defined by Friend (1979) as continuous ribbons of sediment within a channel. Sandy storeys are defined for the Ainsa basin, which follow this definition; however the definition is modified to incorporate MTDs such that MTDs can comprise a storey when present. When MTDs are present in storeys, thicknesses are generally thicker and storeys are classified as mass transport storeys. Sandy storeys are ~300 m wide and ~2 m thick on average; mass transport storeys are larger in dimension at ~700 m wide and ~6 m thick. Storeys can follow fining upward or coarsening upward trends (Campion *et al.,* 2005). Commonly, they are coarsening upward in axial environments and fining upwards in off-axis/marginal environments. Storeys may be erosive or purely depositional and are composed of one or more bedsets.

3.5.6. ELEMENT

Elements (Fig. 3.28, 3.29 and 3.30) are 5th order depositional bodies and are comprised of channel fill elements and mass transport elements. Channel fill elements are classified into environmental regions (axis, off-axis, margin and levee). They typically have erosive bases and fine upwards in axial positions (Campion *et al.,* 2005). Mass transport elements are commonly erosive and have various internal structures (see section 3.3). Both elements are ~1000 m wide and ~14 m thick. Both elements are comprised of one or more storeys order sandy storey or MTD, respectively.

3.5.7. COMPLEX

Complexes (Figs. 3.28, 3.29 and 3.31) represent 6th order depositional bodies and are represented by MTCs and channel complexes. MTC are comprised by one or more MTD; channel complexes contain common environments of axis, off-axis, margin and levee, and are composed of one or more elements (Campion *et al.,* 2005). Channel complexes are erosional and may show overall coarsening or fining upwards depending on internal stacking patterns. They are ~1400 m wide and ~37 m thick.

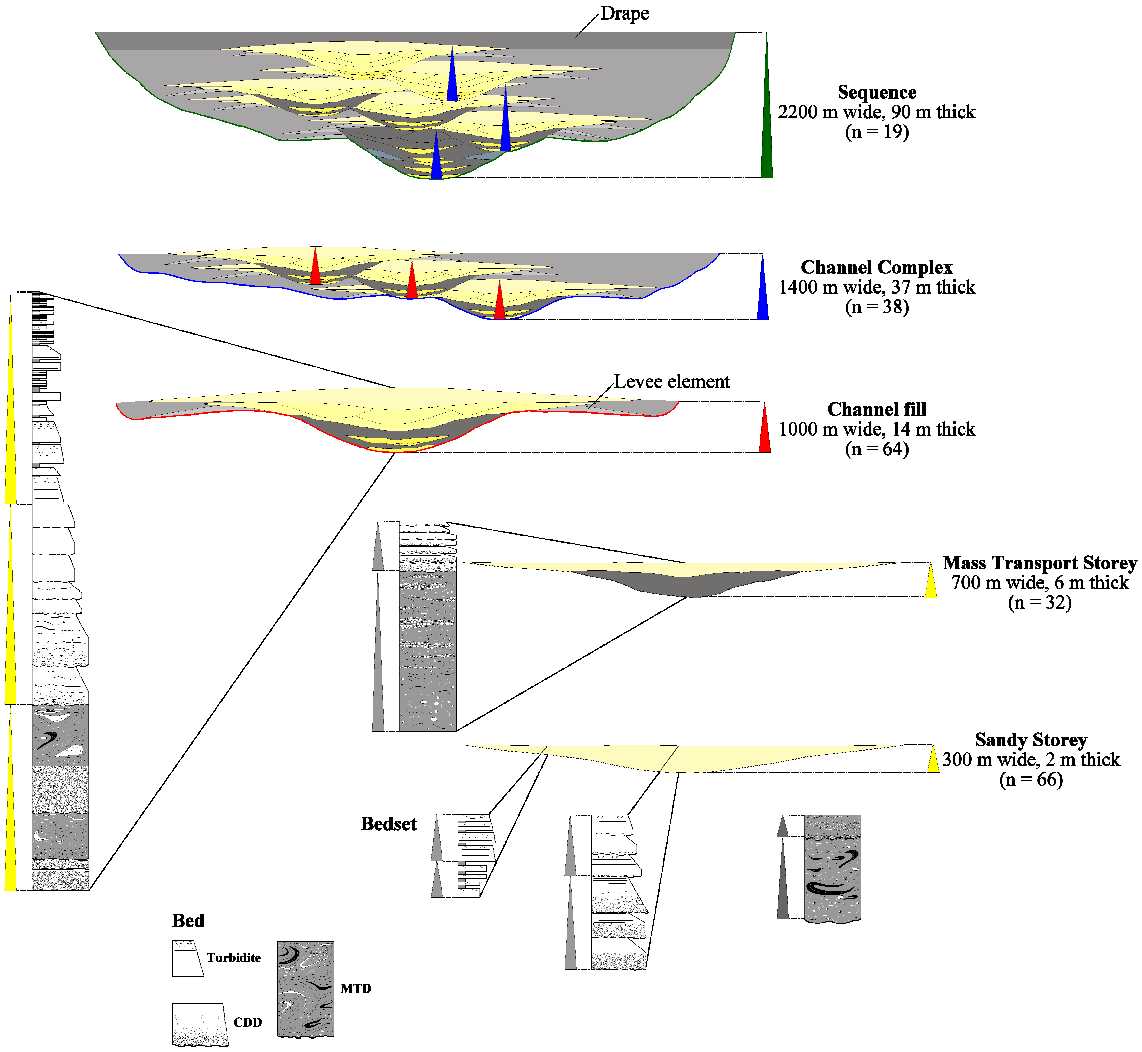

Fig. 3.28. Sectional hierarchical diagram with logs. Basic statistics with representative logs for the Ainsa basin.

3.5.8. SEQUENCE

Sequences (Fig. 3.28) are 7th order depositional bodies, defined at the base by a MTC and characterised at the top by a regional drape or abandonment facies. The base of each sequence represents major basin reorganisation and a shift in depositional axes. Sequences are comprised of complexes and are ~2200 m wide and ~90 m thick.

3.5.9. SYSTEM

Systems are 8th order depositional bodies and represent the focus of this study. Systems are comprised of two or more sequences, and are typically separated from other systems by fine-grained marly sediment. Systems form the Upper and Lower Hecho Groups in this study.

3.5.10. SYSTEM SET

System sets are of 9th order depositional bodies composed of one or more sandy systems that show an overall coarsening-upward trend in the Lower Hecho Group, and a fining-upward trend in the Upper Hecho Group. System sets stack to form a tectonosequence.

3.5.11. GROUP

Groups are 10th order depositional bodies that form the largest sedimentary unit. In this study, the Hecho Group forms the 10th order depositional body in the Ainsa basin.


NE
SW
0
5
10m

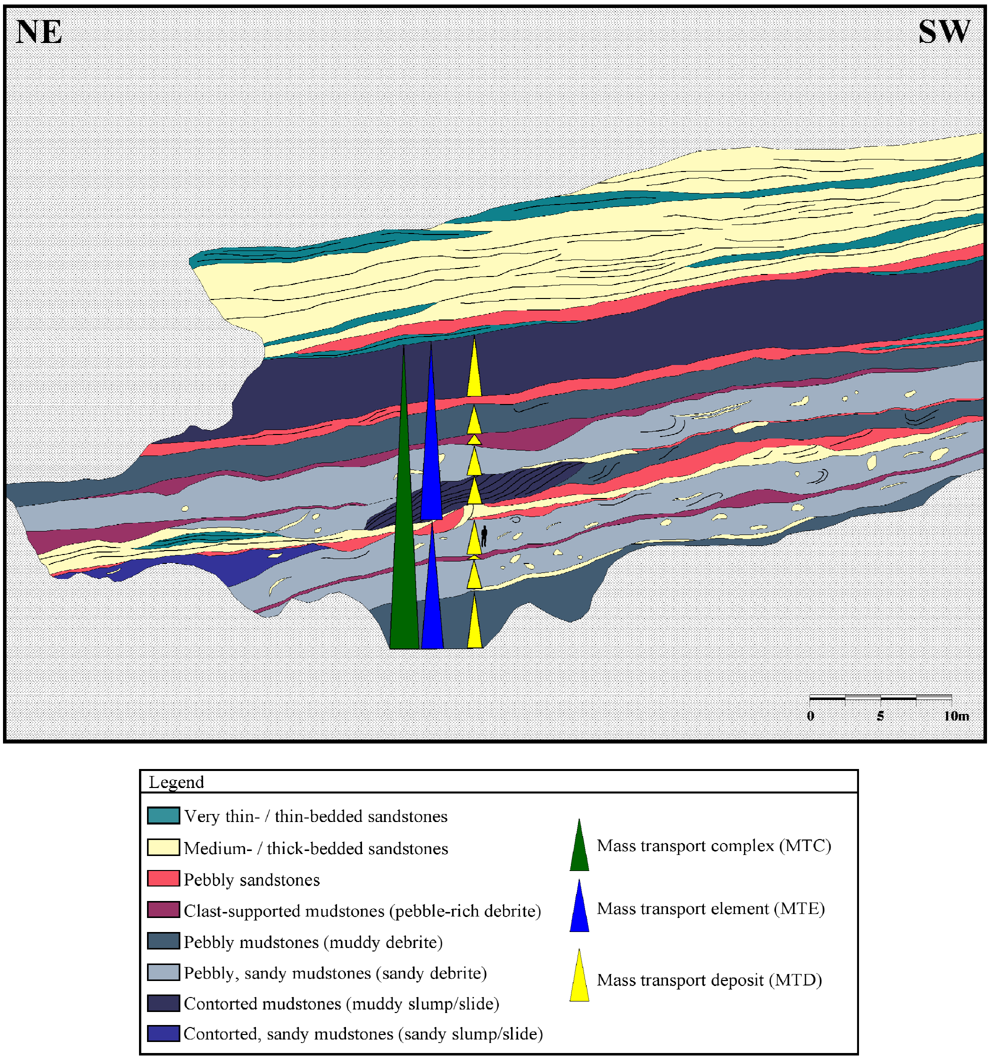
NE
SW
0
5
10m
Legend
Very thin- / thin-bedded sandstones
Medium- / thick-bedded sandstones
Pebbly sandstones
Clast-supported mudstones (pebble-rich debrite)
Pebbly mudstones (muddy debrite)
Pebbly, sandy mudstones (sandy debrite)
Contorted mudstones (muddy slump/slide)
Contorted, sandy mudstones (sandy slump/slide)
Mass transport complex (MTC)
Mass transport element (MTE)
Mass transport deposit (MTD)

Fig. 3.29. Mass transport hierarchical description and application. Palaeoflow is out-of-the-page for this figure. The hierarchy compiling a MTC is shown. Base of Morillo I, locality 42 used as example.

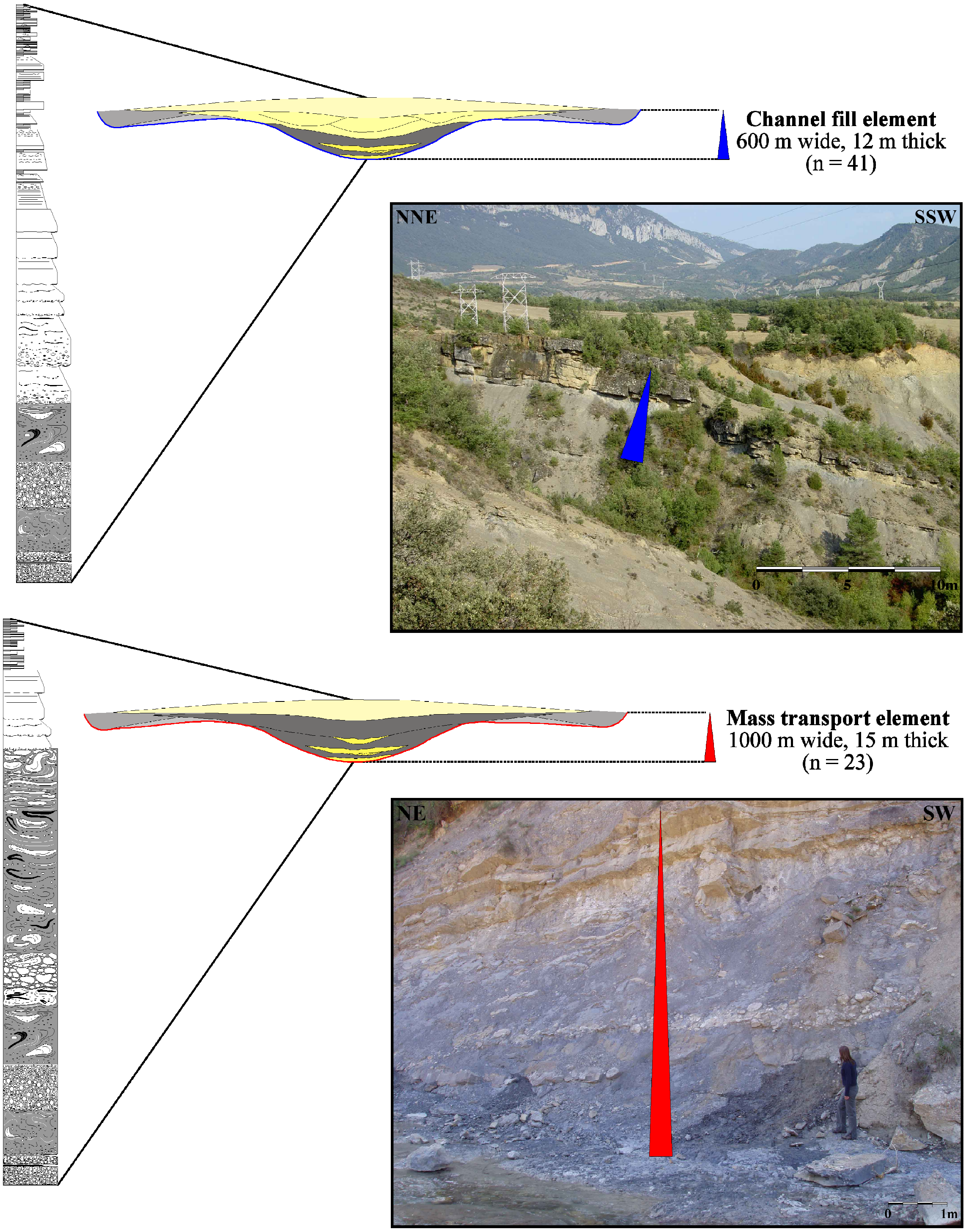

Fig. 3.30. Element order hierarchical representation with accompanying logs.

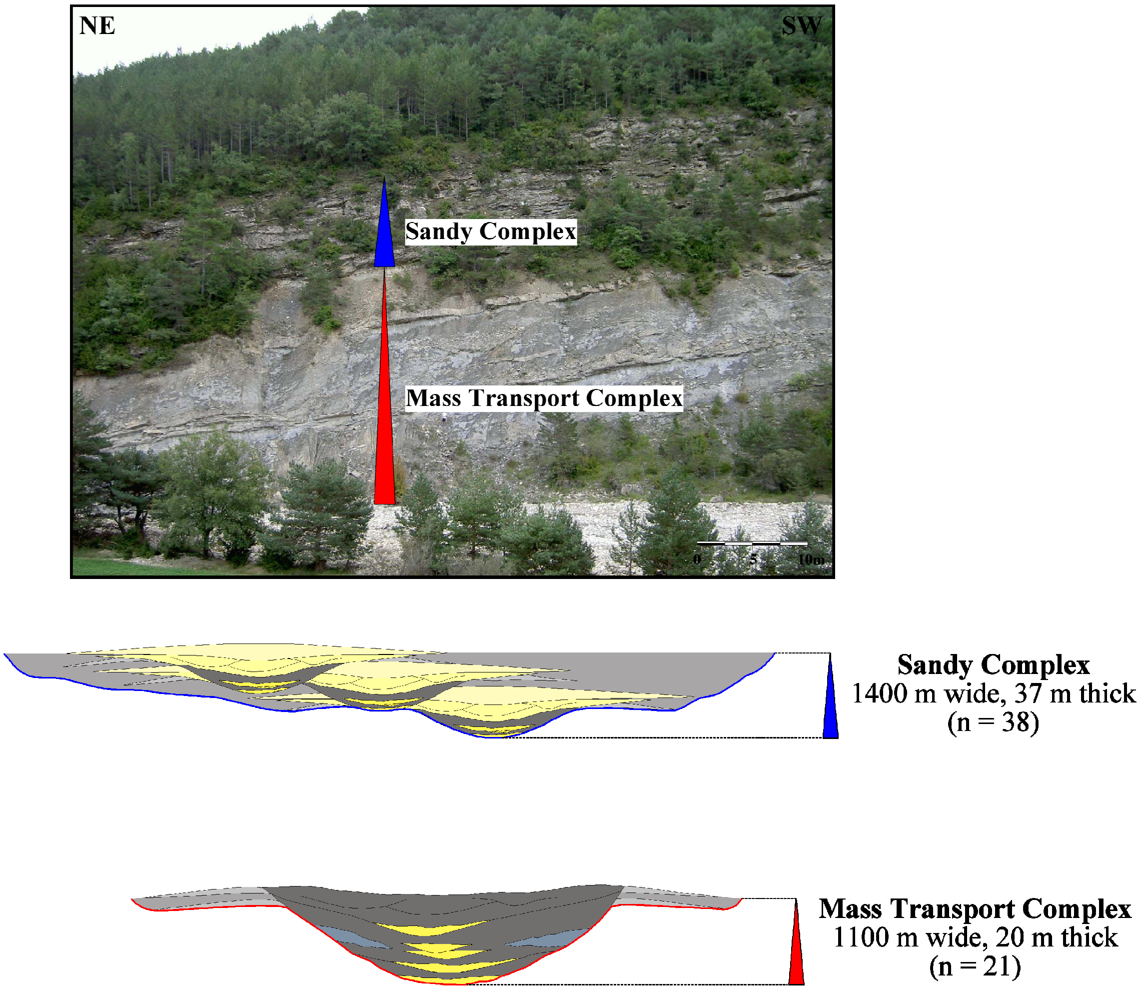

Fig. 3.31. Complex order hierarchical representation with accompanying logs.

CHAPTER 4

THE LOWER HECHO GROUP

4.1. INTRODUCTION

The Lower Hecho Group (the Fosado, Los Molinos, Arro and Gerbe systems) represents the oldest deep-marine siliciclastics sediments in the Ainsa basin during an early stage of basin development during tectonic phase I, forming tectono-sequence I (refer to Section 1.6.4.). The systems comprise the most structurally deformed sediment in the basin due to their proximity to the lateral ramp zone of the SCPU. Therefore, they do not form good quality, extensive outcrops. A total of 11 localities were studied, and ~1,360 m of cumulative measured sections were completed. This chapter provides concise overviews for each depositional system in the Lower Hecho Group, including brief descriptions of facies, architectural elements and depositional styles. The following chapters work chronologically through each depositional system in the study area in order to elucidate the depositional history of the Ainsa basin fill.

4.2. FOSADO SYSTEM

4.2.1. INTRODUCTION

The Fosado system marks the oldest sandy system in the Ainsa basin. It is generally poorly exposed, but forms a discrete outcrop near the village of Fosado, where it has been recognised as a channelised system (Locality 1, Table 2.1; Fig. B1). A number of small ridges, constituting thin sandbodies, are also located around the village of Los Molinos. The abundance of each facies class in the Fosado system is outlined in Figure 4.1. Facies class C, D and E represent the most number of beds measured, whereas the largest proportion of total thickness measured is found within facies class A. Trace fossils are almost absent from the Fosado system, with rare appearances of *Scolicia* and *Thalassinoides* ichnotaxa. This may be a result of the lack of preservation of structures or unfavourable palaeoecological conditions in sustaining a burrowing community.

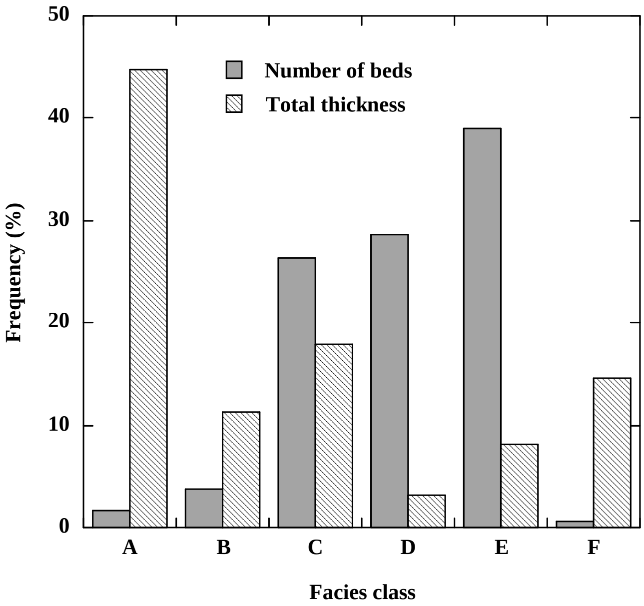

Fig. 4.1. The frequency of facies classes in the Fosado system based on the number of beds and total thickness measured.

4.2.2. SEDIMENTOLOGY AND INTERPRETATION

The total thickness of the Fosado system is ~57 m with an estimated width of ~500 m. Two channel complexes (or sequences), with thicknesses of ~28 m, comprise the Fosado system and are separated by a thin-bedded muddy/marly unit (FA5). Both channel complexes show thinning- and fining-upward trends, and the axes are characterised by FA2 and FA3, with FA4 defining the top of the channels and the channel margins. The outcrop at the village of Fosado (Fig. 4.2) represents one channel complex that consists of two stacked channel elements. Measurements taken at outcrop indicate a palaeoflow averaging ~320°. Mass transport deposits (MTDs) are volumetrically abundance on the outcrop, primarily located at the base of the sandy channel complex, representing a ~8 m thick type Ia MTD (see Chapter 3) in the axis. The MTD passes laterally into a ~14 m MTC in the off-axis environment, which is composed of three muddy MTDs (Fig. B1). The MTDs could indicate the base of the channelised system; although the lower contact of the basal MTD is not exposed, it can be interpreted that it overlies thin-bedded siltstones and mudstones (FA5). The overlying sandbody is ~12 m in the channel axis and is predominantly characterised by thick-bedded, often amalgamated, laterally discontinuous sandstones (FA2) at the base of each channel element. The sandstones are commonly disorganised with a mud-rich sandy matrix and abundant mud-clasts at the base. The top of the channel elements

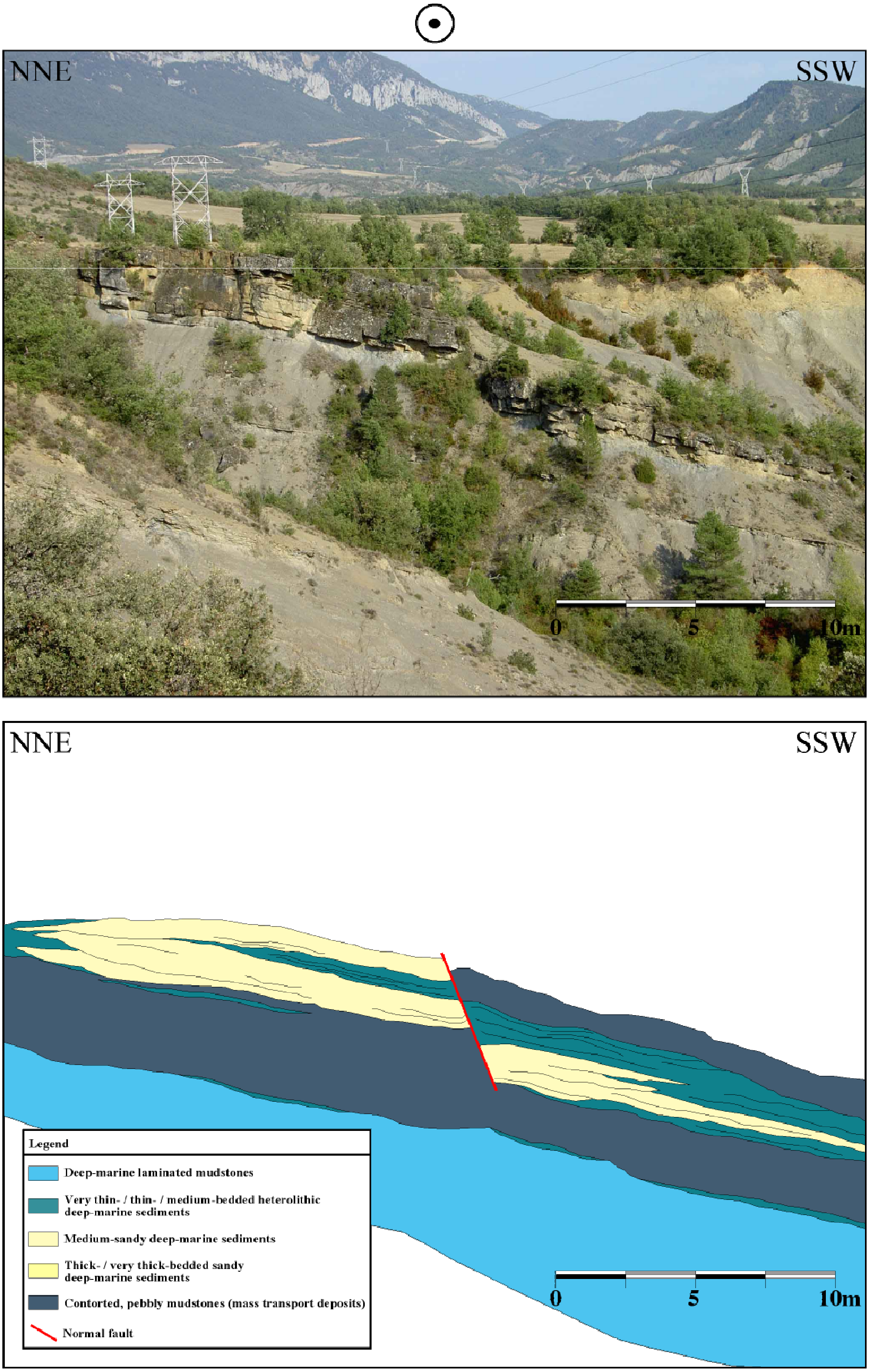

Fig. 4.2. Photo interpretation of a channel complex in the Fosado system at Fosado village. Note the normal fault cutting through the south-southwest channel margin, with a displacement of ~5 m. Palaeoflow is towards the northwest (see Fig. B1).

comprise graded and stratified thin- to medium-bedded sandstones (facies C2.3), followed by thin-bedded, current ripped sandstones (facies C2.4) and mudstones (facies E2), as a fining-upward sequence. Each channel element is ~6 m thick. The top of the channel complex is truncated by a ~7.5 m thick muddy type Ia MTD (Fig. B1), which is exposed in the south-southwest part of the outcrop due to down-faulting (Fig. 4.2). Both channel complex margins are exposed, and are characterised by thin-bedded, fine-grained, current rippled sandstones and mudstones (FA4).

The Fosado system consists of two channel complexes, comprising discrete mid-slope channel elements. The abundance of type Ia MTDs and the disorganised nature of the sandbodies defining the base of channel elements indicate a mid-slope (proximal) setting. The lack of organisation in the basal sandstones and the thin sandy successions could also suggest that the Fosado system represents an immature system with little sorting and low siliciclastic supply. The lack of laterally extensively overbank deposits suggests high confinement on the muddy slope. Due to the erosive nature of the basal MTC, it can be inferred that the event created accommodation laterally adjacent to the main depositional mound, forming a pre-developed master surface for the accumulation of the overlying sandy channel elements. This would account for the observed depositional confinement. It can also be interpreted that the base of the Fosado system signifies the collapse of the upper- to mid-slope to supply the system with chaotic muddy slump and slide material. The association with the overlying sandy sediment suggests a major event supplying sediment of various grades into the basin. Various controls on the sandy system are discussed in Chapter 7. In summary, the Fosado system represents the earliest supply of siliciclastic sediment into deep water during an immature stage of basin development.

4.3. LOS MOLINOS SYSTEM

4.3.1. INTRODUCTION

The Los Molinos system comprises three discrete sandbodies, which are exposed in Barranco Sierra, south of the village of Los Molinos (Locality 2, Table 2.1), and to the north of Ainsa around the abandoned village of Muro Bellos (Fig. 4.3). Originally, these sandbodies were documented by Ramacha *et al.* (2003), and were associated to the Arro system. In this study, they constitute their own system due to: (1) the large volume of thin-bedded, fine-grained deposits between the Arro and Los


NW
SE
0
100
metres

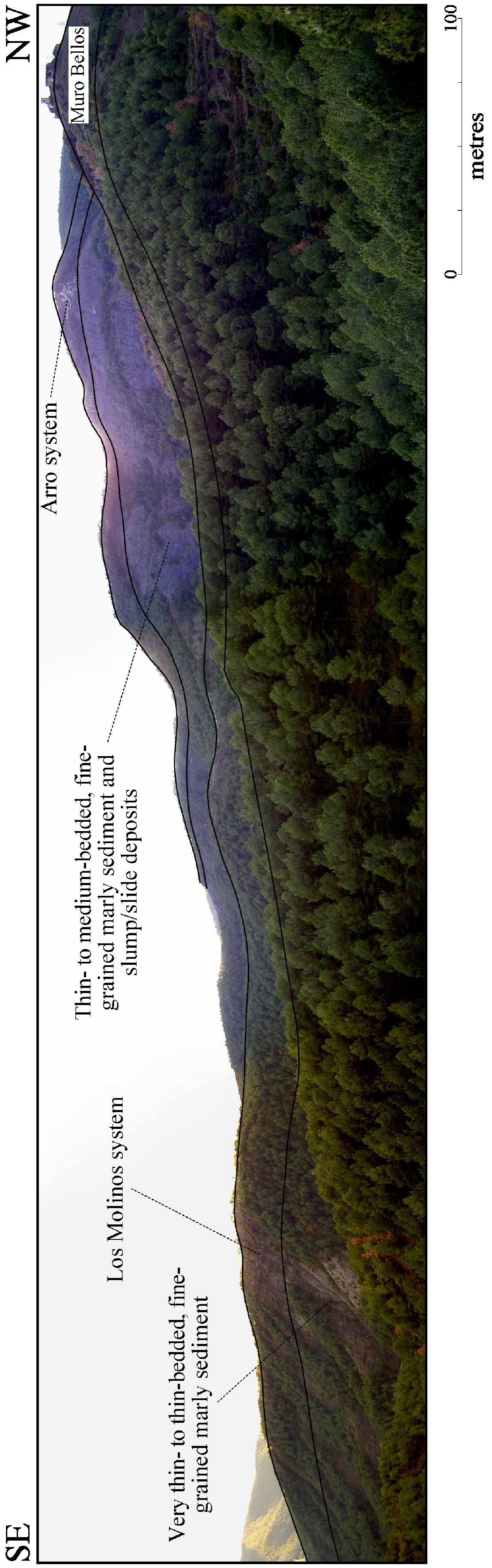
NW
SE
Muro Bellos
Arro system
Thin- to medium-bedded, fine-grained marly sediment and slump/slide deposits
Los Molinos system
Very thin- to thin-bedded, fine-grained marly sediment
0
100
metres

Fig. 4.3. Northern outcrop of the Los Molinos and Arro systems around the abandoned village of Muro Bellos demonstrating the separation between the systems. The Los Molinos systems is defined by a ~40 m thick sandy ridge consisting of thin- to medium bedded sandstones with muddy intercalations. The thin-bedded marly slope sediment between the two systems is thicker at this region (~110 m thick) than the more proximal outcrop along Barranco Sierre (~80 m thick), and contains abundant folded and contorted muddy horizons (slump/slide facies). The Arro system is represented by ~20 m of thick- to very-thick bedded sandstones at this outcrop; true thickness of the Arro system is difficult to determine at this locality due to deformation from folding and thrusting. Palaeoflow is to the right of the plate (~320º).

Molinos systems, ~80 m; (2) the presence of an angular unconformity at the base of the Arro system interpreted as a sequence boundary, which is related to the emplacement of the Atiart thrust (Munoz *et al.*, 1994), slope oversteepening processes and the influx of sediment into the deep marine basin. Other studies (Das Gupta & Pickering, 2008) support this interpretation by demonstrating that the Los Molinos and Fosado systems are petrographically distinct. Figure 4.3 demonstrates the separation of the Los Molinos and Arro systems at a location north of Ainsa, near the town of Escalona. The abundance of each facies class in the Los Molinos system is outlined in Figure 4.4. Facies class C, D and E represent the most number of beds measured, whereas the largest proportion of total thickness measured is found within facies class C and F.

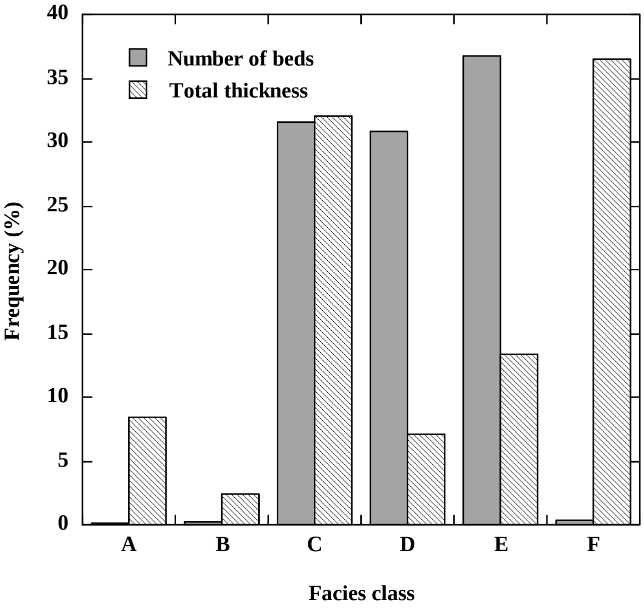

Fig. 4.4. Number of beds and total thickness by facies class for the Los Molinos system.

4.3.2. SEDIMENTOLOGY

The three sandbodies are well exposed at an outcrop in Barranco Sierra, south of Los Molinos village, which are orientated oblique to palaeoflow (Figs. 4.5 and B2). The sandbodies are truncated to the southeast by the Los Molinos thrust (see Section 4.4 for thrust location), and form a ridge trending northwest–southeast from the village of Los Molinos in the south to the abandoned village of Muro Bellos in the north (refer to Fig. 4.3). However, the sandbodies become highly deformed by a thrust and fold system in the northern outcrops. The sandbodies are estimated to have a width of ~700 m and average bed thicknesses of ~5 cm, and are separated by contorted mudstones (mainly type Ia MTDs), thin-bedded sandstones and laminated mudstones (FA5). Thick MTDs (type Ia) characterised by contorted, intraformational mudstones and sandstones, encase the sandbodies and average ~13 m in thickness.

The base of the oldest sandbody is not exposed, but the total thickness is estimated at a few tens-of-metres. A type Ia MTD defines the base, followed by thin-bedded sheet-like sandstones, and thin- to medium-bedded, laterally discontinuous sandstones (FA3). The sandstone beds are characterised by well-developed planar stratification, and in some sandstone beds, extra-formational pebbles, *Nummulites* and intraformational mud-clasts are present at the base. This facies associations is commonly truncated by type Ia MTDs, and often infill the localised topography created by other muddy MTDs. Laterally, the sandbody transitionally passes into finer grained, more muddy sediment (FA4), although the transition between the two facies associations is difficult to determine due to an extensive scree slope covering part of the outcrop. Palaeoflow indicators average ~334° with a dispersion of ~30° (320°–350°) in the basal part of the sandbody, and are more dispersed in the upper part with a range of ~130° (320°–090°). The top of the sandbody is marked by an erosive muddy slump that partially truncates part of the sandbody.

The second sandbody is exposed toward the top of the outcrop in the ridge to the north-northwest of the first sandbody. The base of the sandbody is characterised by thick type I MTDs, interbedded with thinner type II MTDs towards the top (defining the very base of the sandy succession). The type II MTDs are characterised by extra-formational pebbles in a sandy mudstone matrix. The overlying sandy succession is ~9 m thick with a noticeably fining-upwards sequence. Sandstone beds are typically amalgamated and normally graded, with extra-formational pebbles, *Nummulites*

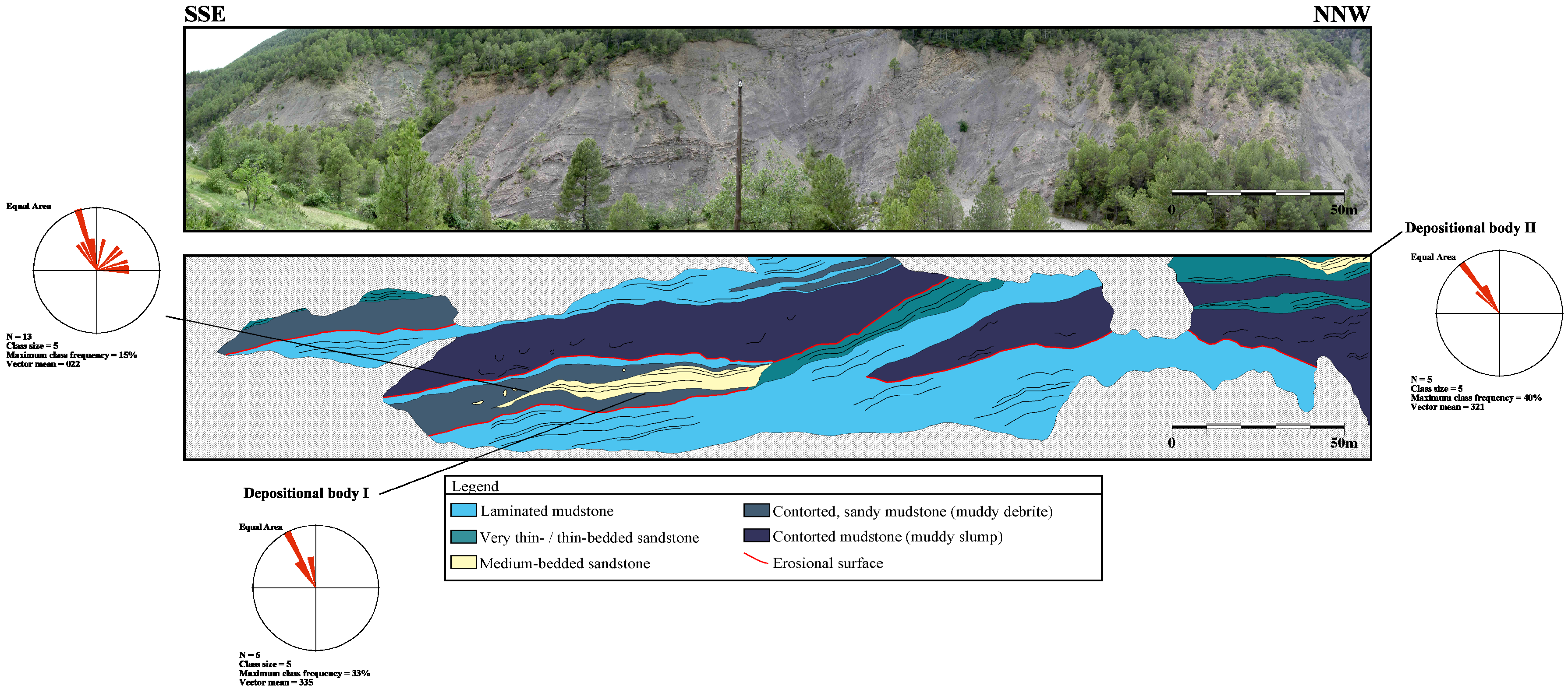

Fig. 4.5. Outcrop interpretation of depositional bodies (labelled I and II) and surrounding sediment, Los Molinos System, Barranco Sierre. Outcrop is orientated oblique to palaeoflow. Rose diagrams show the palaeocurrent directions for current ripples and groove casts (see Fig. B2 for detailed sedimentary log).

and intra-formational mud-clasts. Mean palaeoflow show less dispersion than the previous sandbody and is towards 320°.

The final sandbody is ~50 m thick with a poorly defined base associated with thick-bedded, laterally discontinuous sandstones (FA2) and thin type II MTDs, overlain by thin- to medium-bedded sandstones (FA3). Type II MTDs are apparent throughout the exposure consisting of extra-formational pebbles and shell fragments. Type Ia MTDs are also present consisting of folded, and partially disaggregated thin-bedded sandstone in a muddy matrix. Mean palaeoflow is ~320°.

4.3.3. TRACE FOSSILS

There is a low trace-fossil diversity in the Los Molinos system; the most common ichnotaxa is *Thalassinoides* and *Ophiomorpha*. This may be a result of unfavourable palaeoecological conditions in sustaining a burrowing community, such as a lack of a stable, sandy substrate (the Los Molinos system is dominated by slide and slump deposits).

4.3.4. INTERPRETATION

The Los Molinos slope system comprises three discrete sandbodies encased in type I MTDs (facies F1 and F2), which form a slope apron sequence ~90 m thick. The sandbodies are interpreted as discrete, confined channel elements that infilled composite erosional surfaces created by MTDs. The association of thick type Ia MTDs and confined sandbodies suggests deposition in a mid-slope setting. The type II MTDs at the base of the middle sandbody represents the collapse and redeposition of the outer shelf to littoral zone during the early phase of channel development. The dispersion in palaeoflow observed in the lower sandbody can be attributed to the lack of a source point within the slope apron setting; however, the base of the sandbody generally shows less dispersion indicating depositional confinement within the accommodation created by thick type I MTDs. The younger sandbodies generally show less dispersion, suggesting a temporal increase in confinement between MTDs, related to an increase in the volume of slides and slumps deposited on the slope.

During deposition of the Los Molinos system, turbidity currents originated on the delta front and flowed into the Ainsa basin through a slope apron system, leading to the formation of three channel elements. Thrust-induced slope oversteepening resulted in the contemporaneous collapse of the upper- to mid-slope, leading to the creation of

MTDs that separate the sandbodies by tens-of-metres. During tectonic phase I (see Section 1.6.4), the development of the lateral ramp zone of the SCPU and the propagation of the thrust front in the north created a very active basin margin in the north and east of the basin. The slope apron sequence, therefore, developed in an active setting with thrust-induced oversteepening causing the collapse of the slope environment and the development of volumetrically significant MTDs.

4.4. ARRO SYSTEM

4.4.1. INTRODUCTION

The Arro system is exposed at various localities in the Ainsa basin (Localities 3–8, Table 2.1), extending from Tozal de Charo in the southeast to Morillo de San Pietro in the northwest. The Arro system is stratigraphically located above the Los Molinos system within the Lower Hecho Group. A total of ~460 m of section was measured in six locations. Facies found within the Arro system include laminated mudstones, very thin- to thick-bedded sandstone, and type Ia and Ib MTDs. Figure 4.6 shows facies class abundance in the Arro system, presented by the total number of beds and total thickness measured. There are a large number of beds associated with facies class C and E, whereas facies class F represents a high frequency of total thickness measured (30%).

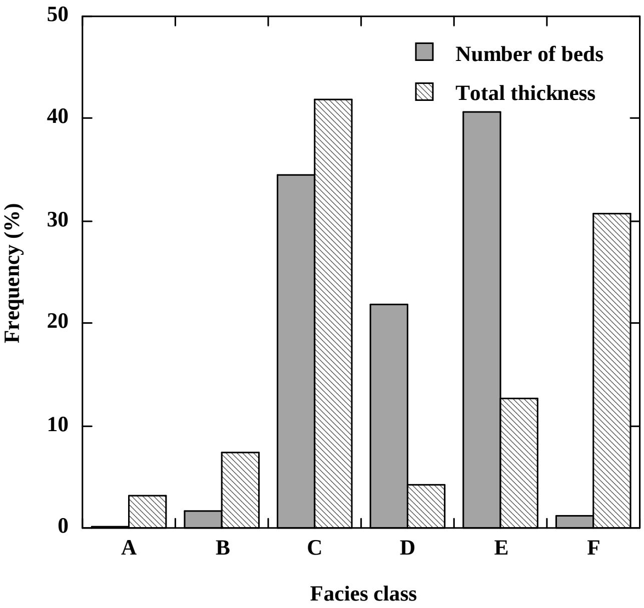

Fig. 4.6. Number of beds and total thickness by facies class for the Arro system.

4.4.2. SEDIMENTOLOGY

The Arro system forms a prominent ridge that can be easily mapped amongst the structural controls in the Ainsa basin (Fig. 4.7). The outcrop at Tozal de Charo represents the most proximal part of the system preserved in the basin, although the succession is poorly exposed and deformed at this locality. The Arro ridge, named the Sarreta d'Arro, extends from the Rio Nata outcrop (Locality 3, Table 2.1) in the south to Barranco Sierre outcrop (Locality 6, Table 2.1) and Santa Catalina ridge in the north (Locality 7, Table 2.1). The most northern outcrop investigated in this study is situated at As Faixas ridge, north of San Vicente (Locality 8, Table 2.1). The Arro system is structurally deformed and is incorporated into the Los Molinos and Arro thrust, forming part of the lateral zone of the SCPU (Fig. 4.7). In the Rio Nata outcrop, the Los Molinos thrust is located ~40 m below the base of the Arro system, and the beds are overturned, dipping at ~80°. The total thickness of the Arro systems varies, with maximum thickness reaching ~200 m in Rio Nata, with an estimated width of ~1,350 m wide at Barranco Sierre. The average sequence thickness is ~70 m.

The sandy succession at Tozal de Charo is ~40 m thick and consists of laterally continuous, medium-to thick-bedded sandstones (FA3), and laterally continuous thin- to medium-bedded sandstone-mudstone couplets (FA4). These facies associations form the lower part of the Charo canyon fill, overlaying a type I MTD and FA6 (slope sediment). Sandstone beds are generally coarse-grained and contain abundant extra-formational material, such as *Nummulite*s, shell fragments and well-rounded pebbles. The sandy succession is interpreted as an off-axis channel complex, which forms part of the Charo canyon fill. The Arro system at Tozal de Charo is erosively overlain by the Gerbe canyon fill (Section 4.5), defined at the base by intra-formational MTDs and an angular unconformity formed as a result of a major phase of tectonic activity marking the onset of the Gerbe system (Millington & Clark 1995b; Fig. B5).

In the Rio Nata outcrop, the Arro system is exposed in the river section and along the adjacent roadside, forming a ~200 m thick sedimentary section (Fig. B3) divided into three sandy sequences. The base of the system is associated with a ~14 m thick MTC comprising muddy slumps interbedded with discrete sandy units (see Fig. B3). The MTC is overlain by a ~34 m thick sandy successions forming the upper part of the Arro I sequence. The sequence is characterised by medium- to thick-bedded, tabular sandstones showing scour-and-fill elements and pinch-and-swell geometries. These sandstones are punctuated by thin, <2 m thick, type I MTDs. The Arro II sequence is

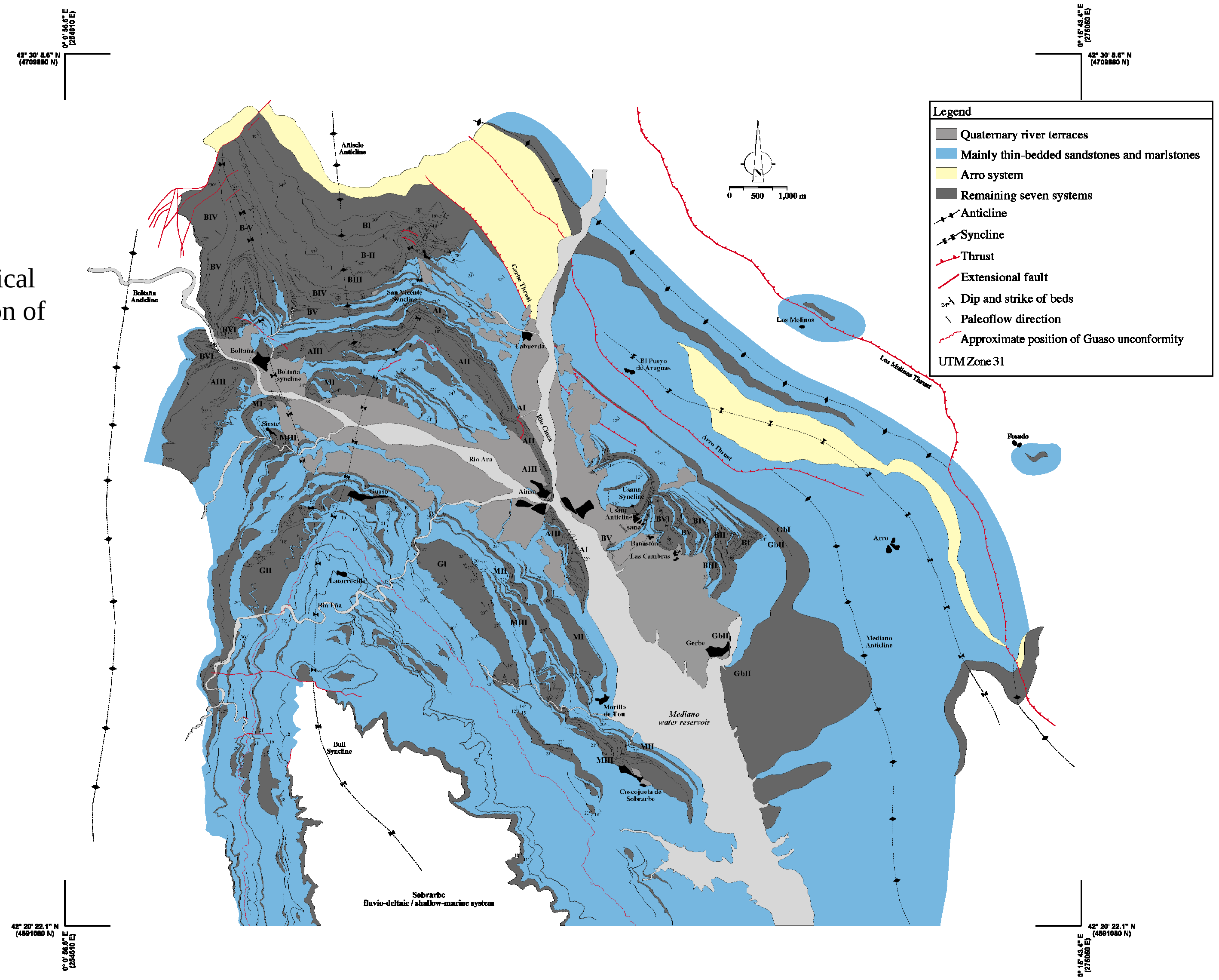

Fig. 4.7. Simplified geological map highlighting the position of the Arro system.

~100 m thick, and is defined at the base by a ~16 m thick muddy MTC. The overlying sandy unit comprises thin- to thick-bedded stratified and graded sandstones, with a large amalgamated sandy unit encased in type I MTDs. The top of the sequence is characterised by thin-bedded, current rippled sandstones, interbedded with muddy slump and slide deposits (type Ia MTDs). The Arro III sequence is ~52 m thick and is predominantly composed of a basal ~19 m thick MTC abundant in *Nummulites* and wood fragments. This is followed by very thin- to thin-bedded, fine-grained sandstones (facies C2.4 and C2.5) and laminated mudstones (facies E2), marking the top of the Arro system.

The Arro sequences are also exposed in the Barranco Sierra and the adjacent road section (Localities 5 and 6, Tables 2.1), forming a ~180 m thick sedimentary section (Fig. B4). The base of the system is associated with an angular unconformity represented by a ~5˚ dip change. Figure 4.8 shows ~60 m of dip-section of the base of the Arro system, where the dip change is recorded. The base of the system, also defining the base of the Arro I sequence, is composed of a ~12 m thick muddy MTC, comprising two type Ia MTDs. A 45 m thick, heterolithic package overlies the basal MTC and consists of laterally extensive, very thin- to medium-bedded tabular sandstones (facies C2.3, C2.4 and C2.5), followed by another ~3 m thick MTD. Medium- to thick-bedded sandstones (facies C2.2) exist at the top of the section that forms a discrete ~7 m thick sandy package, representative of channelised deposits.

The opposite side of the river preserves a sectional outcrop of the middle part of the Arro system (Arro II sequence) at this location (Fig. 4.9). In general, the outcrop shows type Ia and IIb MTDs (facies F1 and F2) forming a ~23 m thick MTC at the base, which becomes more sandy towards the top comprising large rafts of folded mudstones and thin-bedded sandstones. A confined channel element is situated within the upper part of the MTC, which thickens laterally into the river section. The element is characterised by medium- to thick-bedded, amalgamated sandstones in the axis (FA2), overlain by planar stratified, thin-bedded sandstones towards the top (FA3 and FA4). The channel margin element is exposed in the road section, represented by thin type Ia MTDs and thin- to medium-bedded sandstones. A large truncated sandy unit is also situated at this stratigraphic location comprising thick-bedded amalgamated sandstones that are partially eroded by an overlying muddy type Ia MTD. A number of other laterally discontinuous, nummulitic sandy packages are also present, forming wedged-shaped geometries between MTDs. The top of the unit is characterised by medium- to

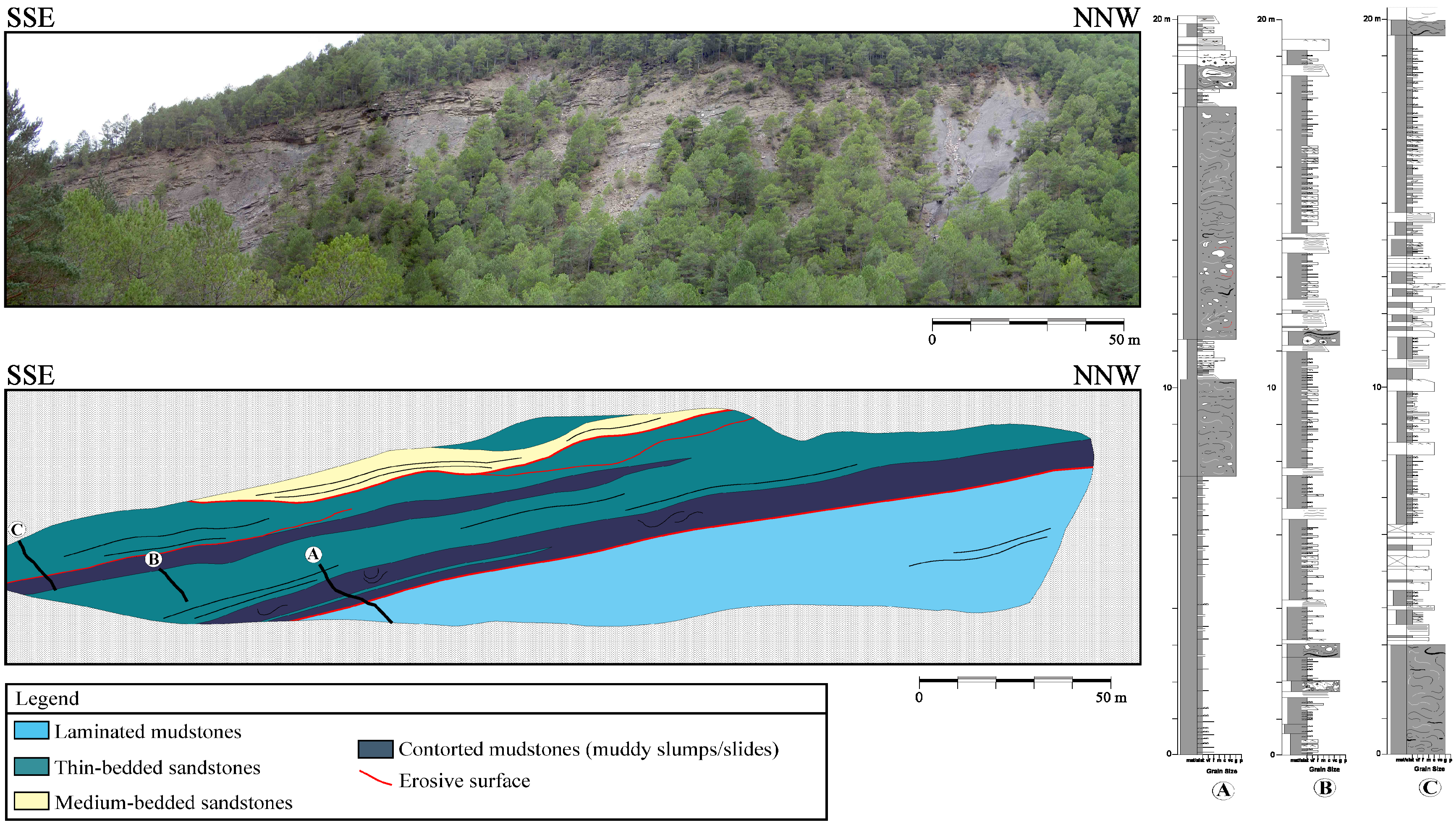

Fig. 4.8. Photo interpretation of the Arro I sequence at Barranco Sierre outcrop, with detailed bed-by-bed sedimentary logs. The base is defined by a slump/slide unit (MTC) overlying muddy slope facies (FA6). Note the predominance of thin-bedded sandstones directly overlying the basal MTC, and the lack of pebbly sediment; a common characteristic of the Arro system. Outcrop is oblique to palaeoflow (palaeoflow is ~312º).

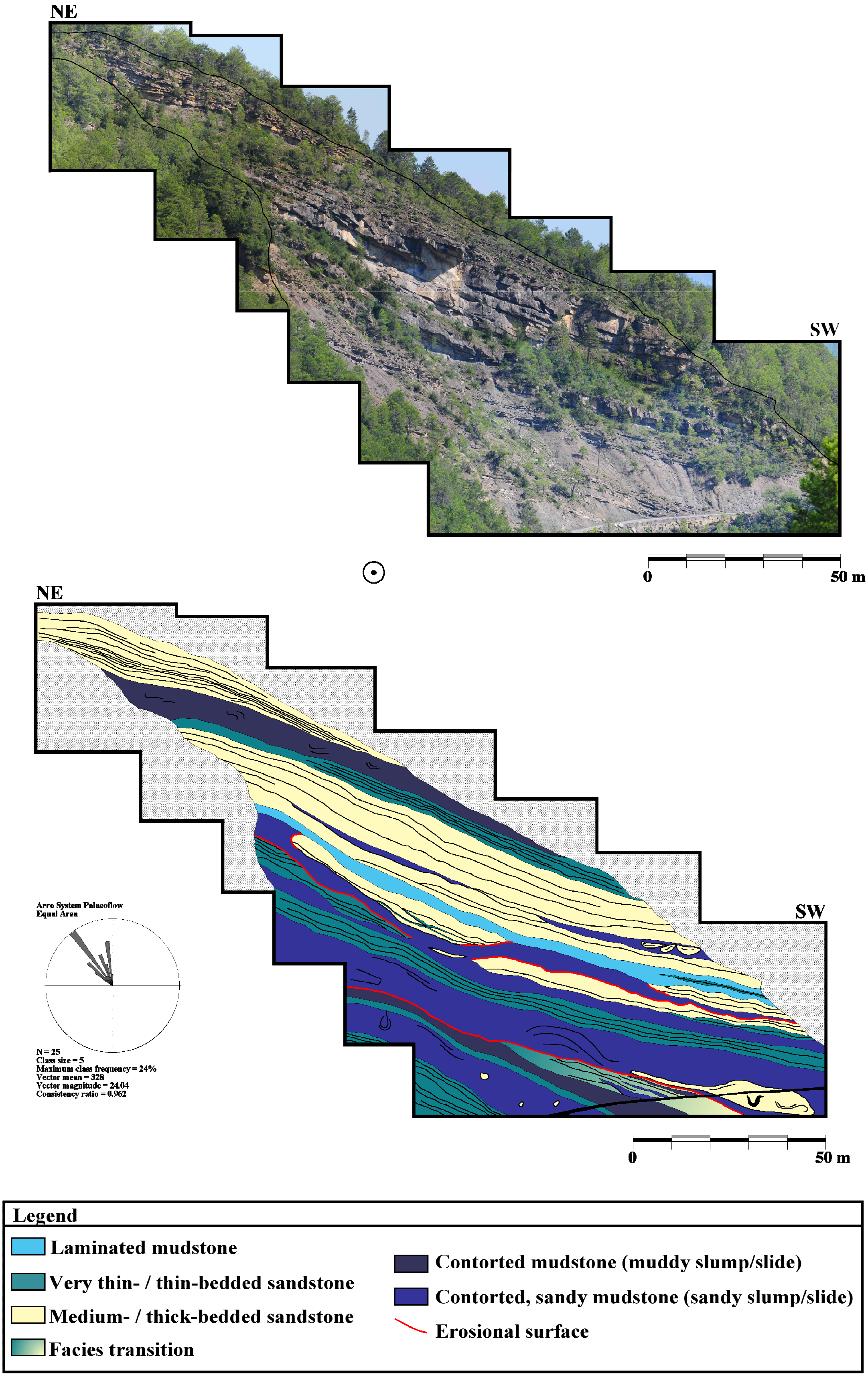

Fig. 4.9. Photo interpretation of the Arro II and III sequences, Barranco Sierre road section. The base of the Arro III sequence is defined by the contorted mudstone deposit situated at the upper part of the plate, which is overlain by a ~15 m thick sandy package.

thick-bedded sandstones (facies C2.1 and C2.2) that form semi-amalgamated channel elements, capped by a type Ia MTD defining the base of the Arro III sequence. These sandstones are characterised by erosive bases and flat to current rippled tops, which thin laterally into the river section. They are characterised by an abundance of nummulitic and woody material. Mean palaeoflow is to the northwest (~328˚).

Figure 4.10 is a correlation between the measured sections taken at both outcrops previously discussed. Erosion is easily identified at sequence boundaries where type Ib MTDs are present. Cut-down associated with this erosion is on the order of 10–20 m. Units of thin-bedded sandstones and medium- to thick-bedded sandstones are laterally continuous, unless they have been truncated. The Arro III sequence is characterised by a ~15 m thick basal MTC (see Fig. 4.10) interbedded with thin packets of thin-bedded sandstones and overlain by tens-of-metres of thin-bedded sandstones representing the top of the Arro system.

4.4.3. TRACE FOSSILS

The trace fossil assemblage in the sandy depocentres of the Arro system is typical of a channel axis environment, predominated by post-depositional trace. The most common ichnotaxa are *Ophiomorpha*, a dwelling/*domichnial* trace; *Halopoa* and *Scolicia*, grazing/*pascichnial* traces. The highest diversity and abundance of trace fossils is found in the thin- to medium-bedded, fine- to coarse-grained sandstones of the Arro I sequence; the sandy succession is indicative of less erosive sediment gravity flows, and therefore, contains a higher preservation potential for burrows. The enrichment of the Arro system in organic matter (i.e., nutrients for trace makers) could be responsible for the lack of pre-depositional structures, particularly graphoglyptids. The graphoglyptids represent a specialised, K-selected equilibrium strategy of colonisation, adapted to surviving in oligotrophic (low nutrient) conditions, whereas the post-depositional ichnotaxa were formed from opportunistic organisms that thrived in eutrophic conditions (Ekdale, 1985; Uchman, 1995; Rodríguez-Tovar *et al.*, 2010).

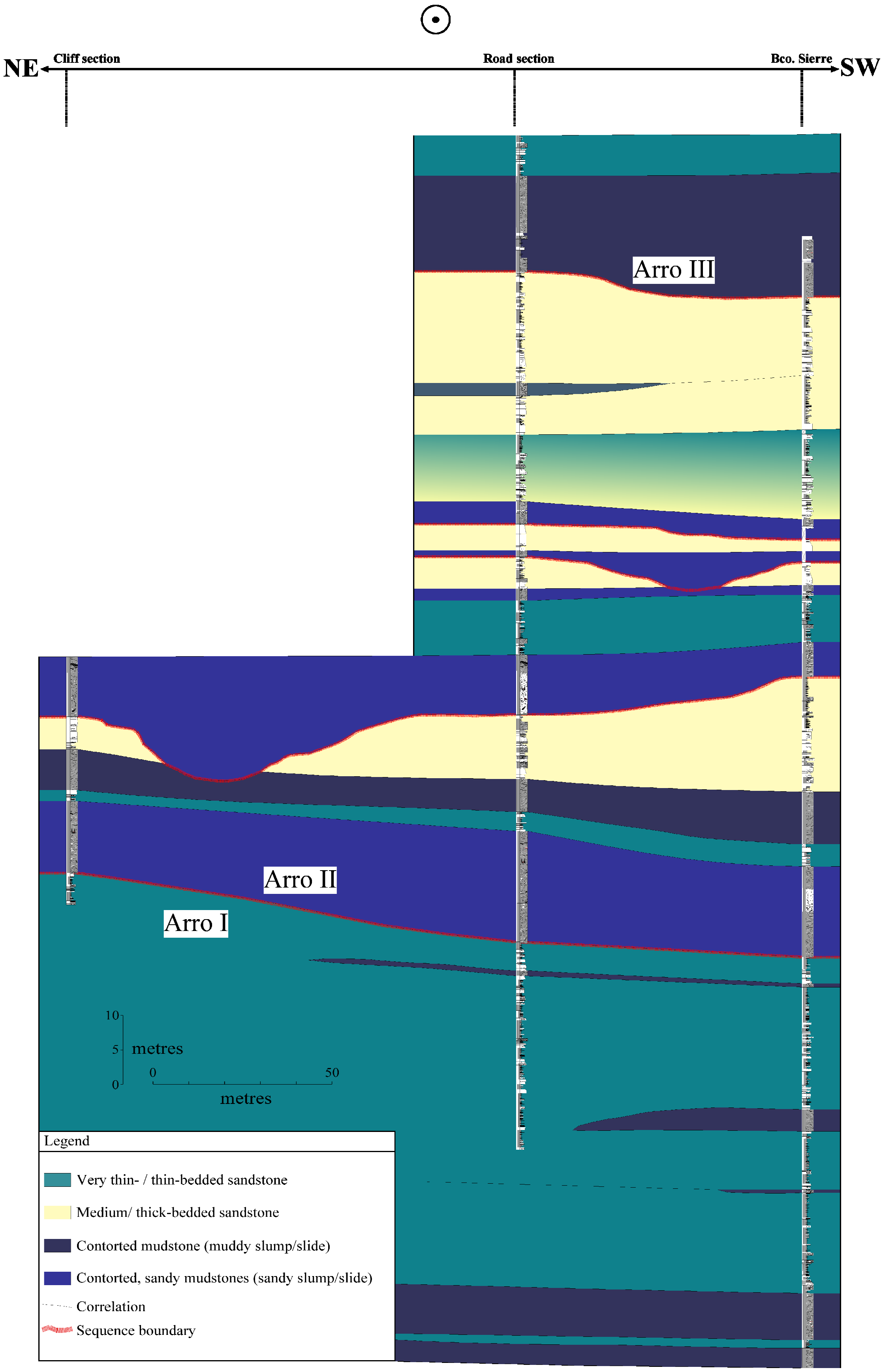

Fig. 4.10. Sectional correlation panel for the Arro sequences, labelled Arro I–III. Interpretation ties to Figures 4.8 and 4.9. Note the addition of sandy slumps (type Ib MTDs) towards the top of the system. See Figure B4 for detailed sedimentary logs.

4.4.4. INTERPRETATION

The study of Millington and Clark (1995a,b) concluded that the Arro system is a canyon-mouth sheet system. However, the various environments preserved in the Arro system represent an upper/mid-slope canyon to lower-slope channel system, composed of three sandy sequences. The sandy part of Arro I sequence at the Rio Nata outcrop indicates a proximal, canyon mouth setting comprising erosive, nummulitic-rich, thick-bedded sandstones, interbedded with slide and slump deposits (type Ia MTDs). This sandy package rapidly thins downslope to tabular, thin- to medium-bedded sandstones preserved in the Barranco Sierre outcrop, forming a thick heterolithic unit. This observed change in facies possibly marks a break in slope as density flows exited the confines of the canyon and underwent a hydraulic jump in response to changes in the slope gradient. The development of the Atiart thrust at that time (Munoz *et al.,* 1994) probably enhanced slope gradients and structurally controlled the position of the slope. The emplacement of this thrust was related to the development of the upper tectonic complex (see Section 1.6.4), involving the lateral expansions of the SCPU. The angular unconformity at the base of the Arro system thus suggests a tectonic-controlled setting. The abundance of erosive type Ib MTDs, particularly towards the base of the Arro II sequence, signifies a very mobile slope setting and probably reflects slope-oversteepening processes during tectonic activity. The MTDs were highly erosive and incorporated partially lithified sediment from the seafloor as disaggregated sandy rafts.

It can also be speculated that the deposition of the Arro system was contemporaneous with the early growth of the Los Molinos thrust and the Mediano detachment fold (see Fig. 4.7 for location), providing further structural control. However, although the development of the Mediano anticline initiated during the late Ypresian/early Lutetian (Bentham & Burbank, 1996, their fig. 19), prominent growth of the anticline did not commence until the middle Lutetian. Poblet *et al*. (1998) documented pre-tectonic strata of Ypresian age that showed no thickness changes across the structure; this is in agreement with observations made in this study, whereby no onlap patterns were observed in tectono-sequence sediment. Thus, the Mediano anticline did not form a significant seafloor high prior to this time, including during deposition of the Arro system.

It can be inferred that a major phase of tectonic uplift in the proximal parts of the South Pyrenean foreland basin reduced accommodation in the delta and shifted the depositional zone basinwards into the Ainsa basin. Intra-basinal tectonic activity (related to this major tectonic event) led to the collapse of the upper- to mid-slope and the subsequent formation of MTDs, which controlled the spatial location of the three sequences. The younger MTDs and sandstones (in the Arro II and III sequences) are rich in organic detritus, including wood fragments, suggesting a temporal increase in the influence of fluvio-deltaic sources, possibly suggesting progradation of the sedimentary system through time. There is also an overall trend of increasing confinement between the sequences in the Arro system, reflecting depositional confinement due to the topography created by the deposition of type Ia MTDs during thrust propagation. The paucity of pebble–cobble grade sediment throughout the Arro systems may indicate a lack of well-developed alluvial fans in the Tremp–Graus basin during this early phase of basin development. The upper section of the Arro system, in the Arro III sequence, is dominated by type Ia MTDs, which are interpreted as the final collapse and healing of the slope conduits marking the end of sedimentation in the system. The overlying finer-grained sandy sediment reflects waning tectonic activity and the deposition of low concentration turbidity currents during an abandonment phase when accommodation was probably restored in the delta area.

4.5. GERBE SYSTEM

4.5.1. INTRODUCTION

The Gerbe system marks the uppermost system of the Lower Hecho group, residing stratigraphically above the Arro system. A total of 300 m of section was measured over three locations (Localities 9, 10 and 11, Table 2.1). Figure 4.11 shows facies class abundance in the Gerbe system, presented by the total number of beds and total thickness measured. There are a large number of beds associated with facies class C and E, whereas facies class A and C represent the highest frequency of total thickness measured. The Gerbe system is composed of two sandy sequences, averaging 105 cm thick and characterised by gravels (facies A1.1-A1.3 and A2.1-2.3), pebbly sandstones and pebble-rich MTDs (type III, facies A1.1, A1.4).

4.5.2. SEDIMENTOLOGY

The Gerbe system (Fig. 4.12) is exposed southeast of Ainsa cropping out at Tozal de Charo (Locality 9, Table 2.1), along the Rio Nata and N-260 road section (Locality 10, Table 2.1), as well as to the north of Ainsa forming a ridge located around

San Vicente (Locality 11, Table 2.1). The total thickness of the Gerbe system is ~210 m. The lower sequence, Gerbe I, is ~60 m thick and represents a type I channel along Rio Nata; Gerbe II is ~150 m thick and is interpreted as a type II mixed channel cropping out at Gerbe and a type I channel cropping out at San Vicente (*sensu* Mutti & Normark, 1987).

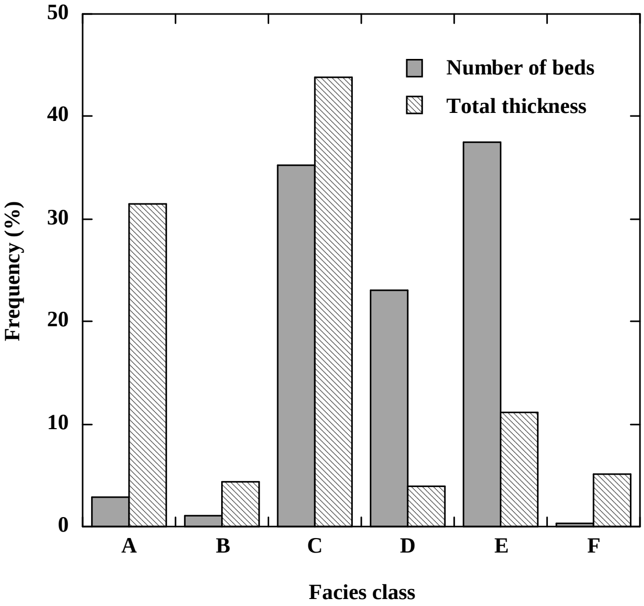

Fig. 4.11. Number of beds and total thickness by facies class for the Gerbe system.

The Gerbe canyon fill is located at Tozal de Charo and is defined at the base by intra-formational MTDs, overlying an angular unconformity formed as a result of a major phase of tectonic activity marking the onset of the Gerbe system (Millington & Clark, 1995b; Fig. B5). The basal surface cuts into the underlying fine-grained slope sediment forming a major erosional surface with several tens-of-metres of cut down. The canyon fill (Fig. 4.13) is characterised by localised, lens-shaped, sandy and muddy gravels (facies A1.1, A2.1 and A2.3) and pebble-rich, muddy MTDs (facies A1.2 and A1.3). Small channel elements <8 m thick may be developed between the MTDs. These sandbodies typically have erosive bases and are confined by the topography created by the underlying cohesive MTDs. The sandbodies are generally thin- to medium-bedded and fine- to medium-grained, abundant in extra-formational wood and coral fragments, *Nummulites* and well-rounded pebbles.

Figure 4.14 represents the exposed part of Gerbe I sequence along the Rio Nata/N-260 section. The outcrop is ~60 m thick and ~500 m wide. Three sections were

Fig. 4.12. Simplified geological map highlighting the position of the Gerbe system.

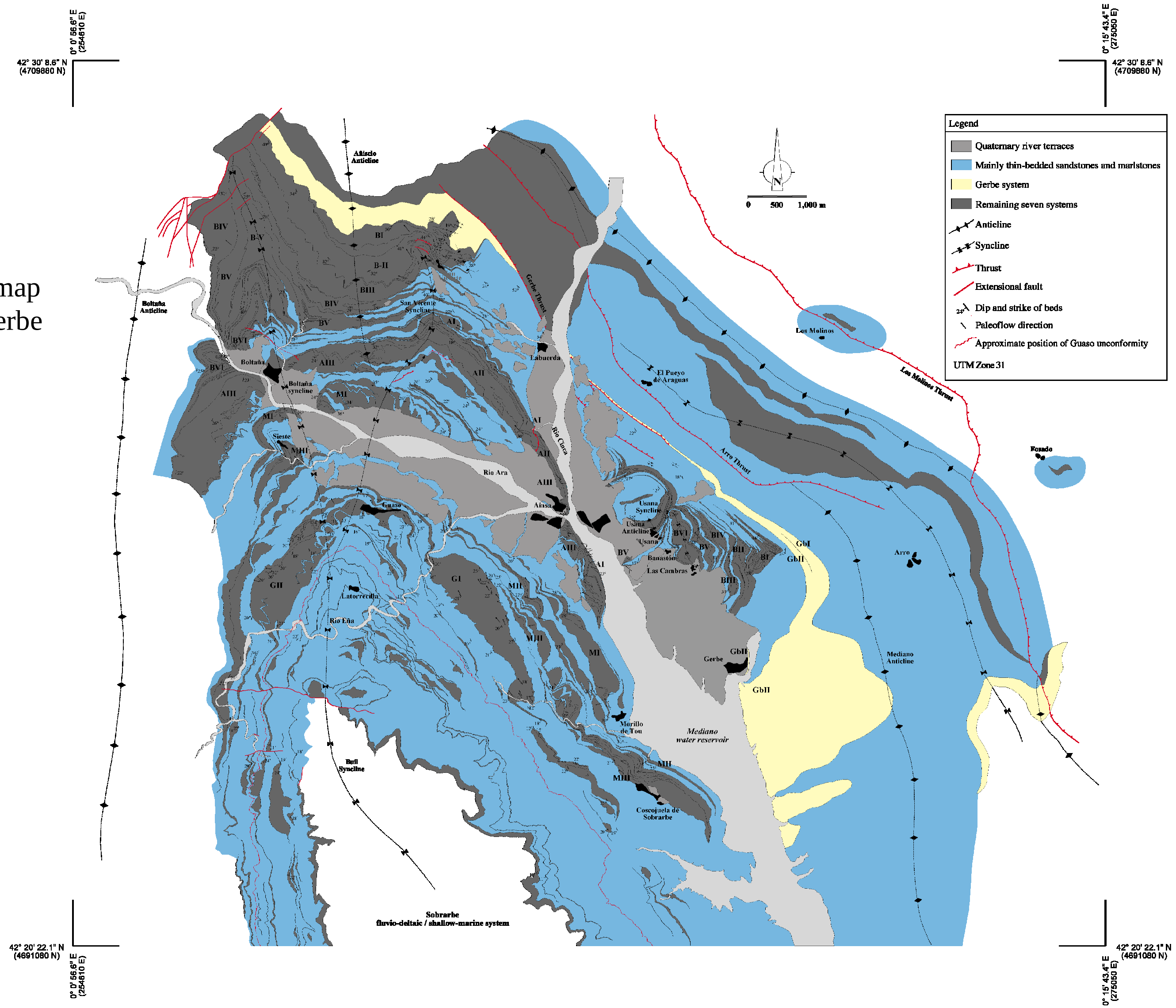

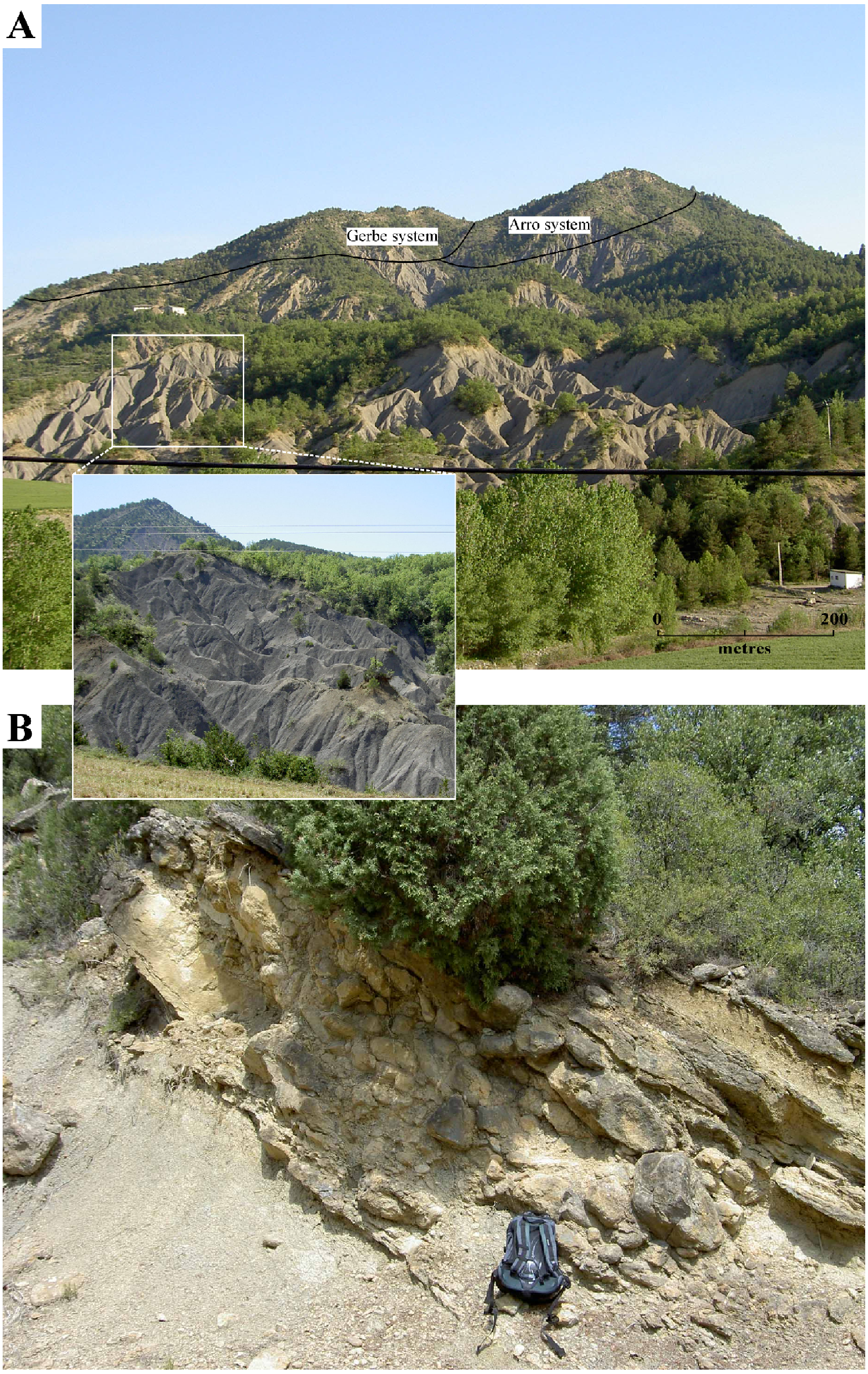

Fig. 4.13. (A) The Charo canyon showing the relationship between the Arro and Gerbe systems. Inset image is of the slope sediment (FA6) the canyon eroded into. (B) Representative facies of the Gerbe canyon fill (facies A1.1). See Fig. B5 for detailed sedimentary log through the Charo canyon.

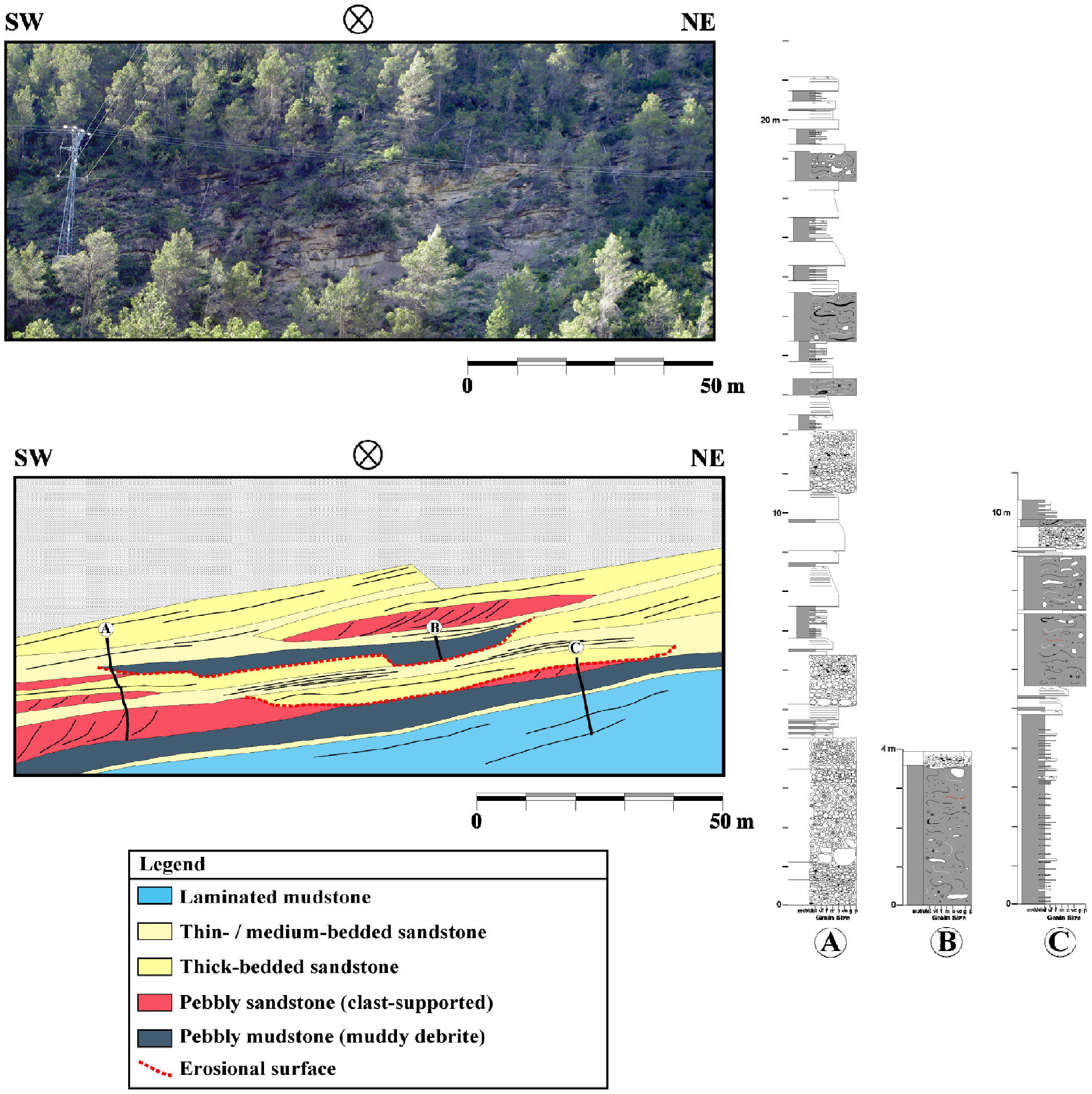

Fig. 4.14. Interpretation of the Rio Nata/N-260 section, showing the complex architecture and lenticular geometry of the lateral accretion barforms in the lower slope canyon-channel transition of the Gerbe I sequence. Accompanying sedimentary logs illustrate the overall fining upward trend. Note that the erosion surfaces are linked to both MTDs and thick-bedded sandstones.

measured at this outcrop. The base of the Gerbe system is defined by thin- to medium-bedded sandstones (~1 m thick) followed by mud-filled scours, laterally discontinuous, lens-shaped conglomerates and muddy debrites (FA1). Erosion occurs throughout and is related to thick-bedded sandstone and MTD deposition. In gravelly deposits, normal grading, stratification and inclined barforms typically exist (Fig. 4.15). The main

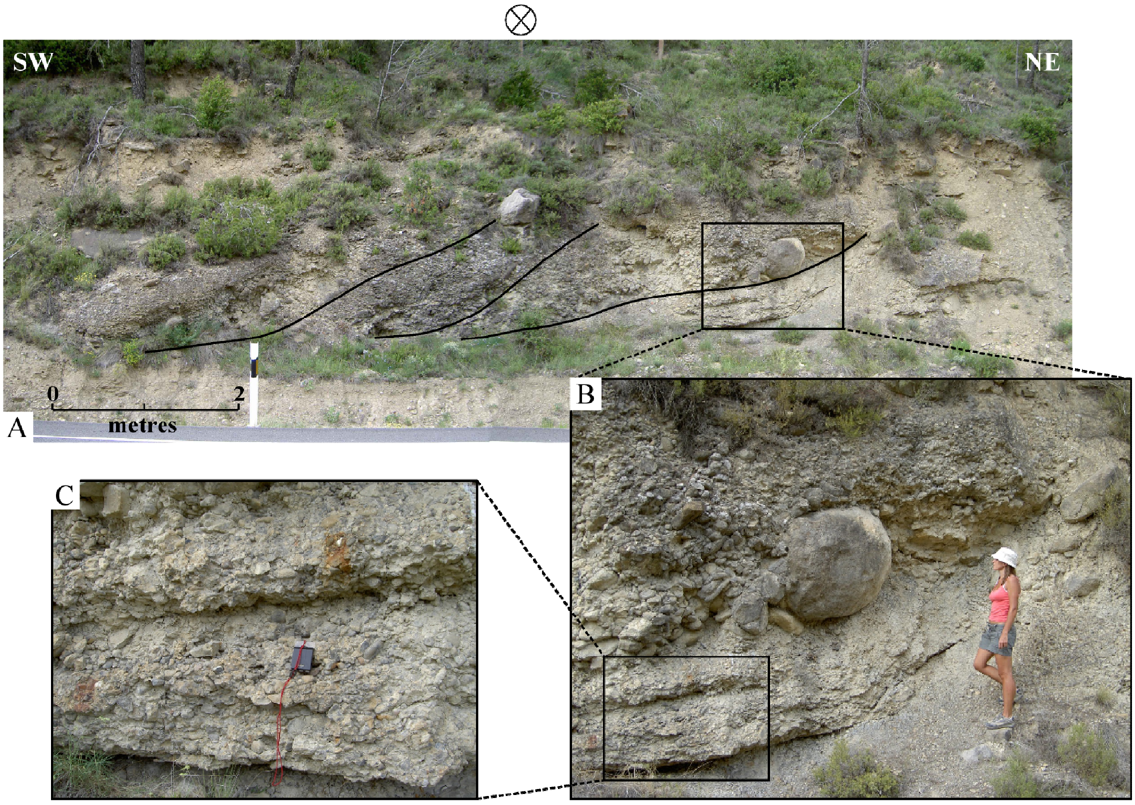

Fig. 4.15. Gravel bars in the lower-slope, erosional-channels, Gerbe I sequence, N-260 road section. (A) Gravel bar element with macro-scale lateral accretion surfaces, showing fining-up trends and some pebble imbrication. Inclined surface dip to the left of the photo (southwest). Mean palaeoflow is ~320°. (B) Disorganised gravel (facies A1.1). Large clast recording frictional freezing of the elutriated heads of hyperconcentrated flows. (C) Each laterally inclined package is defined by a fining-upwards sequence (facies A2.3).

sandbody is ~17 m thick and comprises a number of discrete, laterally offset stacked storey elements with a mean palaeoflow of ~315º. The base of each storey is characterised by discontinuous, clast-supported gravel or a type II MTD <2 m thick, overlain by thick-bedded amalgamated sandstones (facies C2.2) and thin-bedded sandstones (facies C2.4) forming a fining- and thinning-upward sequence <5 m thick. The gravel beds are often lens-shaped, laterally discontinuous with inclined surfaces. These deposits (facie A2.1) characterise the Gerbe I sequence and are interpreted as pebbly barform elements (Fig. 4.15). They range between 2–5 m thick, are laterally discontinuous over ~30 m. The deposits are clast-supported, normally graded and are typically imbricated. The dipping surfaces represent lateral accretion elements, orientated normal to the main palaeoflow, towards the southwest (mean palaeoflow is ~320°).

The Gerbe II sequence is exposed at Gerbe in the south and San Vicente in the north (see Fig. 4.12 for location). The southern outcrop is composed of a discrete sandy channel complex consisting of thin- to thick-bedded, fine- to coarse-grained, laterally continuous sandstones (FA2, FA3 and FA4). Alternatively, the northern outcrop is exposed in Barranco Pasata and is characterised by a similar facies association (FA1) as the Grebe I sequence (Fig. B6). The succession is represented by gravelly barforms interbedded with type II MTDs, typically ~2–3 m thick. The thicker MTDs mainly comprise clast-supported lower divisions and cohesive muddy upper divisions, forming bipartite deposits. Sandy packages consist of planar laminated, medium- to thick-bedded sandstones (facies C2.2 and C2.3) and thin sandy lenses (facies C2.4). A slight coarsening-upward sequence is observed towards the top of the section (Fig. B6).

4.5.3. Trace fossils in the Gerbe sequences

The lower-slope, channelised GI and GII sequences are characterised by a moderate diversity of trace fossils, including *Arenicolites, Ophiomorpha* (dwelling/*domichnial* traces), *Halopoa*, *Scolicia* (grazing/*pascichnial* traces), *Megagrapton* and *Paleodictyon* (traps and gardening/*agrichnial* traces). Among these ichnotaxa, *Arenicolites, Ophiomorpha, Halopoa* and *Scolicia* are post-depositional, representing opportunistic traces makers that excavated vertically into newly deposited sediment. *Megagrapton* and *Paleodictyon* are pre-depositional and formed within a more stable environment between the deposition of turbidites (Kern, 1980; Ekdale, 1985; Taylor *et al.,* 2003; Rodríguez-Tovar *et al.,* 2010). Figure 4.16 represents a typically trace fossil assemblage preserved on the sole of a bedding plane from a medium-bedded, coarse-grained sandstone bed in the GI sequence, showing the preservation of pre- and post-depositional trace fossils.

The highest abundance of trace fossils is found in the channelised sandy units of Gerbe I and Gerbe II sequences, where thin- to medium-bedded, medium- to coarse-grained sandstones prevail, i.e., above the lower gravel division. The occurrence of pre-depositional trace fossils in the depocentre of sequences suggests optimum conditions for more specialised organisms and a high preservation potential in the sandy divisions. The turbidity currents were less erosive than more concentrated density flows, thus providing a more stable environment on the seafloor for the preservation of shallow-tier structures (*sensu* Heard & Pickering, 2008). Sediment gravity flows passing through the axial parts of the channelised Gerbe I and Gerbe II sequences were responsible for the replenishment of organic matter and oxygen to the deep-marine environment, sustaining a diverse population of trace makers (Wilson *et al*., 1985; Wetzel & Uchman, 2001). However, the gravel-dominated lower divisions of the sequences are indicative of lower abundances of trace fossils and are predominated by a deep-tier, post-depositional trace-fossil suite (including, *Ophiomorpha*, *Halopoa* and *Scolicia*). The erosive capabilities of concentrated and hyperconcentrated flows eroded the top of the seafloor, removing the shallow-tier structures. Additionally, a gravelly sea floor would have been a deterrent to most trace-making organisms. The post-depositional ichnotaxa were formed by robust, deeply burrowing organisms that were adapted to surviving burial by the newly deposited sediment (Wetzel & Uchman, 2001).

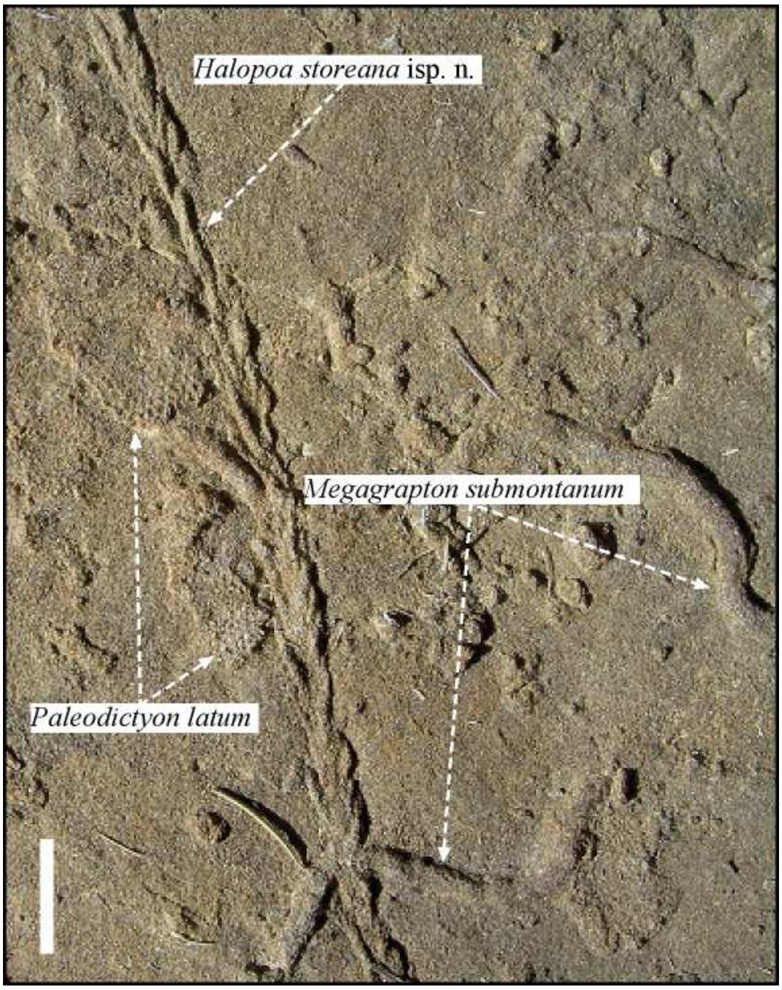

Fig. 4.16. Representative trace-fossil assemblage preserved on the sole of a bedding plane in a channel axis, GI sequence, Rio Nata. *Halopoa storeana* isp. n. (Uchman, 2001), hypichnial full-relief. See Uchman (2001) for discussion; *Megagrapton submontanum* (Azpeitia Moros, 1933), hypichnial semi-relief. See Uchman (1998) for discussion; *Paleodictyon latum* (Vialov & Golev, 1965), hypichnial semi-relief. See Uchman (1995) for discussion. Scale bar is 2 cm.

4.5.4. FIRMGROUND DEVELOPMENT IN GRAVELLY DEPOSITS

The gravel bars underlying the main sandy succession of the GI sequence in the lower-slope canyon-channel transition are abundant in *Arenicolites* burrows. The trace fossils commonly occur in concentrations at the base of disorganised gravel beds or within overlying medium-bedded, coarse-grained sandstones. Individual U-shaped burrow shafts are ~1 cm in diameter and up to ~50 cm long. Despite the abundance of this ichnotaxa, other vertical burrows, such as *Thalassinoides, Skolithos* and *Diplocraterion*, are rare.

Hubbard & Shultz (2008) documented a *Glossifungites* ichnofacies from Cretaceous strata of the Cerro Toro Formation in the Magallanes basin in Chile that represented a significant stratigraphic discontinuity within a debrite-dominated mass transport complex. The trace-fossil suite comprised *Skolithos*, *Diplocraterion* and *Arenicolites* ichnotaxa, which burrowed into a firmground following the exhumation of dewatered, consolidated sediment by erosive turbidity currents. A similar process and mechanism is proposed for the concentration of *Arenicolites* burrows in the GI sequence: an initial bypass phase characterised by erosive, concentrated and hyperconcentrated density flows defined the onset of sequence development, which exposed a diachronous, consolidated surface (but not necessarily a significant firmground) for colonization. Lag deposits (gravel bars), situated in the thalweg of the channel complex defined the stratigraphic horizon. The excavation of trace fossils into the media denotes a period of non-deposition and bypass in the open conduit prior to the deposition of the overlying sandy succession (interpreted as the filling phase). The burrowing organisms were mainly suspension-feeding annelids (Ekdale & Lewis, 1991), and were highly adapted to varying environmental conditions and fluctuating food availability (Cadée, 1984). During low sedimentation rates and the formation of a firm substrate, effective feeding strategies and quiescence on the seafloor enabled the organisms to thrive. The stratigraphic horizon is temporally significant in the evolution of a deep-marine sequence and delineates distinct phases in the formation of architectural elements, e.g., bypass and filling phases in channel fill elements.

4.5.5. INTERPRETATION

The Gerbe system comprises two sequences deposited in an upper/mid-slope canyon to lower-slope erosional channel setting. The abundance of type Ia and II MTDs in the canyon fill suggests mass wasting and collapse of the outer shelf and upper slope environments, excavating a large master surface to confine the Gerbe sequences at this proximal location. As a consequence, erosional confinement caused bypass and localised erosion, forming large scours that were infilled by pebbly lag deposits. The finer-grained sandy packages in the canyon probably represent the products of backfill in the final filling stages of channel elements or complexes.

The Gerbe I sequence at the Rio Nata/N-260 section can be interpreted as an erosional canyon-channel transition area, situated on the lower slope. It can be postulated that the sequence is confined within an irregular erosional surface created by an initial bypass phase prior to the infilling of the conduit. The highly heterogeneous fill containing stratified gravelly lags represent an erosive regime, indicating substantial sediment bypass. The Gerbe II sequence at Barranco Pasata has similar attributes and was deposited in a lower slope setting. These sequences can be related to major phases of tectonic activity causing an increase in slope gradients and the subsequent influx of sediment from the delta and slope environments. The high slope gradients encouraged erosion and the formation of barforms in high-energy braided environments. Nijman (1998) documented a high sedimentation rate at the onset of UM-A megasequence (interpreted as the proximal counterpart to the Gerbe system in this study), which would account for the supply of gravelly material into the basin during this time. This marks a peak supply of conglomerates into the basin and progradation of the depositional zone. This first significant volume of gravelly sediments to enter the Ainsa basin can be attributed to intense tectonic activity and the subsequent increase in sediment supply from the hinterland via alluvial fans. The Gerbe system, therefore, represents a transitional tectonic regime, marking the onset of significant basin reorganisation and the end of tectonic phase I. The Gerbe II sequence at Gerbe village possibly represents a backfilling sequence, migrating upslope during the final stages of sedimentation during a phase of tectonic waning, involving a reduction in sediment supply to deep water.

CHAPTER 5

UPPER HECHO GROUP: BANASTÓN SYSTEM

5.1. INTRODUCTION

This chapter documents a rare example of deep-marine siliciclastic environments associated with a lower-slope canyon-channel transition to proximal basin-floor channel system. The Banastón system defines the base of the Upper Hecho Group and represents a major phase of basin reorganisation (Remacha *et al.*, 2003; 2005). The system preserves six lower-slope, erosional canyon-channel fills that correlate with six associated proximal basin-floor, laterally offset-stacked low-sinuosity, channel-overbank complexes (designated BI–BVI). Detailed mapping, sedimentary logging and palaeocurrent measurements leads to both: (1) the documentation of the transition from erosional lower-slope to proximal basin-floor environments; (2) the development of a new depositional model for low-sinuosity, coarse-grained, erosional-depositional, channel-overbank systems. The Banastón system has received relatively little attention in literature, partly because of poor exposures in the type area (around the villages of Banastón, Usana and San Vicente; Fig. 5.1), although there are excellent outcrops several km away from vehicle access. In addition, new major road cuttings immediately north of Boltaña have afforded unprecedented sections through many tens-of-metres of the system. A brief overview of the Ainsa system follows the description and interpretation of the Banastón system.

5.2. SYSTEM OVERVIEW

Mapping of the Banastón system at a scale of 1:20,000, by combining outcrop mapping, aerial photo interpretation, and logging (Fig. 5.1), has led to a significant understanding of the distribution of sediment facies, depositional architecture, and evolution of this system. A very wide range of sediment facies is recognised in the Banastón system, particularly facies class A, C, D and E (Fig. 5.2). Facies class C, D and E represent the greatest number of beds measured, whereas facies class A and C represent the highest total thickness of all beds measured. Figure 5.3 shows the dimensions of various channelised hierarchical elements in the Banastón system. The

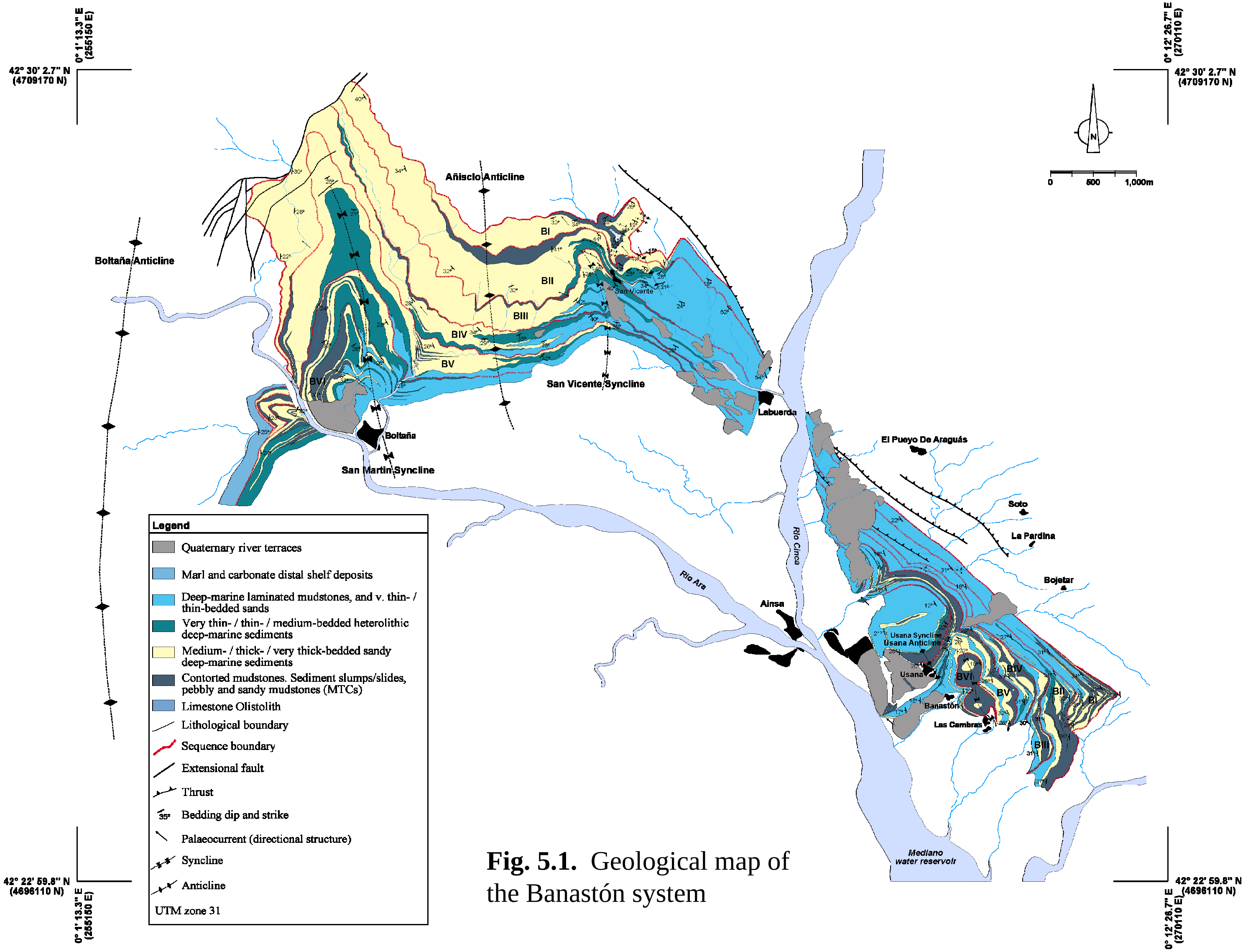

Fig. 5.1. Geological map of the Banastón system

six sequences form the largest depositional bodies in the system and contain the lowest aspect ratio, whilst storeys form the smallest depositional bodies and have the highest aspect ratio.

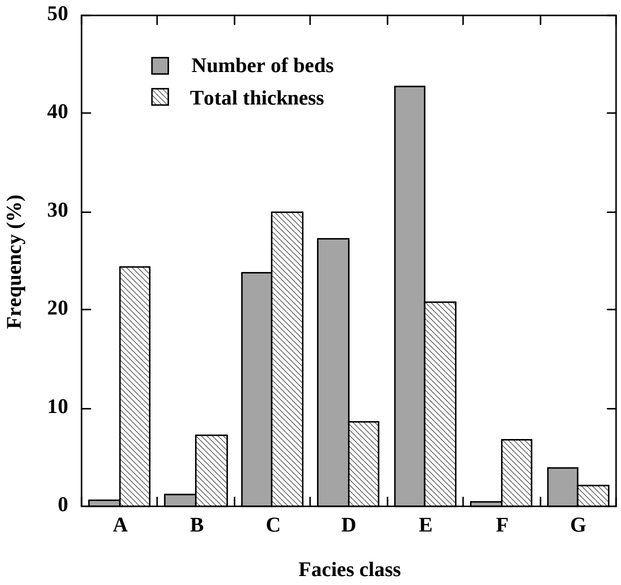

Fig. 5.2. Facies class abundance in the Banastón system.

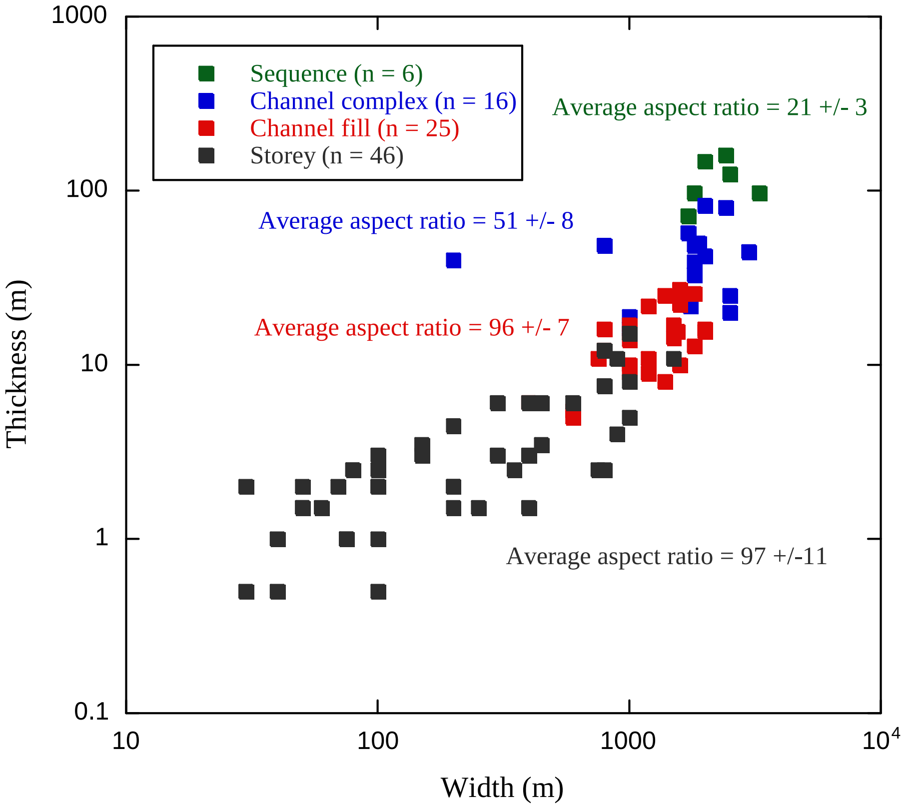

Fig. 5.3. Hierarchical element dimensions in the Banastón system.

The six depositional sequences comprising the Banastón system are persevered in both the Banastón-Usana and San Vicente-Boltaña areas. These sequences are grouped into two stages (stage I and stage II), which will be discussed below. The cumulative thickness of the Banastón system ranges from ~510 m in the Banastón-Usana area, to ~700 m in the San Vicente-Boltaña area. Sequences are recognised by a combination of: (1) a mappable erosional base, usually overlain by (2) a MTC (typically comprising type II MTDs), then (3) a package of sands and/or heterolithics, with (4) a subtle, lateral displacement in the depositional axis for the succeeding sequence in the Boltaña-Usana area and (5) a significant WSW shift in the depositional axis for the succeeding sequence, in the Boltaña-San Vicente area. The general characteristics of each sequence in the Banastón system are outlined in Table 5.1.

The early stages of the Banastón sequences are associated with aerially extensive and thick MTCs, which are generally composed of type II MTDs. These deposits mainly comprise contorted mudstones with local sandy lenses and pebble horizons. Erosion at the base of these deposits occurs on a scale of tens-of-metres. Sand rafts ranging from metres to hundreds of metres in scale occur within the contorted muds. The first sands overlying the basal MTCs typically occur as thick-bedded, granule- to very coarse-grained sandstone turbidite beds (facies class A, B). Locally, small sub-rounded pebbles are present in the lower beds.

In the Banastón sequences, most beds are thick- to medium-bedded, coarse- to medium-grained, amalgamated beds (facies class B, C). Some of the Banastón sequences show an overall fining upward trend (e.g., Banastón II, III, IV and V).

Measurements of the sole structures, cross-stratification and current ripples in the San Vicente-Boltaña area generally show palaeoflow towards the north-northwest, with relatively little dispersion (~320º) in the Banastón I to III sequences (Fig. 5.4). The youngest two sequences (Banastón BV and VI) show more dispersion in the outcrops north of Boltaña, although they represent a more westerly component overall. However, in the Banastón-Usana area, palaeocurrents from the Banastón I to III sequences, where considerably fewer palaeocurrents could be measured, have the greatest dispersion, but suggest a more westerly component (~290º), overall. Palaeocurrent readings from Banastón IV to VI sequences in this area are more consistent, towards ~315º. This pattern of palaeoflow reflects the two depositional stages in the Banastón system (discussed in more detail below).

Sequence		**BI**	**BII**	**BIII**	**BIV**	**BV**	**BVI**
Dimension	Thickness (m)	98	149	72	124	97	160
	Width (m)	1800	200	1700	2500	3300	2400
	Aspect ratio (W/D)	18.4	13.4	23.6	20.2	34	15
Number of beds measured	Total number	407	3541	1836	2834	1475	1451
	Total thickness	98	232	123	187	195	259
	% amalgamated	12	3	2	5	7	6
Bed thickness (cm)	Average	24	7	7	8	13	18
	S.D.	177	33	34	19	60	94
	Min/Max	1/3460	1/1100	1/1020	1/510	1/1290	1/1620
Basal MTC (m)	Thickness	42	24	19	12	33	40
	Width	800	1500	1000	1000	1800	1800
	Aspect ratio (W/D)	19.0	62.5	52.6	83.3	54.54	45
Facies class abundance (%)	Class A	3.4	0.7	0.6	1.2	3.1	2.5
	Class B	8.4	1.5	1.7	4.2	4.7	3.7
	Class C	29.7	26.4	35.2	31.9	32.9	31.4
	Class D	12.8	23.4	20.2	25.8	23.5	17.1
	Class E	44.0	47.6	42.0	36.5	35.4	45.1
	Class F	1.7	0.4	0.3	0.5	0.5	0.3
	Class G	0.0	0.0	0.0	0.0	0.0	0.0
	Class H	0.0	0.0	0.0	0.0	0.0	0.0

Table 5.1. General characteristics of each sequence in the Banastón system

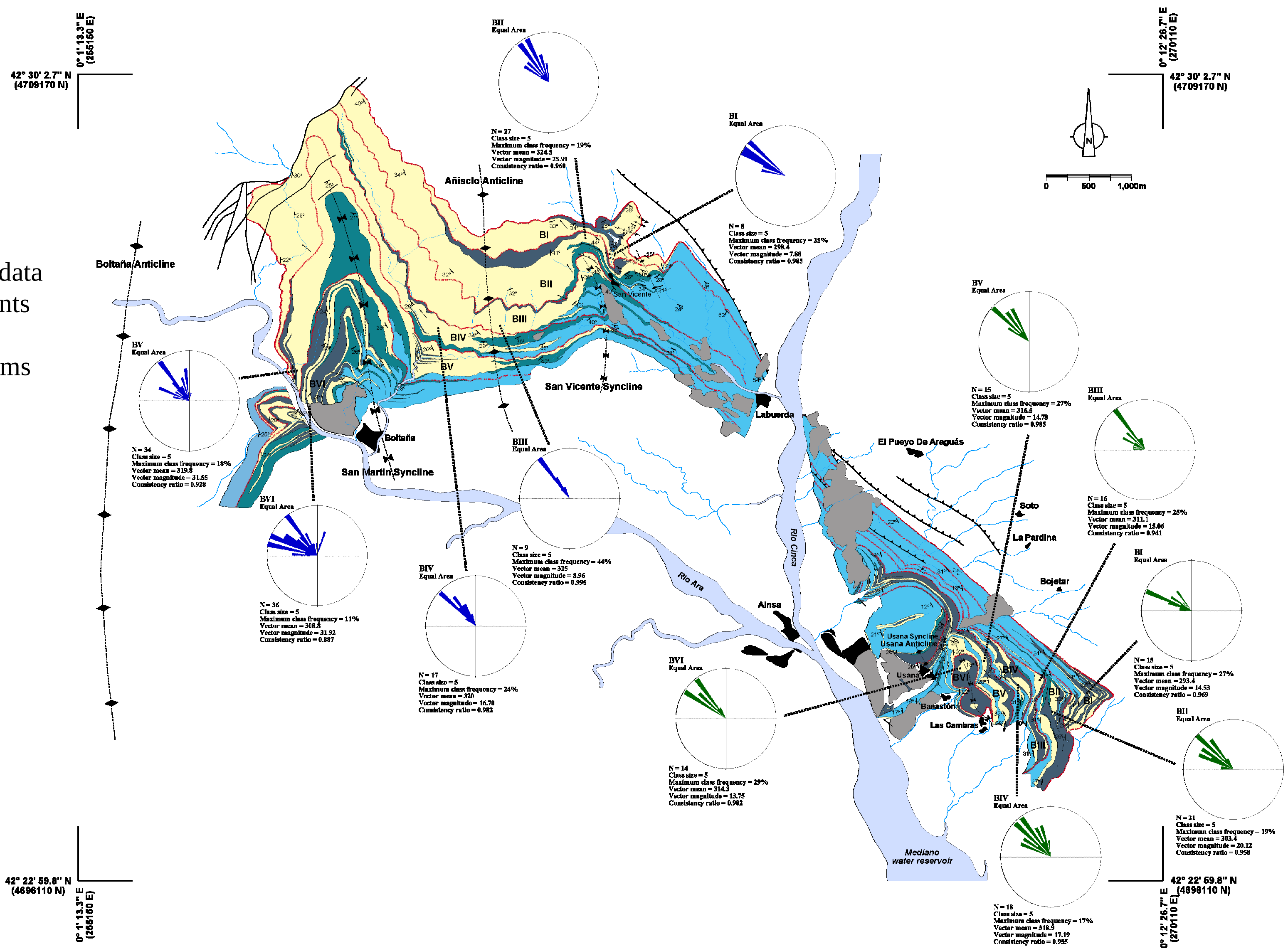

Fig. 5.4. Palaeocurrent data from various environments in the Banastón system, illustrated in rose diagrams

5.3. LOWER-SLOPE TO PROXIMAL BASIN-FLOOR TRANSITION

5.3.1. STAGE I

The base of the Banastón system, the Banastón I sequence, is associated with ~165 m of erosion into the underlying thin-bedded sandstones and laminated mudstones of the Gerbe system; at outcrop level, this feature is expressed as a major v-shaped erosional cut, ~730 m wide. A ~25 m thick type I MTD immediately overlies this surface, representing the initial deposition within the Banastón I sequence. The MTD is characterised by an abundance of contorted, intraformational sediment reworked from the underlying system and subsequently incorporated into the muddy matrix (facies F2). A few nummulitic limestone clasts are also commonly found within the deposit. Although type I MTDs are found within the remaining fill, aerially extensive type II MTDs predominate the sequence. The MTCs are typically a few tens-of-metres thick, containing a mixture of both extraformational and intraformational components within a sandy mudstone matrix. Sub angular carbonate clasts, plant material, remobilised shelfal fauna and sub-rounded pebbles are all common constituents. Localised sandy conglomerate and gravel horizons (facies class A) occur within the MTC, but more distinctively, sandbodies, typically < 8 m thick, overlie each successive complex. Each sandbody consists of thick-bedded, coarse-grained amalgamated sandstones (facies class B), commonly interbedded with thin debris-flow deposits. The base of each sandstone bed is characteristically uneven, with common flute and load cast structures. Deposition of the underlying MTDs caused the partial confinement of each sandbody. Large limestone olistolith blocks are found scattered throughout the entire sequence; the largest measuring 15 m x 7 m x 3 m, and it is located mid-sequence within the upper surface of an inversely graded, pebbly type II MTD. The upper part of the Banastón I sequence is associated with an increase in the volume of extraformational material (such as sub-rounded pebbles, coral fragments and reworked nummulites) found within the type II MTDs, and an increase in the thickness and lateral continuity of the succeeding sandbodies. Figure 5.5 outlines the representative facies in the canyon-channel transition during stage I of deposition.

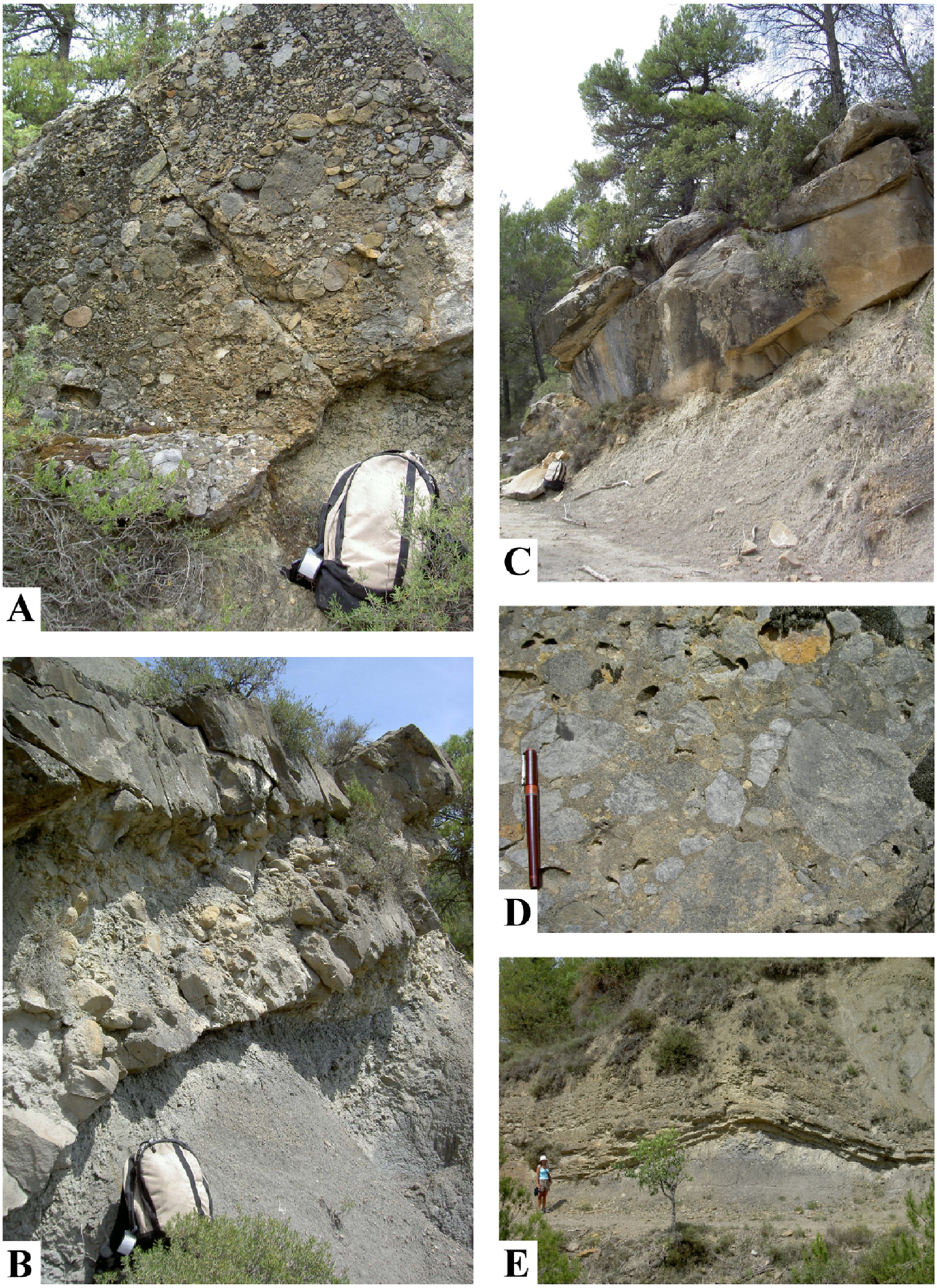

Fig. 5.5. Representative facies in the canyon-channel transition area during stage I of deposition in the Banastón system. (A) Crudely stratified, clast-supported gravel bed (facies A2.1) situated within the MTC defining the base of the BI sequence, east of Las Cambras. The gravel bed has a lens-shaped geometry and pinches out laterally over a distance of ~50 m in both directions. (B) Discontinuous, thin channelised element situated within the MTC defining the base of Banastón II sequence, Betato ridge. Note the predominance of carbonate clasts in the MTD (facies A1.2). (C) Carbonate

olistolith, Banastón I sequence, east of Las Cambras. (D) Angular carbonate clasts in disorganised pebbly sandstone (facies A1.4), Banastón II sequence, Betato ridge. (E) Deformed channel element hydraulically incorporated into a thick MTD as a large sand raft, Banastón III sequence, east of Las Cambras.

The lower boundary of the Banastón system is also observed within the San Vicente-Boltaña area in the northernmost outcrops, immediately north of the village of San Vicente (Fig. C1). The basal surface marks ~55 m of erosion (negative relief) into the underlying Gerbe system with an erosional width of ~1230 m. Within this area, the Banastón I sequence has a cumulative thickness of ~218 m and is predominantly characterised by facies class A and B deposits, with type II MTDs becoming more volumetrically significant towards the upper part of the section. The conglomerates and gravels are typically matrix-supported, normally-graded, with some parallel stratification. Erosive bases with incorporated mud clasts are a common feature. The type II MTDs contain a high proportion of reworked carbonate and sandstone clasts, which mainly occur at the base of the muddy complexes to form bipartite deposits. This is probably the result of eroding upstream Cretaceous-Paleogene carbonate platforms that were exposed through thrusting of the lateral ramp zone of the SCPU over the eastern margin of the deep-marine Ainsa basin.

A ~15 m thick, muddy type I MTD, containing an abundance of sandstone clasts, divides the lower part of the Banastón I sequence from the remaining Cortaroles river section outcrop, adjacent to the town of San Vicente. This area is characterised by stratified, thick-bedded, coarse-grained sandstones (facies class B2), which can be arranged into ~8 m thick, amalgamated units. The bases of individual beds are commonly irregular with flute clasts and outsized scattered pebbles. The beds are generally well-graded, stratified and commonly show current ripples. The bases of the units are defined by a muddy type II MTD, typically showing a few tens of centimetres of erosion throughout the extent of the outcrop. The top of the Banastón I sequence does not show a thinning- or fining-up sequence, but there is a general increase in sandstone-mudstone couplets (facies class C).

Within the Banastón-Usana area, the onset of the Banastón II sequence marks a significant erosional cut into the underlying Gerbe system in addition to the partial truncation of the Banastón I sequence to the south (Fig.5.6).

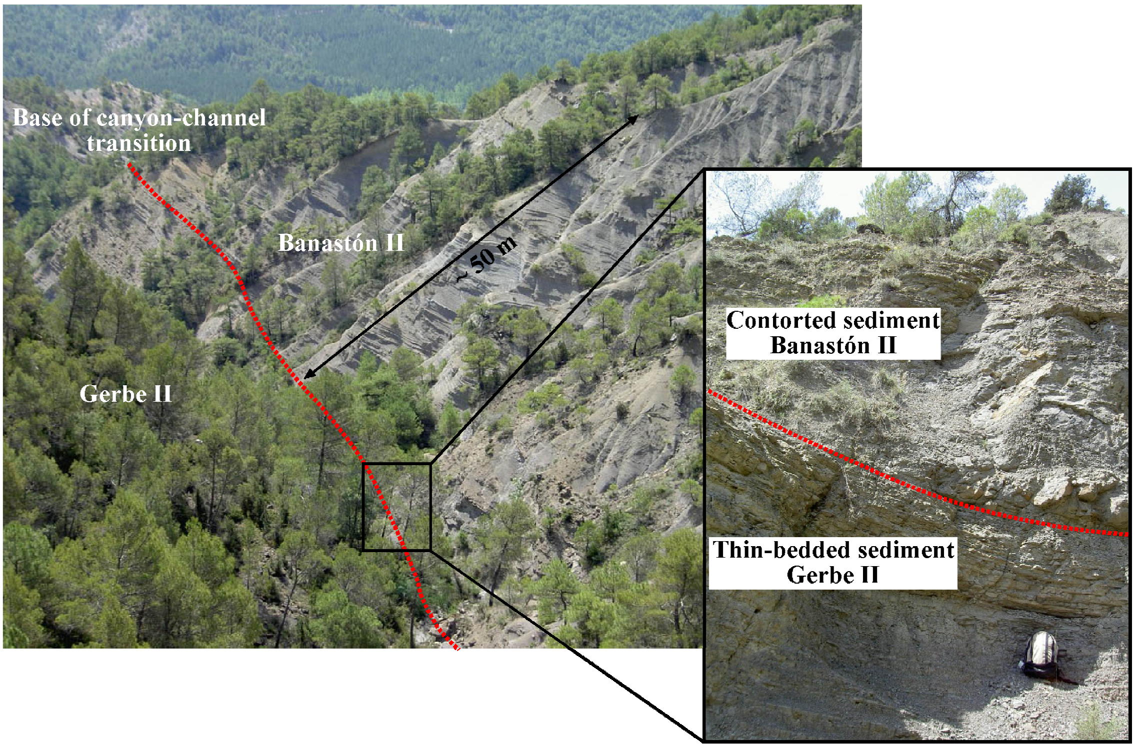

Fig. 5.6. Southern extension of the base of the canyon-channel transition area, showing cutdown into the Gerbe system (~170 m in total), Banastón II sequence, Betato ridge. The erosional processes generated the MTDs by incoporating the eroded material from the underlying sequence (Gerbe II). The cutdown even represents a major phase of tectonic activity causing collapse of shelf and slope region.

The maximum width of the sequence in outcrop is ~1,360 m, with a cumulative thickness of ~95 m. A localised, ~15 m thick type I MTD defines the base, which consists of mainly folded, attenuated and partially disaggregated thin-bedded sandstones and mudstones. An aerially extensive ~70 m thick MTC overlies this deposit. The MTC is characterised by an abundance of fossiliferous material, including shallow-marine shells, coral fragments and reworked nummulites. The matrix is predominantly mudstone, with only localised sandy lenses. A number of discrete matrix- and clast-supported gravel beds (facies class A) punctuate this complex and create local scour depressions, into which they fill. These deposits are laterally irregular and predominantly consist of sub-angular to sub-rounded limestone clasts within a sandy mudstone matrix. Thick-bedded, coarse-grained sandstones are also associated with these deposits, commonly containing flute and load casts at their bases. Limestone olistolith blocks are common throughout, the largest being situated within the upper parts of the ~70 m thick MTC. The upper extent of the Banastón II sequence typically consists of thick- to medium-bedded, coarse-grained sandstones (facies class B), with abundant sole structures, namely groove and tool casts. The overlying fill of the sequence is characterised by very thin-bedded, medium-grained sandstones, interbedded with mudstones (facies class C).

The base of the Banastón II sequence within the Boltaña -San Vicente area is similarly associated with substantial cut-down, although less pronounced to that observed within the outcrops in the Banastón-Usana area. A 15 m thick pebbly MTC defines the base of the erosional surface, and consists of large folded and disaggregated sandstone beds, and thin pebble horizons (Fig. 5.7). The overlying sandy succession predominantly consists of coarse-grained, well-stratified, medium- to thin-bedded sandstones of mainly facies class C (Fig. C2). At the very top of the sequence is a discrete channel complex ~40 m thick, comprised of a number of small channels. The individual channels are ~5 m thick, defined at the base by type II MTCs and overlain by medium-bedded, medium- to coarse-grained sandstones (facies class C).

A correlation panel of the Banastón I and II sequences in the San Vicente outcrops is illustrated in Figure 5.8. The base of each sequence depocentre is characterised by a MTC overlain by a mixed sandstones-MTD succession, which thins laterally in channel margin elements and overbank deposits.

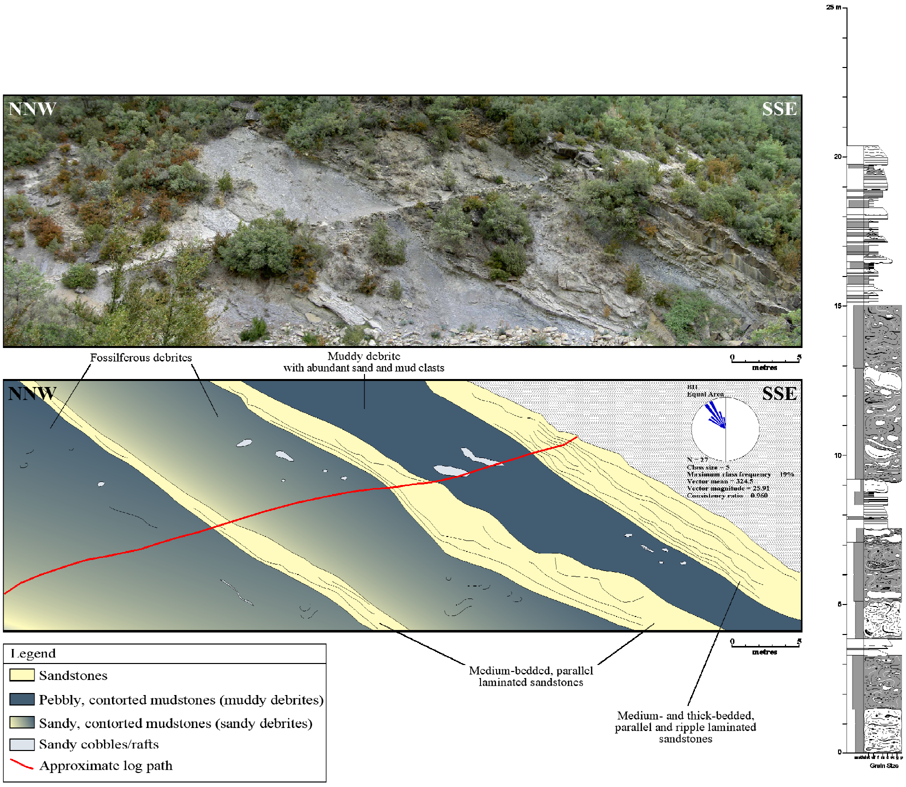

Fig. 5.7. MTC composed of three MTDs (debrites), defining the base of the Banastón II sequence, Barranco Cortaroles, San Vicente. The basal two debrites are products of

highly erosive flows, which eroded sandy material from the seafloor and incorporated the sediment into the flow (refer to Fig. C2 for detailed sedimentary logs).

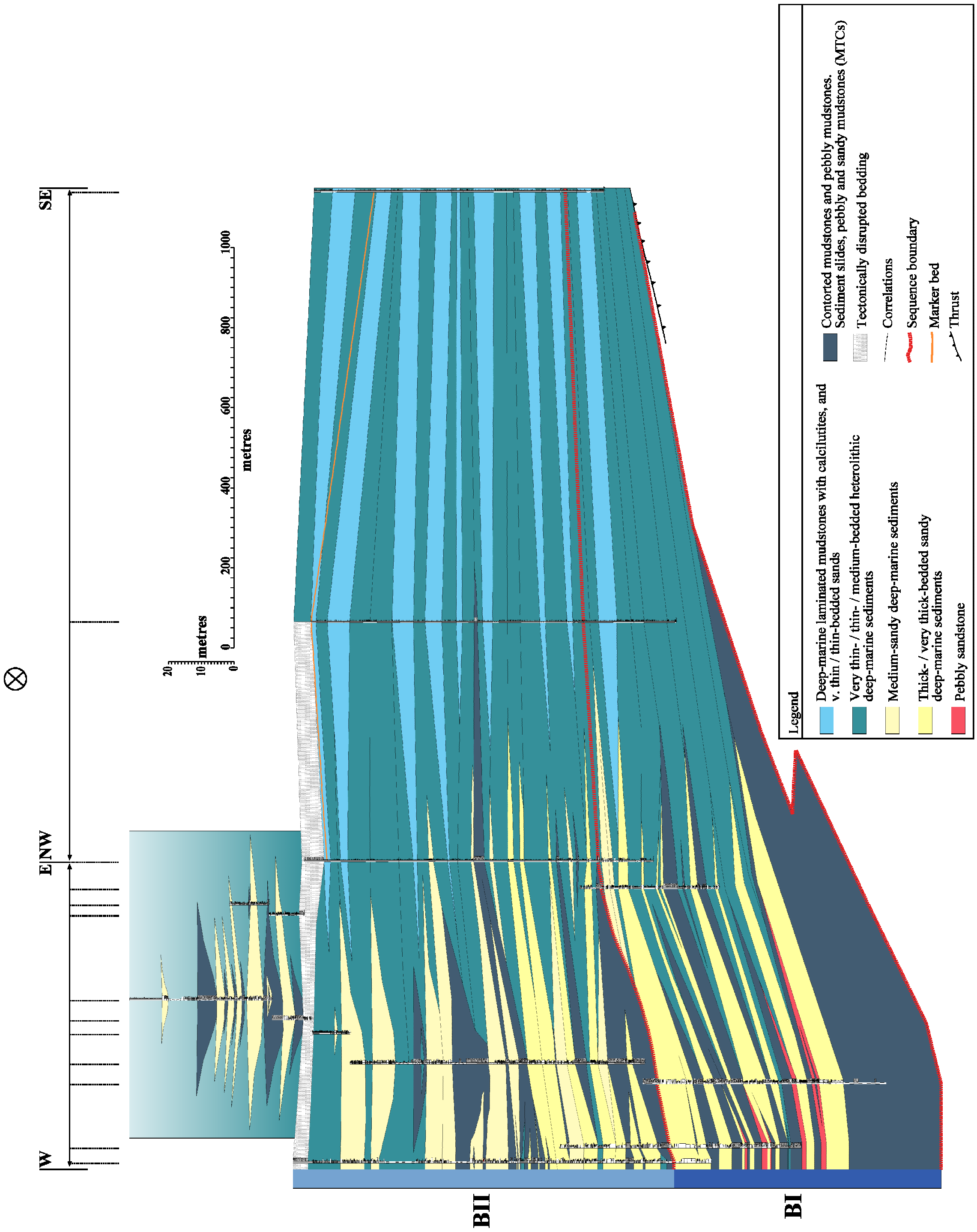

Fig. 5.8. Sectional correlation panel of the Banastón I and II sequences, San Vicente area. See Figures C1 and C2 for detailed sedimentary logs.

The Banastón III sequence is ~55 m thick and ~1,270 m wide within the area of Banastón-Usana. The base is defined by a ~35 m thick lower chaotic unit composed of type II MTDs that are interbedded with dispersed, mainly medium-bedded, disorganised pebbly to coarse-grained sandstones (facies class A and B1). The conglomerates and gravel are predominantly matrix-supported, highly fossiliferous and laterally discontinuous. Erosive beds with sole structures are common. The upper part of the sequence is typically characterised by very thin-bedded, fine-grained sandstones interbedded with siltstones and mudstones (facies class C and D).

The Boltaña -San Vicente area exposes a ~77 m thick section of the Banastón III sequence located mid-ridge between the town of Boltaña and the village of San Vicente (Fig. C3). The base is defined by a ~19 m thick, highly fossiliferous MTC with an abundance of sandstone clasts (Fig. 5.9). The sandstones, which overlie the MTC, are typically medium-bedded, well stratified and coarse- to medium-grained (facies class C). Cross-stratification and current ripples are a common feature of the sandstones, particularly in the off-axis outcrops around the village of San Vicente. The upper part of

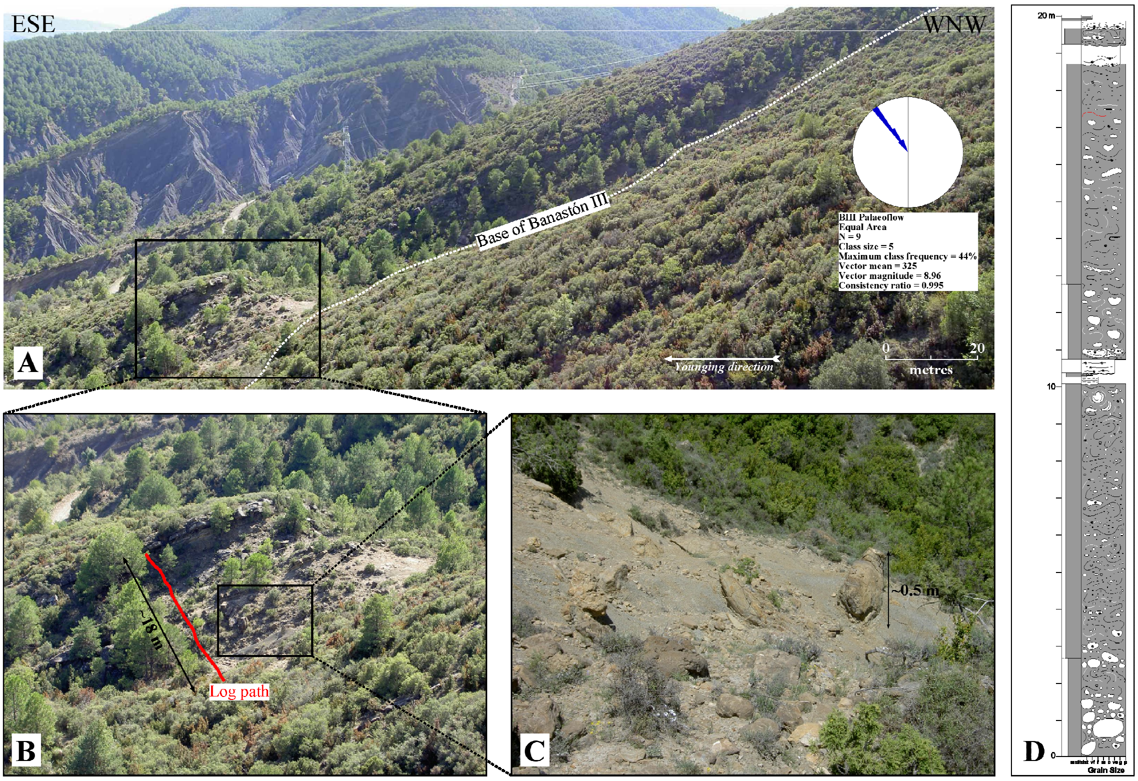

Fig. 5.9. MTC defining the base of the Banastón III sequence, San Miguel ridge, San Vicente. (A) View of the base of the system. Note the ridge forming sany succession overlying the MTC. (B) Detailed view of the MTC, comprising two MTDs separated by thin-bedded, nummulitic sandstones. Red line marks the path of sedimenetary log in (D). (C) Detailed view of the cohesive, muddy matrix of the MTC. (D) Sedimentary log through the MTC (See Fig. C3).

Banastón III sequence contains a well-developed thinning- and fining-upward sequence (facies class C and D), occasionally interrupted by type II MTCs, typically <3 m thick, showing only a small amount of erosion at their bases.

5.3.2. STAGE II

The Banastón IV sequence crops out as a relatively discrete unit ~55 m thick and ~1000 m wide to the east of Banastón village. The base is characterised by a local ~10 m thick, entirely intraformational type I MTD, composed of contorted mudstones and a few attenuated sandstones. The overlying sediment typically comprises type II MTDs and medium- to thin-bedded, gravel- to very coarse-grained, nummulitic sandstones (facies class A and B). The sandstones are predominantly well stratified and normally graded; the gravels are generally matrix-supported with areas of higher clast concentration (facies class A2 and B2). Bed contacts are highly irregular and local cut-down is a common feature. The top of the Banastón IV sequence is characterised by a rapid facies change with an increase in thin-bedded, medium- to fine-grained sandstones, interbedded with silty mudstones (facies class C and D).

The Banastón IV sequence also outcrops in the western region of the Boltaña - San Vicente area. It has a cumulative thickness of ~97 m and ~62 m within the San Martin River section and the Boltaña road section, respectively. Within the river section (Fig. C4), the base is defined by a ~8 m thick muddy type II MTD. An extensive outcrop of thick-bedded, very coarse- to coarse-grained sandstones overlies the MTC (facies class B and C). The sandstones are generally well stratified and show current ripples; the bases are flat and regular, with only localised undulation. The top of the sequence is marked by an increase in mudstone proportion preserved between the sandstone beds, and the decrease in the average bed thickness of the sandy component. The Boltaña road section is characterised by a different facies pattern, with only a very small, <2 m thick, type II MTDs defining the base. There is no evidence for any vertical trends, with medium-bedded, gravel and very-coarse grained sandstones predominating throughout. Small, erosive MTds act to confine the sandstones and form depressions in which the next bed infills (Fig. 5.10). The sandstones locally scour the underlying MTCs and contribute to the irregularity of bedding style observed at this locality.

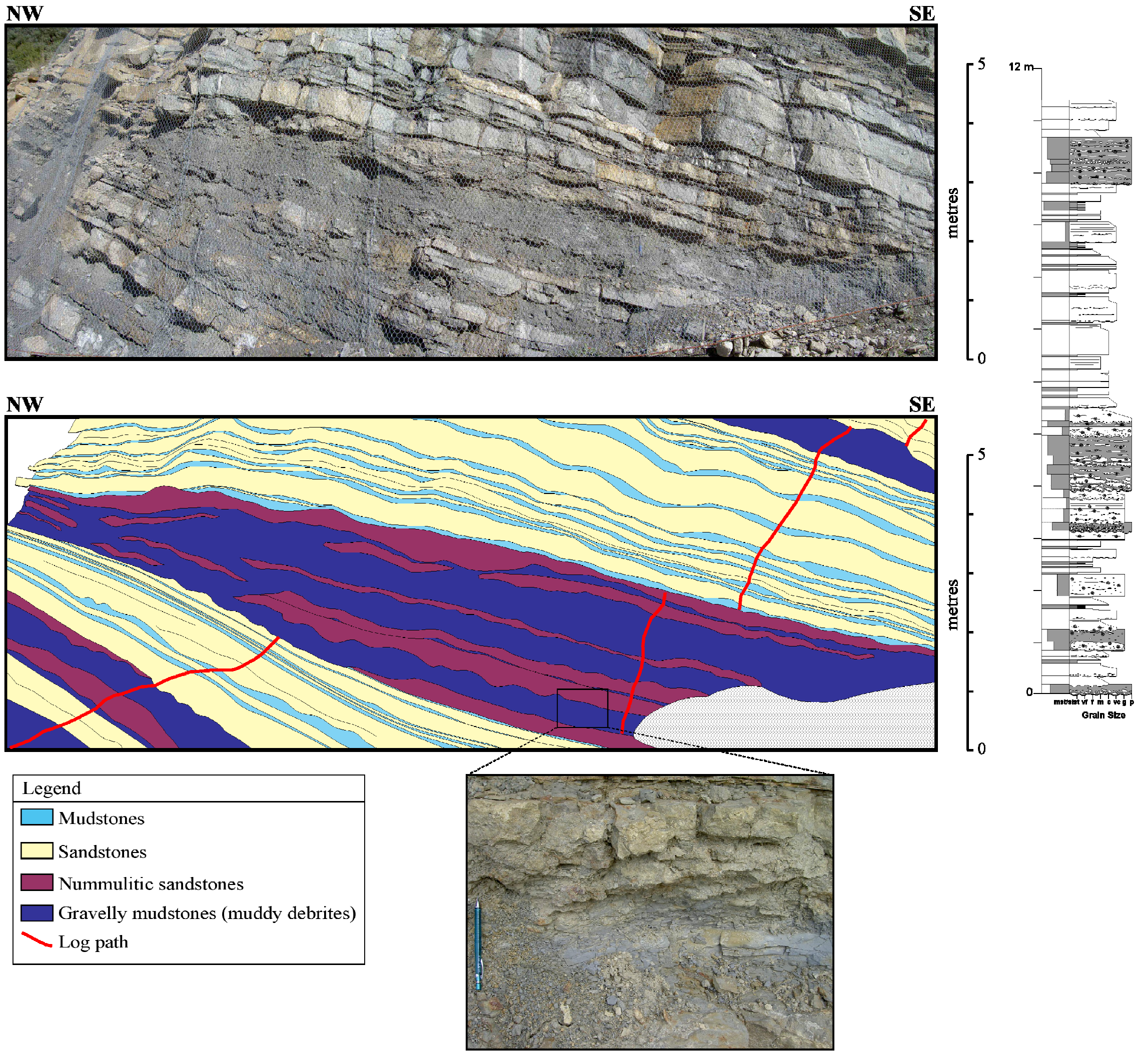

Fig. 5.10. Base of Banastón IV sequence showing the relationship between nummulitic sandstones and gravelly mudstones (inset photo), N-260 road section, north of Boltaña . Debrites locally erode into the underlying sediment and sandstones infill the irregular surface created by the MTDs. This locality represents a slight off-axis environment, which explains the laterally continuity at a bed scale. Deposition of highly nummulitic, carbonate-rich sediment indicates the occurence of substantial erosion into the flanks of the growing intrabasinal high, Boltaña anticline, in the west.

The Banastón V sequence forms an extensive outcrop ~150 m thick and ~1,500 m wide in the Banastón-Usana area. The base is defined by a ~60 m thick, intraformational MTC, containing large, highly contorted and folded sandstone rafts (facies F2). Abundant redeposited shelfal fauna, including coral and oyster fragments, are incorporated into sandy lenses within the mudstone matrix. There is a significant absence of pebbles; however, highly discontinuous gravel horizons (facies class A) punctuate the complex. These horizons consist of sub-angular limestone clasts disorganised within a mudstone matrix. The upper extent of the MTC is characterised by an increase in displaced shelfal fauna, plant material and aligned sand rafts. A limestone olistolith is also present, measuring 7 m by 4 m by 3 m. Laterally extensive sandstone units appear towards the very top part of the MTC and characterise the upper part of the Banastón V sequence. Medium-bedded, matrix-supported conglomerate and gravel beds (facies class A) typically form part of these sandy units, either defining the base of the units, or situated within. Bed contacts are highly irregular with load cast structures commonly found at the bases. The overlying sandstone units comprise medium-bedded, coarse- to medium-grained, relatively tabular sandstones (facies class C). Individual sandstone beds generally contain planar, essentially non-erosive bases, with well-stratified upper proportions. Current ripples are a common attribute. There are at least two sandstone units which can be identified at the top of the sequence and correlated to their off-axis associations; thin-bedded, fine-grained sandstones divide the units. Figure 5.11 illustrates the range of deposits in the canyon-channel system during stage II.

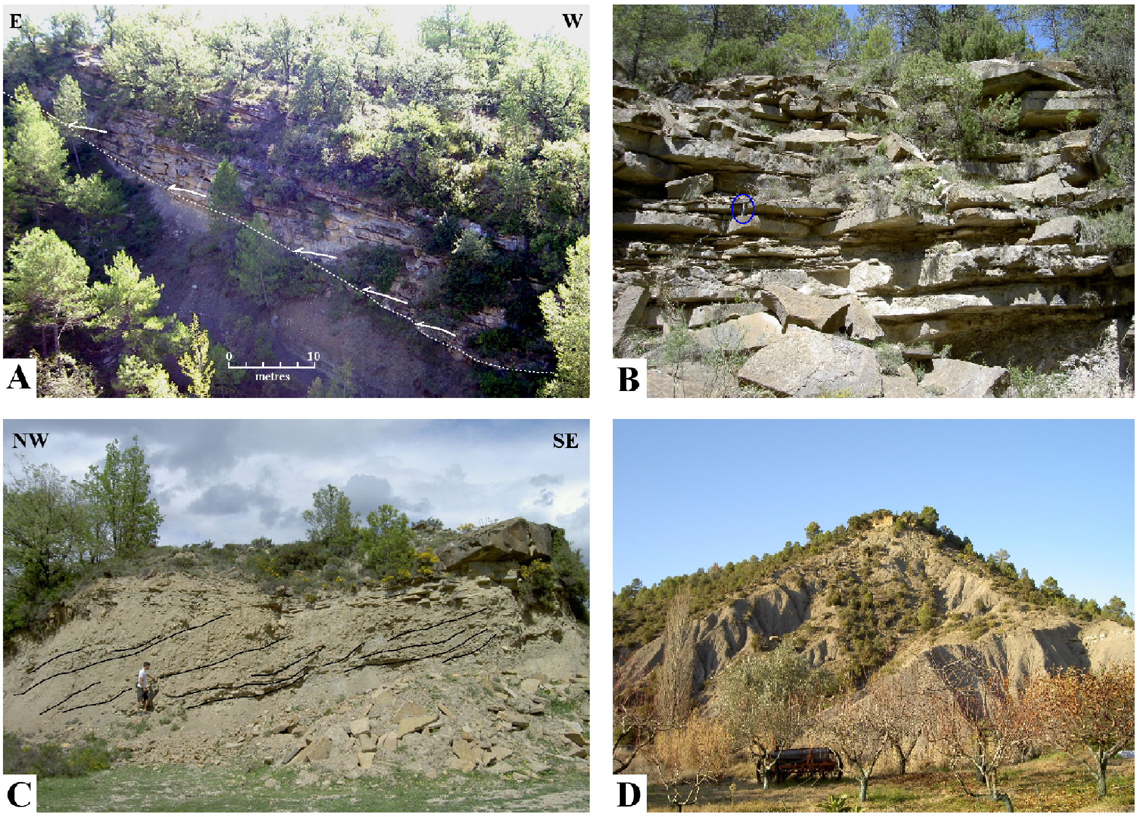

Fig. 5.11. Representative facies and facies associations in the canyon-channel transition area during stage II of deposition in the Banastón system. (A) Stepped channel margin comprising inclined medium to thick-bedded, medium to coarse-grained sandstones (FA2 and FA3) abruptly onlapping the sharply defined basal surface (indicted by arrows), BV sequence, Barranco d’Usana. (B) Tabular, medium-bedded, fine to medium-grained sandstones (FA3) representing the top part of Banastón V sequence, Barranco d’Usana. (C) Large-scale cross-stratification comprising inclined clast

horizons directed down-flow in an imbricated gravel barform (A2.1), Banastón VI sequence, Barranco d'Usana. (D) MTC composed of stacked pebbly mudstones (MTDs) defining the base of Banastón VI sequence, Santa Tecla ridge.

The N-260 road, heading north out of the town of Boltaña, and the San Martin river, both provide representative sections through the Banastón V sequence. A total width of ~4 km is estimated for the sequence, which includes the lateral extent of all the sandstones associated. The Boltaña road section exposes a ~96 m thick section (Fig. C5), defined at the base by a ~35 m thick MTC (Fig 5.12). The MTC is composed of a number of MTDs of varying lithology. The MTC characteristically contains a very high proportion of limestone clasts within a sandy mudstone matrix. Large contorted mudstone horizons, commonly folded around sandy patches of nummulitic material, are predominate in the deposit. Abundant, clast-supported pebble stringers are also a common feature, which are highly irregular and laterally non-persistent. The interbedded sandstone units generally comprise thick-bedded, very coarse- to coarse-grained nummulitic sandstones. Bed contacts are highly irregular, with the top part of the beds generally becoming truncated and incorporated into the succeeding chaotic deposit. A ~20 m thick, medium-bedded, coarse-grained sandstone packet (facies class B) overlies the MTC. The beds are distinctively well-stratified, containing some current ripples and displaying parallel lamination throughout. The overlying ~12 m thick type II MTD consists of a matrix-supported pebbly mudstone, interbedded with a number of clast-supported, imbricated pebble lags. Although this complex forms an extensive outcrop along the road section, it is laterally discontinuous either side of the exposure. The remaining upper part of the sequence predominantly consists of thick- to medium-bedded, very coarse- to coarse-grained nummulitic sandstones (facies class B and C). Occasional very-thick-bedded, very-coarse- to coarse-grained sandstone beds lie within the upper part. The sandstones characteristically show load and dewatering structures at their bases, removing any form of stratification (Fig. 5.13). Thin type II MTDs punctuate the sandy units and vertically continue towards the very top of the sequence. These deposits are highly erosive and commonly form local pebble injectites into the underling sand beds. There is no overall thinning-and-fining-up sequence associated with this section.

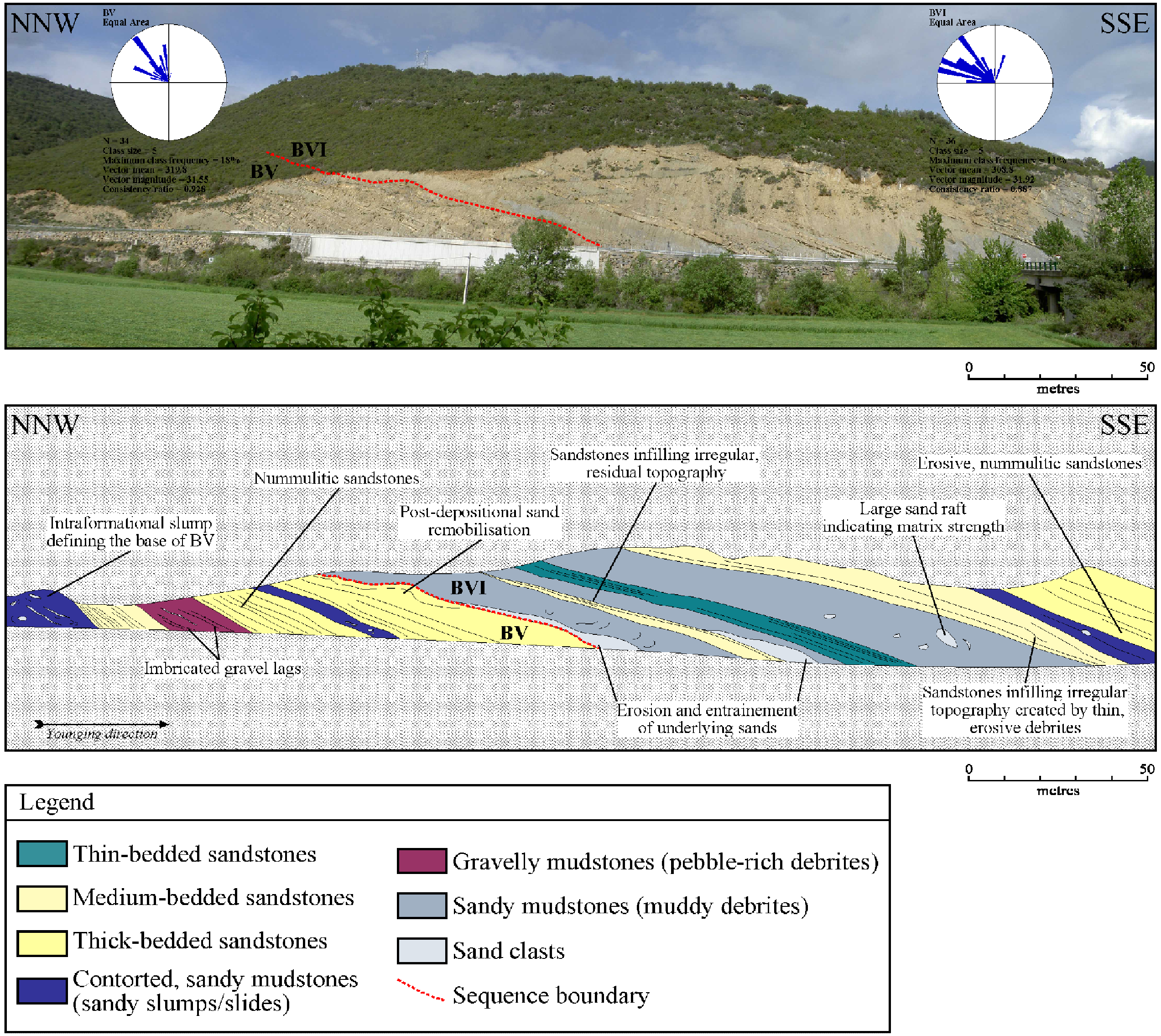

Fig. 5.12. Photo interpretation of the Banastón V and Banastón VI sequences, N-260 road, north of Boltaña. See Figure C5 for detailed sedimentary log.

The San Martin river section is situated to the east of the Boltaña road section and consists of a genetically equivalent but thicker Banastón V sequence, ~152 m thick. Dissimilarly, the base of the sequence contains no MTC and is instead defined somewhere within a gradual coarsening-up sequence situated above the underlying Banastón IV sequence. Thick- to medium-bedded, coarse-grained sandstones, interbedded with highly erosive pebbly mudstones, are predominate in the basal part of the Banastón V sequence. The sandstones are typically normally graded with frequently dispersed, sub-rounded pebbles towards their bases, and show parallel lamination throughout (facies class B2). Type II MTDs are highly erosive and act to partially truncate the underlying sandstones. These chaotic deposits consist of a pebbly lower unit containing a sandy mudstone matrix, and a more mud-dominated, less pebbly upper unit.

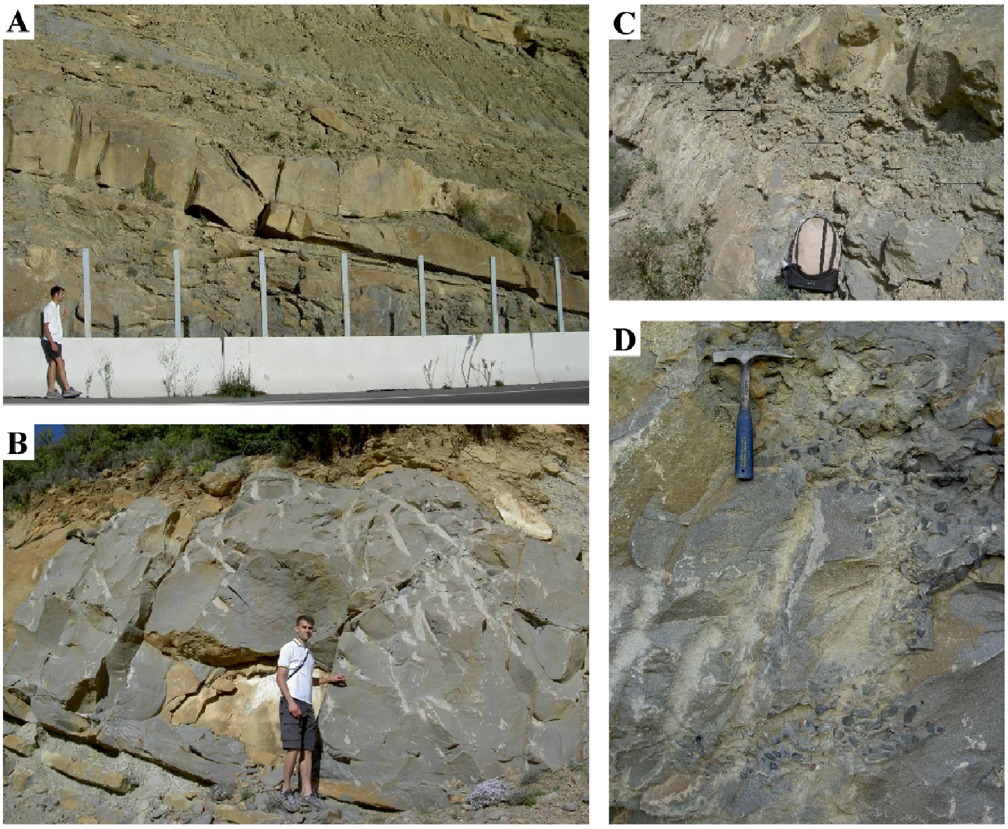

Fig. 5.13. Sediment deformation in the Banastón V sequence, N-260 road section. Deformation was a consequence of rapid sedimentation adjacent to a seafloor high (growing Boltaña anticline). (A) Pinch-and-swell geometry in thick-bedded, coarse-grained turbidite sandstone, inferring post-depositional sand remobilisation (liquefaction). (B) Soft sediment deformation in very thick-bedded sandstones during fluid-escape and liquefaction as a result of loading during rapid burial (Kneller, 1995). (C) Ball-and-pillow structure created by the foundering of sandstone into gravelly mudstone. Arrows point to some of the pseudo-nodules. (D) Load structure; downward injection of rounded mudstone pebbles into a coarse-grained sandstone bed.

Thick- to medium-bedded, pebbly sands commonly overlay these MTCs. The conglomerates are usually clast-supported and normally graded (facies class A2.7). The middle and upper succession of the sequence is associated with medium-bedded, medium- to fine-grained tabular sandstones. The very top part is marked by a well-developed thinning- and fining-up sequence and a reduction in the abundance of pebbly mudstones.

The Banastón VI sequence only exists as a few incomplete outcrops within the Banastón-Usana area. An estimated width and thickness of ~1,230 m and ~45 m respectively, can be assigned to the sequence in order to gain some control on the general characteristics associated. The onset of the sequence is marked by an erosive ~40 m thick MTC, which is characterised by an abundance of sub-rounded pebbles within a contorted mudstone matrix. The pebbles are poorly sorted and generally contain molluscan borings. A number of sub-angular sandstone clasts are also situated within the matrix and contribute to the apparent conglomerate lags comprising the deposit. These conglomerates are well-stratified to form a number of inclined, imbricated horizons. Sporadic, typically <4 m thick, sandstone units sit within the upper part of the complex, and become a more prominent feature towards the off-axis part of the sequence as the MTD decreases in volume. These units comprise thick- to medium-bedded, coarse- to medium-grained sandstones (facies class B), occasionally interbedded with discrete packets of thin-bedded, fine-grained sandstones (facies class C). The beds are commonly very bioturbated and contain a high content of plant material aligned within laminations. The upper surfaces of the individual units are typically flush with the lower surfaces of the overlying pebbly mudstones, with a number of units being deformed and partially incorporated into the chaotic divisions.

The area just north of the town of Boltaña consists of a number of sections exposing more northerly outcrops of the Banastón VI sequence. The maximum width of the exposed sequence is ~2,410 m. The main section, situated along the road just north of Boltaña and extending round to the east, represents the entire sequence measuring ~160 m thick (Fig. C6). A highly erosive, ~40 m thick, type II MTC defines the base (Fig. 5.12). This complex consists of a number of chaotic deposits divided by < 4 m thick sandstone units. The chaotic mudstones that comprise the MTC generally contain lower units of very sandy material incorporated into the muddy matrix. Nummulites and red mud clasts are accompanying attributes. The upper units are characterised by an increase in contorted mudstones and a significant reduction in the volume of sandstone.

Very large sand rafts, the largest measuring ~2 m in length, are intermittently suspended within the muddy matrix. Scattered sub-rounded pebbles, containing molluscan borings, are present throughout. The interbedded sandy units predominantly consist of thick- to medium-bedded, very-coarse- to coarse-grained sandstones (facies class B). The upper boundaries of the units are pervasively disrupted by the overlying pebbly mudstones and commonly show downward pebbly mudstone injectites. Amalgamation is typically rare. The succeeding ~40 m of sediment comprises very-thick- to thick-bedded, gravely to coarse-grained sandstones. Bed contacts are highly irregular and amalgamation is common. Well-developed sole structures and load casts are observed at the base of the beds. Angular mudstone clasts and nummulites are typical constituents. Pebbly mudstones commonly punctuate the sandy succession and are responsible for the truncation of many underlying beds. These beds subsequently form disaggregated rafts or localised sandy lenses within the chaotic deposits. The remaining fill of the Banastón VI sequence is situated to the east of the road section, consisting of semi-continuous outcrops within a vegetated area. The top predominantly contains extensive type II MTDs interbedded with typically <7 m thick sandstone units. The MTDs contain a large amount of sub-angular sandstone clasts and a few scattered small pebbles. The matrix is mainly mudstone, comprising a large volume of redeposited shelfal fauna and plant material. The sandstone units generally consist of thick- to medium bedded, coarse- to medium-grained sandstones (facies class B). Parallel lamination and current ripples are common features. Although more thin-bedded and fine-grained sandstones are present, there is no well pronounced thinning- and fining-up sequence observed.

A correlation panel of the Banastón VI sequence in the Boltaña outcrops is illustrated in Figure 5.14. The lateral margins are confined between the Añisclo anticline in the east and the Boltaña anticline in the west (see Fig. 5.1 for location). There is a distinct stratigraphic increase in MTDs, which punctuate the sandy sequence throughout and is responsible for the wedged geometry between sandbodies.

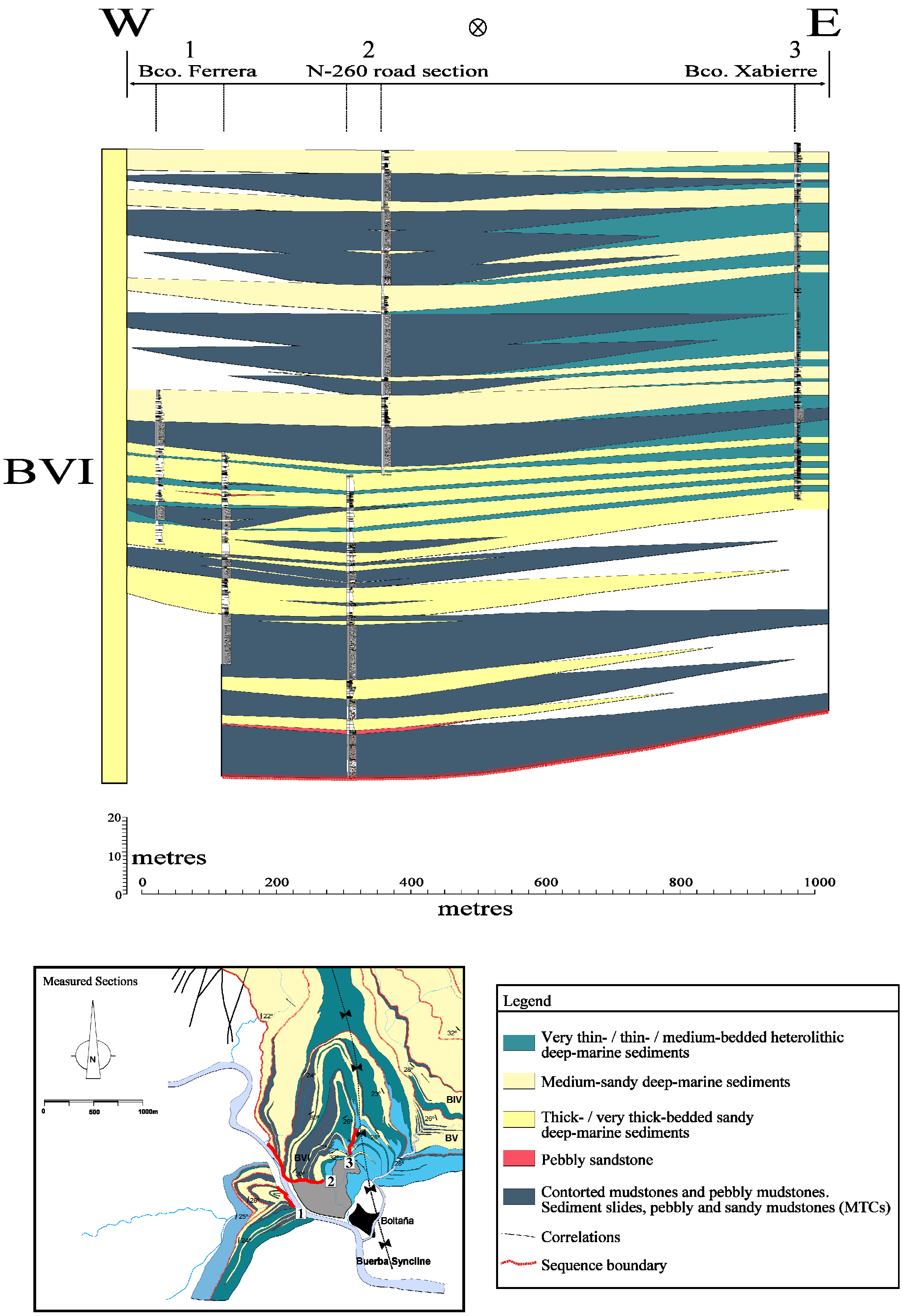

Fig. 5.14. Sectional correlation panel for the Banastón VI sequence, Boltaña area. The inset map shows the sedimentary sections measured in red. See Figure C6 for a more detailed sedimentary log.

5.4. TRACE FOSSILS IN THE BANASTÓN SYSTEM

5.4.1. DISTRIBUTION OF TRACE FOSSILS IN DEEP-MARINE ENVIRONMENTS

The diversity and abundance of trace fossils fluctuates significantly within deep-marine environments in the Banastón system, highlighting the influence of palaeoenvironmental and taphonomical conditions on trace-fossil assemblages. The dynamic controlling factors, including oxygenation, nutrient levels, substrate composition, temperature, salinity (palaeoenvironmental conditions), sediment flux and hydrodynamics of sediment gravity flows (taphonomic conditions), contribute, but not exclusively, to the variation in trace-fossil assemblages (Frey *et al*., 1990; Rodríguez-Tovar *et al.*, 2010).

5.4.1.i. Canyon-channel transition

The lower-slope canyon-channel transition, situated in the Banastón-Usana area, is characterised by the presence of post-depositional trace fossils, i.e., opportunistic traces makers that excavated vertically into newly deposited sediment (*sensu* Kern, 1980; Ekdale, 1985; Taylor *et al.*, 2003; Rodríguez-Tovar *et al.*, 2010). *Thalassinoides* (a feeding/*fodinichnial* trace) and *Ophiomorpha* (a dwelling/*domichnial* trace) are the most common ichnotaxa found in this environment, formed mainly from decapod crustaceans (Frey *et al*., 1978). The burrows are large and robust, deeply excavating the surrounding media. Many of the *Ophiomorpha* burrows are lined with *Nummulites*, providing inferences on the composition of the substrate (Fig 5.15A). There are also abundant *Gastrochaenolites* borings in many of the well-rounded pebbles and cobbles situated in gravelly mudstones (muddy debrites). The bioerosion indicates that the pebbles and cobbles resided for at least some time in the littoral zone prior to remobilisation to deep water (Fig 5.15B). The overall abundance of trace fossils is low, but local concentrations of burrows on individual bedding planes have been observed.

The trace-fossil assemblage is attributed to the unstable environment (fluctuating ecological conditions), where high sediment flux, erosive sediment gravity flows and coarse-grained substrates prevented the intense colonization of the seafloor. The post-depositional ichnotaxa formed by robust, deeply burrowing organisms that were able to survive burial by newly deposited sediment (Wetzel & Uchman, 2001), and thrived in eutrophic conditions as a consequence of fluctuating delivery of abundant organic matter (Rodríguez-Tovar *et al.*, 2010). A number of bedding planes are intensely bioturbated, suggesting the trace makers were opportunistic (Ekdale, 1985) and were able to adapt to a harsh environments (Fig 5.15C). The trace-fossil assemblage almost exclusively occurs within stage II in the evolution of the Banastón system (Banastón IV–VI) as a result of the increase in finer-grained, sandier sediment deposited during the 'spillover' event (see below). In contrast to the lower MTC-dominated stage, the sandy sediment provided a viable environment for organisms, and facilitated the preservation of structures. The concentration of MTCs in stage II in the canyon-channel transition increased the frequency of rapid burial of organisms, providing an inhabitable environment for the development of an infaunal community.

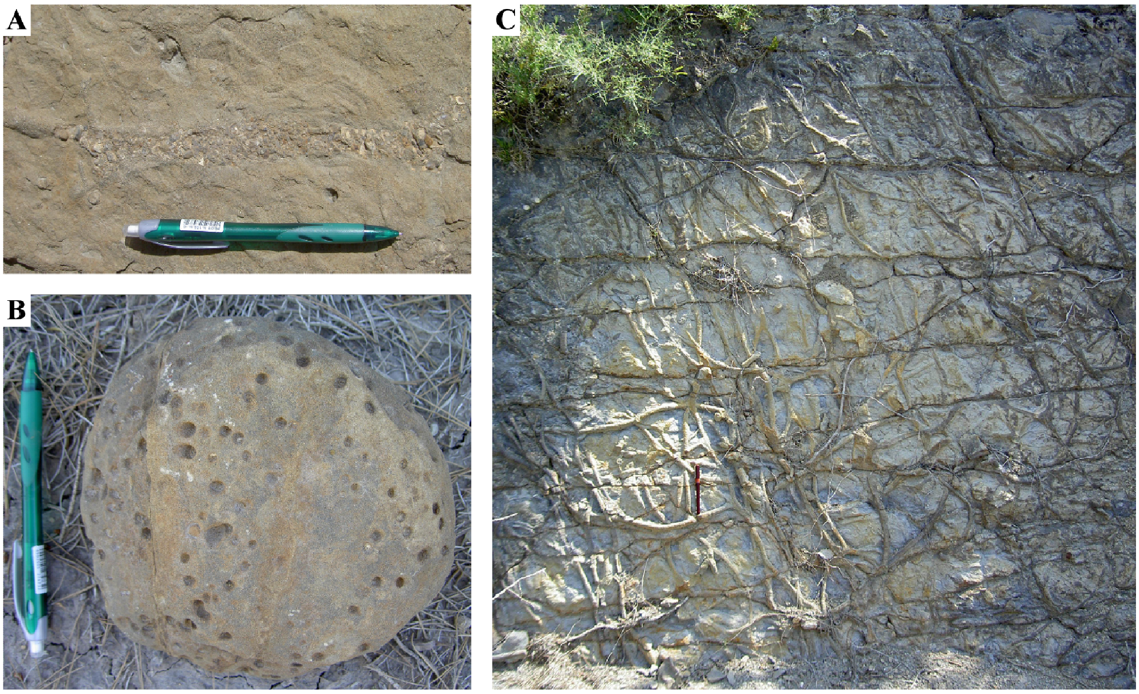

Fig. 5.15. Representative trace fossils and bioerosion in the canyon-channel transition, Banastón system. (A) *Ophiomorpha* burrow lined with *Nummulites*. Epichnial full-relief in Banastón VI sequence, northwest of Banastón village. (B) Cobble-sized extrabasinal clast covered in *Gastrochaenolites* borings produced by molluscs (such as *Lithophaga*), Banastón VI sequence, northwest of Banastón village. (C) Pervasive *Thalassinoides* burrowing produced by crustaceans. Epichnial full-relief in Banastón V sequence, Rio Soto.

5.4.1.ii. Base-of-slope / proximal basin-floor channels

Channel-axis environments

The depocentres of sandy sequences are characterised by an abundance of post-depositional trace-fossil assemblages, including *Halopoa*, *Scolicia* (grazing/*pascichnial* traces), *Thalassinoides* and *Ophiomorpha* ichnotaxa. The overall diversity and abundance is higher than the canyon-channel transition environment, with *Thalassinoides* isp., *Ophiomorpha rudis*, *Scolicia prisca*, *Scolicia strozzii* and Scolicia isp. as the most common ichnospecies. The dominance of *Scolicia* and *Ophiomorpha* ichnotaxa is typical of the *Ophiomorpha rudis* subichnofacies of the deep-marine *Nereites* ichnofacies (refer to Seilacher, 1967 for a detailed description on this ichnofacies). Unfavourable environmental conditions could have been responsible for the apparent low diversity trace-fossil assemblage observed in the channel-axis environments, where only endobenthic, opportunists survived (e.g., *Ophiomorpha* and *Scolicia* trace makers; Wetzel & Uchman, 2001). Heard and Pickering (2008) and Rodríguez-Tovar *et al.* (2010) presented a number of ecological and taphonomical conditions that contributed to this distinct trend, including the non-preservation of shallow-tier structures as a consequence of erosion from high-concentrated density flows, and the affects of 'bull-dozing' traces (mainly consisting of post-depositional ichnotaxa) preventing the formation of, or even destroying, delicate structures due to frequent movements during feeding activity (*sensu* Wetzel, 2002, 2008). The studies also proposed that high sedimentation rates in axial environments prohibited periods of quiescence/stability on the seafloor for the colonization of a diverse burrowing community. Tchoumatchenco & Uchman (1999) considered the influence of sediment grain size on trace-fossil assemblages, suggesting some trace makers were only adapted to fine-grained substrates, thus excluding the dominantly coarse-grained substrate of axial environments.

Off-axis to overbank environments

There is an increase in the number of ichnotaxa recognised from sandy depocentres to off-axis and marginal environments. The most prominent observation is an increase in shallow-tier, pre-depositional structures, especially graphoglyptids (traps and gardening/*agrichnial* traces), including *Helminthorhaphe*, *Desmograpton* and *Paleodictyon*. The most common ichnotaxa are *Scolicia*, *Thalassinoides* and *Ophiomorpha.* This indicates that a variable ethology existed amongst the burrowing community (Heard & Pickering, 2008). Contemporaneous overbank complexes are characterised by low bioturbation.

The appearance of graphoglyptids in environments adjacent to the sandy depocentre represents a lateral shift to more stable conditions on the seafloor between turbidite events. Lower sedimentations rates and deposition from less-concentrated, finer-grained density flows facilitated colonization on the seafloor (Heard & Pickering, 2008). Additionally, reduced seafloor erosion enhanced the preservation potential of shallow-tier trace fossils.

5.4.2. FIRMGROUND DEVELOPMENT IN OVERBANK ENVIRONMENTS

The trace-fossil signature in the Banastón I and II sequences show evidence for firmground development in distal overbank environments where low sedimentation rates prevailed. The *Glossifungites* ichnofacies represents a trace-fossil assemblage excavated in firm, semi-consolidated substrates as a result of exhumation of sediment from erosive turbidity currents following the initial burial and dewatering of soft sediment (Seilacher, 1964; Pemberton *et al.,* 2001). The trace-fossil suite is characterised by robust, vertical to subvertical borrows, including *Arenicolites, Diplocraterion* and *Thalassinoides* ichnotaxa (Uchman *et al.*, 2000, Pemberton *et al.,* 2001). The colonised surfaces are often associated with significant stratigraphic discontinuities, interpreted as time lags between the deposition of sediment and the subsequent bioturbation (*sensu* Savrda, 1991), particularly documented in shallow-marine deposits (e.g., Pemberton & Frey, 1985; Gingras, *et al*., 2000, 2001). Although there has been very little research into firmground identification in deep-marine siliciclastic systems, a mechanism for the generation of firmground surfaces in the Ainsa basin is proposed using the accurate correlation of Banastón I and II sequences into lateral regions and the identification of trace-fossil concentrations at particular stratigraphic horizons.

Barranco Biñés preserves a continuous outcrop along a stream section, exposing a fine-grained, muddy succession situated laterally to the sandy depocentres of the Banastón I, II and III sequences. This overbank zone consists of laterally extensive, very thin- and thin-bedded, current-rippled, very fine-grained sandstones and parallel-laminated, thin-bedded siltstones, interbedded with marly mudstones. These deposits are interpreted to be the products of low-concentration turbidity currents, reflecting deposition from traction and suspension. Overall, bioturbation is low, primarily consisting of *Planolites*; however, two units found within the top of the Banastón I and II overbank sequences containing concentrations of *Arenicolites* burrows have been identified. These units are ~9 m thick and are located ~140 m and ~200 m from the sandy depocentre of Banastón I and II sequences, respectively. The sharp-walled, U-shaped burrows extend vertically into the fine-grained sediment (Fig. 5.16). Individual burrow shafts are ~1 cm in diameter, up to ~180 cm long and are filled with very fine-grained sandstone.

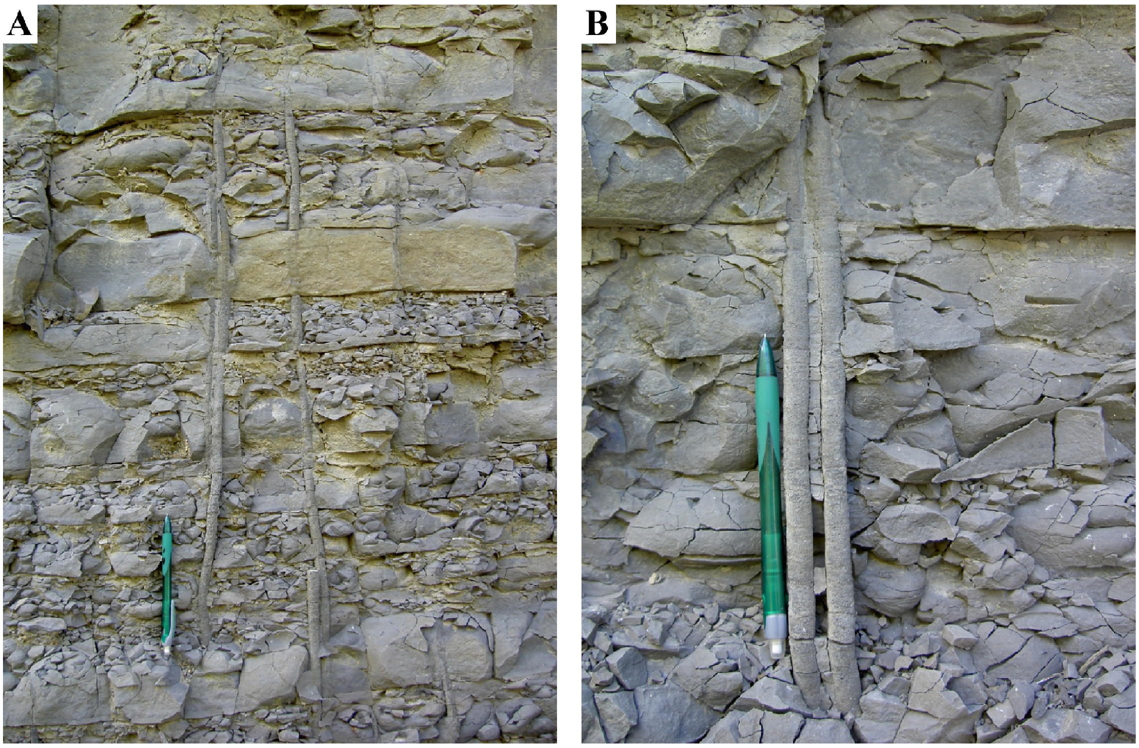

Fig. 5.16. (A) *Arenicolites* isp. Epichnial full-relief in overbank deposits, Banastón I sequence, Barranco Bines. See Ekdale & Lewis (1991) for discussion of ichnogenus. (B) Close-up view of a sharp-walled, U-shaped vertical burrow, showing no indication of structural collapse with compaction. Pencil for scale in (A) and (B) is ~15 cm long.

The characteristics of the *Arenicolites* burrows, including the extreme burrowing depth, passive fills, robust nature and sharp-walls (see Fig. 5.16B) suggests the substrate was a firmground during excavation and indicates a significant stratigraphic horizon in the depositional history of the Banastón I and II sequences. The *Arenicolites* burrows are interpreted as dwelling and feeding structures. The organisms responsible for the trace fossils are suspension-feeding annelids or small crustaceans (Ekdale & Lewis, 1991; Pervesler & Uchman, 2004) that would have thrived during periods of low sedimentation rates when a tranquil setting existed on the seafloor. The depth of the burrows and the feeding strategy of the burrower are consistent with the *Glossifungites* ichnofacies, where organisms were adapted to fluctuating environmental conditions (*sensu* Hubbard & Shultz, 2008). Savrda *et al.* (2001) attributed the development of a firmground in Cenozoic deep-marine slope deposits off the east coast of the United States to a period of sediment starvation and bottom-current winnowing of fines during a rapid transgression. In agreement with this study, the firmgrounds located at the top of the Banastón I and II sequences reflect the diminishing supply of sediment into the Ainsa basin during the final stages of infill of the sequences. The seafloor was subsequently exposed for prolonged periods of time, allowing colonization of the indurated media. It is, therefore, interpreted that these horizons have temporal significance. They represent long-term cessation of siliciclastic sediment into the basin and define the top of sequences, recording relative base-level rise. During this time, coarse sediment was sequestered on the shelf in response to an increase in accommodation in more proximal parts of the foreland basin and exhumed firmgrounds.

5.5. EVOLUTIONARY STAGES IN THE BANASTÓN SYSTEM

Palaeocurrent dispersals, facies variations and trace fossil analysis have identified two discrete stages during accumulation of the Banastón system. There is an apparent decrease in depositional confinement in stage II (from the base of Banastón IV), which can be attributed to a ‘spillover’ event (spill stage of canyon development), in addition to a change in palaeoflow (Fig. 5.17). High confinement of the Banastón I–III sequences (stage I) in the channel-canyon environment was due to erosional downcutting and the filling of excavated conduits (depositional confinement). However, stage I was also characterised by confinement in the north (in the lower-slope/proximal basin-floor environment). This can be attributed to structural confinement between the syndepositional Añisclo anticline in the west, and the advancing thrust front in the east, providing localised accommodation in the basin. Intrabasinal tectonics structurally controlled the northerly palaeoflow during stage I (Fig. 5.18). Conversely, during stage II, involving Banastón IV to VI sequences, a wide dispersal in palaeoflow is observed. This flow pattern may indicate active growth stages of intrabasinal structures, i.e., uplift of the Boltaña and Añisclo anticlines during stage I and inactivity during stage II. Alternatively, stage II could represent an increase in sediment supply and progradation of the depositional zone, causing the splaying observed in stage II (see Fig. 5.18). This two-phase model reflects the balance between locally- and regionally-controlled

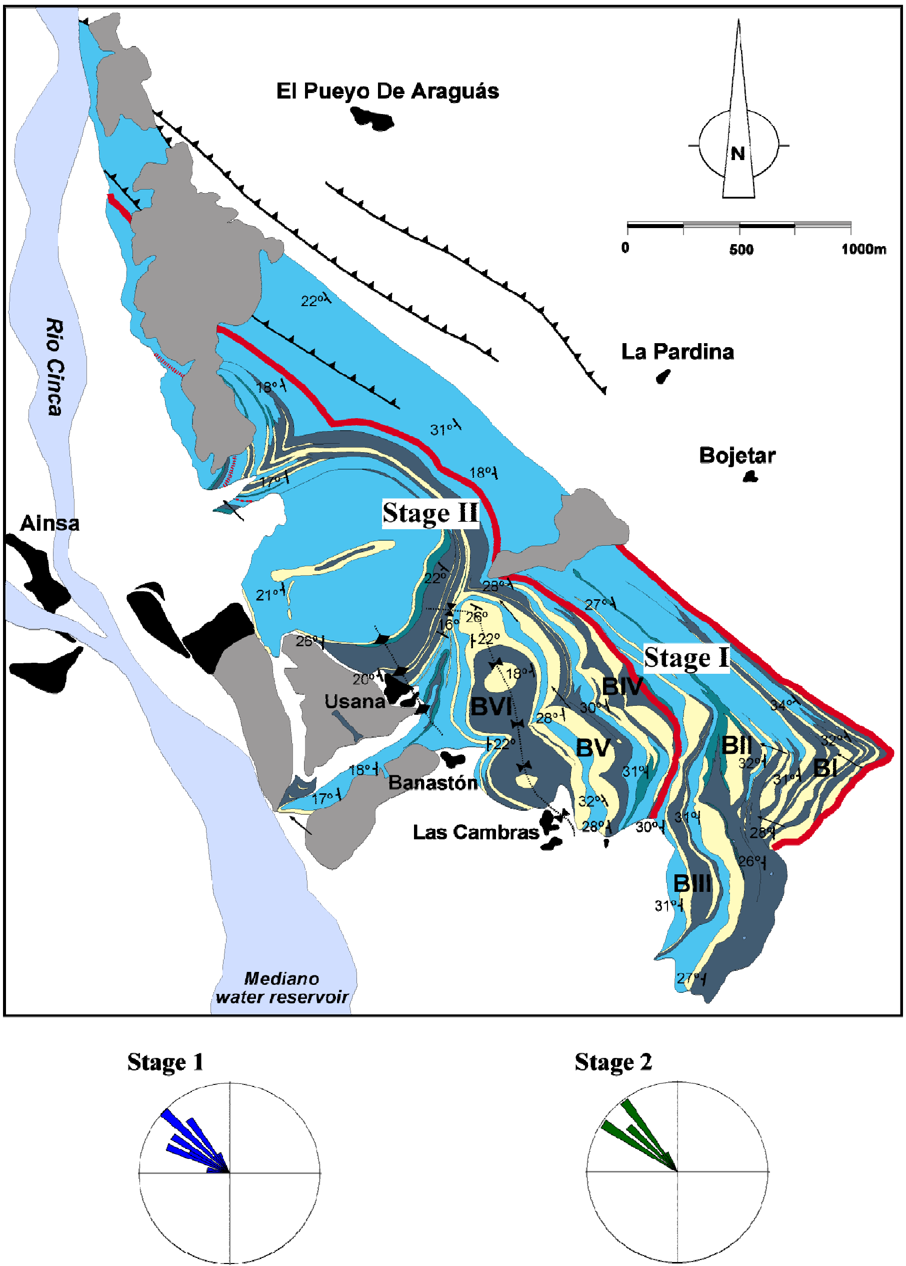

Equal Area
N = 63
Class size = 5
Maximum class frequency = 19%
Vector mean = 303.4
Vector magnitude = 20.12
Consistency ratio = 0.958

Equal Area
N = 55
Class size = 5
Maximum class frequency = 29%
Vector mean = 314.3
Vector magnitude = 13.75
Consistency ratio = 0.982

Fig. 5.17. Map extract showing the division between stage I and stage II at the base of Banastón IV sequence in the canyon-channel transition area, representing a spillover phase in canyon-channel elements.

Stage II: BIV, BV, BVI

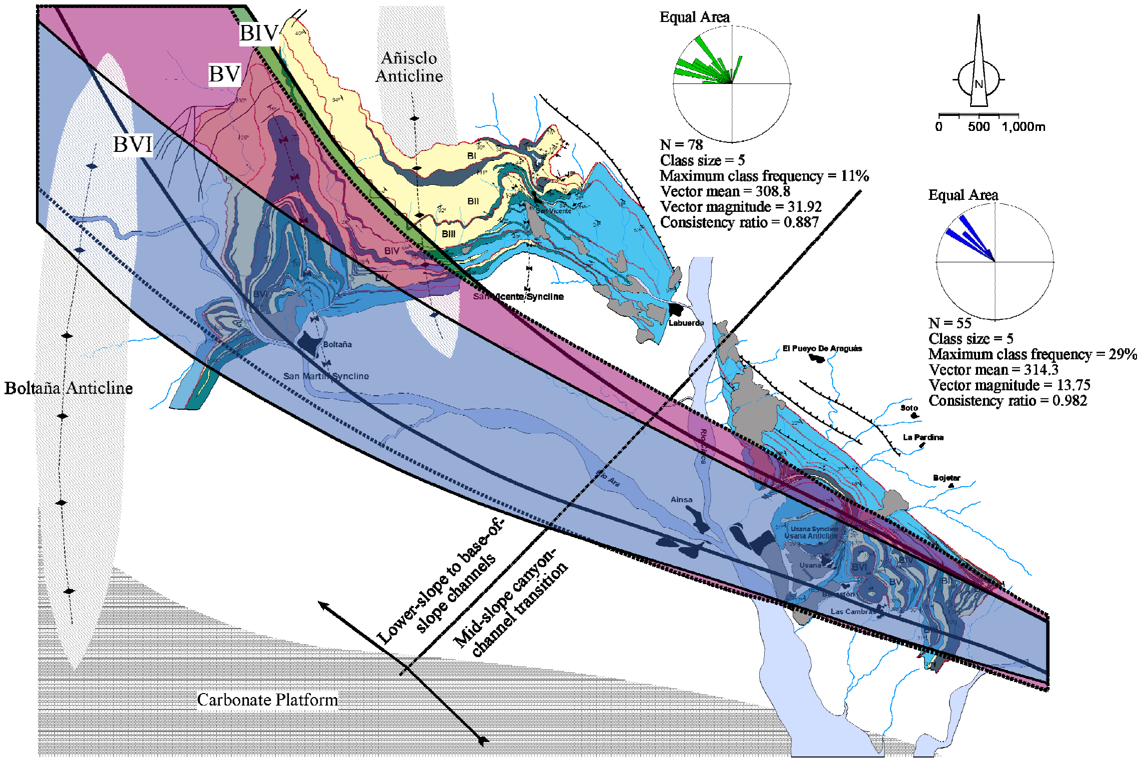

Stage I: BI, BII, BIII

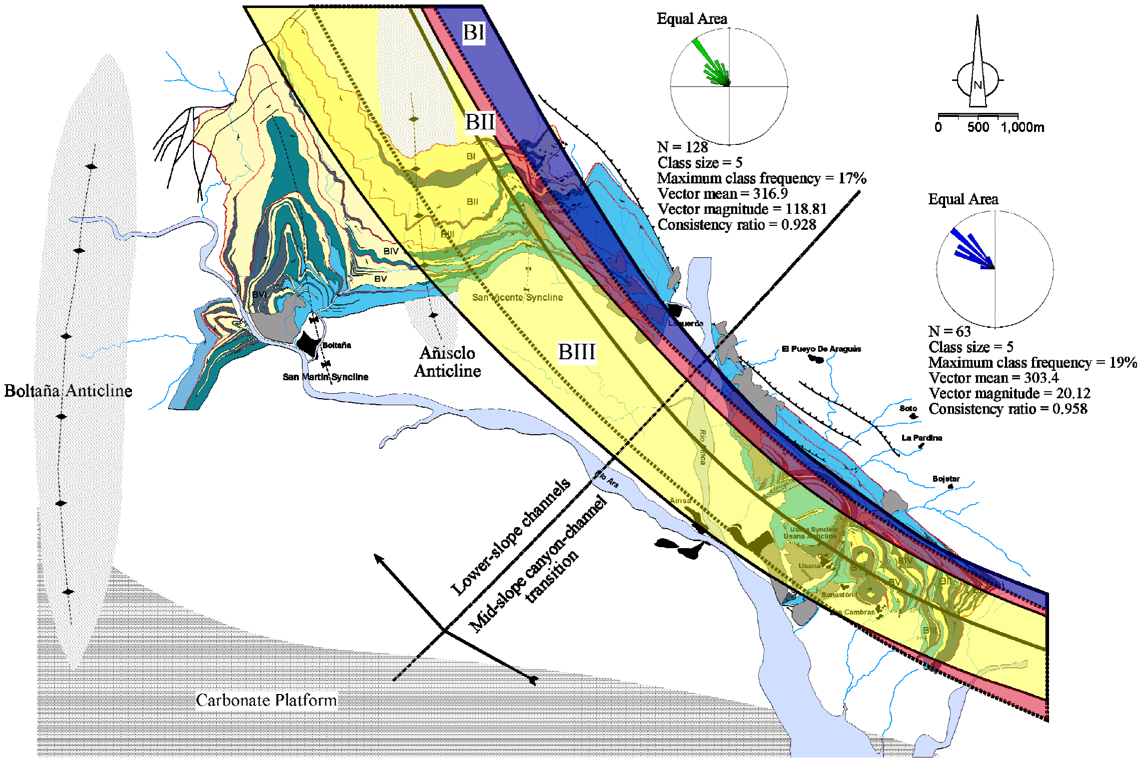

Fig. 5.18. Paleogeography of the Banastón sequences outlining the position of sequence depocentres. Stage I is characterised by structural confinement between

intrabasinal structural highs and the active basin margin, whereas the depocentres in stage II shows a splaying pattern.

subsidence and basin filling (sediment supply/flux). A similar trend is observed by Maestro (2008) for the Eocene Vernet lacustrine piggyback basin in the Pyrenees, where the overall style of sedimentation and regional drainage organisation in the basin is directly related to the movement of the thrusts. This suggests a common depositional pattern that could be applied to other structurally-controlled basins worldwide.

The ~25 m thick, Banastón V channel margin element exposed along Barranco d'Usana is characterised by a stepped profile over a distance of <60 m (Fig. 5.11A). A ~15 m basal lag deposit, comprising disorganised gravels and pebbly sands, define the base of the channel to the west (towards the channel axis), which are interpreted as erosional remnants of the channel thalweg. Medium to thick-bedded, medium to coarse-grained sandstones of the sandy succession overlies the channel thalweg deposits. They are interbedded with thin mudstones and abruptly onlap the sharply defined margin of the channel at its easternmost termination. The sandstones appear to be inclined and dip towards the channel axis (to the west), approximately perpendicular to palaeoflow. The geometry at this locality compares to the inclined strata observed in lateral accretion elements positioned in the inner bend of channels in the Rosario Formation of Baja California, Mexcio (cf. Dykstra & Kneller, 2008) and the Cerro Toro Formation of the Magallanes basin in southern Chile (cf. Hubbard et al., 2008). Although individual sigmoidal bar elements are not recognised at this outcrop, it is plausible to interpret the onlap surfaces as lateral accretion, recording lateral migration of a sinuous channel positioned to the right of the plate (Fig. 5.11) Each inclined surface represents the position of the inner bank of the channel during migration, with the bar elements representing accretion on this inner side of the channel bend. Each laterally offset bar element would truncate successively deeper into the underlying strata, forming the characterisitc sigmoidal cross-sectional geometry, observed in both deep-marine and fluvial settings (Thomas *et al*., 1987; Garcia-Gil, 1993; Miall, 1996; Elliott, 2000; Abreu *et al*., 2003).

It can be interpreted that the sinuous channel represents channel backfilling processes within a confined slope setting. The Upper Cretaceous Canyon San Fernando submarine canyon channel-levee complex of the Rosario Formation, Baja California, Mexico, evolved from a confined submarine canyon, dominated by gravels, to a sandy, slope channel-levee complex (Dykstra & Kneller, 2008, their fig. 4). This ~1 km thick complex shows a similar stratigraphic trend to the canyon-channel transition of the Banastón system, where sinuous, sandy channels (stage II) overlie the confined, gravelly units (stage I). The Upper Carboniferous Ross Formation in the Clare Basin, westeren Ireland shows a temporal evolution of increasing occurrence of sinuous channels towards the top of the formation (Elliot, 2000; Lien *et al.*, 2003). A similar pattern is also observed in the Carboniferous Jackfork Group in the Ouachita Moutains, Arkansas, USA, where sinuous channels are stratigraphically located in the later phases of channel complex sets (Coleman, 2000). A similar interpretation can be inferred for stage I of the Banastón system

5.6. ENVIRONMENTAL INTERPRETATION

The overall sedimentary characteristics of the lower-slope to proximal basin-floor channels in the Banastón system are most consistent with a low-sinuosity, coarse-grained submarine channel (Fig. 5.19).

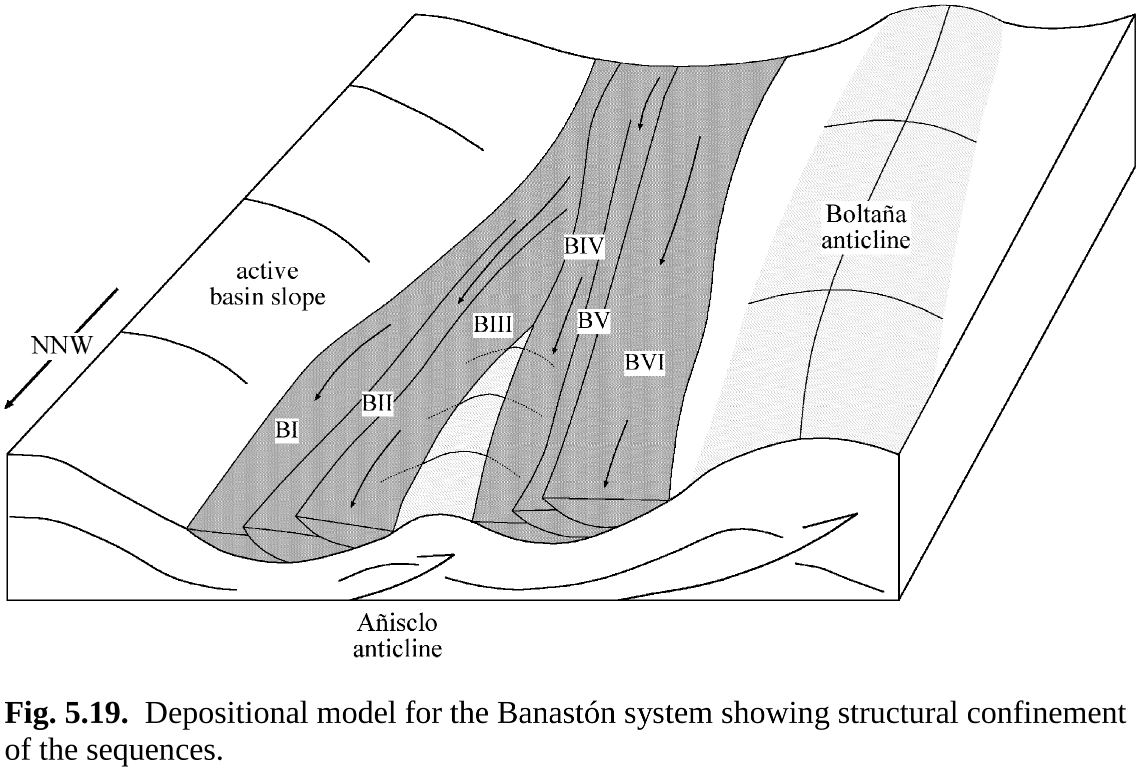

Fig. 5.19. Depositional model for the Banastón system showing structural confinement of the sequences.

The lower-slope erosional channel shows cumulative erosion of ~165 m and contains six unconformity-bounded sequences (Banastón I–VI). The cumulative thickness is ~500 m. The canyon-fill sequences are dominated by pebbly sandstones / conglomerates and very coarse- to coarse-grained sands. Sediment bypass and lag deposits predominate. Banastón I and II are mainly pebbly conglomerates, carbonate-clast-rich debris flow deposits and very coarse-grained sandstones. Banastón III, IV and V have similar deposits but with less pebbly conglomerates. The proximal basin floor (base-of-slope) system has six sequences (Banastón I–VI). Banastón I and II fine upwards, whereas Banastón III, IV, V and VI coarsen upwards with coarse- to very coarse-grained sandy upper parts, including granule-grade sandstones and pebbly mudstones. The youngest sand body shows palaeoflow oriented into the eastern part of Boltaña anticline, demonstrating that the anticline was not a seafloor barrier to sediment gravity flows travelling through the Ainsa basin at this time. Together, these depositional environments record the backfill of six highly confined (channelised) sandbodies. As the sandbodies young, they show progressively less confinement, with the uppermost sand bodies effectively spilling over the previous confines of the canyon, and showing progradation (coarsening-upwards). The Banastón system shows a complete erosional-depositional cycle, from canyon incision to backfill, and complete overspill. The channelised sandbodies are 35–40 m thick. The base of each channelised sandbody is characterised by pebble conglomerates, overlain by sands that fine upwards into marls. In the canyon system, mean palaeoflow is ~290^{o} , compared with ~320^{o} for the proximal basin floor (base-of-slope) system in stage I. This change is interpreted to reflect the lower-most basin slope canyon turning into a typical proximal lowermost slope and basin floor.

Mass transport complexes define the base of each sequence; the thickest MTCs define the base of Banastón I, V and VI sequences. The top part of the Banastón VI sequence is associated with a thick MTC, interpreted as a late-stage coarsening-upward representing progradation of the depositional zone. System development is probably controlled by a high-frequency tectonic driver, where propagation of the active thrust associated with the lateral ramp zone of the SCPU reduced accommodation in the non-marine and shallow-marine setting (Tremp–Graus basin) and induced slope failure into deep water. Nijman (1998) documented a peak supply of conglomerates and a progradation trend within the UM-B megasequence in the Tremp–Graus basin (interpreted as the proximal counterpart to the Banastón system in this study), which would account for the supply of gravelly material into the Ainsa basin and the progradational trends observed in the Banastón system. Although this event can be correlated to the largest Eocene drop in sea level, it was attributed to hinterland uplift and an increase in sediment flux (Nijman, 1998). See Chapter 7 for further discussions on tectonic controls.

5.7. SEAFLOOR TOPOGRAPHY

Intrabasinal thrust-related topography controlling sedimentation is well documented in the literature (Butler & Grasso, 1993; Talling *et al.*, 1995; Dreyer *et al.*, 1999; Haughton, 2000; Hodgson & Haughton, 2004; Gee & Gawthorpe, 2006; Hodgson *et al*, 2006; Mayall *et al*., 2010). Detailed mapping of the Banastón system has revealed the complex evolution of the three-dimensional seafloor bathymetry prior to, and during, the deposition of the six sequences, Banastón I–VI. All six sequences show a significant widening of the area of sand accumulation from the Banastón-Usana to the San Vicente-Boltaña area. In the northern San Vicente-Boltaña area, the Banastón sequences are all confined between the present-day Mediano anticline to the east and the Boltaña anticline to the west. At both lateral margins, the system shows onlap and pinch-out against these structures. During Banastón system times, therefore, linear seafloor ridges were growing along the sites of the present-day Mediano and Boltaña anticlines. An interpreted seismic line (fig. 2 in Bentham *et al*., 1992) suggests that the Boltaña anticline is associated with a thrust that ramped up to form a steep reverse fault on the western limb that cuts the Cuisian to Lower Lutetian Guara Limestone. The interpretation of the same seismic line shows that the core of the Mediano anticline is underlain by a blind thrust. The orientation of the fold axes is consistent with thrusting having a top-to-the-WSW sense of shear (i.e., linked to the emplacement of the Cotiella nappe). Additionally in the San Vicente-Boltaña area, the Banastón sequences show thickness changes, including onlap, onto an intrabasinal seafloor high now mapped as the much tightened Anriscló anticline. This likely represents a synsedimentary growth anticline above a blind thrust.

The Banastón I sequence (oldest part of the Banastón system) is mapped as having its coarsest grained (sandy) deposits restricted between the Mediano in the east, and the Aniscló anticline in the west. Banastón II and III are mapped as showing no significant thickness changes over the Aniscló anticline and, therefore, it is assumed that either this structure had temporarily stopped growing or that sediment flux supply exceeded the rate at which the seafloor high was growing. In contrast, Banastón IV, V and VI have their coarse-grained depocentres confined to the west of the Aniscló anticline, and east of the Boltaña anticline. Therefore, it is inferred that the growth rate of a seafloor high in the present-day area of the Aniscló anticline was greater than the rate of sediment accumulation even though it comprises hundreds of metres of coarse-grained, sandy deposits.

In the most proximal outcrops of the Banastón system, in the Banastón-Usana area, the outcrop patterns in the Banastón system only show the eastern and central (axial) parts of the sequences, and therefore, preclude any detailed understanding of their coarse clastic deposition in relation to the entire basin width. However, it appears that the Banastón I–III sequences show an aggradational stacking pattern confined to lower-slope erosional channels being localised in the same part of the basin slope. This was probably due to a larger (but unexposed) feeder system, such as a submarine canyon. In contrast, Banastón IV, V and VI are significantly less confined and show palaeocurrents that might suggest either a slightly more southerly position for sediment routing down the basin slope, or a reduced seafloor gradient in the region of the lower-slope and base-of-slope, such that depositing flows were less confined. A reduced seafloor gradient would have led to a greater propensity for turbidity currents to overspill the confines of any slope channel, and to turn more rapidly along the basin axis (and thereby show palaeoflow towards ~320^{o}).

A transverse section across the Banastón system shows the lateral migration of the depositional axis of the system, between successive sequences (Fig. 5.20). The gradual thinning of the Banastón sandbodies as they onlap the syndepositional topographical highs of the Boltaña and Mediano anticlines suggests structural confinement by basin-bounding submarine slopes, with intrabasinal highs controlling the precise depositional axes.

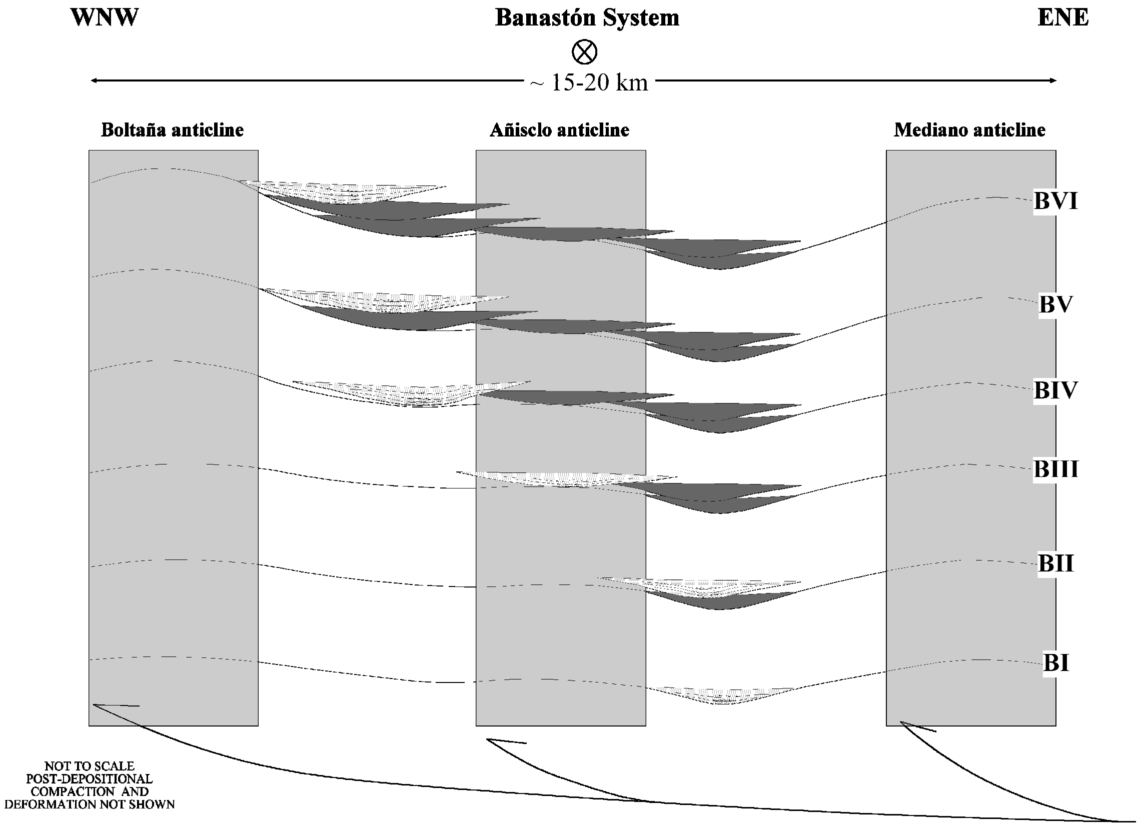

Fig. 5.20. Schematic evolution of seafloor topography during deposition of the sequences in the Banastón System, highlighting the influence of intrabasinal structures on the location of depocentres. Note: active sequence is coloured in white with the underlying sequence shaded dark grey

5.10. DEPOSITIONAL SUMMARY

The Banastón system is characterised by: (1) six depositional sequences characterised by a basal erosional surface, created by extensive mass wasting (sliding and slumping) of finer grained basin-slope marls and thin-bedded turbidites, with up to tens-of-metres of erosion. The canyon excision is interpreted to be related to a phase of thrust-related, tectonically driven over-steepening of the basin slope and linked up-stream environments. The base of the Banastón system is interpreted to record the renewed onset of coarse clastics (after the termination of the underlying Gerbe system) as a basinal response to a significant reduction in relative base level, probably reflecting a major phase of tectonic uplift in the hinterland source area to the east and north, and linked subsidence in the deep Ainsa basin; (2) bases of sequences containing a MTC as pebble-rich mudstones and pebbly sandstones; (3) six depositional sequences, each with ~70 m of accumulated sediment thickness in the basin axis, which can be correlated from channel axis to levee-overbank complexes; (4) lateral (structural) confinement and lateral-offset stacking towards the WSW, away from the rising Pyrenean orogen, associated with the growth of the submarine Mediano anticline. With the renewal of coarse clastic deposition in each sequence, the axis of deposition shifted ~800–1,000 m; (5) development mainly from a range of sediment gravity flows that entered the Ainsa basin from the ESE (flowing towards ~290^o, but with considerable dispersion), and then turned NW (~320^o) transporting sediment down a NNW-dipping slope; (6) marine water depths below storm wave-base, but probably no more than several hundred metres; (7) sandbodies that were confined to a lower-slope canyon in more proximal outcrops, but represent proximal basin floor (mouth-of-canyon) and mainly submarine channels within the axis of the Ainsa basin.

5.11. DISCUSSION

The Banastón system comprises lower-slope (Banastón-Usana area) and proximal basin-floor environments (San Vicente-Boltaña area). The number of feeder channels or slope gullies that supplied the Banastón system is unknown, as the proximal parts of the systems are not exposed. It is likely, however, that a single, relatively straight, canyon fed the more basinal Banastón system. At any time, only one channel-levee-overbank complex appears to have existed, suggesting that the axial part of the Ainsa basin confined sediment pathways to the structurally deepest part, as observed in many modern submarine trenches.

The base of each sandbody is characterised by a MTC, which is consistent with the generic depositional model proposed by Pickering and Corregidor (2005) for other systems in the Ainsa basin. The MTCs formed topography on the seafloor and contributed to the lateral confinement of subsequent sandy sediment gravity flows. As sand supply was gradually switched off (due to the re-equilibration of river graded profiles and the delta front, or shelf healing), the sandbodies thinned and fined upwards, and mud-grade material became the main sediment deposited. This process repeated itself to build six principal sandy sequences.

Each sequence show a lateral offset stacking pattern away from the eastern margin of the Ainsa basin (as has been shown for the underlying Ainsa sandy sequences, Pickering and Corregidor, 2005), due to the increased convergence rates linked to the rising Pyrenean orogen. Intrabasinal tectonics created complex seafloor topography and mobile slope gradients that also influenced the position of the sandy sequences, and contributed to their lateral confinement.

The base of the Banastón systems represents a significant tectonic event, defining the onset of tectonosequence II. This major phase of tectonic uplift and increased erosion played an important role in defining the sedimentary character and depositional style of the system, however, the occurrence of sandy sequences represents a temporal framework that is too frequent to invoke a tectonic driver. It is, therefore, suggested that eustatic sea-level change is favoured, probably driven by global climate change in the Middle Eocene. This is a time when the first significant global deterioration in climate appears to have commenced, as inferred from the stable oxygen/carbon isotope curve of Zachos *et al*. (2003) that are used as a proxy for global climate change.

5.12. THE AINSA SYSTEM

The Ainsa system is ~177 m thick and is stratigraphically located above the Banastón system, forming the second depositional system (from the base) in the Upper Hecho Group. Age dating of the Ainsa basin suggests that deposition of the Ainsa system occurred during the early Lutetian (Payros *et al*., 1999; Remacha & Fernández, 2003; Pickering & Corregidor, 2005). The Ainsa system comprises three sandy sequences (Ainsa I–III) that accumulated in lower-slope erosional channels and proximal basin-floor channel systems. The channels of the Ainsa system show an overall west-southwest migration through time away from the Mediano anticline. This migration is associated with repeated channel incision, sediment bypass and infilling phases of the channels of the three sandy sequences. Figure 5.21 shows facies class abundance in the Ainsa systems, presented by the total number of beds and the total thickness measured. There are a noticeable number of beds associated with facies class C–E, whereas thickness tends to be high for facies class A and C.

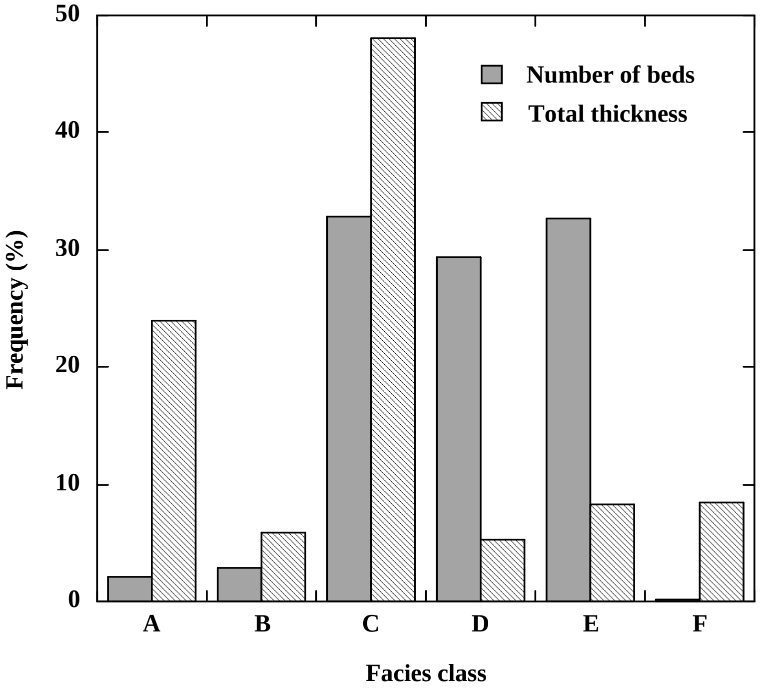

Fig. 5.21. Facies class abundance in the Ainsa system.

A very wide range of facies are recognised in the Ainsa system, particularly a wide variety of MTDs. The following two figures (Fig. 5.22 and 5.23), present an overview of these facies (facies A1.4, B2.1 and C2.1).

The Ainsa quarry section (AI) represents one of the three sequences in the Ainsa system (Fig. 5.24). It has been extensively studied by numerous authors, including Mutti and Normark (1987), Clark and Pickering (1996), Pickering and Corregidor (2000), and Falivene *et al.* (2006a, b, 2010). The base of the quarry section is defined by a poorly exposed MTC comprised of multiple MTDs typically having sand-rich mudstone matrices with abundant pebbles at the base, and mud-rich upper layers. The top of the MTC is irregular and is onlapped by thin-bedded, laterally discontinuous sandstones (FA4) comprising current ripples and interbedded mudstones. These sandstones, ~5 m thick, are characterised as thick-bedded, irregular and laterally discontinuous, having erosive bases. They are commonly composed of angular mud-clasts that form mud-flake breccias. Interbedded are thin, poorly preserved mudstones that show extensive bioturbation. Tabular sandstones overlay these deposits, which are ~10 m thick. An abundance of shallow erosional surfaces appear towards the base of these deposits indicating a weak confinement. Near the top, thin- to medium-bedded sandstones occur with thinning- and fining-upwards sequences. The top of the quarry outcrop is truncated by the erosive base of a MTC. This MTC separates the AI and AII

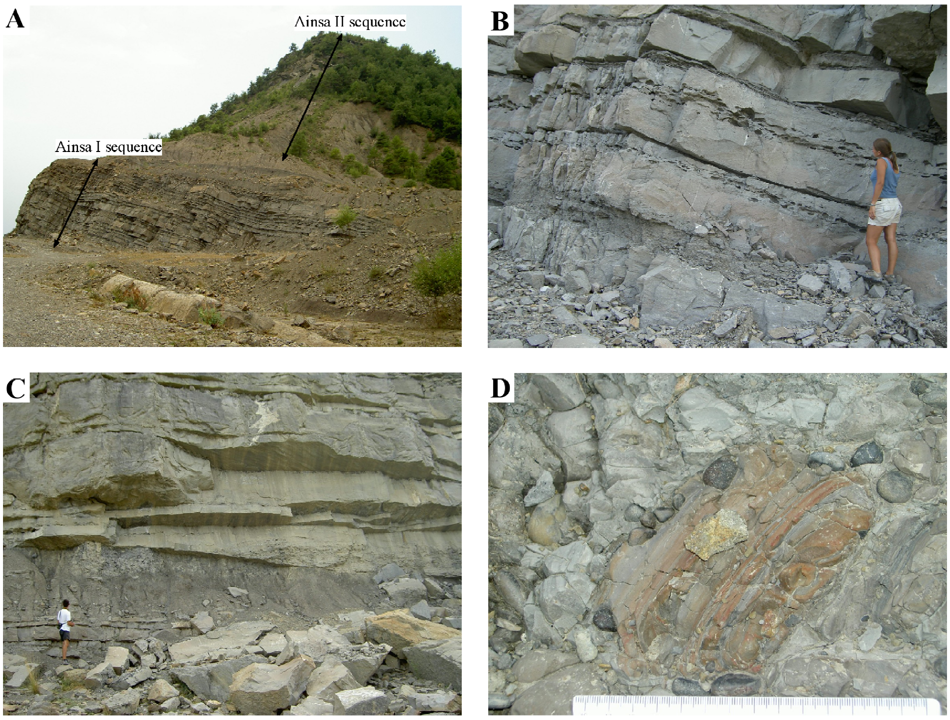

Fig. 5.22. Representative facies and sedimentary architecture in the Ainsa I sequence, Ainsa quarry. (A) Overview of the quarry outcrop highlighting the Ainsa I sequence (~25 m in height) and the Ainsa II sequence (~ 110 m in height). Note the gap between the sequences is represented by ~ 35 m of mud-dominated inter-sequence facies. (B) Thick-bedded, amalgamated sandstone (facies A1.4, B2.1 and C2.1), Ainsa I sandbody. (C) Lower part of the Ainsa I sandbody, with medium-bedded sandstone beds erosively infilling the topography created by a pebbly debrite (type II MTD). Note the erosive contact between the infill sands and the pebbly debrite (D) Red mud clast found within the pebbly debrite in C. Scale is 15 cm long.

sequences (Fig. 5.24).

The AII sequence outcrops north of the town of Ainsa. It is comprised of a stack of sandbodies that is tens-of-metres in thickness. The AII sequence shows a shift in basin orientation, to the southwest, likely due to the growth of the Mediano anticline during depositional times. An overall fining- and thinning-upwards trend is observed through the sequence. Erosion on the order of metres is prevalent. Individual sandbodies typically fine upwards and are coarse to very-fine grained. Bed thicknesses are anywhere from decimetres to metres and are commonly normally-graded.

The Ainsa quarry (Ainsa I sequence) is abundant in *Thalassinoides* and *Ophiomorpha*, particularly *Ophiomorpha rudis* ichnospecies. The majority of the trace fossils are post-depositional, deep structures (formed by endobenthic organisms), suggesting the environment was highly energetic and nutrient-rich (possibly eutrophic),

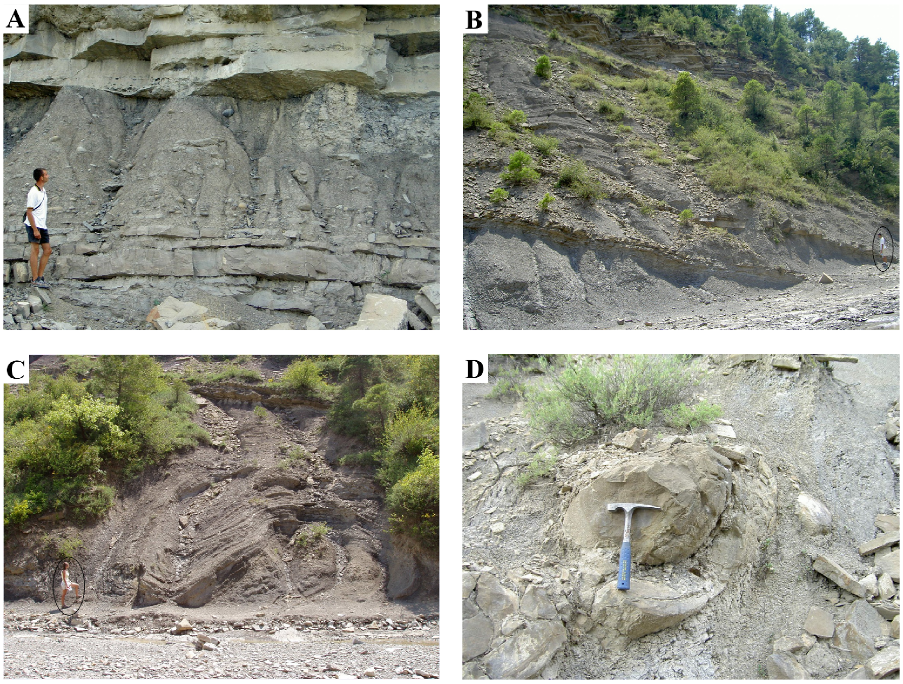

Fig. 5.23. Collection of MTDs from the Ainsa system. (A) Pebbly debrite (type II MTD; facies A1.3) in the lower part of the Ainsa I sequence, Ainsa quarry. (B) MTC comprising of number of muddy slump/slide material (type Ia MTDs; facies F1), at the base of the Ainsa II sequence, Barranco Forcaz. (C) Folded and contorted deposits (type Ia MTDs) forming part of the MTC at the base of the Ainsa II sequence, Barranco Forcaz. (D) Sand raft within a muddy debrite horizon, Ainsa II sequence, Barranco Forcaz.

and the passing sediment gravity flows were erosive; delicate, shallow-tier burrows, such as graphoglyptids were absent on the seafloor or were not preserved. The post-depositional ichnotaxa were formed by robust, deeply burrowing organisms that were able to survive burial by the newly deposited sediment (Wetzel & Uchman, 2001) and thrive in eutropic conditions (Rodríguez-Tovar *et al.,* 2010).

The Ainsa system is interpreted as lower-slope, erosional channels to proximal basin-floor channel systems. These settings contain three, topographically and structurally confined (linear), coarse-grained sequences. Each sandy sequence contains channel complexes and channel elements, typically 5–30 m deep and hundreds of metres wide (~100–600 m), and is defined at the base by a MTC. The sequences comprising the Ainsa system show a lateral southwest shift due to the development of intrabasinal growth anticlines (and structural segmentation) during the thrust-top phase of the Ainsa basin (tectonic phase II). The Ainsa system is finer grained than the Banastón system and forms the fining-upward part of the Banastón-Ainsa system set.

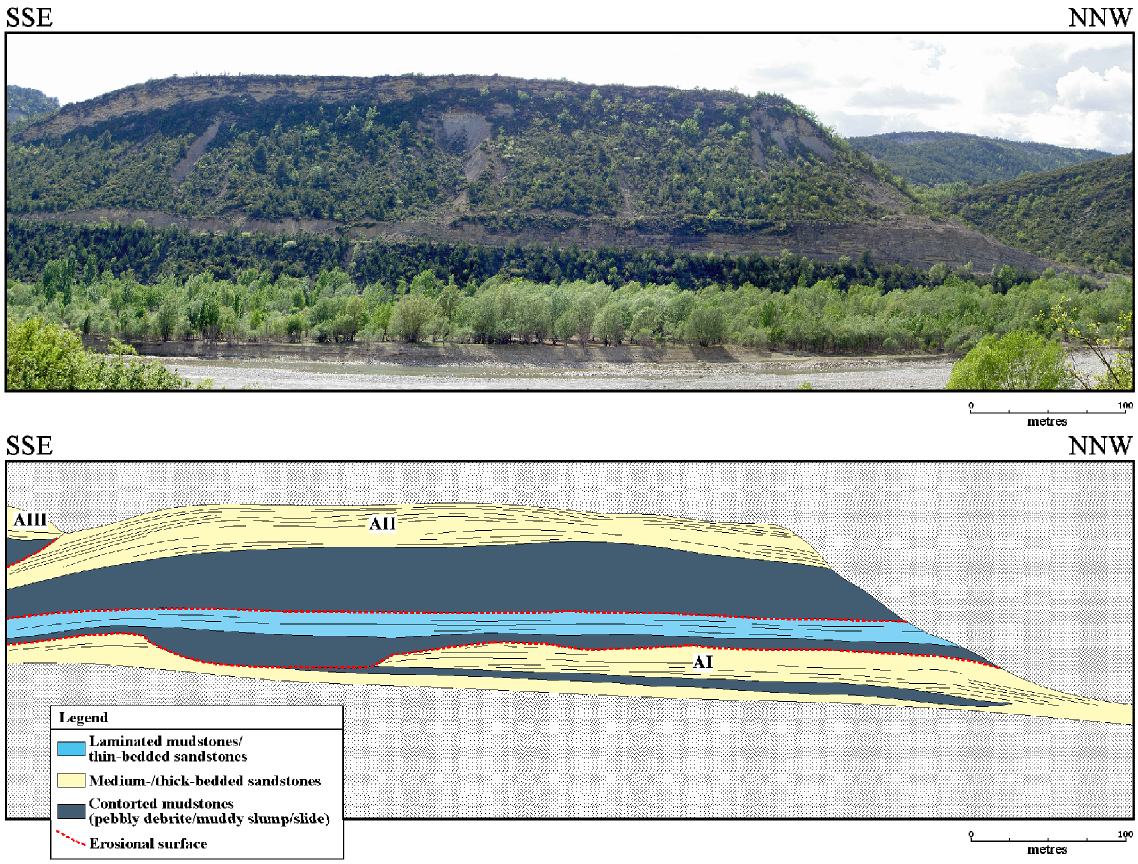

Fig. 5.24. Simplified photo interpretation of the Ainsa quarry outcrop, showing the dominance of contorted, pebbly mudstones (type I and II MTDs) throughout the Ainsa I and II sequences. Note the cutdown of a pebbly MTD into the Ainsa I channel margin element.

CHAPTER 6

THE UPPER HECHO GROUP: MORILLO AND GUASO SYSTEMS

6.1. INTRODUCTION

Studies have shows that there is a complexity of processes influencing the depositional styles of basin fills that can lead to the development of various architectural styles in deep-marine systems (Payros *et al*., 1999; Drzewiecki & Simo, 2000; Gardner *et al*., 2003; Hodgson *et al*., 2006; Amy *et al*., 2007; Hubbard *et al*., 2008; Sutcliffe & Pickering, 2009). The architectural elements comprising each sandy channelised system in the Ainsa basin shows a variation in architectural geometry and facies. This chapter documents examples of the way in which deep-marine systems change their architectural style in response to allocyclic controls. The upper division of the Upper Hecho Group consists of the youngest deep-marine systems in the Ainsa basin, the Morillo and Guaso systems. These systems are stratigraphically significant because they represent the final stages of deep-marine sedimentation in the basin, and record an important tectonic regime of shallowing and depositional confinement. Sedimentological and architectural element analysis is used in this chapter to elucidate basin configuration during deposition of the Morillo and Guaso systems.

6.2. THE MORILLO SYSTEM

6.2.1. INTRODUCTION

The Morillo system is up to ~260 m thick and is stratigraphically located above the Ainsa system, forming the third depositional system (from the base) in the Upper Hecho Group. Age dating of the Ainsa basin suggests the deposition of the Morillo system occurred during the mid Lutetian (Payros *et al*., 1999; Remacha & Fernández, 2003; Pickering & Corregidor, 2005). Nine localities were visited and ~1,110 m of measured section was obtained (Localites 37–43,Table 2.1) from the village of Coscojuela in the south to Sieste in the north, covering a distance of ~9 km. The Morillo system comprises three sandy sequences (Morillo I–III) that accumulated in a mid-slope canyon in the south, to lower-slope, structurally confined channel system in the north (Fig. 6.1).

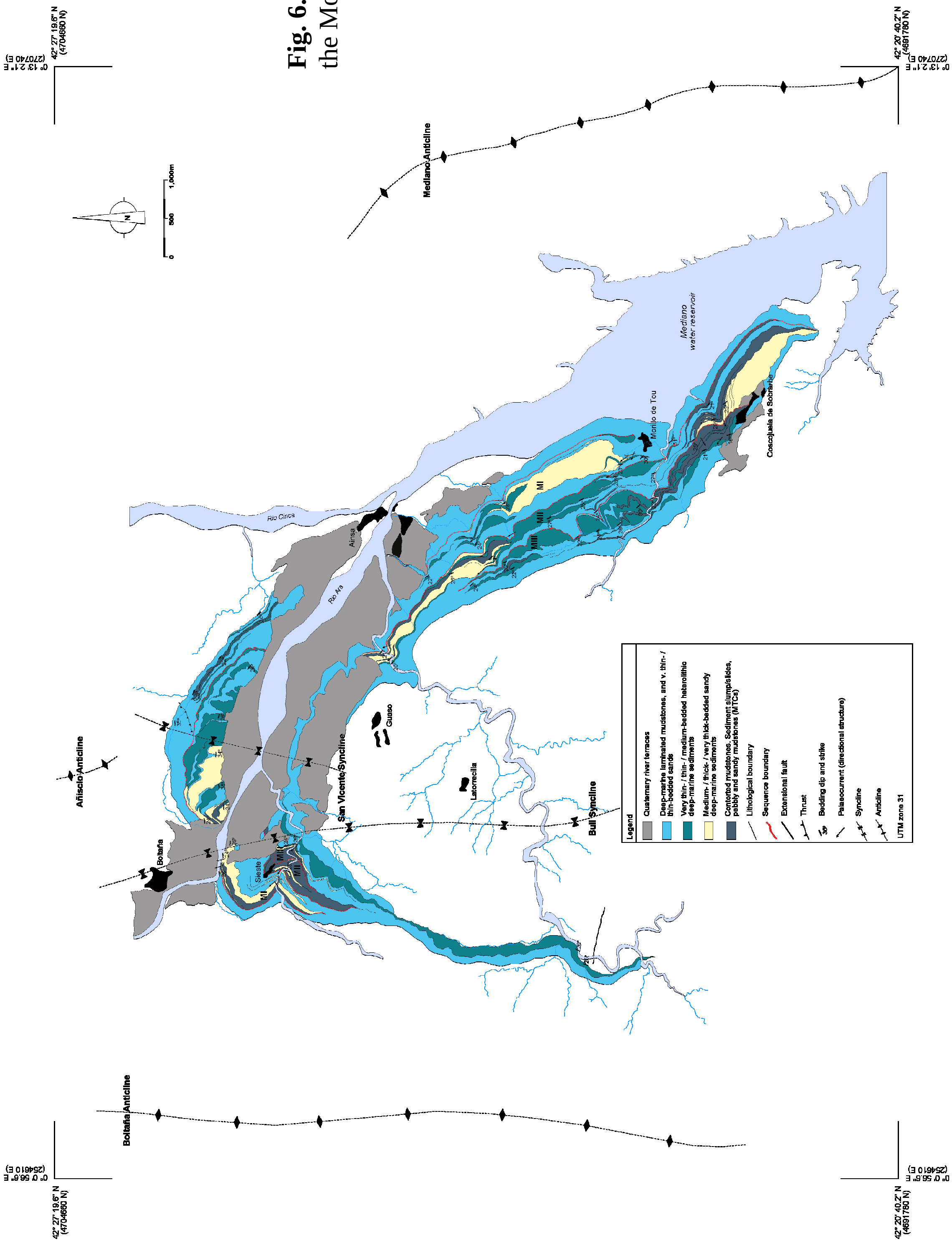

Fig. 6.1. Geological map of the Morillo system

The general characteristics of each sequence are outlined in Table 6.1.

Sequence		**MI**	**MII**	**MIII**
Dimension	Thickness (m)	100	87	72
	Width (m)	2700	2500	2100
	Aspect ratio (W/D)	27.0	28.7	29.2
Number of beds measured	Total number	2785	2265	1244
	Total thickness	188	292	125
	% amalgamated	4	5	3
Bed thickness (cm)	Average	7	13	10
	S.D.	34	102	77
	Min/Max	1/780	1/2755	1/1800
Basal MTC (m)	Thickness	30	9.5	11
	Width	1940	1560	1130
	Aspect ratio (W/D)	64.6	164.2	103
Facies class abundance (%)	Class A	1.1	3.9	0.9
	Class B	1.1	2.1	1.4
	Class C	28.7	23.9	30.1
	Class D	24.6	15.0	24.7
	Class E	44.2	54.9	42.4
	Class F	0.2	0.2	0.5
	Class G	0.0	0.0	0.0
	Class H	0.0	0.0	0.0

Table 6.1. General characteristics of each sequence in the Morillo system.

Figure 6.2 shows facies class abundance in the Morillo systems, presented by the total number of beds and the total thickness measured. There is a noticeable number of beds associated with facies class C–E, and thickness tends to be high for facies class A, C and E.

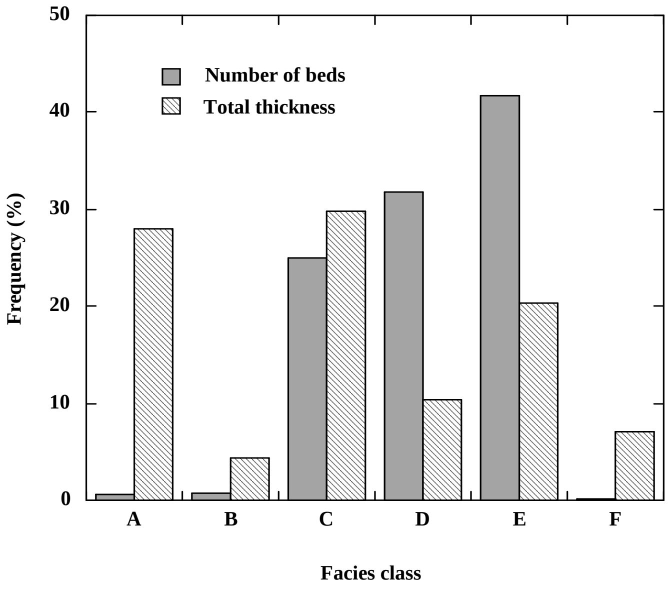

Fig. 6.2. Facies class abundance in the Morillo system

A very wide range of facies are recognised in the Morillo system, particularly a wide variety of MTDs (Fig. 6.3 and 6.4).

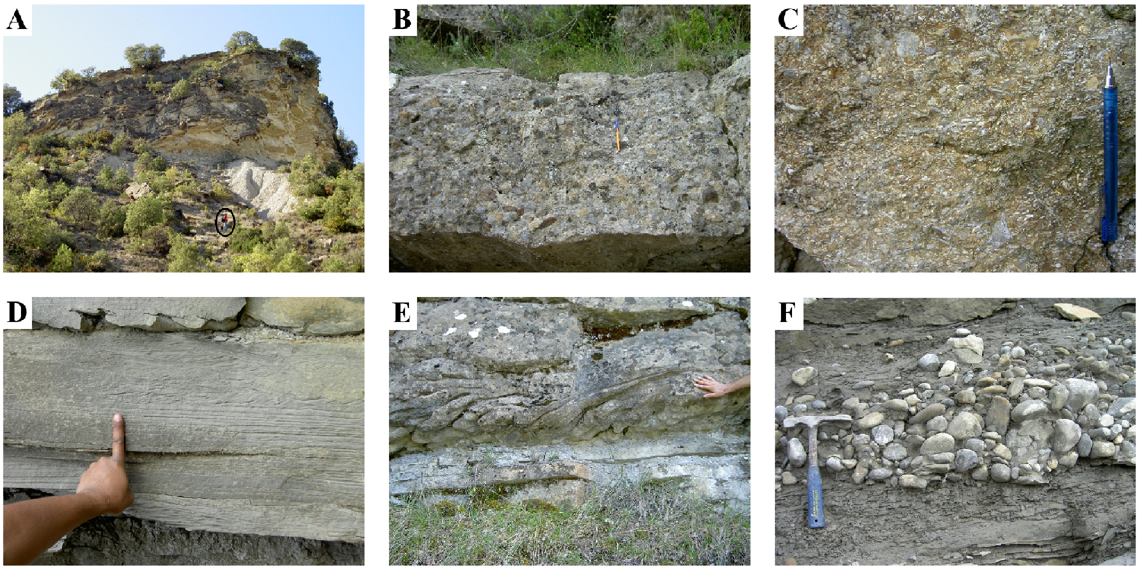

Fig. 6.3. Representative facies in the Morillo system. (A) Very thick-bedded, coarse-grained sandstones (facies B2.1 and C2.1; FA1), MI sequence, Morillo de Tou. (B) Normally-graded gravel (facies A2.3), MII sequence, Rio Sieste. (C) Disorganised, pebbly nummulitic sand (facies A1.4), MII sequence, Rio Sieste. (D) Current-rippled, fine-grained sandstone bed (facies C2.3), MI sequence, Rio Ara (E) Load structures in thick-bedded, disorganised sandstone (facies B1.1), MI sequence, Rio Ara (F) gravel lag (facies A2.1), within basal MTC, MI sequence, Rio Sieste. Note scales in all plates.

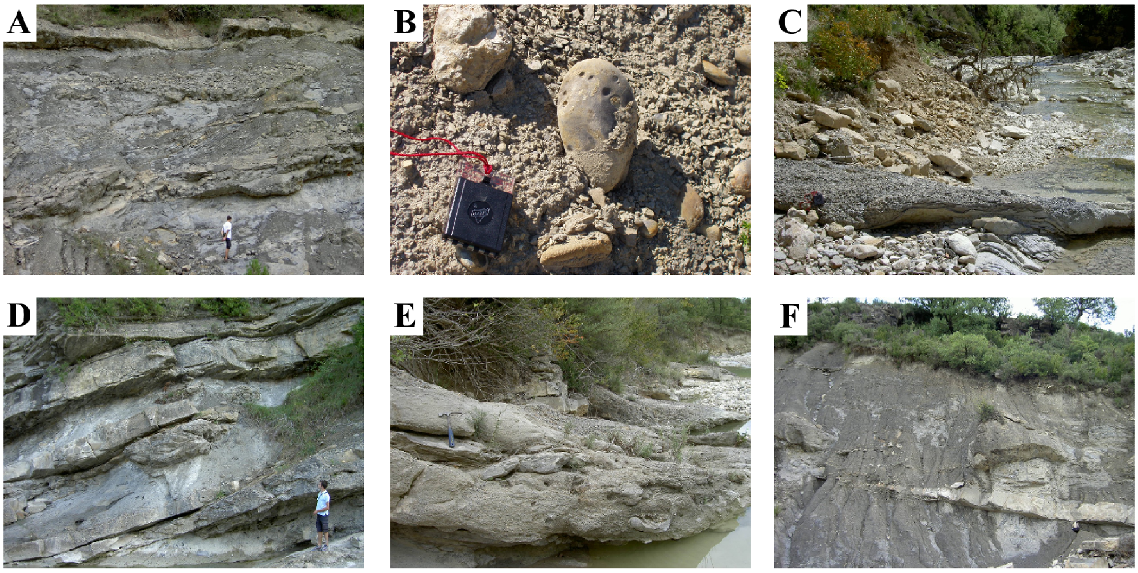

Fig. 6.4. Representative MTDs in the Morillo system. (A) MTC composed of multiple type II MTDs, including a scour infilled with subangular sandstone clasts, MI sequence, Rio Sieste. (B) Detailed view of a pebbly debrite, showing a well-rounded limestone cobble with *Lithophaga* borings formed in the littoral zone prior to redeposition (facies A1.3), MI sequence, Barranco Ranito. (C) Gravel barform (facies A1.1), MII sequence, Rio Sieste. (D) Stacked erosive, muddy debrites/gravelly MTDs with a high proportion

sandstone rafts (facies A1.2 and A1.3), basal part of the MII sequence, Sieste. (E) Sandy debrite with sandstone clasts (facies A1.2), MII, Sieste. (F) Large sand rafts entrained in a highly cohesive muddy slump, indicating matrix strength (facies A1.3). Note the thick-bedded sandstone infilling the topography created by the deposit, MIII sequence, Rio Sieste. Note scales in all plates.

The most common trace fossils in the lower-slope, sandy depocentres of the channelised Morillo sequences are *Ophiomorpha,* a dwelling/*domichnial* trace; *Halopoa, Scolicia*, *Gordia*, grazing/*pascichnial* traces; *Megagrapton* and *Paleodictyon*, traps and gardening/*agrichnial* traces. The Morillo I–III sequences are represented by a moderate diversity, low abundance trace-fossil assemblage; there is an increase in diversity and abundance with lateral distance from the channel axis-environments, and vertically, following a temporal trend of decreasing bed thickness and average grain size of sandstone beds (see Chapter 5 for explanation).

The sequences in the Morillo system are recognised by: (1) a mappable erosional base situated in the depositional axis of sequences, usually overlain by (2) a MTD (typically type II) or a MTC, then (3) a succession of sandstones and/or gravels (FA1 and FA2), followed by (4) heterolithic sediment (FA3) representing backfilling and abandonment. The Morillo sequences are regarded as mixed erosional/depositional type channel complexes (*sensu* Mutti & Normark, 1987).

Measurements of the sole structures in proximal outcrops of the Morillo II and III, around the area of Coscojuela village (Locality 43, Table 2.1), show palaeoflow towards the west-southwest (~260º) with relatively little dispersion (Fig. 6.5), suggesting a consistent point source in the east. However, the measurement of sole structures, cross-stratification and current ripples in the Morillo I sequence at Morillo de Tou (Locality 40, Table 2.1) shows wide palaeoflow dispersion, indicative of a meandering system (mean flow ~290º). Downslope, palaeoflow measurement at Rio Ena (Locality 44, Table 2.1) and Rio Sieste (Locality 41, Table 2.1) become more consistent, towards a northerly direction (~348–357º). This downslope trend in palaeoflow is later discussed in more detail.

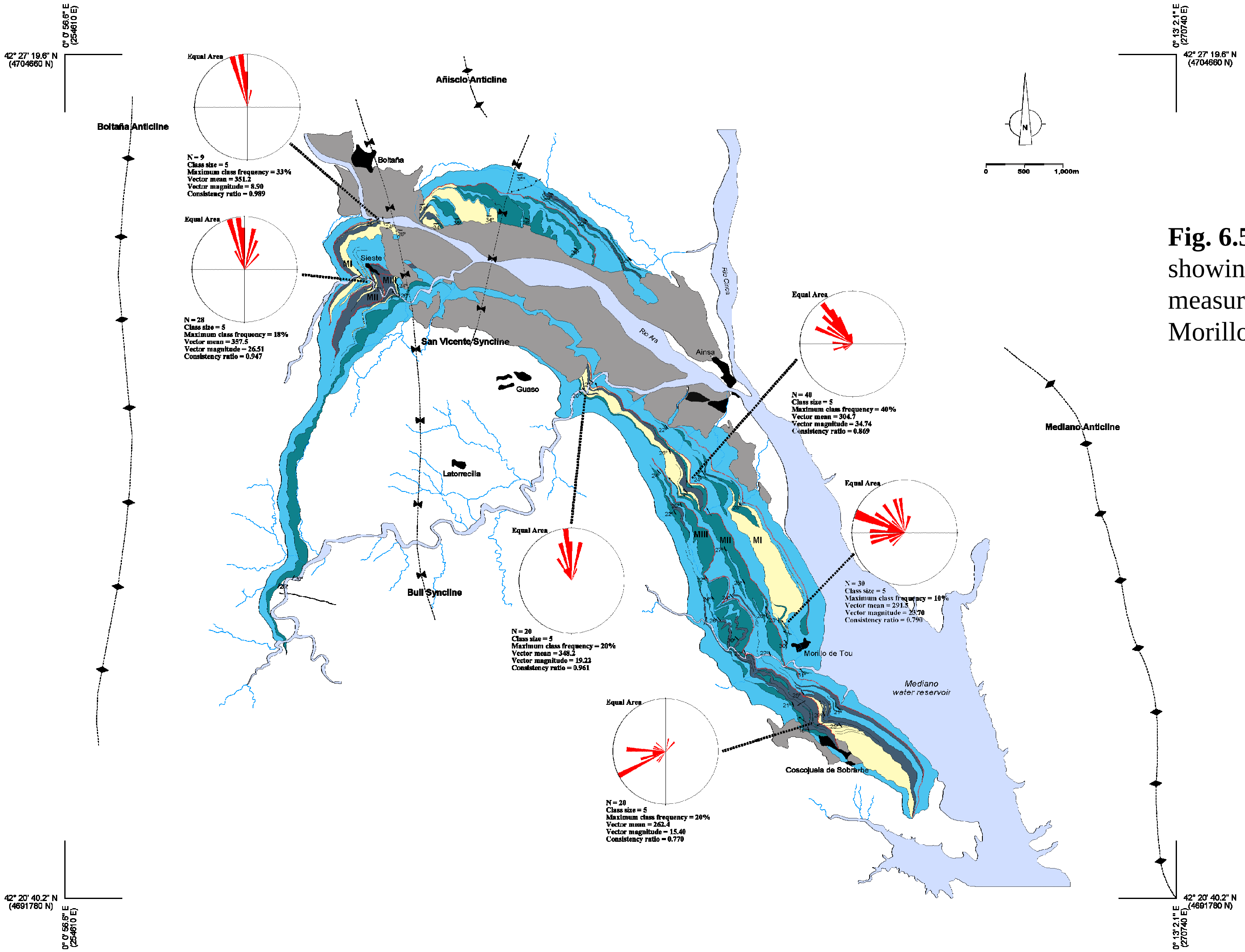

Fig. 6.5. Rose diagrams showing palaeocurrent measurements in the Morillo system

6.2.2. MID-SLOPE CANYON ENVIRONMENT

The mid-slope canyon environment crops out at the village of Coscojuela (Locality 43, Table 2.1) and is particularly well exposed in Barranco Fuen Mazana (Fig. 6.6). The base of the Morillo system is not exposed at this locality, but the top part of Morillo I is defined by a ~26 m thick muddy MTC. This is overlain by a ~27 m thick laminated mud division (FA5) comprising the abandonment facies of the same sequence, followed by a ~92 m thick MTC (FA1) of the Morillo II sequence and a ~54 m thick MTC (FA1) of the MIII sequence. Each MTC is composed of individually stacked MTDs (mainly type II; pebbly mudstones/facies A1.3), containing an abundance of subangular limestone clasts and rafts. These deposits are punctuated by laterally discontinuous, irregular gravel and conglomerate deposits (barforms), which are also defined by a high proportion of limestone clasts (Fig. 6.7A and B). The limestone clasts indicate significant erosional downcutting of the underlying seafloor during canyon excavation. The gravelly MTDs are punctuated by small packets of pebbly sandstones (facies A1.4), typically 2–5 m thick (Fig. 6.7C and D). Some of these gravel beds form amalgamated units of stacked clast-supported pebbly sandstones, often showing reverse grading (facies A2.2; Fig. 6.7E).

The top of Morillo II and III sequences are characterised by normally graded pebbly sandstones (facies A2.4) and parallel laminated, medium- to thick-bedded, coarse-grained sandstones (facies B2.1), representing the backfilling stage of each sequence. This outcrop extends laterally to more marginal deposits in the northwest, where FA1 transitionally pass into thinner units, comprising less extensive MTDs, overlain by finer-grained sandy deposits in the Barranco Moriello stream section. The southern margin of the canyon-fill onlaps against the flanks the Mediano anticline to the south of Coscojuela village, showing abrupt depositional thinning on to the structural high.

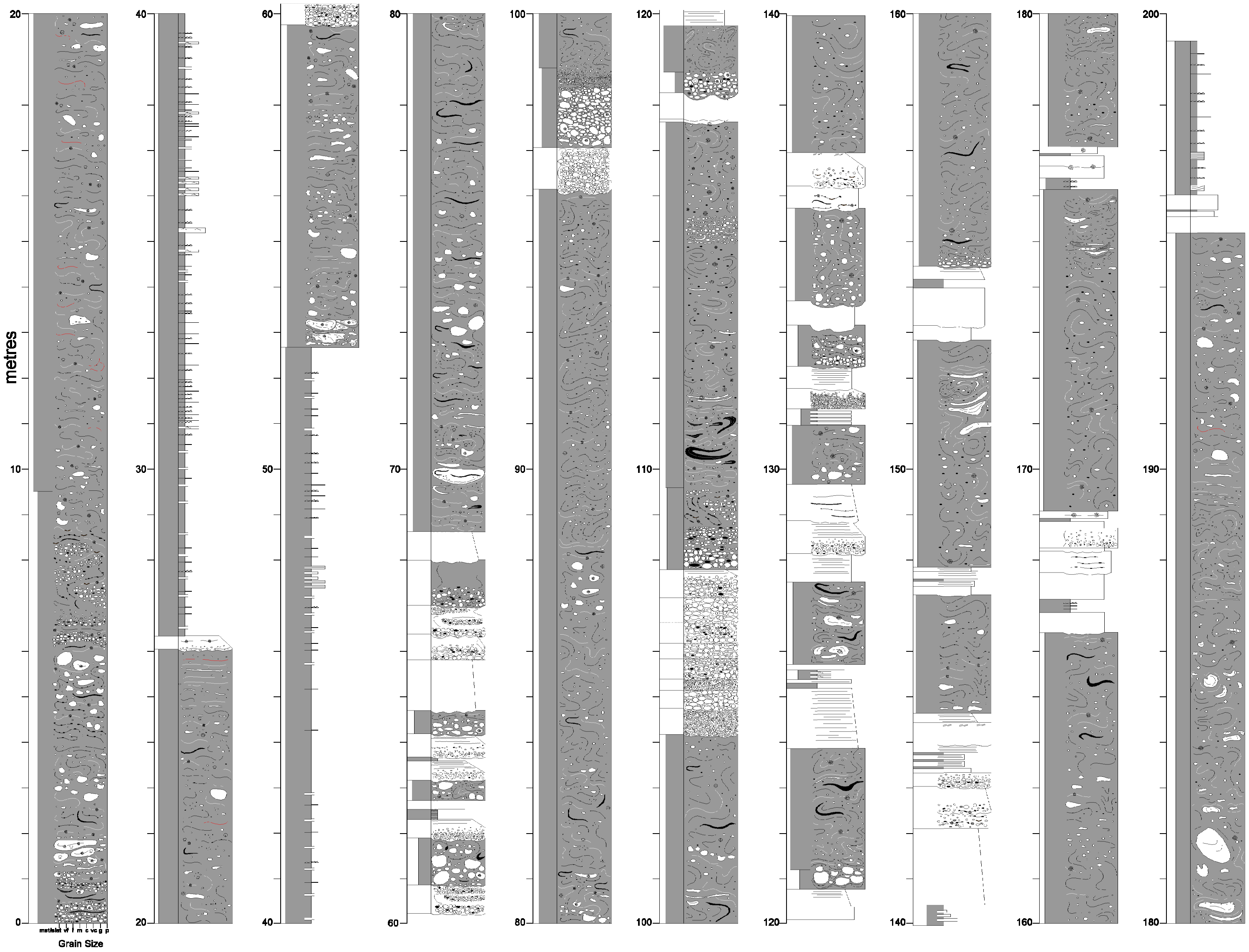

Fig. 6.6. Detailed sedimentary log through the MI–MIII canyon sequences in Barranco Fuen Mazana.

Fig. 6.7. Representative facies and architecture in the mid-slope canyon area, Morillo system, Barranco Fuen Mazana. (A) View of the ridges composing MII and MIII sequences. Palaeoflow from right to left of plate (see rose diagram). (B) Interpretation of plate A showing facies horizons in the foreground and key ridges in the background. Note the thickening of packages towards the left corner of plate marking the sequence axis to the southeast. (C) Carbonate-rich amalgamated unit comprising pebbly sandstone beds (facies A1.4). Thickness of unit is ~210 cm. See B for location (labelled ‘1’). (D) Pebbly sandstone unit (labelled ‘2’ in plate B; facies A1.4), encased in pebble mudstones (Type II MTDs, facies A1.3). Note the cutdown of clast-supported pebbly sandstone in the upper left of plate. (E) Gravelly barform consisting of amalgamated, clast-supported pebbly sandstone beds, often showing reverse grading (facies A2.2). See B for location (labelled ‘2’)

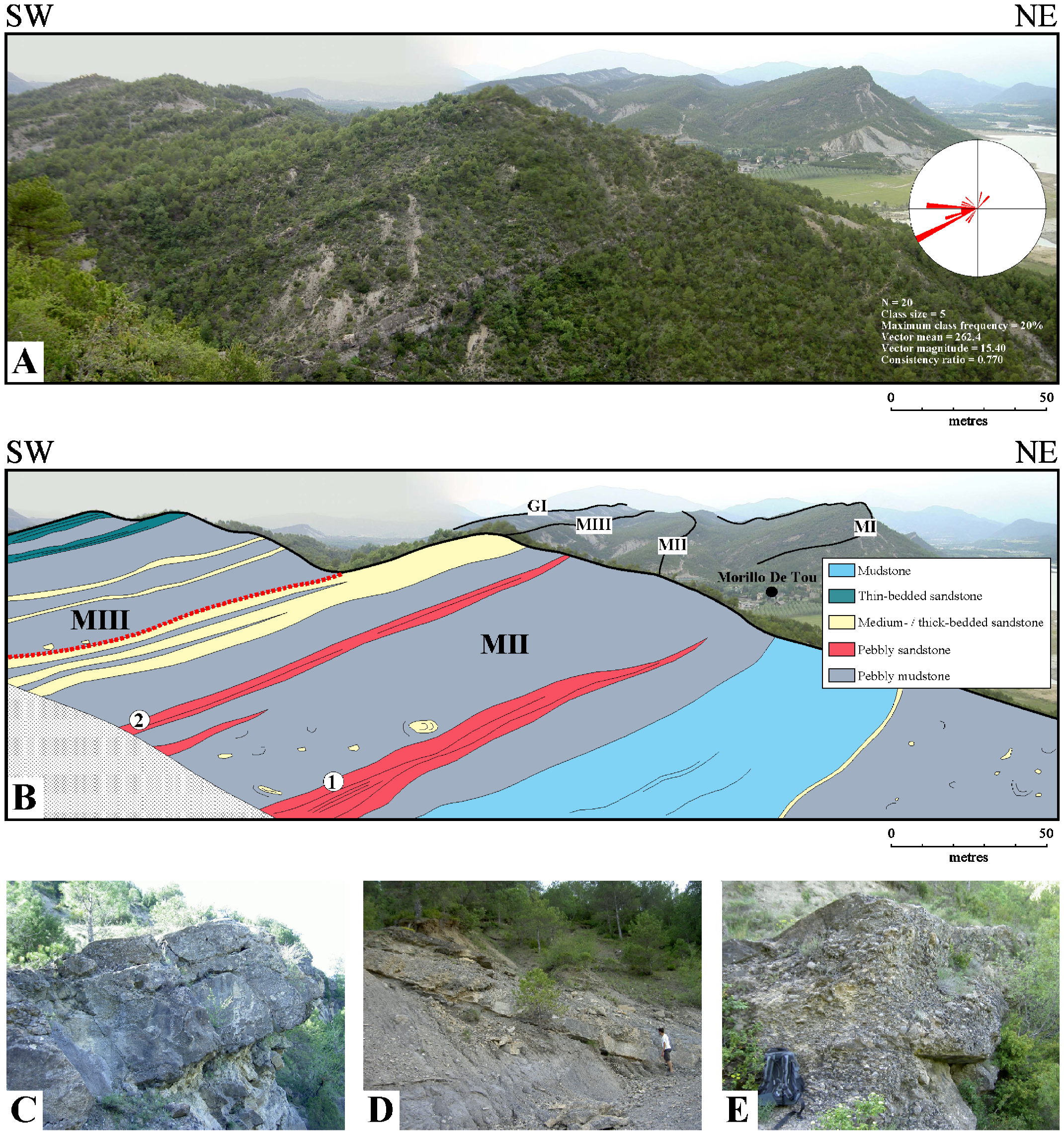

6.2.3. LOWER-SLOPE CHANNELISED ENVIRONMENT

6.2.3.i. Morillo I sequence

The Morillo I sequence has a maximum thickness of ~100 m and forms the thickest sequence in the Morillo system (see Table 6.1 for general characteristics). It contains the highest abundance of facies class C and E, with 4% of beds amalgamated. The sequence is superbly exposed at Morillo de Tou (Locality 40, Table 2.1), forming a ~85 m thick sandy succession defined at the base by a discrete sandy package comprising a channel complex (MIa; Fig.6.8). A ~12 m thick muddy MTD (facies A1.3) defines the base of the main sandy complex (MIb). The sand forms an extensive ridge trending north-northwest–south-southeast (A Sierra Moriello). The top of the ridge is defined by MIc channel complex, which is well-exposed farther downflow, in the northwest of the ridge. The channel complexes are composed of individually stacked channel elements, defined at the base by an erosional surface (Fig. 6.8). As mentioned previously, this outcrop shows a wide dispersal of palaeocurrents, possibly representing sinuous channel elements.

The southwestern margin of Morillo I is exposed in Bco. Cotón, near Morillo de Tou, and is ~85 m thick (Fig. C7). This section shows the transition from sinuous channel fills to laterally equivalent overbank environments. It is characterised by three channel complexes, with well-developed fining-upward sequences, ~20 m thick and separated by several metres of thin-bedded sandstones and siltstones (FA4). Figure 6.9 is a photo interpretation of the outcrop, showing the types of facies comprising the channel margin environment of Morillo I. The lower channel complex is defined by a ~11 m thick type Ia MTD that is overlain by a 5 m thick package of thin- to medium-bedded sandstones (FA3). The main channel element is ~10 m thick and is characterised by medium-bedded, commonly amalgamated sandstones at the base (FA2), and thin- to medium-bedded sandstones (FA3) at the top, forming an overall thinning- and fining-upward sequence. Current ripples are common within the medium-bedded sandstones (FA3). The sandstone have well-developed internal stratification, including parallel and cross lamination. This sandy succession is overlain by very thin- to thin bedded sandstones, siltstones and mudstones (FA4 and FA5).

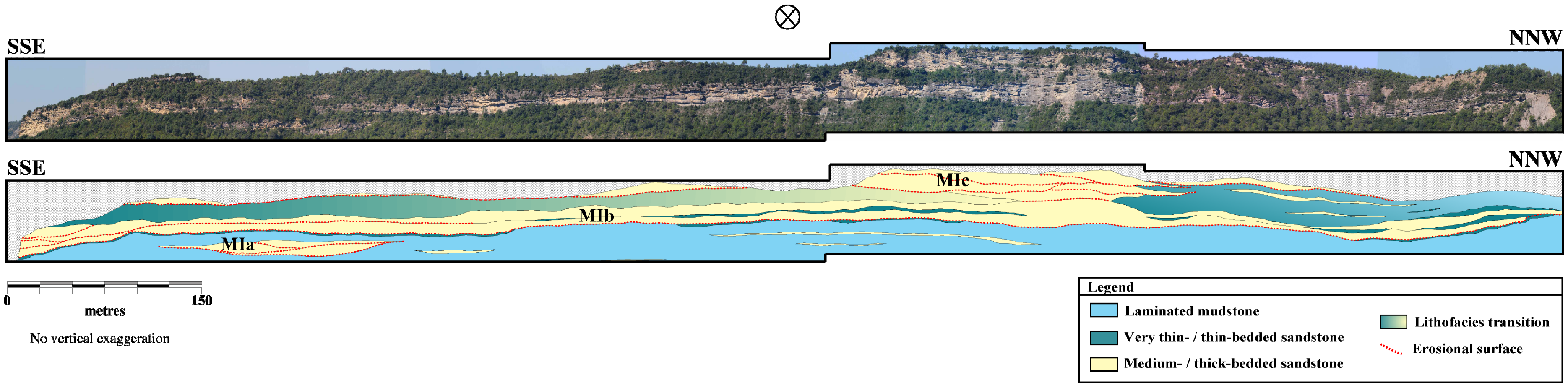

Fig. 6.8. Stacked channel complexes in the MI sequence, A Sierre Moriello ridge. Note that each channel complex comprises a number of channel elements. The spatial relationship and orientation between complexes possibly reflects sinuosity. For example, channel complex MIc shows more confinement than the underlying complexes and could be attributed to sinuosity.

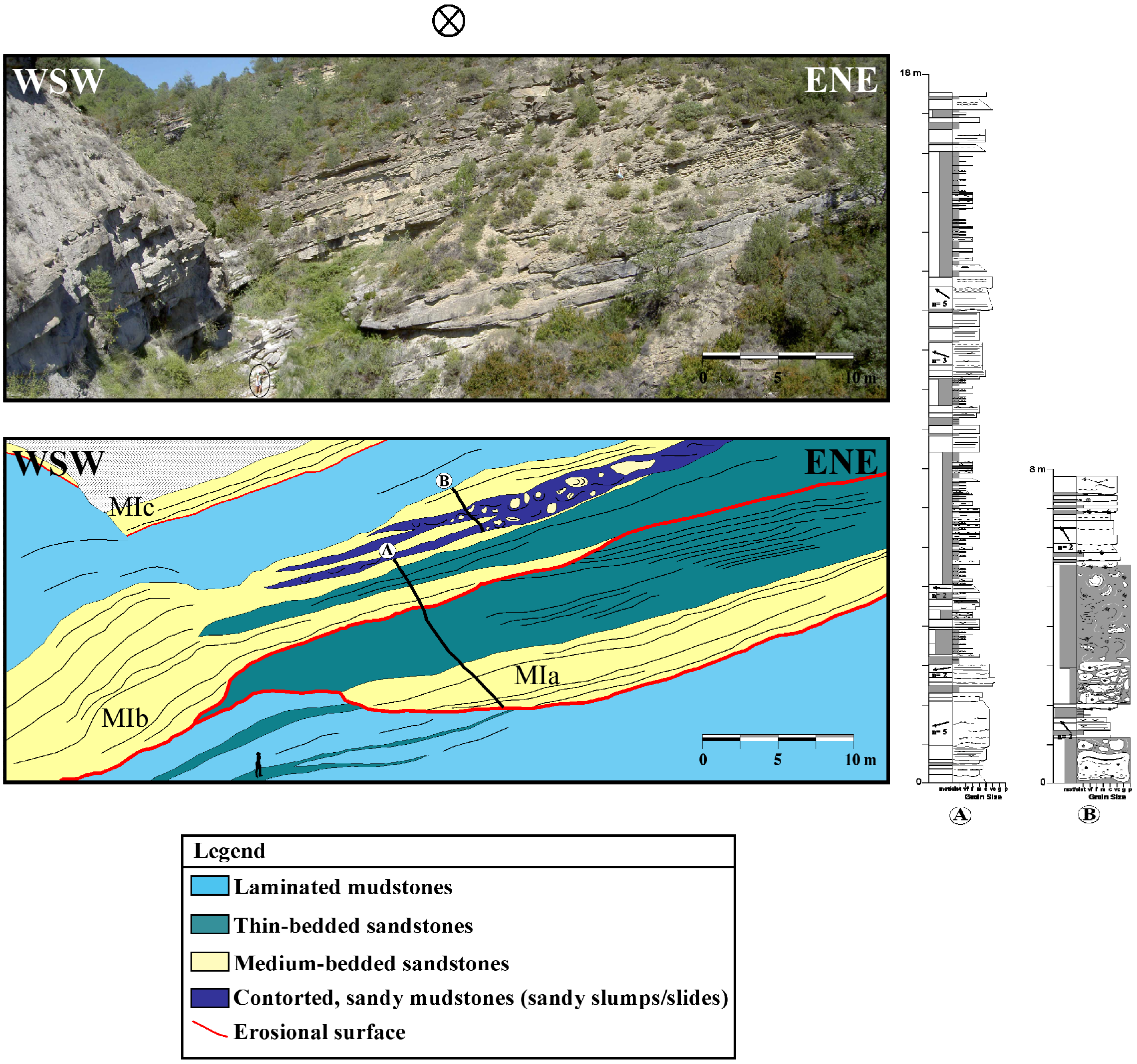

Fig. 6.9. Photo interpretation of the margin environment in MI sequence showing the arrangement of channel complexes (MIa–c). The arrows on the sedimentary logs represent palaeocurrents measurements from tool marks. Person for scale is circled. See Figure C7 for a complete sedimentary log.

The second channel complex comprises two vertically stacked channel elements (see Fig. 6.9), ~10 m thick, with well-developed fining-upward sequences. The sandstones within each channel element are typically amalgamated, with erosive bases (facies A1.4, FA4). Axially (to the northeast), the channel complexes are separated by a ~5 m thick MTD. The MTD can be interpreted as a localised sandy slump deposit (type Ib, facies F2), originating from the collapse of the open conduit farther up-dip. The sandstones overlying this MTD infill the irregular topography created by the depositional mound. The top part of channel complex is overlain by ~8 m of medium- to thin-bedded, fine-grained stratified sandstones (FA5), forming an overall fining-upward sequence. The upper channel complex defining Morillo I consists of a sandy unit ~20 m thick, with thick-bedded sandstones (FA2) at the base, and thin- to medium-bedded sandstones at the top (FA4 and FA4). These sandstones are rarely amalgamated, and have flat bases. Internal stratification is common, including planar and wavy lamination.

Farther north, the northeastern margin of the Morillo I sequence and the constituent channel complexes are exposed in Barranco Ranito (Fig. 6.9). The outcrop represents a more lateral margin environment, and shows ~10–15 m thick marly units separating the channel complexes. Each channel complex is composed of thick- to medium-bedded sandstones at the base (FA2), followed by a finer-grained, upper division containing thin-bedded, fine- to medium-grained sandstone (FA3 and FA4). Channel complex MIb is defined at the base by a ~11 m thick type II MTD (facies A1.3), which confines the overlying sandy package.

The base of the Morillo system is defined in the lower-slope setting (Rio Sieste, Locality 41, Table 2.1) by a ~30 m thick MTC (Figs. 6.10 and C9), characterised by abundant pebbles and sand rafts, with gravel-rich scours and stringers commonly defining the base of individual MTDs. This MTC forms the base of the Morillo I sequence, and is overlain by a sandy complex, ~70 m thick. The base of the Morillo I also crops out at Locality 39 (Table 2.1) parallel to Rio Ara river (Fig. 6.11), which is slightly more off-axis than the Rio Sieste outcrop. The MTC represents a composite unit containing a number of large-scale erosional features that removed thick sandbodies and incorporated the material into the flow. Subsequently, the MTDs are mainly deposits from sandy debrites (MTC type I, facies A1.2) in this area. The upper sandy channel complex predominantly comprises thick- to medium bedded, coarse- to fine-grained sandstones. A characteristic feature of this complex is the abundance of sandy barform elements, showing lateral accretion elements (*sensu lato* Abreu *et al*., 2003). The vector mean bedding orientation in the LAPS strike to the northwest and dips to the northeast (bedding restored to palaeohorizontal; n = 8); and exhibit a vector mean palaeocurrent direction to the north-northwest (~340°; n = 15). Beds commonly consist of a basal pebbly sand (facies A1.4), followed by a thick- to medium-bedded sandstone (facies C2.3 and C2.3) and overlying thin-bedded sandstone and siltstone (facies C2.4 and C2.5), forming a fining-upward trend in each lateral accretion element.

6.2.3.ii. Morillo II sequence

The Morillo II sandy sequence has a maximum thickness of ~87 m at Rio Sieste (see Table 6.1 for general characteristics), and is ~60 m thick in a slight off-axis location in Rio Ena (Fig. C8). The sequence is characterised by a high abundance of facies class C and E, with 5% of beds amalgamated. The northeastern margin of the Morillo II sequence is exposed in Barranco Ranito where it is composed of three, fining-upward channel complexes (FA3 and FA4). The base of the middle channel complex is defined by a ~14 m thick type II MTD (pebbly mudstone, facies A1.3).

The depocentre of Morillo II is located in Rio Sieste (Locality 41, Table 2.1) and is dominated by facies class A deposits (particularly type II MTDs). The base of the sequence is associated with a ~10 m thick pebbly mudstone (type II MTD; facies A1.3), with deformed sandy units (sand rafts) incorporated into the upper part of the deposit. Overlying the MTC is a ~3 m thick unit of thin- to medium-bedded sandstones (FA3).

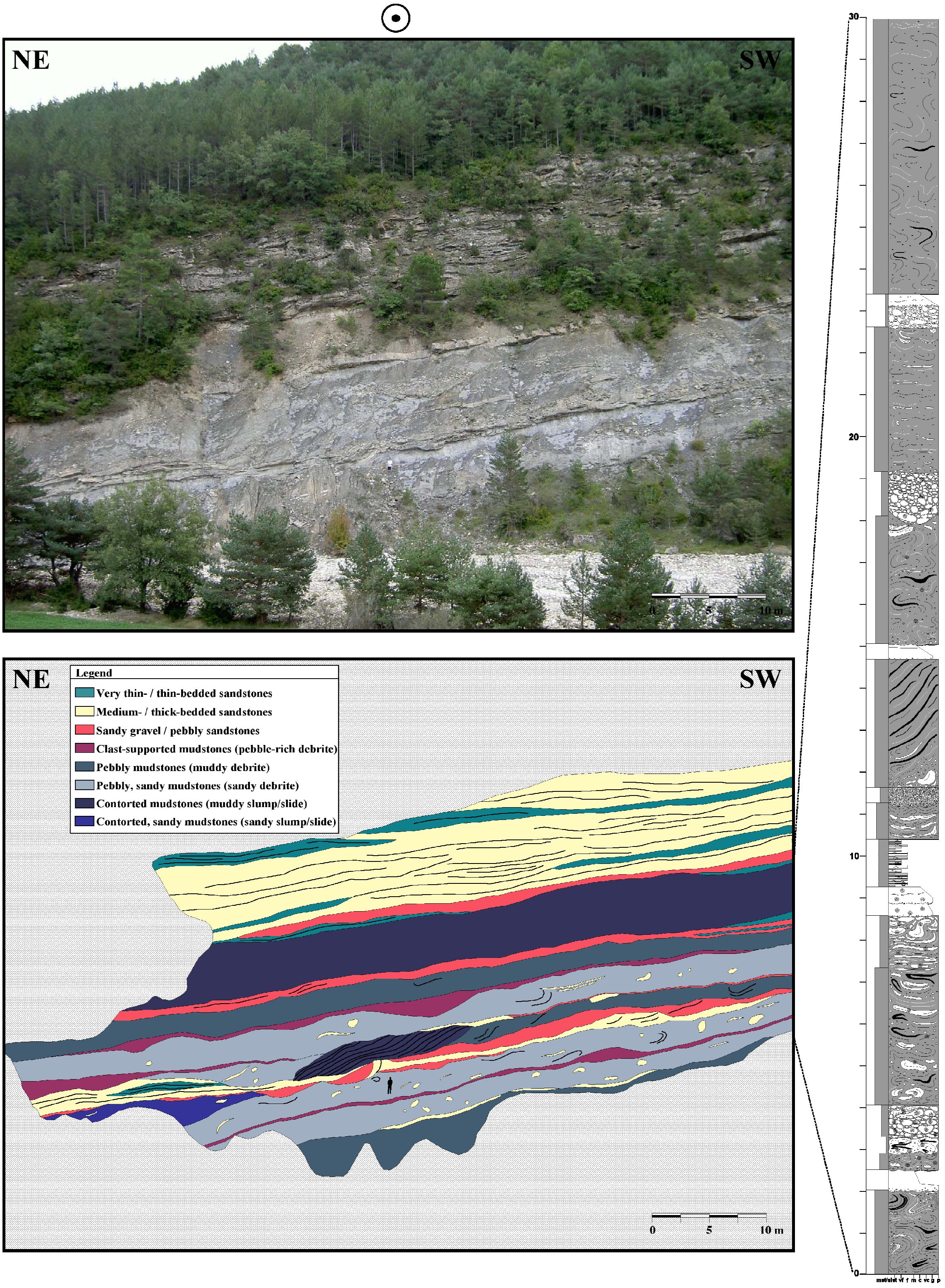

Fig. 6.10. MTC comprising a range of MTDs defining the base of MI sequence, Rio Sieste.

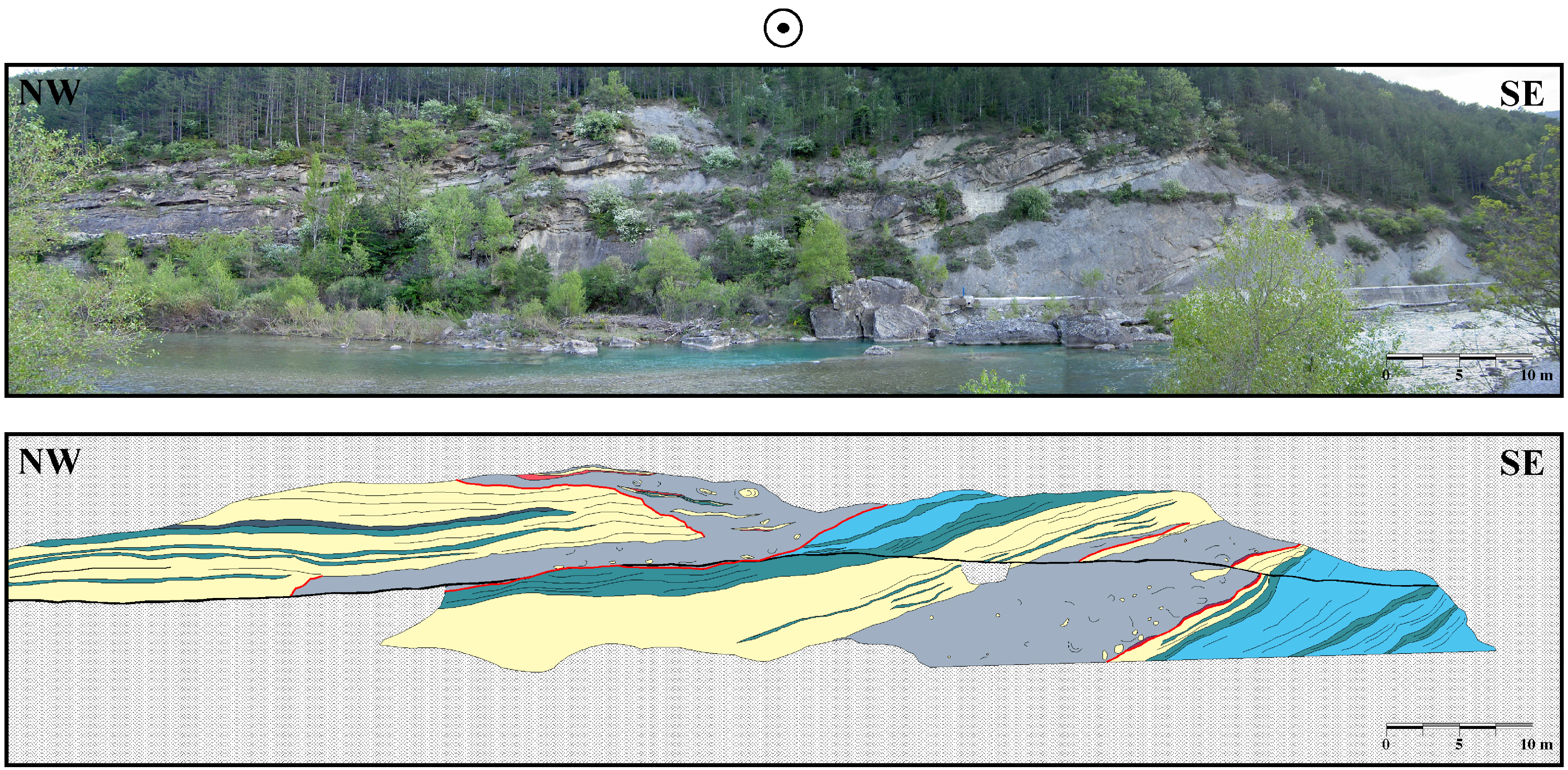

Fig. 6.11. Base of the MII sequence showing large erosional surfaces, Rio Ara.

Legend

🟦	**Laminated mudstones**	🟥	**Clast-supported mudstones (pebble-rich debrite)**
🟩	**Very thin- / thin-bedded sandstones**	■	**Pebbly mudstones (muddy debrite)**
🟨	**Medium- / thick-bedded sandstones**	▨	**Pebbly, sandy mudstones (sandy debrite)**
🟥	**Pebbly sandstones**	/	**Erosional surface**

These deposits are erosively overlain by an amalgamated unit, ~6 m thick, comprising laterally discontinuous gravel and pebbly sandstones (FA1). These deposits form a lens-shaped, gravelly barforms (Fig. 6.12), which show lateral accretion elements. The upper part of Morillo II sequence is characterised by thick- to medium-bedded, amalgamated sandstones with well-developed planar stratification (facies B2.1 and C2.3), interbedded with significant units of muddy MTDs. The majority of the MTDs show internal complexity, with basal gravel divisions and upper muddy divisions, representing multiphase granular flows as described by Parsons *et al*. (2001) and Pickering and Corregidor (2005). The top of the sequence is represented by a ~17 m thick MTD in Rio Sieste, with a pure carbonate matrix (as identified by thin-section analysis) and outsize visco-plastically deformed rafts of intraformational sandstones. A similar, but unrelated deposit is present at the top of the sequence to the south (Barranco Moriello section). These deposits are interpreted as carbonate mass flows.

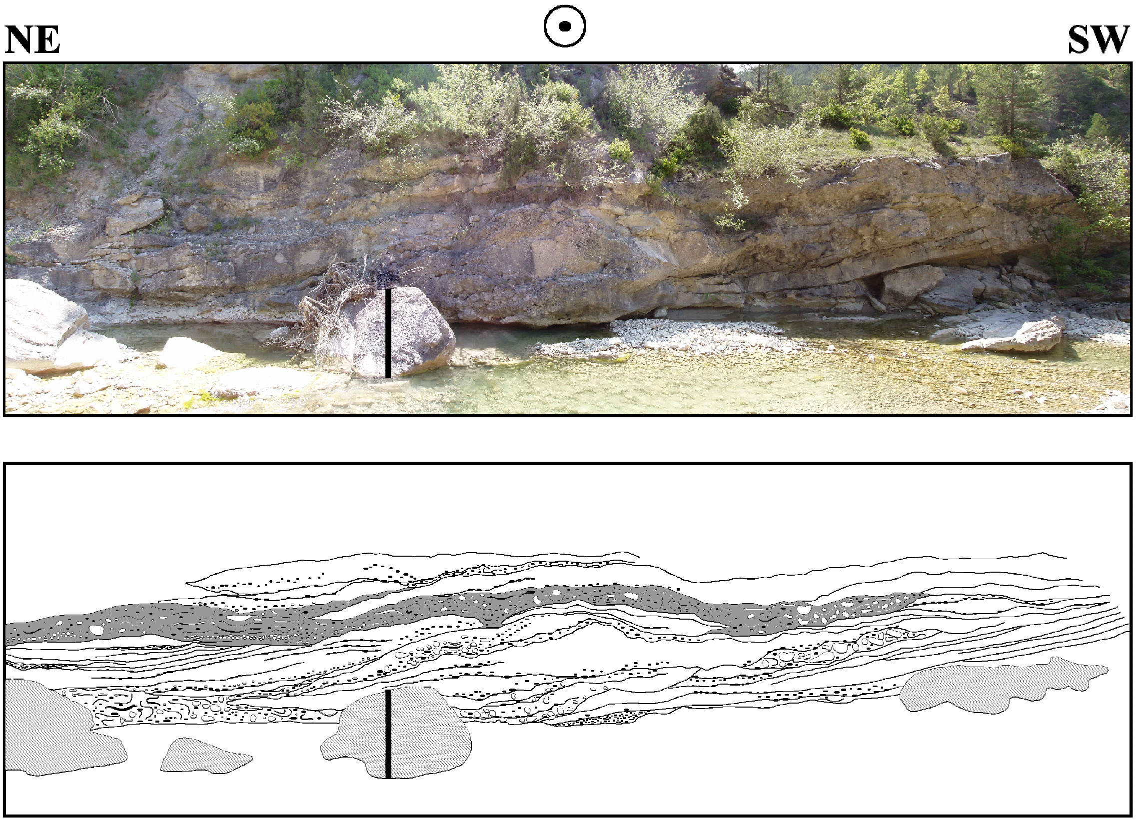

Fig. 6.12. Gravel bar form, MII sequence, Rio Sieste. Scale bar is 2 m.

6.2.3.iii. Morillo III sequence

The Morillo III sequence has a maximum thickness of ~72 m (see Table 6.1 for general characteristics), and is characterised by a high abundance of facies class C and

E, with 3% of beds amalgamated. The sequence is mainly exposed in Rio Sieste (Locality 41, Table 2.1) where it forms a thick MTC (Fig. 6.13 and C9). The MTC comprises a number of stacked MTDs, consisting of discontinuous gravel horizons and sandy mudstones (FA1), interbedded with thick- to medium-bedded, coarse- to medium-grained sandstones (FA2). The heterogeneous fill of this sequence is characterised by rapid lateral facies changes, partly due to the abundance of type II MTDs that formed both the irregular topography upon which the sandstones were deposited, and also eroded many of the sandstone packets.

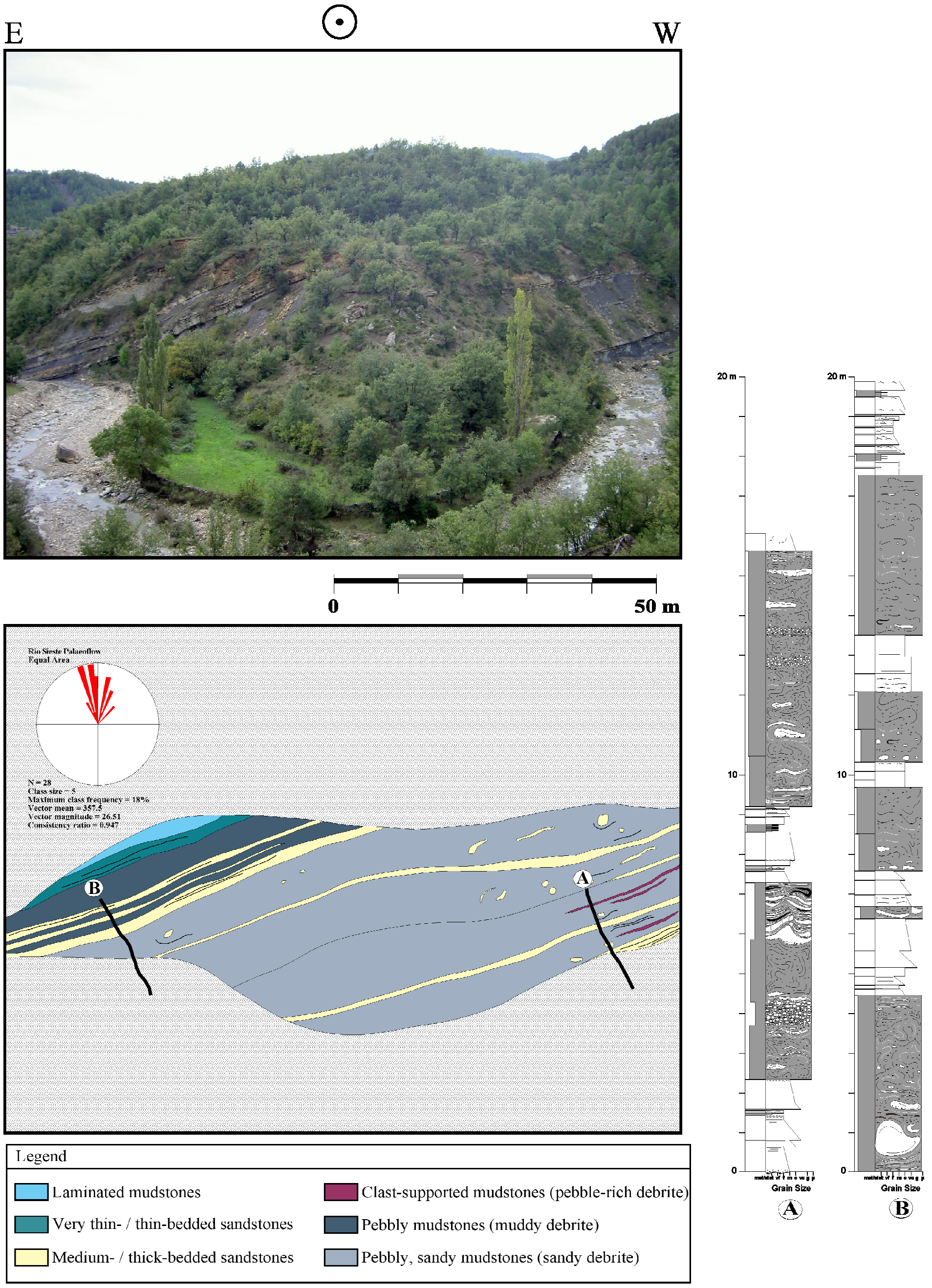

Fig. 6.13. Photo interpretation of the MIII sequence with sedimentary logs. Notice the predominance of pebbly MTDs throughout the sequence (See Fig. C9).

6.2.4. DEPOSITIONAL MODELS

Figure 6.14 illustrates the main palaeogeographic attributes during deposition of the Morillo system, showing the relationship between sequence depocentres. The position of intrabasinal growth anticlines (representing the early stages of growth of the Mediano, Añisclo and Boltaña anticlines) clearly influenced the location of siliciclastic depocentres. The southeastern part of the Ainsa basin, the area surrounding the village of Coscojuela, represents a canyon environment created during deposition of the Morillo system. The Morillo system was fed by a consistent point source in the east-southeast (Fig. 6.14) with the mid-slope canyon funnelling the sediment across the Mediano anticline. The canyon-fill sequences represent an erosional-bypass regime, with thick MTDs representing shelf/mid-slope collapse during slope oversteepening processes and canyon excavation. The deposits in the canyon environment, particularly the abundance of limestone boulders reflects the erosional downcutting through the flanks of the carbonate platform of the Mediano anticline. This would have caused erosional confinement in the canyon, reducing aspect ratios of canyon elements. The highly dispersed pattern of palaeocurrents in the axial part of the Morillo I sequence in the Morillo de Tou location suggests some degree of sinuosity operating at this time,. This is validated by the presence of lateral accretion elements in the northerly outcrop in Rio Sieste. The Morillo I sequence can, therefore, be interpreted as a sandy, sinuous sequence, defined at the base by a thick MTC overlain by sinuous channel elements (Fig. 6.15). The overall sedimentary characteristics of the lower-slope sequences are consistent with a structurally confined channelised system. Abreu et al. (2003) attributed this temporal pattern of increasing sinuosity to an increase in depositional confinement due to changes in gradient and sediment supply as the system evolves. Figure 6.16 shows that the Morillo II and III sequences are more confined than Morillo I sequence, and show a prominent aggradational stacking pattern in Rio Sieste. The stacking patterns reflect the increase in depositional confinement through time from Morillo I to Morillo III sequences. The correlation panel also illustrates the large-scale variations in facies distributions, showing the sandy fill of the Morillo I sequence and the MTD-dominated fills of the Morillo II and III sequences. The abundance of MTDs during deposition of the Morillo II and III sequences reflects the increase in depositional confinement in the basin, and the subsequent generation of mass wasting due to slope oversteepening.

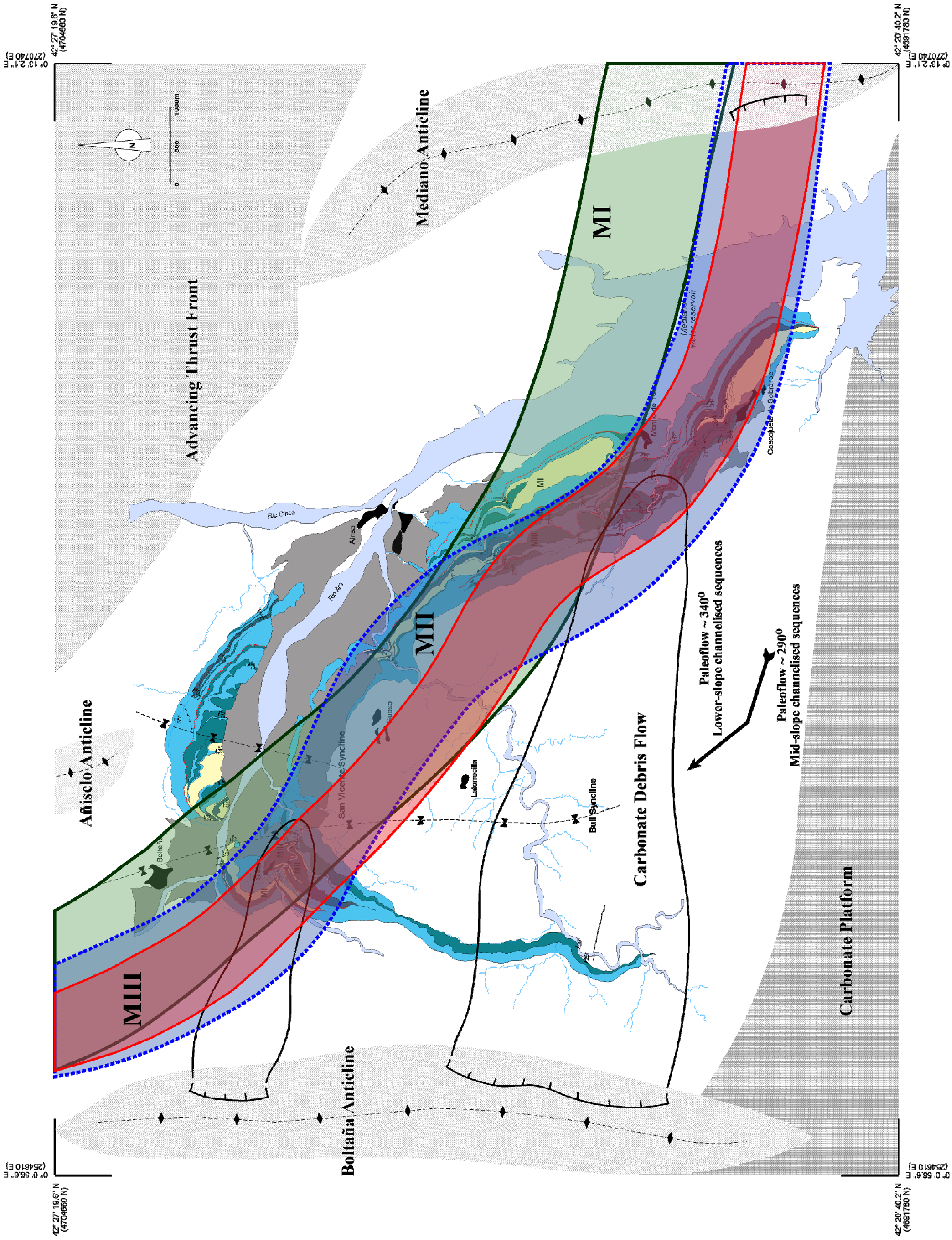

Fig. 6.14. Palaeogeography of the structurally confined Morillo I, II and III sequences with main depocentres outlined. Note: Morillo III is more lateral confined by the growing anticlines, occupying less width and is deflected more northerly. However, all sequences are structurally confined between the Añisclo and Boltaña anticlines. The Morillo times were characterised by the main growth phase of the Mediano anticline when a carbonate platform developed across the emergent structural high and breccias were shed from the flanks as the canyon eroded into the seafloor high.

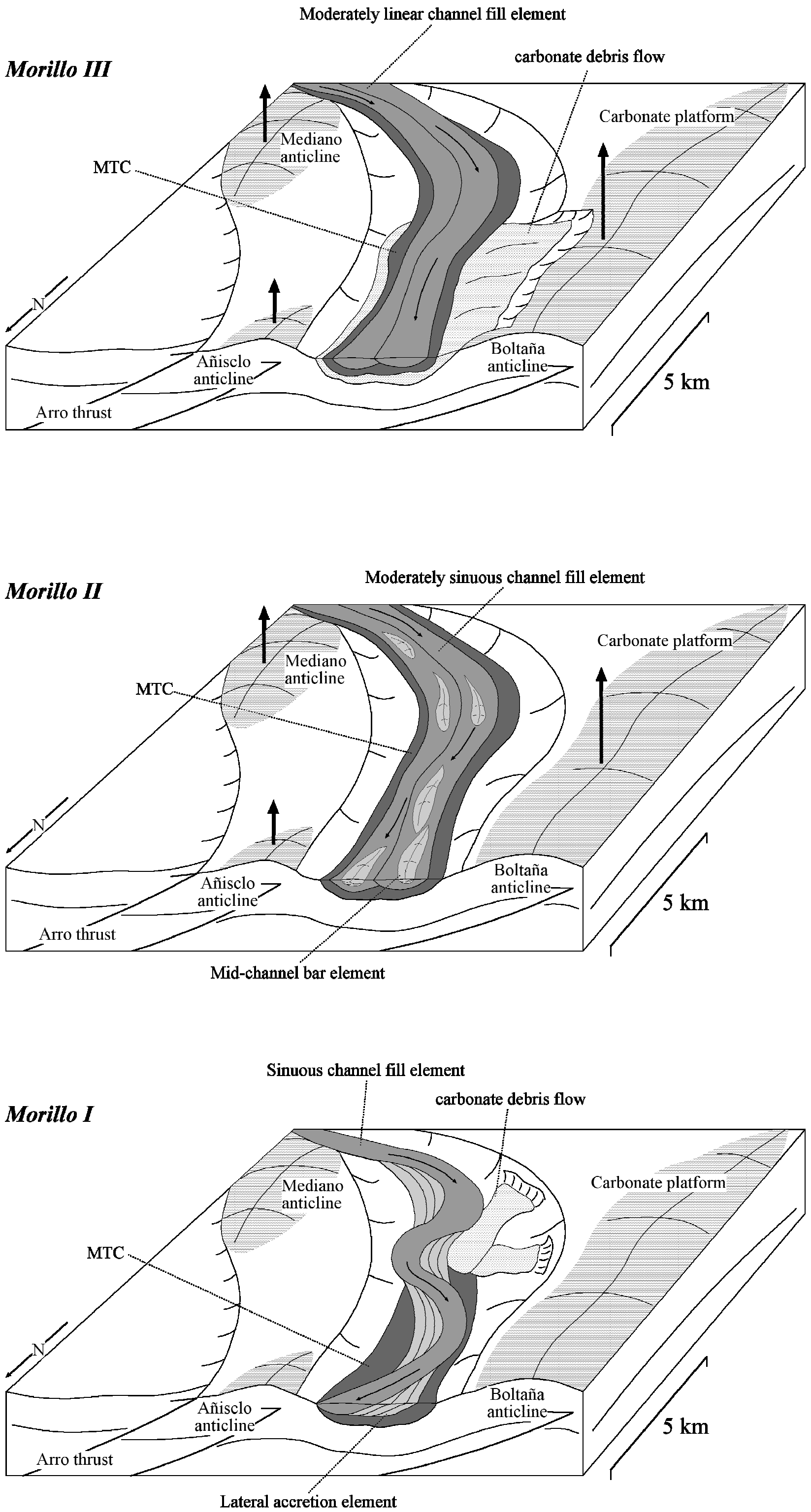

Fig. 6.15. Depositional models for the Morillo I, II and III sequences. Note the tightening of intrabasinal anticlines during deposition of Morillo II and III sequences causing depositional confinement and an increase in slope gradient. See text for more detail.

The abundance of low-angle cross-lamination and imbricated clasts in laterally discontinuous gravels and sandstones are typical of braid bars. These deposits have been well document in other deep-marine environments (Hein & Walker, 1982; Beldersen *et al*., 1984; Harrison & Graham, 1999; Hubbard *et al*., 2008). The barforms in Morillo II sequence therefore suggest a moderately sinuous system, characterised by reworking and bypass processes (Fig. 6.15). Cross-stratification and imbricated clasts are typical of braid bars in fluvial systems (Smith, 1974: Miall, 1992) and of braided channels in deep-marine deposits (Hein & Walker, 1982; Piper & Kontopoulos, 1994). The uplift of intrabasinal structural highs caused the failure of carbonate platforms and the deposition of carbonate mass flows (type Ia MTD). The stratigraphic position of MTDs represent periods of intrabasinal tectonic uplift. The predominance of MTDs in moderately linear channel elements in Morillo III sequence (see Fig. 6.16) is related to progressive depositional confinement and erosion in the Ainsa basin. This is consistent with more northerly-orientated palaeoflows in Morillo II and Morillo III, which suggest flow constriction between the north–south trending Añisclo and Boltaña anticlines.

6.2.5. EVOLUTION OF THE MORILLO SYSTEM

6.2.5.i. Tectonic setting

The Morillo system is part of the Upper Hecho Group and represents a significant tectonic regime during which the Ainsa basin was incorporated into the advancing deformation front. The emplacement of the lower (younger) tectonic complex (Larra-Boltaña / Gavarnie thrust sheets; refer to Chapter I) in the South-Central Pyrenees, and coeval deposition of the Upper Hecho Group in the Ainsa–Jaca basin, signifies the transition between a simple foredeep setting into a complex thrust-top (piggyback) basin.

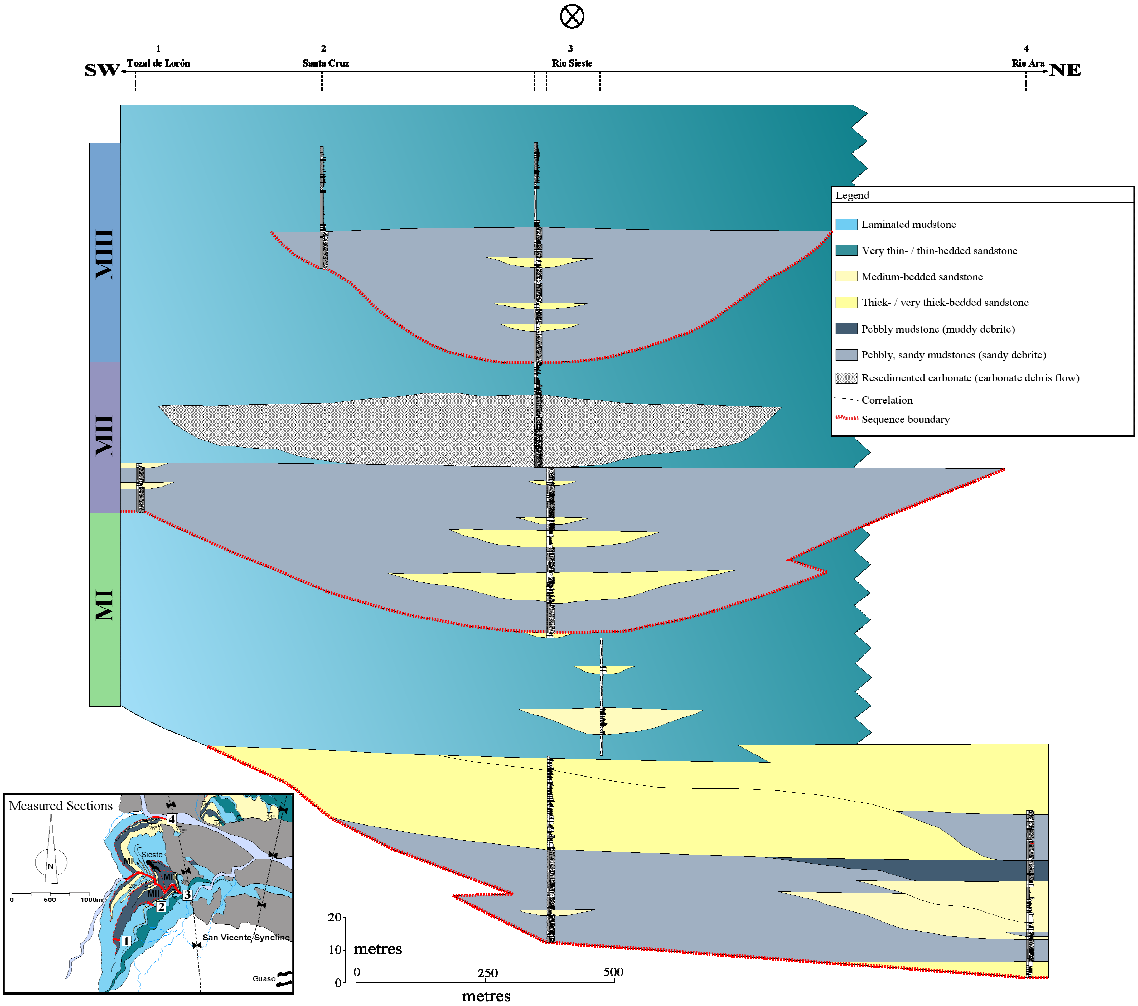

Fig. 6.16. Correlation panel for the Morillo I, II and III sequences in the northwest part of the Ainsa basin, Rio Sieste area. The sequences were confined in the east by the Añisclo anticline and to the west by the Boltaña anticline. See Figure C9 for detailed sedimentary logs.

This transformation represents the initiation of an 'uplift-dominated' phase (tectonic phase II; refer to Chapter 7 for more detail) in the study area, where southwards propagation of basement-involved thrusting (Remacha *et al*., 2003; Fernández *et al*., 2004; Huyghe *et al*., 2009; see Chapter 1 for more detail), incorporated the basin into the hanging wall of the Gavarnie-Sierras Exteriores thrust sheet. This was contemporaneous with the development of the generally north–south-orientated Mediano, Añisclo and Boltaña anticlines in the Ainsa basin. In summary, tectonic phase II (with coeval deposition of the Upper Hecho Group) marks a significant change in the structural configuration of the Ainsa basin, and represents the segmentation and differential structural uplift in the South Pyrenean foreland basin.

6.2.5.ii. Significance of synsedimentary tectonism

Although the Ainsa basin became part of the deforming foreland in the early Lutetian (during the onset of tectonic phase II / early stages of TS-II), a significant change in basin morphology is documented during deposition of the Morillo system (upper part of TS-II) in the mid Lutetian. This period marks a structurally complex stage in the evolution of the Ainsa basin due to the development of both the upper and lower tectonic complexes (Fig. 6.17).

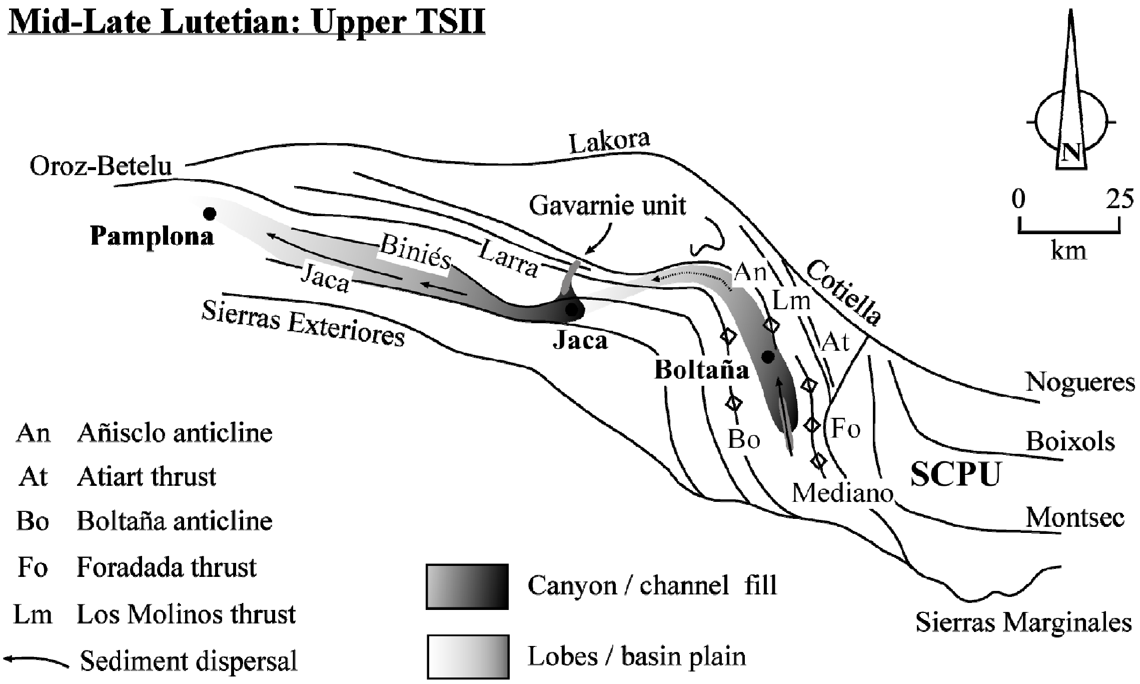

Fig. 6.17. Structural configuration of the southern Pyrenees during deposition of the upper part of tectono-sequence II, during the mid–late Luetian. The Morillo and Guaso systems were fed from a more southern sediment source (see arrow) due to the confinement and structural segmentation of the basin in response to the tightening of growth folds. Redrawn and modified after Remacha *et al.* (2003; 2005) and Das Gupta & Pickering, (2008).

Figure 6.18 provides palaeogeographic reconstructions during tectonic phase II, depicting the continued growth of the intrabasinal anticlines and their influence on sediment dispersal patterns throughout TS-II. Although the Mediano, Añisclo and Boltaña anticlines were incipient bathymetric expressions during the early stages of TS-II and were, therefore, capable of deflecting sandy sequences, larger scale depositional confinement, of the order of siliciclastic systems, within the basin was observed in the later stages of TS-II (discussed in more detail below). During deposition of the Morillo and Guaso systems, flows were deflected around the seafloor topography, as the basin narrowed in response to tectonically-controlled shortening across the Ainsa basin. The Guaso system was subsequently fed from a more southern sediment source within a structurally lower frontal ramp area, deviating around the prominent Mediano anticline (see below). Thus, it is evident that the southwards propagation of basement-involved thrusting (involving the Gavarnie-Sierras Exteriores thrust sheet) during tectonic phase II *progressively* detached and partitioned the Ainsa basin by a series of thrust ramps and associated folds. The influence of intra-basinal deformation was, therefore, more apparent during deposition of the youngest deep-marine clastic systems.

6.2.5.iii. Depositional confinement

Bentham and Burbank (1996) illustrated the large-scale depositional geometry over the Mediano anticline during the Lutetian using litho- and magneto-stratigraphic correlation (their fig. 18). They showed that subsidence and sediment accumulation were most rapid away from the deforming flanks of the structure. This indicates that the basin-bounding anticline posed a control on sediment dispersal patterns in the Eocene Ainsa basin.

During the main phase of uplift and rotation of the Mediano anticline during the middle Lutetian a carbonate platform was developed across the seafloor high (Bentham & Burbank 1996, their fig. 19B), triggering the formation of major carbonate mass flows (types of MTD) originating from the unstable flanks into the Ainsa basin as flows are deflected southwards around the growing structure. Poblet *et al*. (1998) documented the presence of redeposited fossils from Ypresian rocks in Lutetian growth strata of the Mediano anticline, indicating positive relief of the structure and erosional down-cutting during the growth stage. Using a cross-section through the area of greatest fold uplift and maximum observed erosion, they estimated that maximum amount of crestal erosion of the anticline occurred during the middle Lutetian (roughly coinciding with the deposition of the Morillo system), with no net erosion prior to this time. This study implies that prominent growth of the Mediano anticline was during the mid–late Lutetian, driven by footwall deformation related to the development of the SCPU.

A. Early Lutetian: Lower TS-II

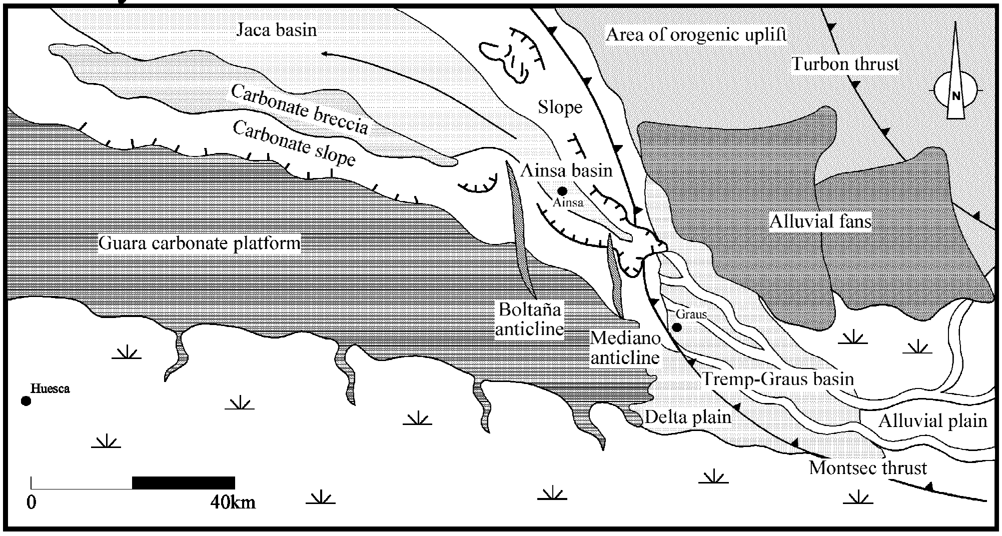

B. Mid Lutetian: Upper TS-II

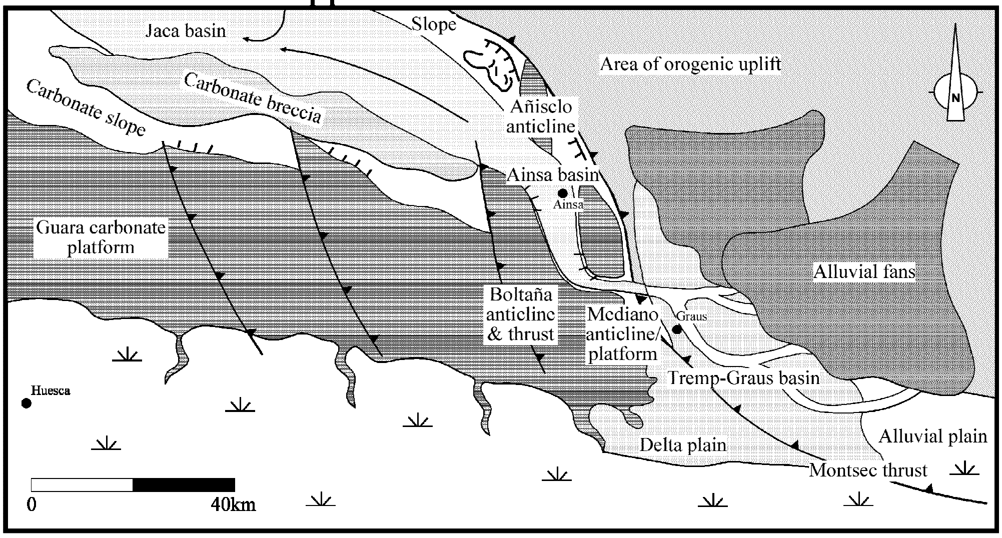

Fig. 6.18. Palaeogeographic reconstructions of the southern foreland basin during tectonic phase II (with coeval deposition of TS-II), depicting thrust propagation and structural influence on basin architecture. (A) Early stage of growth of the Mediano and Boltaña anticline with deposition of the Banastón and Ainsa systems. Redrawn and modified after Dreyer *et al.* (1999). (B) Propagation of thrusting westwards, transforming the Ainsa basin into a thrust-top basin. Basin narrowing and confinement between the Mediano, Añisclo and Boltaña anticlines during deposition of the Morillo and Guaso systems. Note the flow deflection between the intrabasinal highs. Structural and palaeogeographic concepts adapted after Dreyer *et al.* 1999

Muñoz *et al.* (2003) studied the palaeomagnetic history of the Gavarnie thrust sheet in the Ainsa basin and determined a regional clockwise rotation up to 80° in Lower Eocene sediments to accommodate for the southwards thrusting. Provided that rotation decreases with age, so that a precise date for rotation was achieved, it was postulated that rotation was contemporaneous with the development of the major thrust ramp anticlines, the Mediano, Añisclo and Boltaña anticlines. Therefore, the southwards emplacement of the Gavarnie-Sierras Exteriores thrust sheet caused basin narrowing, and depositional confinement due to the coeval development of intrabasinal growth anticlines.

6.2.5.iv. Shallowing of the Ainsa basin

The sedimentological and ichnological analysis of the upper part of the Morillo III sequence indicates the onset of shallowing in the Ainsa basin. The top of the Morillo system is defined by a very thick-bedded, thoroughly laminated unit, which grades upward from very fine-grained sandstone to clay-grade mudstone (Facies D2.1; Fig. 6.19A). The coarser-grained lower division is characterised by sandstone-siltstone alternations or lenses that grade into well-developed parallel to wavy laminations. The base of the bed is gradational and the top is more sharp and planar. The unit forms an extensive ridge running parallel to Barranco Pinares, located to the west of Morillo de Tou village; subsequently, it has been used as a marker bed to correlate depositional bodies in the Morillo III sequence. Tens-of-metres of fine-grained, thin-bedded and laminated marly sediments forming the interfan between the Morillo and Guaso systems, overlies the unit. It can be interpreted that the mode of transport that created the deposit was a sustained, low-concentration turbidity current. Tractional processes produced the pervasive lamination/lenses, followed by suspension sedimentation, associated with a final waning stage, to account for the upper mudstone division. The deposit likely represents the distal product of a quasi-steady, highly efficient, sediment-laden, turbulent flow, possible generated by a hyperpycnal flow exiting a river mouth (Normark & Piper, 1991; Mulder & Syvitski, 1995; Mutti *et al*., 2003). The occurrence of *Asterosoma* ichnotaxa towards the top of the Morillo system is also an indication of shallowing (Fig. 6.19B); the trace fossil is commonly associated with shallow-marine environments (e.g., Stanley & Pickerill 1995; Pemberton *et al*., 2001).

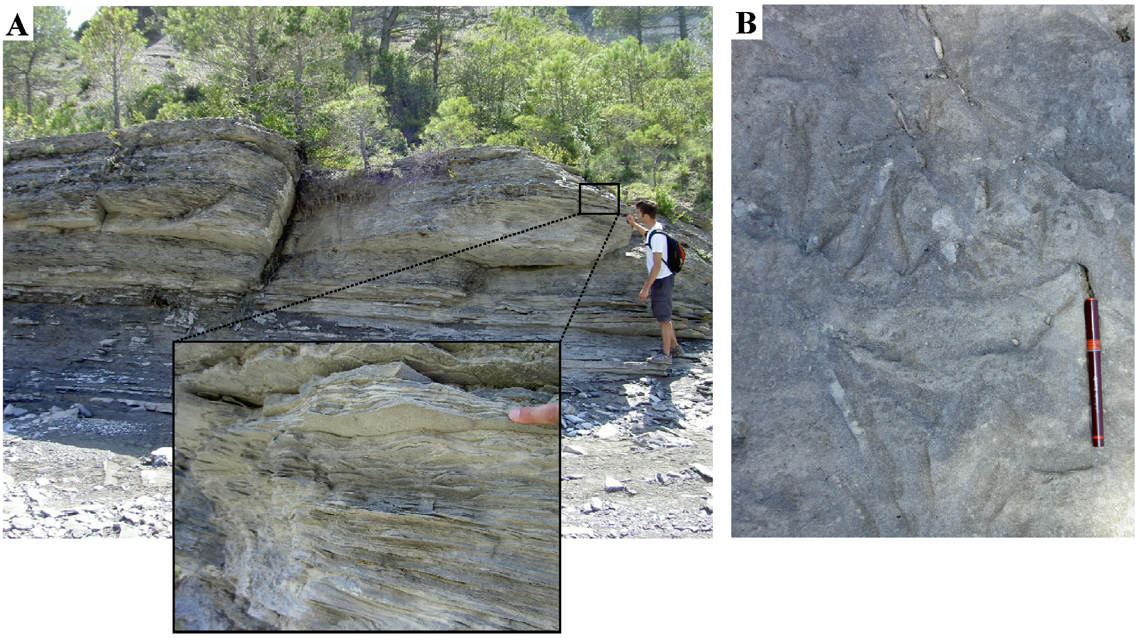

Fig. 6.19. Characteristics of shallowing in the upper part of the Morillo system. (A) Interlaminated unit comprising very fine-grained sandstone and coarse siltstone, showing pervasive horizontal and ripple lamination. Inset photo shows a detailed view of the lamination, with sandy-silty alterations/lenses. (B) *Asterosoma* ispp. Endichnial full-relief. A common trace fossil in the upper part of the Morillo system, indicating a shallow-marine environment of deposition.

The Upper Hecho Group represents a more mature stage of basin development in response to the incremental detachment and accelerated movement on the underlying sole thrust (Remacha *et al*., 1998; Dreyer *et al*., 1999). The end signature of the Morillo system can be related to a phase of tectonically-controlled shortening across the basin and linked differential uplift that led to a significant shallowing of the Ainsa basin. Any thrust-related uplift equalled or exceeded previous basin subsidence rates. Additionally, the emplacement of the Oroz-Betelu massif, in the western boundary of the Central Pyrenees (Remacha *et al*., 2003), was responsible for the western closure of the South Pyrenean foreland basin, preventing connections with the Atlantic Ocean (Remacha *et al*., 2003), and causing the emersion of the inner Pyrenean orogenic wedge (Remacha *et al*., 1998); contributing to the overall shallowing in the area.

A decrease in the rate of differential subsidence allowed sufficient filling and regrading of the slope environment after the main deposition of the Morillo system, ensuing a reduction in relative accommodation and the subsequent basinward shift of the deltaic system post Guaso times. The interlaminated unit in Figure 6.19A may indicate the proximity of the delta to this slope environment, where hyperpycnal flows generate sustained turbidity currents with the capacity and steadiness to flow to distal regions. Alternatively, the unit may represent the deposition of silt-rich buoyant plumes and sediment lofting originating from a low-concentration turbidity currents that represent the final filling stage of the Morillo system.

6.2.6. CONCLUSION

The Morillo system represents a change in sedimentary character in the deep-marine siliciclastic fill due to depositional confinement and the onset of basin shallowing. A phase of differential tectonic uplift prior to and during the accumulation of the Morillo system created a narrower basin morphology related to tectonic phase II. Accelerated movement on the underlying sole thrust caused shallowing in the Ainsa basin, and militated the deposition of structurally-confined braided and sinuous channel sequences. Intrabasinal tectonics has a strong influence on the depositional style of deep-marine sediment, stratal geometry and stacking patterns of depositional bodies.

6.3. THE GUASO SYSTEM

The Guaso system is up to ~155 m thick and is stratigraphically located above the Morillo system, forming the fourth (youngest) depositional system in the Upper Hecho Group. It represents the final stage of deep-marine sedimentation in the Ainsa basin, and is overlain by the Sobrarbe deltaic complex (Dreyer *et al.* 1999). The system can divided into two sequences (Guaso I and II), each characterised by a relatively thin muddy MTD (facies A1.3 or F1) at the base (~5–10 m thick), followed by an extensive sandbody (FA2 and FA3) and associated abandonment facies (FA4) at the top. Each sequence shows an overall fining-upward trend, although there is an overall thickening- and coarsening-upward trend between the sequences (to Guaso II sequence). Age dating of the Ainsa basin suggests the deposition of the Guaso system occurred during the mid–late Lutetian (Payros *et al.*, 1999; Remacha & Fernández, 2003; Pickering & Corregidor, 2005; Dreyer *et al.*, 1999). Only one measured section was recorded from the Guaso system in this study, a ~77 m thick section from the Guaso I sequence in Rio Ena (Locality 45, Table 2.1).

Figure 6.20 shows facies class abundance in the Guaso systems, presented by the total number of beds and the total thickness measured. There are a large number of beds associated with facies class E, although facies class C represents the greatest thickness of beds measured. Unlike the older depositional systems, the Guaso system has a limited number of facies (Fig. 6.21), and is characterised by the lack of gravel-grade sediment (facies class A).

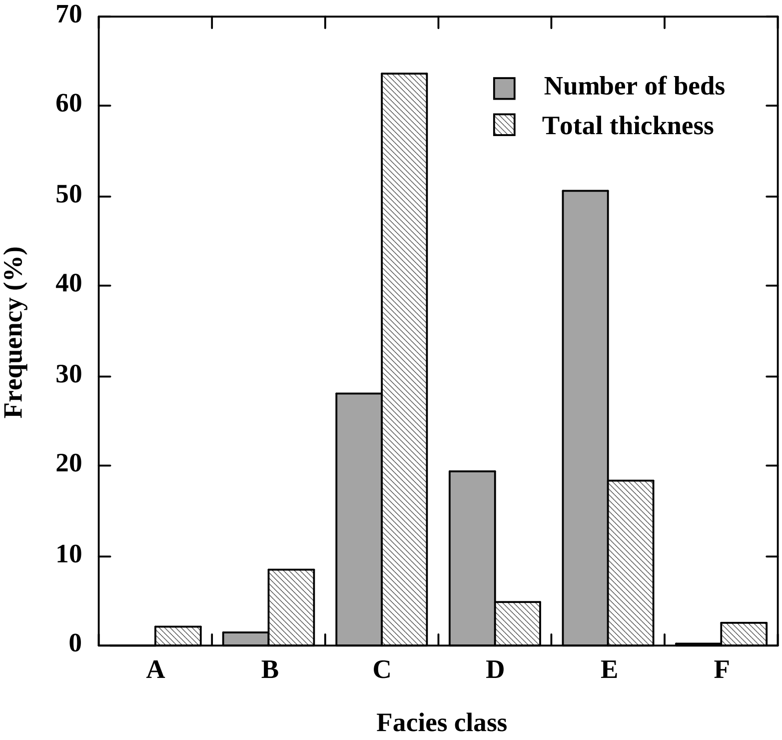

Fig. 6.20. Facies class abundance in the Guaso system

A sandy slump (MTD type Ib, facies F2) defines the base of the Guaso system in the west. It is interpreted as the product of slope collapse during tectonic oversteepening associated with the development of the Boltaña anticline. Within the Rio Ena outcrop, Guaso I sequence is defined by a ~2 m thick MTD (Fig. C10), and thick-bedded, coarse- to medium-grained, amalgamated sandstones (facies B2.1, C2.2 and C2.3). Figure 6.22 illustrates the architectural style of part of the lower sandy succession in Guaso I sequence. Individual channel elements form extensive units of thick to medium-bedded, medium-grained, laminated, sandstones (FA2 and FA3). Ripple, climbing-ripple and convolute lamination is common throughout the middle and upper parts of the channel elements. Towards the top (younger part) of the Guaso I sequence, a change in facies type is observed. It is characterised by the appearance of medium- to thin-bedded, medium-grained sandstones infilling a number of erosional scour elements. The top of the sequences are characterised by thin-bedded sandstone, siltstones and mudstones (FA4).

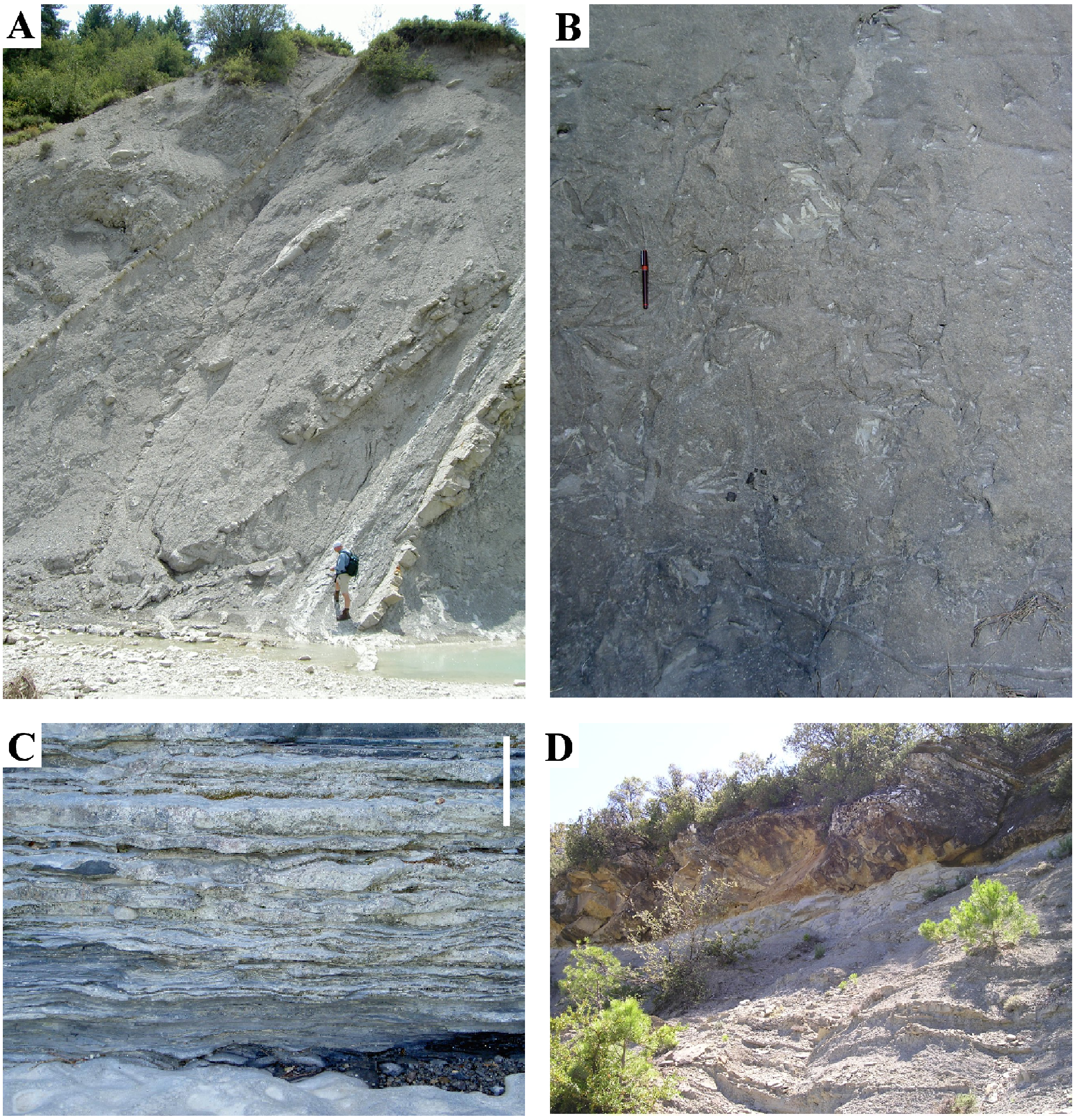

Fig. 6.21. Representative facies, sedimentary structures and architectures in the Guaso system. (A) Slumping and sediment creep horizons (defined between thin-bedded sanstone facies) forming part of the ~14 MTC at the very base of the Guaso system, cropping out in the western area near the village of Gabardiella. The deposit is carbonate-rich and is interpreted to have originated from the eastern flank of the Boltaña anticline. (B) *Asterosoma* ispp. Endichnial full-relief. Common trace fossil in the Guaso system, indicating a more shallow-marine environment of deposition.(e.g., Stanley & Pickerill 1995, Pemberton et al. 2001). See Pervesler and Uchman (2004) for discussion of ichnogenus. (C) Flaser bedding in fine-grained sandstones, Guaso I sequence, Rio Ena. (D) Base of the Guaso I sequence, defined by thin-bedded sandstones and mudstones showing post-depositional load structures underlying the main sandy succession, cliff section parallel to Barranco Pinares.

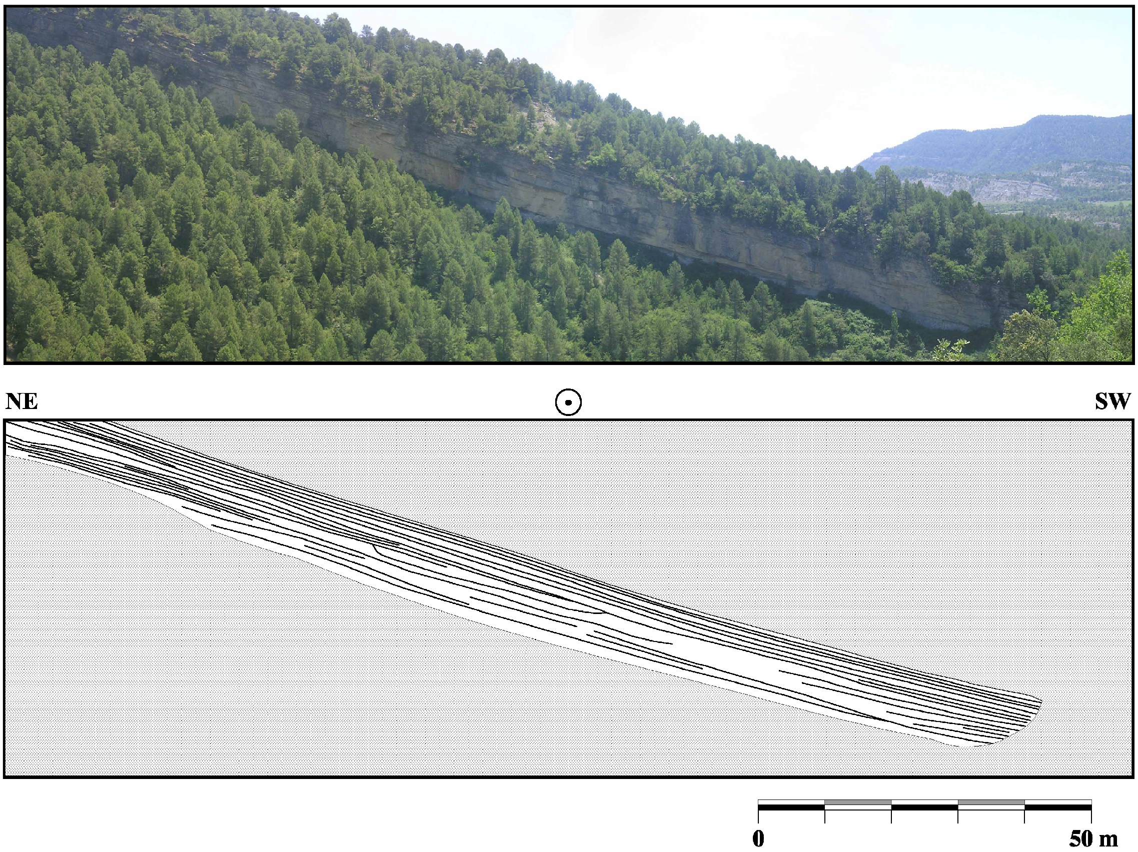

Fig. 6.22. Line interpretation to show the broad channelised character of the Guaso I sequence, outcrop leading into the Rio Ena to the right of the photo. Outcrop comprises a sandy channel complex with thick-bedded sandstones in the axis, which trend laterally into the constituent medium- to thin-bedded sandstone beds. Note the relatively unconfined architectural style of the sequence and the thinning-upward trend. See Figure C10 for detailed sediementary log.

The Guaso II sequence is coarser-grained than Guaso I sequence (Sutcliffe & Pickering, 2009) with a number of type II (pebbly) MTDs defining the base. The sandy succession is characterised by thin- to medium-bedded, coarse-grained sandstones (facies B2.1). Abandonment facies (thin-bedded sandstone, siltstones and mudstones; FA4) form the upper part of Guaso II, as a fining-upward sequence.

6.3.1. TRACE FOSSILS IN THE GUASO SYSTEM

The Guaso system is characterised by a low diversity, medium abundance trace-fossil assemblage, predominantly consisting of post-depositional trace fossils, including *Thalassinoides, Asterosoma* (feeding/*fodinichnia* traces) and *Ophiomorpha* (a dwelling/*domichnial* trace). The occurrence of *Asterosoma* ichnotaxa throughout the Gusao I and II sequences is an indication of shallowing in the Ainsa basin (Fig. 6.21B);

the ichnogenus is commonly associated with shallow-marine environments (e.g., Stanley & Pickerill 1995; Pemberton *et al.*, 2001) and is exclusive to the Morillo and Guaso systems in the Ainsa basin. Additionally, Sutcliffe and Pickering (2009) used the composition of the foraminiferal assemblage in the Guaso system to suggest the sandstones were deposited in upper bathyal water depths.

The low trace fossil diversity in the Guaso system may imply high terrestrial organic matter, (e.g., plant detritus) of low nutritional value in the sandstone beds, producing an unfavourable environment for most burrowers (Rodríguez-Tovar *et al.*, 2010). Seilacher (1977) described specialised burrow structures (i.e., graphoglyptids) that were designed to cultivate microbes as an effective adaptation to break down resistant or organic matter that metazoans were unable to digest. Graphoglyptids are almost absent in the Guaso system, possibly because of the high nutrient levels: they represent a specialised, K-selected equilibrium strategy of colonization, adapted to surviving in oligotrophic (low nutrient) conditions (Ekdale, 1985; Uchman, 1995). The post-depositional ichnotaxa were formed by robust, deeply burrowing organisms that were able to thrive in eutrophic conditions as a consequence of fluctuating delivery of abundant organic matter. The specific presence of *Ophiomorpha rudis* in the Guaso system could reflect the availability of buried plant detritus, formed by crustaceans burrowing deeply into sandstones to obtain organic matter that had already been converted by microbes (Rodríguez-Tovar *et al.*, 2010).

6.3.2. Depositional model

The lack of significant amounts of coarse-grade sediment (facies class A) and slump/slide deposits (facies class F) indicates the Guaso system accumulated in a more unique depositional environment compared to the older systems. Although there is evidence to suggest progradation of the system from, Guaso I to II sequences, there is no evidence to suggest a canyon feeder system. Instead, it seem likely that the Guaso system represents the final filling stages in a structurally-confined, ponded system, which accumulated in a low-gradient setting. The Guaso system is finer grained than the Banastón system and forms the fining-upward part of the Morillo-Guaso system set.

6.3.3. Final stages of basin infill

As discussed in Section 6.2.5, the upper division of the Upper Hecho represents a significant tectonic regime during tectonic phase II. The Guaso system represents a mature stage of basin development, characterised by anticlinal uplift (*sensu* Muñoz *et al*., 1994) in response to the incremental detachment and accelerated movement on the underlying sole thrust (Remacha *et al*., 1998; Dreyer *et al*., 1999), and coeval development of intrabasinal growth anticlines (see above for more detail). As the Ainsa basin became part of the deforming foreland, the final stage of deep-marine sedimentation can be related to a phase of structurally induced uplift, which led to the reduction in seafloor gradients and basin infill. It is assumed that any thrust-related uplift equaled or exceeded previous basin subsidence rates (Sutcliffe & Pickering, 2009), leading to significant shallowing and narrowing of the Ainsa basin during the upper part of tectono-sequence II. However, Dreyer *et al*. (1999) postulated that the generation of time-equivalent regressive unconformities and flooding surfaces within the Ainsa Basin in younger deltaic sediments were due to coeval uplift of thrust-related anticlines and flexural subsidence in the intervening synclines (their figs. 14 & 17). Thus, although there was prevalent regional background uplift caused by thrusting along the Ainsa Basin sole thrust, accommodation space was created by the development of intrabasinal highs including gentle folds such as the Arcusa anticline, in addition to the large-scale structures. Intrabasinal tectonic subsidence was, therefore, able to accommodate the high sedimentation rates during the Late Eocene in order to accumulate the overlying Sobrarbe deltaic complex (*sensu stricto* Dreyer *et al*., 1999). Consequently, the most significant uplift would have been along the intrabasinal anticlines (Mediano, Añisclo and Boltaña anticlines) during the 'uplift-dominated phase' (tectonic phase II), providing structural confinement during deposition of the Guaso system.

As the basin became part of the deforming foreland, there was an overall shallowing in the area due to regional background uplift caused by thrusting along the Ainsa Basin sole thrust. This resulted in net uplift, coeval with the growth of thrust-ramp anticlines, and progradation of the Sobrarbe deltaic complex across the Ainsa basin and into the Jaca basin, as sediment supply exceeded accommodation in the foreland. The deltaic systems were forced to enter the Ainsa basin in the structurally lower frontal ramp area to the south (Dreyer *et al*., 1999), deflecting around the topography created by the development of the lateral ramp zone of the SCPU. Poblet *et al*. (1998) documented syngrowth strata *overlapping* the crest of the Mediano anticline, which was defined by an angular unconformity separating the sediment from the underlying growth strata *onlapping* the fold limbs of the structure (see their fig. 9).

Palaeomagnetic data determined that the entire syngrowth strata were Lutetian to Bartonian in age (Holl & Anastasio, 1993); thus, it can be surmised that the sediment overlapping the Mediano anticline was part of the middle–upper Lutetian Sobrarbe deltaic complex (Dreyer *et al*., 1999), deposited when uplift along the Mediano anticline was diminishing (Bentham & Burbank, 1996, their fig.19) and sedimentation rates exceeded anticlinal uplift rate during delta progradation over the study area. The final part of the Eocene basin fill consists of an alluvial redbed succession of the Escanilla Formation overlying the Sobrarbe deltaic complex, which spread across the crest of the Mediano anticline (Bentham & Burbank, 1996; Dreyer *et al*., 1999).

CHAPTER 7

DISCUSSION: EVOLUTION OF THE AINSA BASIN

7.1. INTRODUCTION

An important outstanding problem in sedimentary basins is the cause and timing of coarse clastic sediment delivery and the interaction between controlling factors. The temporal and spatial variations in geometry and architecture of deep-marine systems are controlled by relative sea-level changes, sediment flux, tectonic accommodation and climate change. At a smaller scale, local tectonics, as documented in this study, can create bathymetry that determines the transport mechanism, location and configuration of siliciclastic sediment. Data from previous chapters are integrated to produce a synthesis of architectural styles in order to assess the depositional history of the Ainsa basin and unravel the relative importance of tectonic processes and climate change in controlling sedimentation.

7.2. STRUCTURAL OVERVIEW

The depositional history of the Ainsa basin is inherently linked to the evolution of the South Pyrenean thrust system (Williams & Fischer, 1984; Williams, 1985). The subdivision of the Hecho Group into two tectono-sequences (TS-I and TS-II) reflects the growth of the Pyrenean orogenic wedge and the development of two tectonic complexes in the south-central Pyrenees. Table 7.1 provides an overview of the structural evolution of the south-central Pyrenees and the stratigraphy of the South Pyrenean foreland basin. The upper (older) tectonic complex (see Section 1.6.4.) involves structures that are part of the ancestral orogen (*sensu* Remacha *et al.*, 2003), and includes detachment and thrust propagation in the SCPU and the Lakora (Eaux-Chaudes) thrusts (Seguret, 1972; Teixell, 1992). Although this complex developed in the Late Cretaceous, it remained active during the late Ypresian, with the generation of new cover thrusts defining *tectonic phase I* in the Ainsa basin (Table 7.2). This period is characterised by very strong flexural subsidence in the foreland controlled by loading during the propagation of basement thrusts, involving the Nogueres unit and Lakora-Eaux Chaudes thrust sheet, where regional, load-driven subsidence controlled

Epoch	Age	Tectonics	Environment / sedimentation pattern	Stratigraphy
Late Cretaceous	Coniacian, Santonian	Plate collision in Eastern Pyrenees, progressed westwards Inversion of earlier extensional structures Subsidence and deepening	Shallow marine	Congost Limestone
	Campanian	Bóixols thrust	Deep-marine fill of the Vallcarga basin	Vallcarga Flysch
	Maastrichtian	Uplift of the Ebro Massif / southeast	Regression Coastal	Arén Sandstone
Palaeocene	Danian, Selandian, Thanetian	Uplift in the northeast Nogueres unit Lakora-Eaux Chaudes thrust sheet Progressive detachment and thrust propagation in the SCPU Subsidence	Shallow marine, Alluvial / fluvial	Tremp Formation
Eocene	Lower–Middle Ypresian	Development of the Montsec thrust Increased crustal shortening with upper crustal detachment Subsidence and deepening to the west	Transgression Shallow marine to deep marine Alveolina Limestone, marls Increased sediment supply from the axial zone Basin axis shift towards foreland	Ager Group
	Upper Ypresian	Enlargement of SCPU: western lateral ramp zone development	**Ainsa basin: TS-I** Delta complex Deep-marine: siliciclastic fill	Lower-middle Montañana Group Lower Hecho Group
	Lower–Middle Lutetian	Larra-Boltaña thrust sheet, early stages of the Gavarnie thrust sheet Continued uplift in the northeast	**Ainsa basin: TS-II** Delta complex Deep-marine: siliciclastic fill	Upper Montañana Group Upper Hecho Group
	Upper Lutetian–Lower Bartonian	Gavarnie thrust sheet, Oroz-Betelu massif	Accommodation reduction, progradation Delta complex, shallow marine	Sobrarbe Complex (including the lower and middle part of the Mondot member)
	Middle Bartonian–Priabonian	Tightening of intrabasinal structures (e.g., the Boltaña anticline), Sierras Exteriores / Guarga thrust	Fluvial to alluvial transition High sediment supply	Escanilla Formation (upper part of the Mondot Member and the Olson Member)
Oligocene - Miocene	Rupelian–Burdigalian	Subsidence in Ebro basin	Molasse stage Alluvial Fan: Fanconglomerates / conglomerates Shift in depositional axis – Ebro basin development: lacustrine - alluvial	Collegats Formation Peraltilla Formation, Sariñena Formation

Table 7.1. Structural evolution of the South-Central Pyrenees and stratigraphy of the Vallcarga–Tremp–Ainsa basin. Information compiled from Nijman *et al.* (1998); Dreyer *et al.* (1999); Remacha *et al.* (2003, 2005); Luzón, (2005).

foreland-basin deposition. The deposition of the Lower Hecho Group in phase I represents the oldest deep-marine siliciclastics sediments in the basin; the sedimentary characteristics of the sandy systems within this tectono-sequence are discussed later.

The Upper Hecho Group represents a more mature stage of basin development, during *tectonic phase II* (Table 7.2), representing locally-controlled piggyback-basin deposition in an uplift-dominated regime. The emplacement of the lower (younger) tectonic complex is mainly characterised by basement-involved thrusting, which propagated to the south and west deforming and uplifting previous thrusts as a forward-breaking sequence. The onset of phase II is marked by the development of the Larra-Boltaña cover thrust and associated folds (Teixell, 1990, 1992, 1996), followed by the Gavarnie-Sierras Exteriores thrust sheet (Labaume, 1983) and the Oroz-Betelu thrust (Remacha & Fernández, 2003). These structures were accompanied by the reactivation of structures of the upper tectonic complex; such structures were mainly out-of-sequence thrusts related to the lateral ramp zone of the SCPU (Remacha *et al.*, 2003), including the Arro and Gerbe thrusts sheets. In summary, this phase marks a significant change in the structural configuration of the Ainsa basin, and represents the segmentation and differential structural uplift in the South Pyrenean foreland basin.

Epoch	**Age**	**Tectonic Phase**	**Thrusting units**	**Structures in the basin**	**Tectono-sequence**	**Turbidite systems**
Eocene	Upper Ypresian	**Phase I: Subsidence** Part of the Upper Tectonic Complex	Generation of new cover thrusts: enlargement of the lateral ramp zone of the South-Central Pyrenean Unit	Thrusts: Foradada, Atiart, Los Molinos Anticline: Mediano	TS-I	Lower Hecho Group: Fosado, Los Molinos, Arro, Gerbe
	Lower – Middle Lutetian	**Phase II: Uplift** Lower Tectonic Complex	Larra-Boltaña / Gavarnie / Oroz-Betelu / reactivation of structures in the Upper Tectonic Complex	Out-of-sequence thrusts: Arro, Gerbe Anticlines: Boltaña, Añisclo	TS-II	Upper Hecho Group: Banastón, Ainsa, Morillo, Guaso

Table 7.2. Structural evolution of the Ainsa basin, outlining the tectonic phases and thrusting units responsible for the growth of structures within the basin, and the division of the Hecho Group into tectono-sequences. Note that the upper tectonic complex was initiated during the Late Cretaceous, but was still active in controlling TS-I during the Late Ypresian. The ages provided mark the onset of development for the intrabasinal structures and do not indicate cessation of growth. Data for tectonic phases, thrusting units and their timing were compiled from Remacha *et al*. (2003).

This is demonstrated in the depositional pattern of Upper Hecho Group (section below). Thus, the evolution of the Ainsa basin was characterised by strong compressive deformation related to these tectonic complexes, which exerted a primary control on the deposition of turbidite systems in the basin.

The Ainsa basin originated as a foredeep to the south and west of the Montsec thrust sheet (Fernández *et al.*, 2004), being controlled by the emplacement of the Lakora (Eaux-Chaudes)-SCPU tectonic complex. Continental and deltaic deposits accumulated in the Tremp–Graus thrust-top basin, which was located on top of the Montsec thrust sheet (Nijman & Nio, 1975; Ori & Friend, 1984; Puigdefàbregas *et al.*, 1992; Nijman, 1998). Dreyer *et al*. (1999) interpreted the study area (Ainsa basin) as a transitional foredeep setting in this early stage (Ypresian–early Lutetian), primarily responding to synclinal flexing of an underlying sole thrust during a 'subsidence-dominated' phase (phase I), involving lithospheric loading ahead of the main thrust front. By contrast, phase II of structural growth is characterised by anticlinal uplift (Muñoz *et al.*, 1994) and a shift towards an 'uplift-dominated' phase in response to detachment and accelerated movement on the underlying sole thrust, the Gavarnie-Sierras Exteriores thrust sheet (Verges & Muñoz, 1990; Muñoz, 1992; Dreyer *et al.*, 1999; Remacha *et al.*, 2003; Fernández *et al.*, 2004). Consequently, the subdivision of the Hecho Group marks a depositional transition between a regionally controlled foredeep setting in phase I, to a locally controlled piggyback setting in phase II.

The emplacement of the Gavarnie-Sierras Exteriores thrust sheet was part of a larger sequence of deformation, involving the generation of new thrust systems and related folds that segmented the South Pyrenean foreland basin. The east–west sequence of thrusting and folding, during tectonic phase II in the Lutetian to Priabonian, began in the east with renewed deformation of the Mediano anticline in the early Lutetian: a detachment fold that developed into a fault-propagating fold (Remacha *et al.*, 2003) due to continued movement on the Montsec thrust sheet, propagating to the south and west (Farrell *et al.*, 1987, their fig. 6). The differential uplift segmented the Tremp–Graus basin into a piggyback setting, diminishing relative subsidence and accelerating filling (Bentham & Burbank, 1996). Prominent surface expressions of this thrust-top phase are represented by growth anticlines developed in the proximal part of the foreland basin in the Middle to Late Eocene, as documented by de Boer *et al*. (1991). Westwards, development of tectonic phase II was characterised by the onset of the Larra-Boltaña cover system in the early Lutetian (Teixell, 1990, 1992, 1996; Remacha & Fernández, 2005), followed by the basement-involved Gavarnie thrust sheet in the mid/late Lutetian (Labaume, 1983). The north–south trending Boltaña anticline is a fault-propagating fold developed above the western oblique ramp of the Gavarnie thrust sheet (Holl & Anastasio, 1995) from the Lutetian until early Priabonian (Puigdefàbregas & Souquet, 1986). The fold developed to the west of the Ainsa basin as an intrabasinal growth anticline during deposition of the Upper Hecho Group. Prominent growth of the structure in the mid/late Lutetian indicated the basin had become incorporated into the deformation front and detached as a thrust-top basin. The north–south trending Añisclo anticline is situated to the east of the Boltaña anticline, forming a fault-propagating fold that deforms the hanging wall of the oblique ramp (Remacha *et al.,* 2003). Emergence of the Añisclo anticline was coeval with the Boltaña anticline and forms an additional growth anticline in the Ainsa basin. The Larra thrust splays from the older Lakora thrust (Teixell, 1996) and is connected to the Boltaña anticline through the Monte Perdido thrust (Remacha *et al.,* 2003). Activation of the Gavarnie basement thrust, located in the western part of the Axial Zone, resulted in the deformation of the Larra and Lakora thrusts, and the formation of the Axial Zone antiform (Farrell *et al*., 1987; Schellart, 2002; Teixell, 1996). Huyghe *et al*. (2009) demonstrated that the Gavarnie thrust sheet was genetically related to the younger Guarga thrust using previous zircon and apatite fission-track age data (after Sinclair *et al*., 2005; Jolivet *et al*., 2007) for the timing of thrust activity in the Gavarnie thrust sheet, sedimentological data suggesting coeval development of the Boltaña anticline, and rotation data in the Jaca basin related to the emplacement of the Guarga thrust sheet. This study demonstrates the incremental evolution of the linked thrust system to the present tectonic configuration. It can, therefore, be concluded that the South Pyrenean foreland basin was progressively detached by the Gavarnie-Sierras Exteriores thrust sheet and partitioned by a series of thrust ramps and associated folds from the Middle Eocene to Oligocene. The basin evolved into a system of piggyback sub-basins, which comprised the Tremp–Graus, Ainsa and Jaca sub-basins (Puigdefàbregas *et al*., 1992; Poblet *et al*., 1998). This dynamic structural framework is reflected in the tectono-stratigraphic evolution of the study area, outlined in this chapter.

The deposition of the Hecho Group represented a significant stage of thrust-front advancement in the South Pyrenean foreland basin, and was coeval with maximum rates of tectonic subsidence and shortening (Vergés *et al*., 1995). The depositional history of the Ainsa basin fill is inherently linked to the evolution of the South Pyrnean thrust system (Williams & Fischer, 1984; Williams, 1985), involving the development of two tectonic phases (outlined in this study), where the first-order control on basin accommodation was tectonic (Pickering & Bayliss, 2009).

7.3. DEPOSITIONAL HISTORY OF THE AINSA BASIN

7.3.1. STACKING PATTERNS

The Hecho Group unconformably overlies the Castigaleu Group (predominantly comprising shelf carbonates and marls), and records a major tectonic regime involving the deepening of the Ainsa–Jaca basin (Mutti *et al.*, 1988). The eight depositional systems comprising the Hecho Group (Fig. 7.1) represents a foreland-propagating turbidite wedge, showing a lateral stepwise migration to the southwest in response to the advancement of the active basin margin in the north and east (Fig. 7.2). This indicates a strong tectonic control on basin geometry, accommodation and sediment supply during the Eocene. The oldest six deep-marine systems (Fosado, Los Molinos, Arro, Gerbe, Banastón and Ainsa systems) were fed by a southeast point source, from canyons and erosional channels, which entered the basin across a narrow shelf break, defined by the lateral ramp zone of the SCPU. Sediment gravity flows were directed axially through the basin to the northwest. Syn-depositional propagation of this lateral ramp zone was responsible for the observed stacking pattern. Development of the Mediano anticline initiated during accumulation of the Banastón system (base of the Upper Hecho Group), which progressively emerged to form a carbonate platform in the east. The two youngest systems, the Morillo and Guaso systems, were subsequently fed from a more southern source point to accommodate for this obstruction.

The Lower Hecho Group (TS-I) is characterised by an aggradational stacking pattern of sequences within each system (Fig. 7.3), with minimal lateral shifting due to the maintenance of a steady depocentre occupying the width of the basin (a function of high relative subsidence during tectonic phase I), and high sediment supply. System confinement and stacking in TS-I is a result of forward propagation of the active basin margin, operating on a frequency consistent with system development. An offset (compensational) stacking pattern of the two sandy sequences in the Gerbe system is observed. This marks the initial growth of the Mediano anticline in tectonic phase II, relocating the depositional axis of the second sequence to the southwest. The lateral offset stacking of sandy sequences to the southwest is prevalent within each system in

Fig. 7.1. Simplified geological map of the Ainsa basin (modified after Pickering & Bayliss, 2009)

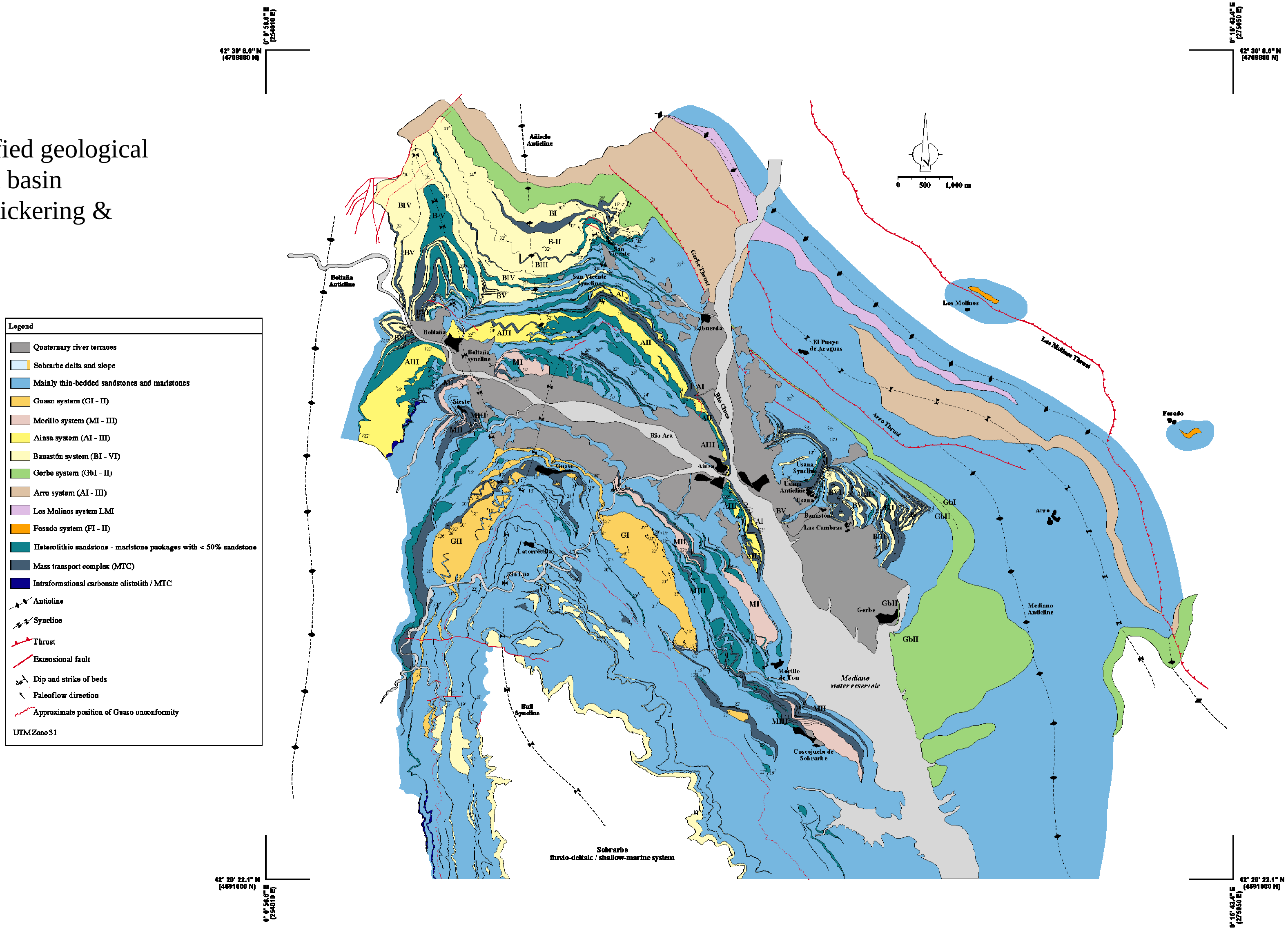

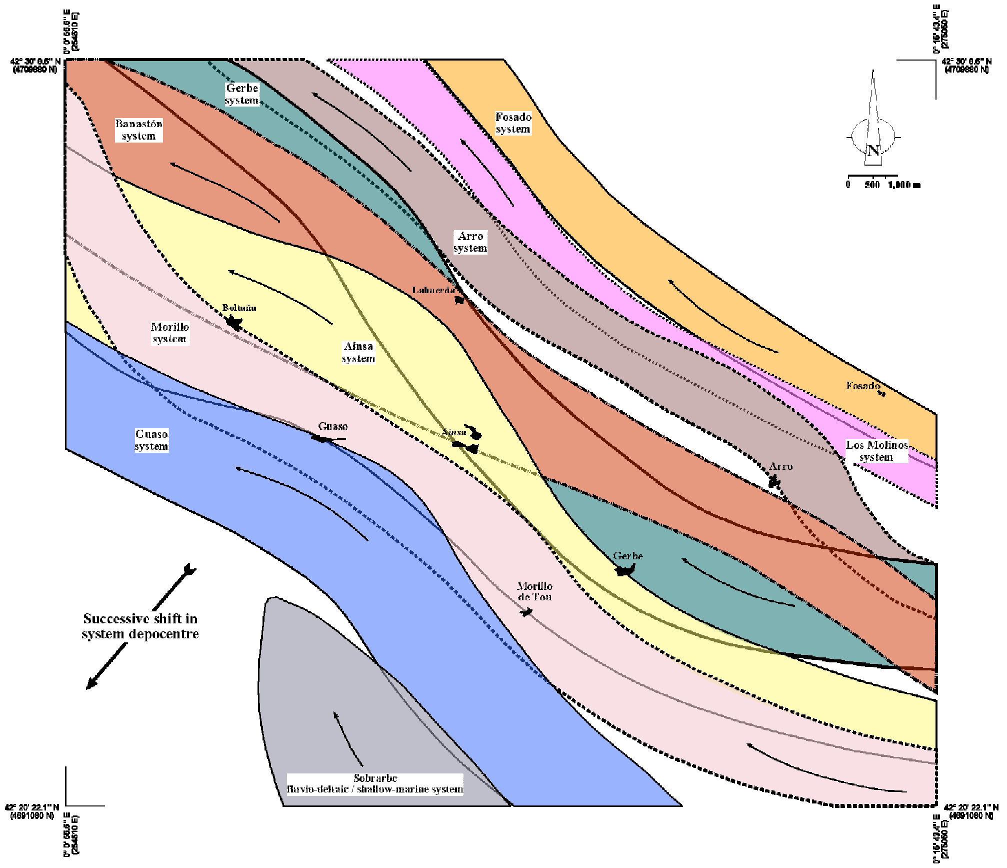

Fig. 7.2. Outline of system depocentres, interpreted from the simplified geological map.

the Upper Hecho Group (TS-II). Eastward (orogenward) relocation of the depocentre of each sandy system is due to the contemporaneous uplift of the Boltaña anticline in the west. As the final sequence in each system reaches the flanks of the structural high, the sequence within the proceeding system is forced to relocate due to a phase of renewed relative uplift of both anticlines. This trend demonstrates that timing of tectonics is able to operate on high frequencies cycles (<1–2 Myr), consistent with the deposition of systems, where the growth of intrabasinal structural highs controlled the position of sandy systems in the Upper Hecho Group.

7.3.2. FACIES TRENDS

Figure 7.4 shows the distribution of three basic facies types (siltstones/mudstones, sandstones and MTDs) in each depositional system. Figure 7.4A illustrates that the largest number of beds measured in the study were siltstones and mudstones, representing an overall abundance of fine-grained, very thin- to thin bedded sediment in the Ainsa basin.

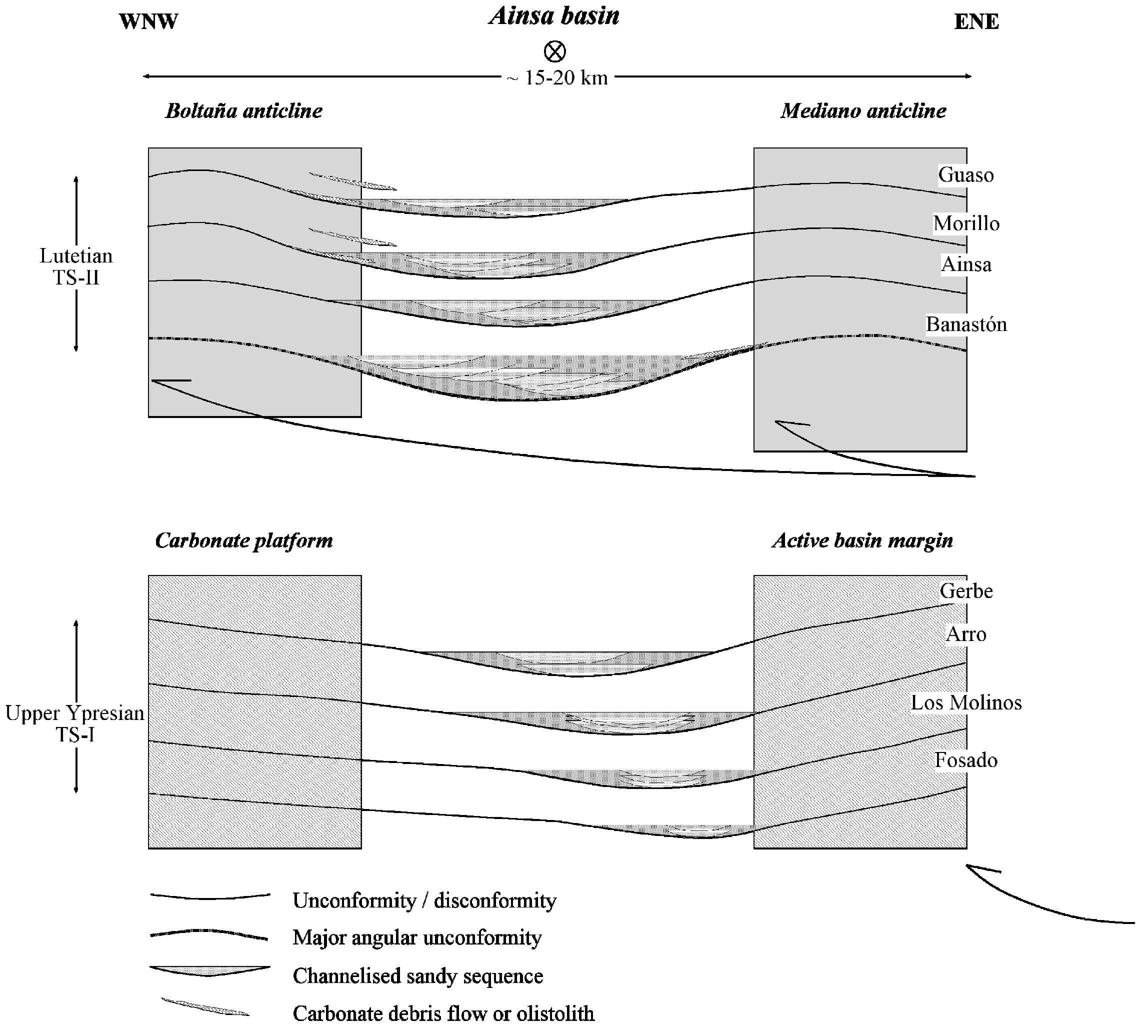

Fig. 7.3. Evolution of the sandy systems in the Ainsa basin, highlighting the influence of intrabasinal structures on the position of depocentres. The base of each system is characterised by forward and southwest depocentre migration, a response to the propagation of the active basin margin in the north and east (consisting of a complex system of lateral and frontal ramps and detachments). Tectono-sequence I is characterised by an aggradational stacking pattern of sequences, whereas tectono-sequence II is represented by the lateral offset stacking of sandy sequences.

Figure 7.4B represents the total thickness of all beds measured. The cumulative thickness of all measured MTDs is greater than the total thickness of siltstones and mudstone, suggesting that MTDs account for a high volume of sediment in the Ainsa basin. Additionally, an overall decreasing trend of MTD total thickness from the oldest to youngest systems is observed. This can be attributed to a highly active slope margin during the Lower Hecho Group (with the development of the lateral ramps zone of the SCPU during tectonic phase I), causing an abundance of upper/mid-slope collapse.

A. Number of beds

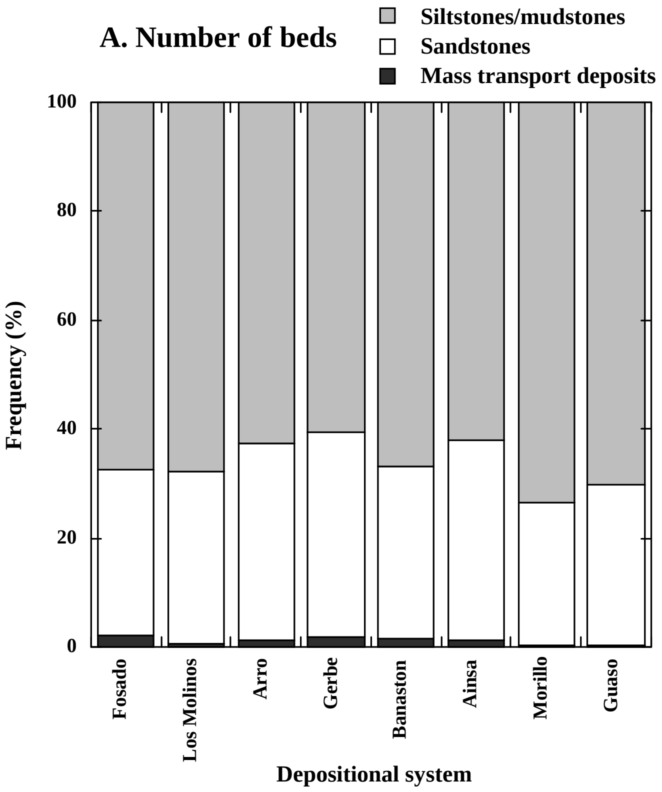

B. Total thickness

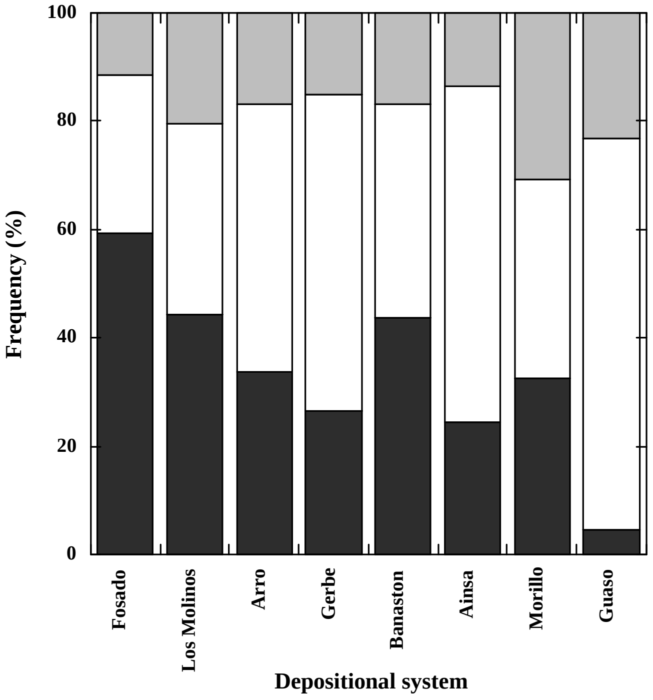

Fig. 7.4. Facies trends by depositional system in the Ainsa basin

As the tectonic regime changed during tectonic phase II, the basin became incorporated into the deformation front and a higher proportion of siltstones, mudstones and sandstones entered the basin. Figure 7.5 shows that the Banastón system is the thickest depositional system (~700 m thick) in the Ainsa basin, representing a major unconformity (defining the base of TS-II), basin reorganisation and high sediment supply. The oldest systems, the Fosado and Los Molinos system, are the least developed because they represent a time period when high accommodation existed in the proximal foreland (Tremp–Graus basin), and therefore, the Ainsa basin received a low volume of sediment. Petrographic studies have shown interesting trends in the composition of sandstones from the Ainsa basin, which can be attributed to the tectonic evolution of the south-central Pyrenees (see Section 7.3.4).

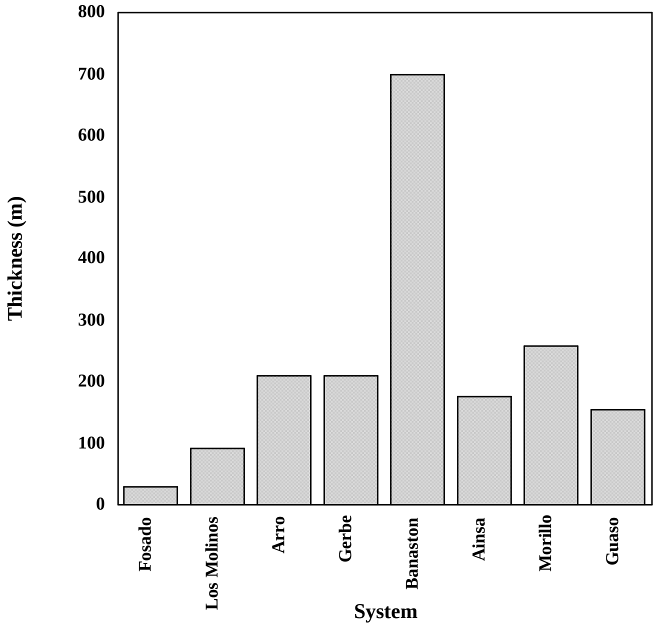

Fig. 7.5. Total thickness of depositional systems in the Ainsa basin

7.3.3. ARCHITECTURAL EVOLUTION OF SANDY SYSTEMS

Studies have shows that there is a complexity of processes influencing the depositional styles of basin fills that can lead to the development of various architectural styles in deep-marine systems (Payros *et al.*, 1999; Drzewiecki & Simo, 2000; Gardner *et al.*, 2003; Hadler-Jacobsen *et al.*, 2005; Hodgson *et al.*, 2006; Amy *et al.*, 2007; Sutcliffe & Pickering, 2009). The architectural elements composing each sandy channelised system show a variation in architectural geometry and facies (Fig. 7.6).

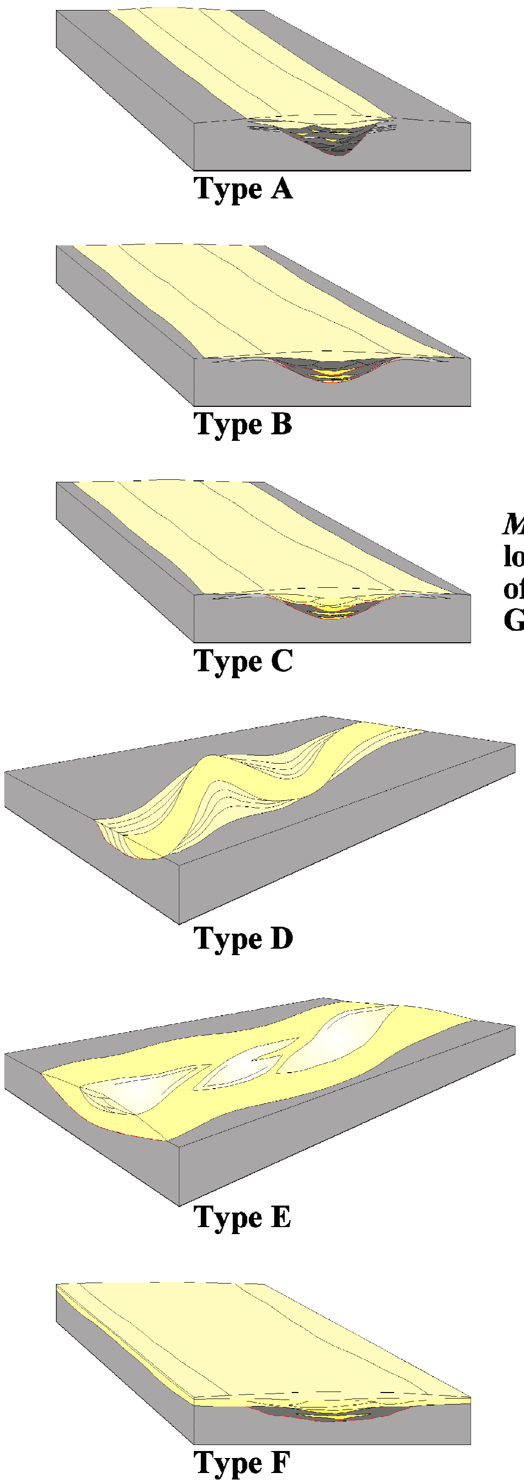

Type A

Canyon-fill element:
mid- to lower-slope environment of the Arro, Gerbe, Banastón and Morillo systems

Type B

Erosional channel-fill element:
lower-slope environment of the Los Molinos system and the Gerbe I, Banastón VI and Morillo III sequences

Type C

Mixed erosional/depositional channel-fill element:
lower-slope to proximal basin-floor environment of the Fosado, Arro and Ainsa systems, and the Gerbe II and Banastón I-V sequences

Type D

Sinuous channel-fill element:
lower-slope to proximal basin-floor environment of the Morillo I sequence

Type E

Braided channel-fill element:
lower-slope to proximal basin-floor environment of the Morillo II sequence

Type F

Depositional channel-fill element:
low-gradient environment of the Guaso system

Fig. 7.6. Sequence-fill models for the Hecho Group. Note that the architectural elements form composite depositional bodies that comprise each deep-marine environment in the sandy sequences.

Channel-fill type A represents the infill of large-scale erosional features that were excavated during the early stages of channel development. The channel fill of this type is characterised by bypass facies and MTDs (FA1), overlain by thin units of FA3, representing the backfilling stages. Channel-fill type B defines erosional slope channels containing an abundance of coarse-grained, lenticular sandstones and MTDs (FA1), with minor amounts of FA2 defining the top of the elements. Channels of this type are mainly filled with gravelly lags representing bypassing flows. Channel-fill type C often forms the downflow counterparts of channel-fill type B. They contain a range of facies associations (FA1, FA2 & FA3), representing a mixed erosional/depositional channel type, and are the most abundant channel fills. An initial erosional-bypass phase defines the base (FA1), followed by a depositional phase (FA2 & FA3). Channel-fill type D represents sinuous sandy regimes that developed lateral accretion elements. This type of fill predominantly contains FA2, FA3 and FA4. Channel-fill type E is characterised by FA1 and FA2, which form gravelly, mid-channel barforms due to flow confinement. Channel-fill type F represents the final filling stages of the deep-marine fill of the Ainsa basin. They are characterised by laterally continuous, sandy deposits of FA2, FA3 and FA4 that accumulated during a significant stage of slope gradient reduction. A brief description of each system is presented in an evolutionary framework below. A summary of the main characteristics of each depositional system is outlined in Table 7.3.

7.3.3.i. Evolution of the Lower Hecho Group

The *Fosado system* is poorly exposed, but consists of two channel complexes. The accumulative thickness of the sandy part of the Fosado system is ~57 m, which includes a local basal type I MTD defining the base of each channel complex. The sandy complexes comprise two small-scale channelised sandbodies, interpreted as mid-slope channel elements based on their geometry, the abundance of surrounding type Ia MTDs, and the proximity to shelf deposits. The Fosado system represents the initial influx of siliciclastic material in the Ainsa basin during a subsidence-dominated tectonic phase. Due to the high accommodation space created in the Tremp–Graus basin and the lack of well-developed alluvial fans during this time, the Fosado system is the product of a low-sediment flux regime.

System	Environment	Total thickness (m)*	Estimated width (m)**	Sequences		Average MTC thickness (m)	Average bed thickness (cm)	% beds amalgamated
				Number of sequences	Average thickness (m)			
Fosado	Discrete, mid-slope channel complexes	57.0	500	2	28.5 +/- 2.1	7.5 +/- 0.7	27.5*** +/- 125.2	9
Los Molinos	Slope apron system with discrete channel elements	89.5	700	1	89.5	12.9 +/- 4.6	5.3 +/- 42.0	1
Arro	Upper/mid-slope canyon to lower slope channel system	210.5	1350	3	70.2 +/- 24.6	17.8 +/- 2.0	7.4 +/- 36.6	1
Gerbe	Upper/mid-slope canyon to lower slope, erosional channel system	210.0	2100	2	105.0 +/- 63.6	8.0 +/- 4.2	9.7 +/- 29.9	5
Banastón	Lower-slope canyon-channel transition to proximal basin-floor channel system	700.0	2500	6	116.7 +/- 33.8	28.3 +/- 12.0	9.8 +/- 67.1	4
Ainsa	Lower-slope erosional channels to proximal basin-floor channel system	176.5	2600	3	58.8 +/- 20.2	13.8 +/- 5.0	8.2 +/- 31.3	5

Table 7.3. Summary of the main characteristics of each depositional system in the Hecho Group

System	Environment	Total thickness (m)*	Estimated width (m)**	Sequences		Average MTC thickness (m)	Average bed thickness (cm)	% beds amalgamated
				Number of sequences	Average thickness (m)			
Morillo	Mid-slope canyon to lower-slope, structurally-confined channel system	259.0	2400	3	86.3 +/- 14.0	16.8 +/- 11.4	8.1 +/- 40.3	5
Guaso	Low-gradient, strucutrally-confined channel system	155.0	2600	2	77.5 +/- 3.5	11.0 +/- 12.7	5.2 +/- 37.8	1

* Thickness derived by cumulative sum of sequence depocentres, excluding overlying muddy successions

** Average width of the sandy part of channel sequences, excluding fine-grained overbank successions

*** High value due to the lack of thin bed measurements

Table 7.3. (Continued)

The *Los Molinos system* comprises three discrete sandbodies encased in type I MTDs (facies F1 and F2), which form a slope apron sequence ~90 m thick. The sandy parts of the sequence frequently consist of basal type II MTDs, followed by a thin package of FA2. Remacha *et al*. (2003) interpreted the sandbodies as part of the Arro system; however, they constitute a system in this study, due to: (1) the large volume of thin-bedded, fine-grained deposits between the Los Molinos and Arro systems (~80 m); (2) an angular unconformity at the base of the Arro system, which is interpreted as a sequence boundary related to the emplacement of the Atiart thrust (Muñoz *et al*., 1994). Additionally, the Los Molinos and underlying Fosado sandstones are petrographically distinct (Das Gupta & Pickering, 2008). The Los Molinos sandbodies are interpreted as slope channels that eroded into the muddy slope. The association of thick type Ia MTDs and confined sandbodies suggests deposition on a mid-slope setting. During tectonic phase I, the development of the lateral ramp zone of the SCPU and the propagation of the thrust front in the north created a very active basin margin in the north and east. The slope apron sequence, therefore, developed in an active setting with thrust-induced oversteepening causing the collapse of upper- to mid-slope (predominantly muddy) material.

The *Arro system* is up to ~210 m thick (lower-slope sandy part), and represents a canyon and channel slope system, subdivided into three sequences. The Arro system developed coevally with the emplacement of the Atiart thrust (Muñoz *et al*., 1994), which structurally controlled and deformed the three sequences. This thrust was also responsible for numerous slope collapses and the subsequent deposition of nummulitic type I MTDs. These chaotic deposits are interbedded with the channelised sandstones (FA2 & FA3). The sandstones of the Arro system are rich in organic detritus, including wood fragments, suggesting that it was probably sourced from fluvio-deltaic systems. However, there is a paucity of pebble–cobble grade sediment, possibly indicating the lack of well-developed alluvial fans in the Tremp–Graus basin. The base of the Arro system is associated with an angular unconformity related to an increase in slope gradient due to the emplacement of the Atiart thrust, representing the development of the upper tectonic complex (involving the Lakora-Eaux Chaudes thrust unit / SCPU). There is an overall trend of increasing confinement between the sequences in the Arro system, reflecting depositional confinement due to the topography created by the deposition of type Ia MTDs during thrust propagation, and from slope oversteepening processes.

The *Gerbe system* contains two sequences that were deposited in an upper/mid-slope canyon to lower-slope erosional channel setting. Total thickness of the Gerbe system is ~210 m. The sandy part of each sequence varies from ~60 m thick for Gerbe I sequence (locality 10, Table 2.1) to ~150 m thick for Gerbe II sequence (locality 11, Table 2.1). Both sequences are characterised by gravels, pebbly sandstones and pebble-rich MTDs forming gravelly barforms in a high-energy, braided environment. The older Gerbe I sequence is a type I channel, and the Gerbe II sequence is a type II mixed channel, with a gravelly base and sandy fill (*sensu* Mutti & Normark, 1987). The Gerbe system records the first major influx of gravelly sediment into the basin, representing uplift in the Axial Zone and the development of alluvial fans in the Tremp–Graus basin (Nijman, 1998). The system accumulated in a transitional tectonic regime between the emplacement of the upper and lower tectonic complexes, and signifies the initial increase in sediment supply in to the basin during renewed tectonic activity in the hinterland. The excavation of the Charo canyon (feeder canyon to the Gerbe sequences) also suggests tectonic-induced slope steepening processes.

7.3.3.ii. Evolution of the Upper Hecho Group

The *Banastón system* comprises six lower-slope, canyon-channel sequences that correlate with six, proximal basin-floor, laterally offset-stacked, coarse-grained, channelised sequences. In the lower-slope, these channels are defined by erosional surfaces with a cumulative cutdown of ~170 m into the underlying Grebe system, overlain by a mixture of type I and II MTDs. The Banastón system preserves a sand-prone, lower-slope and proximal basin-floor transition. The system is ~500 m thick in the lower-slope, and ~700 m thick farther north in the proximal basin-floor, with a maximum across-flow width of ~2 km (basin-slope) to ~4.5 km (proximal basin-floor). Each sequence is defined by gravel-rich, muddy deposits (MTCs).

The base of the Banastón system corresponds with a major angular unconformity defining the base of tectono-sequence II, and the initial emplacement of the lower tectonic complex (tectonic phase II). This system represents significant basin reorganisation and the increase in sediment flux (and a basinward step in the depositional profile) due to a major phase of structural deformation in the south-central Pyrenees. The six sequences were confined between the growing Mediano anticline in the east, the Boltaña anticline to the west, and an additional seafloor high that grew to create the Añisclo anticline (~3 km NW of the Mediano anticline). The growth of these structures signified the transition into a thrust-top (piggyback) setting, and the onset of a uplift-dominated phase in the Ainsa basin. This is reflected in the depositional trends between the six sequences; a progradational shift due to the reduction in accommodation is observed.

The *Ainsa system* is ~180 m thick, and is interpreted as lower-slope, erosional channels to proximal basin-floor channel systems. These settings contain three, topographically and structurally confined (linear), coarse-grained sequences. Each sandy sequence contains channel complexes and channel elements, typically 5–30 m deep and hundreds of metres wide (~100–600 m), and is defined at the base by a MTC. The sequences comprising the Ainsa system show a lateral southwest shift due to the development of intrabasinal growth anticlines (and structural segmentation) during the thrust-top phase of the Ainsa basin.

The *Morillo system* is up to ~260 m thick, and comprises three sequences that accumulated in a mid-slope canyon to lower-slope, structurally confined channel system. The base of the Morillo system is associated with a ~30 m thick MTC, characterised by abundant pebbles and sand rafts, with gravel-rich scours and stringers commonly defining the base of individual MTDs. The Morillo sequences are interpreted as mixed erosional/depositional type channel complexes (*sensu* Mutti & Normark, 1987). The heterogeneous fills are characterised by rapid lateral facies changes, partly due to the abundance of type II MTDs that formed both the irregular topography upon which the sandstones were deposited, and also eroded many of the sandstone packets. Sandy macroform elements define the Morillo I sequence and are interpreted as lateral accretion elements in sinuous channel elements; whereas, pebble-rich intrachannel barforms in Morillo II represent low-sinuosity, braided channels, created by bypassing flows that reworked gravels on the seafloor. Morillo III sequence is abundant in type II MTDs, and represents an increase in confinement, forming relatively straight channel elements.

The abundance of MTDs, pebbly sandstones and barforms indicates significant amounts of bypass, and suggests that seafloor gradients were relatively high during deposition. The heterogeneous nature of the deposits and the abundance of bypass facies, as well as the aggradational stacking pattern of sequences in Rio Sieste, suggests the system may have been confined at this point between the intrabasinal growth anticlines (during tectonic phase II). The occurrence of *Asterosoma* ichnotaxa towards the top of the Morillo system is an indication of shallowing; the trace fossil is commonly associated with shallow-marine environments (e.g., Stanley & Pickerill, 1995; Pemberton *et al*., 2001). This implies that the Ainsa basin had become incorporated into the hanging wall of the basement-involved Gavarnie-Sierras Exteriores thrust sheet (Verges & Muñoz, 1990; Muñoz, 1992; Dreyer *et al*., 1999; Remacha *et al*., 2003; Fernández *et al*., 2004) during this stage. The end signature of the Morillo system can, therefore, be related to a phase of tectonically-controlled shortening across the basin and linked differential uplift that led to a significant shallowing and depositional confinement in the Ainsa basin.

The *Guaso system* is ~155 m thick and comprises two sandy sequences. The system is overlain by ~150–200 m of fine-grained slope and deltaic sediments (Sutcliffe & Pickering, 2009), and represents the end of deep-marine sedimentation in a structurally-confined, low-gradient channel system. The development of intrabasinal anticlines formed a structurally-segmented, ponded basin. The progressive development of the Gavarnie-Sierras Exteriores thrust sheet led to tectonic uplift of the Ainsa basin as it became part of the deforming foreland. Slope gradients were insufficient to excavate canyons of erosional channels, albeit there is a slight overall progradational trend between Guaso I and II sequence. This trend could be due to the reduction of accommodation in more proximal parts of the basin during the uplift regime.

Figure 7.7 illustrates the palaeogeographic reconstruction of the Ainsa basin during deposition of the Upper Hecho Group, and syndepositional thrust propagation. The accumulation of the Banastón system, sourced from uplifted terrains to the north of the Tremp–Graus basin, was contemporaneous with the early stages of growth of the Mediano and Boltaña anticlines (Fig. 7.7A). Southwards and westwards propagation of the thrust front transformed the Ainsa basin into a thrust-top basin. This caused prominent basin narrowing and depositional confinement between the Mediano and the Boltaña anticlines during deposition of the Ainsa, Morillo and Guaso systems (Fig. 7.7B). During the late Lutetian, progradation of deltaic facies (Sobrarbe complex) southwards over the study area was a consequence of progressive uplift in the area (Fig. 7.7C).

A. Early Lutetian

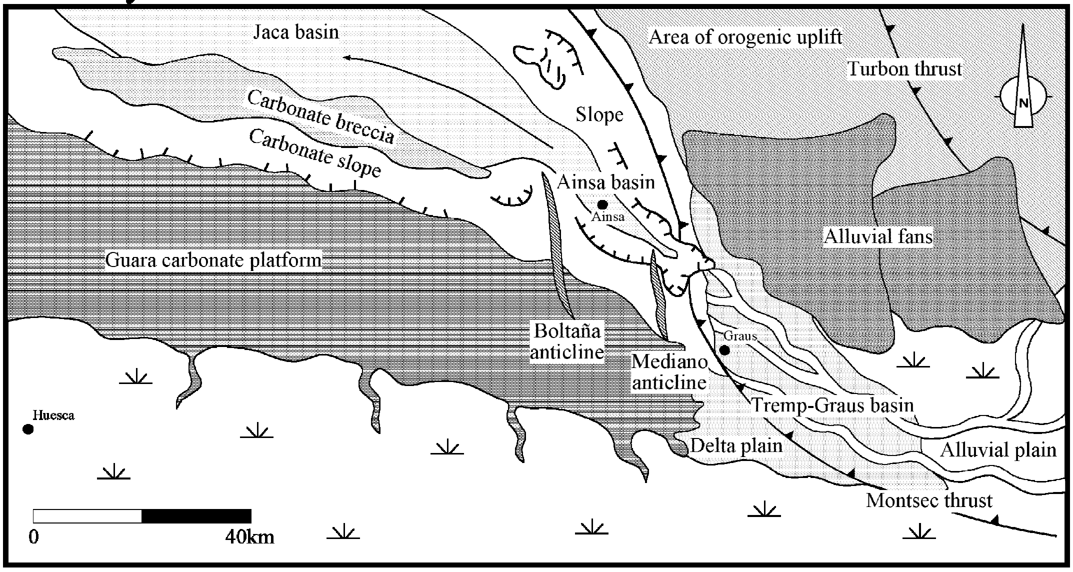

B. Mid Lutetian

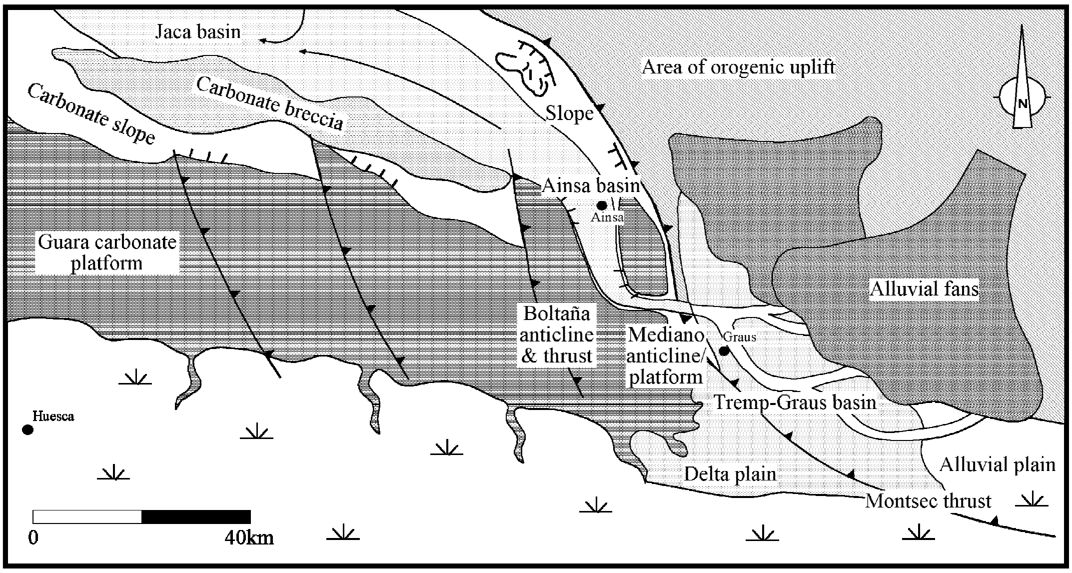

C. Late Lutetian

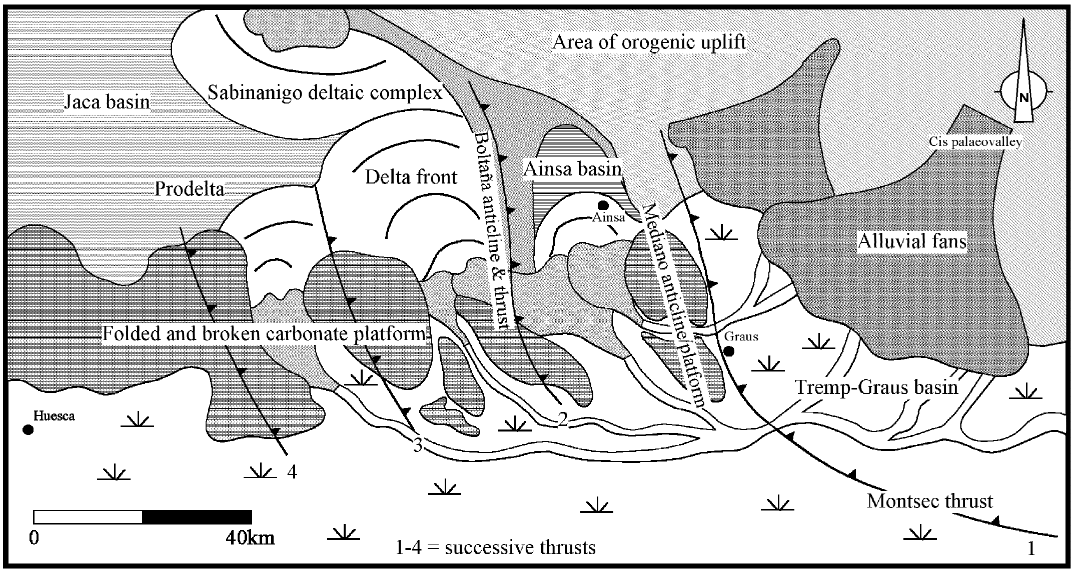

Fig. 7.7. Palaeogeographic reconstructions of the southern foreland basin, specifically the Ainsa basin, depicting thrust propagation and the influence on basin architecture. (A) Early stage of growth of the Mediano and Boltaña anticline during the accumulation of the lower part of the Upper Hecho Group, with the former present as an intraslope lineament, and the latter a subtle seafloor high. Note the Lower Hecho Group were deposited prior to the growth of these intrabsinal structures. (B) Propagation of thrusting southwards and westwards, transforming the Ainsa basin into a thrust-top basin during the upper part of the Upper Hecho Group. Depositional confinement was a function of the development of the Mediano and the Boltaña anticlines. (C) Progradation of deltaic facies over the Ainsa basin as uplift and sediment flux exceeded accommodation in the Tremp–Graus basin. Structural deformation of the carbonate platform as successive thrusts formed isolated structural highs. Note that sediment was sourced from a southerly direction during this time. (A) and (C) redrawn and modified after Dreyer *et al*. (1999).

7.3.4. PETROGRAPHY OF THE AINSA BASIN

7.3.4.i. Introduction

Petrographic studies have shown that sandstone composition can provide useful information on sedimentary basins. This includes the tectonic setting of the basin, the character of sediment provenance, and the nature of the sedimentary processes including flow type, transport pathways and depositional mechanisms (Hiscott, 1978; Ingersoll, 1978; Zuffa, 1991; Fontana *et al*., 1989; Das Gupta & Pickering, 2008).

Despite the considerable amount of research on the sedimentology and stratigraphy of the Ainsa basin, there are only two petrographic studies that attempt to apply petrographic signatures of sandstones (petrofacies) to basin analysis. Fontana *et al*. (1989) addressed the importance of petrography in understanding the complex source areas of the Ainsa–Jaca turbidites. They analysed 40 sandstone samples from the Ainsa–Jaca basin in order to determine the influence of eustasy and tectonism on the carbonate-rich siliciclastic sequences. A more detailed quantitative study was completed by Das Gupta & Pickering (2008), who described and interpreted the petrography of 157 sandstone samples collectively taken from seven of the eight deep-marine sandy systems (including the Los Molinos system with the Arro system) in the Ainsa–Jaca basin. The same methodology was adopted in both studies. The framework grains of the sandstones were divided into four categories, after the criteria of Zuffa (1980), in order to classify each sandy system into a characteristic petrofacies. The four categories, as follows, have different compositional and genetic significance: (i) non-carbonate extrabasinal (NCE); (ii) carbonate extrabasinal (CE); (iii) non-carbonate intrabasinal

(NCI); and (iv) carbonate intrabasinal (CI). Refer to Fontana *et al*. (1989) and Das Gupta & Pickering (2008) for a detailed description on each category. Table 7.4 summaries the petrofacies of Fontana *et al*. 1989 and Das Gupta & Pickering (2008); due to NCI grains being present only in very small proportions in all the samples (typically between 2–4% mean value), this category does not contribute to the discrimination between petrofacies.

Petrofacies	Description	Origin of defining category
1	Sandstone (sensu Zuffa, 1980) or non-carbonate extrarenites. The framework of these rocks is mainly composed of siliciclastic grains (~80% or more); carbonate grains are negligible (~2%).	NCE: Palaeozoic Axial Zone (crystalline basement: granite, gneisses and phyllites)
2	Hybrid arenites (sensu Zuffa, 1980). A distinctive characteristic of this petrofacies is the significant presence of CI grains (~10% or more).	CI: Coeval (Eocene) carbonate shelves (bioclasts and intraclasts)
3	Calcilithite. These rocks contain relatively abundant (~10% or more) CE grains.	CE: Mesozoic (Cretaceous) limestone and dolomite

Table 7.4. Petrofacies in the Ainsa basin (after Fontana *et al*., 1989; Das Gupta & Pickering, 2008).

The results from the petrographic studies of the Ainsa–Jaca basin can be used in conjunction with the dataset from this sedimentological and stratigraphic study to make inferences on the cause and timing of coarse clastic sediment supply to the basin. In keeping with the scope of this study, only the petrographic results from the Ainsa basin are considered. The following section outlines the key results and interpretations from Fontana *et al*. (1989) and Das Gupta & Pickering (2008) and demonstrates how these findings support the depositional trends and basin evolution detailed in this chapter.

7.3.4.ii. Petrographic signatures in the sandy systems

An improved understanding of the stratigraphy in Ainsa basin has recently been achieved through the extensive correlations between outcrops, yielding detailed maps and stratigraphic panels (Pickering & Corregidor, 2000, 2005a, 2005b; Remacha & Fernandez, 2003; Fernandez et al., 2004; Remacha et al., 2005). In Das Gupta & Pickering (2008), this facilitated the accurate sampling of sandy systems at many outcrops; therefore, these petrographic results are considered to be the most reliable. Fontana *et al*. (1989) utilised stratigraphy that is now considered outdated and consequently characterised some of the sandy systems under contrasting petrofacies. These results and interpretations will, therefore, be tentatively analysed in this discussion.

Das Gupta and Pickering (2008) found that standard QFL plots were insufficient in showing any petrographic trends in the arenites of the Ainsa basin. The siliciclastic portion of the samples proved to be too compositionally similar, but NCE-CI-CE classification was more effective due to the significant intrabasinal and extrabasinal carbonate components (Fig. 7.8).

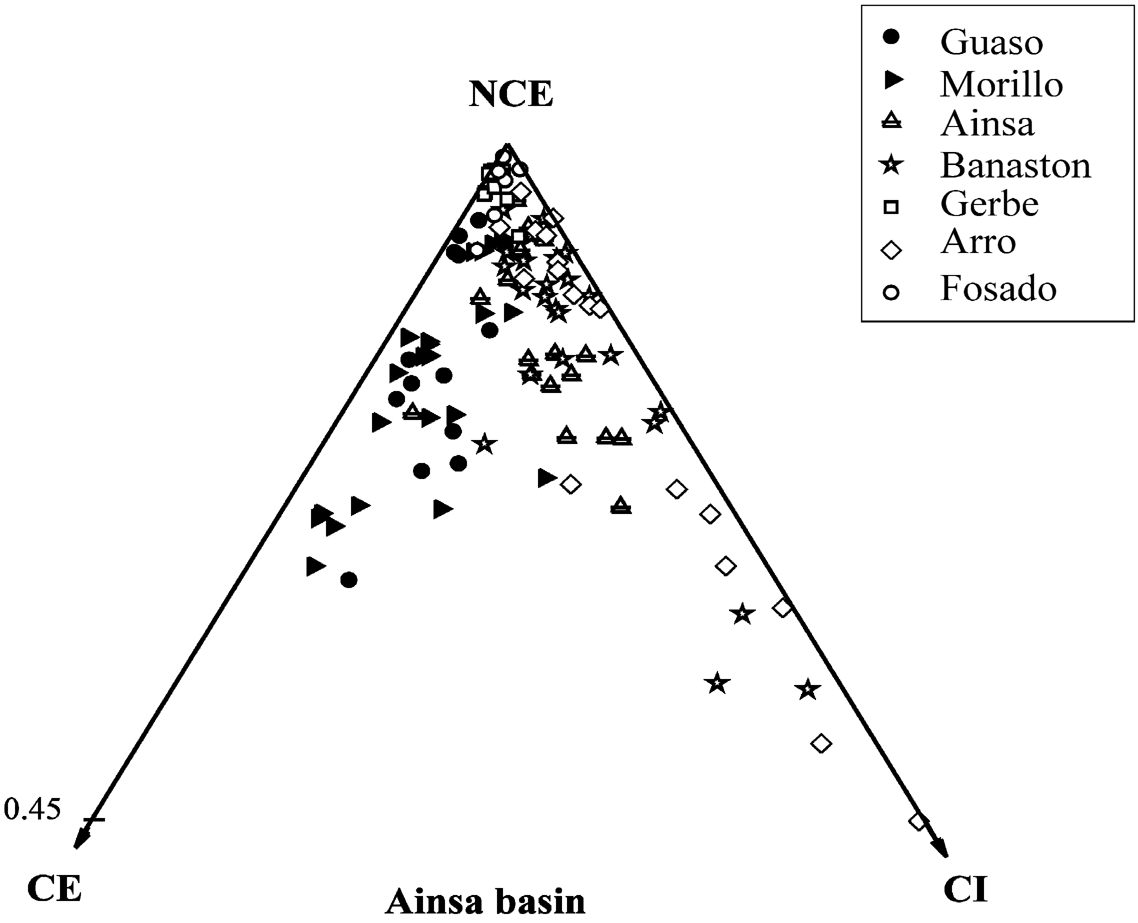

Fig. 7.8. Compositional plot of the arenites from the Ainsa basin (modified after Das Gupta & Pickering, 2008).

Although discrete samples from individual sandy systems appear to cover multiple petrofacies fields, mean values for abundances of framework grains allowed the classification of systems into distinct petrofacies (Table 7.5). The Fosado and Gerbe arenites have typical sandstone framework grains (with high abundances of NCE grains), whereas the Arro and Banastón samples are interpreted as hybrid arenites due to their enrichment in CI grains. The Ainsa arenites generate a transitional signature comprising significant proportions of both CI and CE grains. The Ainsa systems can, therefore, be defined as an intermediate system, with a mixed petrofacies classification between the hybrid arenites and calcilithites. The Morillo and Guaso systems show a change in arenite composition determined by the abundance of CE grains, representative of calcilithites. Alternatively, Fontana *et al.* (1989) classified the Gerbe arenites as hybrid arenites, and the Banastón and Ainsa arenites as calcilithites. Although these contrasting results are overlooked, this earlier study highlights some fundamental tectonostratigraphic concepts operating in the Ainsa basin.

Fosado system	*Petrofacies 1*: ~85% NCE; 1.2% CI; 2% CE; NCI
Arro system	*Petrofacies 2*: 69% NCE; 16%–49% CI; 2% CE
Gerbe system	*Petrofacies 1*: ~84% NCE; 2% CI; 0.9% CE
Banastón system	*Petrofacies 2*: 71% NCE; 11% CI; 3% CE
Ainsa system	*Petrofacies 2–3*: 70% NCE; 9% CI; 5% CE
Morillo system	*Petrofacies 3*: 66% NCE; 4% CI; 13–25% CE
Guaso system	*Petrofacies 3*: 64% NCE; 3 % CI; 10–21% CE

Table 7.5. Petrographic overview of the sandy systems in the Ainsa basin, (after Das Gupta & Pickering, 2008). The composition percentages represent mean values.

7.3.4.iii. Petrographic trends in the tectonosequences

The generalised petrographic trend of arenites in Das Gupta & Pickering (2008) shows an increase in the proportion of carbonate grains (CI and CE grain types) stratigraphically with time (from the oldest to the youngest sandy system). This pattern can be related to the two phases of structural evolution of the South Pyrenean foreland basin, described previously. It also supports the tectonic model presented in this chapter.

With the exception of the Arro system (discussed later), the TS-I arenites (Fosado system to the Gerbe system) are differentiated by the dominance of siliciclastic grains and the lack of carbonate grains. The early development of the South Pyrenean foreland basin was characterised by strong lithospheric flexure in response to the emplacement of basement-involved thrust sheets within the upper tectonic complex (phase I of structural evolution; refer to Chapter 1). Siliciclastic-rich sediment was supplied to the shallow-marine shelfal environments by the denudation of the Axial Zone and transportation via alluvial- and fluvio-deltaic systems. The lack of significant proportions of CI grains indicates the coeval carbonate shelves (carbonate factories) where not exhumed by thrusting at this time, suggesting high rates of subsidence across the young basin (interpreted as a ‘subsidence-dominated’ phase). Additionally, it signifies the basin was not compartmentalised into constituent sub-basins by intrabasinal tectonics. Although accommodation would have been high in the proximal parts of the basin (Tremp basin), as previously stated, flux-driven progradation enabled sediment to reach the deep-marine realm (Ainsa basin).

The TS-II arenites (Banastón system to the Guaso system) are characterised by high proportions of carbonate grains. This petrographic signature can be attributed to the change in tectonic regime in the southern Pyrenees. The advancement of active thrust sheets in phase II of structural evolution (see Chapter 1), distributed deformation forelandwards (southwards and westwards), generating the lower tectonic complex and the enlargement of the lateral ramp zone of the SCPU (Remacha *et al.*, 2003). The incorporation of the basin into the deformation front caused the growth of north-south intrabasinal structures (anticlines) and the subsequent segmentation of the basin. Consequently, an ‘uplift-dominated’ phase prevailed in the proximal parts of the basin as regional and local thrust-induced uplift diminished accommodation. The abundance of CI grains in the Banastón and Ainsa systems originated from uplift and erosion of coeval shelfal sediments. Alternatively, the CE grains in the Ainsa, Morillo and Guaso systems were derived from the uplift and denudation of older, underlying parts of the southern foreland basin, consisting of carbonate platforms formed within Mesozoic basins during the early movement of the Iberian plate (Chapter 1).

The cross-section in Figure 7.9 illustrates the sources of the defining framework grain categories (NCE, CI and CE), showing how forward propagation of the orogenic wedge accounts for the shift in petrographic signature of arenites. The three source areas were active throughout the depositional history of the Ainsa basin, but there is a temporal limitation to the relative importance of each source (Das Gupta & Pickering, 2008). Although the diagram infers the generation of significant abundances of CE grains prior to CI grains, from the sequential uplift forelandwards, the inverse petrographic trend is explained by the dominance of erosion of adjacent shelfal sediments, followed by the denudation of newly exhumed older (underlying) strata.

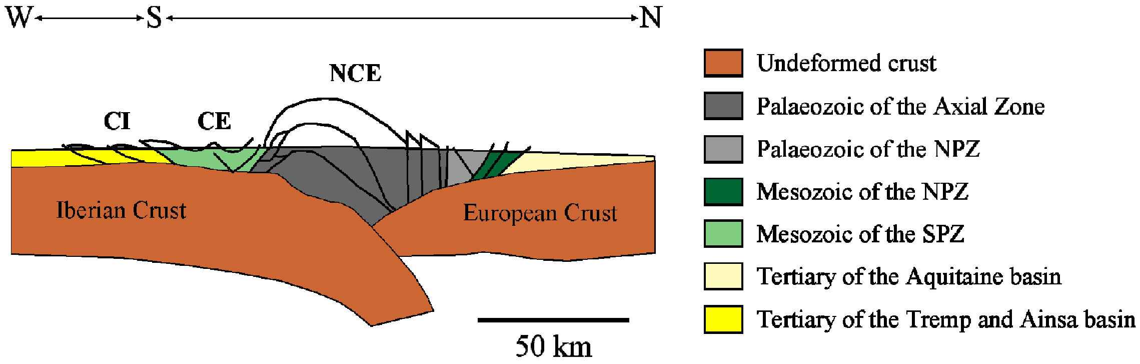

Fig. 7.9. Crustal scale cross-section based on the ECORS-Pyrenees seismic profile showing the sources of the defining framework grain categories (redrawn and modified after Munoz, 1992). The southwards and westwards advancement of the thrust front in the southern Pyrenees exhumed new source areas, influencing the temporal composition of arenites in the Ainsa basin. NCE: non-carbonate extrabasinal; CE: carbonate extrabasinal; CI: carbonate intrabasinal.

7.3.4.iv. Petrographic trends in sandy systems and system sets

Figure 7.10 illustrates the compositional deviations of arenites in the Ainsa basin with every vertical stratigraphic shift between sandy systems (results from Das Gupta & Pickering, 2008). There is an oscillation in composition of sandy systems between NCE and CI abundances up until the younger systems (mainly the Morillo and Guaso systems), which depart towards the enrichment in CE grains. This fluctuating petrographic signature is viewed as evidence for the previously described system set stratigraphic trend in the basin (presented in this chapter), and represents a tectonic influence operating in the basin, in addition to the tectonosequence driver.

The arenite composition of the Fosado system reflects the denudation of the Axial Zone, delivering siliciclastic-rich sediment to a young basin within the ‘subsidence-dominated’ phase. This interpretation can also be applied to the arenites in the overlying Los Molinos system. In accordance with Fontana *et al.* (1989) and Das Gupta & Pickering (2008), it is suggested that the Arro and Banastón systems represent periods of intense tectonic activity, as demonstrated by the significant abundance of CI grains in the arenite samples. This composition is attributed to the uplift, erosion and subsequent resedimentation of adjacent and underlying shelfal sediments. The deep incision of submarine canyons and the formation of major unconformities define the base of these system sets. The erosional unconformity at the base of the Banastón system is more pronounced because it also defines the base of TS-II (the ‘uplift-dominated’ phase) and the transformation of the Ainsa basin from a transitional foredeep setting, into a thrust-top basin. The intense erosion at the base of both system sets is interpreted as a mechanism to reach a new equilibrium slope profile in response to the reduction in accommodation in the proximal foreland basin. The overlying counterparts of these sandy systems (Gerbe and Ainsa systems, respectively) show a reduction in CI grain composition, inferring the decreased erosion and incision into carbonates (i.e. waning tectonic activity/tectonic quiescence) towards the top of the system sets. The petrography of the Morillo and Guaso systems indicate the development of a new source area that supplied extrabasinal carbonates. This implies a renewed episode of thrusting, and, therefore, the occurrence of another system set. Although the Ainsa system shows a transitional petrographic signature, i.e. one that shows high proportion of CE grains, the base of the Morillo system is marked by significant incision, the formation of a submarine canyon and a prominent unconformity.

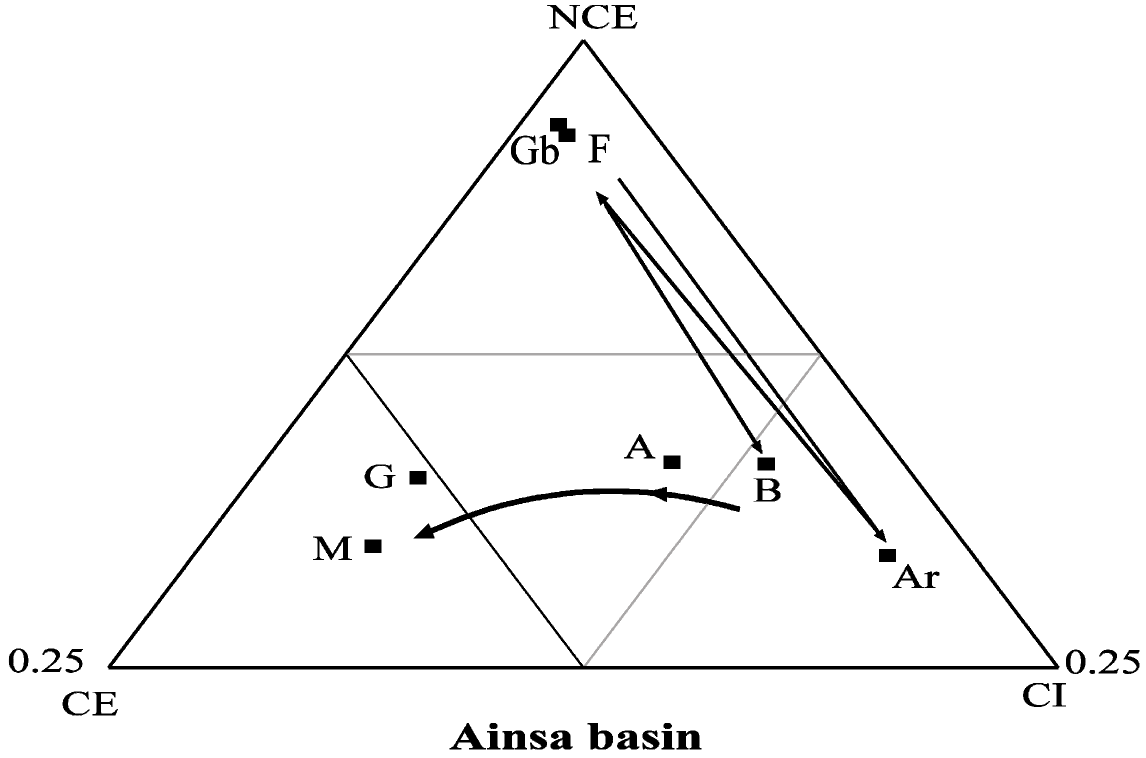

Fig. 7.10. Compositional trends observed in the Ainsa basin (modified after Das Gupta & Pickering, 2008). F: Fosado; Ar: Arro; Gb: Gerbe; B: Banastón; A: Ainsa; M: Morillo; G: Guaso.

Despite the sedimentological complexity and uniqueness of each sandy system, petrographic data supports the stratigraphic classification of the Ainsa basin, and the interpretations made in the study on processes influencing deposition. Using the results obtained in Fontana *et al.* (1989) and Das Gupta & Pickering (2008), the petrographic trend between sandy systems denotes a tectonic driver operating at high frequency modes, at least at a timescale comparable to the deposition of system sets and/or systems to control sandstone compositions. Additionally, the general petrographical pattern of sandstones demonstrates the interaction of multiple source areas in response to tectonic episodes, and supports the tectonic regimes and depositional trends outlined in this chapter.

7.4. CONTROLS ON CYCLIC SEDIMENTATION

Cyclic sedimentation forms the foundation of sequence stratigraphy, and can be identified as either autocyclic or allocyclic. Deep-marine systems reflect the complex interplay between various controlling mechanisms; however, accurately unravelling the relative contributions of such controls remains controversial. This section attempts to provide insight into the interaction between allocyclic controls in the Ainsa basin. A hierarchical approach was employed in this study to deconvolve the relative contributions of tectonism and eustasy in controlling sedimentation at a variety of temporal and spatial scales. Each main depositional tier in the deep-marine stratigraphic hierarchy (see Section 3.5) is addressed below, from the large-scale depositional cycles (tectonosequences) to the small-scale (sequences).

7.4.1. TECTONOSEQUENCES

A long-term 4–5 Myr tectonic driver is recognised in the Ainsa basin, manifest as angular unconformities extending from the shelf to the deep-marine environment. These unconformities divide the stratigraphy into tectono-stratigraphic units (*sensu* Remacha *et al*., 2003; Fernandez *et al*., 2004). Naylor and Sinclair (2007) used a modelling approach to analyse the behaviour of individual thrust units in the context of asymmetric doubly vergent thrust wedges to understand the time scale of punctuated thrust activity. A discrete element model demonstrated that the rates of surface uplift, frontal accretion and exhumation are punctuated on a time scale linked to thrust-sheet geometry and convergence rates. The application of this theory to a number of geological examples, including the Pyrenees, has revealed time scales of tectonic variability, ranging between ~0.1–5 Myr. Using the regional convergence rate of the Montsec and Sierras Marginales thrust sheets in the South-Central Pyrenees of ~6 km Myr $^{-1}$ (Vergés *et al*., 1995), and an average length of ~24 km, Naylor and Sinclair

(2007) calculated an upper limit on the time scale of tectonic variability of 4 Myr. Although this method is simplistic and based on many assumptions, the results are consistent with the long-term 4–5 Myr tectonic driver for the two tectono-sequences recognised in the Ainsa basin.

Bentham and Burbank (1996) used magnetostratigraphy and structural data to determine average sediment accumulation rates and subsidence patterns in the South Pyrenean foreland basin. The purpose of the study was to analyze the deformational history and illustrate the influence of intrabasinal structures on sedimentation. The average rates of compacted deposition for the Tremp–Graus basin were estimated at ~33 cm ky^{-1} in the Ypresian (~55–50 Ma using the timescale of Gradstein *et al*., 2004) and ~16 cm ky^{-1} in the Lutetian (~48.2–42.8 Ma). Conversely, sediment accumulation rates in the Ainsa basin were calculated at ~15 cm ky^{-1} prior to the mid Lutetian (~44.5 Ma) and ~40 cm ky^{-1} during the mid Lutetian (~44.5–43 Ma). The alternating pattern of sediment accumulation rates in the Tremp–Graus and Ainsa basins during the Lutetian (see their fig. 15) was attributed to variations in subsidence modulated by shortening along the lateral ramp zone of the SCPU (represented as a shelf break / intraslope detachment between the basins), specifically the progressive development of the Mediano anticline (see their fig. 19). High sediment accumulation rates in the Tremp–Graus basin prior to the Lutetian were a consequence of strong flexural subsidence controlled by lithospheric loading ahead of the main thrust front (Remacha *et al.,* 2003), particular the high rates of thrusting in the east during the emplacement of the Pedraforca thrust sheet (Vergés & Burbank, 1996). As the southern Pyrenean front propagated southwards, the Tremp–Graus basin was incorporated into the deformation front (Muñoz *et al*., 1994, 1998). The opposing subsidence trend across the flanks of the Mediano anticline culminated from the development of the SCPU involving the growth of the Montsec thrust sheet. The main phase of uplift and rotation of the Mediano anticline caused relative uplift of the Tremp–Graus basin in the east and contemporaneous load-driven subsidence in the Ainsa basin to the west (Bentham & Burbank, 1996). This subsidence trend resulted in a transfer in accommodation between the neighbouring basins causing an overall basinward shift in the locus of sedimentation. It represents the temporal evolution of the South Pyrenean foreland basin depocentre, highlighting the migration from east to west ahead of the advancing thrust front and deforming foreland during the most rapid period of plate collision in the Early to Middle Eocene (Puigdefàbregas *et al*., 1986; Burbank, *et* al., 1992a; Vergés *et al.,* 1995). Furthermore, the trend supports the concept that there was a change in tectonic regime in the South Pyrenean foreland basin during the early/mid Lutetian; it coincides with the shift in tectonic phases that delineates and controls the tectono-sequences.

This study supports the recognition of a 4–5 Myr tectonic driver to explain the two tectonosequences in the deep-marine Ainsa basin that are separated by an angular unconformity; however, the time-averaged driver for higher-frequency depositional sequences is an order of magnitude too fast to be explained by tectonic processes.

7.4.1.i. Turbidite bed-thickness distributions

The power-law frequency distribution of turbidite bed thicknesses has previously been attributed to the external forcing by earthquakes, and could provide an important link between tectonic events and the development of deep-marine depositional sequences. A power-law relationship is given by $N = aT^{-\beta}$, where N is the number of beds thicker than T, T is the bed thickness, β is the power-law scaling exponent, and a is a constant. The scaling exponent (β) is considered an elementary statistic with fractal dimension (*sensu* Turcotte, 1997), thus, inferring scale invariance within turbidite systems and eliminating the application of linear models to explain sedimentation. In order to invoke earthquake triggering as the mechanism responsible for the timing and thickness of turbidite beds, the scaling exponent must be consistent with the distribution of earthquake magnitudes (Bak & Tang, 1989; Beattie & Dade, 1996). Scholtz and Cowie (1990) demonstrated power-law statistics for the magnitude of earthquakes, and a seismic triggering mechanism for turbidity currents has been well documented (eg., the 1929 Grand Banks event; Heezen & Ewing, 1952). Hiscott et al. (1992, 1993) and Beattie and Dade (1996) obtained a power-law fit for the statistical analysis of bed-thickness distributions in the Oligocene Izu-Bonin forearc basin of the western Pacific Ocean. The studies determined similar scaling exponents for both the thickness of turbidites and earthquake magnitudes with power $\beta \approx 1$, demonstrating that sedimentation patterns in a region of intense tectonic activity serves as an estimate of palaeoseismicity (Beattie & Dade, 1996). A similar control could have operated in the Ainsa basin, in which periods of increased seismic activity were responsible for sediment delivery. However, statistical analysis of turbidite bed-thicknesses from the study area would corroborate this theory and facilitate more accurate inferences on processes controlling depositional sequences. Winkler and Gawenda (1999) used the presence of a power-law distribution in siliciclastic turbidite beds from the Palaeocene to lower Eocene Zumaia series in northern Spain to infer enhanced seismic activity as a result of an increasing tectonic influence attributed to the development of the Pyrenees. The study yielded exponential bed-thickness distributions in the older carbonate and transitional systems, which were driven by climatic variations in periods of tectonic quiescence. Thus, the investigation shows that the scaling of turbidite bed-thickness distributions can be applied to distinguish tectonic and climatic signals in turbidite systems, and that siliciclastic sediment input is primarily governed by tectonic activity. Further investigation would be required to test this theory in the Ainsa basin.

7.4.2. SANDY SYSTEMS

Eight depositional systems in the Hecho Group have been identified in this study (Fig. 7.1). In general, the base of each sandy channelized system is defined by a MTC. A predictable, idealized, genetic vertical sequence that tends to fine upward has been proposed using sequence stratigraphic principles, as due to a relative base-level change (Pickering and Corregidor, 2005), either eustatic sea level or induced by tectonic processes. A model is presented below that offers a possible scenario for the control on sandy systems.

If the eight sandy systems in the Ainsa basin accumulated in ~8–10 Myr (duration of the entire deep-marine fill after Puigdefàbregas *et al*., 1975; Dreyer *et al*., 1999; timescale of Gradstein *et al*., 2004), this suggest a time-averaged driver was operating at ~1 Myr cycles, which is consistent with high-frequency tectonic processes. A possible tectonic driver is considered in Figure 7.11. The basic concept of the model is adapted and modified after Posamentier & Allen (1993) and Willis (2000), but integrates the results from modelling the influence of low-angle detachment faults on sedimentation patterns presented by Clevis *et al*. (2004b). The model demonstrates the interplay between tectonic and eustatic cycles in the South Pyrenean foreland basin, and how this relationship controlled sedimentation and the development of sandy systems in the Ainsa basin. During the development of tectono-sequence, periods of crustal shortening and orogenic loading (phase I) and increased rates of subsidence sequestered coarse-grained sediment in proximal areas adjacent to the orogenic load. The rate of regional subsidence always exceeded the rate of eustatic fall (zone A), resulting in a relative rise in sea level and retrogradation of the shoreline, leaving the deep-marine basins starved of sediment. Phase I is, therefore, characterised by slope healing and the deposition of background sedimentation in the Ainsa basin. This phase may also

Tectono-sequence II: Early- to Mid Luetitan

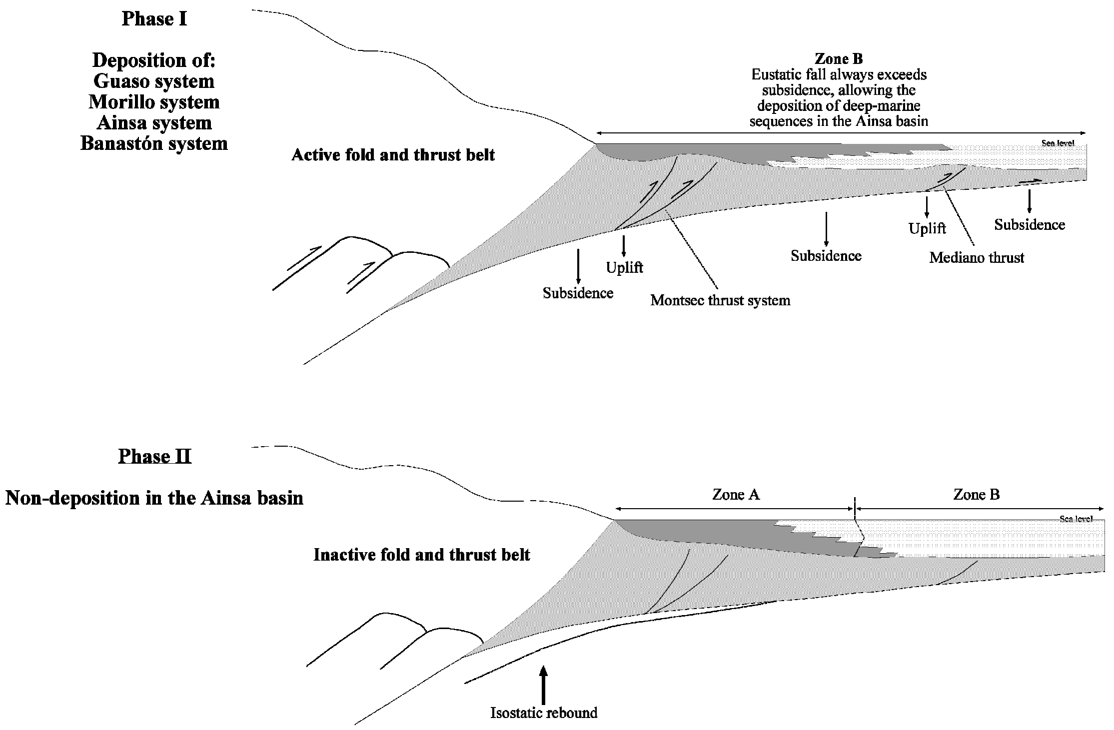

Tectono-sequence I: Late Ypresian

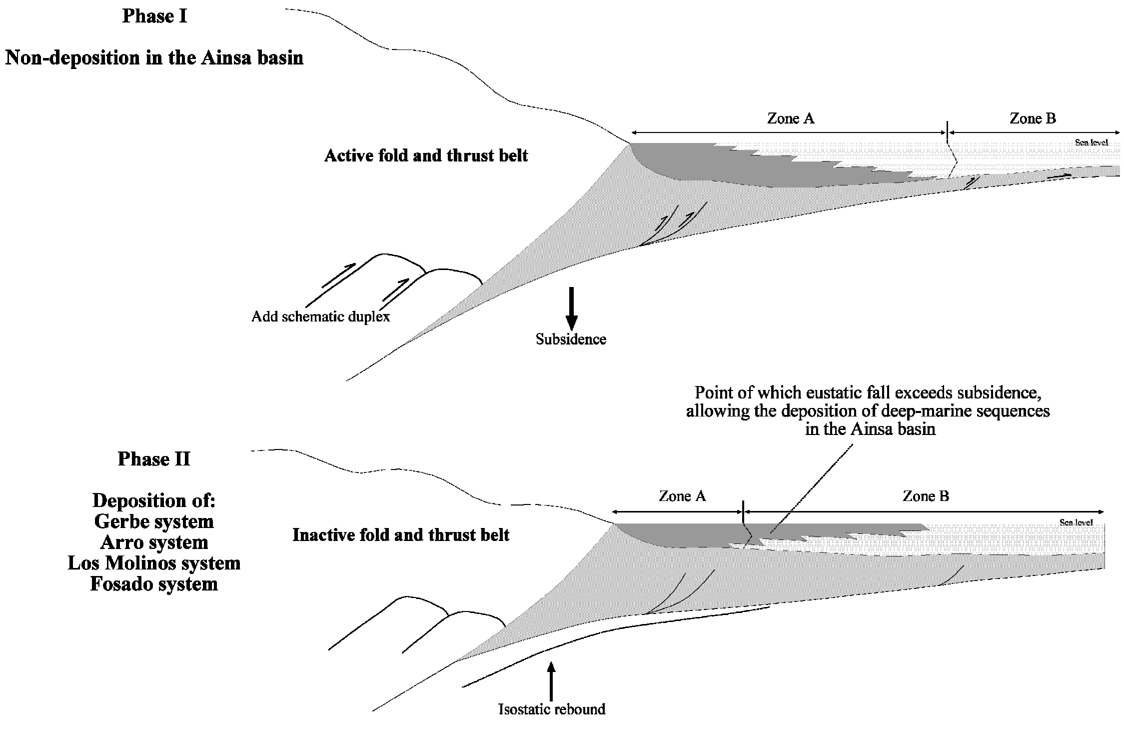

Fig. 7.11. Schematic representation in transverse cross-section of the generalised pattern of sedimentation and geometry in the South Pyrenean foreland basin (model is adapted and modified after Posamentier & Allen, 1993; Wiliis, 2000; Clevis *et al.*, 2004a,b).

account for the products of backfill and abandonment facies in the Ainsa basin, such as low-concentration turbidites occurring after the influx of sediment prior to this phase. Regional isostatic uplift during erosion of the orogenic wedge and increase in sediment flux (phase II) caused a reduction in accommodation and accelerated filling in the proximal foreland basin. This phase allowed the progradation of the shoreline into zone B and the subsequent deposition of coarse clastic sediment into deep water, i.e., the influx of sediment into the Ainsa basin.

Forward propagation of the orogenic wedge during deposition of tectono-sequence II distributed deformation more forelandwards (southwards and westwards), with the progressive horizontal translation over a shallow detachment fault (sole thrust) underlying the basin and the growth of associated intrabasinal thrusts (*sensu* Clevis *et al*., 2004b). This development marks the transition to the next tectonic stage (tectonic stage II, see Section 1.6.4) and the transformation of the Ainsa basin from a transitional foredeep setting into a thrust-top basin (Dreyer *et al*., 1999). During times of thrust activity (phase I), regional load-driven subsidence was always suceeded by regional and local thrust-induced uplift, allowing the fluvio-delta environment to become susceptible to eustatic falls (zone B). The periodic reduction in accommodation initiated progradation, with the subsequent deposition of coarse clastics into the study area. Structural lows, located adjacent to intrabasinal highs, accommodated the influx of sediment basinwards during this time. During quiescence (phase II) relaxation of structures and reduced denudation rates allows flexural subsidence to exceed the rate of eustatics falls, causing backfilling of deep-marine channels and the retrogradation of the shoreline (into zone A) landwards.

Holl and Anastasio (1993) conducted a detailed palaeomagnetic study to determine fold rates in the southern Pyrenees. The investigation recognised the episodic emplacement of the Mediano anticline (part of the Cotiella-Montsec thrust sheet), with intervals of slow fold growth at 2–3 Myr intervals (tilting at 2.2–4.2° yr^{-1}) punctuated by intervals lasting <1.5 Myr when fold growth was 3–5 times faster and produced angular unconformities. These temporal variations in folding rate can be related to synsedimentary tectonic processes operating within the South Pyrenean foreland basin, likely indicating episodic movement along the Cotiella-Montsec thrust sheet. This study suggests a higher frequency tectonic signal operating in the southern Pyrenees and offers an explanation for the frequency of unconformities indentified in the syntectonicstrata of the basin. It is, therefore, reasonable to assume a tectonic driver operating at frequencies comparable to the deposition of sandy systems.

Abreu and Anderson (1998) presented evidence for glaciation in East Antarctica since the middle Eocene using a composite oxygen isotope record, illustrating the first existence of an ice sheet near the lower-middle Eocene boundary (base of the Lutetian) and significant volume changes by late Eocene. This is supported by evidence in marine sedimentary systems for global deterioration in climate associated with Antarctic ice development in the Eocene (e.g., Browning *et al.*, 1997; Miller *et al.*, 2005; Pekar *et al.*, 2005). The study of Abreu and Anderson (1998) also postulated the development of the Antarctic ice sheet was responsible for glacial-eustatic changes for most of the Cenozoic. Accordingly, this suggests that the middle Eocene represents a significant time period for cooling of marine waters, development of ice sheets, and a prominent shift in global climate. The ages of sequence boundaries from six depositional cycles from shallow-marine sediments, obtained from ODP Leg 189 Site 1171 (South Tasman Rise) have been used with other sequence stratigraphic data sets and oxygen isotope records to suggest significant (>10 m) eustatic changes during the early–middle Eocene (Pekar *et al.*, 2005). The synchronicity between the development of sequence boundaries and $\delta^{18}O$ increases indicates a global control, and that glacio-eustasy was the only possible mechanism in the Eocene for rapid sea-level changes (Pekar *et al.*, 2005). Thus, it was interpreted that the periodic development of large, ephemeral ice sheets were responsible for the observed sea-level changes during early–middle Eocene (51–42 Ma). This duration is broadly contemporaneous with the deposition of the deep-marine fill in the Ainsa basin, suggesting that glacio-eustasy could be the mechanism controlling sediment flux, at least on a frequency comparable to the accumulation of systemsets and systems (third-order sequences) and/or higher (see sections below on the control of sequences and sub-sequences) in the study area. Additionally, the study of Pekar *et al.* (2005) used $\delta^{18}O$ records to estimate sea-level changes of ~20 m for the early Eocene (51–49 Ma) and ~25–45 m for the middle Eocene (48–42 Ma). The results and conclusions from these studies demonstrate that the middle Eocene was an important time period for global climate change, and that large, rapid sea-level changes have been observed globally during this time. Consequently, glacio-eustasy provides a reasonable alternative for the supply and delivery of coarse clastics to the Ainsa basin.

Although the depositional styles of the sandy systems can be related to various tectonic phases within the southern Pyrenees (Section 7.3), the occurrence of the eight sandy systems remains ambiguous and requires further investigation to elucidate possible controlling mechanisms. An improved age model for the Ainsa basin would help to constrain the timing and cause of coarse clastic sediment supply.

7.4.3. SANDY SEQUENCES

The depositional systems can be subdivided into 22 sandy sequences, ~30–160 m thick, that are composed of stacked channel complexes and channel fill elements, typically 5–30 m deep and hundreds of metres wide (~300–1,400 m). The base of each sequence is characterised by a composite erosional surface representing an initial bypass phase defined by gravelly lags, which are overlain by a mass transport complex, typically 8–40 m thick that consists of stacked pebbly and contorted mudstones (referred to as mass transport deposits, MTDs). The sandy component of the filling phase generally comprises laterally discontinuous, very-thick to medium-bedded, amalgamated sandstones, with dewatering structures. Above such deposits, channel fills are composed of finer grained, thin- to medium-bedded sandy backfilling-and-abandonment facies associations, which grade laterally into channel margin and overbank environments. Muddy slide and slump deposits (and other MTDs) commonly define the top of sequences and represent collapse of the underfilled conduits during the final plugging phase.

Heard *et al*. (2008) and Pickering and Bayliss (2009) postulated that if ~25 sandbodies (named sequences herein) including the muddy, inter-sequence counterparts in the Ainsa basin were deposited in ~8–10 Myr (duration of the entire deep-marine fill after Puigdefàbregas *et al*., 1975; Dreyer *et al*., 1999; timescale of Gradstein *et al*., 2004), then it could be estimated that a long eccentricity (~400 kyr) Milankovitch frequency was responsible for this apparent division. Albeit this model is simplistic, it employs a non-tectonic driver to explain the accumulation of sandy sequences. The middle Eocene was an important time period for global climate change and offers possible mechanisms for controlling sequences/sub-sequences in the Ainsa basin.

The analysis of clay mineral ratios from inter-turbidite beds from the Zumaia series from northern Spain suggests that tropical to subtropical conditions prevailed in the rising Pyrenean chain in the early Eocene, and the widespread occurrence of kaolinite implies a very warm perennially humid climate with significant precipitation

(Winkler & Gawenda, 1999). This is consistent with middle Eocene palynofloral and microfaunal data obtained from the Ainsa basin (Pickering & Fadell, 2004; Pickering & Corregidor, 2005). Such favourable climatic conditions would enhance weathering. Thus, during periods of tectonic exhumation (possibly causing enhanced gradients), early weathering of newly created source areas would allow rapid delivery of sediment to feeder systems with minimal time delay (therefore imposing no time lag for erosion-denudation release of large volumes of siliciclastics, and sediment transport mechanisms from source to sink). This demonstrates the importance of climate in influencing sedimentation patterns and the formation of depositional cycles in the South Pyrenean foreland basin.

7.4.4. MILANKOVITCH FORCING OF DEPOSITIONAL CYCLES

Many investigations have attributed cyclic sedimentation in the Paleogene as representing Milankovitch orbital forcing on fine-grained sediments (e.g., Van Echelpoel & Weedon, 1990; Machlus *et al*., 2001; Anastasio *et al*., 2005; Coxall *et al*., 2005; Burgess & Pearson, 2007; Heard *et al*., 2008; Westerhold & Rohl, 2009).

Heard *et al*. (2008) conducted a quantitative analysis of bioturbation intensity to investigate the presence of high-frequency cyclicity in the Ainsa basin. The trace fossil data set was acquired from very-thin and thin-bedded sandstones, laminated siltstones and silty mudstones from the Ainsa system in Core A6 (obtained from one of the eight wells drilled in the Ainsa basin as part of a consortia-based research study at University College London). The lithofacies within the core are primarily the products of low-concentration turbidity currents deposited off-axis to the sand-rich depocentres of the Ainsa II and III sequences, and represent channel overbank and ‘inter-sequence’ environments. Spectral analysis was performed on the bioturbation intensity data from ~159 m of core, which included the thin-bedded upper division of the Ainsa II sequence and very thin-bedded, inter-sequence deposits (situated between Ainsa II and III sequences); due to the absence of any cyclicity in bioturbation intensity from the thicker-bedded, coarser-grained sediments in the Ainsa III sequence, this core interval was excluded from the study. The time series analysis yielded two prominent power peaks that were compared to the ~41-kyr obliquity and ~100-kyr short eccentricity orbital frequency bands. It was postulated that this cyclicity in bioturbation intensity was a function of fluctuating environmental conditions operating at two different frequencies. The analysis of total organic carbon produced no significant variations throughout the core, thus suggesting periodic changes in bottom-water oxygenation levels, rather than the supply of organic matter/marine productivity as the principal controlling factor (Heard *et al*., 2008). Although Heard *et al*. (2008) confirmed Milankovitch-scale mechanisms controlling ocean circulation in the Ainsa basin this does not unequivocally determine that global climate change was responsible for deep-marine siliciclastic sedimentation. Consequently, the rôle of eustatic sea-level change (probably glacio-eustasy) as a driver for cyclic depositional elements in the Ainsa basin remains speculative, and further geochemical techniques is required to ascertain environmental conditions during the inhabitation of the seafloor by burrowing organisms.

Anastasio *et al*. (2005) integrated stratigraphic and palaeomagnetic data from the southern margin of the Jaca basin to suggest Milankovitch orbital forcing on cyclic sedimentation in the Eocene. Spectral analysis was conducted on anhysteretic remanent magnetization (ARM) variations from ~1 km of deep-marine marine basinal and prodeltaic sediment. The results produced strong power peaks that aligned to all of the principal orbital frequency bands: long eccentricity (400 kyr), short eccentricity (100 kyr), obliquity (40.4 kyr), long precession (24.4 kyr), and short precession (20 kyr). They proposed global climate modulated carbonate production, variable detrital inputs such as atmospheric dust (varying wind intensity or aridity) or watershed erosion (runoff variation) as possible mechanisms controlling ARM cyclicity. Additionally, bed thickness and grain size analyses also suggested high frequency periodicity, which was attributed to precessional forcing, thus providing more certainty that eustatic sea-level change controlled sub-sequence depositional elements in the Ainsa–Jaca basin. In agreement with this thesis, they also postulated that tectonic processes controlled larger-scale stratigraphic sequences, exemplifying the complex interaction between longer-term tectonic processes and higher-frequency climate variations in controlling sedimentation in the Ainsa basin.

In contrast to the arguments presented above for the regulation of small-scale depositional cycles from Milankovitch forcing, a number of publications have suggested that the advancement of the South Pyrenean thrust system in the Lutetian led to the structural rise of the western boundary of the foreland basin, which likely isolated the Ainsa–Jaca basin from global ocean circulation (e.g., Cámara & Klimowitz, 1985; Remacha *et al*., 1998, 2003, 2005; Remacha & Fernández, 2005). The emplacement of the Oroz-Betelu massif during the development of the upper tectonic complex was responsible for the western closure of the South Pyrenean foreland basin, preventing connections with the Atlantic Ocean (Remacha *et al*., 2003). Remacha *et al*. (2005) documented onlap patterns of megaturbidites onto the Oroz-Betelu massif, and also recorded flow reflections in turbidites indicating ponding in the basin during the deposition of the Banastón system; therefore, constraining the growth of the submarine high as early as the middle Lutetian. The development of basin-margin closure would have subsequently removed climatic influences from the Ainsa–Jaca basin during deposition of the Upper Hecho Group. In which case, the use of bioturbation intensity to infer Milankovitch orbital forcing on cyclic sedimentation in the Ainsa basin would be disregarded. However, the emplacement of the Oroz-Betelu thrust may have restricted ocean circulation, rather than fully isolating the foreland basin from global oceanographic changes. Heard *et al*. (2008) speculated that a submarine sill (using the syndepositional Boltaña anticline as an example, but applying the theory to the Oroz-Betelu massif) could have provided a barrier to the thorough mixing of ocean circulation, such as well-oxygenated marine bottom-water, thus enhancing stratification of the water column and exacerbating cyclical changes on a Milankovitch time scale.

Ichnology and magnetostratigraphy have been used to infer a Milankovitch control on cyclic sedimentation in the Ainsa–Jaca basin (Anastasio *et al*., 2005; Heard *et al*., 2008), demonstrating that global climate change could have operated at various frequency bands to control smaller-scale depositional elements in the study area. However, in the absence of geochemical methods (e.g., ratio of $^{87}Sr/^{86}Sr$) to assess the presence or departure of global isotope signatures in the Ainsa–Jaca basin, it is not possible to *fully* elucidate the importance and relative contribution of Milankovitch processes in controlling sedimentation and the cyclicity of sub-sequence depositional elements.

7.4.5. SUB-MILANKOVITCH CLIMATE OSCILLATIONS IN THE AINSA BASIN

Scotchman *et al*. (*in press*) identified millennial-scale climate oscillations, too rapid to be explained by orbital forcing, within laminated, fine-grained sediments in the A6 core. Two cycles were identified using aluminium-normalised element ratios in the sediment: 1,565-year (469 mm) cycles modulated by a 7,141-year (2157 mm) period. They were interpreted as climatically driven variations in the composition of the sediment supply in the Ainsa basin, and suggested solar emissions as a possible external forcing mechanism. Such climatic oscillations with this period are comparable to

Quaternary Bond (~1,500-year), Dansgaard-Oeschger (~1,470-year) and Heinrich (~7,200-year) climatic events. However, a fundamental difficulty is elucidating if the climatic events were regional or global in extent, and even if they are compared and calibrated with proxy records during this time, there could be associated problems. Roberts (1993) discussed the chronological uncertainty with calibrating data sets with archives of climate change, and also showed that individual proxies have different response times to climate change (e.g., some may lag behind others), which provides uncertainty when implying mechanisms of climate changes. Despite this ambiguity, the observations of Scotchman *et al.* (*in press*) lend support for global climatic variability in the Ainsa basin operating at a range of frequencies, and provide reasonable evidence for high-frequency, climatically-driven cyclic sedimentation.

7.4.6. CONCLUSIONS

The stratigraphic subdivision of sedimentary packages of various scales into a deep-marine scalar hierarchy (presented in this study) can be attributed to the complex interaction between teconic processes and climate change.

The deposition of the Hecho Group represented a significant stage of thrust-front advancement in the South Pyrenean foreland basin, and was coeval with maximum rates of tectonic subsidence and shortening (Vergés *et al*., 1995). The depositional history of the Ainsa basin fill is inherently linked to the evolution of the South Pyrnean thrust system (Section 7.3.3; Williams & Fischer, 1984; Williams, 1985), where the first-order control on basin accommodation was tectonic (Section 7.2; Pickering & Bayliss, 2009). Tectonic phases involving the development of major thrust sheets are reflected in the sedimentary character of tectono-sequences, systems and sequences, e.g., variations in sediment compositions, grain sizes and stratigraphic thicknesses (Section 7.3.2). Intrabasinal tectonics created complex seafloor topography and mobile slope gradients, which controlled the position of the eight sandy systems (Section 7.3.2) and contributed to the formation of various types of system architecture and sequence fills (Fig. 7.6).

The timing of coarse clastic sediment delivery into the deep-marine basin and the occurrence of sedimentary packages can be correlated to glacio-eustatic sea-level changes, where the long-term 4–5 Myr tectonic driver that controlled the development of the two large-scale tectonosequences were overprinted by a higher frequency climate driver. The growth of 22 sandy sequences in the Ainsa basin were controlled by a long eccentricity (~400 kyr) Milankovitch frequency, with higher-frequency orbital bands (short eccentricity and obliquity) influencing the accumulation of channel complexes and channel fill elements (see Section 3.5 for hierarchy). However, the cause and timing of the eight, discrete sandy systems remains ambiguous and requires further investigation to elucidate possible controlling mechanisms.

CHAPTER 8

CONCLUSIONS AND FUTURE RESEARCH

8.1. RESEARCH ACHIEVEMENTS

- The first geological maps of the Banastón and Morillo systems surveyed on 1:20,000 aerial photographs, involving detailed field-based outcrop and aerial photograph interpretation of slope to proximal basin-floor environments.
- A simplified geological map of the Ainsa basin using 1:40,000 topographic maps and covering the entire deep-marine sediments of the basin (~15 km^2). This is the first time individual geological maps of sandy systems have been merged and the remaining areas of the Ainsa basin mapped.
- Detailed bed-scale sedimentary logs compiled from ~4,000 m of measured section from 46 locations, which includes all the eight sandy systems comprising the Ainsa basin. The ~70,000 beds that were recorded were classified into 30 facies divisions for description and analysis.
- A number of correlations panels constructed for the interpretation of the Banastón and Morillo systems, particularly assessing the influence of syn-sedimentary structures on facies distributions and depositional architectures.
- The development of depositional models for erosional slope to proximal basin-floor channelised sequences in the Banastón and Morillo systems, illustrating the location and configuration of depocentres in response to thrust-induced seafloor topography.
- Extensive interpretations of outcrop photomosaics demonstrating facies associations and geometrical relationships in a range of architectural elements from sandy systems in the Ainsa basin.
- A new deep-marine channelised hierarchy for the Ainsa basin and the development of generic models showing the complex internal organisation of each hierarchical level.
- A synthesis of architectural styles in deep-marine systems, and a synopsis of the depositional history of the Ainsa basin integrating the regional stratigraphic and structural evolution of the South Pyrenean foreland basin.

- The tentative identification of tectono-climatic signals and the frequencies each process operates at to control the timing of sediment supply and the resulting hierarchical organisation of depositional bodies in the Ainsa basin.
- The majority of figures in the thesis are original and derived from the results of extensive fieldwork and interpretations drawn from the study. The remaining figures are all redrawn and modified from previous work and referenced accordingly.

8.2. CONCLUSIONS

The analysis of architectural styles, facies distributions, stacking patterns and the stratigraphic hierarchy of sandbodies using detailed geological maps and ~4,000 m of measured section were used to characterise the complex depositional history of the Ainsa basin fill, and document the evolution of the proximal parts of eight, channelised deep-marine systems of the Hecho Group. A hierarchical approach was employed in this study to deconvolve the relative contributions of tectonism and eustasy in controlling sedimentation at a variety of temporal and spatial scales. Tectonic processes were responsible for the large-scale stratigraphic patterns observed in tectono-sequences and systems, whereas the timing of coarse clastic sediment delivery is consistent with known frequencies of global climate change.

The syntectonic Hecho Group can be subdivided into two tectono-sequences related to major phases of thrust propagation in the south-central Pyrenees. The tectono-sequences represent periods of tectonic reorganisation, and the formation of angular unconformities formed by large-scale mass-wasting processes related to slope oversteepening and basin depocentre shift towards the foreland. Tectono-sequence I (TS-I), involving the Lower Hecho Group, accumulated during a period of very strong flexural subsidence ahead of the main thrust front during a foredeep setting in the Ainsa basin. The Lower Hecho Group comprises four discrete depositional systems (Fosado, Los Molinos, Arro and Gerbe systems), and their constituent sandy sequences (eight in total, with a cumulative thickness of ~570 m) that show very little lateral migration due to high basin-scale accommodation. Each depositional system shows a lateral stepwise migration, as a foreland-propagating clastic wedge responding to the advancement of the active basin margin in the north and east. Alternatively, tectono-sequence II (TS-II), involving the Upper Hecho Group, represents a more mature stage of basin development, characterised by anticlinal uplift as the basin became detached and incorporated into the deformation front. The development of intrabasinal growth anticlines signifies this transition into a complex thrust-top (piggyback) basin. The Upper Hecho Group comprises four, structurally-confined depositional systems (Banastón, Ainsa, Morillo and Guaso systems), and their constituent sandy sequences (14 in total, with a cumulative thickness of ~1,290 m). Growth of the north-south trending Mediano, Añisclo and Boltaña anticlines segmented the basin and controlled the position of the depositional systems and their sequences during this period. A pattern of westward lateral offset stacking is observed in the sandy sequences in each depositional system due to the growth of the Mediano anticline in the east; however, eastward (orogenward) relocation of the succeeding depositional system is recorded due to the contemporaneous uplift of the Boltaña anticline in the west. Although the depositional systems of the Hecho Group can be related to third-order seal-level fluctuations, the structural trend in TS-II demonstrates that the timing of tectonic processes operated at frequencies consistent with the accumulation of depositional systems. Several modes of structural control by thrust-sheet emplacement during the evolution of the south-central Pyrenees were considered.

The eight depositional systems range between ~60–700 m thick, comprise 2–6 sandy sequences, and were deposited in a number of deep-marine settings that include mid-slope canyons, lower-slope erosional channels and proximal basin-floor channel systems. Temporal variation in depositional style and architecture between systems reflects the tectonic regimes operating during the accumulation of the tectono-sequences. The depositional systems comprising the Lower Hecho Group are characterised by a high proportion of sediment slide and slump deposits (constituting ~25% of total thickness in TS-I) that originated from the active basin margin, and sandstone-mudstone couplets showing infrequent bed amalgamation. There is an overall thickening- and coarsening-upward trend related to changes in the staging area of the flows. The depositional systems defining TS-II contain higher abundances of pebbly sandstones, gravels and debris flows (representing ~40% of total thickness of TS-II). This is attributed to a basinward-shift in the depositional zone during the thrust-top stage of basin evolution, and an increase in sediment supply derived from the Pyrenean Axial Zone. A significant change in basin morphology is documented during the later stages of TS-II, in the Morillo and Guaso systems, which can be related to a phase of tectonically-controlled shortening across the foreland and linked differential uplift that led to significant shallowing in the Ainsa basin. The development of intra-basinal anticlines led to increasing basin narrowing and depositional confinement, which directed palaeoflow around the growing seafloor highs. As the basin became structurally segmented, the final stage of deep-marine sedimentation was represented by a low-gradient, ponded system.

The depositional systems can be subdivided into 22 sandy sequences, ~30–160 m thick, that are composed of stacked channel complexes and channel fill elements, typically 5–30 m deep and hundreds of meters wide (~200–1,500 m). The sandy sequences were controlled by a long eccentricity (~400 kyr) Milankovitch frequency with higher-frequency orbital bands (short eccentricity and obliquity) influencing the accumulation of channel complexes and channel fill elements. The base of each sequence is characterised by a composite erosional surface representing an initial bypass phase defined by gravelly lags that are overlain by a mass transport complex, typically 10–40 m thick and consisting of stacked pebbly and contorted mudstones (referred to as mass transport deposits, MTDs). MTDs created irregular seafloor topography, and locally controlled the spatial distribution of deposits around the cohesive depositional mounds. The sandy filling phases generally comprise laterally discontinuous, very thick to medium-bedded, amalgamated sandstones, with dewatering structures. Above such deposits, channel fills are composed of finer grained, thin- to medium-bedded backfilling-and-abandonment facies associations, with minor amounts of MTDs. These facies associations grade laterally into channel margin and overbank environments.

An important outcome of this study is the recognition of a complex hierarchical interaction between global climatic and tectonic drivers, operating at a variety of time scales to control the timing of coarse clastic sediment supply and architectural styles of depositional systems. Tectonic processes were responsible for the creation of basin accommodation, and large-scale stratigraphic patterns and sedimentary characteristics observed in the Ainsa basin, whereas the timing and occurrence of coarse clastic sedimentary packages of various scales can be attributed to sedimentation changes associated with glacio-eustasy. This study suggests that the controls on deep-marine basins can be divided into those that control the occurrence of sediment in deep-water environments, and those that control the style of sedimentation.

8.3. FUTURE RESEARCH

The research undertaken in this study has yielded a number of areas of interest that could generate topics for further investigation. The ideas outlined below are aimed to improve the understanding of the evolution of the Ainsa basin and compliment the data set presented in this thesis.

BED-THICKNESS DISTRIBUTIONS: The statistical analysis of bed-thickness distributions, using the ~70,000 measured beds recorded in this study, can be employed in the identification of deep-marine environments to investigate if different statistical distributions are a function of facies type, and to unravel tectonic and climatic forcing in the Ainsa basin. The frequency distribution of turbidite thickness has become increasingly recognised as a tool to: (1) recognise trigger mechanisms for turbidity currents (Hiscott *et al.*, 1992, 1993; Rothman *et al.*, 1994; Beattie & Dade, 1996; Winkler & Gawenda, 1999); (2) determine bed volumes (Malinverno, 1997); (3) interpret depositional processes (Pirmez *et al.*, 1997; Talling, 2001; Awadallah, 2002); (4) predict depositional environments (Carlson & Grotzinger, 2001). Winkler and Gawenda (1999) used turbidite bed scaling in selected intervals from the Palaeocene to lower Eocene Zumaia series in northern Spain to distinguish tectonic and climatic controls in turbidite systems. A temporal trend from exponential bed-thickness distributions, driven by climatic variations, in the carbonate and transitional systems to a power-law distribution in the younger siliciclastic system was interpreted as an increasing tectonic influence due to the rising Pyrenees: Hiscott *et al.* (1992, 1993) and Beattie and Dade (1996) postulated that the thicknesses of beds show a scaling relationship similar to that observed for earthquake magnitudes, and therefore proposed a seismic triggering mechanism for the turbidites obeying power-law statistics. Deviations from the ideal power-law distribution may reflect the complexity of intrabasinal processes and mechanisms acting upon turbidity flows or turbidites (e.g., Drummond, 1999; Talling, 2001; Carlson & Grotzinger, 2001), thus identifying depositional environments. This statistical method could be applied to the Ainsa basin to form an integrated investigation with other techniques (see below) in order to understand the depositional history of the Ainsa basin, and elucidate the triggering mechanisms and intrabasinal processes controlling the deep-marine stratigraphic hierarchy.

CLASSIFICATION AND STRATIGRAPHIC SIGNIFICANCE OF MASS TRANSPORT DEPOSITS AND COMPLEXES: MTDs represent 32% of the ~4,000 m of stratigraphic section measured in this investigation and have been mapped as aerially extensive composite units (MTCs), extending laterally from channelised depocentres to off-axis marginal and overbank environments. Therefore, it can be assumed that they form a volumetrically significant component of sedimentary environments in the Ainsa basin. This study classified MTDs into six categories based on lithological content in order to assess a range of vertical trends that comprise MTCs. A more thorough investigation into their stratigraphic location, depositional processes, geometry and internal characteristics (e.g., grain-size distribution and fabric), with the aim to produce a detailed classification scheme, could lead to an improved understanding of the range of controls and transport mechanisms responsible for MTDs. Additional analysis may involve high-resolution field mapping and correlation of MTCs to research the stratigraphic significance of such units in a temporal and spatial framework. Investigating MTDs in other basins, such as the coarse-grained deposits in the Cerro Toro Formation of the Magallanes foreland basin in Chile, would provide a wider context for understanding the nature of such deposits and the vertical associations forming MTCs.

DETAILED MAPPING OF THE LOWER HECHO GROUP: Geologically mapping of the Lower Hecho Group (including the Fosado, Los Molinos, Arro and Grebe systems) on 1:20,000 aerial photographs (involving field-based outcrop interpretation) would allow the construction of a complete detailed map of the Ainsa basin, and constrain the spatial and temporal distribution of facies associations in the basin. This would provide a better understanding of the early evolution of the Ainsa basin during the emplacement of the upper tectonic complex.

STRUCTURAL TECHNIQUES: The enlargement of the lateral ramp zone of the South-Central Pyrenean Unit deformed much of the earliest parts of the deep-marine fill in the Ainsa basin during tectonic phase I (Ypresian), resulting in a complex structural configuration of many sandy sequences, which was later complicated by out-of-sequence thrusting and related folding during tectonic phase II (Lutetian). This demonstrates an important synsedimentary tectonic influence on deposition within the basin. The construction of structural maps and the acquisition of structural measurements, such as the lineations on fault place surfaces, would constrain the timing and style of kinematics during the evolution of the basin. Radiometric dating (see below) could also be used to precisely constrain the timing of thrusting. Subsequently, the structural configuration of the basin could be placed into a chronostratigraphic framework to reconstruct the status of the basin in a number of time-slices. This would aid in understanding the present-day outcrop relationships for mapping purposes, particularly the structural complications between the Los Molinos and Arro systems, and to provide knowledge on the tectonic processes operating in the basin.

UNRAVELLING TECTONIC AND CLIMATIC SIGNALS USING MORE SOPHISTICATED METHODS OF ANALYSIS: The systematic study of hierarchical organisation of sequences in the Ainsa basin has revealed the complex interplay between factors controlling sedimentation at a variety of temporal and spatial scales; however, only a tentative identification of tectono-climatic signals has been achieved through the investigation of complex stacking patterns and architectural styles. Although information from various publications has been used to distinguish possible drivers of cyclic sedimentation in foreland basins, radiometric and geochemical studies in the Ainsa basin could establish a set of tools that could lend insight into the interaction between global climate change and tectonic processes that exerted an important control on deposition. Fission track thermochronological studies have been used to determine exhumation/denudation histories in orogenic belts, and to elucidate sediment provenance (Hurford & Carter, 1991; Johnson, 1997; Carter & Bristow, 2000; Bernet *et al.*, 2004; Jolivet *et al.*, 2007). Zircon and apatite fission track ages obtained in the Gavarnie thrust constrained the timing of thrust activity (Sinclair *et al.*, 2005; Jolivet *et al.*, 2007) that formed an important component in the tectono-stratigraphic evolution of the thrust-top phase (during deposition of the Upper Hecho Group) in the Ainsa basin. Acquiring additional thermochronological data could constrain the timing and sequence of southward thrusting in the Eocene and delineate structural regimes involving the activity of specific thrust sheets in the denudation history of the hinterland. Providing the age dating of the stratigraphy in the Ainsa basin is accurate, an insight into the relative importance of tectonic processes on the stratigraphic hierarchy can be achieved. Information on sedimentary provenance can also be derived from coarse clastic sediment analysis in the basin to discriminate source regions and to determine the age of the sediments. Das Gupta and Pickering (2008) conducted a petrographic study of sandstone compositions in the Ainsa basin and provided inferences on sediment provenance and dispersal pathways. Integrating gechronometric techniques would be more effective in determining the evolution of basinal sediments and the depositional history of the basin. Collectively, these tools can distinguish the tectonic processes operating in the basin, the age and timescale at which they occur (to control depositional sequences), and the characterisation of hinterland evolution. Alternatively, the contribution of global climate change often depends on the calibration with the eustatic sea-level curve. Geochemical signatures of both sediments and calcareous hard part fossils can assess the relative importance of climate and tectonic controls in a basin by attempting to identify the presence of global ocean circulation (using ^{18}O and ^{13}C records). Remacha *et al*. (2005) documented flow reflections in the Banastón system inferring the western boundary closure of the South Pyrenean foreland basin. The ponding was attributed to the emplacement of the Oroz-Betelu thrust, which prevented connections with the Atlantic Ocean and represented the development of the lower (younger) tectonic complex during deposition of the Upper Hecho Group. Testing this hypothesis with geochemical methods such as the ratio of ^{87}Sr/^{86}Sr would verify the restriction/isolation of the basin if a departure from global oceanic isotope values were observed, thus indicating a strong tectonic influence. Conversely, calibration of this record would reflect global oceanographic changes, which may suggest a global climatic control on the Ainsa–Jaca basin. Flecker and Ellam (1999) applied the same methodology in basins from the Eastern Mediterranean, interpreting ^{87}Sr/^{86}Sr divergence from the global oceanographic curve during the Tortonian as a tectonic-controlled isolation of the Mediterranean basins prior to the Messinian salinity crisis.

The quantitative analysis of faunal successions within the Ainsa basin, such as faunal associations, diversities and abundances, could be used as a tool in unravelling tectonic processes and global climate change. Pedley and Maniscalco (1999) applied this technique to Late Miocene strata of Sicily within the Caltanissetta region to identify faunal associations that were interpreted to reflect changes in base level due to the increasing affect of tectonic-induced shallowing (i.e., the identification of low diversity faunal associations), and the removal of climatic influences (and eustatically-controlled faunal signatures) as the basin became restricted from the open ocean. A more detailed study of faunal patterns in the Ainsa basin would provide information on environmental changes (e.g., salinity, nutrient levels, oxygenation and temperature fluctuations), particularly when integrated with the geochemical values from the basin and alternative controls on fauna distributions can be isolated (e.g., substrate composition and taphonomic conditions). Understanding the timing of tectonic processes, and calibrating the faunal values with available eustatic signatures would provide further relevance in resolving the cause of such palaeoecological trends and the mechanisms responsible for changes in water chemistry. Additionally, spectral analysis could be employed to determine the presence of cyclicity in the biostratigraphy (e.g., faunal abundances, diversities) and lithostratigraphy (e.g., grain-size distributions, rhythmic interlayering in fine-grained sediments) of the Ainsa basin. The mechanisms responsible for the various frequencies operating could be inferred by equating power peaks to known frequencies yielded by various controlling factors. Heard *et al*. (2008) applied spectral analysis on bioturbation abundance of very thin- and thin-bedded siliciclastic turbidites in the Ainsa basin. The observed cyclicity was interpreted to reflect two Milankovitch frequency modes that drove global environmental changes, and therefore likely controlled palaeoecological conditions in the basin. Further spectral analysis is required to elucidate the range of high-frequency mechanisms operating in the Ainsa basin.

DEFINING DEPOSITIONAL BODIES AT VARIOUS HIERARCHICAL LEVELS USING ICHNOLOGY: The analysis of trace fossils in this study has suggested that the seafloor in the Ainsa basin once supported an abundant and/or diverse burrowing community. The investigation into firmground development in overbank environments in the Banastón I and II sequences using the identification of the *Glossifungites* ichnofacies, highlighted the possibility of a new deep-marine stratigraphic tool in defining key horizons. The colonised surfaces are particularly documented in shallow-marine deposits (e.g., Pemberton & Frey, 1985; Gingras, *et al*., 2000, 2001), albeit there has been very little research into firmground identification in deep-marine siliciclastic systems. Hubbard and Shultz (2008) recognised *Glossifungites* ichnofacies in Cretaceous strata of the Magallanes foreland basin in Chile. They interpreted the horizon as a stratigraphic discontinuity associated with a long-term cessation of coarse-grained sediment and used it as a marker horizon to correlate throughout the basin. Thus, this tool may improve correlations in the Ainsa basin stratigraphy, especially between the Tremp–Graus, Ainsa and Jaca sub-basins, and may even permit accurate correlations in other basins worldwide. These horizons have temporal significance, and if integrated with geochemical data and sedimentary characteristics could prove to be a valuable tool in defining stratigraphic horizons and cyclic patterns in the Ainsa basin.

CORRELATION AND ANALYSIS IN THE TREMP–GRAUS BASIN: Nijman (1998) presented an extensive study on the Tremp–Graus basin, detailing stratigraphic cyclicity and depositional trends in the proximal part of the South Pyrenean foreland basin. Integrating this data set with the results outlined in this thesis might develop sedimentological relationships between the fluvio-deltaic systems in the east and the contemporaneous deep-marine slope to proximal basin-floor systems in the west. This could permit the first detailed correlation between the sub-basins; physical correlations have been unsuccessful due to the present-day structural separation by the Mediano anticline. The spatio-temporal evolution of the foreland basin and inferences on the factors controlling deposition could be achieved through further integrated studies on the sub-basins.

GEOLOGICAL MAPPING AND CORRELATION IN THE JACA BASIN: The deep-marine sediments in the Jaca basin have been extensively studied (e.g., Mutti, 1977; Mutti & Johns, 1978; Mutti *et al.*, 1985; Labaume *et al.,* 1987; Remacha *et al.*, 1991, 1995, 2003, 2005; Barnolas & Teixell, 1994; Payros *et al.,* 1999; Remacha & Fernández, 2003, 2005; Heard & Pickering, 2008; Das Gupta & Pickering, 2008), but there has been little attempt to interpret the observations in a wider context (e.g. in terms of the syn-tectonic evolution of the South Pyrenean foreland basin). A comprehensive study in the Jaca basin to describe the spatio-temporal evolution of the deep-marine sandy systems in more distal regions would, therefore, be beneficial in testing the hierarchical levels and depositional trends proposed in this study. This would provide a better understanding of the deep-marine sedimentation history in the central sector of the South Pyrenean foreland basin.

REFERENCES

Abreu, V.S. & Anderson, J.B. 1998. Glacial eustasy during the Cenozoic: sequence stratigraphic implications. AAPG z Bulletin, 82, 1385–1400.

Abreu, V., Sullivan, M., Pirmez, C. & Mohrig, D. 2003. Lateral accretion packages (LAPs): an important reservoir element in deep water sinuous channels. Marine and Petroleum Geology, 20, 631–648.

Ahr, W. M. 1973. The carbonate ramp: an alternative to the shelf model. Gulf Coast Association of Geological Societies Transactions, 23, 221–225.

Amy, L.A., Kneller, B.C. & McCaffrey, W.D. 2007. A generic model for the filling of pondedturbidite basins; interpretation of the Grés de Peïra Cava. Journal of Geological Society of London, 164, 143–162.

Anadón, P., Colombo, F., Esteban, M., Marzo, M., Robles, S., Santanach, P. & Solé Sugrañes, L. 1979. Evolución tectonoestratigráfica de los Catalánides.: Acta Geol. Hispànica, Volum homenatge a Lluís Solé i Sabarís, 14, 242–270.

Anastasio, D.J. & Holl, J.E. 2001. Transverse fold evolution in the External Sierra, southern Pyrenees, Spain. Journal of Structural Geology, 23, 379–392.

Anastasio, D.J., Hinnov, L.A., Newton, M.L. & Kodama, K.P. 2005. Milankovitch Modulated Eocene Growth Strata From the Jaca Piggyback Basin, Spanish Pyrenees. American Geophysical Union, Fall Meeting 2005, Abstract PP51C-0618.

Anderson, K.S., Graham, S.A. & Hubbard, S.M. 2006. Facies, architecture, and origin of a reservoir-scale sand-rich succession within submarine canyon fill: insights from Wagon Caves Rock (Paleocene), Santa Lucia Range, California, U.S.A. Journal of Sedimentary Research, 76, 819–838.

Arbués, P., Muñoz, P.A., Poblet, J., Puigdefàbregas C. & McClay, K. 1998. Significance of submarine truncation surfaces in the sedimentary infill of the Ainsa basin (Eocene of south-central Pyrenees, Spain) (abs.). Abstracts of the 15th International Sedimentological Congress, Alacant, Spain, Publicaciones de la Universidad de Alicante, 145–146.

Arbués, P., Mellere, D., Puig, M. & Marzo, M. 2007. Los Molinos Road, Spain: The Effect of Slumping on Sandstone Distribution in the Arro Turbidites. In: Nilsen, T.H., Shew, R.D., Steffens, G.S. & Studlick, J.R.J. (eds.) Atlas of deep-water outcrops: AAPG Studies in Geology 56, CD-ROM, pp. 17.

Awadallah, S.A.M. 2002. Architecture and depositional history of the lower Cloridorme Formation, Gaspé Peninsula, Quebec, Canada. Unpublished PhD Thesis, Memorial University of Newfoundland, St John's, Canada, pp. 376.

Azpeitia, M. F. 1933. Datos para el studio paleontólogico del Flysch de la Costa Cantábrica y de algunos otros puntos de España. Boletín. Instituto Geológico y Minero de España, 53, 1–65.

Bak, P. & Tang, C. 1989. Earthquakes as a self-organized critical phenomena. Journal of Geophysical Research, 94, 15,635–15,637.

Bakke, K., Gjelberg, J. & Petersen, S.A. 2008. Compound seismic modelling of the Ainsa II turbidite system, Spain: Application to deep-water channel systems offshore Angola. Marine and Petroleum Geology, 25, 1058–1073.

Barnolas, A. & Teixell, A. 1994. Platform sedimentation and collapse in a carbonate dominated margin of a foreland basin (Jaca basin, Eocene, southern Pyrenees). Geology 22, 1107–1110.

Barnolas, A., Samso, J.M., Teixell, A., Tosquella, J. & Zamorano, M. 1991. Evolución sedimentaria entre la cuenca de Graus–Tremp y la cuencade Jaca–Pamplona. I Congreso Grupo Español del Terciario, Libro Guía Excursión 1. Vic.

Beattie, P.D. & Dade, W. B. 1996. Is scaling in turbidite deposition consistent with forcing by earthquakes? Journal of Sedimentary Research, 66, 909–915.

Beldersen, R.H., Kenyon, N.H., Stride, A.H. & Pelton, C.D. 1984. A ‘braided’ distributary system on the Orinoco deep-sea fan. Marine Geology, 56, 195–206.

Bentham, P. & Burbank, D.W. 1996. Chronology of the Eocene foreland basin evolution along the western oblique margin of the south-central Pyrenees. In: Dabrio, C. J. Tertiary Basins of Spain, The Stratigraphic Record of Crustal Kinematics. Cambridge University Press, Cambridge, pp.144–152.

Bentham, P.A., Burbank, D.W. & Puigdefàbregas, C. 1992. Temporal and spatial controls on the alluvial architecture of an axial drainage system: late Eocene Escanilla Formation, southern Pyrenean foreland basin. Spain. Basin Research, 4, 335–352.

Bernet, M., Brandon, M.T., Garver, J.I. & Molitor, B.R. 2004. Fundamentals of detrital zircon fission-track analysis for provenance and exhumation studies with examples from the European Alps. Geological Society of America, 378, 25–36.

Blair, T.C. & Bilodeau, W.L. 1988. Development of tectonic cyclothems in rift, pull-apart, and foreland basin: sedimentary response to episodic tectonism. Geology, 16, 517–520.

Bouma, A. H. 1962. "Sedimentology of some flysch deposits, a graphic approach to facies interpretation". Amsterdam, Elsevier. pp 168.

Bouma, A. H., DeVries, M.B., & Stone, C.G. 1997. Reinterpretation of depositional processes in a classic flysch sequence (Pennsylvanian Jackfork Group), Ouachita Mountains, Arkansas and Oklahoma. AAPG Bulletin, 81, 470–472.

Brongniart, A.T. 1823. Observations sur les Fucoids. Société d'Hist Natur. Paris. Mémoir, 1, 301–320.

Brongniart, A.T. 1828. Histoire des végétaux fossils ou recherches botaniques et géologiques sur les végétaux renfermés dans les diverses couches du globe. Volume 1. G. Dufour and E. d'Ocagne, Paris, pp. 136.

Brookfield, M.E. 1977. The origin of bounding surfaces in ancient aeolian sandstones. Sedimentology, 24, 303–332.

Browning, J.V., Miller, K.G., Van Fossen, M., Liu, C., Pak, D.K., Aubry, M.P. & Bybell, L.M. 1997. Early to middle Eocene sequences of the New Jersey coastal plain and their significance for global climate change. In: Miller, K.G. & Snyder, S.W. (eds.) Proceedings of the Ocean Drilling Program, Scientific results, Volume 150: College Station, Texas, Ocean Drilling Program, pp. 229–242.

Burbank, D.W., Puigdefàbregas, C. & Munoz, J.A. 1992a. The chronology of the Eocene tectonic and stratigraphic development of the eastern Pyrenean foreland basin, north-east Spain. Geological Society of America, Bulletin, 104, 1101–1120.

Burbank, D.W., Vergés, J., Muñoz, J.A. & Bentham, P. 1992b. Coeval hindward- and forward-imbricating thrusting in the south-central Pyrenees, Spain: Timing and rates of shortening and deposition. Geological Society of America Bulletin, 104, 3–17.

Burgess, C.E. & Pearson, P.N. 2007. Milankovitch scale cyclicity in the Eocene Southern Ocean — an integrated micropalaeontological and geochemical approach. Geophysical Research Abstracts, 9, 03065.

Butler, W.H. & Grasso, M. 1993. Tectonic controls on base-level variations and depositional sequences within thrust-top and foredeep basins: examples from the Neogene thrust belt of central Sicily. Basin Research, 5, 137–151.

Cadée, C.G. 1984. Opportunistic feeding, a serious pitfall in trophic structure analysis of (paleo)faunas. Lethaia, 17, 289–292.

Cámara, P. & Klimowitz, J. 1985. Interpretación geodinámica de la vertiente centrooccidental surpirenaica (cuencas Jaca–Tremp). Estudios Geológicos, 41, 391–404.

Campbell, CV. 1967. Lamina, Laminaset, Bed and Bedset. Sedimentology, 8, 7–26.

Campion, K., Sprague, A. & Sullivan M. 2005. Architecture and lithofacies of the Capistrano Formation (Miocene-Pliocene), San Clemente, California. Fullerton, Calif.: Pacific Section SEPM, Society for Sedimentary Geology.

Carlson, J. & Grotzinger, J.P. 2001. Submarine fan environment inferred from turbidite thickness distributions. Sedimentology, 48, 1331–1351.

Carter, A. & Bristow, C.S. 2000. Detrital zircon geochronology: enhancing the quality of sedimentary source information through improved methodology and combined UPb and fission-track techniques. Basin Research,12, 47–57.

Chang, K.H. 1975. Unconformity bounded stratigraphic units. Geological Society of America Bulletin, 66, 1544–1552.

Choukroune, P. & Seguret, M. 1973. Tectonics of the Pyrenees; role of compression and gravity. In: Dejong, K.H. & Schotten, R. (eds.) Gravity and Tectonics. Wiley, New York, pp. 141–156.

Choukroune, P. & ECORS Team. 1989. The ECORS Pyrenean deep seismic profile reflection data and the overall structure of an orogenic belt Tectonics 8, 23–39.

Clark, J.D. 1995. Detailed section across the Ainsa II Channel complex, South Central Pyrenees, Spain. In: Pickering, K.T., Hiscott, R.N., Kenyon, N.H., Ricci Lucchi, F. & Smith, R.D.A. (eds.) Atlas of deep water environments: architectural style in turbidite systems. Chapman and Hall. London, pp. 139–144.

Clark, J.D. & Pickering, K.T. 1996. Submarine channels: Processes and architecture. Vallis Press, London, pp. 232.

Clark, I. & Cartwright, J. 2009. Interactions between submarine channel systems and deformation in deepwater fold belts: Examples from the Levant Basin, Eastern Mediterranean sea. Marine and Petroleum Geology, 26, 1465–1482.

Clevis, Q., de Boer, P. & Nijman, W. 2004a. Differentiating the effect of episodic tectonism and eustatic sea-level fluctuations in foreland basins filled by alluvial fans and axial deltaic systems: insights from a three-dimensional stratigraphic forward model. Sedimentology, 51, 809–835.

Clevis, Q., de Jager, G., Nijman, W. & de Boer, P.L. 2004b. Stratigraphic signatures of translation of thrust-sheet top basins over low-angle detachment faults. Basin Research, 16, 145–163.

Coleman, J. L. 2000. Carboniferous submarine basin development of the Ouachita Mountains of Arkansas and Oklahoma. In Bouma, A. H. & Stone, C. G. (eds.) Fine grained turbidite systems. AAPG Memoir 72/SEPM Special Publication No. 68, 21–32.

Coney, P.J., Muñoz, J.A., Mcclay, K.R. & Evenchick, C.A. 1996. Syntectonic burial and post-tectonic exhumation of the southern Pyrenees foreland fold-thrust belt. Journal of Geological Society, London, 153, 9–16.

Coxall, H.K., Wilson, P.A., Palike, H., Lear, C.H. & Backman, J. 2005. Rapid stepwise onset of Antarctic glaciation and deeper calcite compensation in the Pacific Ocean. Nature, 433, 53–57.

Das Gupta, K. & Pickering, K.T. 2008. Petrography and temporal changes in petrofacies of deep-marine Ainsa–Jaca basin sandstone systems, Early and Middle Eocene, Spanish Pyrenees. Sedimentology, 55, 1083–1114.

DeCelles, P.G., Giles, K.A. 1996. Foreland basin systems. Basin Research, 8, 105–123.

Dercourt, J., Zonensshain, L.P., Ricou, L.E., Kazmin, V.G., Le Pichon, X., Knipper, A.L., Grandjacquet, C., Sbortshikov, I.M., Geyssant, J., Leprevier, C., Pechersky, D.H., Boulin, J., Sibuet, J.C., Savostin, L.A., Sorokhtin, O., Westphal, M., Bazhenov, M.L., Lauer, J.P. & Biju-Duval, B. 1986. Geological Evolution of the Tethys Belt from the Atlantic to Pamirs since the Lias: Tectonophysics, 123, 241–315.

Dreyer, T., Corregidor, J., Arbues, P. & Puigdefàbregas, C. 1999 Architecture of the tectonically influenced Sobrarbe deltaic complex in the Ainsa Basin, northern Spain. Sedimentary Geology, 127, 127–169.

Drummond, C.N. 1999. Bed-thickness structure of multi-sourced ramp turbidites: Devonian Brailler Formation, Central Appalacian Basin. Journal of Sedimentary Research, 69, 115–121.

Drzewiecki, P.A & Simo (TONI), J.A. 2000. Tectonic, eustatic and environmental controls on mid-Cretaceous carbonate platform deposition, south-central Pyrenees, Spain. Sedimentology, 47, 471–495.

Dykstra, M. & Kneller, B. 2008 Lateral accretion in a deep-marine channel complex: implications for channelized flow processes in turbidity currents, Sedimentology, 56, 1411–1432.

ECORS Pyrenees team. 1988. The ECORS deep reflection seismic survey across the Pyrenees. Nature, 331, 508–511.

Ekdale, A.A. 1985. Paleoecology of the marine endobenthos. Palaeogeography, Palaeoclimatology, Palaeoecology, 50, 63–81.

Ekdale, A.A. & Lewis, D.W. 1991. Trace fossils and paleoenvionmental control of ichnofacies in a late Quaternary gravel and loess fan delta complex, New Zealand. Palaeogeography, Palaeoclimatology, Palaeoecology, 81, 253–279.

Elliott, T. 2000. Depositional architecture of a sand-rich, channelized turbidite system: the Upper Carboniferous Ross Sandstone formation, Western Ireland. In: Weimer, P., Slatt, R.M., Bouma, A.H. & Lawrence, D.T. (eds.) Gulf Coast Section Society of Economic Paleontologists and Mineralogists Foundation 20th Annual Research Conference: Deep-water Reservoirs of the World pp. 342–373. GCSSEPM, Houston, TX.

Emery, D. & Myers, K. J. 1996. Sequence Stratigraphy. Blackwell Science, Oxford, pp. 297.

Eschard, R., Albouy, E., Deschamps, R., Euzen, T. & Ayub, A., 2003. Downstream evolution of turbiditic channel complexes in the Pab Range outcrops, Maastrichtian Pakistan. Marine and Petroleum Geology, 20, 691–710.

Falivene, O., Arbués, P., Gardiner, A., Pickup, G., Muñoz, J.A. & Cabrera, L. 2006a. Best practice stochastic facies modeling from a channel-fill turbidite sandstone analog (the Quarry outcrop, Eocene Ainsa basin, northeast Spain). American Association of Petroleum Geologists, Bulletin, 90 (7), 1003–1029.

Falivene, O., Arbués, P., Howell, J., Muñoz, J.A. & Fernández, O. 2006b. Hierarchical geocellular facies modelling of a turbidite reservoir analogue from the Eocene of the Ainsa basin, NE Spain. Marine and petroleum geology, 23 (6), 679–701.

Falivene, O., Arbués, P., Ledo, J., Benjumea, B., Muñoz, J.A., Fernández, O. & Martínez, S. 2010. Synthetic seismic models from outcrop-derived reservoir-scale three-dimensional facies models: The Eocene Ainsa turbidite system (southern Pyrenees). The American Association of Petroleum Geologists, 94, 317–343.

Farrell, S.G. 1984. A dislocation model applied to slump structures, Ainsa basin, south central pyrenees. Journal of structural geology, 6, 727–736.

Farrell, S.G., Williams, G.D. & Atkinson, C.D. 1987. Constraints on the age of movement of the Montsech and Cotiella Thrusts, south central Pyrenees, Spain

Journal of the Geological Society, 144, 907–914.

Fernández, O., Muñoz, J.A., Arbues, P., Falivene, O. & Marzo, M. 2004. Three-dimensional reconstruction of geological surfaces: An example of growth strata and turbidite systems from the Ainsa basin, Pyrenees, Spain. American Association of Petroleum Geologists, Bulletin, 88, 1049–1068.

Ferry, J-N., Mulder, T., Parize O. & Raillard, S. 2005. Concept of equilibrium profile in deep-water turbidite system: effects of local physiographic changes on the nature of sedimentary process and the geometries of deposits. Geological Society, London, Special Publications,244, 181–193.

Fischer, M.W. 1984. Thrust tectonics in the northern Pyrenees. Journal of Structural Geology, 6, 721–6.

Fitzgerald, P.G., Muñoz, J.A., Coney, P.J. & Baldwin, S.L. 1999 Asymmetric exhumation across the Pyrenean orogen: implications for the tectonic evolution of a collisional orogen. Earth and Planetary Science Letters, 173, 157–170.

Flecker, R. & Ellam, R.M. 1999. Distinguishing climatic and tectonic signals in the sedimentary successions of marginal basins using Sr isotopes: an example from the Messinian salinity crisis, Eastern Mediterranean. Journal of the Geological Society, London, 156, 847–854.

Flemings, P.B. & Jordan, T.E. 1990. Stratigraphic modeling of foreland basins; Interpreting thrust deformation and lithosphere rheology. Geology, 18, 430–434.

Fontana, D., Zuffa, G.G. & Garzani, E. 1989. The interaction of eustacy and tectonism from provenance studies of the Eocene Hecho Group Turbidite Complex (South-Central Pyrenees, Spain). Basin Research, 2, 223–237.

Frey, R.W., Howard, J.D. & Pryor, W.A. 1978. *Ophiomorpha*: Its morphologic, taxonomic, and environmental significance. Palaeogeography, Palaeoclimatology, Palaeoecology, 23, 199–229.

Frey, R.W. Pemberton, S.G. & Saunders, T.D. 1990. Ichnofacies and bathymetry: A passive relationship. Journal of Paleontology, 64, 155–158.

Friend, P.F., Slater, M.J. & Williams, R.C. 1979. Vertical and lateral building of river sandstone bodies, Ebro Basin, Spain. Journal of the Geological Society of London, 136, 39–46.

Friend, P.F., Marzo, M., Nijman, W. & Puigdefàbregas, C. 1981. Fluvial sedimentology in the Tertiary South Pyrenean and Ebro Basins, Spain. In: Elliot, T. (ed.) Field Guide to Modern and Ancient Fluvial Systems in Britain and Spain. II

International Conference on Fluvial Sedimentology, Keele University, pp. 4.1–4.50.

Galloway, W.E. 1989a. Genetic stratigraphic sequences in basin analysis I: Application to northwest Gulf of Mexico Cenozoic basin. American Association of Petroleum Geologists Bulletin, 73, 125–142.

Galloway, W.E. 1989b. Genetic stratigraphic sequences in basin analysis II: Application to northwest Gulf of Mexico Cenozoic basin. American Association of Petroleum Geologists Bulletin, 73, 143–154.

Gaspar-Escribano, J.M., van Wees, J.D., ter Voorde, M., Cloetingh, S., Roca, E., Cabrera, L., Muñoz, J.A., Ziegle, P.A. & Garcia-Castellanos, D. 2001. Three-dimensional flexural modelling of the Ebro Basin (NE Iberia). Geophysical Journal International, 145, 349–367.

Garcia-Gil, S. 1993. The fluvial architecture of the upper Buntsandstein in the Iberian Basin, central Spain. Sedimentology, 40, 125–143.

Garcia-Senz, J., Muñoz, J.A., McClay, K. 2000. Inversion of Early Cretaceous extensional basins in the central Spanish Pyrenees. (abs.) AAPG Bulletin, 84, 9, 1428–1429.

Gardner, M.H., Borer, J.M., Melik, J.J., Mavilla, N., Dechesne, M. & Wagerle, R.D. 2003. Stratigraphic process-response model for submarine channels and related features from studies of Permian Brushy Canyon outcrops, West Texas. Marine and Petroleum Geology, 20, 757–788.

Garrido-Megías, A. 1973. Estudio geológico y relación entre la Tectónica y Sedimentación del Secundario y Terciario de la Vertiente Meridional Pirenaica en su Zona Central (Provincias de Huesca y Lérida.) PhD thesis, Granada University, Spain.

Garrido-Megias, A. 1982. Introducción al Análisis Tectosedimentario: aplicación al estudio dinámico de las cuencas. Buenos Aires. V Congreso Latinoamericano de Geología, Actas, 385–402.

Gee, M.J.R. & Gawthorpe, R.L. 2006. Submarine channels controlled by salt tectonics: examples from 3D seismic data offshore Angola. Marine and Petroleum Geology, 23, 443–458.

Ghosh, B. & Lowe, D.R. 1993. The architecture of deepwater channel complexes, Cretaceous Venado Sandstone Member, Sacramento Valley, California. In: Graham, A. & Lowe, D.R. (eds.) Advances in the Sedimentary Geology of the

Great Valley Group, Sacramento Valley, California, SEPM Pacific Section Guidebook, 73, 51–65.

Gingras, M.K., Pemberton, G.S. & Saunders, T. 2000. Firmness Profiles Associated with Tidal-Creek Deposits: The Temporal Significance of Glossifungites Assemblages, Journal of Sedimentary Research, Section A. Sedimentary Petrology and Processes, 70, 1017–1025.

Gingras, M.K., Pemberton, S.G. & Saunders, T. 2001. Bathymetry, sediment texture, and substrate cohesiveness: Their impact on modern *Glossifungites* trace assemblages at Willapa Bay, Washington. Palaeogeography, Palaeoclimatology, Palaeoecology, 169, 1–21.

Gonthier, E.G., Faugeres, J.C. & Stow, D.A.V. 1984. Contourite facies of the Faro Drift, Gulf of Cadiz. In: Stow, D.A.V. & Piper, D.J.W. (eds.) Fine-Grained Sediments: Deep Water Processes and Facies. Geological Society Special Publication, 15, 275–292.

Gradstein, F.M., Ogg, J.G., Smith, A.G., Agterberg, F.P., Bleeker, W., Cooper, R.A., Davydov, V., Gibbard, P., Hinnov, L., House, M.R., Lourens, L., Luterbacher, H.-P., McArthur, J., Melchin, M.J., Robb, L.J., Shergold, J., Villenueve, M., Wardlaw, B.R., Ali, J., Brinkhuis, H., Hilgen, F.J., Hooker,J., Howarth, R.J., Knoll, A.H., Laskar, J., Monechi, S., Powell, J., Plumb, K .A., Raffi, I., RoÅNhl, U., Sanfilipo, A., Schmitz, B., Schakleton, N.J., Shields, G.A., Strauss, H., van Dam, J., Veizer, J., van Kolfschoten, T. & Wilson, D. 2004. A Geologic Time Scale 2004. University Press, Cambridge, UK, pp. 384.

Hackbarth, C. J. & Shew, R.D. 1994. Morphology and stratigraphy of a Mid-Pleistocene turbidite leveed channel from seismic, core, and log data. In: Bouma, A., Weimer, P. & Perkins, B. (eds.) Submarine fan and turbidite systems, 127–133. Houston: GCS-SEPM Foundation.

Hadler-Jacobsen, F., Johannessen, E.E., Ashton, N., Henriksen, S., Johnson, S.D. & Kristensen, J.B. 2005. Submarine fan morphology and lithology distribution, a predictable function of sediment delivery, gross shelf-to-basin relief, slope gradient and basin topography. In: Dope, A.G. & Vining, B.A. (eds.) Petroleum Geology: North West Europe and Global Perspectives. Proceedings of the 6th Petroleum Conference. Geological Society, London, pp. 1121–1145.

Haq, B.U., Hardenbol, J. & Vail, P.R. 1987. Chronology of fluctuating sea levels since the Triassic. Science, 235,1156–1167.

Harrison, C.P. & Graham, S.A. 1999. Upper Miocene Stevens Sandstone, San Joaquin Basin, California: reinterpretation of a petroliferous, sand-rich, deep-sea depositional system. AAPG Bulletin, 83, 898–924.

Haughton, P. 2000. Evolving turbidite systems on a deforming basin floor, Tabernas, SE Spain. Sedimentology, 47, 497–518.

Heard, T. & Pickering, K.T. 2008. Trace fossils as diagnostic indicators of deep-marine environments, Middle Eocene Ainsa –Jaca basin, Spanish Pyrenees: Sedimentology, 55, 809–844.

Heard, T., Pickering, K.T. & Robinson, S.A. 2008. Milankovitch forcing of bioturbation intensity in deep-marine thin-bedded siliciclastic turbidites. Earth and Planetary Science Letters, 272, 130–138.

Heezen, B.C. & Ewing, M. 1952. Turbidity currents and submarine slumps, and the 1929 Grand Banks earthquake. American Journal of Science, 250, 849–873.

Hein, F.J. & Walker, R.G. 1982. The Cambro-Ordovician Cap Enrage Formation, Quebec, Canada; conglomeratic deposits of a braided submarine channel with terraces. Sedimentology, 29, 309–329.

Heller, P.L., Angevine, C.L. & Winslow, N.S. 1988. Two phase stratigraphic model of foreland basin sequences. Geology, 16, 501–504.

Hickson, T.A. & Lowe, D.R. 2002. Facies architecture of a submarine fan channel-levée complex: the Juniper Ridge Conglomerate, Coalinga, California. Sedimentology, 49, 335–362.

Hirst, J.P.P. & Nichols, G.J. 1986. Thrust tectonic controls on Miocene alluvial distribution patterns, southern Pyrenees. In: Allen, P. A. & Homewood, P. (eds.) Foreland Basins, vol. 8. Special Publications of the International Association of Sedimentologists, pp. 247–58.

Hiscott, R.N. 1978. Provenance of Ordovician deep-water sandstones, Tourelle Formation, Quebec and implications for initiation of the Taconic Orogeny. Canadian Journal of Earth Science, 15, 1579–1597.

Hiscott, R.N. 1994. Traction-carpet stratification in turbidites; fact or fiction? Journal of Sedimentary Research, 64 204–208.

Hiscott, R.N. & James, N.P. 1985. Carbonate debris flows, Cow Head Group, western Newfoundland. Journal of Sedimentary Petrology, 55, 735–745.

Hiscott, R.N. & Middleton, G.V. 1979. Depositional mechanics of thick-bedded sandstones at the base of a submarine slope, Tourelle Formation (Lower

Ordovician), Quebec, Canada. In: Doyle, L.J. & Pilkey, O.H. (eds.) Geology of Continental Slopes: SEPM Special Publication, 27, pp. 307–326.

Hiscott, R.N. & Middleton, G.V. 1980. Fabric of coarse deep-water sandstones, Tourelle formation, Quebec, Canada. Journal of Sedimentary Petrology, 50, 703–722.

Hiscott, R.N. & Pickering, K.T. 1984. Reflected turbidity currents on an Ordovician basin floor. Nature, 311, 143–145.

Hiscott, R.N., Colella, A., Pezard, P., Lovell, M.A. & Malinverno, A. 1992. Sedimentology of deep-water volcaniclastics, Oligocene Izu-Bonin Forearc Basin, based on formation microscanner images. In: Taylor, B. & Fujioka, K. (eds.) Ocean Drillin Program, Proceedings and scientific results, Leg 126, Bonin Arc/Trench system. Texas A&M University, College Station, 75–96.

Hiscott, R.N., Colella, A., Pezard, P., Lovell, M.A. & Malinverno, A. 1993. Basin plain turbidite succession of the Oligocene Izu-Bonin intracratonic forearc basin. Marine and Petroleum Geology, 10, 450–466.

Hiscott, R.N., Pickering, K.T., Bouma, A.H., Hand, B.M., Kneller, B.C., Postma, G., & Soh, W. 1997. Basin-floor fans in the North Sea: sequence stratigraphic models vs. sedimentary facies: discussion. American Association of Petroleum Geologists, Bulletin, 81, 662–665.

Hodgson, D.M. & Haughton, P.D. 2004. Impact of syndepositional faulting on gravity current behaviour and deep-water stratigraphy: Tabernas-Sorbas Basin, SE Spain. In: Lomas, S. A. & Joseph, P. (eds.) Confined Turbidite Systems. Geological Society, London, Special Publications, 222, 135–158.

Hodgson, D.M., Flint, S.S., Hodgetts, D., Drinkwater, N.J., Johanessen, E.J. & Luthi, S.M. 2006 Stratigraphic evolution of fine-grained submarine sand systems, Tanqua depocenter, Karoo Basin, South Africa. Journal of Sedimentary Research, 76, 19–39.

Holl, J.E. & Anastasio, D.J. 1993. Paleomagnetically derived folding rates, Southern Pyrenees, Spain. *Geology,* 13, 271–274.

Holl, J.E. & Anastasio, D.J. 1995. Kinematics around a large-scale oblique ramp, southern Pyrenees, Spain. Tectonics, 14, 1368–1379.

Houston, W.S., Huntoon, J.E. & Kamola, D.L. 2000. Modeling of Cretaceous foreland-basin parasequences, Utah, with implications for timing of Sevier thrusting. Geology, 28, 267–270.

Hubbard, S.M. & Shultz, M.R. 2008. Deep Burrows in Submarine Fan-Channel Deposits of the Cerro Toro Formation (Cretaceous), Chilean Patagonia: Implications For Firmground Development and Colonization in the Deep Sea. Palaios, 223–232.

Hubbard, S.M., Romans, B.W., and Graham, S.A. 2008. Deep-water foreland basin deposits of the Cerro Toro Formation, Magallanes basin, Chile: Architectural elements of a sinuous basin axial channel belt, Sedimentology, 55, 1333–1359.

Hubert, J.F. 1966. Sedimentary history of Upper Ordovician geosynclinal rocks, Girvan, Scotland, Journal of Sedimentary Petrology, 36, 677–699.

Hurford, A. J. & Carter, A. 1991. The role of fission track dating in discrimination of provenance. In: Morton, A. C., Todd, S. P. & Haughton, P. D. W. (eds.) Developments in sedimentary provenance studies. London Geological Society Special Publication, 57, 67–78.

Huyghe, D., Mouthereau, F., Castelltort, S., Filleaudeau P.Y. & Emmanuel L. 2009. Paleogene propagation of the southern Pyrenean thrust wedge revealed by finite strain analysis in frontal thrust sheets: Implications for mountain building. Earth and Planetary Science Letters, 288, 421–433.

Ingersoll, R.V. 1978. Petrofacies and petrologic evolution of the late Cretaceous fore-arc basin, northern and central California. Journal of Geology, 86, 335–353.

Ingram, R.L. 1954. Terminology for the thickness of stratification and parting units in sedimentary rocks. Geological Society of America Bulletin, 65, 937–938.

Johnson, C. 1997. Resolving denudational histories in orogenic belts with apatite track thermochronology and structural data: An example from southern Spain. Geology, 25, 623–626.

Johnson, S.D., Flint, S., Hinds, D. & Wickens, H. De V. 2001. Anatomy of basin floor to slope turbidite systems, Tanqua Karoo, South Africa: Sedimentology, sequence stratigraphy and implications for subsurface prediction. Sedimentology, 48, 987–1023.

Jolivet, M., Labaume, P., Monie, P., Brunel, M., Arnaud, N. & Campani, M. 2007. Thermochronology constraints for the propagation sequence of the south Pyrenean basement thrust system (France–Spain). Tectonics, 26, TC5007-1–TC50017.

Jordan, T.E. Allmendinger, R.W., Damanti, J.F. & Drake, R.E. 1993. Chronology of motion in a complete thrust belt: the Precordillera, 30–31 8S, Andres Mountains.

Journal of Geology, 101, 135–146.

Kern, J.P. 1980. Origin of trace fossils in Polish Carpathian flysch. Lethaia, 13, 347–362.

Kneller, B. 1995. Beyond the turbidite paradigm: physical models for the deposition of turbidites and their implications for reservoir prediction. In: Hartley, A.J. & Prosser, D.J. (eds.) Characterisation of deep marine clastic systems. Geological Society of London Special Publication, 94, 29–46.

Książkiewicz, M. 1968. On some problematic organic traces from the flysch of the Polish Carpathians, Part 3. Rocznik Polskiego Towarzystwa Geologicznego, 38, 3–17.

Książkiewicz, M. 1970. Observations on the ichnofauna of the Polish Carpathians. In: Crimes, P.T. & Harper, C. (eds.) Trace Fossils. Geological Journal special Issue, 3, 283–322.

Książkiewicz, M. 1977. Trace fossils in the flysch of the Polish Carpathians. Palaeontologica Polonica, 36, 1–208.

Labaume, P. 1983. Evolution tectono-sédimentaire et megaturbidites du Bassin turbiditique Eocene sud-Pyrénéen [unpublished Ph.D. Thesis]: Université des Sciences et Techniques du Languedoc, Montpellier, France, pp. 195.

Labaume, P., Séguret, M. & Seyve, C. 1985. Evolution of a turbiditic foreland basin and analogy with an accretionary prism: Example of the Eocene South-Pyrenean basin. Tectonics, 4, 661–685.

Labaume, P., Mutti, E. & Seguret, M. 1987. Megaturbidites: a depositional model from the Eocene of the SW-Pyrenean Foreland Basin, Spain. Geomarine Letters 7, 91–101.

Labourdette, R., Crumeyrolle, P. & Remacha, R. 2008. Characterisation of dynamic flow patterns in turbidite reservoirs using 3D outcrop analogues: Example of the Eocene Morillo turbidite system (south-central Pyrenees, Spain). Marine and Petroleum Geology, 25, 255-270.

Ledo, J., Ayala, C., Pous, J., Queralt, P., Marcuello, A. & Muñoz , J.A. 2000. New Geophysical constraints on the deep structure of the Pyrenees. Geophysical Research Letters, 27, 1037–1040.

Léon-Gonzalez, L. 1972. Sintesis paleogeografica y estratigrafica del Paleoceno del norte de Navarra. Paso el Eoceno. Bol. Geol. Min., 83, 234–241.

Lien, T., Walker, R.G. & Martinsen, O.J. 2003. Turbidites in the Upper Carboniferous Ross Formation, western Ireland: reconstruction of a channel and spillover system. Sedimentology, 50, 113–148.

Lowe, D.R. 1982. Sediment gravity flows II. Depositional models with special reference to the deposits of high-density turbidity currents. Journal of Sedimentary Petrology, 52, 279–297.

Lowe, D.R. 1997. Reinterpretation of depositional processes in a classic flysch sequence (Pennsylvanian Jackfork Group), Ouachita Mountains, Arkansas and Oklahoma: Discussion. American Association of Petroleum Geologists Bulletin 81, 460–465.

Lowe, D.R., Guy, M. & Palfrey, A. 2003. Facies of slurry-flow deposits, Britannia Formation (Lower Cretaceous), North Sea: implications for flow evolution and deposit geometry. Sedimentology, 50, 45–80.

Luzón, A. 2005. Oligocene–Miocene alluvial sedimentation in the northern Ebro Basin, NE Spain: Tectonic control and palaeogeographical evolution. Sedimentary Geology, 177, 19–39.

Luzón, A., González, A., Muñoz, A. & Sánchez-Valverde, B. 2002. Upper Oligocene–Lower Miocene shallowing upward lacustrine sequences controlled by periodic and non-periodic processes (Ebro Basin, Spain). Journal of Paleolimnology, 28, 441–446.

Machlus, M., Olsen, P.E., Christie-Blick, N. & Hemming, S.R. 2001. Milankovitch Cyclicity in the Eocene Green River Formation of Colorado and Wyoming. American Geophysical Union, Abstract U12A-0005.

Maestro, E. 2008. Sedimentary evolution of the Late Eocene Vernet lacustrine system (South-Central Pyrenees). Tectono-climatic control in an alluvial-lacustrine piggyback basin. Journal of Paleolimnology, 40, 1053–1078.

Malinverno, A. 1997. On the power law size distribution of turbidites. Basin Research, 9, 263–274.

Marzo, M. & Steel, R.J. 2000. Unsual features of sediment supply-dominated, transgressive-regressive sequences: Paleogene clastic wedges, SE Pyrenean foreland basin, Spain. Sedimentary Geology, 138, 3–15.

Marzo, M., Nijman, W. & Puigdefàbregas, C. 1988. Architecture of the Castissent fluvial sheet sandstones, Eocene South Pyrenees, Spain. Sedimentology, 35, 719–738.

Mayall, M., Lonergan, L., Bowman, A., James, S., Mills, K., Primmer, T., Pope, D., Rogers, L. & Skeene, R. 2010. The response of turbidite slope channels to growth-induced seabed topography. AAPG Bulletin, 94, 1011–1030.

McCaffrey, W.D., Gupta, S. & Brunt, R. 2002. Repeated cycles of submarine channel incision, infill and transition to sheet sandstone development in the Alpine Foreland Basin, SE France. Sedimentology, 49 (3), 623–635.

Meigs, A.J. & Burbank, D.W. 1997. Growth of the South Pyrenean orogenic wedge. Tectonics, 16, 239–258.

Meigs, A., Vergés, J. & Burbank, D.W. 1996. Ten-million-year history of a thrust sheet. Geological Society of American Bulletin, 108, 1608–1625.

Melick, J., Cavanna, G., Benevelli, G., Tinterri, R. & Mutti, E. 2004. The Lutetian Ainsa Sequence: an Example of a Small Turbidite System Deposited in a Tectonically Controlled Basin. Search and Discovery Article #50008.

Miall, A.D. 1985. Architectural-element analysis: a new method of facies analysis applied to fluvial deposits. Earth Science Reviews, 22, 261–308.

Miall, A.D. 1992. Alluvial deposits. In: Facies Models: Response to Sea-Level Change Walker, R.G. & James, N.P. (eds.) GeoText 1, pp. 119–143. Geological Association of Canada, St. John’s.

Miall, A.D. 1996. The geology of Fluvial Deposits: Sedimentary Facies, Basin Analysis, and Petroleum Geology. Springer, New York, pp. 582.

Miller, K.G., Wright, J.D. & Browning, J.V. 2005. Visions of ice sheets in a greenhouse world: Marine Geology, 217, 215–231.

Millington, J. & Clark, J.D. 1995a. Submarine canyon and associated base-of-slope sheet system: the Eocene Charo-Arro system, south-central Pyrenees, Spain. In: Pickering, K.T. & Hiscott, R.N., Kenyon, N.H., Ricci Lucchi, F. & Smith, R.D. A. (eds.) Atlas of Deep Water Environments: Architectural style in turbidite systems, London, Chapman and Hall, pp. 150–156.

Millington, J. & Clark, J.D. 1995b. The Charo/Arro canyon mouth sheet system, south-central Pyrenees, Spain: a structurally influenced zone of sediment dispersal. Journal of Sedimentary Research, B65, 443–454.

Mitchum, R.M. 1985. Seismic stratigraphic expression of submarine fans. AAPG Bulletin, 39, 117–136.

Mitchum, R.M. & Van Wagoner, J.C. 1991. High frequency sequences and their stacking patterns: sequence stratigraphic evidence of high frequency eustatic cycles. Sedimentary Geology, 70, 131–160.

Muñoz, J.A. 1992. Evolution of a continental collision belt: ECORS–Pyrenees crustal balanced cross-section. In: McClay, K.R. (ed.) Thrust Tectonics. Chapman and Hall, London, pp. 235–246.

Muñoz, A. & Casas, A.M. 1997. The Rioja Trough (N Spain): tectosedimentary evolution of a symmetric foreland basin. Basin Research, 9, 65–85.

Muñoz, J.A., Martinez, A. & Verges, J. 1986. Thrust sequences in the Eastern Pyrenees. Journal of Structural Geology, 8, 399–405.

Muñoz, J.A., McClay, K. & Poblet, J. 1994. Synchronous extension and contraction in frontal thrust sheets of the Spanish Pyrenees. Geology 22, 921–924.

Muñoz, J.A., Arbués, P. & Serra-Kiel, J. 1998. The Ainsa Basin and the Sobrarbe oblique thrust system: sedimentological and tectonic processes controlling slope platform sequences deposited synchronously with a submarine emergent thrust system. In: Meléndez Hevia, A & Soria, A.R. (eds.) Field Trip Guidebook of the 15th International Sedimentological Congress, Alicante, pp. 213–223.

Muñoz, J.A., Arenas, C., González, A., Luzón, A., Pardo, G. & Villena, J. 2002. Ebro Basin (Northeastern Spain). In: Gibbons, W. & Moreno, T. (eds.) Geology of Spain, London Geological Society, pp. 301– 309.

Muñoz, J.A., García-Senz, J.M., Fernández, O., Roca, E. & Dinarès-Turell, J. 2003. 3D Regional Deformation Patterns Associated to Thrust Sheet Rotation of the Gavarnie–Sierras Exteriores Thrust Sheet, Spanish Pyrenees. AAPG International Conference Absract, Barcelona, Spain, September 21–24, 2003.

Mutti, E. 1977. Distinctive thin-bedded turbidite facies and related depositional environments in the Eocene Hecho Group South-central Pyrenees, Spain. Sedimentology, 24, 107–131.

Mutti, E. 1983. The Hecho Eocene Submarine Fan System, South-Central Pyrenees, Spain. Geo-Marine Letters, 3, 199-202.

Mutti, E. 1985. Turbidite systems and their relations to depositional sequences. In: Zuffa, G.G. (ed.) Provenance of arenites. NATO, Advanced Scientific Institute, D. Reidel, Dordrecht, Holland, pp. 65–93.

Mutti, E. 1992. Turbidite Sandstones. Agip and Instituto di Geologia, University of Parma. Parma. pp. 275.

Mutti, E. & Johns, D.R. 1978. The role of sedimentary by-passing in the genesis of fan-fringe and basin plain turbidites in the Hecho Group System, South-Central Pyrenees. Memorie della Società Geoligica Italiana, 18, 15–22.

Mutti, E. & Normark, W.R. 1987. Comparing examples of modern and ancient turbidite systems: problems and concepts. In: Legget, J.K. & Zuffa, G.G. (eds.) Marine Clastic Sedimentology: Concept and case studies. London, Graham and Trotman, pp. 1–38.

Mutti, E. & Ricci Lucchi, F. 1972. Le torbiditi dell'Appennino settentrionale; introduzione all' analisi di facies. Memorie Società Geologica Italiana 11, 161–199.

Mutti, E. & Normark, W.R. 1991. An integrated approach to the study of turbidite systems. In: Weimer, P. & Link, M.H. (eds.) Seismic Facies and Sedimentary Processes of Modern and Ancient Submarine Fans, New York, Springer-Verlag, pp. 75-106.

Mutti, E., Luterbacher, H.P., Ferrer, J. & Rosell, J. 1972. Schema estratigrafico e lineamenti di facies del Paleogene marino della zona centrale sudpirenaica tra Tremp (Catalogna) e Pamplona (Navarra). Societá Geologica Italiana, Memorie, 11, 391–416.

Mutti, E., Sgavetti, M. & Remacha, E. 1984. Le relazioni tra piataforme deltizie a sistemi torbiditici nel Bacino Eocenico Sudpirenaico di Tremp–Pamplona. *Giornale di Geologia Ser. 3*, 46, 3–32.

Mutti, E., Remacha, E., Sgavetti, M., Rosell, J., Valloni, R. & Zamorano, M. 1985. Stratigraphy and facies characteristics of the Eocene Hecho Group turbidite systems, south-central Pyrenees. In: Mila, M.D. & Rosell, J. (eds.) International Association of Sedimentologists, 6th European Regional Meeting, Llerida, Excursion Guidebook, pp. 521–576.

Mutti, E., Seguret, M. & Sgavetti, M. 1988. Sedimentation and deformation in the Tertiary sequences of the southern Pyrenees. Special Publication of the American Association of Petroleum Geology, Mediterranean Basin Conference. Institute of Geology, University of Parma, Field trip 7, pp. 153.

Mutti, E., Davoli, G., Mora, S. & Papani, L. 1994. Internal stacking patterns of ancient turbidite systems from collisional basins. In: Weimer, P., Bouma, A.H. & Perkins, B. (eds.) GCSSEPM Foundation 15th Annual Research Conference Submarine Fans and Turbidite Systems, December 4-7 pp. 257–268.

Mutti, E., Tinterri, R., Benevelii, G., di Biase, D. & Cavanna, G. 2003. Deltaic, mixed and turbidite sedimentation of ancient foreland basins. Marine and Petroleum Geology, 20, 733–755.

Naylor, M. & Sinclair, H.D. 2007. Punctuated thrust deformation in the context of doubly vergent thrust wedges: Implications for the localization of uplift and exhumation: Geology, 35, 559–562.

Nijman, W. 1981. Fluvial sedimentology and basin architecture of the Eocene Montafiana Group, South Pyrenean Tremp-Graus Basin. In: Elliott, T. (ed.) Field guides to modern and ancient fluvial systems in Britain and Spain. Proceedings of the 2nd. International Conference on Fluvial Sedimentology, Keele UK, 4.3–4.27.

Nijman, W. 1989. Thrust sheet rotation? - The South Pyrenean Tertiary basin configuration reconsidered. Geodinamica Acta, 3, 17–42.

Nijman, W. 1998. Cyclicity and basin axis shift in a piggyback basin: towards modelling of the Tremp–Ager Basin, South Pyrenees, Spain. In: Mascle, A., Puigdefàbregas, C., Luterbacher, H.P. & Fernández, M. (eds.) Cenozoic Foreland Basins of Western Europe. Geological Society of London Special Publication 134, 135–162.

Nijman, W. & Nio, S.D. 1975. The Eocene Montañana Delta (Tremp–Graus Basin, provinces of Lerida and Huesca, southern Pyrenees, Spain). In: The sedimentary evolution of the Paleogene South-Pyrenean Basin. IX Congress of the International Association of Sedimentologists. Nice Excursion. Guidebook 19, part B, pp. 1–20.

Normark, W.R. & Piper, D.J.W. 1991. Initiation processes and flow evolution of turbidity currents: Implications for the depositional record. In Osborne, R. H. (ed). From Shoreline to Abyss; Contribution in Marine Geology in Honor of Francis Parker Shepard. SEPM (Society for Sedimentary Geology), Special Publication, 46,Tulsa, pp. 207–230.

Olóriz, F., Caracuel, J.E. & Rodríguez-Tovar, F.J. 1995. Using Ecostratigraphic Trends in Sequence Stratigraphy. In: Haq, B.U. (ed.) 1995. Sequence Stratigraphy and Depositional Response to Eustatic, Tectonic and Climatic Forcing. Kluwer Academic, Amsterdam, 59–85.

Ori, G.G. & Friend, P.F. 1984. Sedimentary basins formed and carried piggyback on active thrust sheets. Geology, 12, 475–478.

Pardo, G., Villena, J. & González, A. 1989. Contribución a los conceptos y a la aplicación del análisis tectosedimentario Rupturas y unidades tectosedimentarias como fundamento de correlación estratigráfica. Rev Soc Geol Esp, 2, 199–219.

Parsons, J.D., Whipple, K.X. & Simoni, A. 2001. Experimental study of the grain-flow, fluid-mud transition in debris flows. The Journal of Geology, 109, 427–447.

Payros, A., Pujalte, V. & Orue-Etxebarria, X. 1999. The South Pyrenean Eocene carbonate megabreccias revisited: new interpretation based on evidence from the Pamplona Basin. Sedimentary Geology, 125, 165–194.

Payros, A., Orue-Etxebarria, X. & Pujalte, V. 2006. Covarying sedimentary and biotic fluctuations in Lower–Middle Eocene Pyrenean deep-sea deposits: palaeoenvironmental implications. Palaeogeography. Palaeoclimatology. Palaeoecology, 234, 258–276.

Payros, A., Pujalte, V. & Orue-etxebarria, X. 2007. A point-sourced calciclastic submarine fan complex (Eocene Anotz Formation, western Pyrenees): facies architecture, evolution and controlling factors. Sedimentology, 54, 137–168.

Pedley, M. & Maniscalco, R. 1999. Lithofacies and faunal succession (faunal phase analysis) as a tool in unravelling climatic and tectonic signals in marginal basins; Messinian (Miocene), Sicily. Journal of the Geological Society, 156 855–863.

Pekar, S.F., Hucks, A., Fuller, M. & Li, S. 2005. Glacioeustatic changes in the early and middle Eocene 51–42 Ma: Shallow-water stratigraphy from ODP Leg 189 Site 1171 South Tasman Rise and deep-sea $\delta^{18}O$ records. Geological Society of America Bulletin, 117, 1081–1093.

Pemberton, S.G. & Frey, R.W. 1985. The *Glossifungites* ichnofacies: Modern examples from the Georgia coast, U.S.A. In: Curran, H.A. (ed.) Biogenic Structures: Their Use in Interpreting Depositional Environments. SEPM (Society for Sedimentary Geology) Special Publications, 35, 237–259.

Pemberton, S.G., Zhou, Z. & MacEachern, J. 2001. Modern ecological interpretation of opportunistic r-selected trace fossils and equilibrium K-selected trace fossils. Acta Palaeontologica Sinica, 40, 134–142.

Pervesler, P. & Uchman, A. 2004. Ichnofossils from the type area of the Grund Formation Miocene, Lower Badenian in Northern Lower Austria Molasse Basin. Geologica Carpathica, 55, 103–110.

Peybernes, B. & Souquet, P. 1984. Basement blocks and tectosedimentary evolution in the Pyrenees during Mesozoic times. Geological Magazine, 121, 397–405.

Pickering, K.T. 1982. The shape of deep-water siliciclastic systems - a discussion. Geo-

Marine Letters, 2, 41–46.

Pickering, K.T. 1984. Facies, facies-associations and sediment transport/deposition processes in a late Precambrian upper basin-slope/prodelta, Finnmark, N. Norway. In: Stow, D.A.V. & Piper, D.J.W. (eds.) Fine-Grained Sediments: Deep-Water Processes and Facies. Special Publication of The Geological Society London, 15, pp. 343–362.

Pickering, K.T. & Bayliss, N. J. 2009. Deconvolving tectono-climatic signals in deep-marine siliciclastic, Eocene Ainsa basin, Spanish Pyrenees: Seesaw tectonics versus eustasy. Geology, 37, 203–206.

Pickering, K.T. & Corregidor, J. 2000. 3D reservoir scale study of Eocene confined submarine fans, South Central Spanish Pyrenees. In: Weimer. P., Slatt. R.M., Coleman. J., Rosen, N.C., Nelson, H., Bouma, A.H., Styzen, M.J. & Lawrence. D.T. (eds.) Deep water reservoirs of the world: Gulf Coast Section. SEPM Foundation 20th Annual Bob F. Perkins Research Conference, pp. 776–781.

Pickering, K.T. & Corregidor, J. 2005. Mass-transport complexes (MTCs) and tectonic control on basin-floor submarine fans, Middle Eocene, South Central Spanish Pyrenees. Journal of Sedimentary Research, 75, 761–783.

Pickering, K.T. & Fadell, M. 2004. Micropalaeontology of the Mid Eocene Ainsa I fan channel-levee-overbank complex, Ainsa system, South Central Pyrenees, Spain. Unpublished Report (BP and UCL).

Pickering, K.T. & Hiscott, R.N. 1985. Contained (reflected) turbidity currents from the Middle Ordovician Cloridorme Formation, Quebec, Canada: an alternative to the antidune hypothesis. Sedimentology, 32, 373–394.

Pickering, K.T., Clark, J.D., Smith, R.D.A., Hiscott, R.N., Ricci Lucchi, F. & Kenyon, N.H. 1995. Architectural element analysis of turbidite systems, and selected topical problems for sand-prone deep-water systems. In: Pickering, K.T., Hiscott, R.N., Kenyon, N.H., Ricci Lucchi, F. & Smith, R.D.A. (eds.) Atlas of deep water environments: architectural style in turbidite systems. Chapman and Hall. London, pp. 1–10.

Pickering, K.T. Hiscott, R.N. & Hein, F.J. 1989. Deep marine environments. London. Harper-Collins (now Chapman and Hall), pp. 416

Pickering, K.T., Stow, D., Watson, M. & Hiscott, R. 1986. Deep-Water facies, processes and models: A review and classification scheme for modern and ancient sediments. Earth-Science Reviews, 23, 75–174.

Piper, D.J.W. 1973. The sedimentology of silt turbidites from the Gulf of Alaska. In: Initial Reports of the Deep Sea Drilling Project. U.S. Government Printing Office, Washington, 18, 847–867.

Piper, D.J.W. 1978. Turbidites, muds and silts on deep-sea fans and abyssal plains. In: Standley, D.J. & Kelling, G. (eds.) Sedimentation in Submarine Canyons, Fans and Trenches. Dowden, Hutchinson and Ross, Stroudsburg, PA. pp. 163–176.

Piper, D.J.W. & Brisco, C.D. 1975. Deep-water continental-margin sedimentation, DSDP Leg 28, Antarctica. In: Hayes, D.E. & Frakes, L.A. (eds.) Initial Reports of the Deep Sea Drilling Project. U.S. Government Printing Office, Washington, 28, 727–755.

Piper, D.J.W. & Kontopoulos, N. 1994. Bed forms in submarine channels: comparison of ancient examples from Greece with studies of recent turbidite systems. Journal of Sedimentary Research, 64, 247–252.

Pirmez, C., Hiscott, R.N. & Kronen, J.D. 1997. Sandy turbidite successions at the base of channel-levee systems of the Amazon Fan revealed by FMS logs and cores: unravelling the facies architecture of large submarine fans. In: Flood, R.D., Piper, D.J.W., Klaus A. &. Peterson, L.C. Proceedings of the Ocean Drilling Program, Scientific Results, 155, 7–33.

Pirmez, C., Beaubouef, R.T., Friedmann, S.J. & Mohrig, D.M. 2000. Equilibrium profile and baselevel in submarine channels: examples from Late Pleistocene systems and implication for the architecture of deepwater reservoirs. In: Weimer, P., Slatt, R.M. & Coleman, J. (eds.) Deep-Water Reservoirs of the World. Gulf Coast Section SEPM, Foundation 20th Annual Bob F. Perkins Research Conference, pp. 782–805.

Poblet, J. & Hardy, S. 1995. Reverse modelling of detachment folds; application to the Pico del Aguila anticline in the South Central Pyrenees (Spain). Journal of Structural Geology, 17, 1707–1724.

Poblet, J., Muñoz, J.A., Travé, A. & Serra-Kiel, J. 1998. Quantifying the kinematics of detachment folds using three-dimensional geometry: Application to the Mediano anticline (Pyrenees, Spain). Geological Society of America Bulletin, 110, 111–125.

Posamentier, H.W. & Allen, G.P. 1993. Siliciclastic sequence stratigraphic patterns in foreland ramp-type basins. Geology, 21, 445–458.

Posamentier, H.W. & Kolla, V. 2003. Seismic Geomorphology and Stratigraphy of Depositional Elements in Deep-Water Settings. Journal Sedimentary Research, 73, 367–388.

Puigdefàbregas, C. & Souquet, P. 1986. Tecto-sedimentary cycles and depositional sequences of the Mesozoic and Tertiary from the Pyrenees. Tectonophysics, 129, 173–203.

Puigdefàbregas, C., Rupke, N.A. & Sole Sedo, J. 1975. The sedimentary evolution of the Jaca Basin. In: Rosell, J. & Puigdefàbregas, C. (eds.) The Sedimentary Evolution of the Paleogene South Pyrenean Basin. 9th Congress of the International Association of Sedimentologists, Nice, Field-trip 19, part C, pp. 33.

Puigdefàbregas, C., Muñoz, J.A. & Marzo, M. 1986. Thrust belt development in the Eastern Pyrenees and related depositional sequences in the southern foreland basins. In: Allen, P.A. & Homewood, P. (eds.) Foreland Basins, vol. 8. Special Publications of the International Association of Sedimentologists, pp. 229–246.

Puigdefàbregas, C., Muñoz, J.A. & Vergés, J. 1992. Thrusting and foreland basin evolution in the southern Pyrenees. In: McClay, K. R. (ed.) Thrust Tectonics. Chapman and Hall, London, pp. 247–253.

Quatrefages, De M.A.1849. Note sur la *Scolicia prisca* A. de Q. annélide fossile de la Craie. Annales des Sciences Naturelles, 3 série, Zoologie, 12, 265–266.

Reading, H.G. & Richards, M. 1994. Turbidite systems in deep-water basin margins classified by grain size and feeder system. American Association of Petroleum Geologists, Bulletin, 78(5). 792–822.

Remacha, E. & Fernández, L.P. 2003. High resolution correlation patterns in the turbiditic systems of the Hecho Group South-Central Pyrenees, Spain. Marine Petroleum Geology, 20, 711–726.

Remacha, E. & Fernández, L.P. 2005. The transition between sheet-like lobe and basin-plain turbidites in the Hecho Basin (South-Central Pyrenees, Spain). Journal of Sedimentary Research, 75, 798–819.

Remacha, E., Pickart, J. & Oms, O. 1991 The Rapitán turbidite channel. In: Colombo, F., Ramos-Guerrero, E. & Riera, S. (eds.) First Congress of the Spanish Group on the Tertiary, pp. 280–282.

Remacha, E., Oms, O. & Coello, J. 1995. The Rapitán turbidite channel and its related eastern levee-overbank deposits, Eocene Hecho group, south-central Pyrenees, Spain. In: Pickering, K.T. & Hiscott, R.N., Kenyon, N.H., Ricci Lucchi F. &

Smith, R.D.A. Atlas of deep water environments: architectural style in turbidite systems, Chapman & Hall, London., pp. 145–149.

Remacha, E., Fernández, L.P., Maestro, E., Oms, O., Estrada, R. & Teixell, A. 1998. Excursion A1. The Upper Hecho Group turbidites and their vertical evolution to deltas (Eocene, South-central Pyrenees). Association of Sedimentologists 15 th International Sedimentological Congress, Alicante, Spain, Field Trip Guidebook, pp. 25.

Remacha, E., Oms, O., Gual, G., Bolaño, F., Climent, F., Fernández, L.P., Crumeyrollle, P., Pettingill, H., Vicente, J.C. & Suarez, J. 2003. Sand-rich turbidite systems of the Hecho Group from slope to basin plain. Facies, stacking patterns, controlling factors and diagnostic features. Geological Field Trip 12. South-Central Pyrenees. American Association of Petroleum Geologists International Conference and Exhibition, Barcelona, Spain, September 21–24, pp. 78.

Remacha, E., Fernández, L.P. & Maestro, E. 2005. The transition between sheet-like lobe and basin-plain turbidites in the Hecho Basin South-Central Pyrenees, Spain. Journal of sedimentary research, 75, 795–819.

Riba, O., Reguant, S. & Villena, J. 1983. Ensayo de síntesis estratigráfica y evolutiva de la Cuenca terciaria del Ebro. In: Libro Jubilar JM Ríos, (ed.) Geología de España, Tomo II. Instituto Geológico y Minero de España, pp. 131–59.

Ricci Lucchi, F. 1975. Miocene paleogeography and basin analysis in teh Peri-adriatic Apennines. In: Squyres, C.H. (ed.) Geology of Italy: Petroleum Exploration Society of Libya, Tripoli, 2, pp. 129–236.

Ricci Lucchi, F. 1985. Influence of transport processes and basin geometry on sand composition. In: Zuffa, G.G. (ed.) Provenance of Arenites. NATO, Advance Scientific Institute, Reidel, Dordrecht, pp. 19–45.

Richards, M. & Bowman, M. 1998. Submarine fan and related depositional systems II: variability in reservoir architecture and wireline log character. Marine Petroleum Geology, 15, 821–839.

Richards, M., Bowman, M. & Reading, H. 1998. Submarine-fan systems. I: Characterization and stratigraphic prediction. Marine and Petroleum Geology 15, 689–717.

Roberts, N. 1993. Sub-Milankovitch palaeoclimatic events: Their recognition and correlation. Climatic Change, 24, 175–178.

Rodríguez-Tovar, F. J., Uchman, A., Payros , A., Orue-Etxebarria , X., Apellaniz , E. & Molina, E. 2010. Sea-level dynamics and palaeoecological factors affecting trace fossil distribution in Eocene turbiditic deposits (Gorrondatxe section, N Spain). Palaeogeography, Palaeoclimatology, Palaeoecology, 285, 50–65.

Rothman, D.H., Grotzinger, J.P. & Flemings, P. 1994. Scaling in turbidite deposition. Journal of Sedimentary Research, 64A, 59–67.

Roure, F., Choukroune, P., Berastegui, B., Muñoz, J. A., Villian, A., Matheron, P., Bareyt, M., Séguret, M., Camara, P. & Déramond, J. 1989. ECORS deep seismic data and balanced cross-sections: geometric constraints to trace the evolution of the Pyrenees. Tectonics, 8, 41–50.

Ruiz, M., Gallarta, J., Díaza, J., Oliverab, C., Pedreirac, D., Lópezc, C., González-Cortinac, J.M. & Pulgar, J.A. 2006. Seismic activity at the western Pyrenean edge. Tectonophysics, 412, 217–235.

Sadler, P.M. 1981. Sediment accumulation rates and the completeness of stratigraphic sections. Journal of Geology, 89, 569–584.

Santanach, P. 1997. The Ebro Basin in the structural framework of the Iberian Plate. In: Busson, G. & Schreiber, B.C. (eds.) Sedimentary deposition in rift and foreland basins in France and Spain (Paleogene and Neogene). Columbia University Press, New York, pp. 305–313.

Savi, P. & Meneghini, G.G. 1850. Osservazioni stratigrafische e paleontologische concernati la geologia della Toscana e dei paesi limitrofi. Appendix in: Memoria sulla struttura geologica delle Alpi, degli Apennini e dei Carpazi. R.I. Murchison Stemparia granucale, Firenze.

Savrda, C.E. 1991. Ichnology in sequence stratigraphic studies: An example from the Lower Paleocene of Alabama, Palaios, 6, 39–53.

Schellart, W.P. 2002. Alpine deformation at the western termination of the Axial Zone, Southern Pyrenees. In: Rosenbaum, G. & Lister, G.S. 2002. Reconstruction of the evolution of the Alpine-Himalayan Orogen. Journal of the Virtual Explorer, 8, 35–55.

Schuppers, J.D. 1993. Quantification of turbidite facies in a reservoir-analogous submarinefan channel sandbody, south-central Pyrenees, Spain. In: Flint, S.S. & Bryant, I.D. (eds.) The Geologic Modelling of Hydrocarbon Reservoirs and Outcrop Analogues. Special Publications of the International, Association of Sedimentologists, pp. 99-112.

Scotchman, J.I., Pickering, K.T. & Robinson, S. A. In press. Sub-Milankovitch millennial-scale climate variability in Middle Eocene deep-marine sediments.

Séguret, M. 1972. Étude tectonique des nappes et séries decollées de la partie central du vesant sud des Pyrénées. Caractère synsedimentaire, rôle de la compresión et de la gravité. Publ. USTELA. Série Géol. Struct 2, Montpellier, France, 155.

Séguret, M. & Daigneres, M. 1986. Crustal scale balanced cross-section of the Pyrenees, discussion. Tectonophysics, 129, 303– 18.

Seilacher, A. 1964. Biogenic sedimentary structures. In: Imbrie, J. & Newell, N. (eds.) Approaches to Paleoecology. Wiley, New York, pp. 296–316.

Seilacher, A. 1967. Bathymetry of trace fossils. Marine Geology, 5, 413–428.

Seilacher, A. 1977. Pattern analysis of *Paleodictyon* and related trace fossils. In: Crimes, T.P., and Harper, J.C. (eds.) Trace Fossils 2, Geology Journal Special Issue 9, pp. 289–334.

Shanmugam, G. 1997. The Bouma sequence and the turbidite mind set. Earth Science Reviews 42, 201–229.

Shanmugam, G. 2000. 50 years of the turbidite paradigm (1950s—1990s): deep-water processes and facies models—a critical perspective. Marine and Petroleum Geology, 17, 285–432.

Shanmugam, G., Moiola. R.J., & Wagner, J.B. l997. Turbidite paradigm and sequence stratigraphy: a critical perspective. American Association of Petroleum Geologists, Annual Convention Official Program, pp. A106

Simó, A. 1986. Carbonate platform depositional sequences, Upper Cretaceous, south-central Pyrenees (Spain). Tectonophysics, 129, 205–231.

Simó, A. & Puigdefàbregas, C. 1985. Transition from shelf to basin on an active slope, Upper Cretaceous, Tremp area, southern Pyrenees. In: Mila, M. D. & Rosell, J. (eds.) International Association of Sedimentologists, 6th European Regional Meeting, Llerida, Excursion Guidebook. International Association of Sedimentologists, pp. 63–108.

Simpson, G.H.D. 2006. Modelling interactions between fold-thrust belt deformation, foreland flexure and surface mass transport: Basin Research, 18, 125–143.

Sinclair, H.D. 2000. Delta-fed turbidites infilling topographically complex basins: a new depositional model for the Annot sandstones, SE France. Journal of Sedimentary Research, 70, 504–519.

Smith, N.D. 1974. Sedimentology and bar formation in the Upper Kicking Horse River, a braided outwash stream. Journal of Geology, 82, 205–224.

Sinclair, H.D., Gibson, M., Naylor, M. & Morris, R.G. 2005. Asymmetric growth of the Pyrenees revealed through measurement and modeling of orogenic fluxes. American Journal of Science, 305, 369–406.

Sohn, Y.K., Choe, M.Y. & Jo, H.R. 2002. Transition from debris flow to hyperconcentrated flow in a submarine channel (the Cretaceous Cerro Toro Formation, southern Chile). Terra Nova, 14, 405–415.

Soler, M. & Puigdefàbregas, C. 1970. Lineas generales de la geologia del Alto Aragón occidental. - Pirineos, Jaca, 96, 5–19.

Souriau, A. & Granet, M.A. 1995. A tomographic study of the lithosphere beneath the Pyrenees from local and teleseismic data. Journal of Geophysical Research, 100, 18117–18134.

Srivastava, S.P., Schouten, H., Roest, W.R., Klitgord, K.D., Kovacs, L.C., Verhoef, J. & Macnab, R. 1990. Iberian plate kinematics: a jumping plate boundary between Eurasia and Africa. Nature, 344, 756–759.

Stefani, De C.1895. Description Paleontologique. In: Stefani, De C., Major C. J. F. & Barbcy, W. (eds.) Karpathos: Etude Geologique, Paleontologique et Botanique, pp. 165–174. Georges Bridel, Lausanne.

Stanley, D.J., & Maldonado, A. 1981. Depositional models for fine-grained sediment in the Western Hellenic Trench, Eastern Mediterranean. Sedimentology, 28, 273–290.

Stanley, D.J., Knight, R.J., & Stuckenrath, R. 1978. High Sedimentation rates and variable dispersal patterns in the Western Hellenic Trench. Nature, 273, 110–113.

Stow, D.A.V. 1984. Deep-sea clastics: where are we and where are we going?. In: Brenchley, P.J. & William, B.P.J. (eds.) Sedimentology: Recent Developments and Applied Aspects. Geologial Society of London Special Publication, pp. 67–93.

Stow, D.A.V. & Bowen, A.J. 1980. A physical model for the transport and sorting of fine-grained sediment by turbidity currents. Sedimentology, 27, 31–46.

Stow, D.A.V. & Mayall, M. 2000. Deep-water sedimentary systems: new models for the 21st century. Marine and Petroleum Geology, 17, 125–135.

Stow, D.A.V. & Piper, D.J.W. 1984. Deep-water fine-grained sediments: facies models. In: Stow, D.A.V. and Piper, D.J.W (eds.) Fine-Grained Sediments: Deep-Water

Processes and Facies, Geologial Society of London Special Publication, 15, 611–645.

Stow, D.A.V. & Shanmugam, G. 1980. Sequence of structures in fine-grained turbidites; comparison of recent deep-sea and ancient flysch sediments. Sedimentary Geology, 25, 23–42.

Sutcliffe, C. & Pickering, K.T. 2009. End-signature of deep-marine basin-fill, as a structurally confined low-gradient clastic slope: the Middle Eocene Guaso system, south-central Pyrenees.

Talling, P.J. 2001. On the frequency distribution of turbidite thickness. Sedimentology, 48, 1297–1329.

Talling, P.J., Lawton, T.F., Burbank, D.W. & Hobbs, R.S. 1995. Evolution of the latest Cretaceous-Eocen nonmarine deposystems in the Axhandle piggyback basin of central Utah. Geological Society of America Bulletin, 107, 297–315.

Tanaka, K. 1970. Sedimentation of the Cretaceous flysch sequence in the Ikushumbetsu area, Hokkaido, Japan. Geological Survey of Japan, Report, 236, 1–102.

Taylor, A.M., Goldring, R. & Gowland, S. 2003. Analysis and application of ichnofabrics. Earth-Science Reviews, 60, 227–25.

Tchoumatchenco, P. & Uchman, A. 1999. Lower and Middle Jurassic flysch trace fossils from the eastern Stara Planina Mountains, Bulgaria: A contribution to the evolution of Mesozoic ichnodiversity. Neues Jahrbuch für Geologie und Paläontologie, 213(2), 169–199.

Teixell, A. 1990. Alpine thrusts at the western termination of the Pyrenean Axial Zone. Bull. Soc. Géol. France, 8(VI), 241–249.

Teixell, A. 1992. Estructura alpina en la transversal de la terminación occidental de la Zona Axial Pirenaica. Unpublished PhD Thesis, Universitat de Barcelona, Spain, pp. 252

Teixell, A. 1996. The Ansó transect of the southern Pyrenees: basement and cover thrust geometries. Journal Geological Society of London, 153, 301–310.

Teixell, A. 1998. Crustal structure and orogenic material budget in the west central Pyrenees. Tectonics, 17, 395–406.

Thomas, R.G., Smith, D.G., Wood, J.M., Visser, J., Anne Calverley-Range, E. & Koster, E.H. 1987. Inclined heterolithic stratification–terminology, description, interpretation, and significance. Sedimentary Geology, 53, 123–179.

Torell, O.M. 1870. Petrifacta Suecana Formationis Cambricae. Lunds University, 6 (2) 1–14.

Tucker, M.E. & Wright, V. P. 1990. Carbonate Sedimentology. Blackwell Science, pp. 482.

Turcotte, D.L. 1997. Fractals and Chaos in Geology and Geophysics. Cambridge University Press, Cambridge, pp. 398.

Uchman, A. 1995. Taxonomy and palaeocology of flysch trace fossils: The Marnoso-arenacea Formation and associated facies, Miocene, Northern Apennines, Italy. Beringeria, 15, 3–115.

Uchman, A. 1998. Taxonomy and ethology of flysch trace fossils: revision of the Marian Ksiazkiewicz collection and studies of complementary material. Annales Societatis Geologorum Poloniae, 68, 105–218.

Uchman, A., Bubniak, I. & Bubniak, A. 2000. Glossifungites ichnofacies in the area of its nomenclatural archetype, Lviv, Ukraine. Ichnos, 7(3), 183–193.

Uchman, A. 2001, Eocene flysch trace fossils from the Hecho Group of the Pyrenees, northern Spain. Beringeria, 28, 3–41.

Vail, P.R. 1987. Seismic-stratigraphy interpretation using sequence stratigraphy: Part. 1: Seismic stratigraphy interpretation procedures. Atlas of seismic stratigraphy, American Association of Petroleum Geologists Studies in Geology, 27, 1–10.

Vail, P.R., Hardenbol, J. & Todd, R.G. 1984. Jurassic unconformities, chronostratigraphy and sea-level changes from seismic stratigraphy and biostratigraphy. In: Schlee, J.S. (ed.) Interregional Unconformities and Hydrocarbon Accumulation, vol. 36. American Association of Petroleum Geologists Memoir, pp. 129–144.

Van Echelpoel, E. & Weedon, G.P. 1990. Milankovitch cyclicity and the Boom Clay formation; an Oligocene siliciclastic shelf sequence in Belgium. Geological Magazine; November, 127(6), 599–604.

Van Lunsen, H. 1970. Geology of the Ara-Cinca Region, Spanish Pyrenees, Province of Huesca. PhD Thesis, Utrecht University, Geologica Ultraiectina 16, 1–119.

Van Wagoner, J.C., Mitchum, R.M., Campion, K.M. & Rahmanian, V.D. 1990. Siliciclastic Sequence Stratigraphy in Well Logs, Core, and Outcrops: Concepts for High-Resolution Correlation of Time and Facies, AAPG Methods, in Exploration Series No. 7, The American Association of Petroleum Geologists, Tulsa OK, pp. 55.

Van Wagoner, J.C. 1996. Overview of sequence stratigraphy of foreland basin deposits: terminology, summary of papers, and glossary of sequence stratigraphy (64). Sequence Stratigraphy of Foreland Basin Deposits, American Association of Petroleum Geologists, ix–xxi.

Verges, J. & Muñoz, J.A. 1990. Thrust sequences in the southern Central Pyrenees. Bulletin. Société Géologique de France, 8, 265–271.

Vergés, J. & Burbank, D.W. 1996. Eocene–Oligocene Thrusting and Basin Configuration in the Eastern and Central Pyrenees (Spain), in Friend, P.F. & Dabrio, C.J. (eds.) Tertiary Basins of Spain. The Stratigraphic Record of Crustal Kinematics, Cambridge University Press. World and Regional Geology, 120–133.

Vergés, J., Muñoz, J.A. & Martínez, A. 1992. South-Pyrenean fold-and-thrust belt: Role of foreland evaporitic levels in thrust geometry. In: McClay, K. (ed). Thrust Tectonics. Chapman and Hall, London, 225–264.

Vergés, J., Millan, H., Roca, E., Muñoz, J.A., Marzo, M., Cires, J., Denbezemer, T., Zoetemeijer, R. & Cloetingh, S. 1995. Eastern Pyrenees and related foreland basins — Precollisional, syncollisional and postcollisional crustal-scale cross-sections. Marine and Petroleum Geology, 12, 903–915.

Vergés, J., Marzo, M., Santaeularia, T., Serra-Kiel, J., Burbank, D.W., Munoz, J.A. & Gimenez-Montsant, J. 1998. Quantified vertical motions and tectonic evolution of the SE Pyrenean foreland basin. In: Mascle, A., Puigdefàbregas, C., Luterbacher, H.P. & Fernández, M. (eds.) Cenozoic foreland basins of western europe, Geological Society of London, Special Publication, 134, pp. 107–134.

Vergés, J., Fernàndez, M. & Martínez, A. 2002. The Pyrenean orogen: pre-, syn-, and post-collisional evolution. In: Rosenbaum, G. and Lister, G. S. 2002. Reconstruction of the evolution of the Alpine-Himalayan orogeny. Journal of the Virtual Explorer, 8, 57–76.

Vialov, O.S. & Golev, B.T. 1965. O drobnom podrazdieleni gruppy Paleodictyonidae. Byulletin Moskovskovo Obshczhestva Ispityvania Prirody, Odtiel Gieologii, 40, 93–114.

Vissers, R.L.M. 1992. Variscian extension in the Pyrenees. Tectonics, 11, 1369–1384.

Walker, R.G. 1978. Deep-water sandstone facies and ancient submarine fans: models for exploration for stratigraphic traps. AAPG Bulletin 62, 932–966.

Wang, D. & Hesse, R. 1996. Continental slop sedimentation adjacent to an ice-margin; Glaciomarine depostional facies on Labrador Slope and glacial cycles. Marine

Geology, 135, 65–96.

Wentworth, C.K. 1922. A scale of grade and class terms for clastic sediments. Geology, 30, 377–392.

Westerhold, T. & Röhl, U. 2009. High resolution cyclostratigraphy of the early Eocene – new insights into the origin of the Cenozoic cooling trend. Climate of the Past, 5, 309–327.

Wetzel, A. & Uchman, A. 2001. Sequential colonization of muddy turbidites: examples from Eocene Beloveža Formation, Carpathians, Poland. Palaeogeography, Palaeoclimatology, Palaeoecology, 168, 171–186.

Wetzel, A. 2002. Modern Nereites in the South China Sea—ecological association with redox conditions in the sediment. Palaios, 17, 507–515.

Wetzel, A. 2008. Recent bioturbation in the deep South China Sea: a uniformitarian ichnologic approach. Palaios, 23, 601–615.

Williams, G.D. 1985. Thrust tectonics in the south central Pyrenees. Journal of Structural Geology, **7**, 11–17.

Williams, G.D. & Fischer, M.W. 1984. A balanced section across the pyrenean orogenic belt. Tectonics, 3, 773–80.

Willis, A. 2000. Tectonic control of nested sequence architecture in the Sego Sandstone, Neslen Formation and Upper Castlegate Sandstone (Upper Cretaceous), Sevier Foreland Basin, Utah, USA. Sedimentary Geology 136, 277–317.

Winkler, W. & Gawenda, P. 1999. Distinguishing climatic and tectonic forcing of turbidite sedimentation, and the bearing on turbidite bed scaling: Palaeocene – Eocene of northern Spain. Journal of the Geological Society, London, 156, 791–800.

Wilson, T.R.S., Thomson, J., Colley, S., Hydes, D.J. & Higgs, N.C. 1985. Early diagenesis: the significance of progressive subsurface oxidation fronts in pelagic sediments. Geochimica et Cosmoschimica Acta, 49, 811–822.

Wiltschko, D.V. & Dorr, J.A. 1983. Timing of deformation in overthrust belt and foreland of Idaho, Wyoming and Utah. Bulletin of the American Association of Petroleum Geologists, 67, 1304–22.

Wright, V.P. & Burchette, T.P. 1996. Shallow-water carbonate environments. In: Reading, H.G. (ed.) Sedimentary Environments: Processes, Facies and Stratigraphy: Blackwell, Oxford, 325–392.

Winn, R.D. & Dott Jr., R.H. 1979. Deep-water fan-channel conglomerates of Late Cretaceous age, southern Chile. Sedimentology 26, 203–228.

Ziegler, P.A. 1988. Evolution of the Arctic-North Atlantic and the Western Tethys. Tulsa, American Association Petroleum Geology Memoir, pp. 198.

Zoetemeijer, R., Sassi, W., Roure, E. & Cloetingh, S. 1992. Stratigraphic and kinematic modelling of thrusts evolution, northern Apennines, Italy. Geology, 20, 1035–1038.

Zoetemeijer, R., Cloetingh, S., Sassi, W. & Roure, E. 1993. Modelling of a piggyback-basin: record of tectonic evolution. Tectonophysics, 226, 253–269.

Zuffa, G.G. 1980. Hybrid arenites: their composition and classification. Journal of Sedimentary Petrology, 50, 21–29.

Zuffa, G.G. 1991. On the use of turbidite arenites in provenanc studies: critical remarks. In: Morton, A.C. Todd, S.P. & Haughton, P.D.W. (eds.) Developments in Sedimentary Provenance Studies, Geological Society of London Special Publication, 57, 23–29.

Zwart, H.J. 1979. The Geology of the Central Pyrenees. Leidse Geologische Mededelingen, 50, 1–44.

Architecture and processes of deep-marine sandbodies, Ainsa basin, Spanish Pyrenees

Appendices

Nicole Joanna Bayliss

2010

University College London

APPENDIX A

GEOLOGICAL MAPPING

This appendix contains photocopies of various maps produced during the mapping process to create the composite geological maps found in the text. The main aerial photographs used in the interpretations are added to geographically locate the maps that follow. Each map presented within this appendix was completed at a scale of 1:20,000, using aerial photographs as base maps (see Section 2.2).

Field slips were created through field mapping and calibrating observations with aerial photogragh analysis; whereas, the fair copy maps represent the compilation of the field slips and stereopair interpretation.

The photocopied maps contained within this appendix are organised according to their geographical area, which can be located within the preceding aerial photograph.

Banastón System: San Vicente-Boltaña area

Morillo System


OLD
BAN
CAN
TASA
J. CARLOS
BROTONS
212 D 01
N
KODAK SAFETY FILM
km
0.5
1
2

Fig. A1.

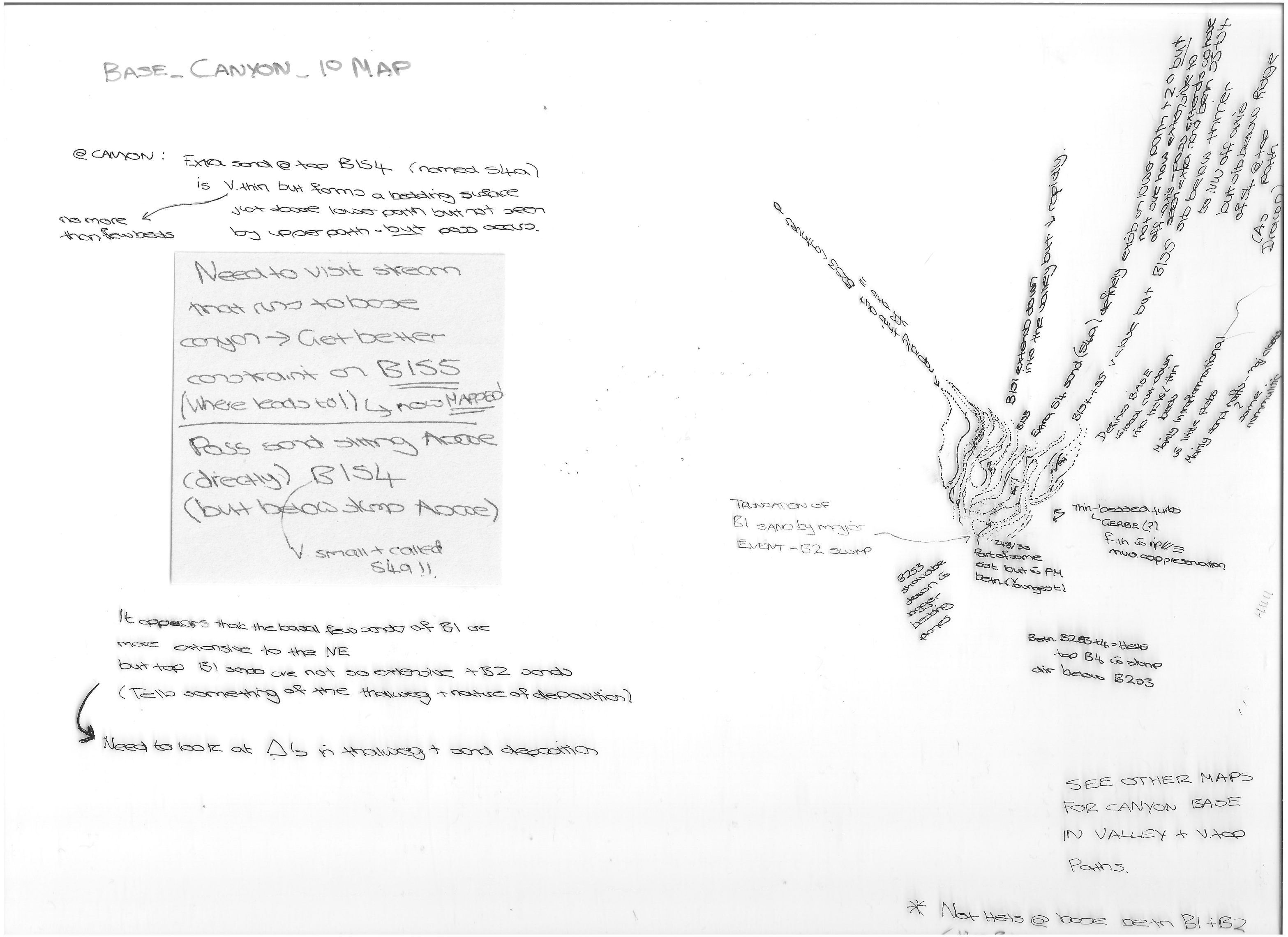

BASE_CANYON_1° MAP

@ CANYON: Extra sand @ top B154 (named S4a)
is V. thin but forms a bedding surface
just above lower path but not seen
by upper path - but poss occurs.

no more than few beds

Need to visit stream
that runs to base
canyon → Get better
constraint on B155
(where leads to!) ↳ now MAPPED

Poss sand sitting Above
(directly) B154
(but below slump Above)

V. small + called S4a !!

It appears that the basal few sands of B1 are
more extensive to the NE
but top B1 sands are not so extensive + B2 sands
(Tells something of the thalweg + nature of deposition)

Need to look at Δ's in thalweg + sand deposition

SEE OTHER MAPS
FOR CANYON BASE
IN VALLEY + V.top
Paths.

* Not beds @ base betn B1+B2

Fig. A2.

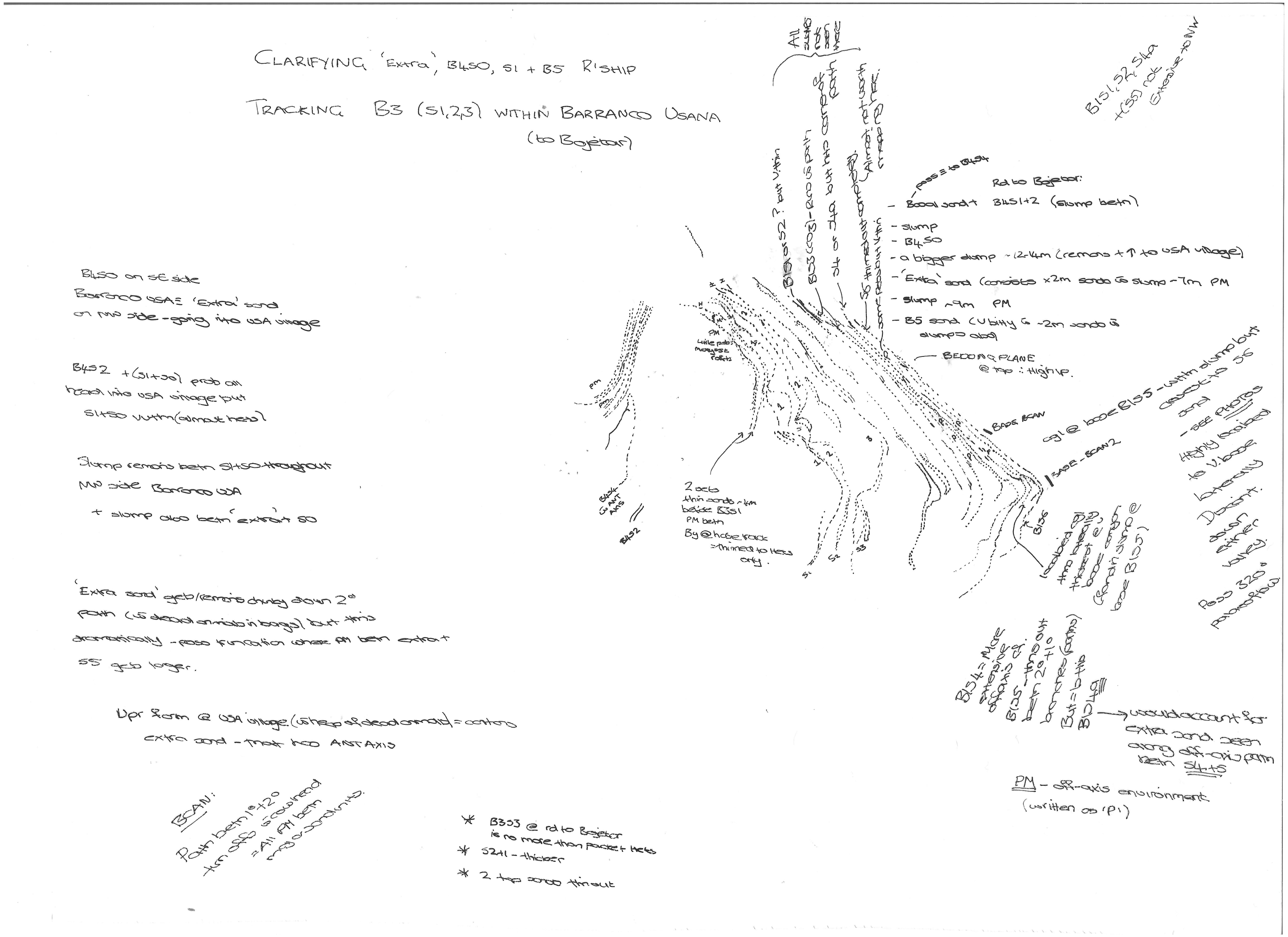

CLARIFYING 'Extra', B450, S1 + B5 R'SHIP

TRACKING B3 (S1,2,3) WITHIN BARRANCO USANA
(to Bojetar)

B450 on SE side
Barranco USA = 'Extra' sand
on NW side - going into USA village

B452 + (S1+S0) prob all
head into USA village but
S1+S0 within (almost here)

Slump remains betn S1+S0 throughout
NW side Barranco USA
+ slump also betn 'extra' + S0

'Extra sand' gets/remains chunky down 2° path (is dead animals in bags) but thins dramatically - poss function where PM betn extra + S5 gets larger.

Upr Form @ USA village (w/ heap of dead animals) = contains extra sand - that has ANT AXIS

BSAN:
Path betn 1°+2° thin S5S scoured = All PM betn major sand units.

- * B353 @ rd to Bojetar is no more than pocket + hets
- * S241 - thicker
- * 2 top sands thin out

B151, 52, 54a +(55) not Extensive to NW

Rd to Bojetar:
poss ≡ to B454
- Basal sand + B451+2 (slump betn)
- slump
- B450
- a bigger slump ~12-14m (remains + ↑ to USA village)
- 'Extra' sand (consists x2m sands & slump ~7m PM
- Slump ~9m PM
- B5 sand (v bitty & ~2m sands & slumps also)

BEDDING PLANE @ top : High'p.

B15 or S2 ? but thin

B53 (cg1) - Rd to path

S4 or S4a but top contact of path

S6 thinned out [illegible]

some pebbles but thin

Almost not [illegible]

All [illegible]

cgl @ base B155 - within slump but closest to S6 sand - SEE PHOTOS Highly localised to v. base laterally. Doesn't [illegible] either valley. Poss 320° palaeoflow.

localised B156 thin laterally + thickest @ base cgl (grading into slump @ base B155)

B154 = More extensive across cgl. B155 - thins out betn 20+10 becomes (poorly) But = b thin B154 → would account for extra sand seen along off-axis path betn S4+S5

PM - off-axis environment (written as 'P1')

2 sets thin sands ~4m below B351 PM betn
By @ hose rack = thinned to Hets only.

Fig. A3.

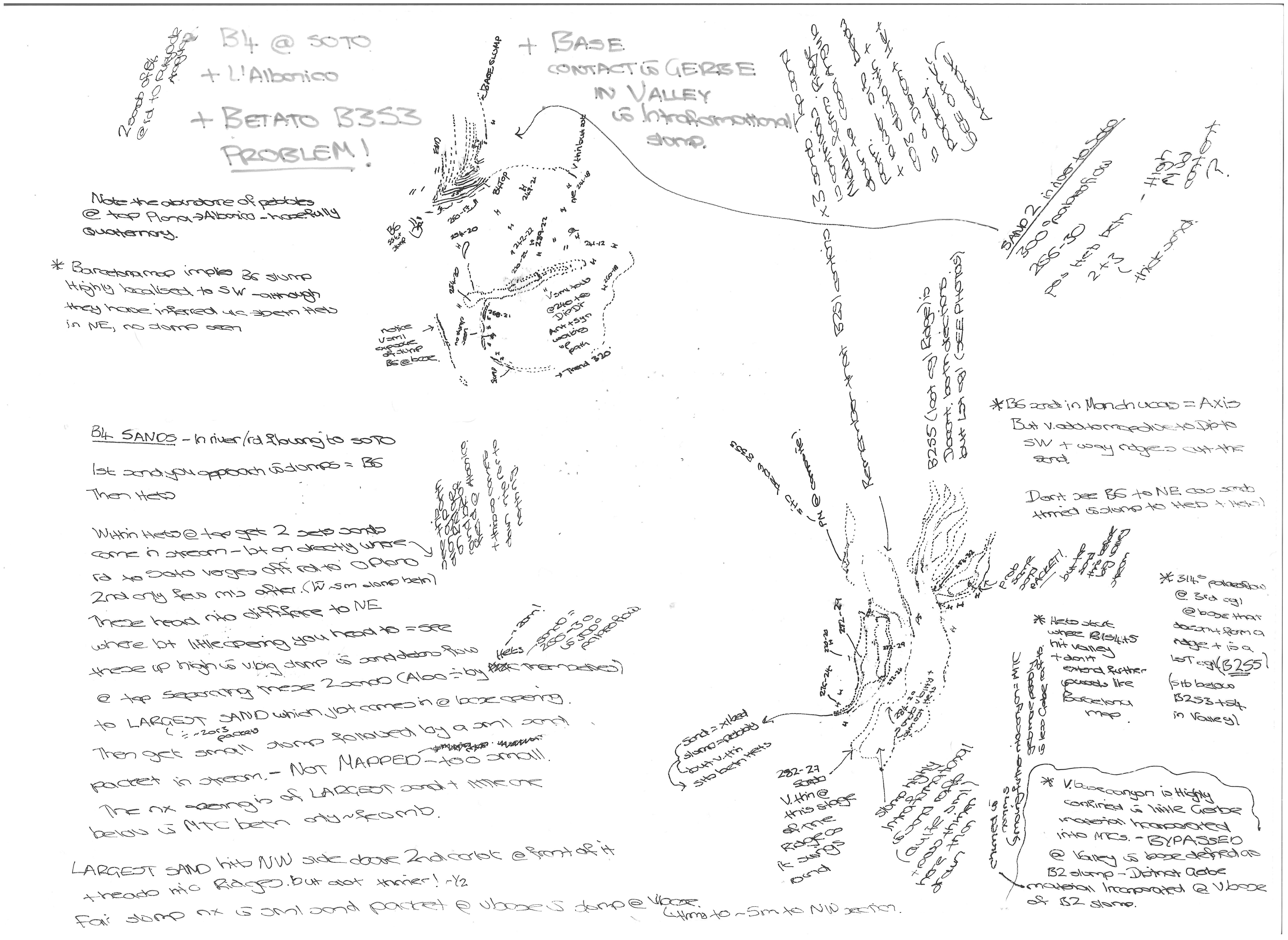

B4 @ SOTO

+ L'Albonico

+ BETATO B353

PROBLEM!

2 sands of Hets @ rd to Albonico

+ BASE CONTACT is GERBE IN VALLEY is Intraformational slump.

Note the abundance of pebbles @ top Plana→Albonico – hopefully Quaternary.

* Barcelona map implies B6 slump Highly localised to SW – although they have inferred it's between Hets in NE, no slump seen

x3 sands. Ridge [illegible] (SEE photos)

SAND 2 in river to Soto 300° palaeoflow 256-30 Pos. Hets betw. 2 + 3 – High angle of R. thick sand.

B255 (lost of Ridge) is Doesn't form decline but [illegible] (SEE PHOTOS)

* B6 sand in Manchucas = Axis But v. difficult to map due to Dip to SW + way ridges cut the sand.

Don't see B6 to NE as sands thinned is slump to Hets + Hets)

* 314° palaeoflow @ 3rd cgl @ base that doesn't form a ridge + is a 1st cgl (B255) (sits below B253 + 54 in Valley)

* Hets start where B1 &4+5 hit valley + don't extend further upwards like Barcelona map.

MTC = [illegible] is less Gerbe [illegible]

* V. base canyon is Highly confined is little Gerbe material incorporated into MTCs. – BYPASSED @ Valley is base defined as B2 slump – Distinct Gerbe material Incorporated @ V. base of B2 slump.

B4 SANDS – In river/rd following to SOTO

1st sand you approach w/ slumps = B6

Then Hets

Within Hets @ top get 2 sets sands come in stream – but on directly where rd to Soto verges off rd to O Plana 2nd only few m's after. (W ~5m slump betn) These head into difference to NE where but little opening you head to = see these up high is v. big slump is sand debris flow @ top separating these 2 sands (Also ÷ by ~~[illegible]~~ themselves) to LARGEST SAND which just comes in @ base opening. (÷ ~2 or 3 packets)

Then get small slump followed by a small sand packet in stream. – NOT MAPPED – too small.

The nx opening is of LARGEST sand + little one below is MTC betn only ~5 or 6 m.

Hets – sand = 266-30 is 300° palaeoflow – ~2m!

Bet Hets of thin beds @ Albonico + thin sands in Hets of 2nd

LARGEST SAND hits NW side above 2nd carbs @ front of it + heads into Ridges. but alot thinner! ~½

Fair slump nx is small sand packet @ v. base is slump @ V. base. (thins to ~5m to NW section.

Fig. A4.

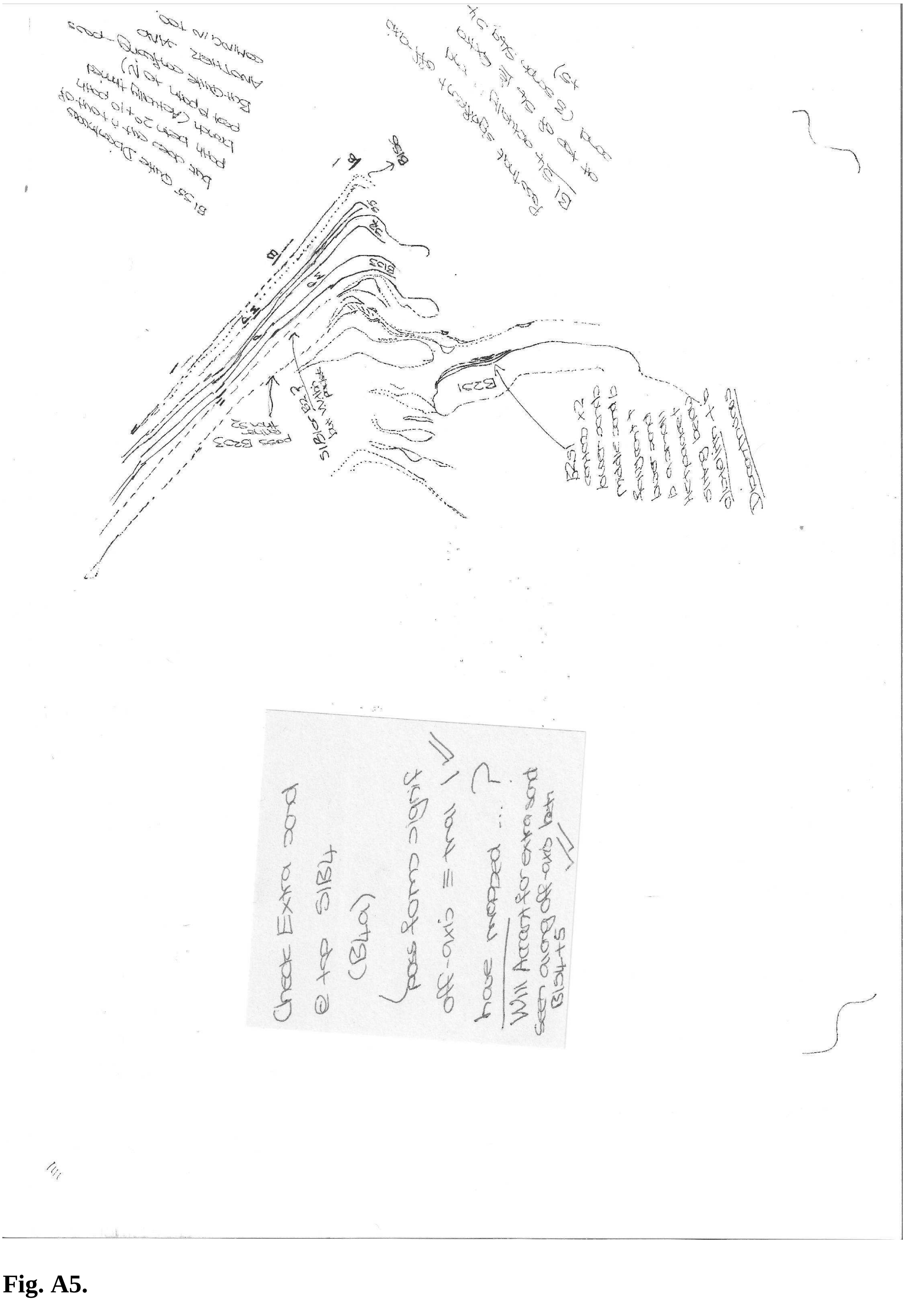

B1 55 Quite Discontinuous
but does cut n tout of
Path betn 20+10 path
branch (Actually thinned
past point to N)
But Quite confused - poss
Another sand
coming in too.

Poss that significant off-axis
B1 54 actually ∴ thin
at top of 54 ie Extra
sand (3 sands 54a, 54
+5)

B251
contacts x2
lower sands
middle sand is
Significant +
lower sand
is a small
Het packet
sitting below
olistolith + is
Discontinuous

Check Extra sand
@ top S1B4
(B4a)
poss forms signif
off-axis = trail ✓✓
have mapped ... ?
Will Account for extra sand
seen along off-axis betn
B1S4+5 ✓✓

Fig. A5.

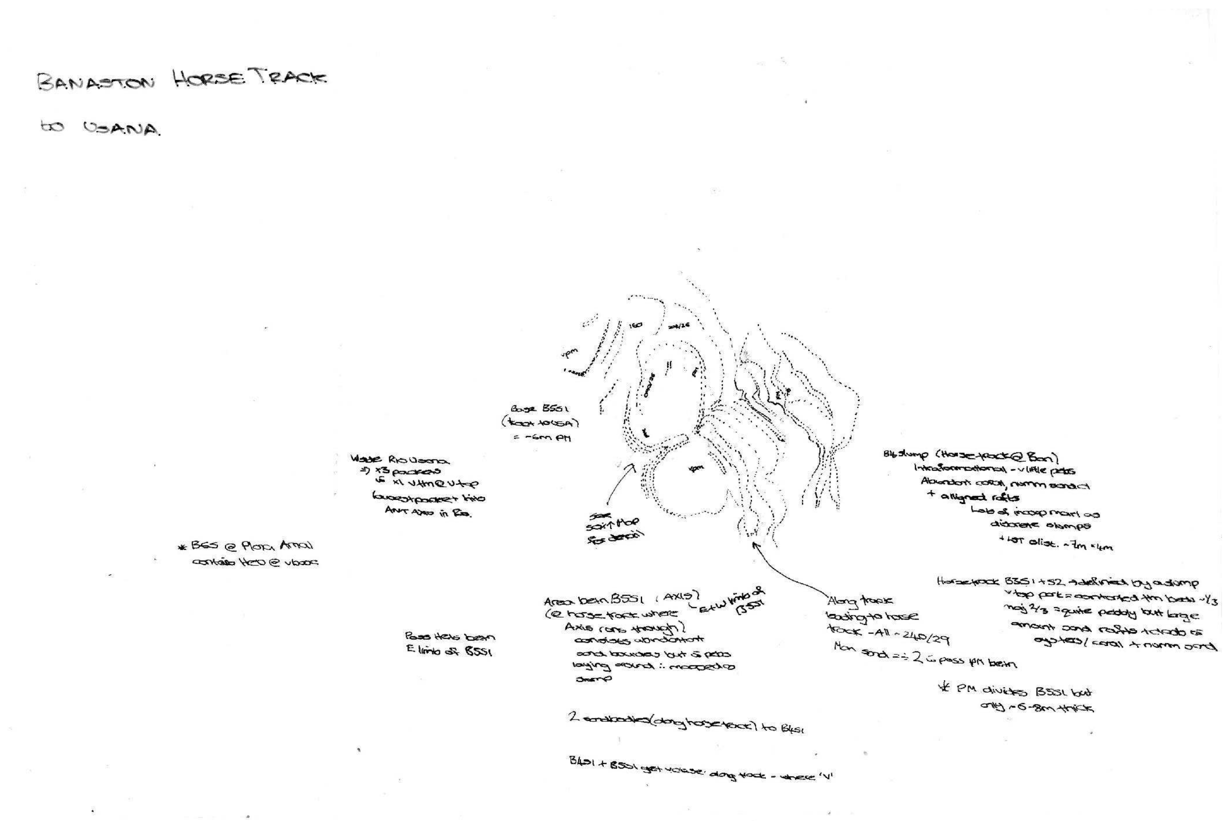

BANASTON HORSE TRACK
to USANA.

Base B5S1
(track to USA)
= ~6m PM

Wade Rio Usana
⇒ ×3 packets
∴ ×1 vthn @ v top
lowest packet into
Ant Axis in Rio.

* B6S @ Plora Amal
contains HEO @ vbase

see soil ↑ map
for detail

B4 slump (Horse-track @ Ban)
Intraformational - v little pebs
Abundant coral, numm sand
+ alligned rafts
Lots of incorp marl as
discrete clumps
+ 1 OT olist. ~7m × 4m

Horsetrack B5S1 + S2 → defined by a slump
v top part = contorted thn beds ~1/3
maj 2/3 = quite pebbly but large
amount sand rafts + clasts of
oysters / coral + numm sand

Along track
leading to horse
track - All ~ 240/29
Mon sand = ∴ 2 ∵ pass PM betn

* PM divides B5S1 but
only ~6-8m thick

Area betn B5S1 (AXIS) ← E+W limbs of B5S1
(@ horse track where
Axis runs through)
consists abundant
sand boulders but & pebs
laying around ∴ mapped as
slump

Pass Here betn
E limb of B5S1

2 sandbodies (along horse track) to B4S1

B4S1 + B5S1 get close along track - where 'V'

Fig. A6.

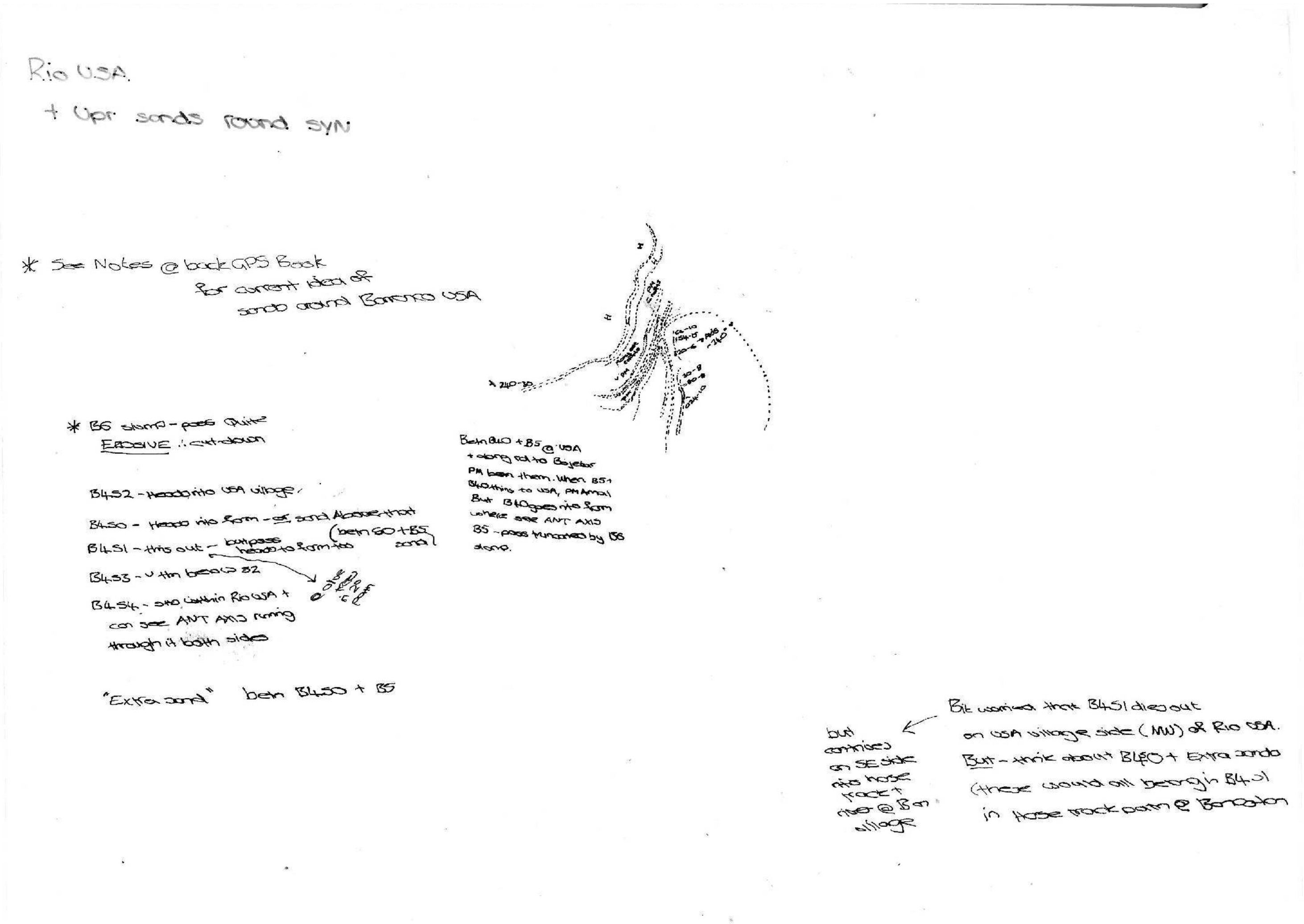

Rio USA.

+ Upr sands round SYN

* See Notes @ back GPS Book
for current idea of
sands around Barranco USA

* B6 slump - poss Quite
EROSIVE ∴ cut-down

B4.52 - heads into USA village.

B4.50 - Heads into farm - SE sand Above that

B4.51 - thins out - but pass heads to farm too (betn 50 + B5 sand)

B4.53 - v thn below 52

B4.54 - sits within Rio USA + can see ANT AXIS running through it both sides

"Extra sand" betn B4.50 + B5

Betn B40 + B5 @ USA
+ along rd to Bajebar
PM betn them. When B5 +
B40 thins to USA, PM Amal
But B40 goes into farm
where see ANT AXIS
B5 - poss truncated by B6
slump.

Bit worried that B4.51 dies out
on USA village side (NW) of Rio USA.
But - think about B4.50 + Extra sands
(these would all belong in B4.5)
in Horse track path @ Barranco

but
continues
on SE side
into horse
track +
river @ B on
village

Fig. A7.

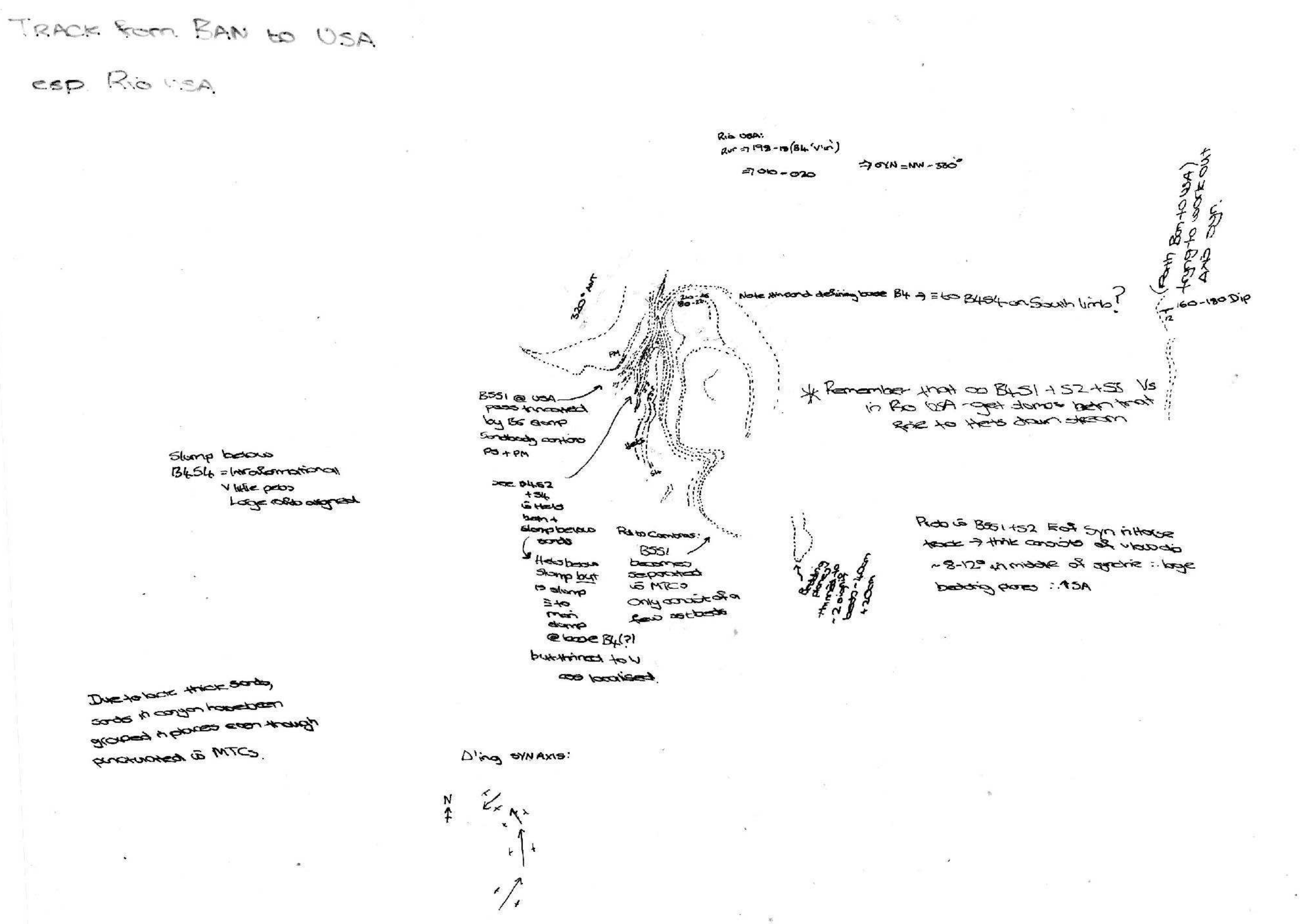
TRACK from BAN to USA
esp Rio USA
Rio USA:
Rvr → 193-13 (B4 'V'in')
→ 010-020
→ SYN = NW-330°
320° Ant
Note diamond defining base B4 → ≡ to B4S4 on South limb?
(Path Ban to USA)
trying to work out
AXD Dip.
160-180 Dip
12
* Remember that ∞ B4S1 + S2 + S5 Vs in Rio USA - get domes betn that rise to Hets down stream
PM
Hets
S4
B5S1 @ USA pass truncated by B6 slump
Sandbody contains PS + PM
see B4S2 + S4 is Hets betn + slump below sands
Hets below slump but is slump ≡ to main slump @ base B4(?) but thinned to W as localised.
Rio to Cambras:
B5S1 becomes separated ū MTCs
Only consist of a few ss beds
Bedding planes of thinning ~20cm beds ~40cm +20cm
Rido is B5S1+S2 E of Syn in those track → think consists of v low dip ~8-12° in middle of syncline ∴ large bedding planes ∴ USA
Slump below B4S4 = intraformational
V little pebs
Large clasts aligned
Due to lack thick sands, sands in canyon have been grouped in places even though punctuated ū MTCs.
D'ing SYN AXIS:
N

Fig. A8.

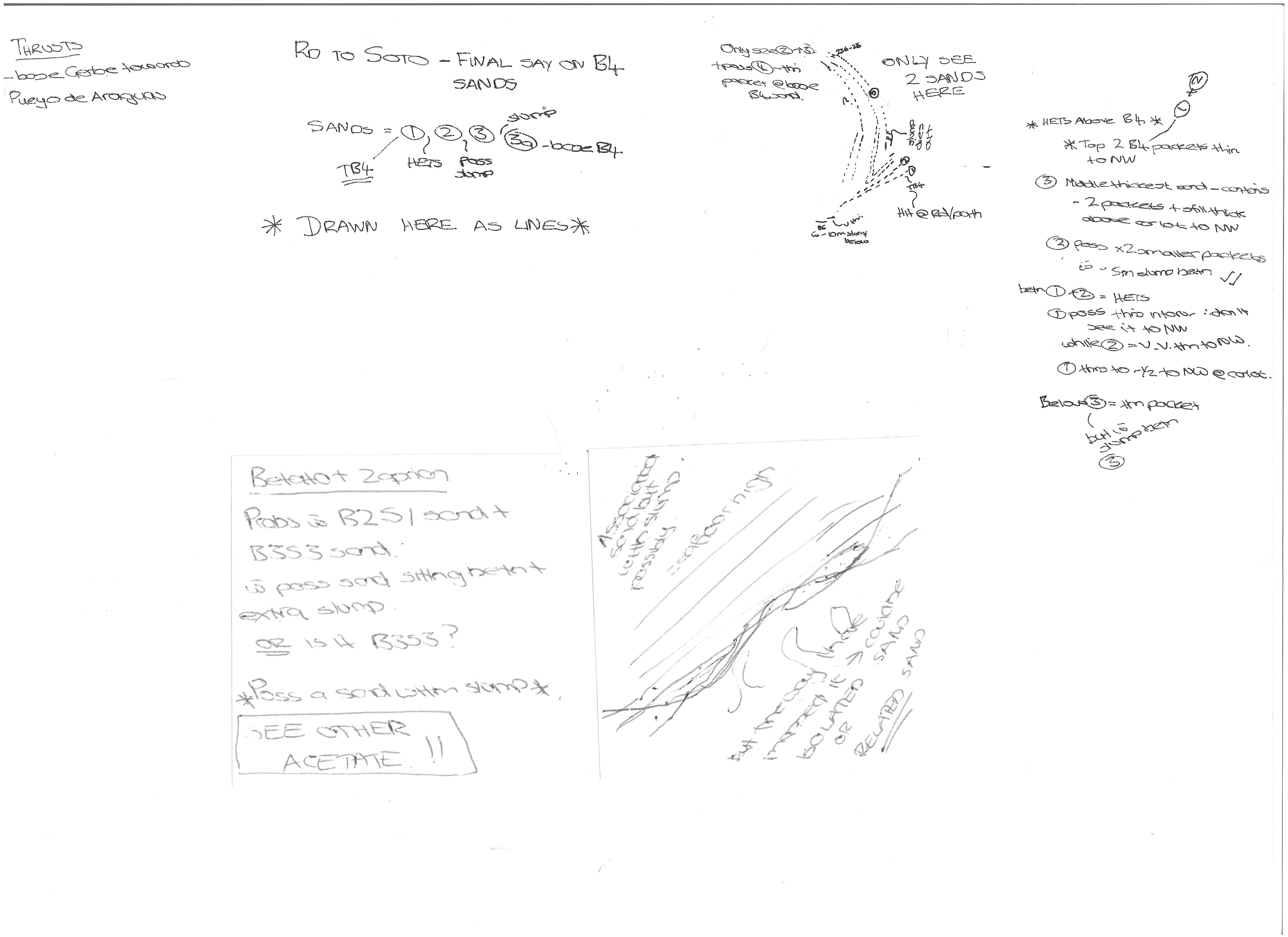

THRUSTS
- base Gerbe towards
Pueyo de Araguas

RD TO SOTO – FINAL SAY ON B4 SANDS

SANDS = ①, ② ③ ③a – base B4
TB4 HETS Poss slump slump

* DRAWN HERE AS LINES *

Only see ② + ③ + poss ④ – thin packet @ base B4 sand.

ONLY SEE 2 SANDS HERE

* HETS Above B4 *

* Top 2 B4 packets thin to NW

③ Middle thickest sand – contains ~2 packets + still thick above or lot to NW

② poss x2 smaller packets w ~5m slump betn ✓✓

betn ① + ② = HETS
① poss thin interv. ∴ don't see it to NW
while ② = v.v. thin to NW.

① thins to ~½ to NW @ contact.

Below ③ = thin pocket
but w slump betn ③

Betato + Zaprion

Probs = B2S1 sand + B3S3 sand.
w poss sand sitting betn + extra slump
OR is it B3S3?

Poss a sand within slump

SEE OTHER ACETATE !!

Associated sand but with possibly slump

seafloor high

but the way imaged it → could be ISOLATED OR RELATED SAND

Fig. A9.

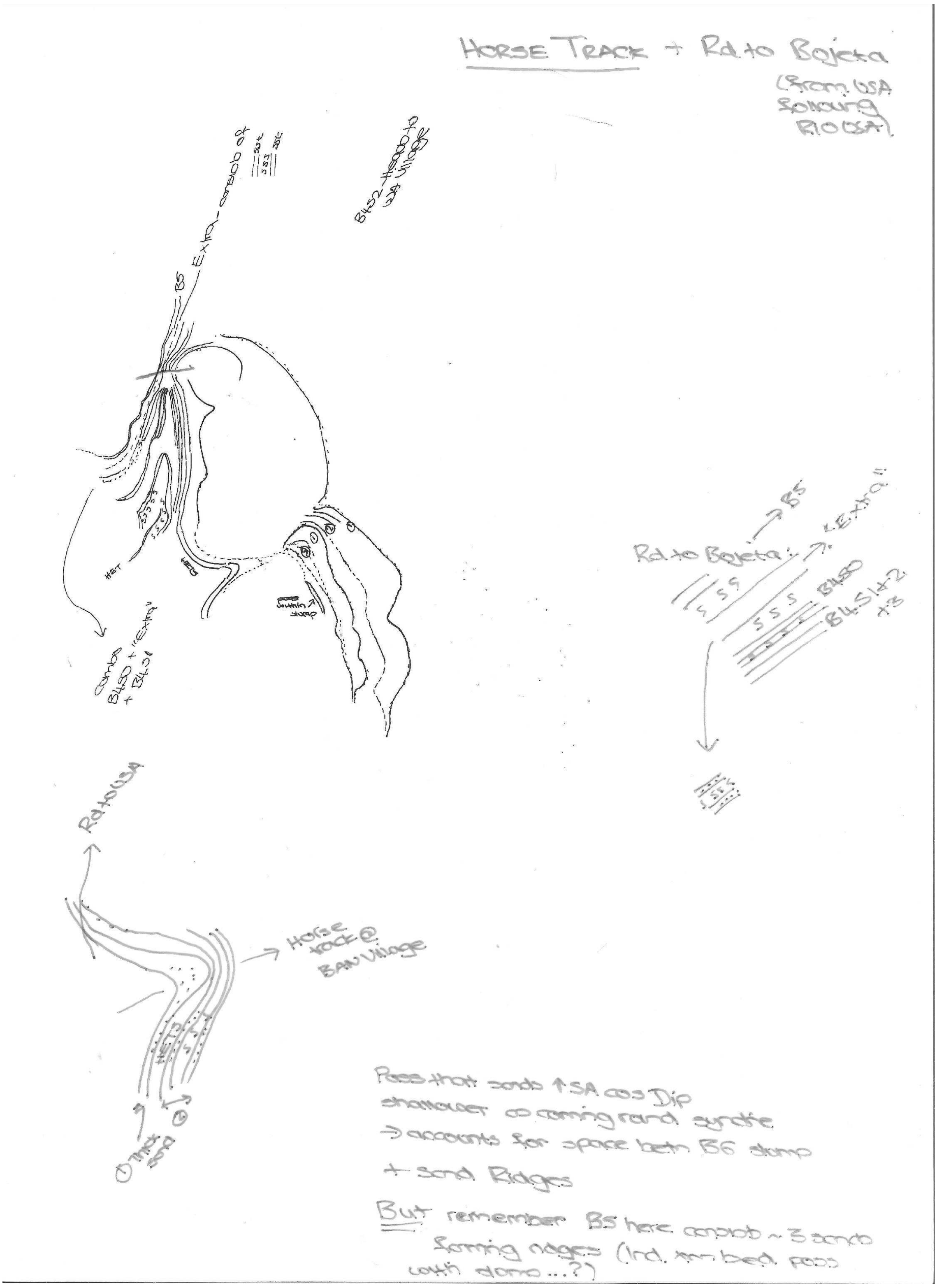

Pass that sands ↑ SA cos Dip shallower as coming round syncline
⇒ accounts for space betn B6 dump + sand Ridges

<u>But</u> remember B5 here combo ~ 3 sands forming ridges (incl. thin bed. poss with dump...?)

Fig. A10.

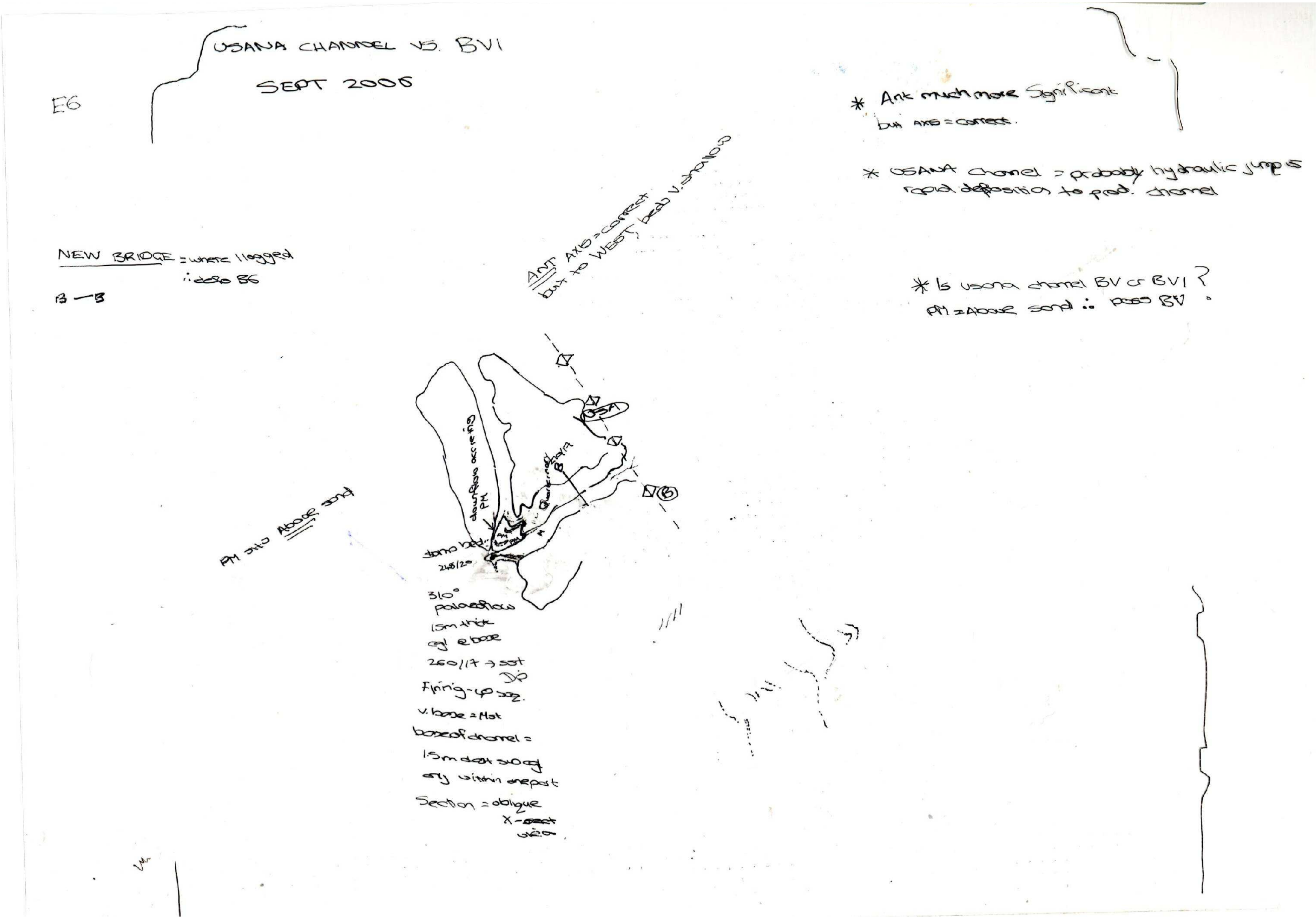

USANA CHANNEL VS. BVI

SEPT 2006

E6

NEW BRIDGE = where I logged
∴ also B6

B — B

ANT AXIS = correct but to WEST, beds v. shallow

PM into Above sand

310° palaeoflow
1.5m thick
cgl @ base
260/17 → sst Dip
fining-up seq.
v. base = Mst
base of channel = 1.5m deep so cgl only within one part
Section = oblique X-sect view.

* Ant much more Significant but AXIS = correct.

* USANA channel = probably hydraulic jump & rapid deposition to prod. channel

* Is usana channel BV or BVI ? PM = Above sand ∴ poss BV.

Fig. A11.

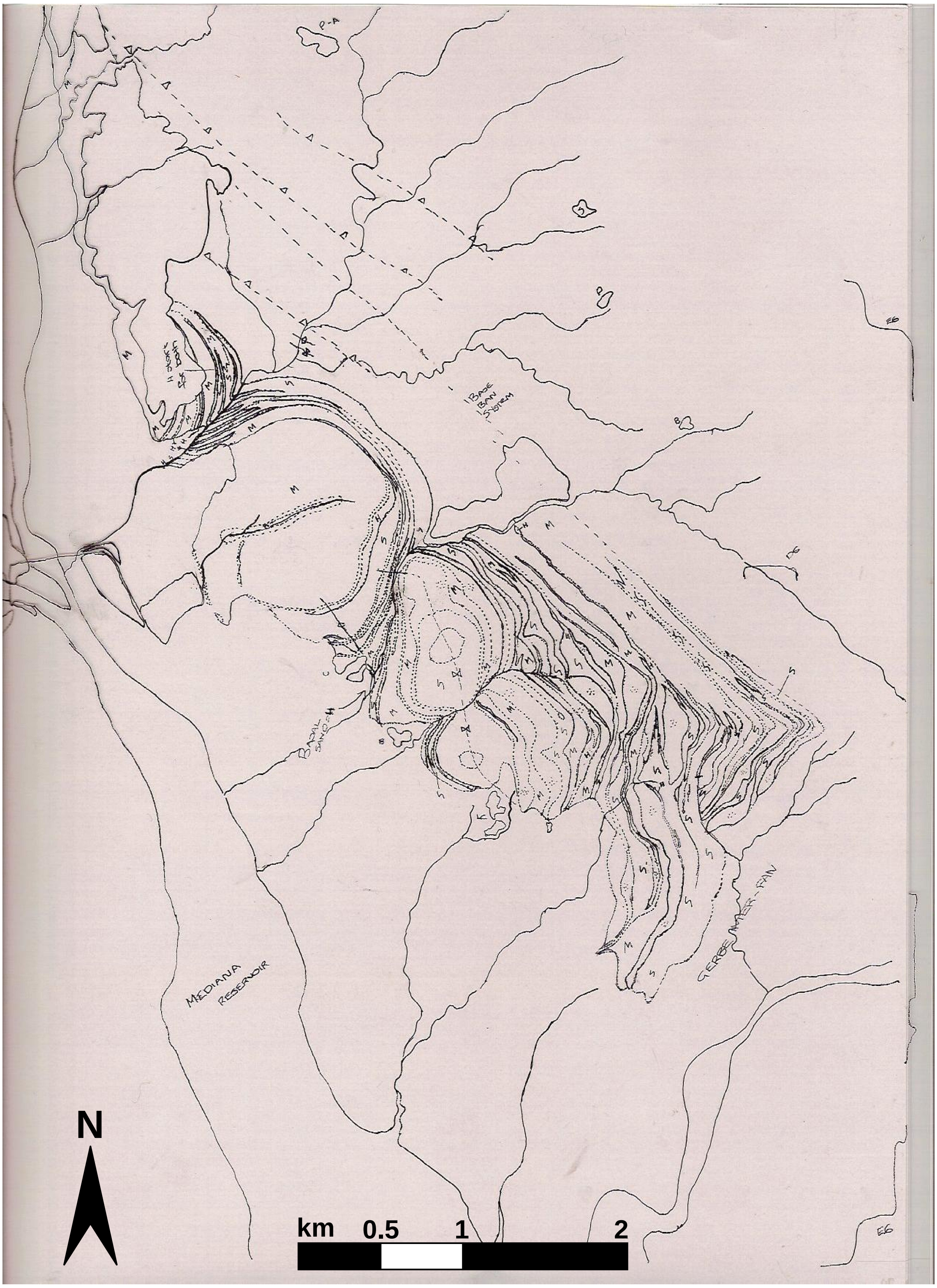

Fig. A12.

M	Mud	-△-△-△-	Thrust fault
∿	Contorted sediment	—◇—	Anticline
——	Lithological contact	--⧖--⧖--	Syncline
-------	Uncertain / inferred lithological contact		

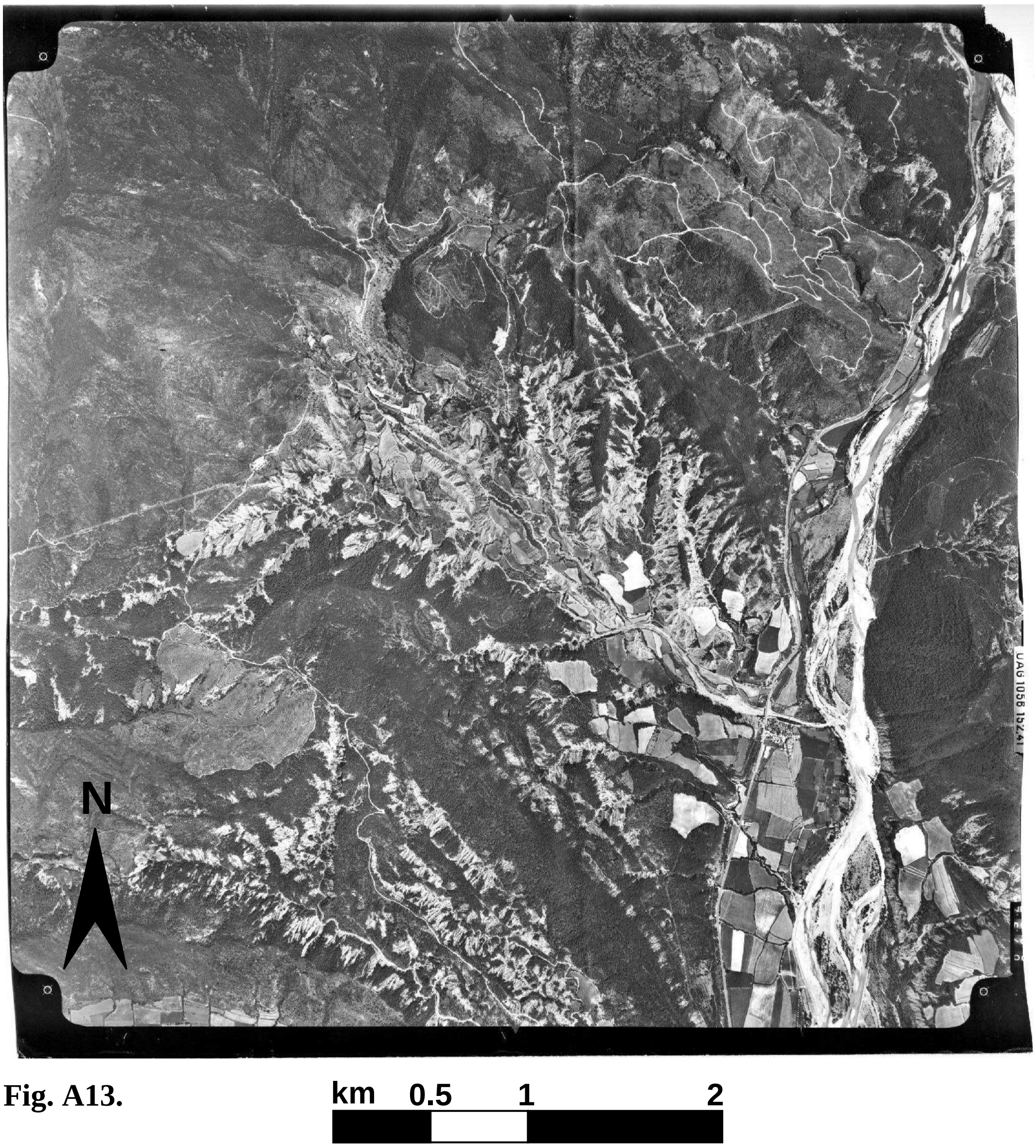

Fig. A13.

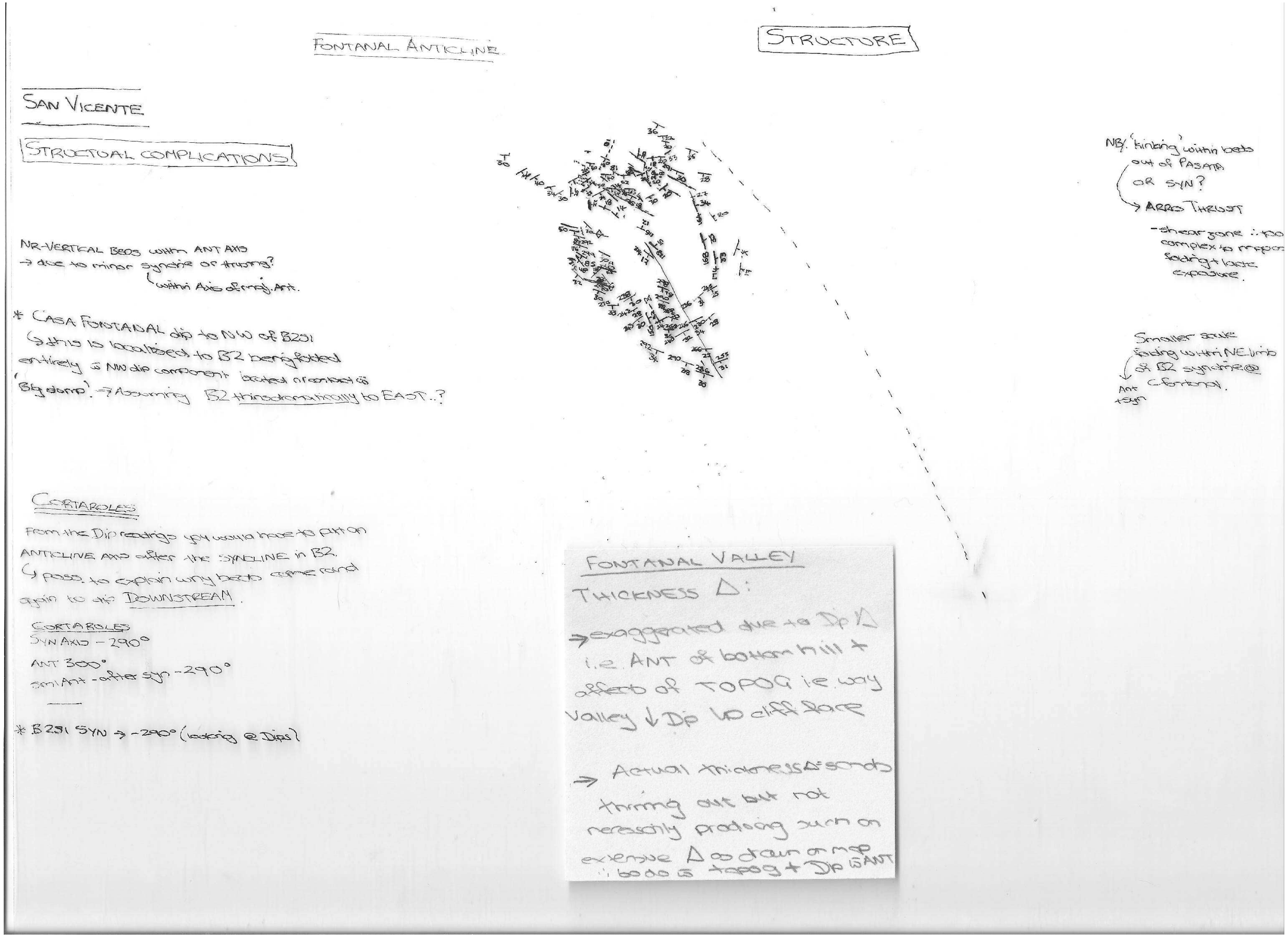

FONTANAL ANTICLINE

STRUCTURE

SAN VICENTE

STRUCTUAL COMPLICATIONS

NR-VERTICAL BEDS with ANT AXIS
→ due to minor syncline or thrusting?
within Axis of maj. Ant.

* CASA FONTANAL dip to NW of B251
↳ this is localised to B2 being folded
entirely ∴ NW dip component located nr contact of
'Big dome'. → Assuming B2 thins dramatically to EAST..?

CORTAROLES

From the Dip readings you would have to put an
ANTICLINE AXIS after the SYNCLINE in B2.
↳ poss. to explain why beds come round
again to dip DOWNSTREAM.

CORTAROLES
SYN AXIS – 290°
ANT 300°
smi Ant – after syn – 290°

* B251 SYN → ~290° (looking @ Dips)

FONTANAL VALLEY

THICKNESS Δ:

→ exaggerated due to Dip Δ
i.e. ANT at bottom hill +
affect of TOPOG i.e. way
Valley ↓ Dip to cliff face

→ Actual thickness Δ: sands
thinning out but not
necessarily producing such an
extensive Δ as drawn on map
∴ bc due to topog + Dip w ANT

NB/. 'kinking' within beds
out of PASATA
OR SYN?
→ ARRO THRUST
– shear zone ∴ too
complex to map on
folding + lack
exposure.

Smaller scale
folding within NE limb
of B2 syncline @
C. Fontanal.
→ Ant + syn

Fig. A14.

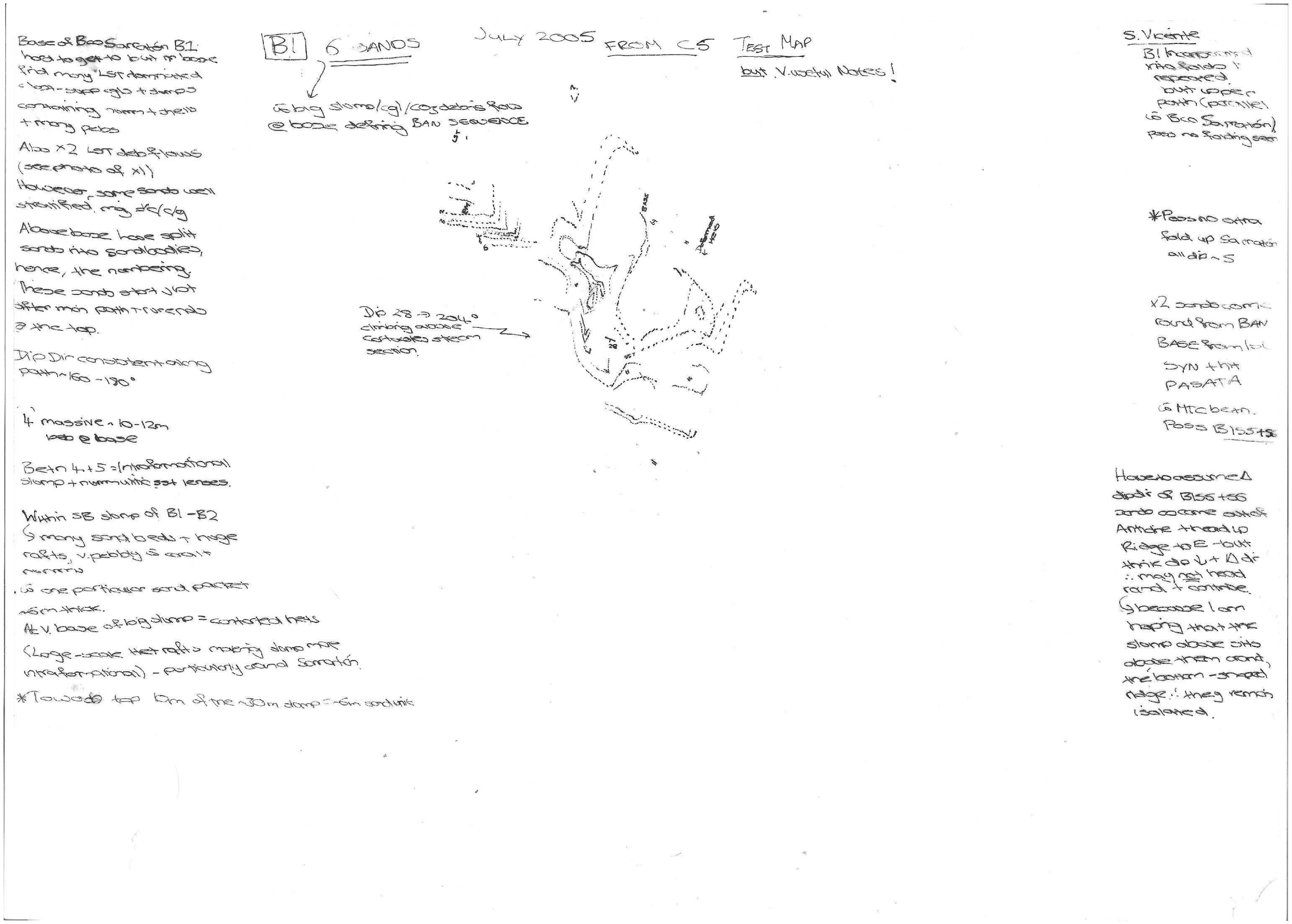

B1 6 BANDS July 2005 FROM C5 TEST MAP
but V.useful Notes!

Base of Bco Sarratón B1
hard to get to but @ base
find many LST dominated
< bdr-size cgls + slumps
containing numm + shells
+ many pebs

Also x2 LST deb flows
(see photo of x1)
However, some sands well
stratified. mg ±c/c/g
Above base have split
sands into sandbodies,
hence, the numbering.
These sands start just
after main path + run ends
@ the top.

Dip Dir consistent along
path ~160 - 180°

4 massive ~ 10-12m
beds @ base

Betn 4 + 5 = Intraformational
slump + nummulitic sst lenses.

Within SB slump of B1 - B2
↳ many sand beds + huge
rafts, v.pebbly & coral +
numms
↳ one particular sand packet
~5m thick.
At v. base of big slump = contorted hets
(Large-scale het rafts ⇒ making slump more
intraformational) - particularly around Sarratón.

*Towards top 10m of the ~30m slump = ~6m sand unit

↳ big slump/cgl/cong debris flow
@ base defining BAN SEQUENCE

Dip 28 → 204°
climbing above
contorted stream
section.

S. Vicente
B1 incorporated
into folds +
repeated.
but upper
path (parallel
↳ Bco Sarratón)
poss no folding seen

*Poss no extra
fold up Sarratón
all dip ~S

x2 sands come
round from BAN
BASE from loc
Syn + hit
PASATA
↳ Mtc bean.
Poss B1SS+SS

Have to assume Δ
dip dir of B1SS + SS
sands occur out of
Anticline + head up
Ridge to E - but
think dip ↓ + Δ dir
∴ may not head
round + continue.
↳ because I am
hoping that the
slump above sits
above them around,
the 'bottom-shaped'
ridge ∴ they remain
isolated.

Fig. A15.

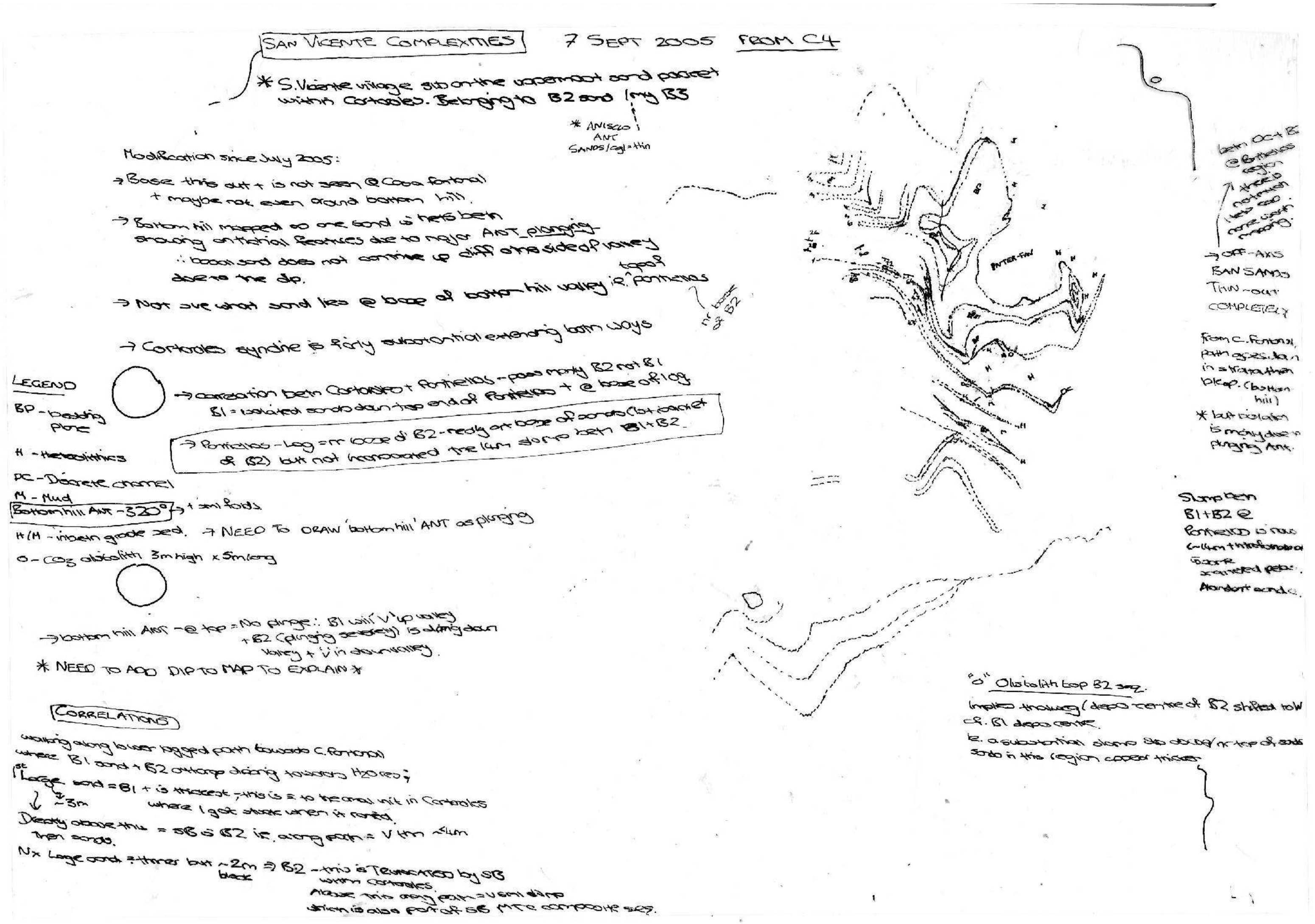

SAN VICENTE COMPLEXITIES 7 SEPT 2005 FROM C4

* S.Vicente village sits on the uppermost sand packet within Cortadas. Belonging to B2 and /my B3

* ANISCO ANT SANDS/cgl = thin

Modification since July 2005:

→ Base this out + is not seen @ Casa fontanal + maybe not even around bottom hill.

→ Bottom hill mapped as one sand is here been showing antiterial features due to major ANT plunging ∴ basal sand does not continue up cliff other side of valley due to the dip.

→ Not sure what sand lies @ base of bottom hill valley i.e. top of Fontanelas
nr base of B2

→ Cortadas syncline is fairly substantial extending both ways

→ correlation betn Cortadas + Fontanelas - poss mostly B2 not B1 + @ base of log
B1 = isolated sands down top end of Fontanelas

→ Fontanelas - Log = nr base of B2 - really at base of sands (1st packet of B2) but not incorporated the 14m slump betn B1 + B2

LEGEND
BP - bedding plane
H - heterolithics
DC - Discrete channel
M - Mud
Bottom hill ANT - 320° → + small folds
H/M - inbetn grade sed.
→ NEED TO DRAW 'bottom hill' ANT as plunging
O - CO3 olistolith 3m high x 5m long

→ bottom hill ANT - @ top = No plunge ∴ B1 will 'V' up valley + B2 (plunging seaward) is along down valley + 'V' in downvalley.

* NEED TO ADD DIP TO MAP TO EXPLAIN *

CORRELATIONS

walking along lower logged path towards C.Fontanal where B1 sand + B2 outcrop dipping towards H2O res;
1st Large sand = B1 + is thickest, this is ≡ to the one unit in Cortadas where I got stuck when it rained. ~3m
Directly above this = SB is B2 i.e. along path = V thin <4m then sands.
Nx Large sand ≈ thinner but ~2m ⇒ B2 - this is TRUNCATED by SB within Cortadas. block
Above this along path = v small slump which is also part of SB in the composite seq.

betn Oct + B2 @ Fontanelas region there is not much less sand more cont mapping.
→ OFF-AXIS BAN SANDS THIN-OUT COMPLETELY

From C.Fontanal, path goes down in stratigraphic order. (bottom hill)
* but isolation is mainly due to plunging Ant.

Slump betn B1 + B2 @ Fontanelas is now c. 14m thick sandy scratched pebs. Abundant sands.

"O" Olistolith top B2 seq.
Implies thrusting (depo centre of B2 shifted to W cf. B1 depo centre.
i.e. a substantial slump has developed nr top of sands sands in this region appear thicker

Fig. A16.

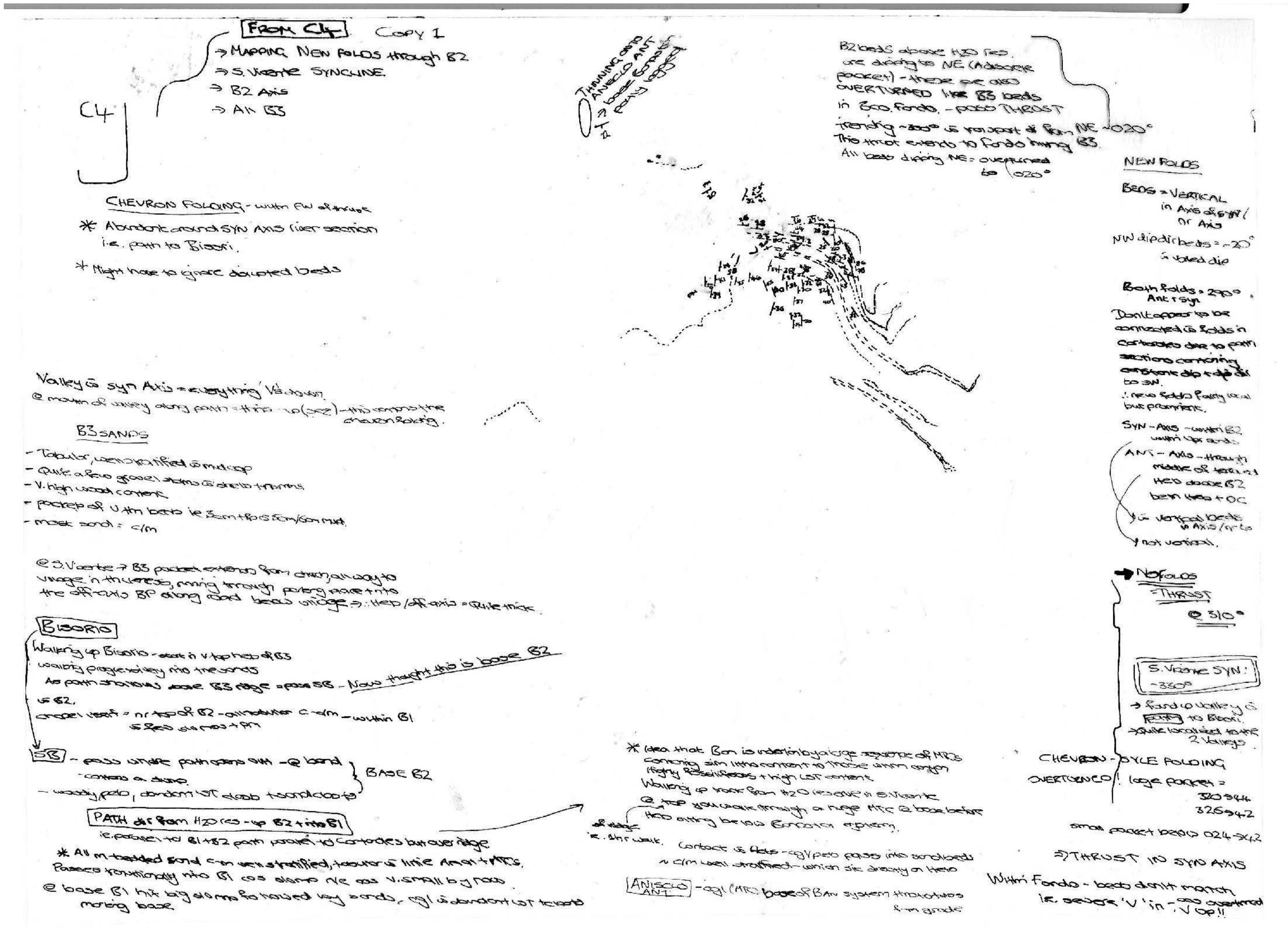

C4

FROM C4 COPY 1

→ MAPPING NEW FOLDS through B2
→ S. Vicente SYNCLINE
→ B2 Axis
→ Ant B3

CHEVRON FOLDING - within FW of thrust

✱ Abundant around SYN AXIS river section i.e. path to Bisorri.

✱ Might have to ignore disrupted beds

Valley = syn Axis = everything 'V's down.
@ mouth of valley along path = thins [illegible] (see) - this confirms the chevron folding.

B3 SANDS

- Tabular, well stratified & mudcap
- Quite a few gravel [illegible] & shells [illegible]
- V. high wood content
- pockets of v thin beds ie 3cm + [illegible] 50cm/60cm mud.
- most sand = c/m

@ S. Vicente → B3 pocket extends from church, all way to village in the trees, running through parking place + into the off-axis BP along road below village ⇒ ∴ Het / off-axis = Quite thick.

BISORRIO

Walking up Bisorrio - start in v. top Het of B3 walking progressively into the sands
As path shallows above B3 ridge = pass SB - Now thought this is base B2 ie B2.
Gravel [illegible] = nr top of B2 - all tabular c-v/m - within B1 [illegible]

SB - pass under path [illegible] - @ band - contains a slump. - woody, pebbly, abundant WT [illegible] + sand clasts } BASE B2

PATH dir from H2O res - up B2 + into B1 ie. parallel to B1+B2 path parallel to Cortondes but over ridge.

✱ All m-bedded sand c-m well stratified, tabular & little Amal + MTCs.
Passes transitionally into B1 as slump [illegible] v. small by now.
@ base B1 hit big slump [illegible] followed by sands, cgl & abundant WT [illegible] marking base.

B2 beds above H2O res. are dipping to NE (Atiart pocket) - these are also OVERTURNED like B3 beds in Eco. Fondo. - [illegible] THRUST trending ~300° is transport dir from NE ~020°
This thrust extends to Fondo [illegible] B3.
All beds dipping NE = overturned to 020°

NEW FOLDS

BEDS = VERTICAL in Axis of syn / nr Axis
NW dip dir beds = ~20° [illegible] dip

Both folds = 290° Ant + Syn
Don't appear to be connected to folds in Cortondes due to path sections containing constant dip + dip dir to SW.
∴ new folds fairly local but prominent.

SYN - AXIS - within B2 within upr sands
ANT - Axis - through middle of vertical Het above B2 betw Het + OC
→ vertical beds in Axis / nr to
→ not vertical.

→ NO FOLDS = THRUST @ 310°

S. Vicente SYN: ~330°

→ found in Valley & PATH to Bisorri.
→ Quite localised to the 2 Valleys.

CHEVRON - STYLE FOLDING OVERTURNED! large pocket = 320 344 326 342
small pocket below 024 342
⇒ THRUST in SYN AXIS

Within Fondo - beds don't match ie. severe 'V' in - [illegible] overturned V OP!!

✱ Idea that Ban is underlain by a large [illegible] of MTCs containing sim litho content to those within canyon
Highly fossiliferous + high WT content
Walking up track from H2O reservoir in S. Vicente
@ top you walk through a huge MTC @ base before Het sitting below Escanilla system.
of ridge ie. 1hr walk.
Contact to Hets - cgl / pebbly pass into sand beds ~ c/m well stratified - which sit directly on Hets

ANISCLO ANT - cgl (MTC) base of Ban system throughout fining up grade

Fig. A17.

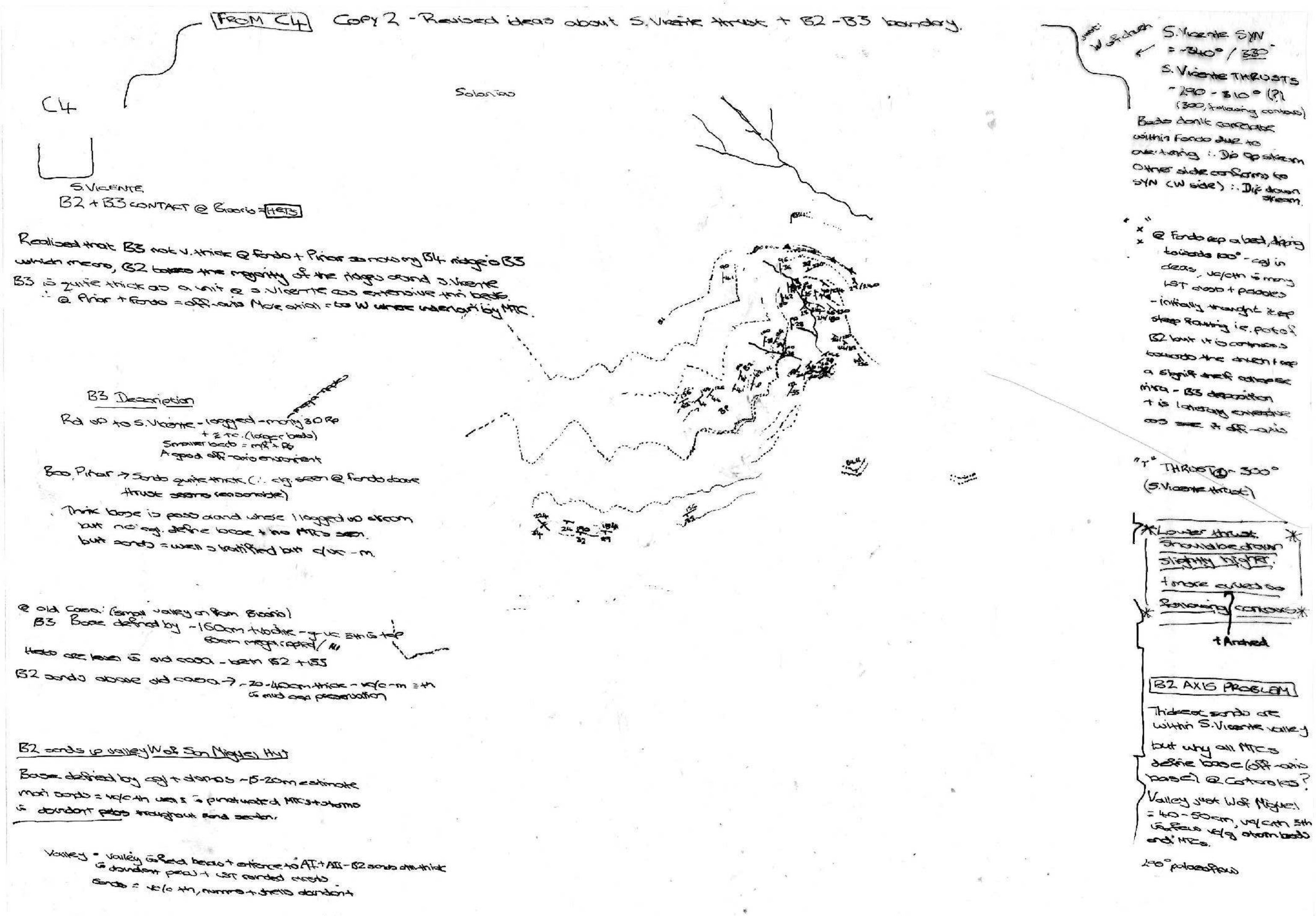

FROM C4 Copy 2 - Revised ideas about S.Vicente thrust + B2-B3 boundary.

C4

S.VICENTE
B2 + B3 CONTACT @ Bioario = HETS

Solanias

Realised that B3 not v. thick @ Fondo + Pinar as now my B4 ridge is B3 which means, B2 takes the majority of the ridges around S.Vicente
B3 is quite thick as a unit @ S.Vicente as extensive thin beds.
∴ @ Pinar + Fondo = off-axis More axial = to W where underlain by MTC.

B3 Description

Rd up to S.Vicente - logged - mainly 30 Fp + 2 Tc. (larger beds)
Smaller beds = mP + Fb
A good off-axis environment

Bco. Pinar → Sands quite thick (∴ cgl seen @ Fondo above thrust seems reasonable)

Think base is poss around where I logged up stream but no cgl. define base + no MTCs seen. but sands = well stratified but c/vc - m.

@ old Casa: (small valley on from Bioario)
B3 Base defined by ~160cm thick - g-vc [illegible] 80cm mega rippled / [illegible]
Hets are lower [illegible] old casa - betw B2 + B3
B2 sands above old casa → ~20-400cm thick - vc/c-m [illegible] mud [illegible] preservation

B2 sands up valley W of San Miguel Hut

Base defined by cgl + slumps ~15-20m estimate
main sands = vc/c-th [illegible] punctuated MTCs + slumps
& abundant pebbles throughout sand section.

Valley = valley [illegible] beds + entrance to AI + AII - B2 sands [illegible] thick
& abundant pebbles + LST rounded clasts
Sands = vc/c th, nummulites + shells abundant

W of church

S.Vicente SYN
= ~340° / 330°
S.Vicente THRUSTS
~290 - 310° (?)
(300, following contours)
Beds don't correlate within Fondo due to overturning ∴ Dip up stream
Other side conforms to SYN (W side) ∴ Dip down stream.

@ Fondo exp a bed, dipping towards 100° - cgl in clasts, vc/cth is many LST clasts + pebbles
- initially thought it [illegible] steep flowing i.e. part of B2 but it is continuous towards the church + [illegible] a signif [illegible] change [illegible] - B3 deposition + is laterally extensive [illegible] off-axis

"T" THRUST ① ~300°
(S.Vicente thrust)

Lower thrust should be drawn slightly higher, + more curved so following contours
+ Arched

B2 AXIS PROBLEM

Thickest sands are within S.Vicente valley but why all MTCs define base (off-axis base) @ Cortoracas?
Valley just W of Miguel = 40-50cm, vc/cth [illegible] vc/g [illegible] beds and MTCs.

290° palaeoflow

Fig. A18.

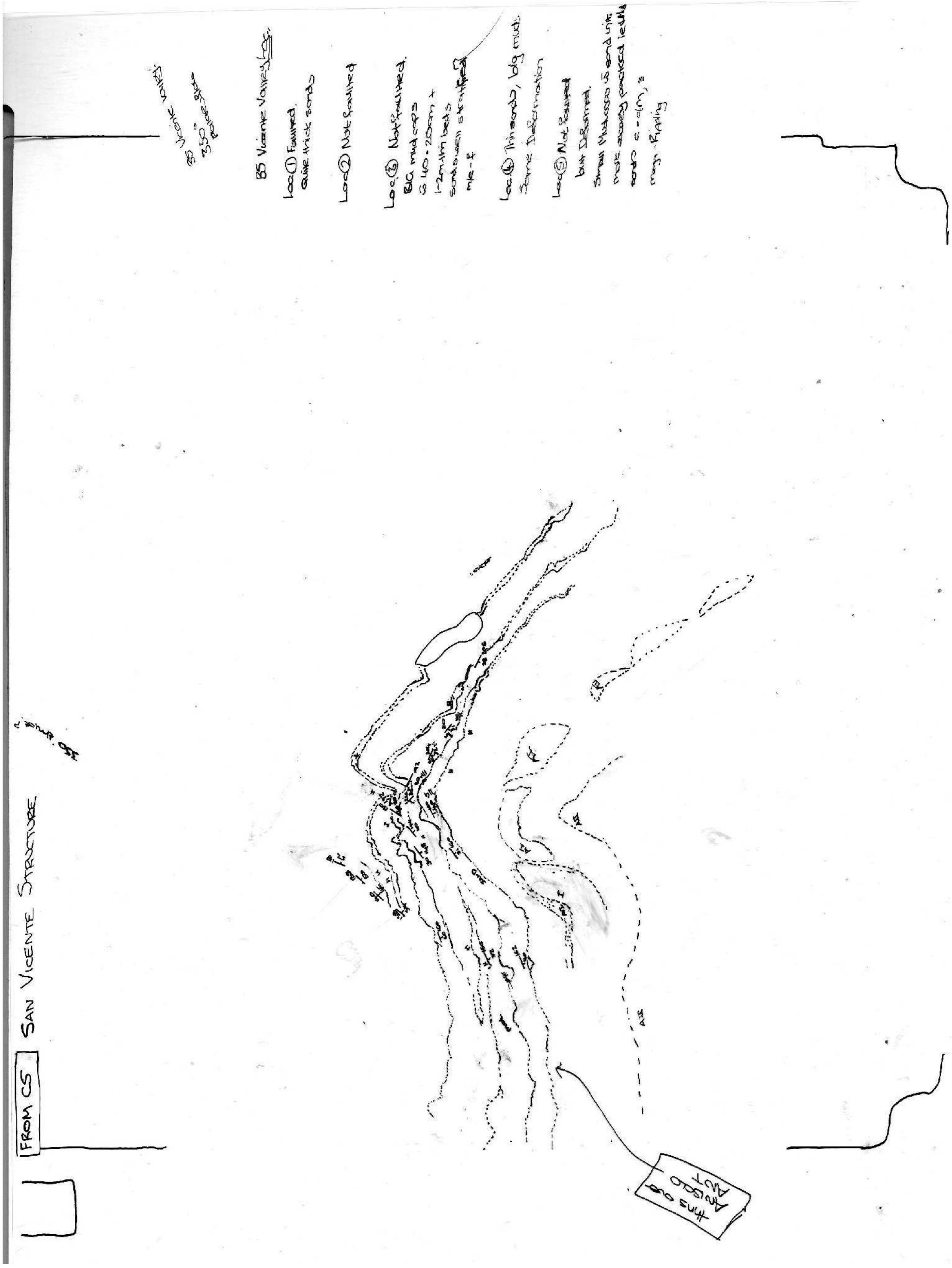
FROM CS
SAN VICENTE STRUCTURE
35° dip 8
35 Vicente Valleys;
350° bedding plane
BS Vicente Valleys Loc.
Loc ① Faulted. Quite thick sands
Loc ② Not faulted
Loc ③ Not faulted. Big mud caps is 40-20cm + 1-2m thin beds sands well stratified m/e-f
Loc ④ Thin sands, big muds. Some Deformation
Loc ⑤ Not faulted but Deformed. Small Mudcaps is sand unit. most closely packed ie(4) sands c-cm, 3 mass Rippling
AXIS
this one AXIS of ANT

Fig. A19.

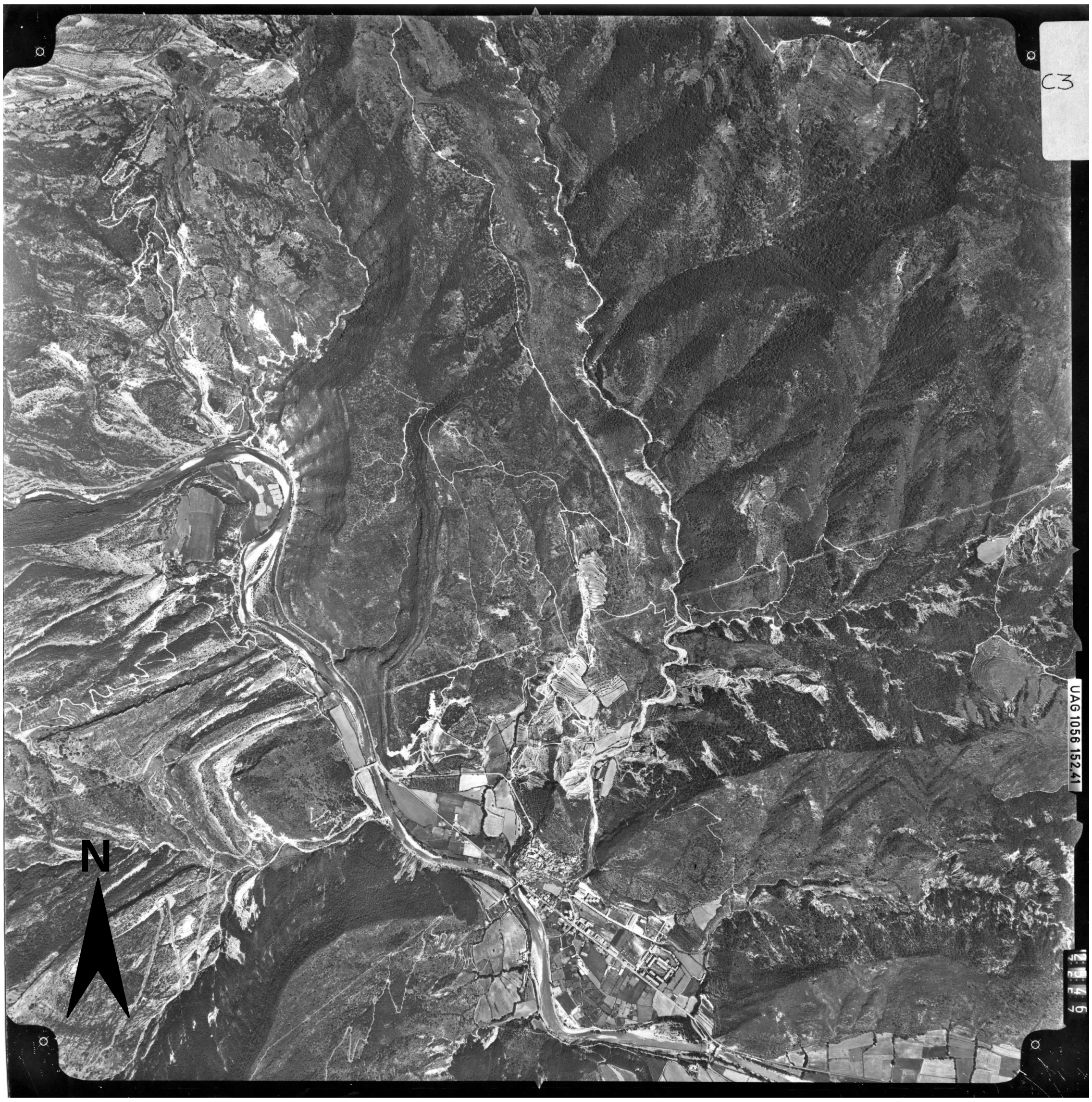

Fig. A20.

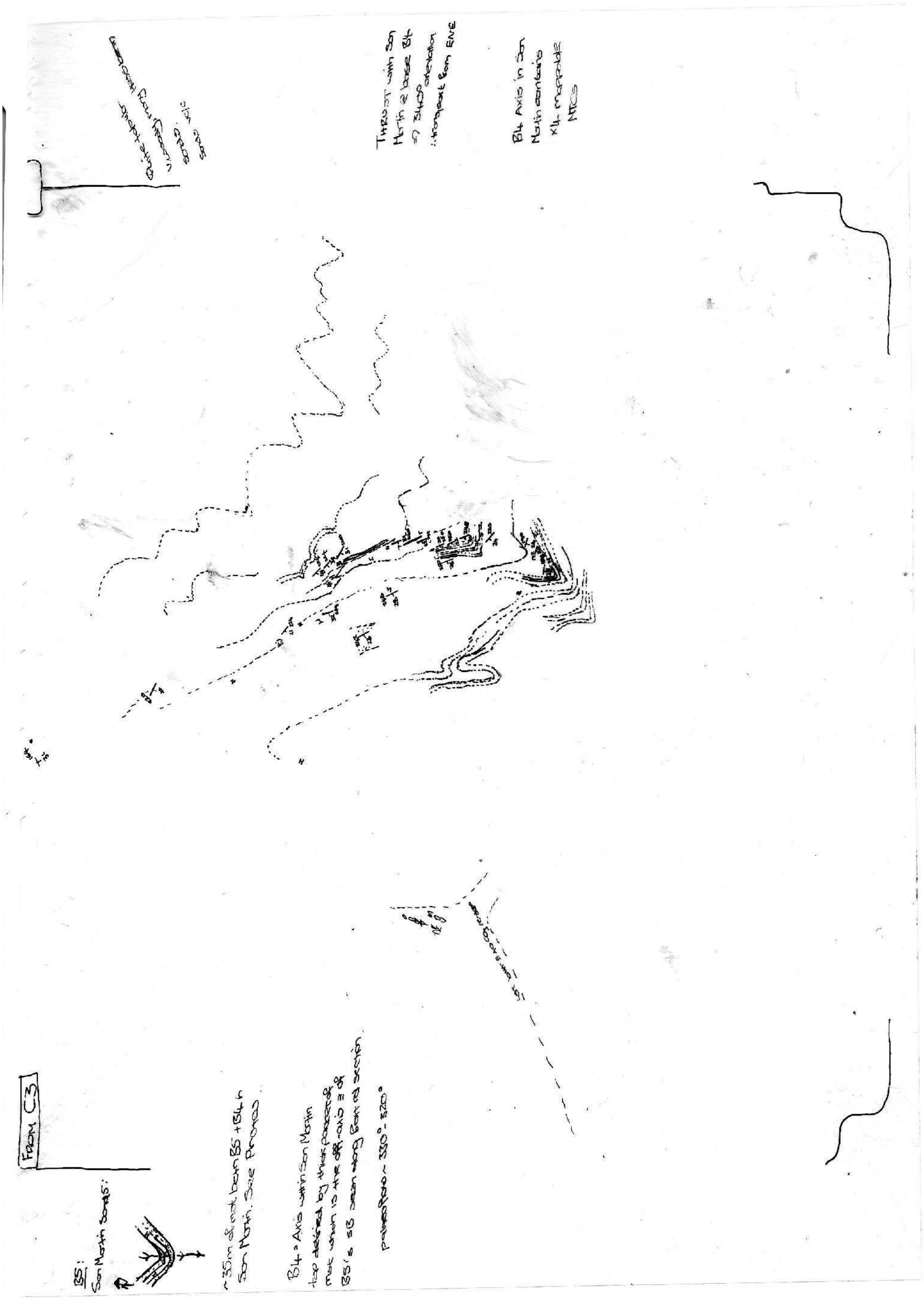
FROM C3
B5:
San Martin sands:
~35m of mat betn B5 + B4 in
San Martin. See Photos
B4 = Axis within San Martin
top defined by thick packet of
mat which is the off-axis ≡ of
B5's SB seen along Barranco section
palaeoflow ~ 330° - 320°
Quite tabular
v. woody, many
sands.
Sands vc/c
THRUST with San
Martin @ base B4
=> 340° orientation
∴ transport from ENE
B4 Axis in San
Martin contains
x4 mappable
MTCs

Fig. A21.

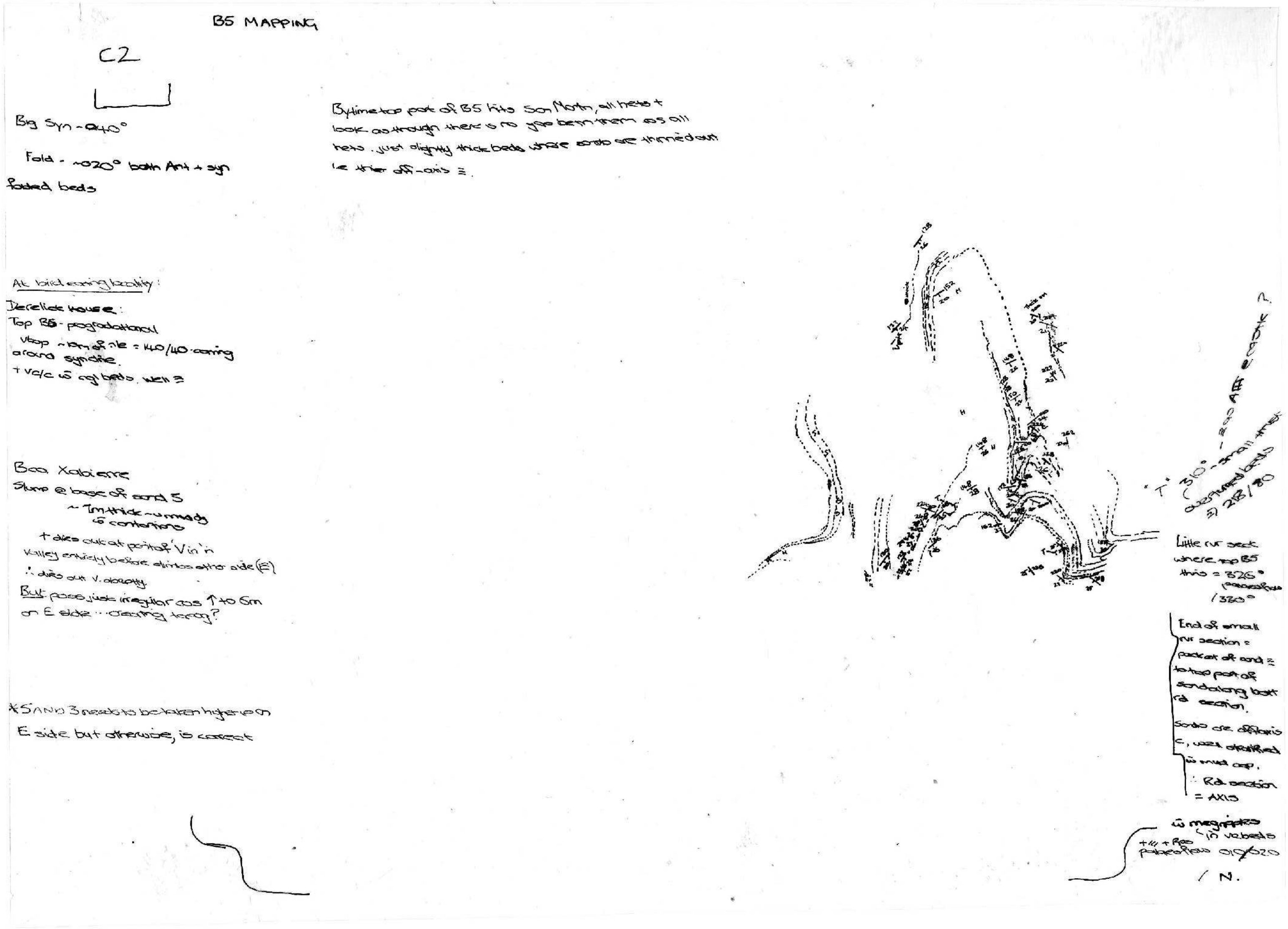

B5 MAPPING

C2

Big Syn - ~040°

Fold - ~020° both Ant + syn
folded beds

By time top part of B5 hits San Martin, all hets +
look as though there is no gap betw them as all
hets. just slightly thick beds where sands are thinned out
ie thier off-axis ≡.

At bird-eating locality:

Derelict house:
Top B5 - progradational
vtop ~1m of sle = 140/40 - coming
around syncline.
+ vc/c w̄ cgl beds, well ≡

Boo. Xabierre
Slump @ base of sand 5
~7m thick - unmag
w̄ contortions
+ dies out at point of 'V' in
valley entirely before climbs other side (E)
∴ dies out v. abruptly.
But poss just irregular as ↑ to 6m
on E side ∴ creating topog?

*5 AND 3 needs to be taken higher ie on
E side but otherwise, is correct

"T" 310° - small thrust
(overturned beds
⇒ 218/80
- 300 A[illegible] [illegible]

Little riv sect
where top B5
thins = 326°
palaeoflow
/ 330°

End of small
riv section =
packet of sand ≡
to top part of
sand along bott
rd section.
Sands are off axis
C, well stratified
w̄ mud cap.
∴ Rd. section
= AXIS

w̄ megaripples
in v.beds
+ III + Res
palaeoflow 010/020

/ N.

Fig. A22.

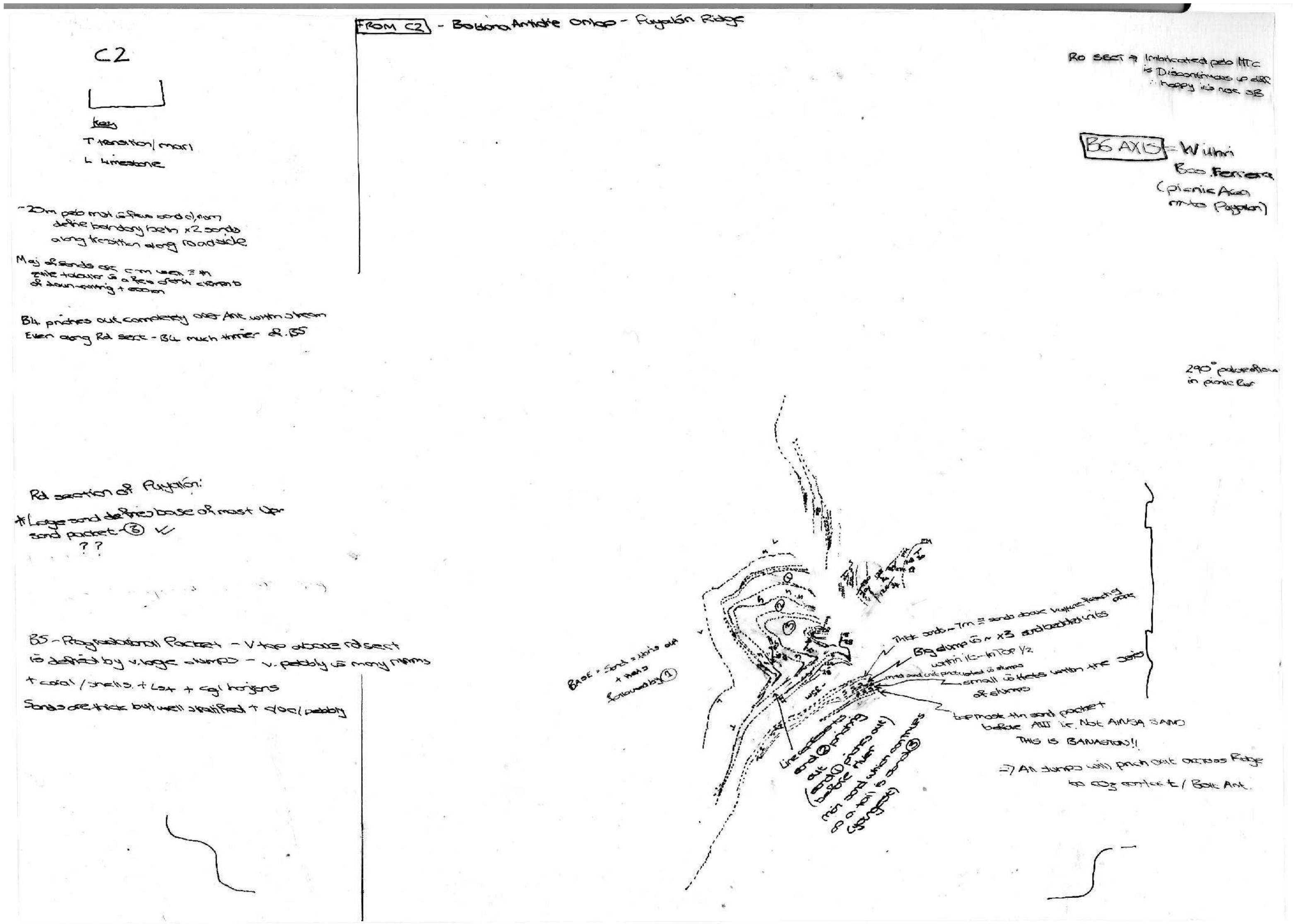

C2

Key
T transition / marl
L limestone

~20m pebb mat (& few sand cl, nom) define boundary betw x2 sands along transition along roadside

Maj of sands occ c-m [illegible] pale to [illegible] a few of th [illegible] elements of down-cutting + erosion

B4 pinches out completely over Ant within stream
Even along Rd sect - B4 much thinner & B5

Rd section of Puyalón:
* Large sand defines base of most Upr sand packet - ③ ✓
??

B5 - Progradational Packet - V top above rd sect is defined by v. large slumps - v. pebbly w many [illegible]
+ coral / shells + Lst + cgl horizons
Sands are thick but well stratified + v.c. / pebbly

FROM C2 - Boltaña Anticline Onlap - Puyalón Ridge

Ro sect ∴ Imbricated pebb MTC is Discontinuous w diff ∴ happy it's not SB

B6 AXIS = Within Bco. Ferrera (picnic Area onto Puyalón)

290° palaeoflow in picnic Bar

Thick sands ~7m ≡ sands above Vulture feeding area
Big slump is ~ x3 and bedded units within it - in top 1/2
med sand unit punctuated w slumps
small w [illegible] within the series of slumps
top most thin sand packet before AIII i.e. Not AINSA SAND
THIS IS BANASTON!!
⇒ All slumps will pinch out across Ridge to occ contact / Bolt. Ant.

BASE = Sand = thins out + thens followed by ①

Line of contacts sand ② pinching out (sand ① pinches out before river) thin sand which continues as a tail is sand ③ (Banastón)

Fig. A23.

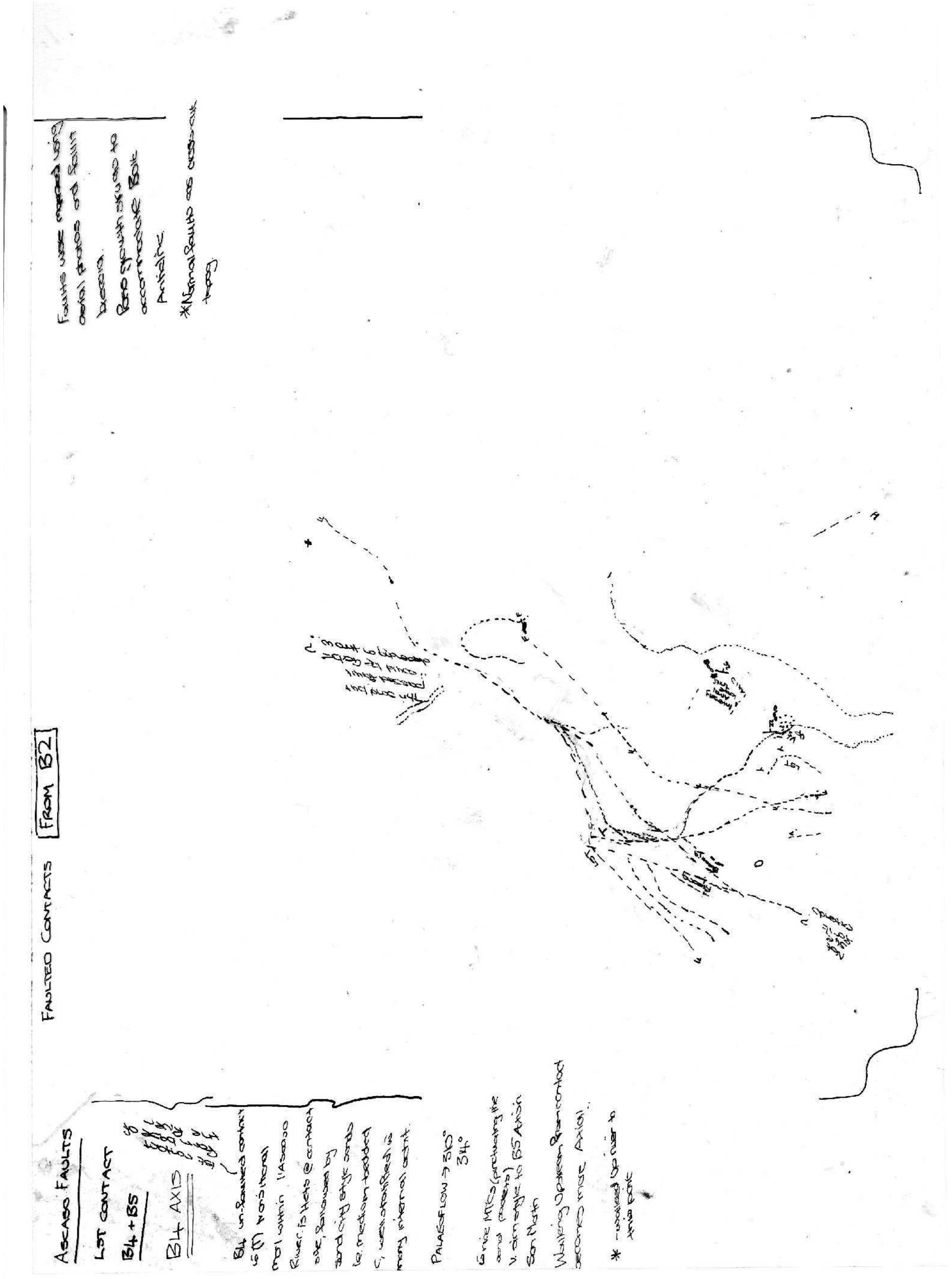

B4 un-faulted contact is (?) transitional marl within l'Ascaso River. Fs Hets @ contact ok, followed by sand city style sands ie. medium-bedded c, well stratified w many internal amalg.

PALAEOFLOW → 310°
34°

Some nice MTCs (punctuating the sand packets)
V. sim style to B5 Axis in San Martin

Walking Upstream from contact becomes more Axial.

* - walked up river to this point

Faults were mapped using aerial photos and fault breccia.
Paso growth strata to accommodate Bolt Anticline.

*Normal faults as cross-cut topog.

Fig. A24.

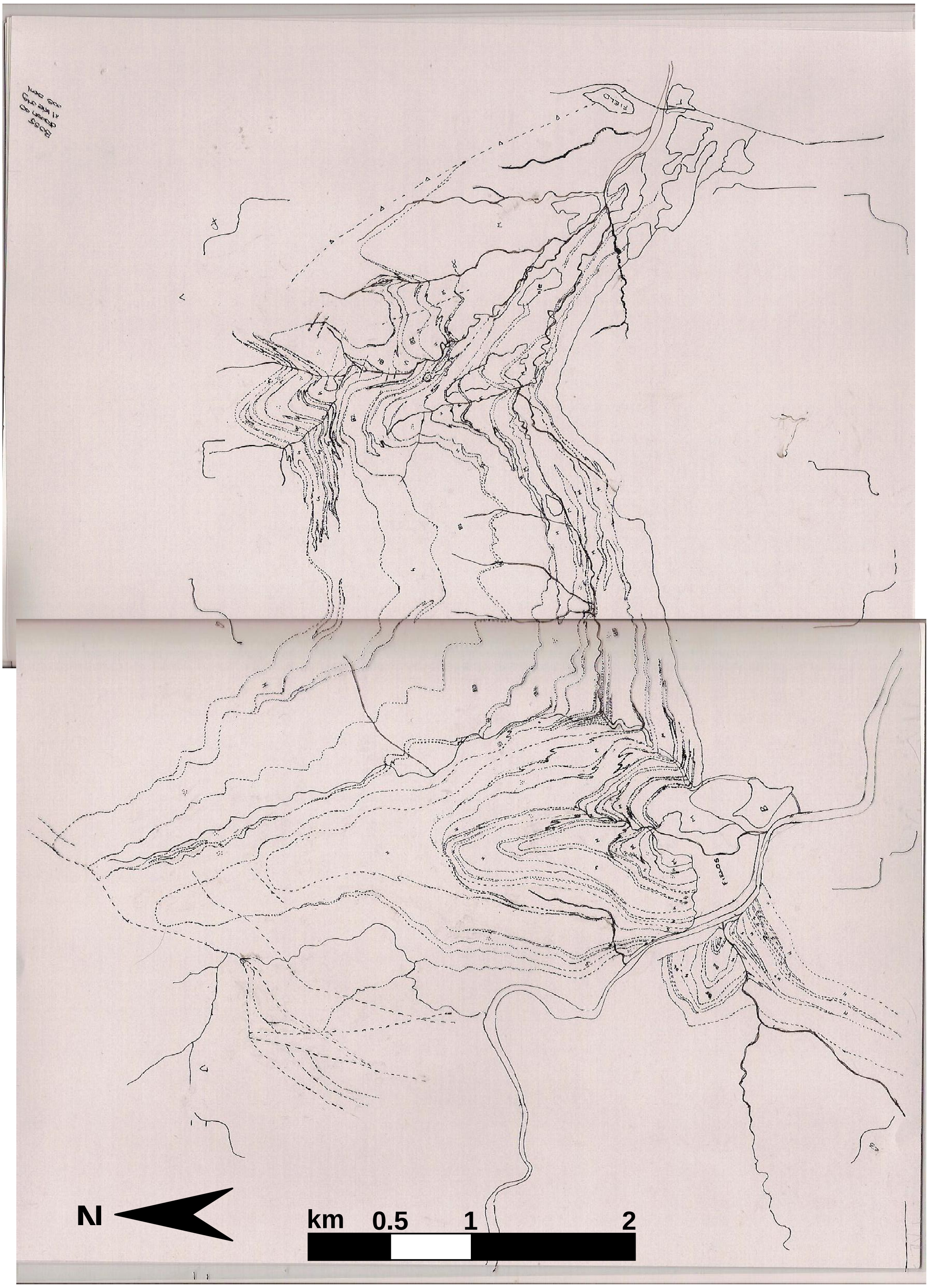

Fig. A25.

M	Mud	- △ - △ - △ -	Thrust fault
∿	Contorted sediment	—◇—	Anticline
——	Lithological contact	- - ⧖ - - - ⧖ - - -	Syncline
- - - - - - -	Uncertain / inferred lithological contact		

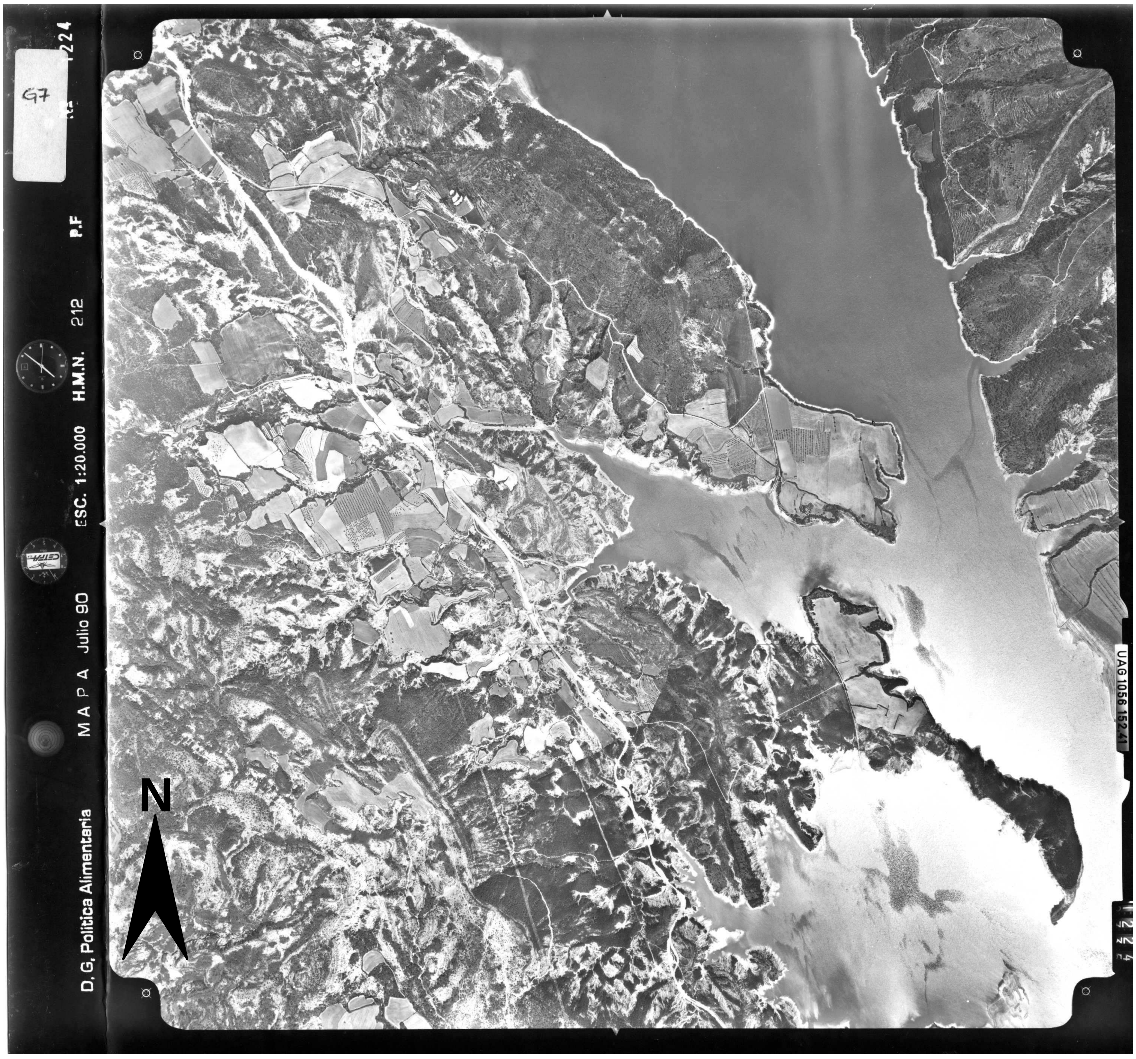
G7
1224
P.F
H.M.N. 212
ESC. 1:20.000
M A P A Julio 90
D.G. Politica Alimentaria
N
UAG 1056 152.41
1224

Fig. A26.

km 0.5 1 2

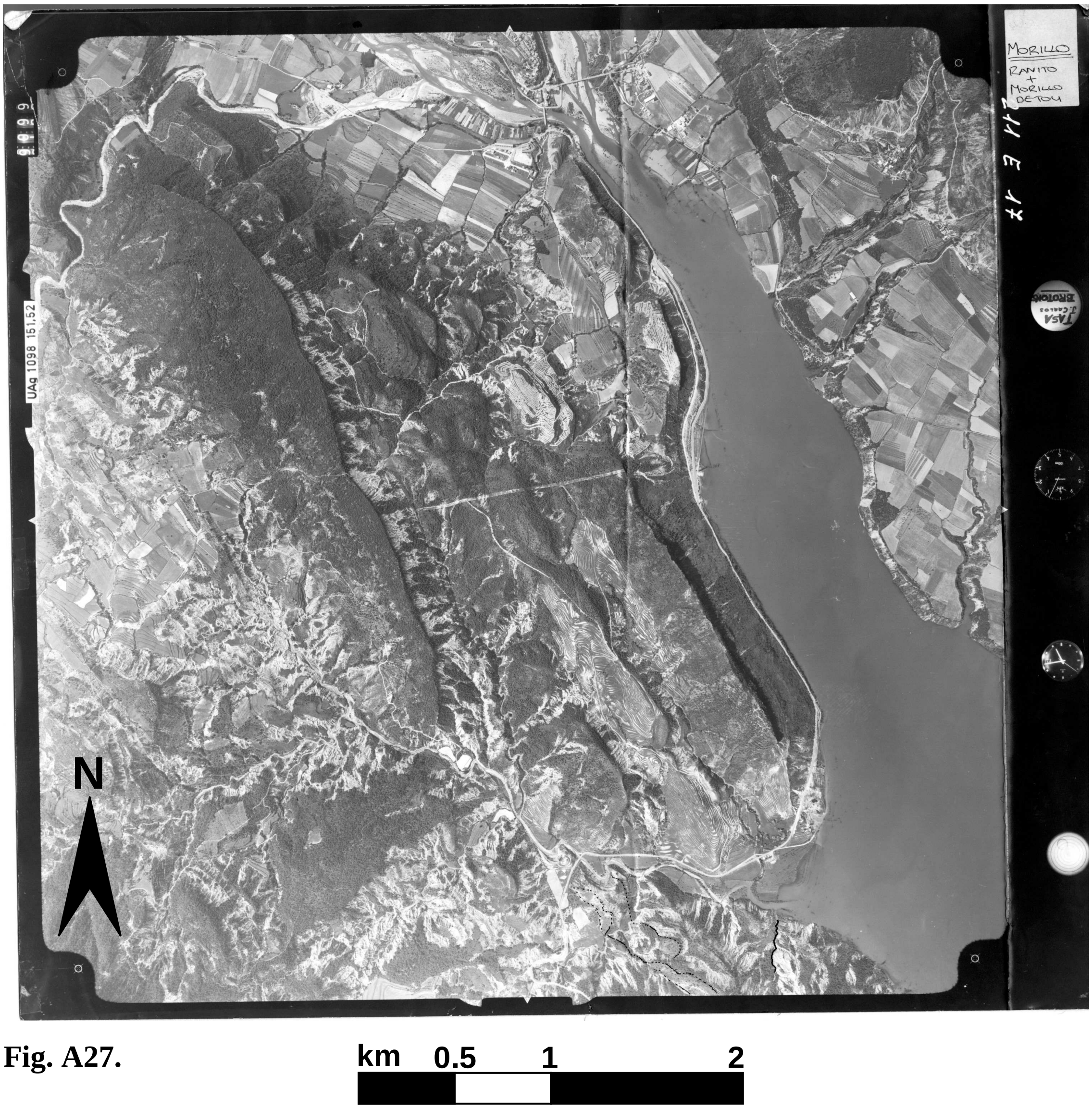
MORILLO
RANITO
+
MORILLO
DE TOU
211 E 17
TASA
J. Carlos
BROTONS
UAg 1098 151,52
N
km
0.5
1
2

Fig. A27.

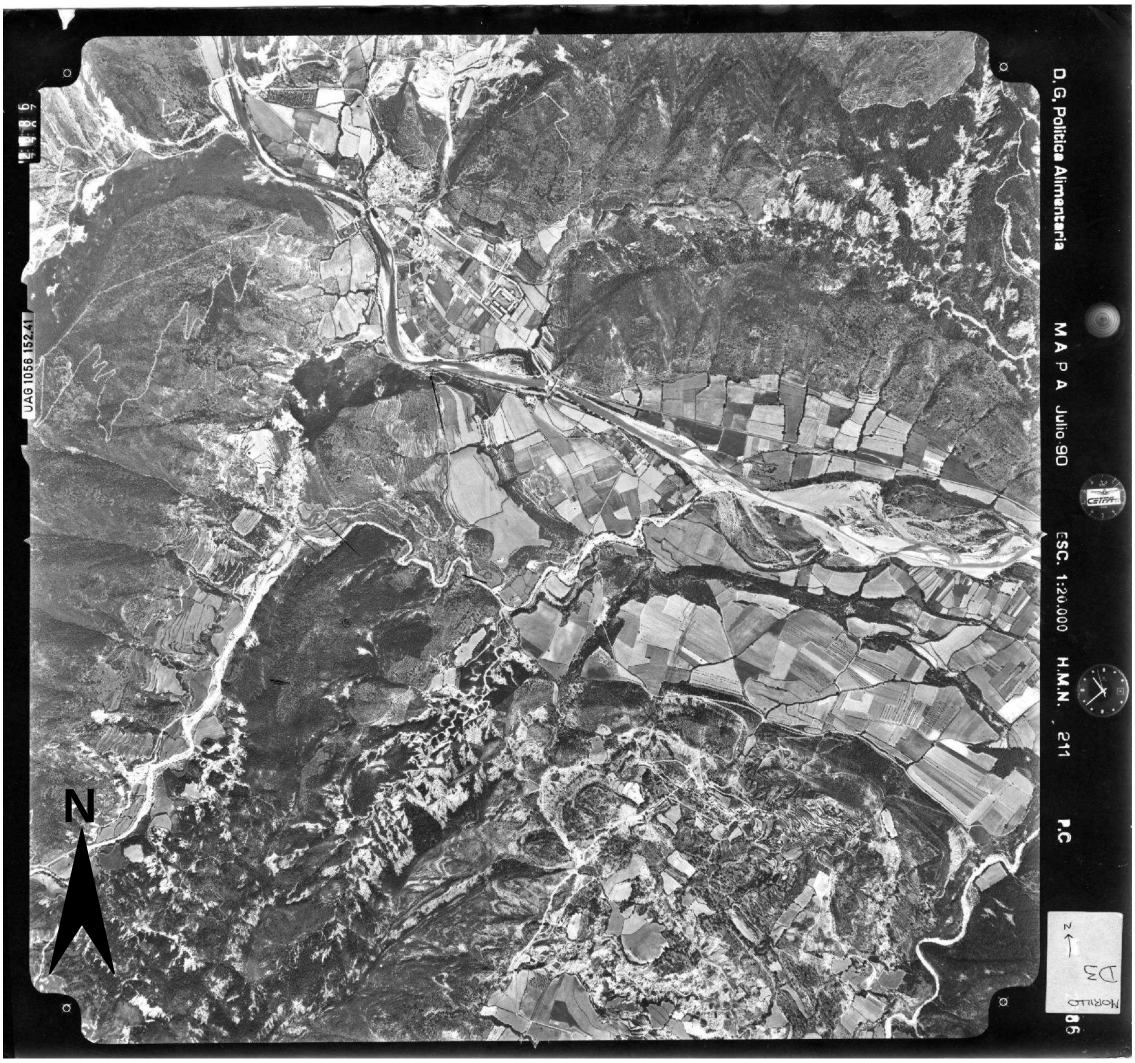
D.G. Politica Alimentaria
M A P A Julio 90
ESC. 1:20.000 H.M.N. 211
P.C
UAG 1056 152.41
N
D3
MORILLO
km 0.5 1 2

Fig. A28.

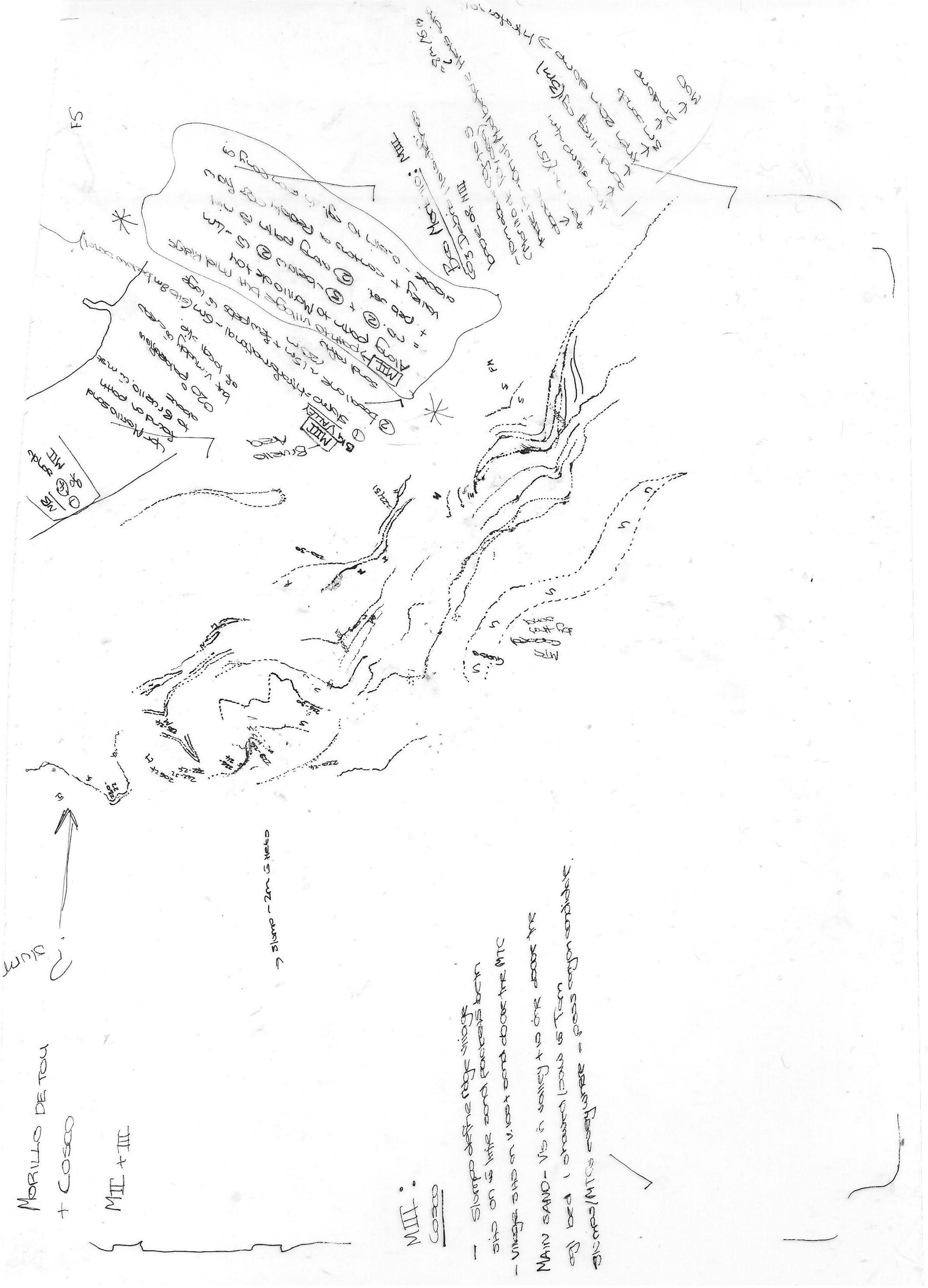

Fig. A29.

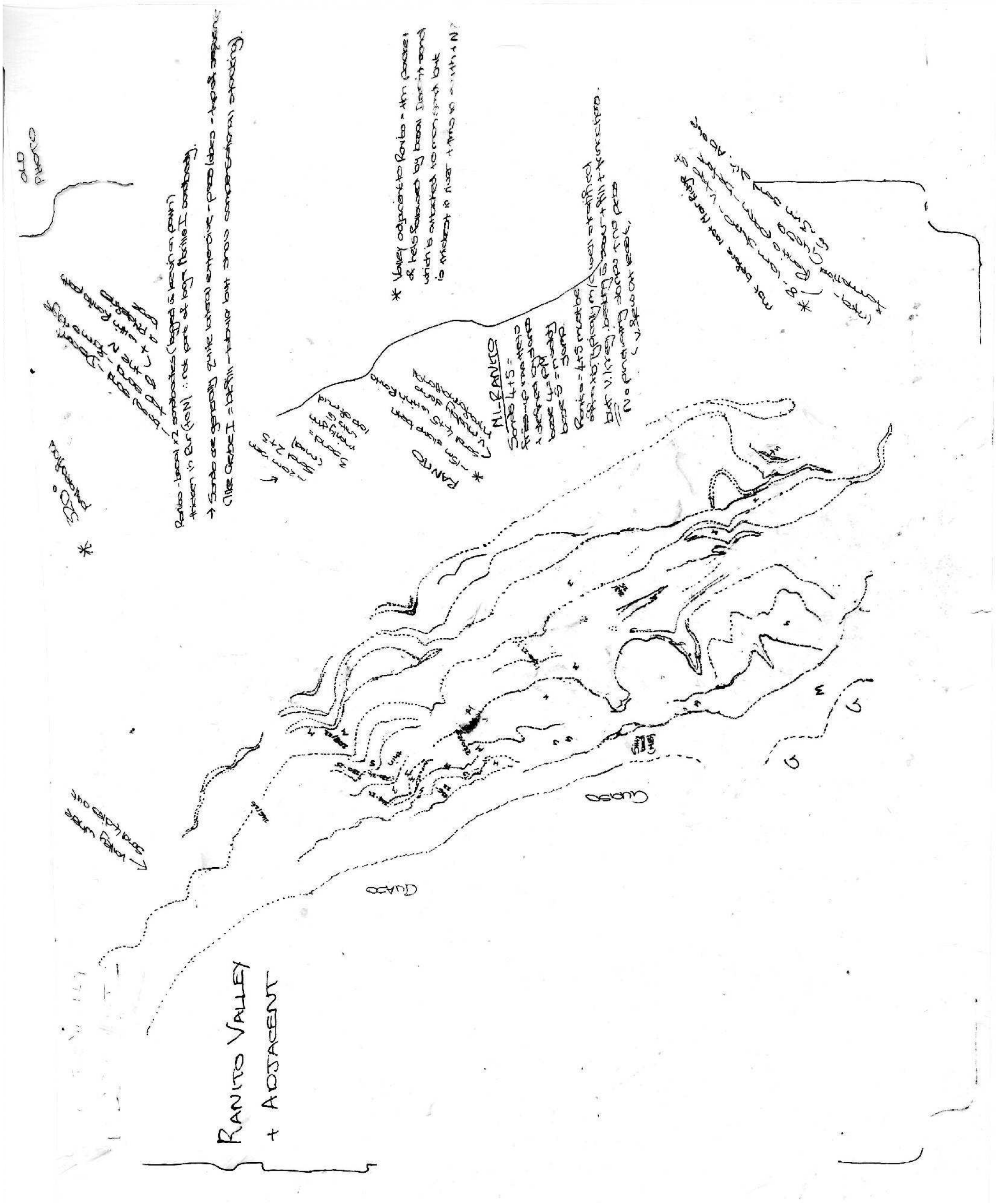
RANITO VALLEY
+ ADJACENT
OLD PHOTO
* 320° palaeoflow
– basal sand – Doesn't
top sand – forms ridge
to the N
↳ + with Ranito part
a pebbly
base
Ranito – basal ×2 sandbodies (logged & kevin on pown) thicken in Bur (to N) ∴ not part of logs Rotillo I sandbody.
→ Sands are generally quite lateral extensive – poss lobes – top of sequence (like Gebe I = bk fill – tabular but show compensational stacking).
↓ ~20m of sand 2+3 (mud)
3 sand = mainly thin units & lots of mud
RANITO
* ~15m sharp base sand 4+5 within Ranito (v. muddy sand transformational
MI-RANITO
Sands 4+5 = fines-up matrix + defined by sands
base 4 = PM
base 5 = muddy sand.
Ranito = 4+5 must be offshore typically m/c well stratified but v. irreg. bedding & scour + fill + truncation.
No pinching sands + no pebs (v. few at least,
* Valley adjacent to Ranito = thin pockets & hets followed by basal [illegible] sand which is attached to main sand but is thickest in river + thins to south + N?
mst before last Mar Ridge of
* 8–10m thick – v. top of
(Ranito form – before
Interp – formation Guasa
~3m sand dir. Above
Valley where sand kicks out
Guado
Guado
G
M
G

Fig. A30.

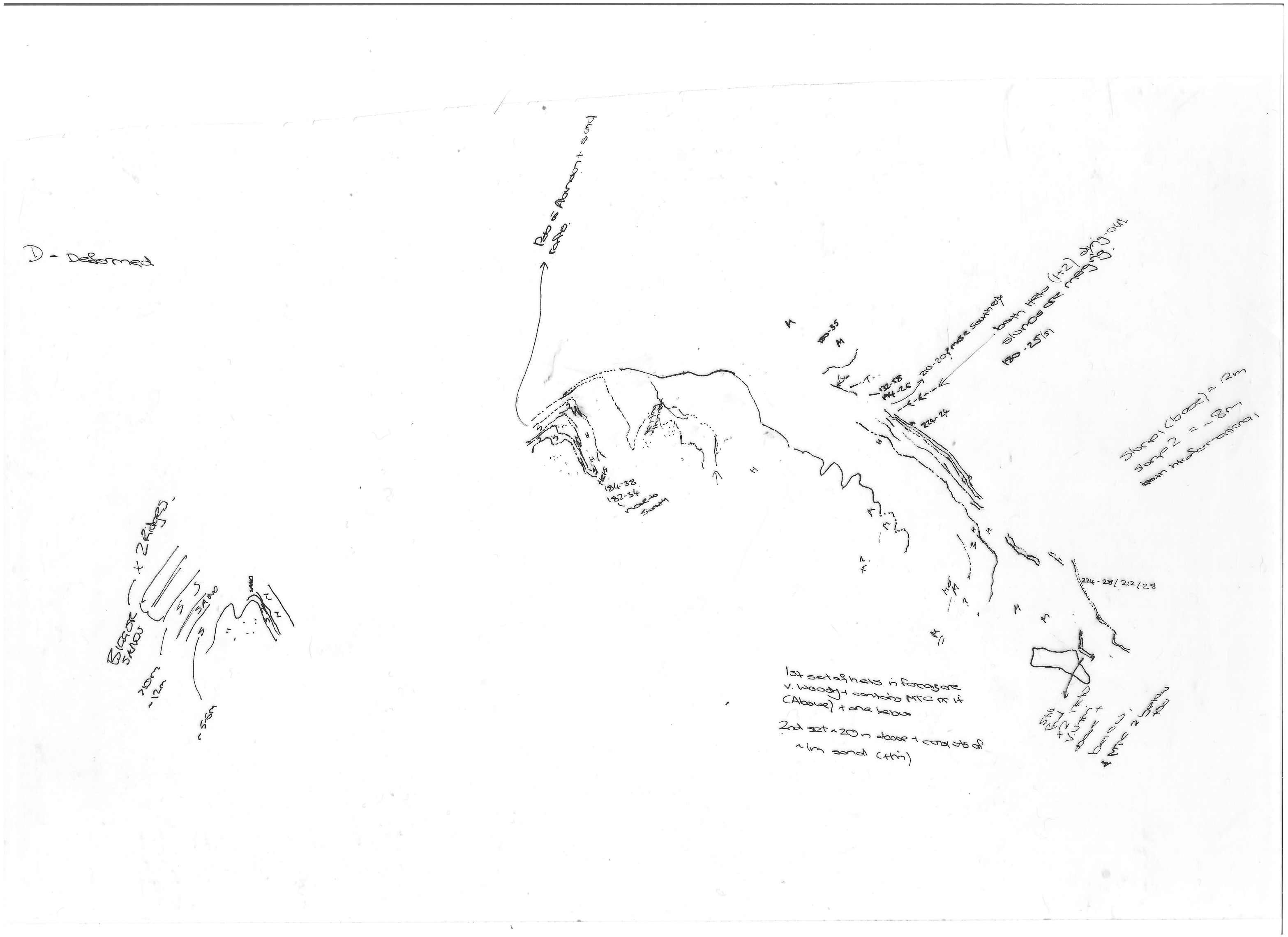
D - Deformed
Rip is Abandon + sand
cuts.
M
180-35
M
132-58
144-26
210-20? more southerly
both HETs (1+2) dying out
slumps are merging.
180-25(s)
224-24
Slump 1 (base) = 12m
slump 2 = ~8m
both intraformational
H
M
184-38
182-34
more to South
224-28/212/28
M
1st set of HETs in foreground
v. woody + contains MTC on it
(Above) + one below
2nd set ~20 m above + consists of
~1m sand (thin)
Bigger sands
+ 2 Ridges.
S
SAND
~10m
~12m
~5-6m
H

Fig. A31.

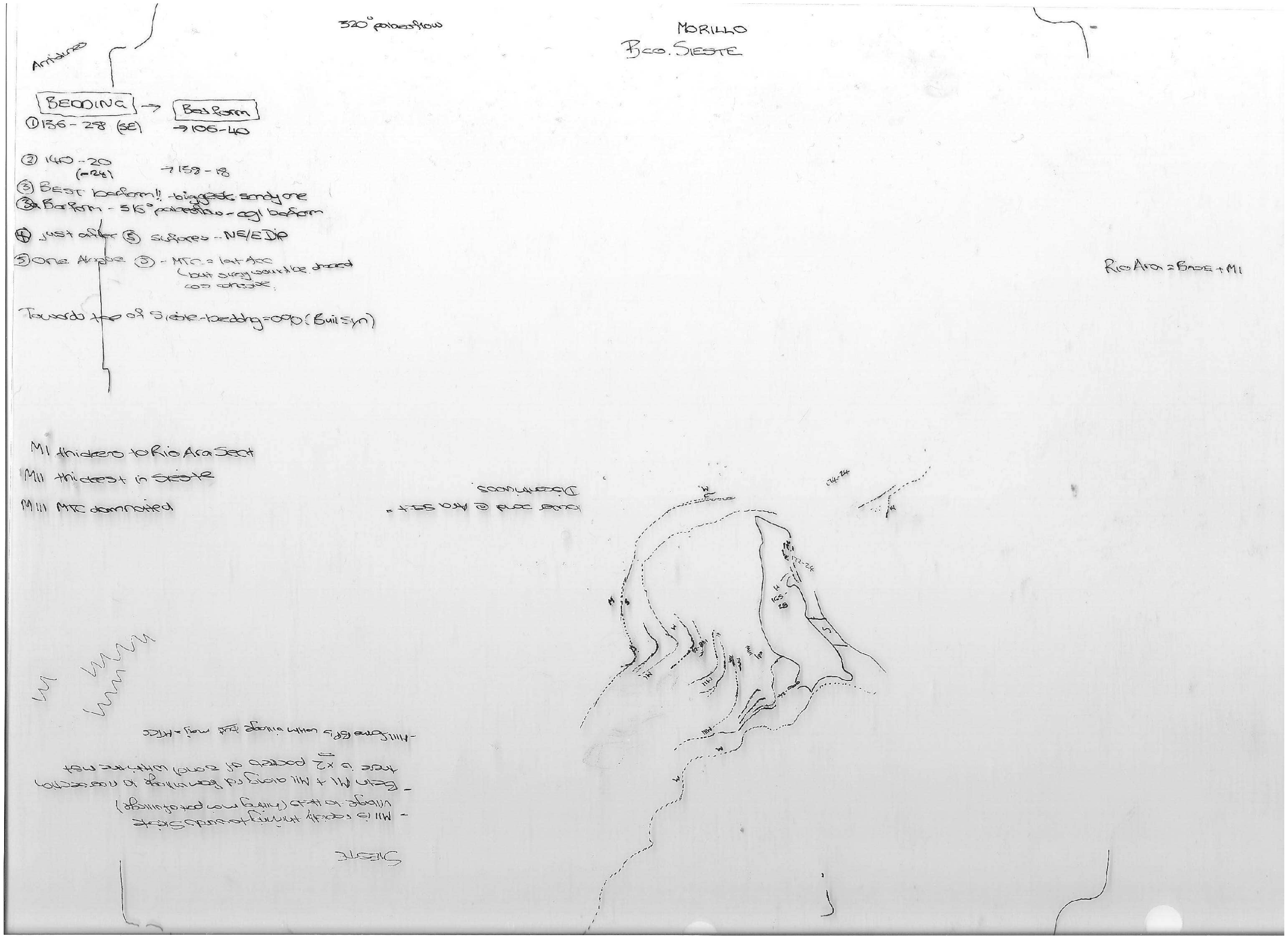

MORILLO
Bco. SIESTE

320° palaeoflow

Arridures

BEDDING → Bedform
① 136 - 28 (SE) → 106-40

② 140 - 20 (=24) → 158 - 18

③ BEST bedform!! - biggest sandy one
③a Bedform - 316° palaeoflow - cgl bedform

④ just after ⑤ surfaces - NE/E Dip

⑤ One Above ⑤ - MTC = lat Acc
(but surely would be draped cos cohesive.

Towards top of Sieste - bedding = 090 (Buil Syn)

Rio Ara = Base + MI

MI thickens to Rio Ara Sect
MII thickest in Sieste
MIII MTC dominated

Discontinuous
basal sand @ Ara Sect. =

SIESTE
- MII is rapidly thinning towards Sieste village to the (hitting main part of village)
- Betn MI + MII along rd from village to river section there is x2 pockets of sand within the mst
- MIII some BPs within village but maj = MTCs

Fig. A32.

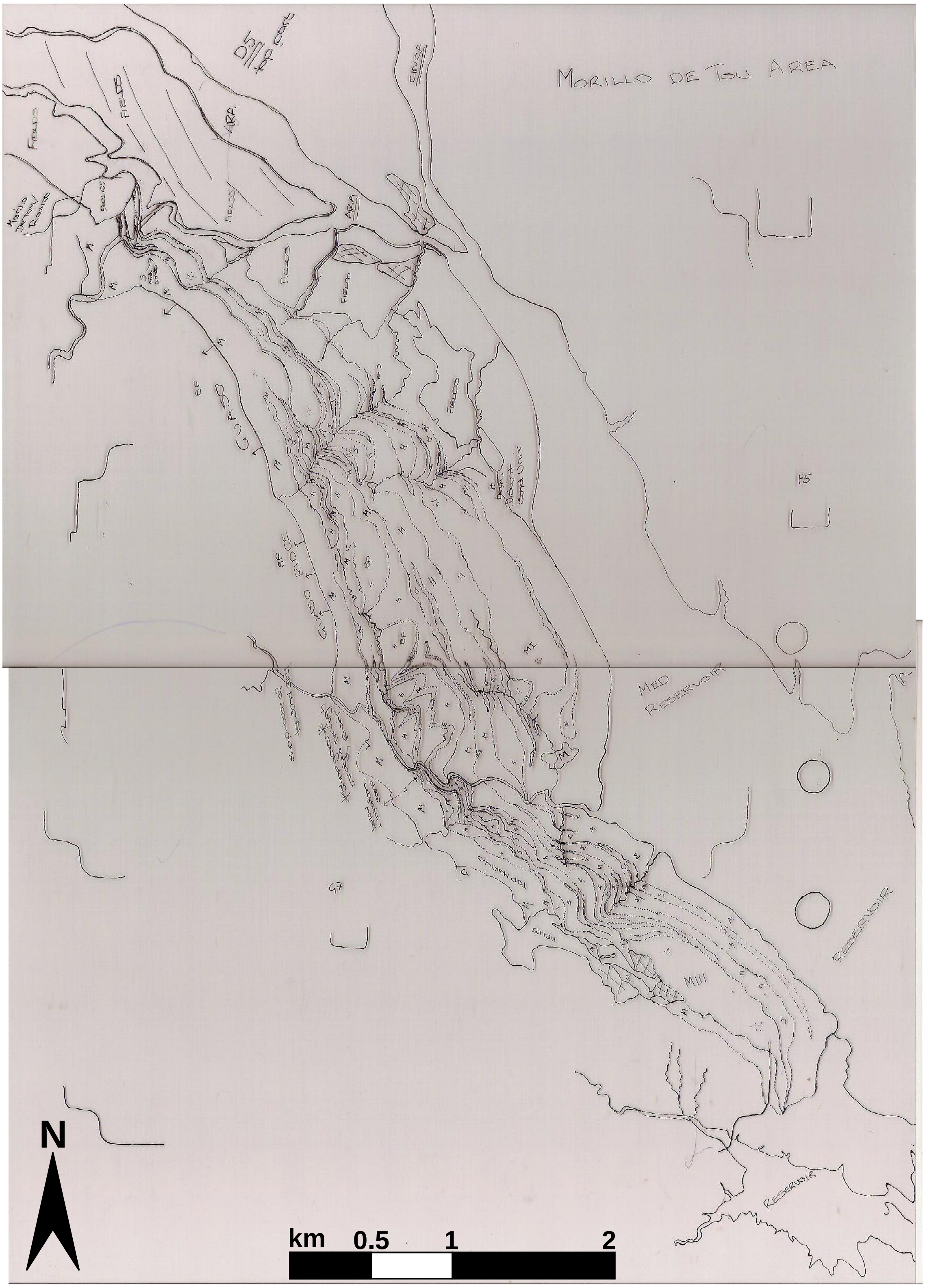

Fig. A33.

M	Mud	-△-△-△-	Thrust fault
∿	Contorted sediment	—◇—	Anticline
———	Lithological contact	--⧖---⧖---	Syncline
-------	Uncertain / inferred lithological contact		

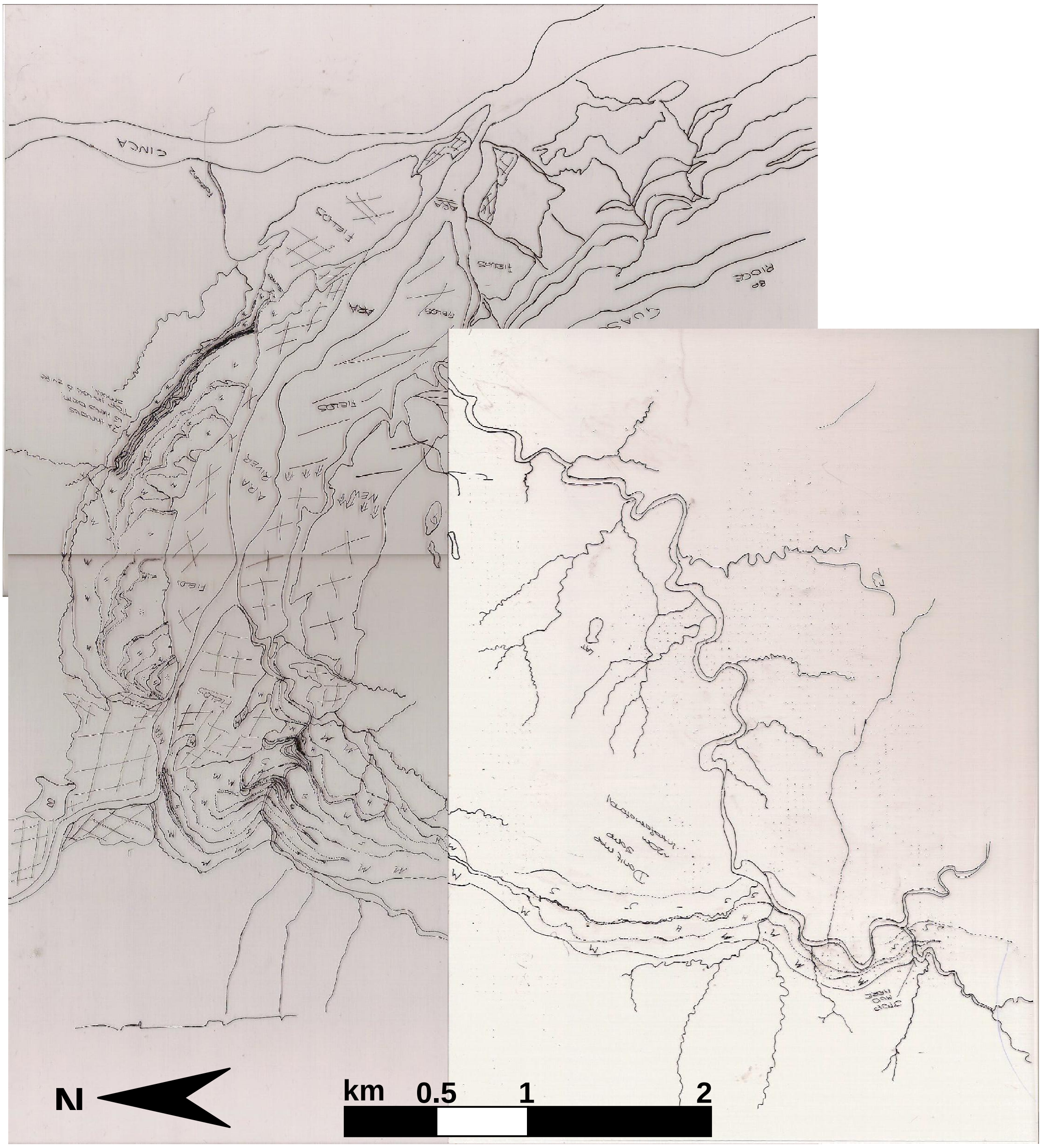

Fig. A34.

M	Mud	-△-△-△-	Thrust fault
∿	Contorted sediment	—◇—	Anticline
———	Lithological contact	--⧗---⧗---	Syncline
- - - - - - -	Uncertain / inferred lithological contact		

APPENDIX B

THE LOWER HECHO GROUP

This appendix is composed of representative sedimentary logs of each sandy system in the Lower Hecho Group. The location of each measured section is provided; refer to Figure 2.4 for a locality map. Each log illustrates the sedimentary characteristics of the outcrop, measured and analysed at a bed-by-bed scale. See Figure B0 for the symbols used in the sedimentary logs.

Fig. B1. Detailed sedimentary log through the Fosado channel complex, Fosado village. Latitude 42 25' 46.326" N; Longitude 0 15' 17.650" E (locality 1, Figure 2.4).
Fig. B2. Detailed sedimentary log through the Los Molinos system, Barranco Sierre. Latitude 42 26' 10.820" N; Longitude 0 12' 50.623" E (locality 2, Figure 2.4).
Fig. B3. Detailed sedimentary log through the Arro system, Rio Nata. Latitude 42 24' 25.909" N; Longitude 0 14' 22.762" E (locality 3, Figure 2.4).
Fig. B4. Detailed sedimentary log through the Arro system, Barranco Sierre. Latitude 41 31' 36.091" N; Longitude 0 15' 40.003" E (locality 6, Figure 2.4).
Fig. B5. Detailed sedimentary log through the Gerbe system, Charo canyon. Latitude 42 23' 30.933" N; Longitude 0 15' 8.906" E (locality 9, Figure 2.4).
Fig. B6. Detailed sedimentary log through the Gerbe II sequence, Barranco Pasata. Latitude 42 28' 50.944" N; Longitude 0 6' 36.950" E (locality 11, Figure 2.4).

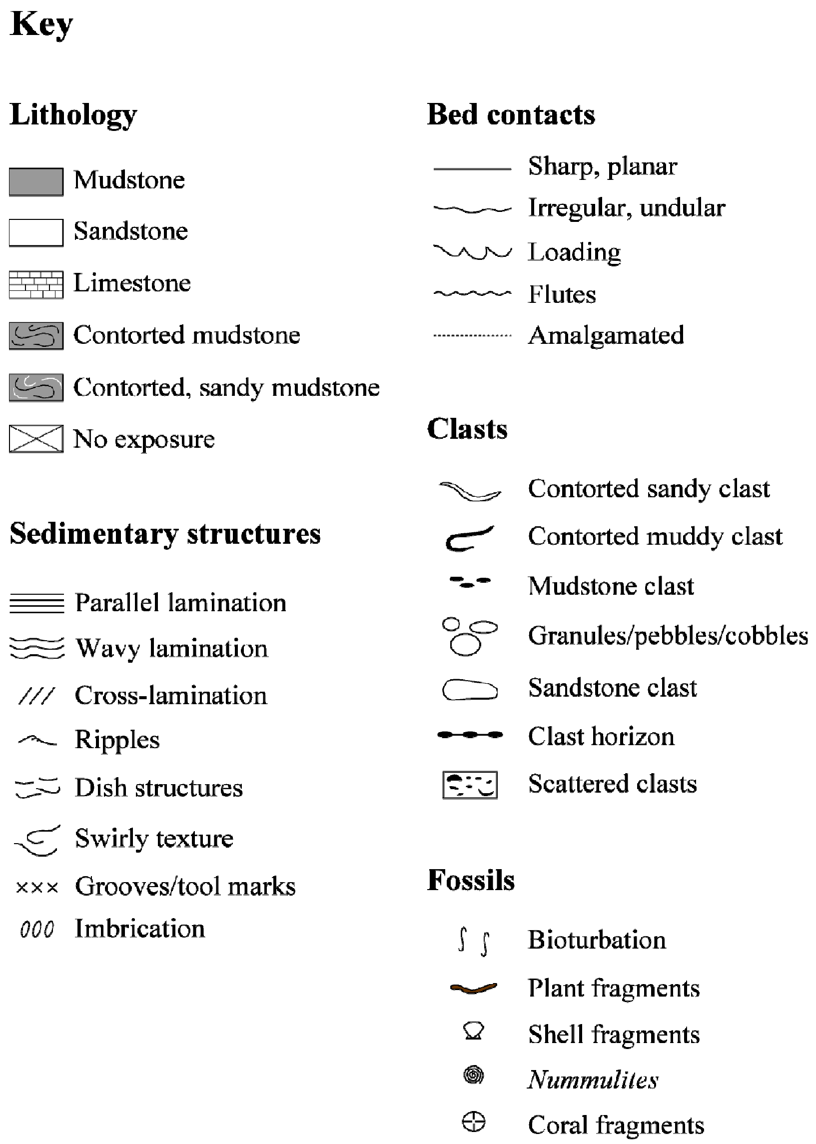

Fig. B0. Key for symbols used in sedimentary logs.

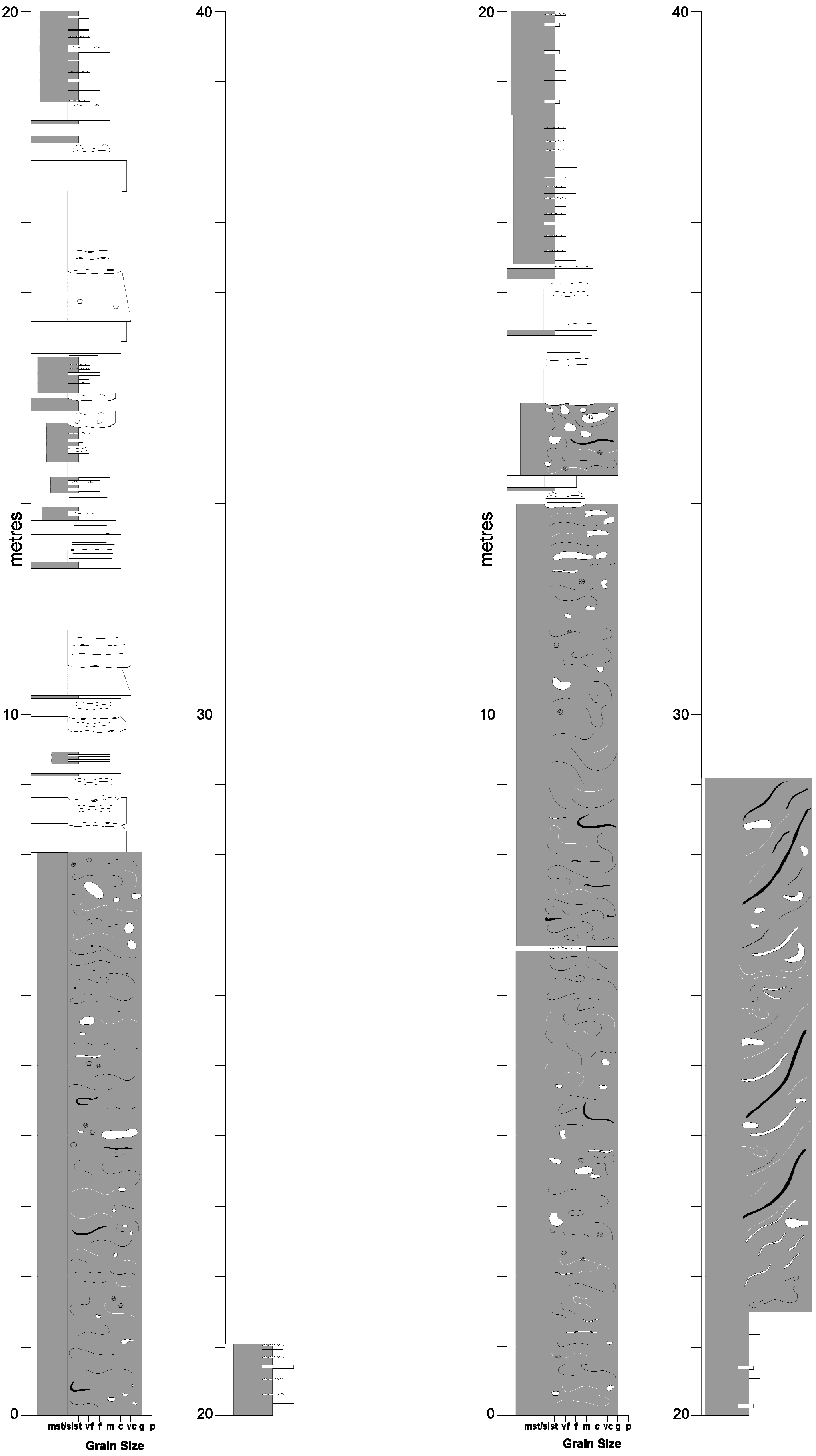

Fig. B1. ***Axis*** ***Off-axis***

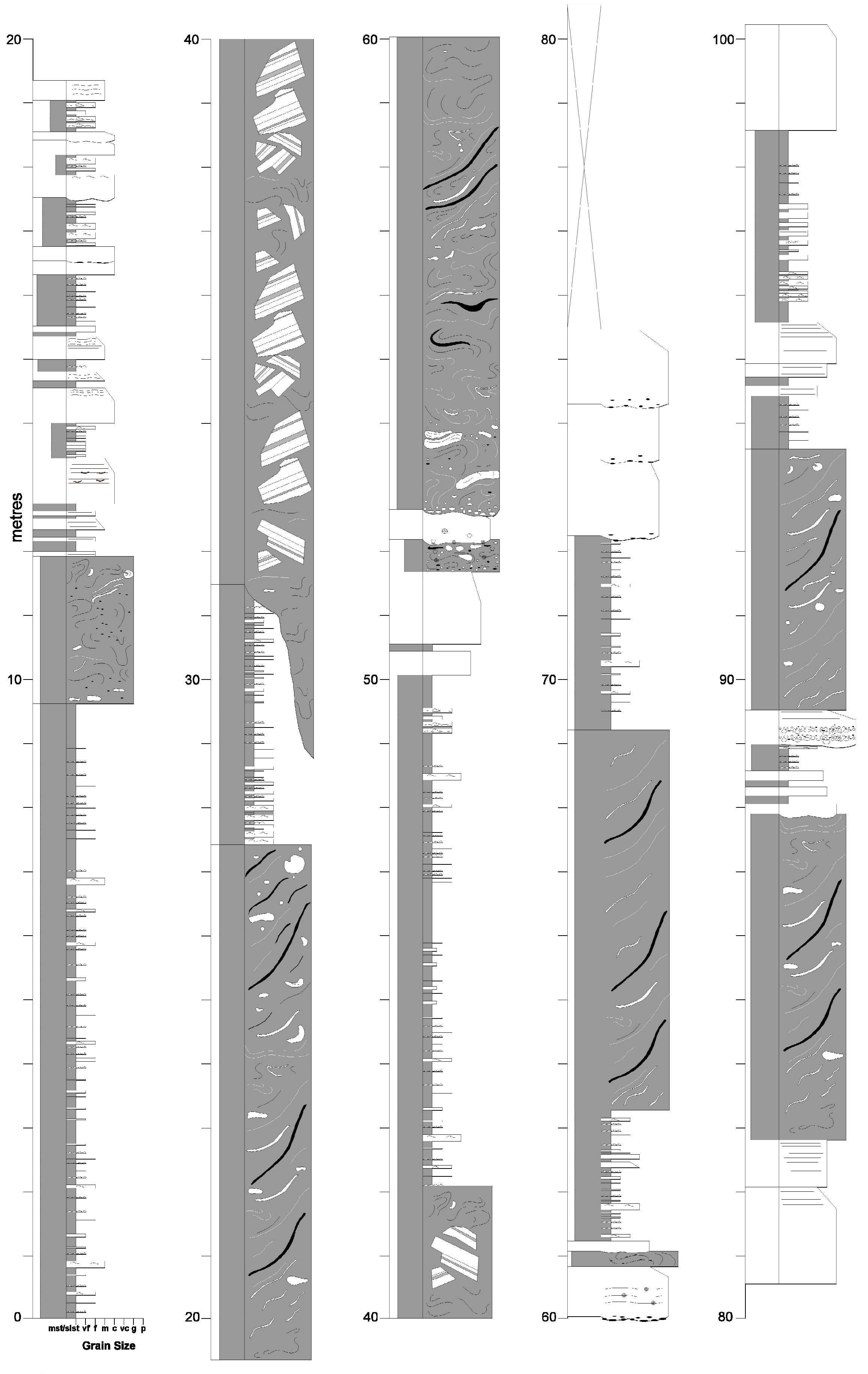
20
10
0
metres
mst/slst vf f m c vc g p
Grain Size
40
30
20
60
50
40
80
70
60
100
90
80

Fig. B2.

Fig. B3.

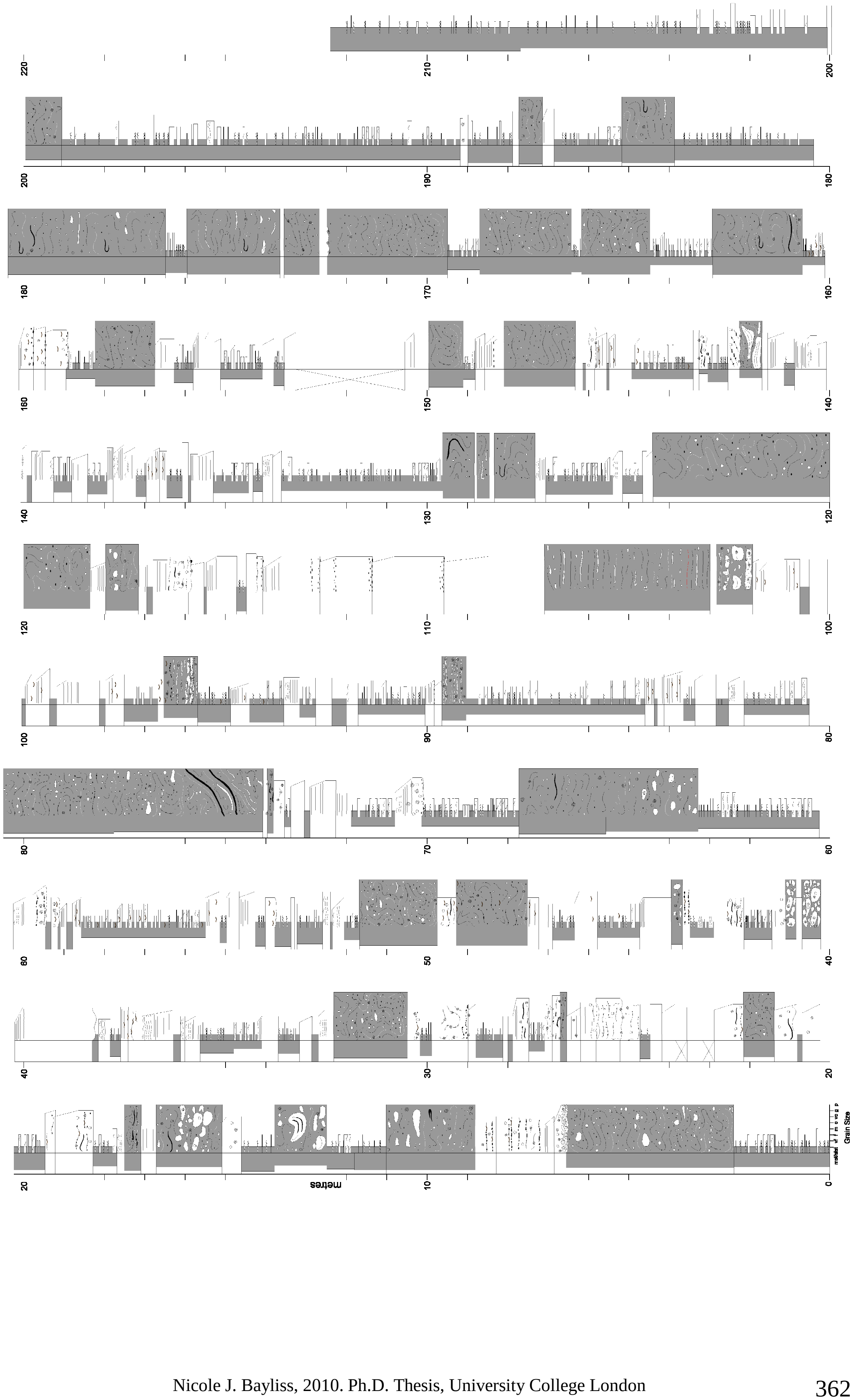
220
210
200
190
180
170
160
150
140
130
120
110
100
90
80
70
60
50
40
30
20
10
0
metres
mst/slst
vf
f
m
c
vc
g
p
Grain Size

Fig. B4.

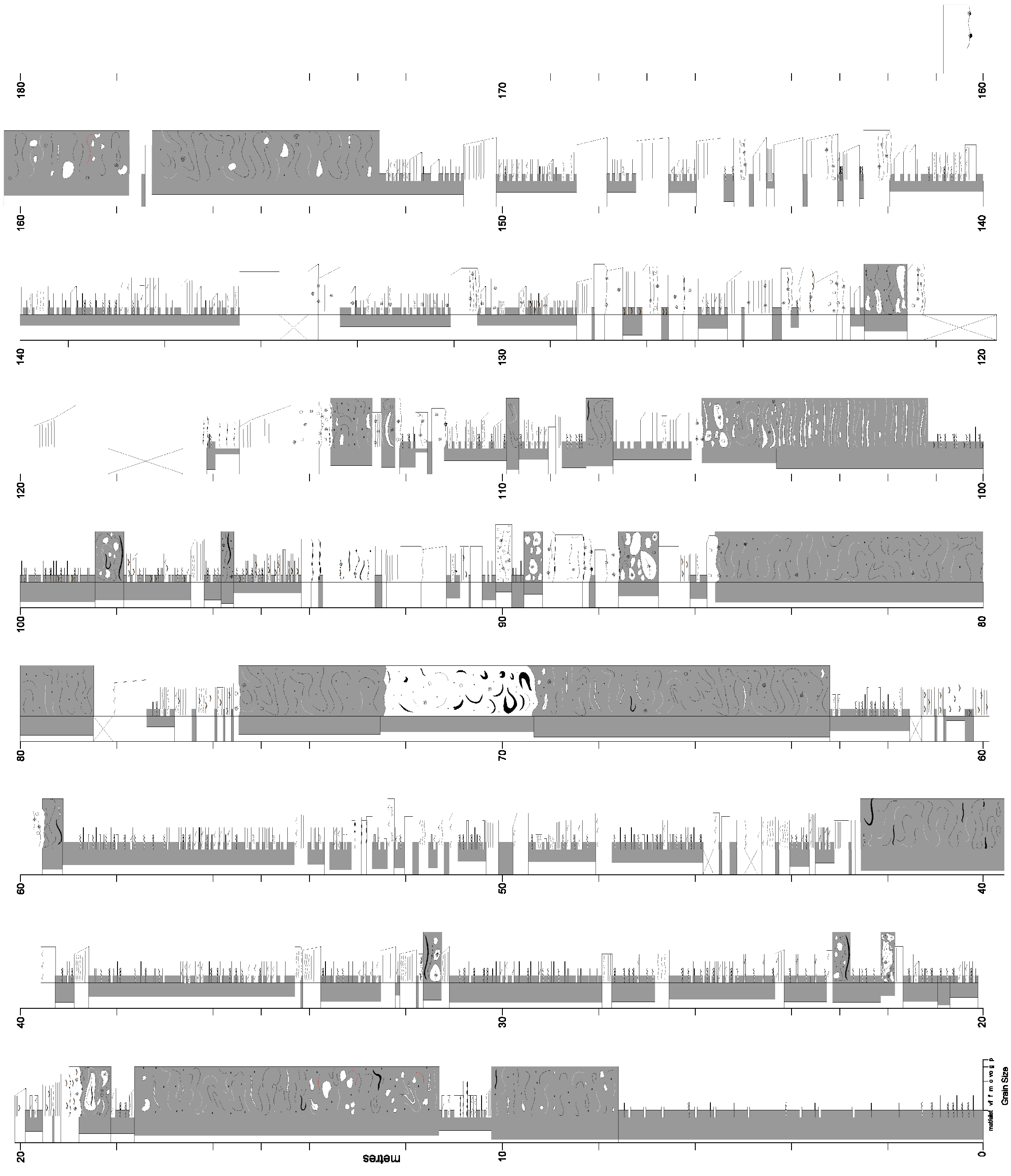
0
10
20
20
30
40
40
50
60
60
70
80
80
90
100
100
110
120
120
130
140
140
150
160
160
170
180
metres
Grain Size
mat/silt
vf
f
m
c
vc
g
p

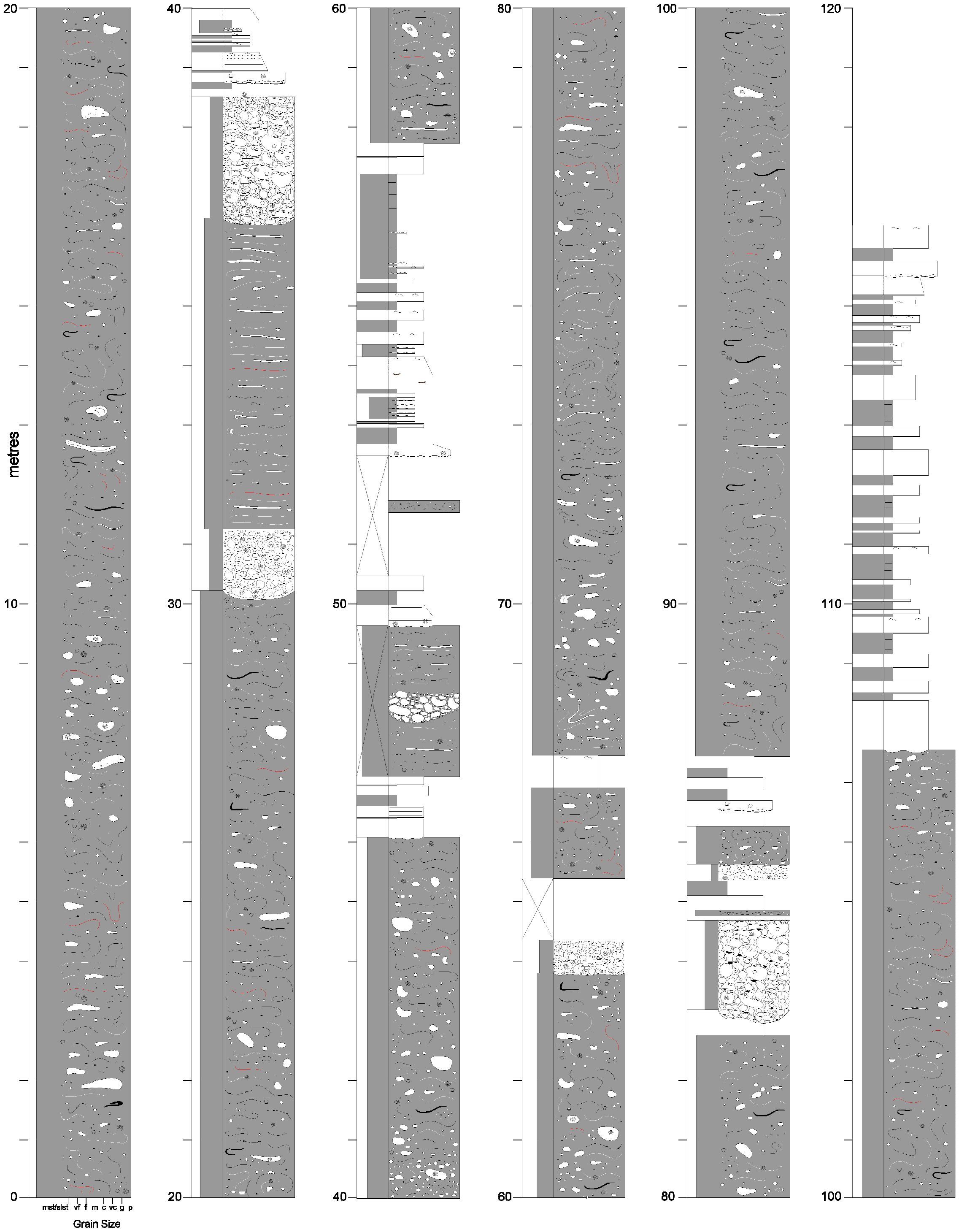

20
10
0
metres
mst/slst vf f m c vc g p
Grain Size
40
30
20
60
50
40
80
70
60
100
90
80
120
110
100

Fig. B5.

Fig. B6.

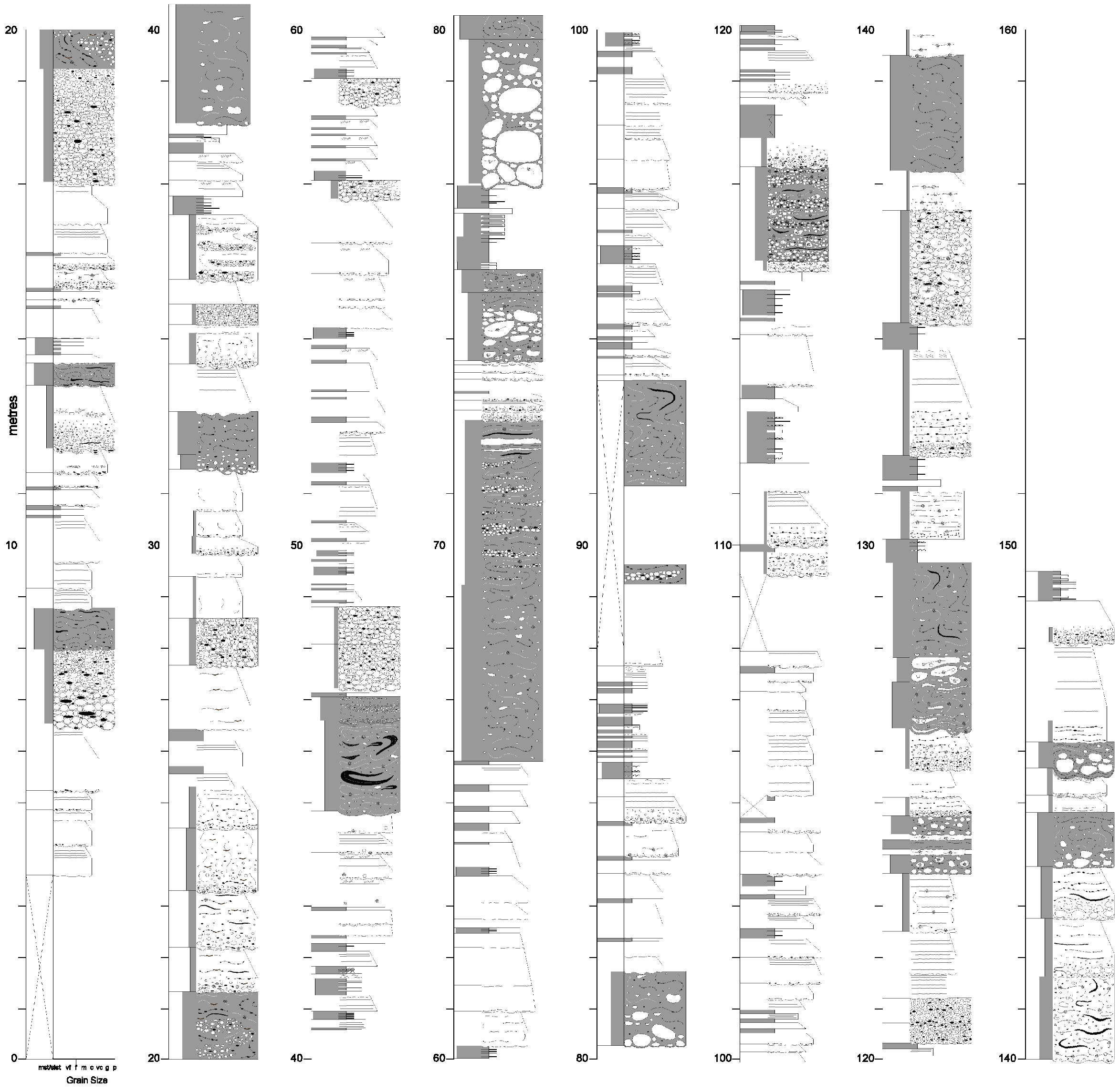
0
10
20
metres
30
40
50
60
70
80
90
100
110
120
130
140
150
160
mst/slst vf f m c vc g p
Grain Size

APPENDIX C

THE UPPER HECHO GROUP

This appendix is composed of representative sedimentary logs of each sandy system in the Upper Hecho Group. The location of each measured section is provided; refer to Figure 2.4 for a locality map. Each log illustrates the sedimentary characteristics of the outcrop, measured and analysed at a bed-by-bed scale. See Figure C0 for the symbols used in the sedimentary logs.

Fig. C1. Detailed sedimentary log through the Banastón I sequence, Barranco Pasata. Latitude 42 28’ 44.782” N; Longitude 0 6’ 36.796” E (locality 17, Figure 2.4).

Fig. C2. Detailed sedimentary log through the Banastón II sequence, Barranco Cortaroles. Latitude 42 28’ 14.354” N; Longitude 0 6’ 38.635” E (locality 22, Figure 2.4).

Fig. C3. Detailed sedimentary log through the Banastón III sequence, San Miguel. Latitude 42 28’ 5.250” N; Longitude 0 6’ 11.905” E (locality 24, Figure 2.4).

Fig. C4. Detailed sedimentary log through the Banastón IV sequence, Barranco San Martin. Latitude 42 27’ 50.011” N; Longitude 0 4’ 42.416” E (locality 27, Figure 2.4).

Fig. C5. Detailed sedimentary log through the Banastón V sequence, N-260 road, Boltaña. Latitude 42 27’ 22.103” N; Longitude 0 3’ 25.351” E (locality 30, Figure 2.4).

Fig. C6. Detailed sedimentary log through the Banastón VI sequence, N-260 road, Boltaña. Latitude 42 27’ 17.258” N; Longitude 0 3’ 26.017” E (locality 32, Figure 2.4).

Fig. C7. Detailed sedimentary log through the Morillo I and II sequences, Barranco Cotón, Morillo de Tou. Latitude 42 22’ 55.135” N; Longitude 0 9’ 4.913” E (locality 40, Figure 2.4).

Fig. C8. Detailed sedimentary log through the Morillo II sequence, Rio Ena. Latitude 42 25’ 13.350” N; Longitude 0 6’ 46.955” E (locality 44, Figure 2.4).

Fig. C9. Detailed sedimentary log through the Morillo I, II and III sequences, Rio Sieste. Latitude 42 25’ 53.390” N; Longitude 0 4’ 7.579” E (locality 41, Figure 2.4).

Fig. C10. Detailed sedimentary log through the Guaso I sequence, Rio Ena. Latitude 42 24’ 44.315” N; Longitude 0 6’ 39.758” E (locality 45, Figure 2.4).

Key

Lithology

- ▩ Mudstone
- □ Sandstone
- ▦ Limestone
- ▩ Contorted mudstone
- ▩ Contorted, sandy mudstone
- ⊠ No exposure

Sedimentary structures

- ≡ Parallel lamination
- ≋ Wavy lamination
- /// Cross-lamination
- ⌒ Ripples
- ⌣ Dish structures
- ∽ Swirly texture
- ××× Grooves/tool marks
- 000 Imbrication

Bed contacts

- ― Sharp, planar
- ∼ Irregular, undular
- ﹏ Loading
- 〰 Flutes
- ┈ Amalgamated

Clasts

- ∼ Contorted sandy clast
- ⌒ Contorted muddy clast
- -•- Mudstone clast
- ○ Granules/pebbles/cobbles
- ⬭ Sandstone clast
- •–•–• Clast horizon
- ⊡ Scattered clasts

Fossils

- ʃ ʃ Bioturbation
- ∼ Plant fragments
- ◡ Shell fragments
- ◎ *Nummulites*
- ⊕ Coral fragments

Fig. C0. Key for symbols used in sedimentary logs

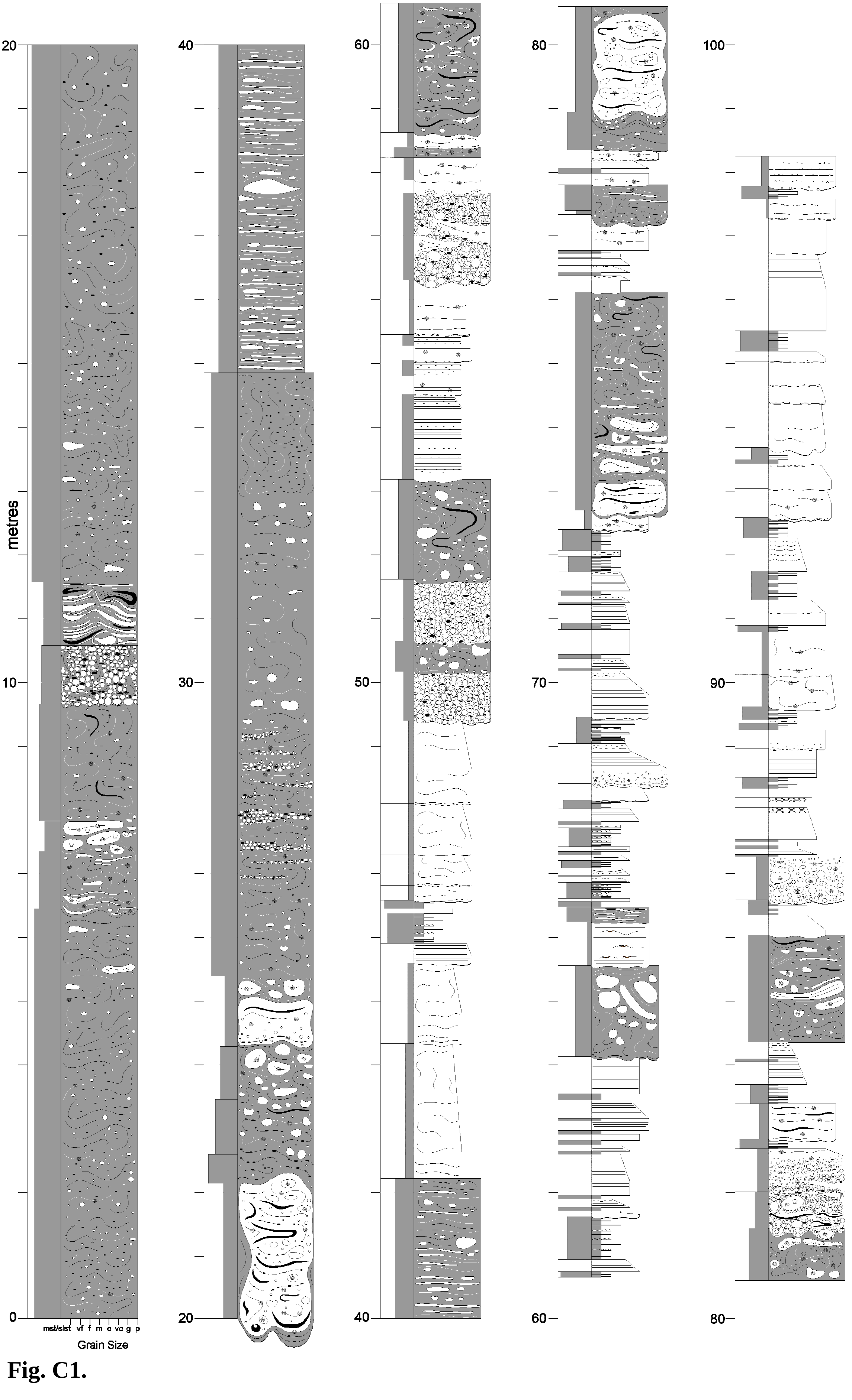
20
10
0
metres
mst/slst vf f m c vc g p
Grain Size
40
30
20
60
50
40
80
70
60
100
90
80

Fig. C1.

Fig. C2.

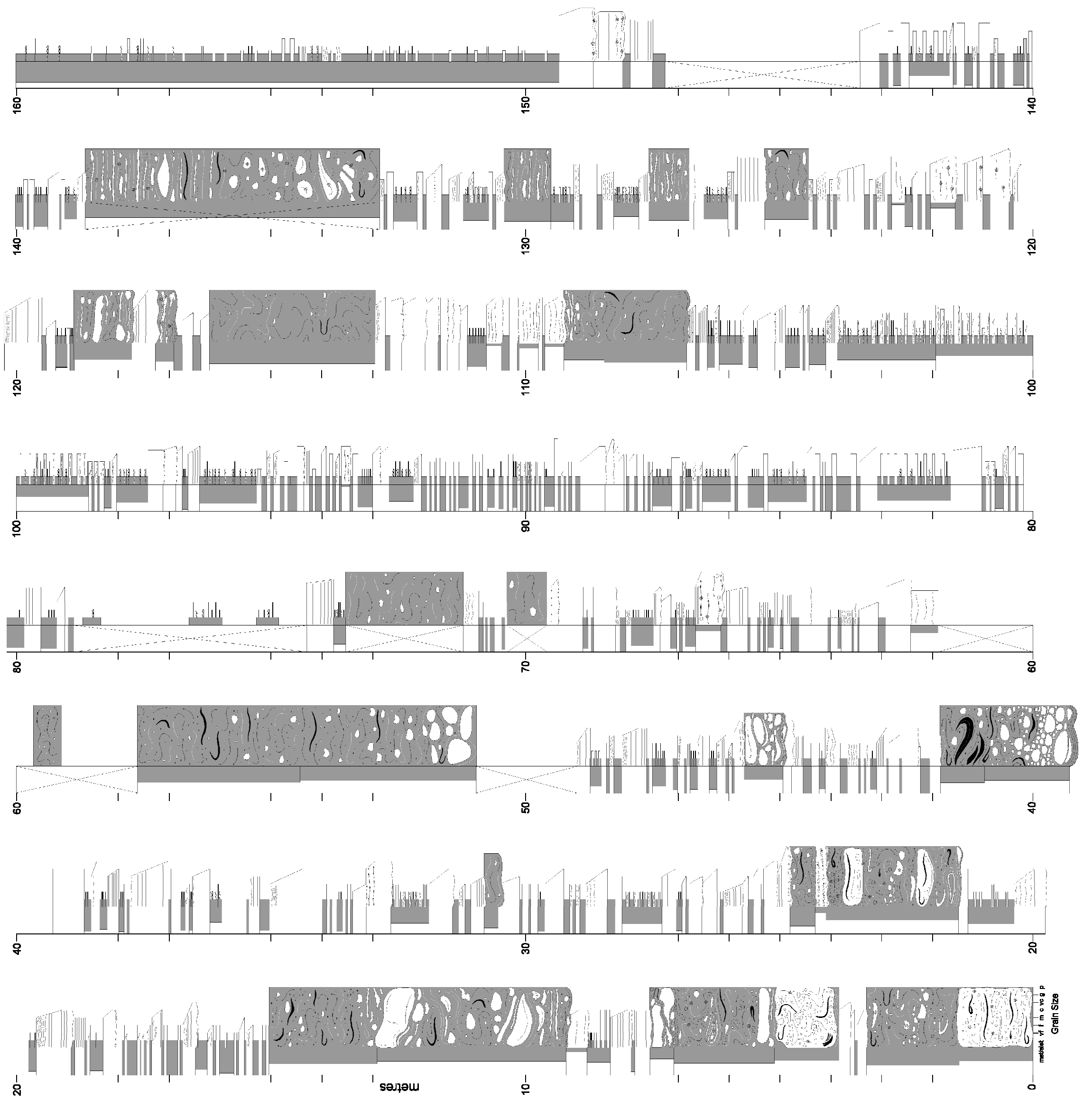

160
150
140
130
120
110
100
90
80
70
60
50
40
30
20
10
0
metres
mud/silt
vf
f
m
c
vc
g
p
Grain Size

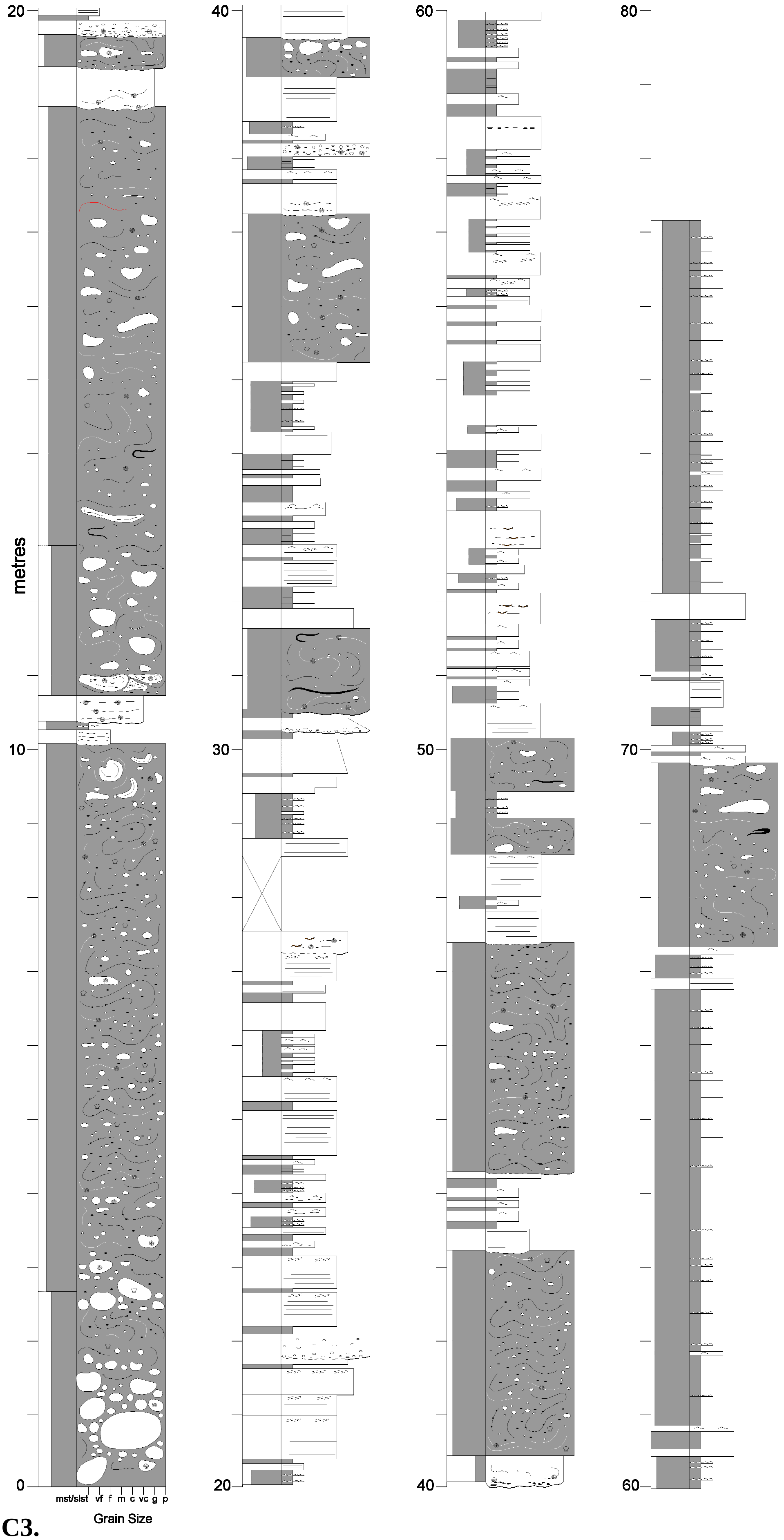
20
10
0
metres
40
30
20
60
50
40
80
70
60
mst/slst vf f m c vc g p
Grain Size

Fig. C3.

Fig. C4.

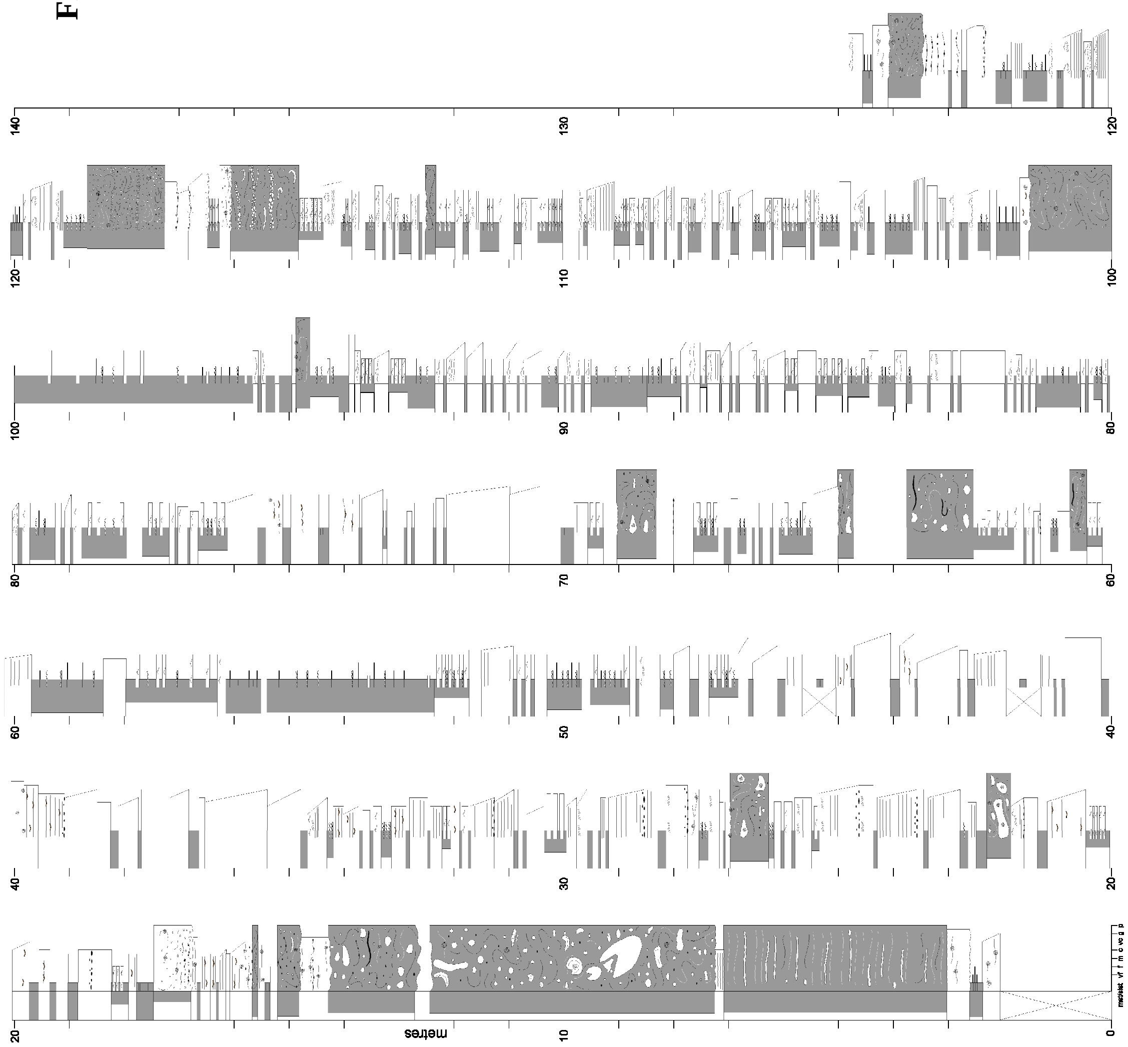
0
10
20
30
40
50
60
70
80
90
100
110
120
130
140
metres
mud/silt vf f m c vc g p
Grain Size

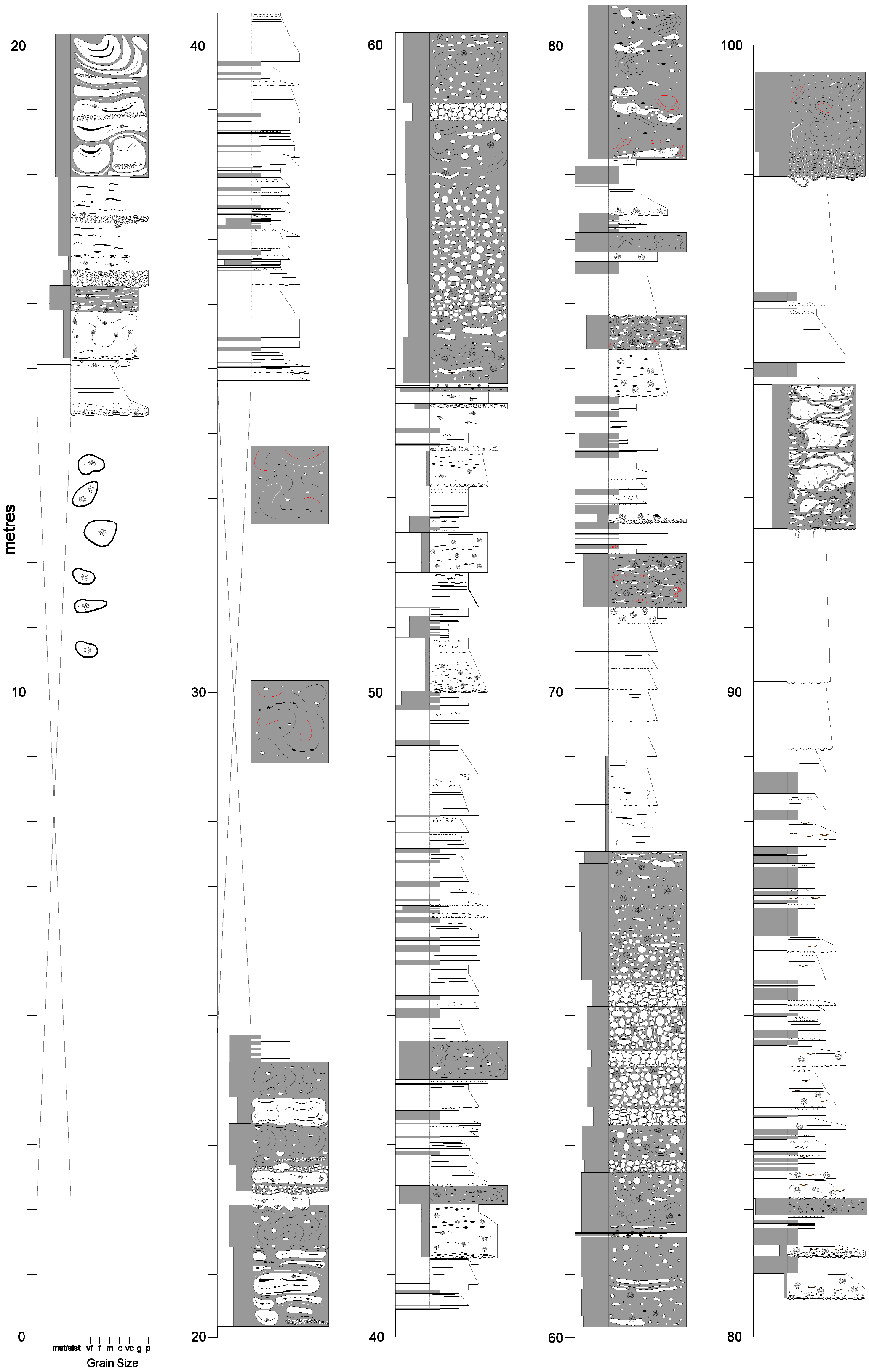
metres
0
10
20
30
40
50
60
70
80
90
100
mst/slst vf f m c vc g p
Grain Size

Fig. C5.

Fig. C6.

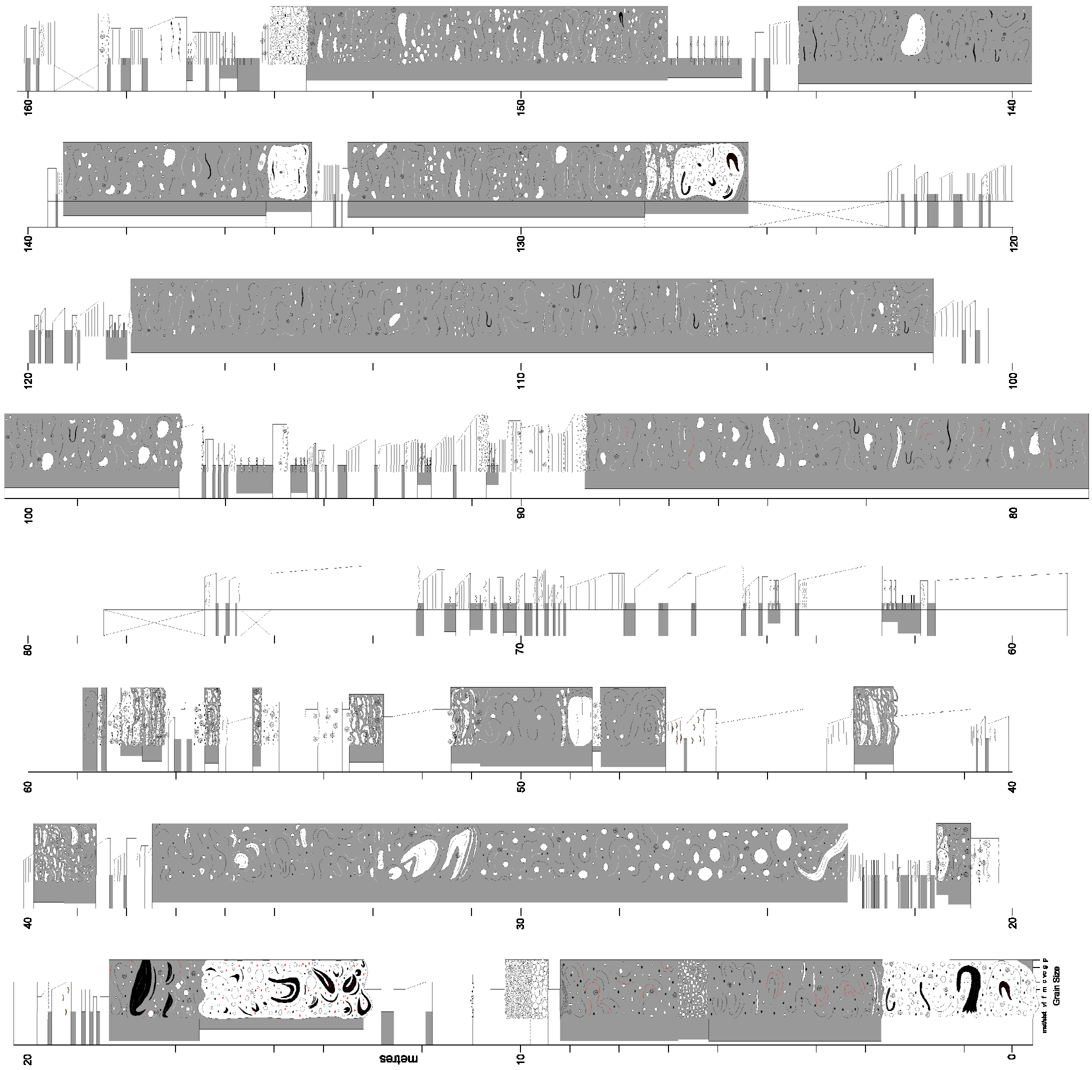

160
150
140
140
130
120
120
110
100
100
90
80
80
70
60
60
50
40
40
30
20
20
metres
10
0
mud/silt vf f m c vc g p
Grain Size

Fig. C7.

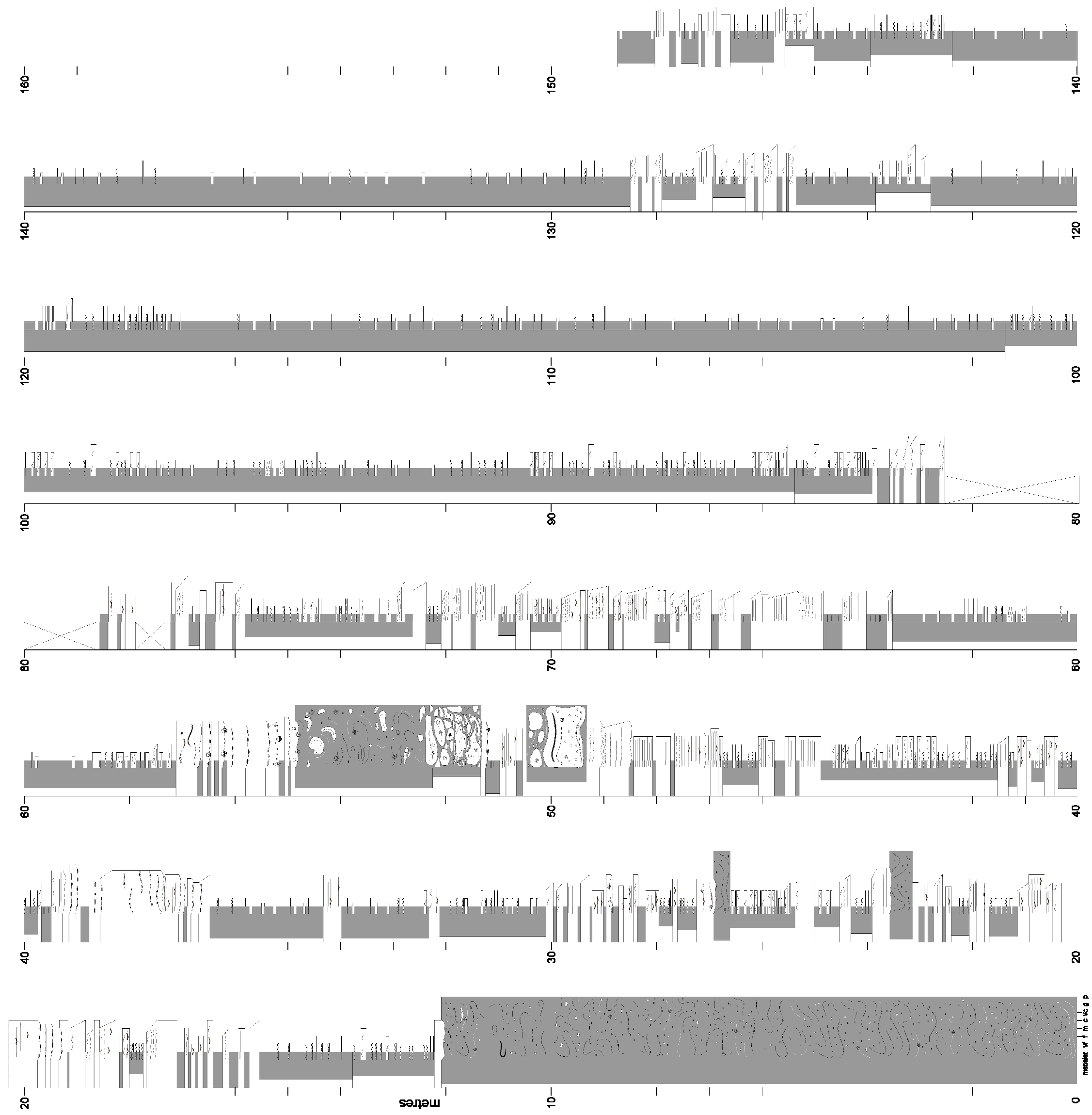
0
10
20
30
40
50
60
70
80
90
100
110
120
130
140
150
160
metres
mst/slst vf f m c vc g p
Grain Size

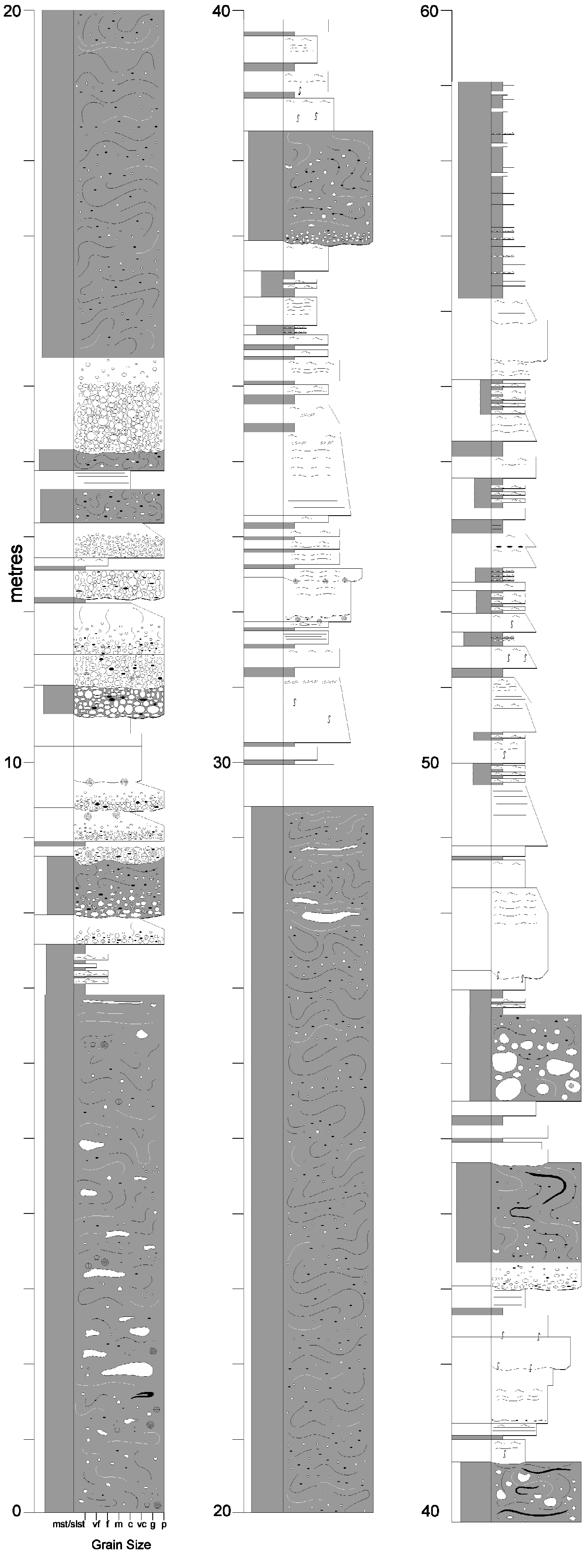

Fig. C8.

Fig. C9.

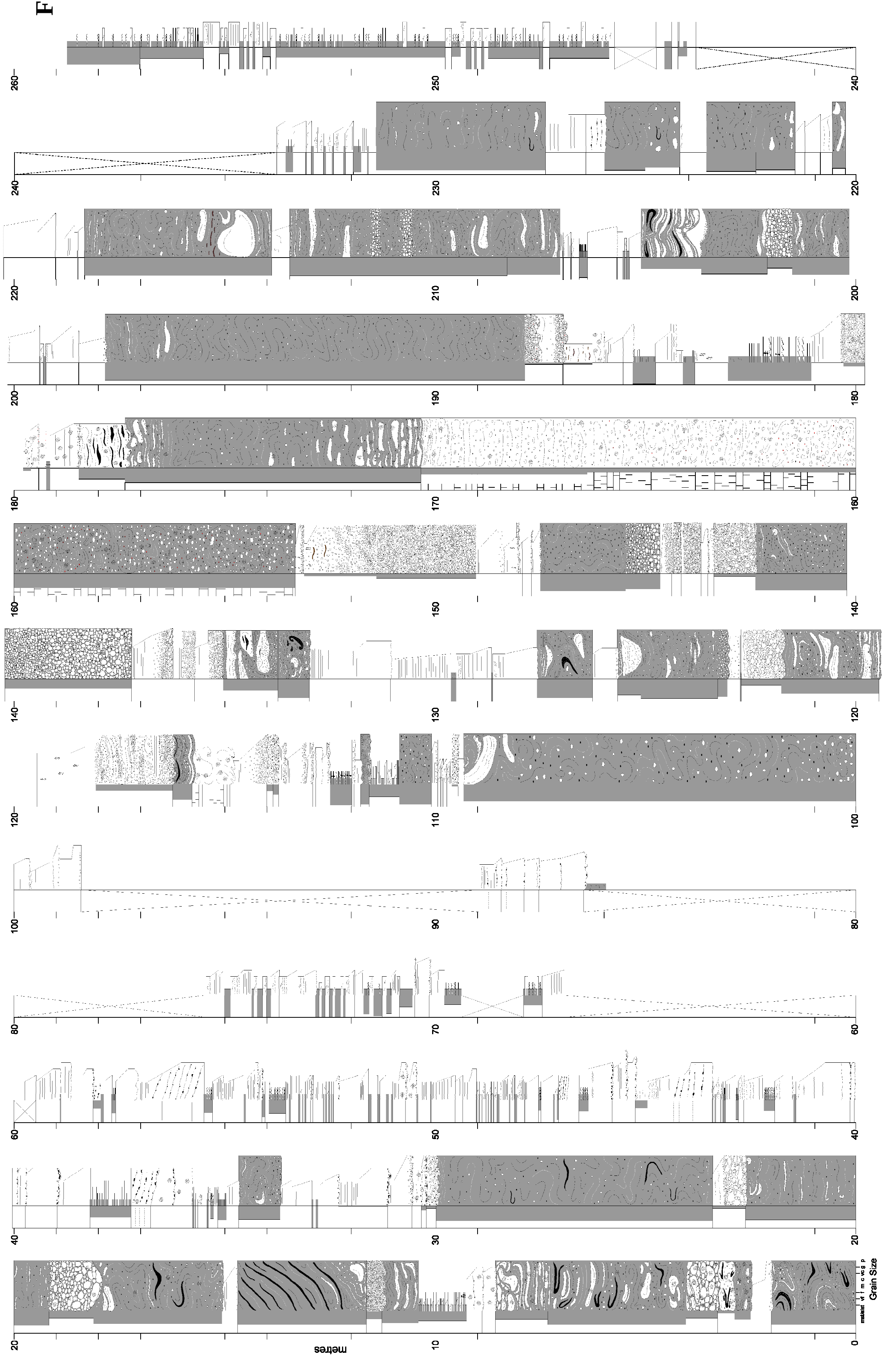
260
250
240
230
220
210
200
190
180
170
160
150
140
130
120
110
100
90
80
70
60
50
40
30
20
10
0
metres
mud/silt vf f m c vc g p
Grain Size

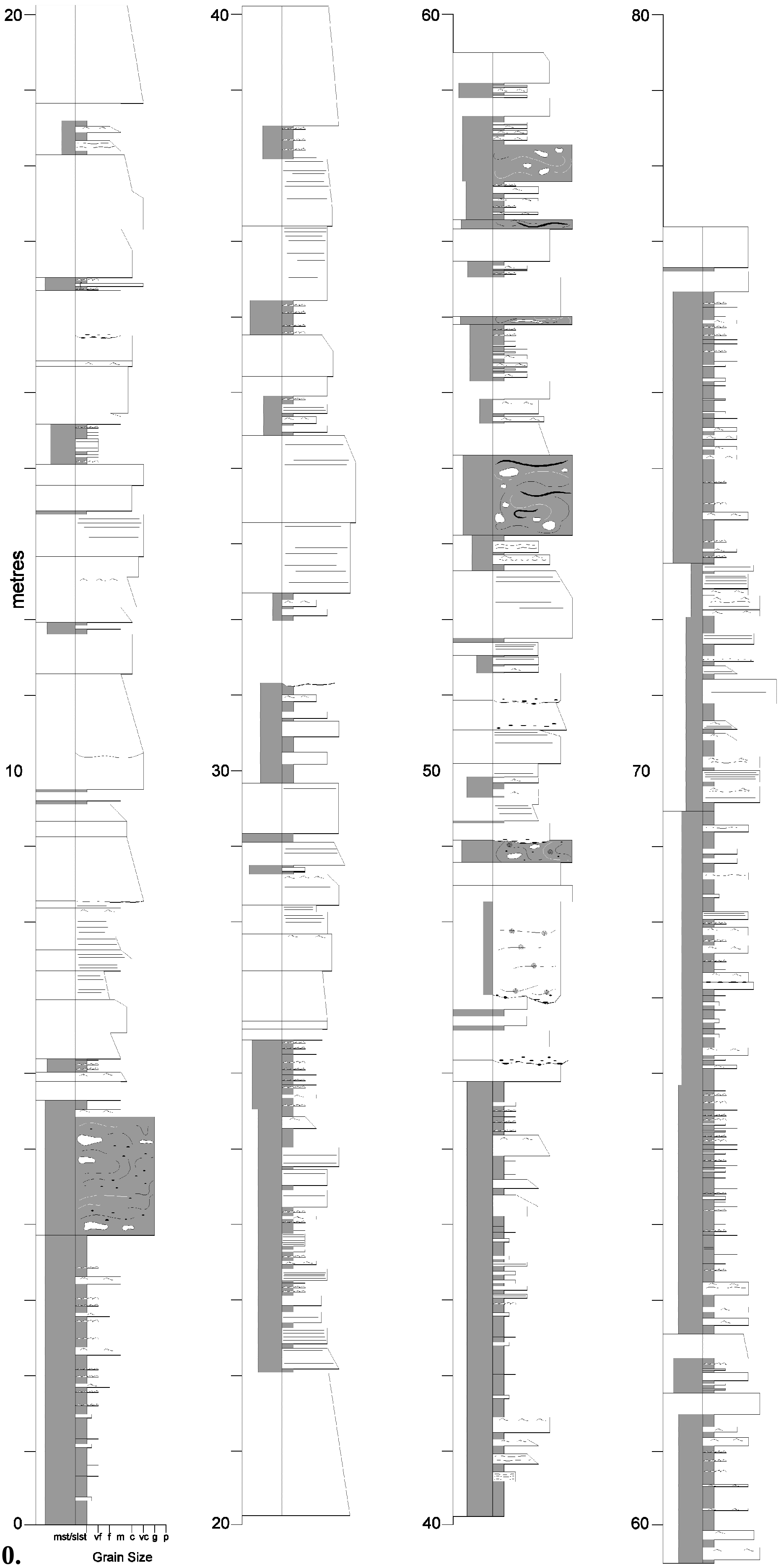
20
10
0
metres
mst/slst
vf
f
m
c
vc
g
p
Grain Size
40
30
20
60
50
40
80
70
60

Fig. C10.

APPENDIX D

PUBLISHED WORK

This thesis has discovered various important scientific contributions in the area of deep-water stratigraphy, which will be consolidated into a number of scientific publications. This appendix contains the first published paper derived from this study; others are to follow.